

NISTIR 8271 DRAFT SUPPLEMENT

Face Recognition Vendor Test (FRVT) Part 2: Identification

Patrick Grother
Mei Ngan
Kayee Hanaoka
*Information Access Division
Information Technology Laboratory*

This document is a draft supplement of [NIST Interagency Report 8271](#)

2022/02/23



NISTIR 8271 DRAFT SUPPLEMENT

Face Recognition Vendor Test (FRVT) Part 2: Identification

Patrick Grother
Mei Ngan
Kayee Hanaoka
*Information Access Division
Information Technology Laboratory*

This document is a draft supplement of [NIST Interagency Report 8271](#)

February 2022



U.S. Department of Commerce
Gina M. Raimondo, Secretary

National Institute of Standards and Technology
James K. Olthoff, Performing the Non-Exclusive Functions and Duties of the Under Secretary of Commerce for Standards and Technology & Director, National Institute of Standards and Technology

RELEASE NOTES

2022-02-23: The 1:N track of the FRVT remains open.

- ▷ This document is the fourteenth draft update to [NIST Interagency Report 8271](#). It includes results for algorithms recently submitted by two first-time participants: Cloudwalk - Moontime Smart Technology, Decatur Industries Inc, NotionTag Technologies Private Limited, and Reveal Media Ltd.
- ▷ The document also includes results for algorithms from five returning developers: Cognitec Systems GmbH, Sensemte Group, and Viettel Group
- ▷ The [1:N results page](#) has been updated.

2022-01-20: The 1:N track of the FRVT remains open.

- ▷ This document is the fourteenth draft update to [NIST Interagency Report 8271](#). It includes results for algorithms recently submitted by two first-time participants: Daon and SQIsoft.
- ▷ The document also includes results for algorithms from five returning developers: Cyberlink Corp, NEC, Neurotechnology, Paravision, and Rank One Computing.
- ▷ The [1:N results page](#) has been updated.

2021-12-16: The 1:N track of the FRVT remains open.

- ▷ This document is the thirteenth draft update to [NIST Interagency Report 8271](#). It includes results for algorithms from six returning developers: Dahua Technology, Imagus Technology, Line Corporation, N-Tech Lab, Qnap Security, and Realnetworks Inc.
- ▷ The [1:N results page](#) has been updated.

2021-11-22: The 1:N track of the FRVT remains open.

- ▷ This document is the twelfth draft update to [NIST Interagency Report 8271](#). It includes results for algorithms recently submitted by three first-time participants Clearview AI, Griaule, and Mantra Softech India.
- ▷ This document and the [1:N results page](#) also include results for algorithms from six returning developers: Acer Incorporated, Canon, Dermalog, Samsung S1, VisionLabs, and Veridas Digital Authentication.

2021-10-28: The 1:N track of the FRVT remains open.

- ▷ This document is the eleventh draft update to [NIST Interagency Report 8271](#). It includes results for algorithms recently submitted by three first-time participants (20Face, Fujitsu Research and Development Center, and Vision-Box), and five returning participants (Alchera, Gorilla Technology, Tevian, Thales-Cogent, and Visidon). Visidon
- ▷ Both the main [1:N results page](#) and the small-gallery [paperless travel page](#) have been updated.

2021-09-21: The 1:N track of the FRVT remains open. Three news items:

- ▷ This document is the tenth draft update to [NIST Interagency Report 8271](#). It includes results for algorithms recently submitted by six first-time developers: Cubox, Fincore, HyperVerge, Qnap Security, Staqu Technologies, and Tripleize (Aize, 3-ize).
- ▷ It includes results also for four returning developers: Cognitec Systems, Incode Technologies, Innovatrics, Neurotechnology, and Rank One Computing.

2021-08-02: The 1:N track of the FRVT remains open. Three news items:

- ▷ This document is the ninth draft update to [NIST Interagency Report 8271](#). It includes results for algorithms recently submitted by eight participants: Cyberlink Corp, NEC Corp, N-Tech Lab, Realnetworks Inc., Sensetime Group, Veridas Digital, Viettel Group, and Vigilant Solutions.
- ▷ Algorithms submitted since July 24 will be included in the next update scheduled for September 9, 2021.
- ▷ A new report, NIST Interagency Report 8381 - FRVT Part 7: Identification for Paperless Travel and Immigration, has been released [[PDF](#), [webpage](#)]. It documents the use of FRVT 1:N algorithms in positive access control and immigration status update travel applications where the enrolled population size is as low as 420 people for aircraft boarding, and 42 000 for an airport security line. These population sizes are much smaller than those used in the main [1:N evaluation](#). Going forward, we will update the report and webpage with results for new algorithms.

2021-07-07: The 1:N track of the FRVT remains open. One update:

- ▷ This document is the eighth draft update to [NIST Interagency Report 8271](#). It include results for an algorithm from one participant: Kakao Enterprises.

2021-06-22: The 1:N track of the FRVT remains open. Three updates:

- ▷ This is the seventh draft of the update to [NIST Interagency Report 8271](#). It includes results for algorithms from three new participants: Line Corporation, Rendip, and Samsung S1 Corp.
- ▷ We have also added results for algorithms from five returning developers: Imagus Technology, Kneron, Tevian, Visidon, and Xforward AI Technology.
- ▷ The algorithm-specific report cards (examples: [1](#), [2](#), and [3](#)) now include figures showing how low threshold values can be used to reduce candidate list lengths for human review, while (usually) elevating miss rates (FNIR) only modestly. The reports also feature some minor additions and clarifications.

2021-03-26: The 1:N track of the FRVT remains open. Three updates:

- ▷ This is the sixth draft of the update to [NIST Interagency Report 8271](#). It includes results for algorithms from three returning developers: Neurotechnology, Guangzhou Pixel Solutions, and Tech5 SA.
- ▷ We have added results on the webpage and in the report for a new ageing dataset in which border crossing photos are searched against a gallery of border crossing photos collected between 10 and 15 years prior to the mated search photos. See section [2](#) for a description of the images. Table [1](#) has a new entry describing the experiment.
- ▷ We will mostly discontinue running the mugshot ageing test, reserving it for algorithms that show high accuracy on the new border-crossing set.

2021-03-26: Regarding the fifth draft of the update to [NIST Interagency Report 8271](#):

- ▷ In addition have added results for first algorithms from two new participants: Viettel Group and Veridas Digital Authentication Solutions.
- ▷ We have added results for algorithms from two returning developers: Idemia and Cognitec Systems.
- ▷ In addition to the report, the [results page](#) and its hyperlinked [report cards](#) have been updated.

2021-02-08: Regarding the fourth draft of the update to [NIST Interagency Report 8271](#):

- ▷ We have added results for eight algorithms submitted by eight developers: Cyberlink, Dermalog, Imagus, Paravision, Sensetime, Trueface, Vigilant Solutions, and X-Forward AI. With the exception of Trueface, all of these developers have participated previously.
- ▷ We anticipate updating this report again in the first week of March 2021.

- ▷ The main [results page](#) has been revised with tabs for the investigative and lights-out identification tables, and a new tab dedicated to speed and resource consumption.
- ▷ The report cards (example [here](#)) hyperlinked from the [results page](#) have been revised to improve content and format.

2020-12-14: Regarding third draft of the update to [NIST Interagency Report 8271](#):

- ▷ We have added results for fifteen algorithms submitted by thirteen developers. The four first-time participants are: Acer, Akurat Satu Indonesia, Canon, and Xforward AI Technology. The ten returning developers are: AllGoVision, Cyberlink Corp, Dahua Technology, Deepglint, Guangzhou Pixel Solutions, IIT Vision, Innovatrics, Rank One Computing, Scanovate, Sensetime Group, Synesis, and VisionLabs.
- ▷ We have added two new datasets to the evaluation: First a set of “visa-border” photos, representing search of an airport immigration lane photo against a database of closely ISO standard portraits; second a “visa-kiosk” set representing search of a photo collected in a registered traveller kiosk against the same ISO portrait gallery. The images are described in section [2.1](#).
- ▷ As in previous reports, we include results for searching mugshots against a mugshot gallery containing a single image of each of 12 million people. However we have suspending running searches against a gallery in which multiple lifetime photos per person are present, because this is computationally expensive. We retain a $N = 3$ million search test dedicated to ageing in which mugshots taken up to 18 years after the first photograph are searched - see Table [7](#).
- ▷ Tables containing computational resource information, Table [2](#) . . . , now include duration of the finalization step, in which search algorithms can, at their option, build fast-search data structures.
- ▷ We have linked revised per-algorithm PDF report cards from the main [results page](#).
- ▷ We have regenerated all figures and tables to drop algorithms submitted before June 2018. Results for prior algorithms appear in [archived editions](#) of this report.
- ▷ Going forward, we anticipate producing more frequent updates to this report. Developers may submit one algorithm to this evaluation every four calendar months.

2020-03-24: Regarding the second draft of the update to [NIST Interagency Report 8271](#):

- ▷ Adds results for three algorithms from three developers, Dermalog, Innovatrics, and Synesis.
- ▷ Adds Table [7](#) on ageing showing the increase in false negative rates with time elapsed between two photos. Some of the results were contained in graphs in prior editions of this report, but the table adds results for some newly submitted algorithms.
- ▷ Adjusts frontal mugshot results (for recent and lifetime consolidated galleries) to include the effect of removing some images that should not have been included in image test sets. These images were mostly profile views, images of tattoos containing faces, images of faces on tee shirts, and images of photographs on walls behind the intended subject. This affects many tables and reduces false negative identification rates for all algorithms. The reduction is larger for “recent” enrollments than for “lifetime consolidated” ones with the consequence that accuracy on recent images is now superior.

2020-02-26: Regarding the first draft of the update to [NIST Interagency Report 8271](#):

- ▷ Adds results for 38 algorithms from 31 different developers, eleven of whom are entirely new to the 1:N track of FRVT. These are Allgovision, Cyberlink, Deepsea Tencent, Farbar F8, Imperial College London, Intsys MSU, Kedacom, Kneron, Pixelall, and Scanovate.

DISCLAIMER

Specific hardware and software products identified in this report were used in order to perform the evaluations described in this document. In no case does identification of any commercial product, trade name, or vendor, imply recommendation or endorsement by the National Institute of Standards and Technology, nor does it imply that the products and equipment identified are necessarily the best available for the purpose.

INSTITUTIONAL REVIEW BOARD

The National Institute of Standards and Technology's Research Protections Office reviewed the protocol for this project and determined it is not human subjects research as defined in Department of Commerce Regulations, 15 CFR 27, also known as the Common Rule for the Protection of Human Subjects (45 CFR 46, Subpart A).

ACKNOWLEDGMENTS

The authors are grateful for the support and collaboration of the the Department of Homeland Security's Science & Technology Directorate (S&T), Office of Biometric Identity Management (OBIM), and Customs and Border Protection (CBP).

Additionally, the authors are grateful to staff in the NIST Biometrics Research Laboratory for infrastructure supporting rapid evaluation of algorithms.

Executive Summary

This document is a draft revision of the September 2019 report [NIST Interagency Report 8271](#). That report gave extensive documentation of face recognition applied to mugshots. This report extends that by adding more two more challenging datasets containing images with serious departures from canonical frontal image standards. The report also adds results for algorithms submitted to NIST since in 2019 and 2020. The algorithms, which implement one-to-many identification of faces appearing in two-dimensional images, are prototypes from the research and development laboratories of mostly commercial suppliers, and are submitted to NIST as compiled black-box libraries implementing a NIST-specified C++ test interface. The report therefore does not describe how algorithms operate. The report lists accuracy results alongside developer names and will therefore be useful for comparison of face recognition algorithms and assessment of absolute capability. The report is accompanied by a [webpage](#) with sortable results.

The evaluation uses six datasets: frontal mugshots, profile view mugshots, desktop webcam photos, visa-like immigration application photos, immigration lane photos, and registered traveler kiosk photos. These datasets are sequestered at NIST, meaning that developers do not have access to them for training or testing. This aspect is important because face recognition algorithms are very often deployed without the developer having access to the customers image data. A possible exception to this would be in a cloud-based application where the operational image data is uploaded to a cloud operated by a face recognition developer.

The major result in NIST IR 8271 was that massive gains in accuracy have been achieved in the years 2013 to 2018 and these far exceed improvements made in the prior period, 2010 to 2013. While the industry gains were broad - at least 30 developers' algorithms outperformed the most accurate algorithm from late 2013, there remains a wide range of capability. While this report shows accuracy gains only over the period 2018-2020, the most accurate algorithm reported here is substantially more accurate than anything reported in NIST IR 8271. This is evidence that face recognition development continues apace, and that FRVT reports are but a snapshot of contemporary capability.

From discussion with developers, the accuracy gains stem from the adoption of deep convolutional neural networks. As such, face recognition has undergone an industrial revolution, with algorithms increasingly tolerant of poorly illuminated and other low quality images, and poorly posed subjects. One related result is that a few algorithms correctly match side-view photographs to galleries of frontal photos, with search accuracy approaching that of the best c. 2010 algorithms operating on purely frontal images. The capability to recognize under a 90-degree change in viewpoint - pose invariance - has been a long-sought milestone in face recognition research.

With good quality portrait photos, the most accurate algorithms will find matching entries, when present, in galleries containing 12 million individuals, with rank one miss rates of approaching 0.1%. The remaining errors are in large part attributable to long-run ageing, facial injury and poor image quality. Given this impressive achievement - close to perfect recognition - an advocate might claim that cooperative face recognition is a solved problem, a statement that can be refuted with the following context and caveats:

- ▷ **Mugshots vs. less constrained captures:** The low error rates reported here are attained using mostly excellent cooperative live-capture mugshot images collected with an attendant present. Recognition in other circumstances, particularly those without a dedicated photographic environment and human or automated quality control checks, will lead to declines in accuracy. This is documented here for side-view images, poorer quality webcam images, and, particularly, for newly introduced ATM-style kiosk photos that were not originally intended for automated face recognition. In this case, recognition error rates are much higher, often in excess of 20% even with the more accurate algorithms which variously remain intolerant of face cropping (at image edge) and of large downward head pitch.
- ▷ **Algorithm accuracy spectrum:** Recognition accuracy is very strongly dependent on the algorithm and, more

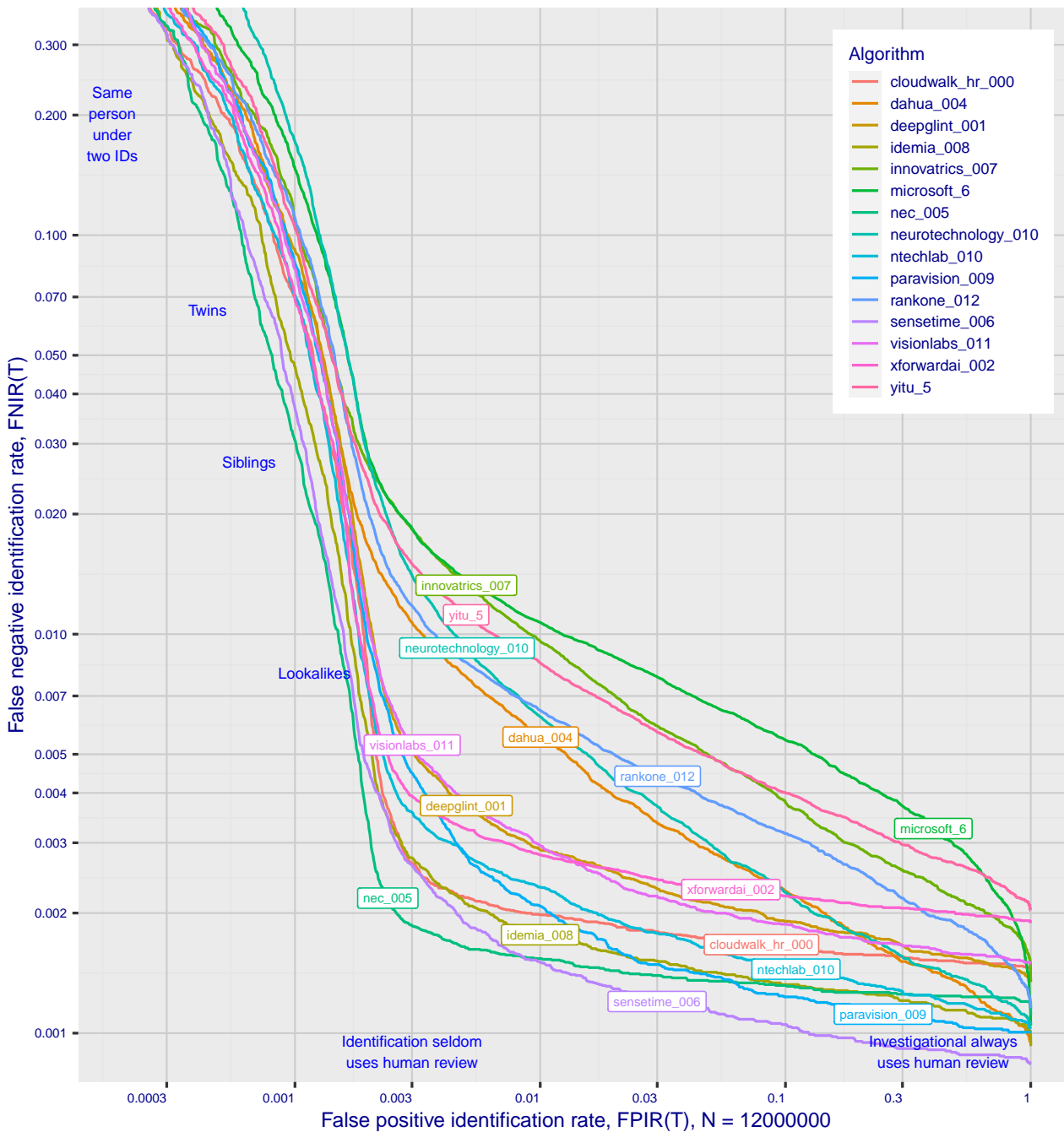


Figure 1: Identification miss rates across the false positive range. $N = 12$ million individuals are enrolled with one recent image.

generally, on the developer of the algorithm. False negative error rates in a particular scenario range from a few tenths of one percent to beyond fifty percent. This is tabulated exhaustively later: For example Table 10 shows accuracy across datasets. Figure 1 here compares algorithms on mugshot searches in a consolidated gallery of 12 million subjects and 12 million photos. Many algorithms do not achieve the low error rates noted above, and while many of those may still be useful and valuable to end-users, only the most accurate excel on poor quality images and those collected long after the initial enrollment sample.

▷ **Versioning:** While results for up to ten algorithms from each developer are reported here, the intra-provider

accuracy variations are usually smaller than the inter-provider variations. That said different versions give an order of magnitude fewer misses. Some developers demonstrate speed-accuracy tradeoffs¹. See Figs. 18, 19.

- ▷ **Low similarity scores:** In thousands of mugshot cases the correct gallery image is returned at rank 1 but its similarity score is nevertheless low, below some operationally required score threshold. This is not so important when face recognition is used for “lead generation” in investigational applications because human reviewers are specifically required to review potentially long candidate lists and the threshold is effectively 0. In applications where search volumes are higher and labor is not available to review the results from searches, a higher threshold must be applied. This reduces the length of candidate lists and false positive identification rates at the expense of increased false negative miss rates. The tradeoff between the two error rates is reported extensively later.
- ▷ **Population size:** As the number of enrolled subjects grows, some mates are displaced from rank one, decreasing accuracy. As tabulated later for N up to 12 million, false negative rates generally rise slowly with population size. This enables use of face recognition in very large populations. However in most positive and negative identification applications², a score threshold is set to limit the rate at which non-mate searches produce false positives. This has the consequence that some mated searches will report the mate below threshold, i.e. a miss, even if it is at rank 1. The utility of this is that many non-mated searches will return no candidate identities at all. As the error-tradeoff characteristic shows, investigational miss rates on the right side are very low but then rise steadily (in the center region) as threshold is increased to support “lights-out” applications, and ultimately rise quickly (left side) as discussed below. Thus, if we demand that just one in one thousand non-mate searches produce any false positives, the most accurate algorithms there (Sensetime-004 and NEC-3) would fail on between 3 and 5% of mated searches. Even though the graph shows results for the most accurate algorithms, all but two would fail to find the mate in more than 8% of mated searches. While the two most accurate algorithms produce a relatively flat error tradeoff until the threshold is raised to limit false positives to about 1 in 400 non-mated searches³.

Thereafter, as the threshold is raised to further reduce false positives, miss rates rise rapidly. This means that low false positive identification rates are inaccessible with these algorithms, a result that does not apply for ten-finger identification algorithms. The rapid rise occurs because the lower mate scores are mixed with very high non-mate scores, the low scores from poor image quality and ageing, the high non-mates from the presence of lookalikes persons (doppelgangers), twins (discussed next) and, ultimately, the presence of a few unconsolidated subjects i.e. persons present under multiple IDs.

- ▷ **False negatives from ageing:** A large source of error in long-run applications where subjects are not re-enrolled on a set schedule is ageing. Changes in facial appearance increase with the time elapsed between photographs. These will depress similarity scores and eventually cause false negatives. All faces age and while this usually proceeds in a graceful and progressive manner, drug use can accelerate this [28]. Elective surgery may be effective in delaying it although this has not been formally quantified with face recognition. As ageing is essentially unavoidable, it can only be mitigated by scheduled re-capture, as in passport re-issuance. To quantify ageing effects, we used the more accurate algorithms to enroll the earliest image of 3.1 million adults and then search

¹For example, NEC-0 prepares templates much faster than NEC-2 but gives twenty times more misses. Dermalog-5 executes a template search much more quickly than Dermalog-6 but is also much less accurate.

²In a positive identification application such as a registered traveler system, a user is making an implicit claim to be enrolled in the system - most users will be. In a negative application, such as with deportees, the implicit claim is that the subject is not enrolled - most will not be.

³The gallery size here is 12 million people, one image per person. Given 331 201 non-mated searches, an exhaustive implementation of one-too-many search would execute almost 4 trillion comparisons. At a false positive identification rate of 0.0025 the number of false positives is, to first order, 828 corresponding to single-comparison false match rate of $828 / 4 \text{ trillion} = 2.1 \times 10^{-10}$ i.e. about 1 in 5 billion. Strictly this FMR computation is meaningful only for algorithms that implement 1:N search using N 1:1 comparisons, which is not always the case.

with 10.3 million newer photos taken up to 18 years after the initial enrollment photo. Figure 2 puts ageing into context by contrasting it with the increase in false negatives that occurs when the number of individuals in an enrollment database becomes larger and the chance of a false positive increases such that higher thresholds may become necessary⁴.

The Figure shows, from top to bottom, increases in false negative identification rates (FNIR) with the algorithm being tested. This applies to increases due to N on the left side, and increases due to ageing on the right side. The relative spacing of the dots shows that for all algorithms the dependency of FNIR on N (up to 12 million) is considerably less than on ΔT (up to 18 years).

In the inset table, accuracy is seen to degrade progressively with time, as mate scores decline and non-mates displace mates from rank 1 position. More accurate algorithms tend to be less sensitive to ageing. The more accurate algorithms give fewer errors after 18 years of ageing than middle tier algorithms give after four. Note also we do not quantify an ageing rate - more formal methods [2] borrowed from the longitudinal analysis literature have been published for doing so (given suitable repeated measures data). See Figures 60, 82 and 93.

⁴Some algorithms implement strategies to automatically adjust scores to account for increased population size. This relieves the system owner of having to increase thresholds as N increases.

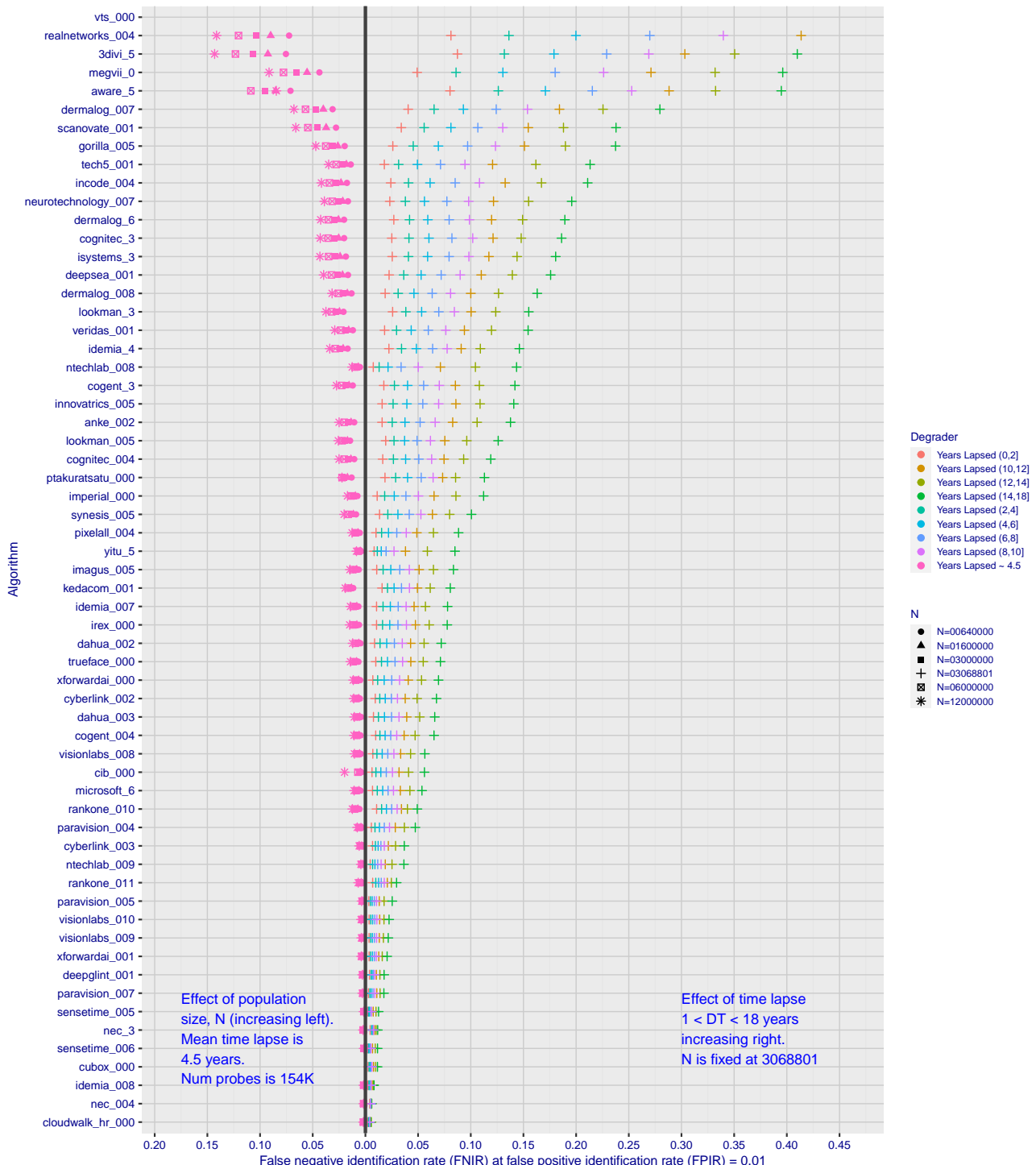


Figure 2: Identification miss rates as a function of enrolled population size, N , and time-lapse, ΔT .

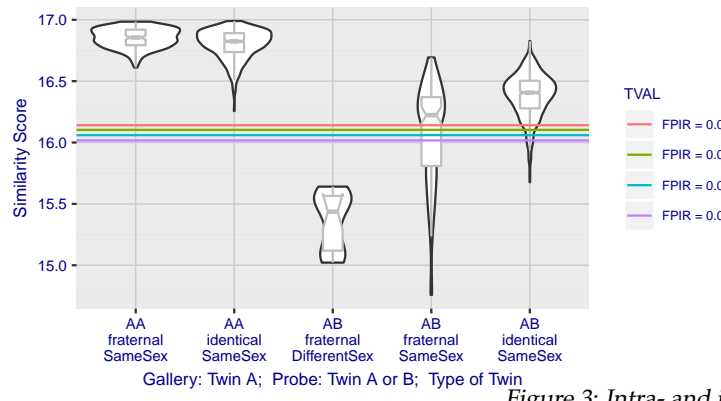


Figure 3: Intra- and inter-twin scores

▷ **False positives from twins:** By enrolling 640 000 mugshots, adding photos of one twin, and then searching photos of those subjects and their twin the inset figure shows, for one typical algorithm, the similarity is generally greater when searching twins against themselves (A) than when searching twins against their sibling (B) but very often still above even stringent thresholds i.e. those corresponding to one in one thousand searches producing a false positive. Thus twins will very often produce a high-scoring non-match on a candidate list and a false alarm in an online identification system. The plot of Fig. 3 shows that fraternal twins are sometimes correctly rejected at those thresholds - including most different sex twins (at center). Figure ?? shows substantially similar behavior for all algorithms tested. In an investigative search, a twin would typically appear at rank 1, or rank 2 if their sibling happened to also be the gallery. Twins (and triplets etc.) constituted 3.3% of all live births [17] in recent years⁵, and because that number is higher today than when the individuals in current adult databases were born, the false positives that arise from twins are now, and will increasingly be, an operational problem. Relative to the United States, twins are born with considerable regional variation. For example they are much less common in East Asia, and much more common in Sub-Saharan Africa [21].

The presence of twins in the mugshot database is inevitable given its size, around 12.3 million people. As this is not an insignificant sample of the domestic United States population, people with other familial ties will be present also. The data was collected over an extended period and because location information is not available, we are unable to estimate the proportion of the domestic population that is present in the dataset. However, if we assume twins are neither more or less disposed to arrest than the general population, we can estimate that hundreds of thousands of individuals in the dataset are twins. This will affect false positive rates because we randomly set aside 331 201 individuals for nonmate searches, and some proportion of those will be twins with siblings in the gallery.

▷ **Database integrity:** An operational error rate should be added to all false negative rates in this report reflecting the proportion of images in a real database that are un-matchable. Such anomalies arise from images that: do not contain a face; include multiple persons; cannot be decoded; are rotated by 90° or 180°; depict a face on clothing; and others introduced by a long tail of various clerical errors. While the mugshot trials in this report have been constructed to minimize such effects, they are a real problem in actual operations.

This report is being updated continuously as new algorithms are submitted to FRVT, and run on new datasets. Participation in the [one-to-many identification track](#) is independent of participation in the [one-to-one verification track](#) of FRVT.

⁵See the CDC's National Vital Statistics Report for 2017: https://www.cdc.gov/nchs/data/nvsr/nvsr67/nvsr67_08-508.pdf

Scope and Context

Audience: This report is intended for developers, integrators, end users, policy makers and others who have some familiarity with biometrics applications. The methods and metrics documented here will be of interest to organizations engaged in tests of face recognition algorithms. Some of these have been incorporated in the ISO/IEC 19795 Part 1 Biometric Testing and Reporting Framework standard, now nearing publication.

Prior benchmarks: Automated face recognition accuracy has improved massively in the two decades since initial commercialization of the various technologies. NIST has tracked that improvement through its conduct of regular independent, free, open, and public evaluations. These have fostered improvements in the state of the art. This report serves as an update to the [NIST Interagency Report 8271](#) on performance of face identification algorithms, published in September 2019.

Demographics: In December 2019, NIST published a first report on demographic dependencies in face recognition, [NIST Interagency Report 8280](#) that documented age, sex and race differentials in one-to-one and one-to-many false positive and false negative rates.

Scope: NIST IR 8271 documented recognition results for four databases containing in excess of 30.2 million still photographs of 14.4 million individuals. That constituted the largest public and independent evaluation of face recognition ever conducted. It includes results for accuracy, speed, investigative vs. identification applications, scalability to large populations, use of multiple images per person, images of cooperative and non-cooperative subjects.

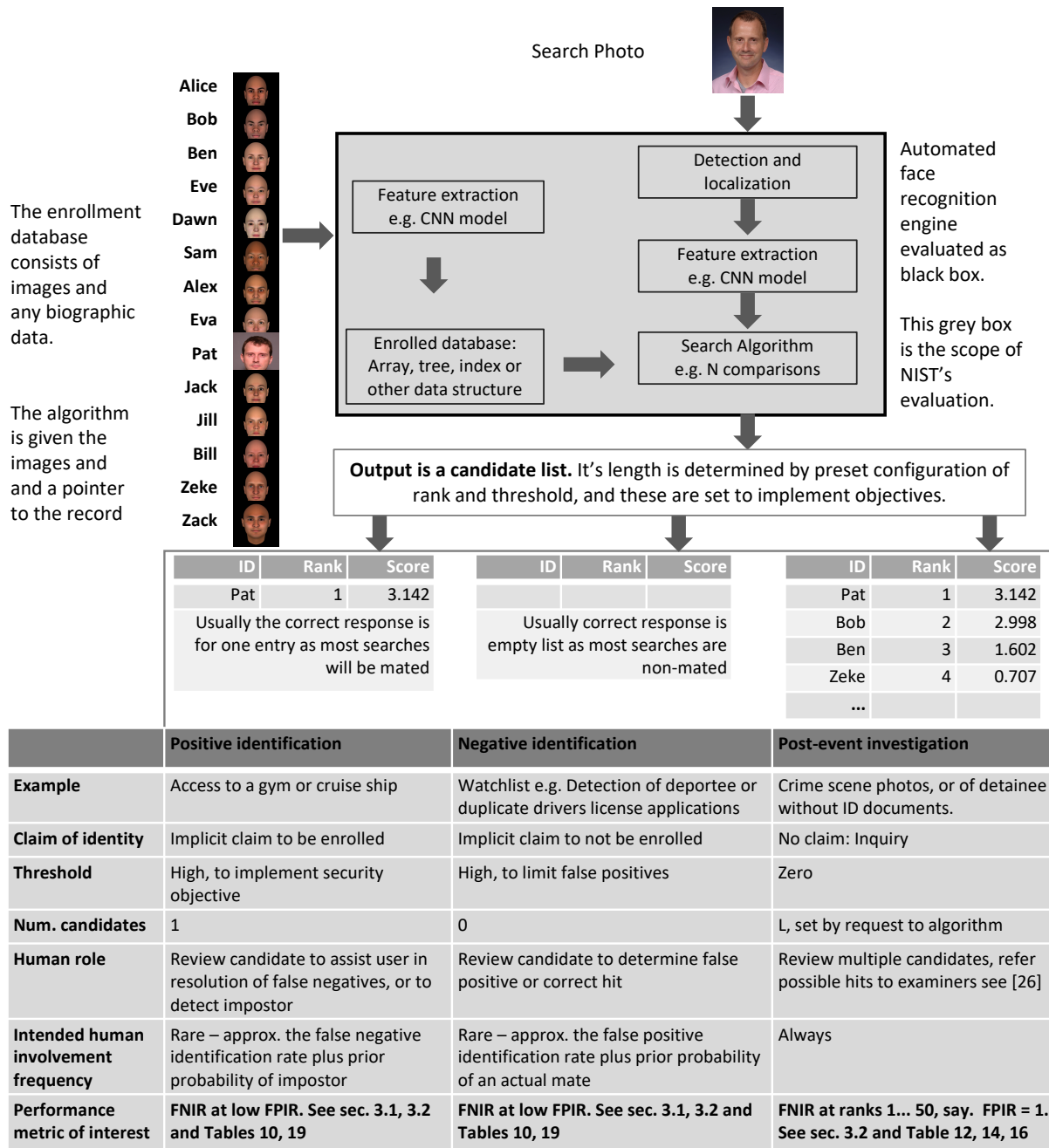
The report also includes results for ageing, recognition of twins, and recognition of profile-view images against frontal galleries. It otherwise does not address causes of recognition failure, neither image-specific problems nor subject-specific factors including demographics. Separate reports on demographic dependencies in face recognition will be published in the future. Additionally out of scope are: performance of live [human-in-the-loop transactional systems](#) like automated border control gates; human recognition accuracy as used in forensic applications; and recognition of persons in video sequences (which NIST evaluated separately [9]). Some of those applications share core matching technologies that *are* tested in this report.

Images: Five kinds of images are employed; these are either compared with images of the same kind, or against others from different capture environments as follows. The primary dataset is a set of law enforcement mugshot images (Fig. 5) which are enrolled and then searched with three kinds of images: other mugshots (i.e. within-domain); profile-view photographs (90 degree cross-view); and lower quality webcam images (Fig. 6) collected in similar detention operations (cross-domain). Additionally we compare high quality visa-like photos collected in immigration offices, with: medium quality border crossing images collected in primary immigration lanes; poor quality images collected in ATM-like registered traveller kiosks.

Participation and industry coverage: The report includes performance figures for prototype algorithms from the research laboratories of commercial developers and a few universities. This represents a substantial majority of the face recognition industry, but only a tiny minority of the academic community. Participation was open worldwide. While there is no charge for participation, developers incur some software engineering expense in implementing their algorithms behind the NIST application programming interface (API). The test is a black-box test where the function of the algorithm, and the intellectual property associated with it, is hidden inside pre-compiled libraries.

Recent technology development: Most face recognition research with deep convolutional neural networks (CNNs) has been aimed at achieving invariance to pose, illumination and expression variations that characterize photojournalism and social media images. The initial research [18, 22] employed large numbers of images of relatively few ($\sim 10^4$) individuals to learn invariance. Inevitably much larger populations ($\sim 10^7$) were employed for training [11, 20] but the benchmark, Labeled Faces in the Wild with (essentially) an equal error rate metric [12], represents an easy task,

one-to-one verification at very high false match rates. While a larger scale identification benchmark duly followed, Megaface [15], its primary metric, rank one hit rate, contrasts with the high threshold discrimination task required in most large-population applications of face recognition, namely credential de-duplication, and background checks. There, identification in galleries containing up to 10^8 individuals must be performed using a) very few images per individual and b) stringent thresholds to afford very low false positive identification rates. This track of FRVT was launched to measure the capability of the new technologies, including in these two cases. FRVT has included open-set identification tests since 2002, reporting both false negative and positive identification rates [7].



Performance metrics for applications: This report documents the performance of one-to-many face recognition algorithms. The word "performance" here refers to recognition accuracy and computational resource usage, as measured

by executing those algorithms on massive sequestered datasets.

This report includes extensive tabulation of recognition error rates germane to the main use-cases for face search technology. The Figure below, inspired by the Figure 1 in [23] differentiates different applications of the technolgy. The last row directs readers to the main tables relevant to those applications, respectively threshold-based and rank-based metrics that are special cases of the metrics given in section 3. The terms negative identification and positive identification are taken from the ISO/IEC 2382-37:2017 standardized biometrics vocabulary.

The algorithms are specifically configured for these applications by setting thresholds and candidate list lengths. Both rank-based metrics and threshold-based metrics include tradeoffs. In investigation, overall accuracy will be reduced if labor is only available to review a few candidates from the automated system. Note that when a fixed number of candidates are returned, the false positive identification rate of the automated face recognition engine will be 100%, because a probe image of anyone not enrolled will still return candidates. In identification applications where false positives must be limited to satisfy reviewer labor availability or a security objective, higher false negative rates are implied. This report includes extensive quantification of this threshold-based tradeoff.

See Sec. 3

Template diversity: The FRVT is designed to evaluate black-box technologies with the consequence that the templates that hold features extracted from face images are entirely proprietary opaque binary data that embed considerable intellectual property of the developer. Despite migration to CNN-based technologies there is no consensus on the optimal feature vector dimension. This is evidenced by template sizes ranging from below 100 bytes to more than four kilobytes. This diversity of approaches, suggests there is no prospect of a standard template something that would require a common feature set to be extracted from faces. Interoperability in automated face recognition remains solidly based on images and documentary standards for those, in particular the ICAO portrait [27] specification deriving from the ISO/IEC 19794-5 Token frontal [24] standard, which are similar to certain ANSI/NIST Type 10 [26] formats.

Training: The algorithms submitted to NIST have been developed using image datasets that developers do not disclose. The development will often include application of machine learning techniques and will additionally involve iterative training and testing cycles. NIST itself does not perform any training and does not refine or alter the algorithm in any way. Thus the model, data files, and libraries that define an algorithm are fixed for the duration of the tests. This reflects typical operational reality where recognition software, once installed, is fixed and constant until upgraded. This situation persists because on-site training of algorithms on customer data is atypical essentially because training is not a turnkey process.

Automated search and human review: Virtually all applications using automated face search require human review of the outputs at some frequency: Always for investigational applications; rarely in positive identification applications, after rejection (false or otherwise); and rarely in negative identification applications, after an alarm (false or otherwise). The human role is usually to compare a reference image with the query image or the live-subject if present, to render either a definitive decision on “exclusion” (different subjects), or “identification” (same subject), or a declaration that one or both images have “no value” and that no decision can be made. Note that automated face recognition algorithms are not built to do exclusion - low scores from a face comparison arise from different faces *and* poor quality images of the same face.

Human reviewers make recognition errors [5, 19, 25] and are sensitive to image acquisition and quality. Accurate human review is supported by high resolution - as specified in the Type 50, 51 acquisition profiles of the ANSI/NIST Type 10 record [26], and by multiple non-frontal views as specified in the same standard. These often afford views of the ear. Organizations involved in image collection should consider supporting human adjudication by collecting high-resolution frontal and non-frontal views, preparing low resolution versions for automated face recognition [24], and retaining both for any subsequent resolution of candidate matches. Along these lines, the ISO/IEC Joint Technical

Committee 1 subcommittee 37 on biometrics has just initiated projects on image quality assessment and face-aware capture.

Release Notes

FRVT Activities: Since February 2017, NIST has been evaluating one-to-one verification algorithms on an ongoing basis. NIST then restarted FRVT's one-to-many track in February 2018, inviting participants to send up to prototype algorithms. Both tracks allows developers to submit updated algorithms to NIST at any time but no more frequently than four calendar months. This more closely aligns development and evaluation schedules. Results are posted to the web within a few weeks of submission. Details and full report are linked from the [Ongoing FRVT site](#).

FRVT Reports: The results of the FRVT appear in the series NIST Interagency Reports tabulated below. The reports were developed separately and released on different schedules. In prior years NIST has mostly reported FRVT results as a single report; this had the disadvantage that results from completed sub-studies were not published until all other studies were complete.

Date	Link	Title	No.
2014-03-20	PDF	FRVT Performance of Automated Age Estimation Algorithms	7995
2015-04-20	PDF	Face Recognition Vendor Test (FRVT) Performance of Automated Gender Classification Algorithms	8052
2014-05-21	PDF	FRVT Performance of face identification algorithms	8009
2017-03-07	PDF	Face In Video Evaluation (FIVE) Face Recognition of Non-Cooperative Subjects	8173
2017-11-23	PDF	The 2017 IARPA Face Recognition Prize Challenge (FRPC)	8197
2018-11-27	PDF	Face Recognition Vendor Test - Part 2: Identification	8271
2019-09-11	PDF	Face Recognition Vendor Test - Part 2: Identification	8271
2019-12-11	PDF	Face Recognition Vendor Test - Part 3: Demographic Effects	8280
2020-01-03	WWW	Face Recognition Vendor Test (FRVT) - Part 1 Verification	Draft

Details appear on pages linked from <https://www.nist.gov/programs-projects/face-projects>.

Appendices: This report is accompanied by appendices which present exhaustive results on a per-algorithm basis. These are machine-generated and are included because the authors believe that visualization of such data is broadly informative and vital to understanding the context of the report.

Typesetting: Virtually all of the tabulated content in this report was produced automatically. This involved the use of scripting tools to generate directly type-settable L^AT_EX content. This improves timeliness, flexibility, maintainability, and reduces transcription errors.

Graphics: Many of the Figures in this report were produced using the **ggplot2** package running under **R**, the capabilities of which extend beyond those evident in this document.

Contents

Release Notes	1
Disclaimer	4
Institutional Review Board	4
Acknowledgments	4
Executive Summary	5
Scope and Context	11
Release Notes	15
1 Introduction	17
2 Evaluation datasets	18
3 Performance metrics	24
4 Results	40
Appendices	75
A Accuracy on large-population FRVT 2018 mugshots	75
B Effect of time-lapse: Accuracy after face ageing	120
C Effect of enrolling multiple images	178
D Accuracy with poor quality webcam images	185
E Accuracy for profile-view to frontal recognition	195
F Search duration	199
G Gallery Insertion Timing	206

1 Introduction

One-to-many identification represents the largest market for face recognition technology. Algorithms are used across the world in a diverse range of biometric applications: detection of duplicates in databases, detection of fraudulent applications for credentials such as passports and driving licenses, token-less access control, surveillance, social media tagging, lookalike discovery, criminal investigation, and forensic clustering.

This report contains a breadth of performance measurements relevant to many applications. Performance here refers to accuracy and resource consumption. In most applications, the core accuracy of a facial recognition algorithm is the most important performance variable. Resource consumption will be important also as it drives the amount of hardware, power, and cooling necessary to accommodate high volume workflows. Algorithms consume processing time, they require computer memory, and their static template data requires storage space. This report documents these variables.

1.1 Open-set searches

FRVT tested open-set identification algorithms. Real-world applications are almost always “open-set”, meaning that some searches have an enrolled mate, but some do not. For example, some subjects have truly not been issued a visa or drivers license before; some law enforcement searches are from first-time arrestees⁶. In an “open-set” application, algorithms make no prior assumption about whether or not to return a high-scoring result, and for a mated search, the ideal behaviour is that the search produces the correct mate at high score and first rank. For a non-mate search, the ideal behavior is that the search produces zero high-scoring candidates.

Many academic benchmarks execute only closed-set searches. The proportion of mates found in the rank one position is the default accuracy metric. This hit rate metric ignores the score with which a mate is found; weak hits count as much as strong hits. This ignores the real-world imperative that in many applications it is necessary to elevate a threshold to reduce the number of false positives.

⁶Operationally closed-set applications are rare because it is usually not the case that all searches have an enrolled mate. One counter-example, however, is a cruise ship in which all passengers are enrolled and all searches should produce exactly one identity. Another example is forensic identification of dental records from an aircraft crash.

2 Evaluation datasets

This report documents accuracy for four kinds of images - mugshots, webcam, profiles and wild - as described in the following sections.

2.1 Immigration-related images

This report includes benchmark tests sharing a common enrollment of high quality frontal portrait images collected while subject make applications for various immigration benefits. We then search that with two kinds of images, webcam images collected during in-bound immigration and also images collected from registered travelers using a ATM-style kiosk. These are described below and depicted in Figure 4.



Figure 4: Example photos.

- ▷ **Application reference photos:** The images are collected in an attended interview setting using dedicated capture equipment and lighting. The images, at size 300x300 pixels, are smaller than normally indicated by ISO. The images are all high-quality frontal portraits collected in immigration offices and with a white background. As such, potential quality related drivers of high false match rates (such as blur) can be expected to be absent. The images are encoded as ISO/IEC 10918-1 i.e. JPEG. Older images had a compression ration of about 16:1, while newer images, since 2010, are more lightly compressed at 4:1. When these images are provided as input into the algorithm, they are labeled with the type "iso". This report enrols 1 600 000 application images, one per person.
- ▷ **Border crossing photos:** Most images are have width 320 and height 240 pixels. They are JPEG compressed at 16:1 i.e. filesize just below 15KB. The images present challenges for face recognition in that subjects often exhibit non-zero yaw and pitch (associated with the rotational degrees of freedom of the camera mount), low contrast (due to varying and intense background lights), and poor spatial resolution (due to inexpensive cameras). There are often subjects standing in the background, usually at very low resolution (see Figure 4b). In such cases, algorithms should detect all faces and determine which is the largest and most centered. When these images are provided as input into the algorithm, they are labeled with the type "wild".
- ▷ **Kiosk photos:** These photos were collected from subjects whose attention was focused on interaction with an immigration kiosk. They images were not intended for use with automated face recognition. The camera is situated above a display which the user touches, and is triggered either without directing the subject to look at it, or without waiting for the subject to comply. The images are therefore characterized by pitch-down pose, sometimes exceeding 45 degrees, as in Figure 4c. Yaw-angle variation is mild, with most images close to frontal. The images

have width 320 pixels and height 240 pixels and therefore tall individuals are sometimes cropped. This is often just above the eyes and can occur at the nose or mouth. Conversely, short individuals are sometimes cropped such that only the top part of the face is visible. In a quite small number of cases, there other subjects standing just behind the primary subject such that algorithms should detect all faces and determine which is the largest and most centered. Background ceiling lighting is often visible and this sometimes leads to under-exposure of the face. When these images are provided as input into the algorithm, they are labeled with the type "wild".

2.2 Law enforcement images

The main mugshot dataset used is referred to as the FRVT 2018 set. This set was collected over the period 2002 to 2017 in routine United States law enforcement operations. This set yields three subsets

- ▷ **Mugshots:** Mugshots comprise about 86% of the database. They have reasonable compliance with the ANSI/NIST ITL1-2011 Type 10 standard's subject acquisition profiles levels 10-20 for frontal images [26]. The most common departure from the standard's requirements is the presence of mild pose variations around frontal - the images of Figure 5 are typical. The images vary in size, with many being 480x600 pixels with JPEG compression applied to produce filesizes of between 18 and 36KB with many images outside this range, implying that about 0.5 bits are being encoded per pixel. When these images are provided as input into the algorithm, they are labeled with the type "mugshot".

Example images appear in Fig. 5

[NIST Interagency Report 8238](#) includes a comparison of this set of mugshots with the smaller and easier sets of mugshots used in tests run in 2010 and 2014.

- ▷ **Profile images:** Profile-view images have been collected in law enforcement for more than 100 years, as human capability is improved with orthogonal information. The profile images used in this report were collected during the same session as the frontal mugshot photograph, in the same standardized photographic setup. These would not therefore be used with automated face recognition. A small subset, 200 000 images, were set aside for testing. When these images are provided as input into the algorithm, they are labeled with the type "wild".

Example images appear in Fig. 7

- ▷ **Webcam images:** The remaining 14% of the images were collected using an inexpensive webcam attached to a flexible operator-directed mount. These images are all of size 240x240 pixels, that are in considerable violation of most quality-related clauses of all face recognition standards. As evident in the figure, the most common defects are non-frontal pose (associated with the rotational degrees of freedom of the camera mount), low contrast (due to varying and intense background lights), and poor spatial resolution (due to inexpensive camera optics) - see examples in Fig 6. The images are overly JPEG compressed, to between 4 and 7KB, implying that only 0.5 to 1 bits are being encoded per color pixel. When these images are provided as input into the algorithm, they are labeled with the type "wild".

Example images appear in Fig. 6

These are drawn from NIST Special Database 32 which may be downloaded [here](#).

These images were partitioned in galleries and probesets for the various experiment listed in Table 1.

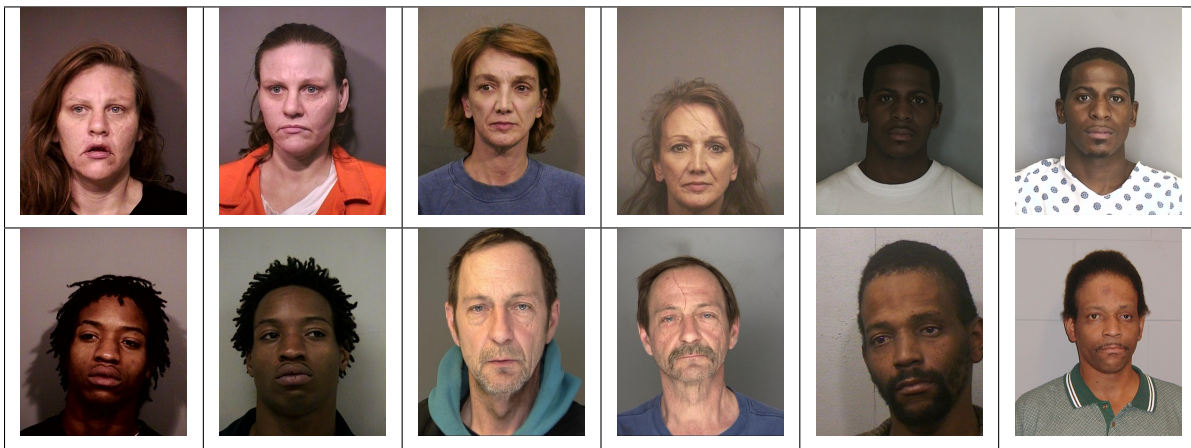


Figure 5: Six mated mugshot pairs representative of the FRVT-2014 (LEO) and FRVT-2018 datasets. The images are collected live, i.e. not scanned from paper. Image source: NIST Special Database 32 the Multiple Encounter Deceased Subjects dataset.



Figure 6: Twelve webcam images representative of probes against the FRVT-2018 mugshot gallery. The first eight images are four mated pairs. Such images present challenges to recognition including pose, non-uniform illumination, low contrast, compression, cropping, and low spatial sampling rate. Image source: NIST Special Database 32 the Multiple Encounter Deceased Subjects dataset.



Figure 7: **[Profile views]** The three images are a frontal enrollment, subsequent frontal probe, and same-session ninety degree profile view. While collection of both frontal and profile views has been typical in law enforcement for more than a century, the recognition of profile to frontal views has essentially been impossible. However, reasonably high accuracy results is now possible - see section E.

Image				
Encounter	1	...	$K_i - 1$	K_i
Capture Time	T_1	...	$T_{K_i - 1}$	T_{K_i}
Role RECENT	Not used	Not used	Enrolled	Search
Role LIFETIME	Enrolled	Enrolled	Enrolled	Search

Figure 8: Depiction of the “recent” and “lifetime” enrollment types. Image source: NIST Special Database 32

2.3 Enrollment strategies

Many operational applications include collection and enrollment of biometric data from subjects on more than one occasion. This might be done on a regular basis, as might occur in credential (re-)issuance, or irregularly, as might happen in a criminal recidivist situation [4]. The number of images per person will depend on the application area. In civil identity credentialing (e.g. passports, driver’s licenses), the images will be acquired approximately uniformly over time (e.g. ten years for a passport). While the distribution of dates for such images of a person might be assumed uniform, a number of factors might undermine this assumption⁷. In criminal applications, the number of images would depend on the number of arrests. The distribution of dates for arrest records for a person (i.e. the recidivism distribution) has been modeled using the exponential distribution but is recognized to be more complicated⁸.

In any case, the 2010 NIST evaluation of face recognition showed that considerable accuracy benefits accrue with retention and use of *all* historical images [6].

To this end, the FRVT API document provides $K \geq 1$ images of an individual to the enrollment software. The software is tasked with producing a single proprietary undocumented “black-box” template⁹ from the K images. This affords the algorithm an ability to generate a *model* of the individual, rather than to simply extract features from each image on a sequential basis.

As depicted in Figure 8, the i -th individual in the FRVT 2018 dataset has K_i images. These are labelled as x_k for $k = 1 \dots K_i$ in chronological order of capture date. To measure the utility of having multiple enrollment images, this report evaluates three kinds of enrollment:

- ▷ **Recent:** Only the second most recent image, $x_{K_i - 1}$ is enrolled. This strategy of enrollment mimics the operational policy of retaining the imagery from the most recent encounter. This might be done operationally to ameliorate the effects of face ageing. Obviously retaining only the most recent image should only be done if the identity of the person is trusted to be correct. For example, in an access control situation retention of the most recent successful *authentication* image would be hazardous if it could be a false positive.
- ▷ **Lifetime-consolidated:** All but the most recent image are enrolled, $x_1 \dots x_{K_i - 1}$. This subject-centric strategy might be adopted if quality variations exist where an older image might be more suitable for matching, despite the ageing effect.

⁷For example, a person might skip applying for a passport for one cycle, letting it expire. In addition, a person might submit identical images (from the same photography session) to consecutive passport applications at five year intervals.

⁸A number of distributions have been considered to model recidivism, see for example [3].

⁹There are no formal face template standards. Template standards only exist for fingerprint minutiae - see ISO/IEC 19794-2:2011.

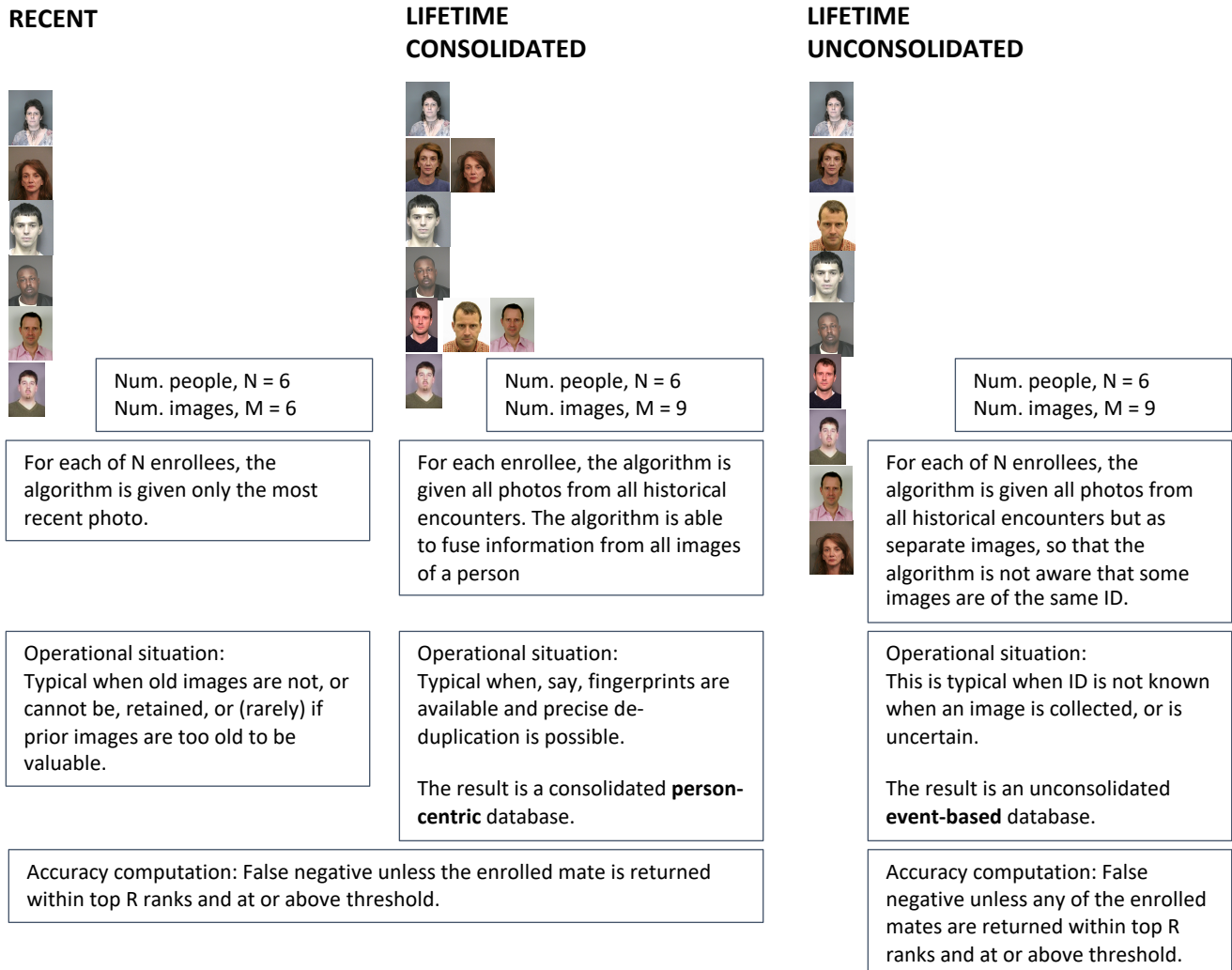


Figure 9: Enrollment strategies. The figure shows the three kinds of enrollment databases examined in this report. Image source: NIST Special Database 32

	ENROLLMENT				SEARCH			
	TYPE SEE SECTION 2.3	POPULATION FILTER	N-SUBJECTS	N-IMAGES	MATE N-SUBJECTS	NON-MATE N-IMAGES	N-SUBJECTS	N-IMAGES
Mugshot trials from enrollment of single images								
1	RECENT	NATURAL	640 000	640 000	154 549	154 549	331 254	331 254
2	RECENT	NATURAL	1 600 000	1 600 000				
3	RECENT	NATURAL	3 000 000	3 000 000				
4	RECENT	NATURAL	6 000 000	6 000 000				
5	RECENT	NATURAL	12 000 000	12 000 000				
Cross-domain								
13	MUGSHOTS AS ON ROW 2				82 106 WEBCAM	82 106 WEBCAM	331 254 WEBCAM	331 254 WEBCAM
Cross-view								
14	MUGSHOTS AS ON ROW 2				100 000 PROFILE	100 000 PROFILE	100 000 PROFILE	100 000 PROFILE
Mugshot ageing								
17	OLDEST	NATURAL	3 068 801	3 068 801	2 853 221	10 951 064	0	0
Border crossing ageing								
17	OLDEST	NATURAL	1 600 000	1 600 000	903 655	1 922 393	1 393 076	1 680 000
Visa-border								
19	PRIOR	NATURAL	1 600 000 VISA	1 600 000 VISA	80 000 BORDER	80 000 BORDER	80 000 BORDER	80 000 BORDER
20	VISA AS ON ROW 18				21 016 BORDER	21 016 BORDER	21 016 BORDER	21 016 BORDER

Table 1: Enrollment and search sets. Each row summarizes one identification trial. Unless stated otherwise, all entries refer to mugshot images. The term “natural” means that subjects were selected without heed to demographics, i.e. in the distribution native to this dataset. The probe images were collected in a different calendar year to the enrollment image. Missing values in rows 2-12 are the same as in row 1.

▷ **Lifetime-unconsolidated:** Again all but the most recent image are enrolled $x_1 \dots x_{K_i-1}$ but now separately, with different identifiers, such that the algorithm is not aware that the images are from the same face. This kind of event- or encounter-centric enrollment is very common when operational constraints preclude reliable consolidation of the historical encounters into a single identity. This aspect also prevents the recognition algorithm from a) building a holistic model of identity (as is common in speaker recognition systems) and b) implementing fusion, for example template-level fusion of feature vectors, or post-search score-level fusion. The result is that searches will typically yield more than one image of a person in the top ranks. This has consequences for appropriate metrics, as detailed in section 3.2.1

NIST first evaluated this kind of enrollment in mid 2018, and the results tables include some comparison of accuracy available from all three enrollment styles.

In all cases, the most recent image, x_{K_i} , is reserved as the search image. For the 1.6 million subject enrollment partition of the FRVT 2018 data, $1 \leq K_i \leq 33$ with $K_i = 1$ in 80.1% of the individuals, $K_i = 2$ in 13.4%, $K_i = 3$ in 3.7%, $K_i = 4$ in 1.4%, $K_i = 5$ in 0.6%, $K_i = 6$ in 0.3%, and $K_i > 6$ is 0.2% for everyone else. This distribution is substantially dependent on United States recidivism rates.

We did not evaluate the case of retaining only the highest quality image, since automated quality assessment is out of scope for this report. We do not anticipate that such strategies will prove beneficial when the quality assessment apparatus is imperfect and unvalidated.

3 Performance metrics

This section gives specific definitions for accuracy and timing metrics. Tests of open-set biometric algorithms must quantify frequency of two error conditions:

- ▷ **False positives:** Type I errors occur when search data from a person who has never been seen before is incorrectly associated with one or more enrollees' data.
- ▷ **Misses:** Type II errors arise when a search of an enrolled person's biometric does not return the correct identity.

Many practitioners prefer to talk about "hit rates" instead of "miss rates" - the first is simply one minus the other as detailed below. Sections 3.1 and 3.2 define metrics for the Type I and Type II performance variables.

Additionally, because recognition algorithms sometimes fail to produce a template from an image, or fail to execute a one-to-many search, the occurrence of such events must be recorded. Further because algorithms might elect to not produce a template from, for example, a poor quality image, these failure rates must be combined with the recognition error rates to support algorithm comparison. This is addressed in section 3.5.

Finally, section 3.7 discusses measurement of computation duration, and section 3.8 addresses the uncertainty associated with various measurements. Template size measurement is included with the results.

3.1 Quantifying false positives

It is typical for a search to be conducted into an enrolled population of N identities, and for the algorithm to be configured to return the closest L candidate identities. These candidates are ranked by their score, in descending order, with all scores required to be greater than or equal to zero. A human analyst might examine either all L candidates, or just the top $R \leq L$ identities, or only those with score greater than threshold, T . The workload associated with such examination is discussed later, in 3.6.

False alarm performance is quantified in two related ways. These express how many searches produces false positives, and then, how many false positives are produced in a search.

False positive identification rate: The first quantity, FPIR, is the proportion of non-mate searches that produce an adverse outcome:

$$\text{FPIR}(N, T) = \frac{\text{Num. non-mate searches where one or more enrolled candidates are returned with score at or above threshold}}{\text{Num. non-mate searches attempted.}} \quad (1)$$

Under this definition, FPIR can be computed from the highest non-mate candidate produced in a search - it is not necessary to consider candidates at rank 2 and above. FPIR is the primary measure of Type I errors in this report.

Selectivity: However, note that in any given search, several non-mate may be returned above threshold. In order to quantify such events, a second quantity, selectivity (SEL), is defined as the *number* of non-mates returned on a candidate list, averaged over all searches.

$$\text{SEL}(N, T) = \frac{\text{Num. non-mate enrolled candidates returned with score at or above threshold}}{\text{Num. non-mate searches attempted.}} \quad (2)$$

where $0 \leq \text{SEL}(N, T) \leq L$. Both of these metrics are useful operationally. FPIR is useful for targeting how often an

adverse false positive outcome can occur, while SEL as a number is related to workload associated with adjudicating candidate lists. The relationship between the two quantities is complicated - it depends on whether an algorithm concentrates the false alarms in the results of a few searches or whether it disburses them across many. This was detailed in FRVT 2014, NISTIR 8009. It has not yet been detailed in FRVT 2018.

3.2 Quantifying hits and misses

If L candidates are returned in a search, a shorter candidate list can be prepared by taking the top $R \leq L$ candidates for which the score is above some threshold, $T \geq 0$. This reduction of the candidate list is done because thresholds may be applied, and only short lists might be reviewed (according to policy or labor availability, for example). It is useful then to state accuracy in terms of R and T , so we define a “miss rate” with the general name **false negative identification rate** (FNIR), as follows:

$$\text{FNIR}(N, R, T) = \frac{\text{Num. mate searches with enrolled mate found outside top } R \text{ ranks or score below threshold}}{\text{Num. mate searches attempted.}} \quad (3)$$

This formulation is simple for evaluation in that it does not distinguish between causes of misses. Thus a mate that is not reported on a candidate list is treated the same as a miss arising from face finding failure, algorithm intolerance of poor quality, or software crashes. Thus if the algorithm fails to produce a candidate list, either because the search failed, or because a search template was not made, the result is regarded as a miss, adding to FNIR.

Hit rates, and true positive identification rates: While FNIR states the “miss rate” as how often the correct candidate is either not above threshold or not at good rank, many communities prefer to talk of “hit rates”. This is simply the **true positive identification rate**(TPIR) which is the complement of FNIR giving a positive statement of how often mated searches are successful:

$$\text{TPIR}(N, R, T) = 1 - \text{FNIR}(N, R, T) \quad (4)$$

This report does not report true positive “hit” rates, preferring false negative miss rates for two reasons. First, costs rise linearly with error rates. For example, if we double FNIR in an access control system, then we double user inconvenience and delay. If we express that as decrease of TPIR from, say 98.5% to 97%, then we mentally have to invert the scale to see a doubling in costs. More subtly, readers don’t perceive differences in numbers near 100% well, becoming inured to the “high nineties” effect where numbers close to 100 are perceived indifferently.

Reliability is a corresponding term, typically being identical to TPIR, and often cited in automated (fingerprint) identification system (AFIS) evaluations.

An important special case is the **cumulative match characteristic**(CMC) which summarizes accuracy of mated-searches only. It ignores similarity scores by relaxing the threshold requirement, and just reports the fraction of mated searches returning the mate at rank R or better.

$$\text{CMC}(N, R) = 1 - \text{FNIR}(N, R, 0) \quad (5)$$

We primarily cite the complement of this quantity, $\text{FNIR}(N, R, 0)$, the fraction of mates *not* in the top R ranks.

The **rank one hit rate** is the fraction of mated searches yielding the correct candidate at best rank, i.e. $\text{CMC}(N, 1)$. While this quantity is the most common summary indicator of an algorithm’s efficacy, it is not dependent on similarity scores, so it does not distinguish between strong (high scoring) and weak hits. It also ignores that an adjudicating reviewer is often willing to look at many candidates.

3.2.1 False negative rates for unconsolidated galleries

As detailed in section 2.3 a common type of gallery, here referred to as the lifetime unconsolidate type, is populated with all images of an individual without any association between them. That is, the gallery construction algorithm is not provided with any ID labels that would support processing of a person's images jointly. This contrasts with the lifetime consolidate type where an algorithm may explicitly fuse features from multiple images of a person, or select a best image. In such cases, where the number of enrolled images is a random variable, we define two false negative rates as follows.

The first demands that the algorithm place any of the K_i mates in the top $R \geq 1$ ranks. The proportion of searches for which this does not occur forms a false negative identification rate:

$$\text{FNIR}_{\text{any}}(N, R, T) = 1 - \frac{\text{Num. mate searches where any enrolled mate is found in the top } R \text{ ranks and at-or-above threshold}}{\text{Num. mate searches attempted.}} \quad (6)$$

The second demands that the algorithm place all K_i mates in the top $R \geq K_i$ ranks. The proportion of searches for which this does not occur forms a false negative identification rate:

$$\text{FNIR}_{\text{all}}(N, R, T) = 1 - \frac{\text{Num. mate searches where all enrolled mates are found in the top } R \text{ ranks and at-or-above threshold}}{\text{Num. mate searches attempted.}} \quad (7)$$

Placing all mates in the top ranks is a more difficult task than correctly retrieving any image, so it holds that: $\text{FNIR}_{\text{all}} \geq \text{FNIR}_{\text{any}}$. This is evident in the results presented for November 2018 algorithms in Tables starting at ??.

The information retrieval community might prefer to compute and plot *precision* and *recall*; this is a valid approach, but we advance the two metrics above because they relate to our normal definition of consolidated FNIR, and they cover the two extreme use-cases of wanting any hit vs. all hits.

3.3 DET interpretation

In biometrics, a false negative occurs when an algorithm fails to match two samples of one person – a Type II error. Correspondingly, a false positive occurs when samples from two persons are improperly associated – a Type I error.

Matches are declared by a biometric system when the native comparison score from the recognition algorithm meets some threshold. Comparison scores can be either similarity scores, in which case higher values indicate that the samples are more likely to come from the same person, or dissimilarity scores, in which case higher values indicate different people. Similarity scores are traditionally computed by fingerprint and face recognition algorithms, while dissimilarities are used in iris recognition. In some cases, the dissimilarity score is a distance possessing metric properties. In any case, scores can be either mate scores, coming from a comparison of one person's samples, or nonmate scores, coming from comparison of different persons' samples.

The words "genuine" or "authentic" are synonyms for mate, and the word "impostor" is used as a synonym for non-mate. The words "mate" and "nonmate" are traditionally used in identification applications (such as law enforcement search, or background checks) while genuine and impostor are used in verification applications (such as access control).

An error tradeoff characteristic represents the tradeoff between Type II and Type I classification errors. For identification this plots false negative vs. false positive identification rates i.e. FNIR vs. FPIR parametrically with T. Such plots

are often called detection error tradeoff (DET) characteristics or receiver operating characteristic (ROC). These serve the same function – to show error tradeoff – but differ, for example, in plotting the complement of an error rate (e.g. $TPIR = 1 - FNIR$) and in transforming the axes, most commonly using logarithms, to show multiple decades of FPIR. More rarely, the function might be the inverse of the Gaussian cumulative distribution function.

The slides of Figures 10 through 15 discuss presentation and interpretation of DETs used in this document for reporting face identification accuracy. Further detail is provided in formal biometrics testing standards, see the various parts of ISO/IEC 19795 Biometrics Testing and Reporting. More terms, including and beyond those to do with accuracy, appear in ISO/IEC 2382-37 Information technology – Vocabulary – Part 37: Harmonized biometric vocabulary.

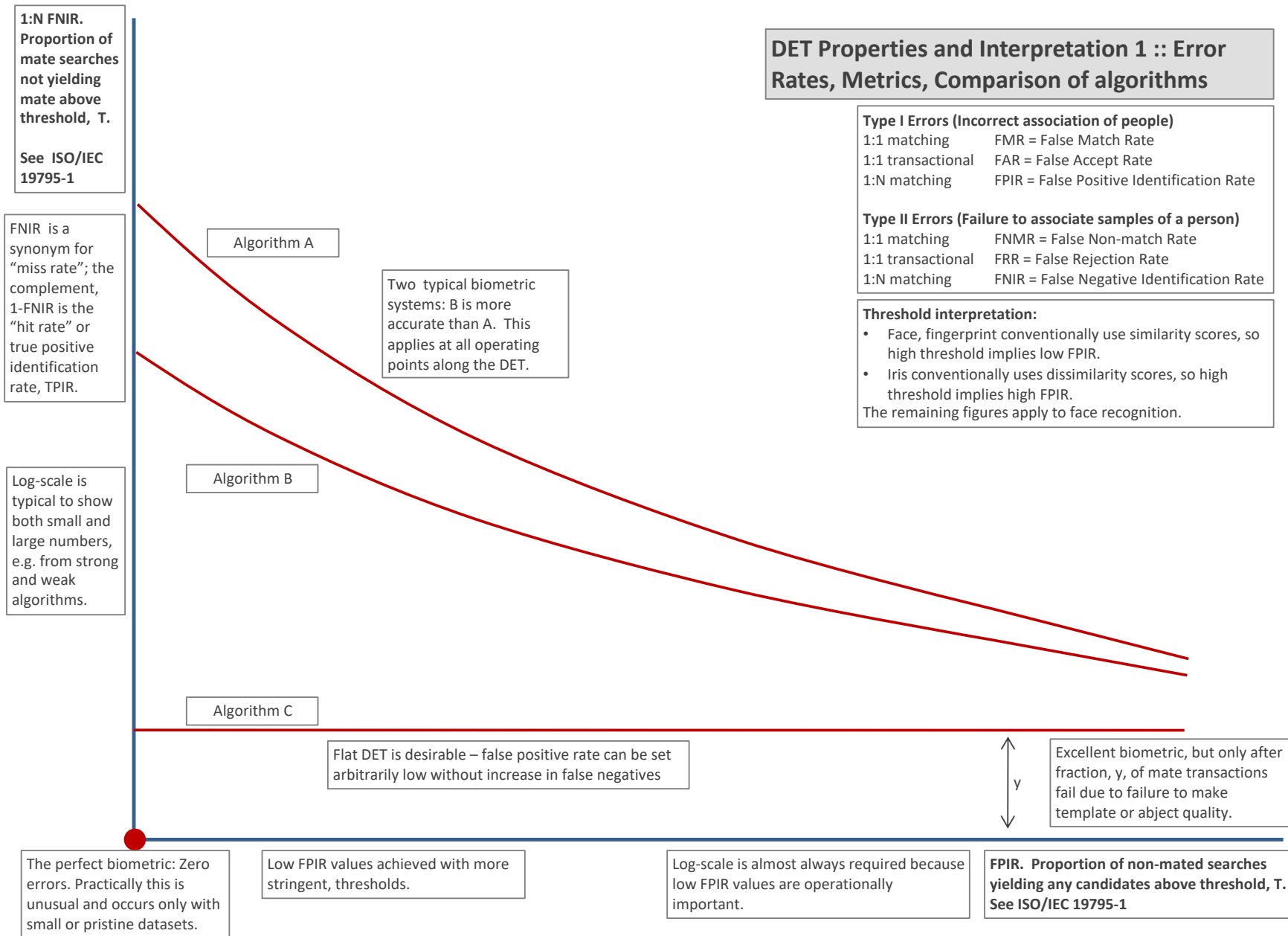


Figure 10: DET as the primary performance reporting mechanism.

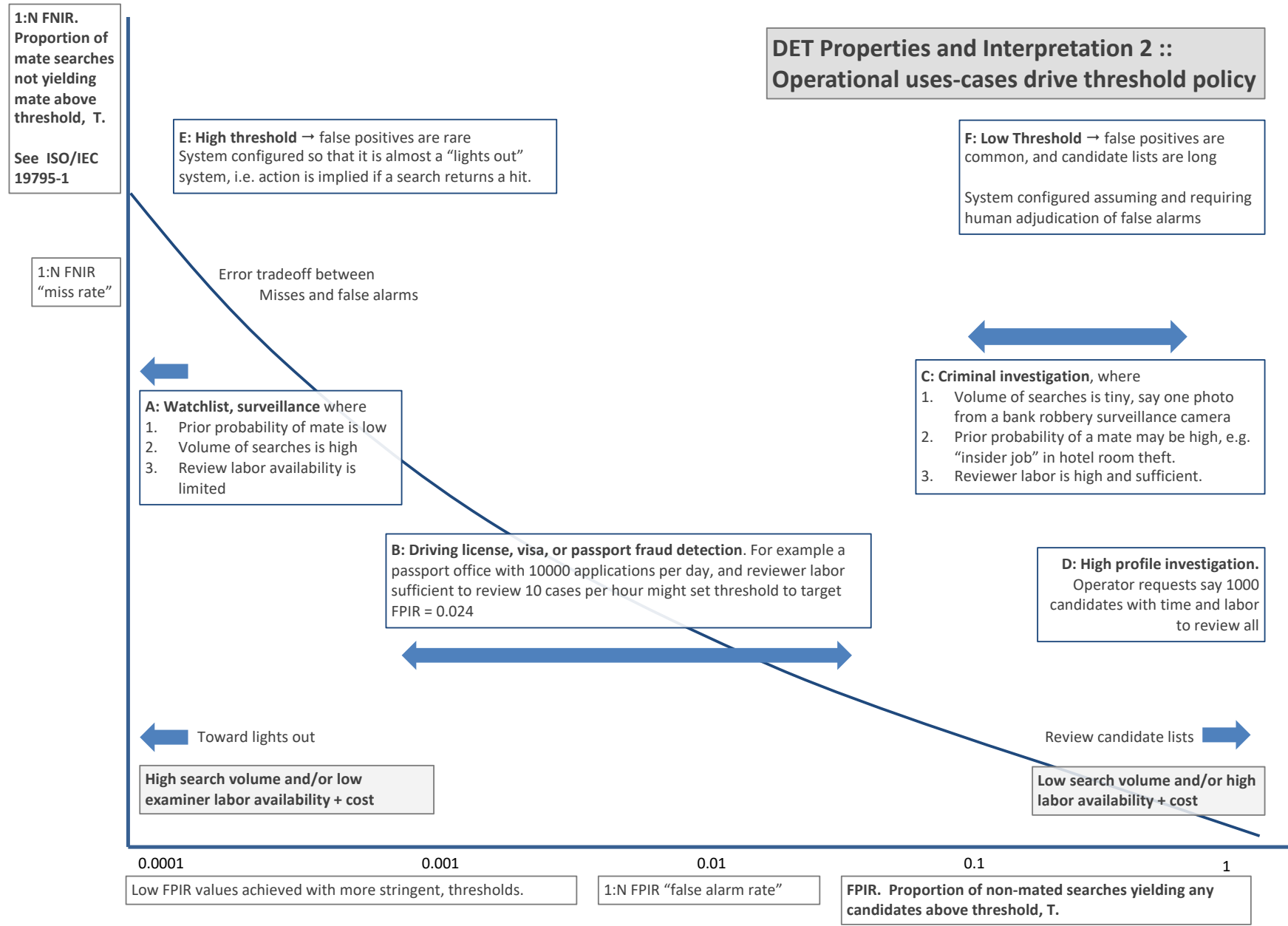
2022/02/23
14:06:29FNIR(N, R, T) = False neg. identification rate
FPIR(N, T) = False pos. identification rate
N = Num. enrolled subjects
R = Num. candidates examined
T = ThresholdT = 0 → Investigation
T > 0 → Identification

Figure 11: DET as the primary performance reporting mechanism.

2022/02/23
14:06:29

$\text{FNIR}(N, R, T) =$ False neg. identification rate
 $\text{FPIR}(N, T) =$ False pos. identification rate

N = Num. enrolled subjects
 R = Num. candidates examined

T = Threshold
 $T = 0 \rightarrow$ Investigation
 $T > 0 \rightarrow$ Identification

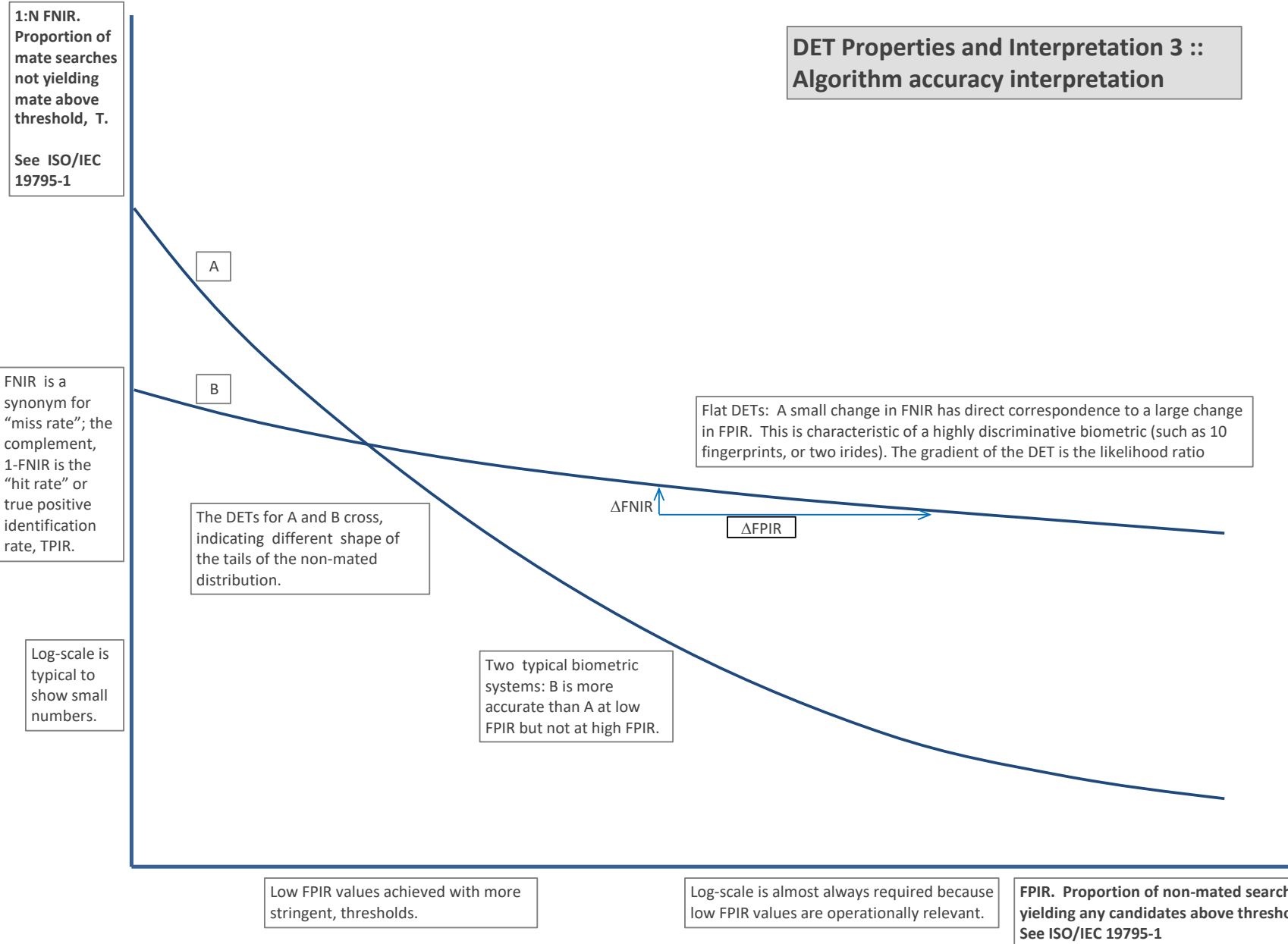


Figure 12: DET as the primary performance reporting mechanism.

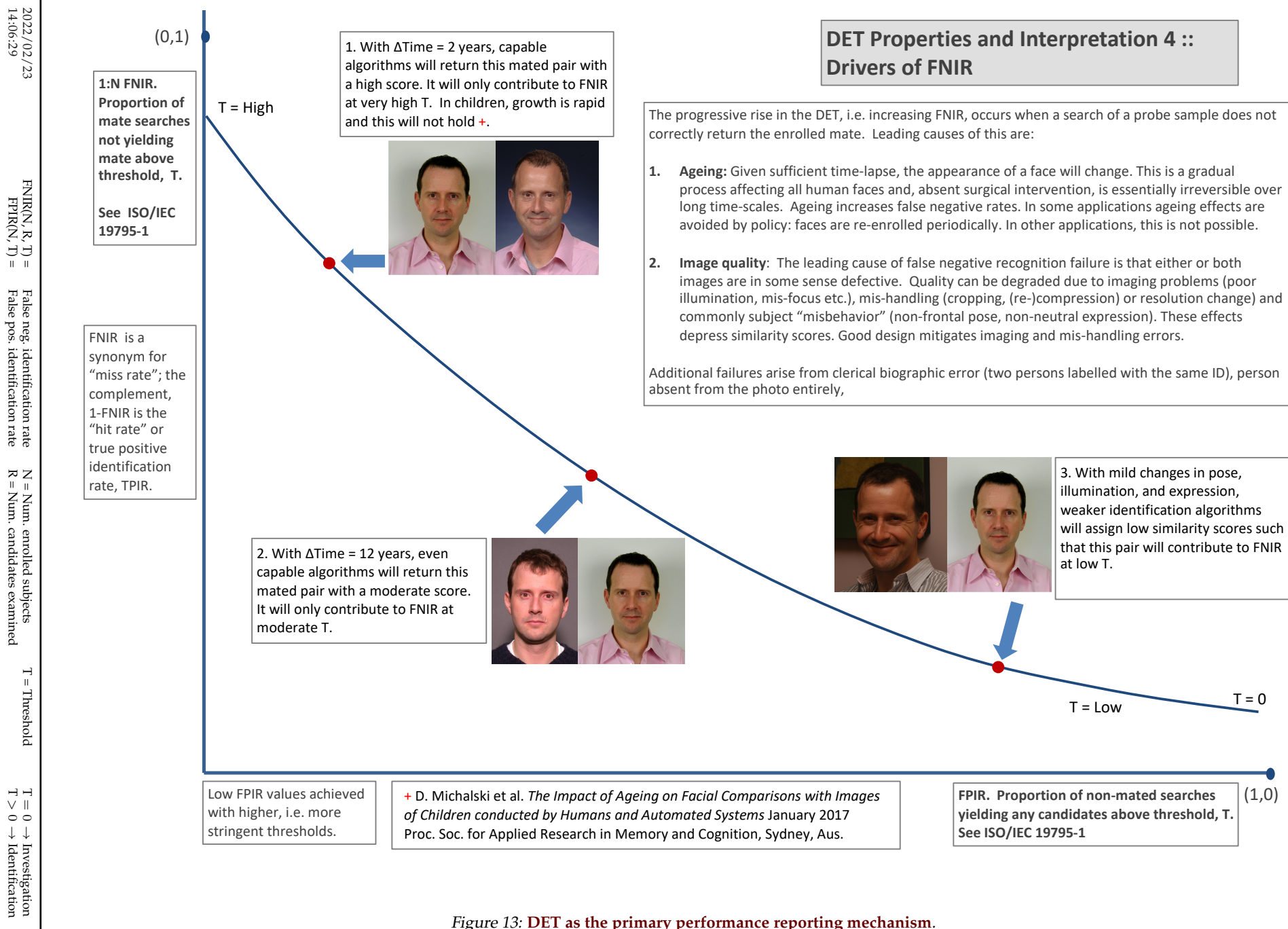


Figure 13: DET as the primary performance reporting mechanism.

2022/02/23
14:06:29

$\text{FNIR}(N, R, T) =$ False neg. identification rate
 $\text{FPIR}(N, T) =$ False pos. identification rate

$T = \text{Threshold}$

$T = 0 \rightarrow \text{Investigation}$
 $T > 0 \rightarrow \text{Identification}$

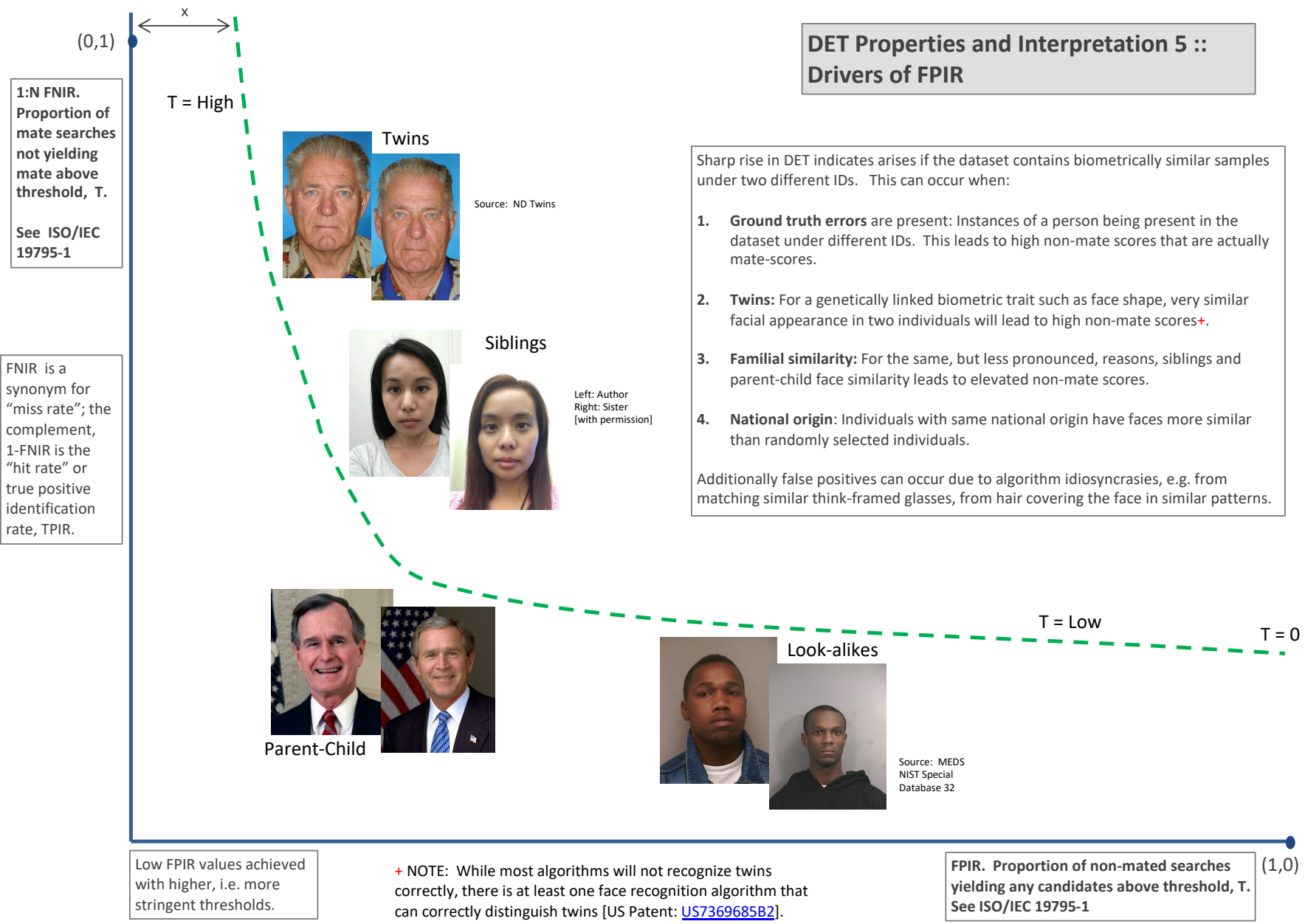


Figure 14: DET as the primary performance reporting mechanism.

2022/02/23
14:06:29

$\text{FNIR}(N, R, T) =$
False neg. identification rate
 $\text{FPIR}(N, T) =$
False pos. identification rate

$N =$ Num. enrolled subjects
 $R =$ Num. candidates examined

$T =$ Threshold

$T = 0 \rightarrow$ Investigation
 $T > 0 \rightarrow$ Identification

1:N FNIR.
Proportion of mate searches not yielding mate above threshold, T .
See ISO/IEC 19795-1

Algorithm X,
Condition 1

Algorithm X,
Condition 2

If system X is used with images of different properties, say from different imaging systems, or from different populations, generally both FNIR and FPIR will change. The dotted line joins points of the same threshold. Horizontal (vertical) lines indicate change in FPIR (FNIR) only. Two cases concerning population size are shown below (A and B), for the blue curves.

FNIR is a synonym for "miss rate"; the complement, 1-FNIR is the "hit rate" or true positive identification rate, TPIR.

Log-scale is typical to show small numbers.

Algorithm Y,
Condition 1

Algorithm Y,
Condition 2

If DETs are computed for two categories (men and women) or (cameras A and B) or (indoor vs. outdoor), generally the Type I and Type II errors will differ and the line of constant threshold will be neither horizontal nor vertical.

The ideal situation in most applications is that a fixed threshold yields a fixed FPIR so that system owners see no change in false alarms across populations or conditions.

Low FPIR values achieved with higher, i.e. more stringent, thresholds.

Log-scale is often required because low FPIR values are operationally relevant.

FPIR. Proportion of non-mated searches yielding any candidates above threshold, T . See ISO/IEC 19795-1

Figure 15: DET as the primary performance reporting mechanism.

DET Properties and Interpretation 7 :: Effect of enrolled population size.

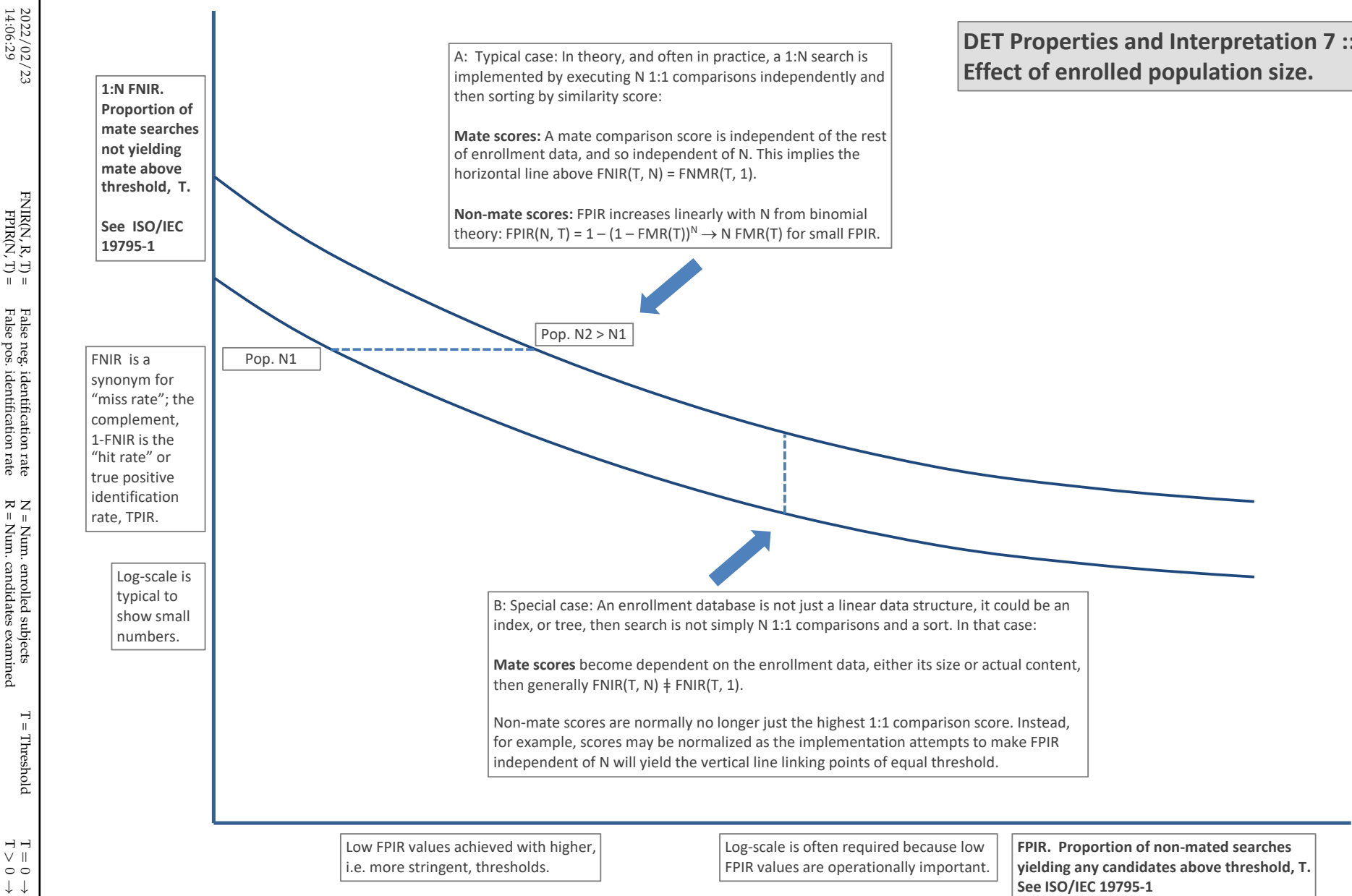


Figure 16: DET as the primary performance reporting mechanism.

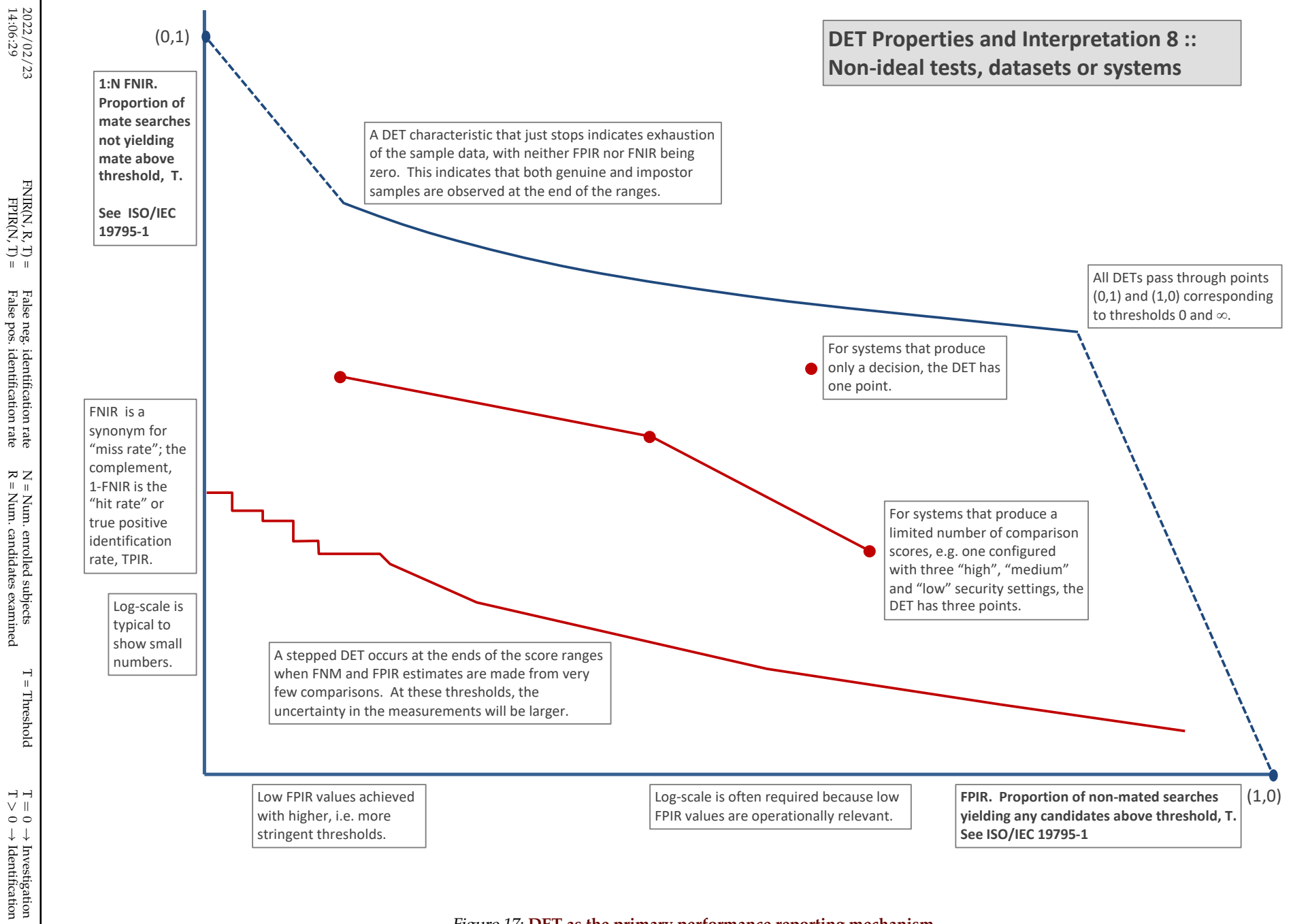


Figure 17: DET as the primary performance reporting mechanism.

3.4 Best practice testing requires execution of searches with and without mates

FRVT embeds 1:N searches of two kinds: Those for which there is an enrolled mate, and those for which there is not. The respective numbers for these types of searches appear in Table 1. However, it is common to conduct only mated searches¹⁰. The cumulative match characteristic is computed from candidate lists produced in mated searches. Even if the CMC is the only metric of interest, the actual trials executed in a test should nevertheless include searches for which no mate exists. As detailed in Table 1 the FRVT reserved disjoint populations of subjects for executing true non-mate searches.

3.5 Failure to extract features

During enrollment some algorithms fail to convert a face image to a template. The proportion of failures is the failure-to-enroll rate, denoted by FTE. Similarly, some search images are not converted to templates. The corresponding proportion is termed failure-to-extract, denoted by FTX.

We do not report FTX because we assume that the same underlying algorithm is used for template generation for enrollment and search.

Failure to extract rates are incorporated into FNIR and FPIR measurements as follows.

- ▷ **Enrollment templates:** Any failed enrollment is regarded as producing a zero length template. Algorithms are required by the API [10] to transparently process zero length templates. The effect of template generation failure on search accuracy depends on whether subsequent searches are mated, or non-mated: Mated searches will fail giving elevated FNIR; non-mated searches will not produce false positives so, to first order, FPIR will be reduced by a factor of $1 - \text{FTE}$.
- ▷ **Search templates and 1:N search:** In cases where the algorithm fails to produce a search template from input imagery, the result is taken to be a candidate list whose entries have no hypothesized identities and zero score. The effect of template generation failure on search accuracy depends on whether searches are mated, or non-mated: Mated searches will fail giving elevated FNIR; Non-mated searches will not produce false positives, so FPIR will be reduced. Thus given a measurement of false negative and positive rates made over only those where failures-to-extract did not occur, those rates - call them FNIR^\dagger and FPIR^\dagger - could be adjusted by an explicit measurement of FTX as follows

$$\text{FNIR} = \text{FTX} + (1 - \text{FTX})\text{FNIR}^\dagger \quad (8)$$

$$\text{FPIR} = (1 - \text{FTX})\text{FPIR}^\dagger \quad (9)$$

This approach is the correct treatment for positive-identification applications such as access control where cooperative users are enrolled and make attempts at recognition. This approach is not appropriate to negative identification applications, such as visa fraud detection, in which hostile individuals may attempt to evade detection by submitting poor quality samples. In those cases, template generation failures should be investigated as though a false alarm had occurred.

¹⁰For example, the [Megaface benchmark](#). This is bad practice for several reasons: First, if a developer knows, or can reasonably assume, that a mate always exists, then unrealistic gaming of the test is possible. A second reason is that it does not put FPIR on equal footing with FNIR and that matters because in most applications, not all searches have mates - not everyone has been previously enrolled in a driving license issuance or a criminal justice system - so addressing between-class separation becomes necessary.

3.6 Fixed length candidate lists, threshold independent workload

Suppose an automated face identification algorithm returns L candidates, and a human reviewer is retained to examine up to R candidates, where $R \leq L$ might be set by policy, preference or labor availability. For now, assume also that the reviewer is not provided with, or ignores, similarity scores, and thresholds are not applied. Given the algorithm typically places mates at low (good) ranks, the number of candidates a reviewer can be expected to review can be derived as follows. Note that the reviewer will:

- ▷ Always inspect the first ranked image Frac. reviewed = 1
- ▷ Then inspect those candidates where mate not confirmed at rank 1 Frac. reviewed = 1-CMC(1)
- ▷ Then inspect those candidates where mate not confirmed at rank 1 or 2 Frac. reviewed = 1-CMC(2)

etc. Thus if the reviewer will stop after a maximum of R candidates, the expected number of candidate reviews is

$$M(R) = 1 + (1 - CMC(1)) + (1 - CMC(2)) + \dots + (1 - CMC(R - 1)) \quad (10)$$

$$= R - \sum_{r=1}^{R-1} CMC(r) \quad (11)$$

A recognition algorithm that front-loads the cumulative match characteristic will offer reduced workload for the reviewer. This workload is defined only over the searches for which a mate exists. In the cases where there truly is no mate, the reviewer would review all R candidates. Thus, if the proportion of searches for which a mate does exist is β , which in the law enforcement context would be the recidivism rate [3], the full expression for workload becomes:

$$M(R) = \beta \left(R - \sum_{r=1}^{R-1} CMC(r) \right) + (1 - \beta)R \quad (12)$$

$$= R - \beta \sum_{r=1}^{R-1} CMC(r) \quad (13)$$

3.7 Timing measurement

Algorithms were submitted to NIST as implementations of the application programming interface(API) specified by NIST in the Evaluation Plan [10]. The API includes functions for initialization, template generation, finalization, search, gallery insert, and gallery delete. Two template generation functions are required, one for the preparation of an enrollment template, and one for a search template.

In NIST's test harness, all functions were wrapped by calls to the C++ std::chrono::high_resolution_clock which on the dedicated timing machine counts 1ns clock ticks. Precision is somewhat worse than that however.

3.8 Uncertainty estimation

3.8.1 Random error

This study leverages operational datasets for measurement of recognition error rates. This affords several advantages. First, large numbers of searches are conducted (see Table 1) giving precision to the measurements. Moreover, for the two mugshot datasets, these do not involve reuse of individuals so binomial statistics can be expected to apply to recognition error counts. In that case, an observed count of a particular recognition outcome (i.e. a false negative or false positive) in M trials will sustain 95% confidence that the actual error rate is no larger than some value.

As an example, the minimum number of mugshot searches conducted in this report is $M = 154\,549$, and for an observed FNIR around 0.002, the measurement supports a conclusion that the actual FNIR is no higher than 0.00228 at 99% confidence level. On the false positive side, we tabulate FNIR at FPIR values as low as 0.001. Given estimates based on 331 254 non-mate trials, the actual FPIR values will be below 0.00115 at 99% confidence. In conclusion, large scale evaluation, without reuse of subjects, supports tight uncertainty bounds on the measured error rates.

3.8.2 Systematic error

The FRVT 2018 dataset includes anomalies discovered as a result of inspecting images involved in recognition failures from the most accurate algorithms. Two kinds of failure occur: False negatives (which, for the purpose here, include failures to make templates) and false positives.

False negative errors: We reviewed 600 false negative pairs for which either or both of the leading two algorithms did not put the correct mate in the top 50 candidates. Given 154 549 searches, this number represents 0.39% of the total, resulting in $\text{FNIR} \sim 0.0039$. Of the 600 pairs:

- ▷ **A: Poor quality:** About 20% of the pairs included images of very low quality, often greyscale, low resolution, blurred, low contrast, partially cropped, interlaced, or noisy scans of paper images. Additionally, in a few cases, the face is injured or occluded by bandages or heavy cosmetics.
- ▷ **B: Ground truth identity label bugs:** About 15% of the pairs are not actually mated. We only assigned this outcome when a pair is clearly not mated.
- ▷ **C: Profile views:** About 35% included an image of a profile (side) view of the face, or, more rarely, an image that was rotated 90 degrees in-plane (roll).
- ▷ **D: Tattoos:** About 30% included an image of a tattoo that contained a face image. These arise from mis-labelling in the parent dataset metadata.
- ▷ **E: Ageing:** There is considerable time-lapse between the two captures.

All these estimates are approximate. Of these, the tattoo and mislabelled images can never be matched. These constitute an accuracy floor in the sample implying that FNIR cannot be below 0.0018¹¹. The profile-views, low-quality images, and images with considerable ageing can, in principle, be successfully matched - indeed some algorithms do so - so are not part of the accuracy floor.

¹¹This value is the sum of two partial false negative rates: $\text{FNIR}_B = 0.15 * 0.0039$ plus $\text{FNIR}_D = 0.3 * 0.0039$

For the microsoft-4 algorithm the lowest miss rate from (recent entry in Table 22) is $\text{FNIR}(640\,000, 50, 0) = 0.0018$. This is close to the value estimated from the inspection of misses. It is below the 0.0039 figure because the algorithm does match some profile and poor quality images, that the yitu-2 algorithm does not.

For many tables (e.g. Table 22), the FNIR values obtained for the FRVT-2018 mugshots could be corrected by reducing them by 0.0018. The best values would then be indistinct from zero. The results in this report *were not* adjusted to account for this systematic error.

False positive errors: As shown in Figure 1 and discussed in Figure 14 many of the DET characteristics in this report exhibit a pronounced turn upward at low false positive rates. The shape can be caused by identity labelling errors in the ground truth of a dataset, specifically persons present in the database under two IDs such that some proportion of non-mate pairs are actually mated. To look for such possibilities, we merged the highest 1000 non-mate pairs produced by three different algorithms which resulted in 1839 unique pairs. This constitutes 0.56% of all non-mate searches. We assert that it is *very* difficult for human reviewers to assign the pairs into the following three categories: twins; doppelgangers; or ground-truth errors (instances of the same person under two IDs). Given this difficulty we made no attempt to correct any possible ground truth errors except by removing 57 pairs in the following categories:

- ▷ **A: Profile views:** Thirteen pairs included one or two profile-view images. As described in Figure 130, these can cause false positives.
- ▷ **B: Same-session photographs:** For twelve pairs, the images were identical or trivially altered (e.g. cropped) versions of the same photo. These were present under a different ID likely due to some clerical or procedural mistake.
- ▷ **C: Tattoos of faces:** There were fourteen instances of tattoo photographs that contained faces causing false matches.
- ▷ **D: T-shirt faces:** There were six instances of T-shirt photographs (of Bob Marley and Che Guevara) being detected instead of the face and causing false positives.
- ▷ **E: Background faces:** There were twelve instances of one subject appearing in the background of two otherwise correct portrait photos.

Note we did not remove any images where there was a chance that the pair was actually a different person.

In any case, the results in this report have not been adjusted for this systematic error.

4 Results

This section gives extensive results for algorithms submitted to FRVT 2018. Three page “report cards” for each algorithm are contained in a [separate supplement](#). Performance metrics were described in section 3. The main results are summarized in tabular form with more exhaustive data included as DET, CMC and related graphs in appendices as follows:

- ▷ The three tables 2-4 list algorithms alongside full developer names, acceptance date, size of the provided configuration data, template size and generation time, and search duration data.
 - The **template generation duration** is most important to applications that require fast response. For example, an eGate taking more than two seconds to produce a template might be unacceptable. Note that GPUs may be of utility in expediting this operation for some algorithms, though at additional expense. Two additional factors should be considered¹²¹³.
 - The **search duration** is the time taken for a search of a search template into a gallery of N enrollment templates. This performance variable, together with the volume of searches, is influential on the amount of hardware needed to sustain an operational deployment. This is measured here with the algorithm running on a single core of a contemporary CPU. Search is most simply implemented as N computations of a distance metric followed by a sort operation to find the closest enrollments. However, considerable optimization of this process is possible, up to and including fast-search algorithms that, by various means, avoid computation of all N distances.
 - The **template size** is the size of the extracted feature vector (or vectors) and any needed header information. Large template sizes may be influential on bus or network bandwidth, storage requirements, and on search duration. While the template itself is an opaque data blob, the feature dimensionality might be estimated by assuming a four-bytes-per-float encoding. There is a wide range of encodings. For the more accurate algorithm, sizes range from 256 bytes to about 2KB bytes, indicating essentially no consensus on face modeling and template design.
 - The **template size multiplier** column shows how, given k input images, the size of the template grows. Most implementations internally extract features from each image and concatenate them, and implement some score-level fusion logic during search. Other implementations, including many of the most accurate algorithms, produce templates whose size does not grow with k . This could be achieved via selection of the best quality image - but this is not optimal in handling ageing where the oldest image could be the best quality. Another mechanism would be feature-level fusion where information is fused from all k inputs. In any case, as a black-box test, the fusion scheme is proprietary and unknown.
 - The size of the **configuration data** is the total size of all files resident in a vendor-provided directory that contains arbitrary read-only files such as parameters, recognition models (e.g caffe). Generally a large value for this quantity may prohibit the use of the algorithm on a resource-constrained device.

¹²The FRVT 2018 API prohibited threading, so some gains from parallelism may be available on multiple-cores or multiple processors, if the feature extraction code could be distributed across them.

¹³Note also that factors of two or more may be realizable by exploiting modern vector processing instructions on CPUs. It is not clear in our measurements whether all developers exploited Intel’s AVX2 instructions, for example. Our machine was so equipped, but we insisted that the same compiled library should also run on older machines lacking that instruction. The more sophisticated implementations may have detected AVX2 presence and branched accordingly. The less sophisticated may be defaulted to the reduced instruction set. Readers should see the FRVT 2018 API document for the specific chip details.

▷ Tables 22-23 report core rank-based accuracy for mugshot images. The population size is limited to $N = 1.6$ million identities because this is the largest gallery size on which all algorithms were executed. Notable observations from these tables are as follows:

- **Accuracy gains since 2018:** NIST Interagency Report 8238 documented massive gains over those reported in the FRVT 2014 report, NIST Interagency Report 8009. Further gains are documented in this report. Comparing the most accurate algorithm in November 2018, NEC-3, the value of $\text{FNIR}(N, L, T)$ reduced from 0.0031 to 0.0024 for the Sensetime-004 algorithm with $N = 12$ million recent images. The tables show broader gains: many developers have made advances since 2018 with between two and five-fold reduction in errors.
- **Wide range in accuracy:** The rank-1 miss rates vary from $\text{FNIR}(N, 1, 0) = 0.0012$ for sensetime-004 up to about 0.5 for the very fast but inaccurate microfocus-x algorithms. Among the developers who are superior to NEC in 2013, the range is from 0.002 to 0.035 for camvi-3. This large accuracy range is consistent with the buyer-beware maxim, and indicates that face recognition software is far from being commoditized.

▷ Tables 26-27 report threshold-based error rates, $\text{FNIR}(N, L, T)$, for $N = 1.6$ million for mugshot-mugshot accuracy on FRVT 2014, FRVT 2018, and also (in pink) mugshot-webcam accuracy using FRVT 2018 enrollments. Notable observations from these tables are as follows:

- **Order of magnitude accuracy gains since 2014:** As with rank-based results, the gains in accuracy are substantial, though somewhat reduced. At $\text{FPIR} = 0.01$, the best improvement over NEC in 2014 is a 27 fold reduction in FNIR using the NEC_2 algorithm. At $\text{FPIR} = 0.001$, the largest gain is a six-fold reduction in FNIR via the NEC_3 algorithm.
- **Broad gains across the industry:** About 19 companies realize accuracy better than the NEC benchmark from 2014. This is somewhat lower than the 28 developers who succeeded on the rank-1 metric. This may be due to the ubiquity of, and emphasis on, the rank-1 metric in many published algorithm development papers.
- **Webcam images:** Searches of webcam images give $\text{FNIR}(N, T)$ values around 2 to 3 times higher than mugshot searches. Notably the leading developers with mugshots are approximately the same with poorer quality webcams. But some developers e.g. Camvi, Megvii, TongYi, and Neurotechnology do improve their relative rankings on webcams, perhaps indicating their algorithms were tailored to less constrained images.

▷ Tables 16, 19, 20 and show, respectively, high-threshold, rank 1, and rank 50 FNIR values for all algorithms performing searches into five different gallery sizes, $N = 640\,000$, $N = 1\,600\,000$, $N = 3\,000\,000$, $N = 6\,000\,000$ and $12\,000\,000$. The $\text{FPIR} = 0.001$ table is included to inform high-volume duplicate detection applications. The Rank-1 table is included as a primary accuracy indicator. The Rank-50 table is included to inform agencies who routinely produce 50 candidates for human-review. The notable results are:

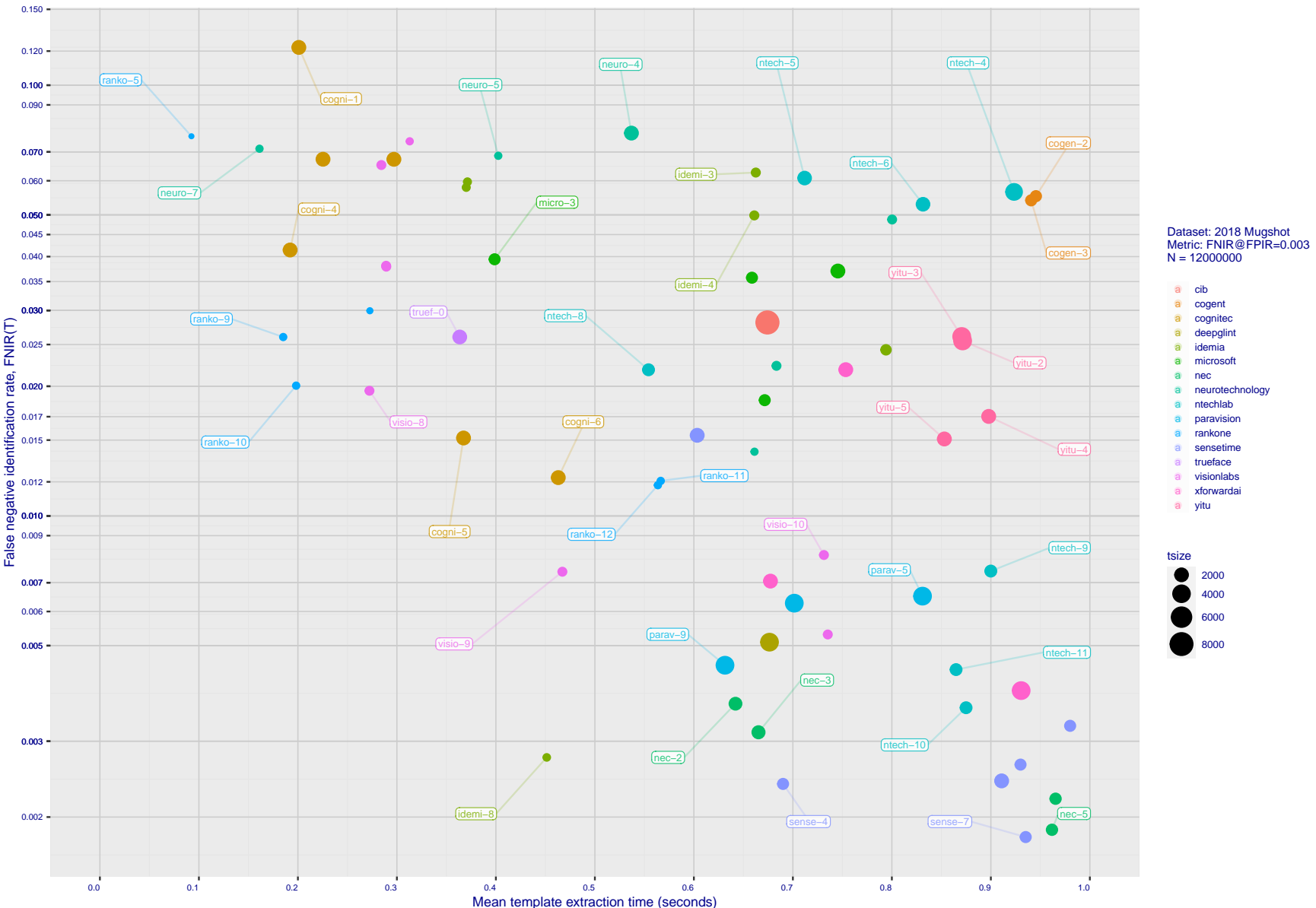
- **Slow growth in rank-based miss rates:** $\text{FNIR}(N, R)$ generally grows as a power law, aN^b . From the straight lines of many graphs of Figure 20 this is clearly a reasonable model for most, but not all, algorithms. The coefficient a can be interpreted as FNIR in a gallery of size 1. The more important coefficient b indicates scalability, and often, $b \ll 1$, implies very benign growth in FNIR. The coefficients of the models appear in the Tables 19 and 20.
- **Slow growth in threshold-based miss rates:** $\text{FNIR}(N, T)$ also generally grows as a power law, aN^b except at the high threshold values corresponding to low FPIR values. This is visible in the plots of Figure 36 which

show straight lines except for $FPIR = 0.001$, which increase more rapidly with N above 3 000 000. Each trace in those figures shows $FNIR(N, T)$ at fixed $FPIR$ with both N and T varying. Thus at large N , it is usually necessary to elevate T to maintain fixed $FPIR$. This causes increased $FNIR$. Why that would no-longer obey a power-law is not known. However, if we expect large galleries to contain individuals with familial relations to the non-mate search images - in the most extreme case, twins - then suppression of false positives becomes more difficult. This is discussed in the Figures starting at Fig. 10

▷ Figure ?? shows false positives from twins against their enrolled siblings, broken out by type of twin: fraternal or identical. The Figure is based on the enrollment of 104 single images on one of a pair of twins, and then the search of 2354 second images. Note that the dataset is heavily skewed towards identical twins which is not representative of the true population. There is also a skew towards same sex fraternal twin pairs compared to different sex fraternal twin pairs again not representative of the true population.

The notable results are:

- For all algorithms tested, the 1087 mated searches (Twin A vs. Twin A) produce scores almost always above typical operational thresholds, with (not shown) matches at rank 1. The images are of good quality, so this is the result expected from the rest of this report.
- For the 1066 identical twin searches (AB), almost all produce the twin at rank 1, with a few producing the mate at further down the candidate lists rank and low score.
- For the 169 fraternal searches (AB) from same sex pairs, most algorithms give a large number of very high scores, implying false positives at all thresholds. However, there are long tails containing lower scores that are correctly below threshold. In general, scores that are higher in this distribution are all rank 1 whereas the lower scores have much higher ranks.
- (Not shown) Of the 169, there are 24 fraternal searches (AB) involving different sex twins. Here most algorithms correctly report scores well below the lowest threshold, and usually not on the candidate list at all.

2022/02/23
14:06:29

14:06:29

FPIR(N, T) = False pos. identification rate
R = Num. candidates

R = Num. candidates examined

242

$T > 0 \rightarrow$ Identification

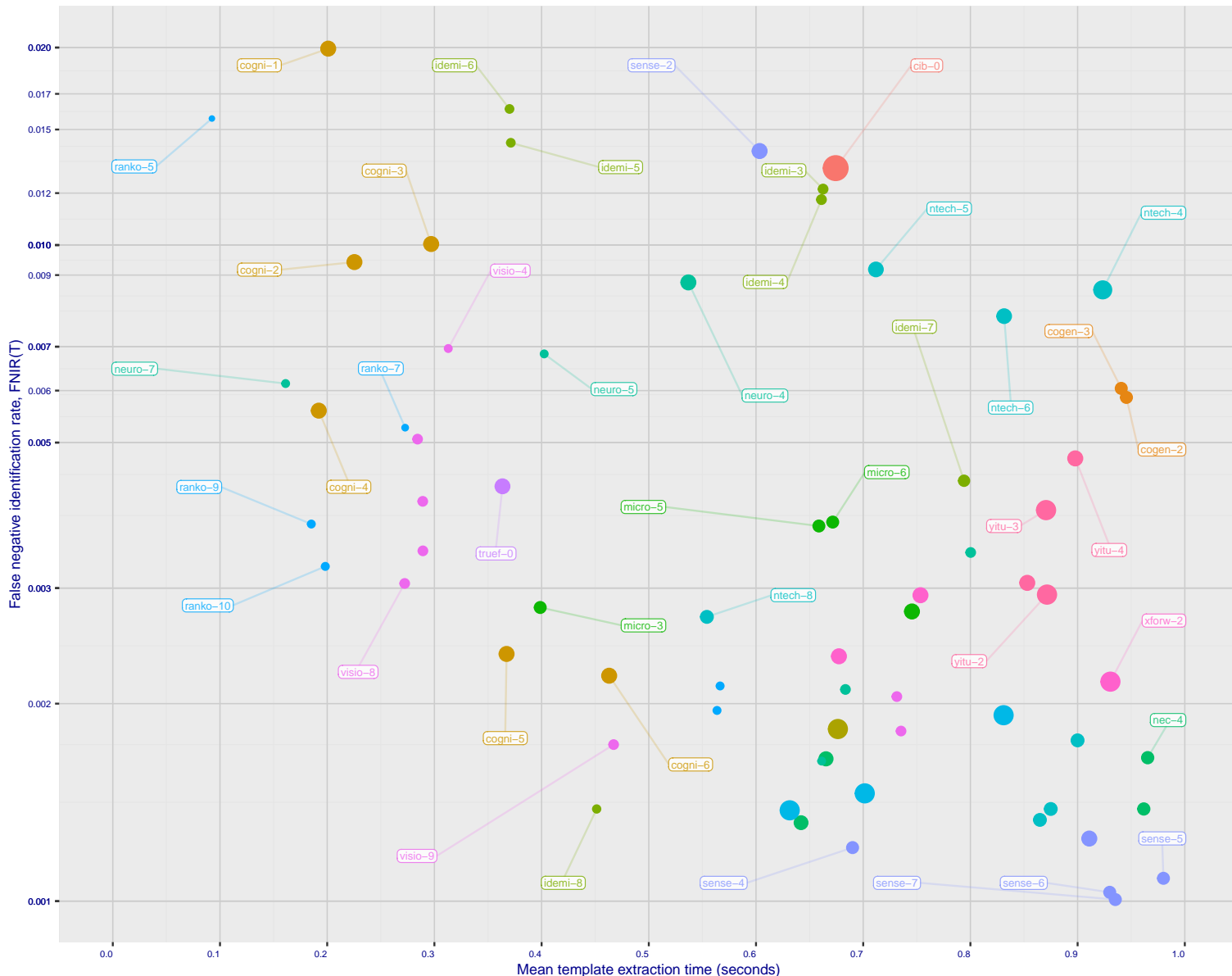


Figure 19: [Mugshot Dataset] Speed-accuracy tradeoff. For developers of the more accurate algorithms the plot shows the tradeoff of rank-one recognition miss-rates, FNIR($N, 1, 0$), and template generation time. Developers are coded by color. Template size is encoded by the size of the circle. Some labels are quite distant from the respective point, to avoid superposing text. Without any other influences, the assumption would be that taking time to localize the face, and extract features, would lead to better accuracy. This occurs for NEC with their slower algorithm being much accurate than the version that extract features in fewer than 90 milliseconds.

Developer	Full Name	Short	Seq.	Validation	Config ¹	Lib ¹	Template Generation		Finalize ²	Search Duration ⁵					Millisecond
		Name	Num.	Date	Data (MB)	Data (MB)	Size (B)	Mult ³	Time (ms) ⁴	Time (s)	L=1	L=50	L=50	L=50	Power Law
							N=1.6M	N=1.6M	N=3M	N=6M	N=12M	(μs)			
1	20Face	20face	000	2021-10-01	112	319	114	2048	-	20	236	62	9	(196)	6355
2	3DDivi	3divi	5	2018-10-26	186	51	186	4096	k	16	28	(89)	538	(87)	537
3	3Divi	3divi	6	2018-10-26	187	51	37	528	k	107	640	26	5	(12)	33
4	Acer Incorporated	acer	000	2020-08-12	35	67	30	512	-	15	198	4	295	(56)	295
5	Acer Incorporated	acer	001	2021-11-08	42	610	104	2048	-	11	184	59	9	(100)	619
6	Akurat Satu Indonesia	ptakuratsatu	000	2020-10-23	0	572	39	538	-	196	905	209	28633	(6)	15
7	Alchera Inc	alchera	2	2018-10-30	7	14	97	2048	k	6	114	190	63	(174)	2923
8	Alchera Inc	alchera	3	2018-10-30	251	14	87	2048	k	85	531	191	63	(175)	2955
9	Alchera Inc	alchera	004	2021-09-17	476	24	144	2048	-	177	853	175	35	(197)	6657
10	Alivia / Innovation Sys	isystems	3	2018-10-30	350	784	137	2048	1	167	825	133	16	(68)	385
11	AllGoVision	allgovation	000	2019-07-30	168	150	94	2048	k	52	404	89	12	(178)	3226
12	AllGoVision	allgovation	001	2020-07-14	283	126	110	2048	-	154	777	95	13	(177)	3174
13	Anke Investments	anke	0	2018-10-30	779	27	177	2072	k	59	429	131	16	(102)	675
14	Anke Investments	anke	1	2018-10-30	779	27	174	2072	k	60	430	125	15	(107)	707
15	Anke Investments	anke	002	2019-06-27	341	401	167	2056	k	10	623	104	13	(101)	624
16	Aware	aware	5	2018-10-30	368	27	184	3100	k	160	792	173	34	(16)	95
17	Aware	aware	6	2018-10-30	368	27	2	124	k	159	789	3	2	(32)	158
18	Ayonix	ayonix	1	2018-10-29	74	2	57	1036	k	2	12	84	11	(51)	279
19	Ayonix	ayonix	2	2018-10-30	74	2	58	1036	1	11	110	14	(51)	279	
20	Camvi Technologies	camvitech	4	2018-10-30	233	220	45	1024	1	123	686	171	31	(13)	33
21	Camvi Technologies	camvitech	5	2018-10-30	257	220	48	1024	1	145	751	169	31	(11)	31
22	Canon Inc	cib	000	2020-10-19	426	127	210	8196	-	17	674	113	(179)	3589	
23	Canon Inc	canon	001	2021-10-27	1139	91	193	4096	-	189	885	148	21	(199)	6804
24	Clearview AI Inc	clearviewai	000	2021-11-12	358	316	194	4096	-	150	765	166	30	(112)	802
25	Cloudwalk - Hengrui AI Technology	hr	000	2021-02-10	501	392	96	2048	-	197	905	118	15	(53)	282
26	Cloudwalk - Moontime Smart Technology	cloudwalk	mt	2022-01-31	716	573	132	2048	-	183	869	77	10	(78)	440
27	Cognitec Systems GmbH	cognitec	2	2018-10-30	463	26	167	2052	k	17	225	156	27	(154)	1733
28	Cognitec Systems GmbH	cognitec	3	2018-10-30	465	26	156	2052	k	30	297	129	16	(153)	1719
29	Cognitec Systems GmbH	cognitec	004	2021-03-08	384	60	147	2052	-	14	192	102	13	(152)	1673
30	Cognitec Systems GmbH	cognitec	005	2021-07-30	460	61	152	2052	-	39	367	64	9	(144)	1556
31	Cognitec Systems GmbH	cognitec	006	2022-02-10	689	61	145	2052	-	69	463	74	10	(123)	1006
32	Cubox	cubox	000	2021-08-24	529	298	98	2048	-	201	917	73	10	(180)	3646
33	Cyberlink Corp	cyberlink	000	2019-06-12	217	93	148	2052	1	110	654	165	30	(104)	696
34	Cyberlink Corp	cyberlink	001	2019-10-07	459	102	161	2052	1	59	423	162	28	(108)	698
35	Cyberlink Corp	cyberlink	002	2020-07-31	333	109	204	4140	-	138	724	200	6875	(141)	1353
36	Cyberlink Corp	cyberlink	003	2021-01-05	333	100	208	6212	-	126	691	177	35	(84)	488
37	Cyberlink Corp	cyberlink	004	2021-07-16	371	100	208	6212	-	140	728	152	23	(84)	492
38	Cyberlink Corp	cyberlink	005	2022-01-07	371	100	207	6212	-	142	733	168	30	(80)	489
39	DAON	daon	000	2021-12-23	274	2	171	2069	-	91	583	46	8	(88)	524
40	Dahua Technology Co Ltd	dahua	0	2018-10-29	276	167	86	2048	k	44	374	150	22	-	(49)
41	Dahua Technology Co Ltd	dahua	1	2018-10-29	276	167	92	2048	k	40	369	158	28	-	(48)
42	Dahua Technology Co Ltd	dahua	002	2019-12-02	607	137	140	2048	k	122	685	144	19	(43)	243
43	Dahua Technology Co Ltd	dahua	003	2020-11-18	889	154	87	2048	-	137	723	137	18	(54)	283
44	Dahua Technology Co Ltd	dahua	004	2021-11-18	812	116	131	2048	-	148	758	79	11	(75)	423
45	Decatur Industries Inc	decatur	000	2022-02-09	411	383	158	2052	-	179	863	66	9	(155)	1761
46	Deepglint	deepglint	001	2019-11-15	448	265	196	4096	-	119	676	174	35	(103)	677
47	Dermalog	dermalog	5	2018-10-26	0	440	4	128	1	84	528	199	3155	(1)	0
48	Dermalog	dermalog	6	2018-10-26	0	453	13	256	1	81	507	4	2	(29)	142
49	Dermalog	dermalog	007	2020-02-12	0	424	3	128	1	54	410	1	1	(22)	98
50	Dermalog	dermalog	008	2021-01-25	0	531	28	512	-	41	370	18	4	(62)	335
51	Dermalog	dermalog	009	2021-11-09	0	318	31	512	-	35	347	13	3	(47)	253
52	FarBar Inc	f8	001	2019-10-03	266	19	102	2048	k	164	810	107	14	-	-

Notes	
1	Configuration size does not capture static data present in libraries. Libraries are included but the size also includes any ancillary libraries for image processing (e.g. openCV) or numerical computation (e.g. blas).
2	Finalization is the processing of converting $N = 1600000$ templates into a searchable data structure an operation which can be a simple copy, or the building of an index or tree, for example. The duration of the operation may be data dependent, and may not be linear in the number of input templates.
3	This multiplier expresses the increase in template size when k images are passed to the template generation function.
4	All durations are measured on Intel®Xeon®CPU E5-2630 v4 @ 2.20GHz processors. Estimates are made by wrapping the API function call in calls to std::chrono::high_resolution_clock which on the machine in (3) counts 1ns clock ticks. Precision is somewhat worse than that however.
5	Search durations are measured as in the prior note. The power-law model in the final column mostly fits the empirical results in Figure 131. However in certain cases the model is not correct and should not be used numerically.

Table 2: Summary of algorithms and properties included in this report. The blue superscripts give ranking for the quantity in that column. Missing search durations, denoted by “-”, are absent because those runs were not executed, usually because we did not run on the larger galleries. Caution: The power-law model is sometimes an incorrect model. It is included here only to show broad sublinear behavior, which is flagged in green. The models should not be used for prediction.

2022/02/23
14:06:29

$\text{FNK}(N, K, 1) = \text{False neg. identification rate}$
 $\text{FPIR}(N, T) = \text{False pos. identification rate}$

$N = \text{Num. enroled subjects}$
 $R = \text{Num. candidates examined}$

$I = 0 \rightarrow$ investigation
 $T > 0 \rightarrow$ Identification

DEVELOPER FULL NAME	SHORT NAME	SEQ. NUM.	VALIDATION DATE	CONFIG ¹ DATA (MB)	LIB ¹ DATA (MB)	TEMPLATE GENERATION SIZE (B) MULT ³	FINALIZE ² TIME (S)	SEARCH DURATION ⁵ MILLISEC						POWER LAW (μ s)
								L=1 N=1.6M	L=50 N=1.6M	L=50 N=3M	L=50 N=6M	L=50 N=12M		
53 Fincore Ltd	fincore	000	2021-08-18	250	224	135/2048 -	73/475	56/9	(95)562	(92)560	-	-	-	-
54 Fujitsu Research and Development Center	fujitsulab	000	2021-10-12	497	337	50/1032 -	207/945	28/5	(151)1668	(148)1657	(128)3140	(125)6320	(124)12723	67 0.78 N ^{1.0}
55 Gorilla Technology	gorilla	2	2018-10-29	91	1252	65/1132 k	34/338	154/24	(30)145	(30)146	(26)293	(25)612	(27)1509	126 0.02 N ^{1.1}
56 Gorilla Technology	gorilla	3	2018-10-26	94	1252	177/2156 k	87/559	204/12020	-	(161)2047	-	-	-	-
57 Gorilla Technology	gorilla	004	2020-01-06	182	1244	178/2192 k	47/388	179/41	(55)286	(56)285	(77)1191	(77)2416	(72)5036	164 0.00 N ^{1.3}
58 Gorilla Technology	gorilla	005	2021-02-22	306	1420	209/6288 -	76/483	193/78	(111)802	(111)799	(90)1514	(100)4454	(94)8820	150 0.05 N ^{1.2}
59 Gorilla Technology	gorilla	006	2021-09-30	377	691	211/8326 -	151/767	197/99	(147)1626	(145)1612	(108)4222	(99)4422	(99)9363	66 0.59 N ^{1.0}
60 Griaule	griaule	000	2021-11-01	0	584	151/2052 -	56/417	40/8	(192)5827	(194)6150	(161)11473	(159)22952	(156)46070	31 3.89 N ^{1.0}
61 Guangzhou Pixel Solutions Co Ltd	pixelall	002	2019-07-01	0	165	180/2560 k	13/190	122/15	(138)1296	(138)1334	(115)2526	(110)5136	(114)11045	87 0.52 N ^{1.0}
62 Guangzhou Pixel Solutions Co Ltd	pixelall	003	2019-11-05	0	690	182/2560 k	131/703	151/22	(135)1273	(134)1307	(112)2474	(111)5198	(115)11141	96 0.46 N ^{1.0}
63 Guangzhou Pixel Solutions Co Ltd	pixelall	004	2020-07-02	0	538	181/2560 k	61/449	136/17	(134)1259	(133)1300	(111)2465	(116)5492	(116)11443	109 0.34 N ^{1.1}
64 Guangzhou Pixel Solutions Co Ltd	pixelall	005	2021-03-23	0	717	179/2560 -	173/840	83/11	(146)1606	(143)1528	(117)2609	(107)4926	(119)11770	59 0.73 N ^{1.0}
65 Hikvision Research Institute	hikvision	5	2018-10-29	593	9	70/1408 1	96/607	128/16	(117)883	(117)895	(97)1908	(92)3792	(100)9387	137 0.10 N ^{1.1}
66 Hikvision Research Institute	hikvision	6	2018-10-29	593	9	71/1408 1	94/598	130/16	(115)871	(116)877	-	-	-	-
67 HyperVerge Inc	hyperverge	001	2021-08-11	1791	212	49/1024 -	175/845	24/5	(106)705	(101)681	(81)1346	(82)2681	(78)5680	74 0.32 N ^{1.0}
68 Idemia	idemia	5	2018-10-29	417	48	22/352 1	43/371	25/5	(26)137	(27)138	(31)437	(30)724	(28)1630	158 0.01 N ^{1.2}
69 Idemia	idemia	6	2018-10-29	417	48	21/352 1	42/370	22/4	(27)137	(26)138	(32)442	(32)827	(29)1646	160 0.01 N ^{1.2}
70 Idemia	idemia	007	2020-01-17	738	113	44/860 1	161/794	108/14	(31)151	(31)152	(52)683	(55)1481	(52)3022	169 0.00 N ^{1.4}
71 Idemia	idemia	008	2021-03-15	378	65	21/300 -	63/451	14/3	(25)132	(25)131	(23)247	(22)501	(21)1013	54 0.07 N ^{1.0}
72 Imagus Technology Pty Ltd	imus	005	2021-01-15	222	311	103/2048 -	158/786	108/14	(42)236	(61)313	(50)651	(50)1361	(40)2461	135 0.03 N ^{1.1}
73 Imagus Technology Pty Ltd	imus	006	2021-05-27	248	369	142/2048 -	196/904	67/9	(60)317	(41)234	(37)499	(48)1273	(43)2727	156 0.01 N ^{1.2}
74 Imagus Technology Pty Ltd	imus	007	2021-11-16	248	366	143/2048 -	97/609	52/9	(41)234	(42)238	(33)442	(33)881	(31)1765	26 0.16 N ^{1.0}
75 Imperial College London	imperial	000	2019-08-28	461	15	119/2048 1	90/577	94/13	(65)360	(70)379	(91)1626	(95)4057	(112)10291	172 0.00 N ^{1.5}
76 Incode Technologies Inc	incode	2	2018-10-29	71	31	105/2048 1	29/289	12/5	(73)411	(74)404	-	-	-	-
77 Incode Technologies Inc	incode	3	2018-10-29	133	31	138/2048 1	129/697	117/15	(72)408	(76)412	(88)847	(87)1608	(66)4486	130 0.05 N ^{1.1}
78 Incode Technologies Inc	incode	004	2019-06-24	254	50	108/2048 1	72/475	82/12	(66)365	(69)378	(88)1482	(99)1660	(50)2954	107 0.12 N ^{1.1}
79 Incode Technologies Inc	incode	005	2021-07-29	259	21	100/2048 -	78/500	72/10	(59)316	(80)454	(63)890	(65)1843	(59)3640	119 0.07 N ^{1.1}
80 Innovatrics	innovatrics	4	2018-10-30	0	400	62/1076 k	48/399	201/10902	(5)8	(4)8	(4)11	(2)9	(3)13	9 668.38 N ^{0.2}
81 Innovatrics	innovatrics	005	2019-09-30	0	455	38/538 1	169/827	203/11897	(4)8	(5)8	(3)9	(3)9	(2)9	1 4055.65 N ^{0.1}
82 Innovatrics	innovatrics	007	2021-08-16	175	58	49/538 -	153/777	109/14	(21)197	(22)100	(18)188	(19)378	(18)788	23 0.09 N ^{1.0}
83 IraxAI	irex	000	2021-02-09	724	46	183/3080 -	174/844	143/19	(99)616	(96)600	(72)1120	(79)2477	(79)5863	113 0.13 N ^{1.1}
84 Kakao Enterprise	kakao	000	2021-06-23	404	124	157/2052 -	172/835	42/8	(40)213	(39)215	(38)510	(37)971	(35)1955	115 0.05 N ^{1.1}
85 Kedacom International Pte	kedacom	001	2019-09-16	239	36	179/292 1	80/507	52/2	(109)764	(108)760	(98)1940	(88)2983	(86)6623	91 0.31 N ^{1.0}
86 Kneron	kneron	000	2020-03-03	366	13	120/2048 k	83/523	93/13	(171)2535	(172)2506	(147)4752	(145)9696	(146)20926	92 0.95 N ^{1.0}
87 Kneron	kneron	001	2021-06-10	270	69	89/2048 -	71/472	57/9	(172)2690	(174)2642	-	-	-	-
88 Line Corporation	line	000	2021-06-02	138	397	123/2048 -	75/481	47/8	(187)5433	(189)5418	(159)10144	-	-	29 3.65 N ^{1.0}
89 Line Corporation	line	001	2021-11-21	471	396	129/2048 -	199/907	48/8	(157)1872	(158)1934	(134)3647	(135)7675	-	97 0.64 N ^{1.0}
90 Lomonosov Moscow State University	instsysmu	000	2019-08-19	375	168	112/2048 1	99/614	103/13	(76)430	(78)431	(61)860	(60)1730	(79)5353	145 0.03 N ^{1.1}
91 Lookman Electroplast Industries	lookman	3	2018-10-28	203	24	20/292 1	33/336	12/3	(108)739	(106)745	(85)1394	(84)2817	(91)8286	123 0.13 N ^{1.1}
92 Lookman Electroplast Industries	lookman	4	2018-10-28	184	24	42/548 1	31/320	21/4	(120)981	(120)998	-	-	-	-
93 Lookman Electroplast Industries	lookman	005	2019-09-16	239	36	41/548 1	79/506	17/4	(122)1005	(122)1008	(116)2597	(115)5446	(95)8939	121 0.19 N ^{1.1}
94 Mantra Softech India	mantra	000	2021-10-28	460	61	159/2052 -	55/412	71/10	(119)916	(118)910	(93)1714	(91)3411	(88)6841	35 0.57 N ^{1.0}
95 Megvii/Face++	megvii	1	2018-10-28	1703	41	188/4096 1	103/631	172/32	(91)552	(93)561	(79)1222	(75)2321	(80)5968	129 0.08 N ^{1.1}
96 Megvii/Face++	megvii	2	2018-10-28	1735	42	195/4096 1	105/635	170/31	(92)553	(90)558	-	-	-	-
97 MicroFocus	microfocus	5	2018-10-29	94	26	11/256 k	24/262	8/2	(37)182	(36)186	(29)354	(29)708	(25)1425	49 0.11 N ^{1.0}
98 MicroFocus	microfocus	6	2018-10-29	94	26	12/256 k	23/262	10/2	(38)183	(35)186	-	-	-	-
99 Microsoft	microsoft	5	2018-10-29	381	155	46/1024 1	111/658	85/11	(145)1606	(149)1673	(127)3076	(124)6302	(127)13160	65 0.79 N ^{1.0}
100 Microsoft	microsoft	6	2018-10-29	478	155	47/1024 1	115/671	121/15	(148)1642	(147)1618	(136)3710	(126)6401	(125)12892	82 0.68 N ^{1.0}
101 N-Tech Lab	ntech	5	2018-10-30	1685	113	82/1940 k	135/711	188/55	(45)243	(46)246	(40)538	(40)1100	(46)2867	141 0.02 N ^{1.1}
102 N-Tech Lab	ntech	6	2018-10-30	1686	117	83/1940 k	171/831	189/63	(44)243	(45)246	(42)546	(41)1104	(47)2873	143 0.02 N ^{1.1}
103 N-Tech Lab	ntechlab	007	2019-06-25	2450	51	185/3348 k	162/795	192/73	(66)393	(77)427	(56)780	(63)1768	(58)3499	90 0.16 N ^{1.0}
104 N-Tech Lab	ntechlab	008	2020-01-06	1111	51	69/1300 k	86/554	178/36	(36)179	(33)184	(28)341	(28)683	(24)1395	46 0.11 N ^{1.0}

Notes

- Configuration size does not capture static data present in libraries. Libraries are included but the size also includes any ancillary libraries for image processing (e.g. openCV) or numerical computation (e.g. blas).
- Finalization is the processing of converting $N = 1600000$ templates into a searchable data structure an operation which can be a simple copy, or the building of an index or tree, for example. The duration of the operation may be data dependent, and may not be linear in the number of input templates.
- This multiplier expresses the increase in template size when k images are passed to the template generation function.
- All durations are measured on Intel®Xeon®CPU E5-2630 v4 @ 2.20GHz processors. Estimates are made by wrapping the API function call in calls to std::chrono::high_resolution_clock which on the machine in (3) counts 1ns clock ticks. Precision is somewhat worse than that however.
- Search durations are measured as in the prior note. The power-law model in the final column mostly fits the empirical results in Figure 131. However in certain cases the model is not correct and should not be used numerically.

Table 3: Summary of algorithms and properties included in this report. The blue superscripts give ranking for the quantity in that column. Missing search durations, denoted by “-”, are absent because those runs were not executed, usually because we did not run on the larger galleries. Caution: The power-law model is sometimes an incorrect model. It is included here only to show broad sublinear behavior, which is flagged in green. The models should not be used for prediction.

2022/02/23

14:06:29

FNIR(N, R, T) =

False neg. identification rate

N = Num. enrolled subjects

R = Num. candidates examined

T = Threshold

T = 0 → Investigation

T ∨ 0 → Identification

	DEVELOPER	SHORT	SEQ.	VALIDATION	CONFIG ¹	LIB ¹	TEMPLATE GENERATION	FINALIZE ²	SEARCH DURATION ⁵ MILLISEC							
									TIME (S)	L=1	L=50	L=50	L=50	POWER LAW		
										N=1.6M	N=1.6M	N=3M	N=6M	N=12M		
105	N-Tech Lab	ntechlab	009	2021-03-01	1208	42	68 1300	-	194 899	176 35	(35) 178	(34) 184	(27) 336	(27) 676	(30) 1704	108 0.05N ^{1.1}
106	N-Tech Lab	ntechlab	010	2021-06-24	351	213	67 1280	-	185 874	29 6	(77) 440	(79) 435	(57) 821	(58) 1645	(55) 3337	60 0.22N ^{1.0}
107	N-Tech Lab	ntechlab	011	2021-12-07	679	208	66 1280	-	180 864	31 6	(82) 488	(81) 483	(64) 912	(66) 1869	(70) 5003	125 0.07N ^{1.1}
108	NEC	nec	2	2018-10-30	705	35	78 1616	k	108 642	140 18	(70) 405	(74) 409	(70) 1072	(61) 1755	(65) 4255	132 0.06N ^{1.1}
109	NEC	nec	3	2018-10-30	774	110	79 1712	k	113 665	141 21	(3) 7	(3) 14	(9) 40	(10) 82	(15) 151	0.00N ^{1.2}
110	NEC	nec	004	2021-07-19	971	63	63 1104	-	211 965	32 7	(63) 349	(64) 351	(51) 662	(49) 1330	(42) 2685	50 0.20N ^{1.0}
111	NEC	nec	005	2021-12-13	922	88	64 1104	-	210 961	33 7	(80) 473	(88) 551	(68) 1017	(69) 2091	(63) 4242	57 0.28N ^{1.0}
112	Neurotechnology	neurotech	5	2018-10-30	266	53	12 256	k	50 402	9 2	(113) 835	(113) 839	(92) 1690	(90) 3219	(96) 8955	114 0.19N ^{1.1}
113	Neurotechnology	neurotech	6	2018-10-30	564	53	10 256	k	139 726	7 2	(114) 839	(114) 842	-	-	-	-
114	Neurotechnology	neurotech	007	2019-10-03	57	51	8 256	k	7 161	6 2	(127) 1118	(126) 1110	(103) 2143	(98) 4397	(97) 9045	64 0.55N ^{1.0}
115	Neurotechnology	neurotechnology	008	2021-03-22	355	49	36 514	-	163 800	20 4	(130) 1167	(129) 1149	(105) 2266	(103) 4573	(104) 9586	70 0.55N ^{1.0}
116	Neurotechnology	neurotechnology	009	2021-09-01	246	82	35 513	-	121 683	11 3	(125) 1035	(124) 1049	(100) 1977	(96) 4270	(92) 8756	101 0.32N ^{1.1}
117	Neurotechnology	neurotechnology	010	2022-01-07	247	83	14 256	-	112 661	2 2	(121) 986	-	-	-	-	-
118	Newland Computer Co Ltd	newland	2	2018-10-30	96	27	109 2048	-	178 855	123 15	(202) 8741	(205) 8854	(173) 17892	(170) 39356	-	127 1.32N ^{1.1}
119	Noblis	noblis	1	2018-10-30	114	176	124 2048	1	17 206	119 15	(136) 1273	(132) 1272	-	-	-	-
120	Noblis	noblis	2	2018-10-30	153	176	205 6144	1	82 517	181 43	(170) 2513	(173) 2522	(148) 5649	(149) 12432	(155) 44262	162 0.04N ^{1.3}
121	NotionTag Technologies Private Limited	notiontag	000	2022-01-14	265	945	176 2120	-	64 453	75 10	(201) 8619	(204) 8705	(172) 16652	(169) 38794	(166) 90607	131 1.15N ^{1.1}
122	Paravision (EverAI)	everai	2	2018-10-30	224	304	115 2048	1	38 366	16 30	(50) 278	(55) 283	-	-	-	-
123	Paravision (EverAI)	everai	3	2018-10-30	438	304	95 2048	1	136 717	160 28	(49) 278	(54) 281	(44) 572	(42) 1146	(37) 2278	83 0.12N ^{1.0}
124	Paravision (EverAI)	everai-paravision	004	2019-06-19	527	128	197 4096	1	116 672	184 45	(93) 559	(91) 559	(118) 2611	(127) 6445	(130) 14519	170 0.00N ^{1.5}
125	Paravision (EverAI)	paravision	005	2019-12-11	543	154	189 4096	1	170 830	186 48	(94) 561	(94) 564	(69) 1056	(72) 2298	(69) 4966	105 0.16N ^{1.1}
126	Paravision (EverAI)	paravision	007	2021-02-01	529	235	192 4096	-	130 701	18 48	(96) 569	(89) 558	(71) 1086	(70) 2111	(64) 4254	20 1.11N ^{0.9}
127	Paravision	paravision	009	2021-12-14	672	300	199 4100	-	104 631	194 82	(181) 3690	(184) 4230	(156) 8037	(155) 16532	(151) 31422	85 1.62N ^{1.0}
128	Qnap Security	qnap	000	2021-07-28	182	15	113 2048	-	65 457	60 9	(132) 1231	(153) 1763	-	-	-	-
129	Qnap Security	qnap	001	2021-12-09	191	13	116 2048	-	98 613	43 8	(150) 1666	(141) 1429	(131) 3472	(132) 7375	(135) 15159	148 0.11N ^{1.2}
130	Quantasoft	quantasoft	1	2018-10-30	276	452	88 2048	k	46 385	30 6	(203) 15422	(206) 14858	(170) 14717	-	(139) 18323	-
131	Rank One Computing	rankone	4	2018-10-09	0	101	1 85	k	3 36	34 7	(23) 101	(25) 101	(19) 190	-	-	27 0.07N ^{1.0}
132	Rank One Computing	rankone	5	2018-10-24	0	101	5 133	k	4 92	35 7	(28) 140	(28) 144	(24) 266	(23) 525	(22) 1049	24 0.11N ^{1.0}
133	Rank One Computing	rankone	006	2019-06-03	0	133	7 165	k	22 245	41 8	-	-	-	-	-	-
134	Rank One Computing	rankone	007	2019-11-12	0	137	6 165	k	25 272	37 7	(24) 116	(24) 115	(21) 2125	(21) 439	(19) 877	48 0.07N ^{1.0}
135	Rank One Computing	rankone	009	2020-06-26	0	105	15 260	k	12 185	82 11	(17) 95	(20) 96	(16) 181	(16) 362	(17) 727	37 0.06N ^{1.0}
136	Rank One Computing	rankone	010	2020-11-05	0	135	17 261	-	16 198	76 10	(18) 95	(16) 95	(14) 178	(14) 357	(15) 714	33 0.06N ^{1.0}
137	Rank One Computing	rankone	011	2021-08-27	0	175	18 261	-	89 566	49 8	(20) 96	(17) 95	(17) 183	(17) 370	(14) 714	44 0.06N ^{1.0}
138	Rank One Computing	rankone	012	2021-12-27	0	257	18 261	-	88 563	39 8	(19) 95	(18) 95	(15) 179	(15) 361	(16) 718	36 0.06N ^{1.0}
139	Realnetworks Inc	realnetworks	2	2018-10-30	105	104	201 4104	k	21 241	152 28	(158) 2008	(162) 2048	(130) 4194	(138) 8642	(134) 1842	58 1.08N ^{1.0}
140	Realnetworks Inc	realnetworks	003	2019-06-12	93	102	81 1848	k	10 173	93 13	(129) 1145	(127) 1132	(102) 2142	(112) 5241	(113) 10495	118 0.21N ^{1.1}
141	Realnetworks Inc	realnetworks	004	2019-10-17	94	102	80 1848	1	9 171	81 11	(128) 1143	(128) 1137	(104) 2149	(105) 4740	(107) 9693	100 0.36N ^{1.0}
142	Realnetworks Inc	realnetworks	005	2021-06-23	168	209	168 2056	-	32 332	55 9	(149) 1654	(146) 1616	(126) 3030	(122) 6068	(122) 12134	41 1.01N ^{1.0}
143	Realnetworks Inc	realnetworks	006	2021-12-02	250	56	166 2056	-	36 348	44 8	(90) 543	(86) 531	(67) 996	(68) 1998	(62) 3991	40 0.33N ^{1.0}
144	Remark Holdings	remarkai	0	2018-10-30	187	847	139 2048	k	92 593	112 14	(190) 5685	(192) 5723	-	-	-	-
145	Remark Holdings	remarkai	000	2019-06-12	234	1092	107 2048	k	109 650	92 12	(191) 5776	(191) 5703	(162) 11604	(168) 32133	(167) 91436	163 0.05N ^{1.3}
146	Remark Holdings	remarkai	1	2018-10-30	187	847	101 2048	k	58 427	118 14	(189) 5680	(193) 5761	(165) 12475	(166) 28726	(164) 59618	153 0.37N ^{1.2}
147	Rendip	rendip	000	2021-05-21	0	416	141 2048	-	191 890	63 9	(46) 249	(66) 368	(54) 697	(54) 1452	(49) 2926	111 0.08N ^{1.1}
148	Reveal Media Ltd	revealmedia	000	2022-02-02	287	196	154 2052	-	45 383	70 10	(162) 2322	(159) 2019	(138) 2838	(136) 7816	(138) 16559	88 0.78N ^{1.0}
149	SQISoft	sqisoft	001	2021-12-20	271	377	163 2056	-	68 462	61 9	(139) 1310	(136) 1319	(110) 2456	(106) 4906	(109) 9755	28 0.90N ^{1.0}
150	Samsung S1 Corp	s1	000	2021-06-03	257	196	191 4096	-	181 865	145 20	(198) 6715	(201) 6794	(169) 13032	(165) 26372	(163) 55723	81 2.82N ^{1.0}
151	Samsung S1 Corp	s1	001	2021-11-01	240	198	136 2048	-	165 813	50 8	(164) 2415	(171) 2491	(146) 4718	(144) 9614	(147) 24472	116 0.53N ^{1.1}
152	Scanovate Ltd	scanovate	000	2020-01-15	250	446	117 2048	-	132 705	114 14	(143) 1419	(140) 1412	(125) 3008	(146) 11616	(120) 12012	154 0.10N ^{1.2}
153	Scanovate Ltd	scanovate	001	2020-09-10	250	446	128 2048	-	118 675	91 13	(140) 1321	(137) 1320	(111) 2502	(109) 5047	(110) 10163	61 0.65N ^{1.0}
154	Sensetime Group	sensetime	0	2018-10-30	525	6	202 4104	k	128 693	180 41	(85) 498	(82) 501	(78) 1212	(71) 2281	(71) 5032	124 0.09N ^{1.1}
155	Sensetime Group	sensetime	1	2018-10-30	525	6	203 4104	k	102 628	184 48	(87) 516	(83) 502	(74) 1146	(73) 2301	(67) 4765	122 0.09N ^{1.1}
156	Sensetime Group	sensetime	002	2019-06-03	523	6	165 2056	k	95 603	138 18	(64) 359	(67) 370	(96) 1897	(101) 4508	(103) 9543	173 0.00N ^{1.5}

Notes													
1	Configuration size does not capture static data present in libraries. Libraries are included but the size also includes any ancillary libraries for image processing (e.g. openCV) or numerical computation (e.g. blas).												
2	Finalization is the processing of converting $N = 1600000$ templates into a searchable data structure an operation which can be a simple copy, or the building of an index or tree, for example. The duration of the operation may												

	DEVELOPER	SHORT NAME	SEQ. NUM.	VALIDATION DATE	CONFIG ¹	LIB ¹	TEMPLATE GENERATION SIZE (B) MULT ³	TIME (MS) ⁴	FINALIZE ² TIME (S)	SEARCH DURATION ⁵ MILLISEC							
										N=1.6M	N=1.6M	N=1.6M	N=3M	N=6M	N=12M		
157	Sensetime Group	sensetime	003	2019-12-02	769	76	164 2056	1	200 910	142 19	(185) 4885	(489) 12325	(161) 24712	(158) 49445	134	0.67N ^{1.1}	
158	Sensetime Group	sensetime	004	2020-08-10	456	29	56 1032	-	125 690	91 12	(169) 2490	(168) 2477	(144) 4654	(143) 9402	(145) 19651	63	1.22N ^{1.0}
159	Sensetime Group	sensetime	005	2020-12-17	631	39	52 1032	-	212 980	80 11	(166) 2459	(182) 3939	(154) 7398	(152) 14768	(144) 19016	18	14.03N ^{0.9}
160	Sensetime Group	sensetime	006	2021-07-26	526	54	51 1032	-	202 929	38 7	(163) 2414	(167) 2422	(142) 4527	(140) 9128	(140) 18640	52	1.35N ^{1.0}
161	Sensetime Group	sensetime	007	2022-01-15	526	37	55 1032	-	204 935	51 8	(165) 2432	(166) 2406	(141) 4513	(139) 8998	(142) 18796	56	1.28N ^{1.0}
162	Shaman Software	shaman	6	2018-10-26	0	200	106 2048	k	133 706	113 14	(98) 603	(99) 612	-	-	-	-	
163	Shaman Software	shaman	7	2018-10-26	0	200	127 2048	k	134 707	113 14	(97) 602	(98) 614	(78) 1187	(78) 2448	(74) 5083	84	0.25N ^{1.0}
164	Shanghai Yitu Technology	yitu	4	2018-10-30	2119	136	173 2070	1	193 897	183 45	(137) 1288	(131) 1203	(109) 2440	(113) 5241	(106) 9671	80	0.52N ^{1.0}
165	Shanghai Yitu Technology	yitu	5	2018-10-30	2043	136	172 2070	1	176 853	187 44	(133) 1237	(130) 1199	(114) 2513	(108) 5013	(105) 9620	76	0.55N ^{1.0}
166	Smilart	smilart	4	2018-10-30	65	89	29 512	k	8 167	19 4	(204) 16137	(207) 15633	-	-	-	-	
167	Smilart	smilart	5	2018-10-30	562	89	99 2048	k	62 450	111 14	-	-	-	-	-	-	
168	StaQu Technologies	staqu	000	2021-08-30	1018	690	198 4096	-	168 826	155 24	(186) 4950	(187) 4933	-	-	-	-	
169	Synesis	synesis	003	2019-07-04	143	17	134 2048	k	18 211	81 12	(86) 507	(84) 502	(106) 2297	(102) 4564	(101) 9452	168	0.00N ^{1.4}
170	Synesis	synesis	3	2018-10-30	237	150	190 4096	k	5 99	163 29	(110) 789	(112) 801	(99) 1941	(94) 3888	(93) 8810	142	0.07N ^{1.1}
171	Synesis	synesis	005	2020-09-08	494	24	200 4104	-	147 756	153 24	(116) 877	(115) 865	(120) 3182	(104) 4658	(108) 9750	155	0.06N ^{1.2}
172	Tech5 SA	tech5	001	2019-08-19	1394	116	72 1536	k	190 887	67 10	(67) 383	(109) 766	(120) 2767	(123) 6149	(82) 6178	153	0.12N ^{1.1}
173	Tech5 SA	tech5	002	2021-04-07	727	112	34 513	-	205 940	15 4	(184) 4682	(199) 6689	(166) 12541	(162) 25145	(160) 50239	39	4.18N ^{1.0}
174	Tencent Deepsea Lab	deepsea	001	2019-07-29	250	323	93 2048	1	144 737	91 12	(124) 1021	(123) 1020	(121) 2774	(119) 5767	(123) 12341	150	0.06N ^{1.2}
175	Tevian	tevian	5	2018-10-30	773	15	98 2048	1	53 405	120 15	(71) 405	(73) 408	(59) 854	(62) 1757	(57) 3380	99	0.14N ^{1.0}
176	Tevian	tevian	006	2021-04-16	769	19	54 1032	-	93 597	68 10	(57) 295	(58) 295	(45) 578	(44) 1187	(45) 2741	112	0.06N ^{1.1}
177	Tevian	tevian	007	2021-10-12	703	19	53 1032	-	155 777	23 4	(58) 297	(59) 298	(46) 579	(43) 1179	(39) 2418	93	0.11N ^{1.0}
178	Thales	cogent	2	2018-10-30	681	39	60 1043	k	208 945	152 17	(159) 2017	(164) 2144	(140) 4298	(137) 8472	(137) 16429	62	1.08N ^{1.0}
179	Thales	cogent	3	2018-10-30	681	39	59 1043	k	206 940	65 9	(131) 1230	(135) 1311	(119) 2687	(114) 5398	(111) 10184	71	0.62N ^{1.0}
180	Thales	cogent	004	2021-02-10	1376	59	162 2053	-	209 947	105 14	(173) 2903	(156) 1911	(132) 3566	(133) 7498	(136) 16370	98	0.64N ^{1.0}
181	Thales	cogent	005	2021-09-13	1043	56	61 1062	-	152 769	27 5	(118) 912	(119) 996	(99) 1872	(93) 3845	(89) 7555	23	0.44N ^{1.0}
182	TigerIT Americas LLC	tiger	2	2018-10-29	416	518	153 2052	k	66 461	124 15	(156) 1816	(157) 1921	(137) 3833	(134) 7526	(132) 14820	78	0.83N ^{1.0}
183	TigerIT Americas LLC	tiger	3	2018-10-30	416	518	150 2052	k	67 461	211 37431	(39) 191	(37) 189	-	-	-	-	
184	Toshiba	toshiba	0	2018-10-30	961	105	77 1548	k	187 876	86 12	(195) 6153	(195) 6236	(163) 12221	(163) 25355	(159) 49448	149	0.36N ^{1.2}
185	Toshiba	toshiba	1	2018-10-30	961	105	170 2060	k	186 875	212 44701	(194) 6007	(197) 6355	-	-	-	-	
186	Tripleize	aize	001	2021-08-06	262	150	118 2048	-	49 402	58 9	(176) 3087	(177) 3080	-	-	-	-	
187	Trueface.ai	trueface	000	2021-01-27	247	119	84 2000	-	37 363	96 13	(48) 271	(63) 327	(48) 614	(46) 1239	(41) 2678	69	0.15N ^{1.0}
188	Veridas Digital Authentication Solutions S.L.	veridas	001	2021-03-05	347	875	133 2048	-	184 872	97 13	(188) 5493	(190) 5469	(160) 10350	(158) 20655	(154) 41264	42	3.40N ^{1.0}
189	Veridas Digital Authentication Solutions S.L.	veridas	002	2021-07-06	347	870	121 2048	-	188 877	78 10	(61) 322	(61) 325	(53) 685	(51) 1365	(44) 2730	106	0.09N ^{1.1}
190	Veridas Digital Authentication Solutions S.L.	veridas	003	2021-11-09	346	870	91 2048	-	182 867	55 9	(79) 440	(62) 327	(55) 699	(52) 1401	(61) 3954	152	0.02N ^{1.2}
191	Viettel Group	vts	000	2021-03-12	250	257	126 2048	-	77 492	198 2295	(2) 4	(2) 4	(2) 6	(4) 11	-	13	0.61N ^{0.6}
192	Viettel Group	vts	001	2021-07-16	352	600	125 2048	-	192 891	147 21	(167) 2477	(170) 2487	(143) 4644	(141) 9313	(141) 18713	41	1.53N ^{1.0}
193	Viettel Group	vts	002	2022-02-08	244	600	130 2048	-	195 903	164 29	(168) 2485	(169) 2485	(145) 4678	(142) 9370	(143) 18833	47	1.49N ^{1.0}
194	Vigilant Solutions	vigilant	5	2018-10-30	335	122	75 1544	k	149 762	141 19	-	(151) 1720	-	-	-	-	
195	Vigilant Solutions	vigilant	6	2018-10-30	337	122	76 1544	k	166 816	147 21	-	(150) 1713	-	-	-	-	
196	Vigilant Solutions	vigilantsolutions	007	2021-01-08	340	51	73 1544	-	100 616	135 16	(142) 1354	(139) 1352	(123) 2911	(121) 5966	(117) 11466	117	0.27N ^{1.1}
197	Vigilant Solutions	vigilantsolutions	008	2021-07-23	340	51	74 1544	-	51 403	101 13	(126) 1062	(125) 1061	(107) 2330	(117) 5520	(102) 9499	138	0.11N ^{1.1}
198	Visidon	visidon	1	2018-10-30	166	42	155 2052	k	114 667	126 15	(182) 4370	(186) 4472	(157) 8454	(156) 17262	(152) 34288	55	2.40N ^{1.0}
199	Visidon	vd	002	2021-05-18	248	42	146 2052	-	124 687	54 9	(160) 2089	(165) 2336	-	-	-	-	
200	Visidon	vd	003	2021-10-12	497	43	149 2052	-	127 692	45 8	(161) 2095	(163) 2082	-	-	-	-	
201	Visiob-Box	visionbox	000	2021-09-17	252	274	169 2059	-	74 481	134 16	(74) 422	(65) 359	(60) 855	(26) 631	(36) 2096	16	2.46N ^{0.8}
202	VisionLabs	visionlabs	6	2018-10-30	360	17	21 512	1	28 289	208 20290	(14) 36	(14) 36	(12) 39	(11) 44	(9) 53	8	3211.93N ^{0.2}
203	VisionLabs	visionlabs	7	2018-10-30	360	17	25 512	1	27 289	210 34666	(15) 63	(15) 63	(13) 72	(13) 80	(11) 115	10	2076.32N ^{0.2}
204	VisionLabs	visionlabs	008	2019-06-18	348	17	27 512	1	26 272	206 12747	(19) 23	(8) 24	(7) 26	(6) 29	(5) 33	6	2539.61N ^{0.2}
205	VisionLabs	visionlabs	009	2020-08-04	689	20	31 512	-	70 467	207 13245	(10) 23	(9) 29	(8) 34	(7) 61	(12) 145	12	8.88N ^{0.6}
206	VisionLabs	visionlabs	010	2021-02-05	1042	20	33 512	-	141 731	202 11837	(7) 21	(11) 32	(10) 36	(8) 39	(6) 43	7	3183.79N ^{0.2}
207	VisionLabs	visionlabs	011	2021-10-20	1042	20	29 512	-	143 735	205 12255	(8) 21	(7) 23	(6) 26	(7) 34	(8) 51	11	301.26N ^{0.3}
208	Vocord	vocord	5	2018-10-30	1035	185	43 768	k	156 780	36 7	(33) 158	(38) 204	(30) 383	(31) 767	(26) 1466	45	0.12N ^{1.0}

Notes
1 Configuration size does not capture static data present in libraries. Libraries are included but the size also includes any ancillary libraries for image processing (e.g. openCV) or numerical computation (e.g. blas).
2 Finalization is the processing of converting $N = 1600000$ templates into a searchable data structure an operation which can be a simple copy, or the building of an index or tree, for example. The duration of the operation may be data dependent, and may not be linear in the number of input templates.
3 This multiplier expresses the increase in template size when k images are passed to the template generation function.
4 All durations are measured on Intel®Xeon®CPU E5-2630 v4 @ 2.20GHz processors. Estimates are made by wrapping the API function call in calls to std::chrono::high_resolution_clock which on the machine in (3) counts 1ns clock ticks. Precision is somewhat worse than that however.
5 Search durations are measured as in the prior note. The power-law model in the final column mostly fits the empirical results in Figure 131. However in certain cases the model is not correct and should not be used numerically.

2022/02/23
14:06:29FNIR(N, R, T) = False neg. identification rate
FPIR(N, T) = False pos. identification rateN = Num. enrolled subjects
R = Num. candidates examined

T = Threshold

T = 0 → Investigation
T > 0 → Identification

	DEVELOPER	SHORT	SEQ.	VALIDATION	CONFIG ¹	LIB ¹	TEMPLATE GENERATION			FINALIZE ²	SEARCH DURATION ⁵ MILLISEC					
							SIZE (B)	MULT ³	TIME (MS) ⁴		TIME (S)	L=1	L=50	L=50	L=50	POWER LAW
FULL NAME	NAME	NUM.	DATE	DATA (MB)	DATA (MB)	N=1.6M	N=1.6M	N=1.6M	N=3M	N=6M	N=12M	(μs)				
209	Vocord	vocord	6	2018-10-30	1035	185	²¹² 10240	k	¹⁵⁹ 785	¹⁹ 243	⁽³⁴⁾ 170	⁽⁴⁰⁾ 216	-	-	-	
210	Xforward AI Technology	xforwardai	000	2020-07-24	236	171	¹²² 2048	-	¹⁴⁶ 753	¹⁰³ 13	⁽¹⁸³⁾ 4603	⁽²⁰³⁾ 7647	⁽¹⁷¹⁾ 15723	⁽¹⁶⁰⁾ 23900	⁽¹⁶²⁾ 53729	¹³⁹ 0.56N ^{1.1}
211	Xforward AI Technology	xforwardai	001	2021-01-21	332	50	¹¹¹ 2048	-	¹²⁰ 677	¹³² 16	⁽¹⁹³⁾ 5887	⁽¹⁸⁵⁾ 4384	⁽¹⁵⁸⁾ 8798	⁽¹⁵⁷⁾ 18553	⁽¹⁵⁷⁾ 48993	¹⁴⁴ 0.32N ^{1.1}
212	Xforward AI Technology	xforwardai	002	2021-05-24	691	50	¹⁸⁷ 4096	-	²⁰³ 930	¹³⁹ 18	⁽²⁰⁰⁾ 6957	⁽¹⁹⁸⁾ 6400	⁽¹⁶⁷⁾ 12659	⁽¹⁶⁷⁾ 31077	⁽¹⁶⁵⁾ 65158	¹⁴⁴ 0.52N ^{1.1}

Notes

- Configuration size does not capture static data present in libraries. Libraries are included but the size also includes any ancillary libraries for image processing (e.g. openCV) or numerical computation (e.g. blas).
- Finalization is the processing of converting N = 1600000 templates into a searchable data structure an operation which can be a simple copy, or the building of an index or tree, for example. The duration of the operation may be data dependent, and may not be linear in the number of input templates.
- This multiplier expresses the increase in template size when k images are passed to the template generation function.
- All durations are measured on Intel®Xeon®CPU E5-2630 v4 @ 2.20GHz processors. Estimates are made by wrapping the API function call in calls to std::chrono::high_resolution_clock which on the machine in (3) counts 1ns clock ticks. Precision is somewhat worse than that however.
- Search durations are measured as in the prior note. The power-law model in the final column mostly fits the empirical results in Figure 131. However in certain cases the model is not correct and should not be used numerically.

Table 6: Summary of algorithms and properties included in this report. The blue superscripts give ranking for the quantity in that column. Missing search durations, denoted by “-”, are absent because those runs were not executed, usually because we did not run on the larger galleries. Caution: The power-law model is sometimes an incorrect model. It is included here only to show broad sublinear behavior, which is flagged in green. The models should not be used for prediction.

#	ALGORITHM	INVESTIGATION, FNIR(N, R = 1, T = 0)								IDENTIFICATION, FNIR(N, R = L, T ≥ 0) FOR FPIR = 0.001								
		(0, 2]	(2, 4]	(4, 6]	(6, 8]	(8, 10]	(10, 12]	(12, 14]	(14, 18]	(0, 2]	(2, 4]	(4, 6]	(6, 8]	(8, 10]	(10, 12]	(12, 14]	(14, 18]	
1	3DIVI-005	⁹⁷ 0.0207	⁹⁷ 0.0304	⁹⁷ 0.0415	⁹⁷ 0.0533	⁹⁷ 0.0646	¹⁰⁸ 0.0735	¹⁰⁸ 0.0884	¹⁰⁶ 0.1148	¹⁰⁷ 0.1580	⁹⁸ 0.2316	⁹⁸ 0.3033	⁹⁸ 0.3740	⁹⁸ 0.4285	¹⁰⁸ 0.4742	¹⁰⁷ 0.5329	¹⁰⁸ 0.5975	
2	ANKE-000	⁹⁵ 0.0162	⁹⁵ 0.0245	⁹⁵ 0.0333	⁹⁵ 0.0428	⁹⁵ 0.0515	¹⁰³ 0.0615	¹⁰³ 0.0780	¹⁰² 0.1028	⁹⁶ 0.1132	⁹⁵ 0.1761	⁹⁶ 0.2402	⁹⁶ 0.3057	⁹⁵ 0.3640	¹⁰³ 0.4200	¹⁰³ 0.4928	¹⁰³ 0.5680	
3	ANKE-002	⁴⁷ 0.0055	⁵⁰ 0.0074	⁵⁰ 0.0090	⁴⁹ 0.0103	⁴⁸ 0.0116	⁵⁷ 0.0135	⁵⁶ 0.0162	⁵⁵ 0.0202	⁵⁴ 0.0329	⁵⁴ 0.0560	⁵⁶ 0.0843	⁵⁷ 0.1169	⁵⁷ 0.1481	⁶⁵ 0.1820	⁶⁵ 0.2280	⁶⁴ 0.2831	
4	AWARE-005	¹⁰⁶ 0.0328	¹⁰⁶ 0.0519	¹⁰⁶ 0.0712	¹⁰⁹ 0.0910	¹⁰⁴ 0.1078	¹¹² 0.1235	¹¹² 0.1457	¹¹² 0.1831	¹⁰⁸ 0.3605	¹⁰⁷ 0.4949	¹⁰⁷ 0.5948	¹⁰⁷ 0.6783	¹⁰⁸ 0.7393	¹¹⁶ 0.7905	¹¹⁶ 0.8408	¹¹⁷ 0.8831	
5	AWARE-006	¹¹⁰ 0.0702	¹¹¹ 0.1110	¹¹¹ 0.1502	¹¹⁸ 0.1899	¹¹⁹ 0.2253	¹²⁶ 0.2614	¹¹⁸ 0.3045	¹¹⁸ 0.3659									
6	AYONIX-002	¹¹³ 0.3360	¹¹⁴ 0.4389	¹¹⁴ 0.5144	¹¹⁴ 0.5814	¹¹⁴ 0.6340	¹²² 0.6818	¹²² 0.7297	¹²³ 0.7774	¹¹⁶ 0.8288	¹¹¹ 0.9013	¹¹¹ 0.9375	¹¹¹ 0.9603	¹¹¹ 0.9744	¹²⁰ 0.9837	¹²⁰ 0.9893	¹²⁰ 0.9927	
7	CAMVI-004	¹⁰⁹ 0.0623	¹⁰⁹ 0.0944	¹⁰⁸ 0.1243	¹⁰⁸ 0.1548	¹⁰⁸ 0.1812	¹¹⁶ 0.2056	¹¹⁶ 0.2344	¹¹⁴ 0.2672	⁹¹ 0.0810	⁹¹ 0.1267	⁸⁸ 0.1721	⁸⁸ 0.2203	⁸⁸ 0.2619	⁹⁴ 0.3040	⁹³ 0.3543	⁸⁹ 0.4124	
8	CAMVI-005	¹¹¹ 0.0849	¹¹¹ 0.1255	¹¹¹ 0.1631	¹¹¹ 0.1989	¹¹⁷ 0.2298	¹¹⁸ 0.2585	¹¹⁷ 0.2915	¹¹⁷ 0.3246									
9	CANON-001						¹⁹ 0.0052	¹⁸ 0.0057	¹⁴ 0.0042						²⁴ 0.0491	²⁴ 0.0606	²⁴ 0.0826	
10	CIB-000	¹⁴ 0.0022	¹⁴ 0.0030	¹⁵ 0.0037	¹⁵ 0.0044	¹⁷ 0.0049	²³ 0.0057	²³ 0.0069	²⁵ 0.0062	²⁵ 0.0139	²⁶ 0.0240	²⁷ 0.0373	²⁸ 0.0525	²⁸ 0.0689	³² 0.0859	³³ 0.1109	³³ 0.1454	
11	CLEARVIEWAI-000	⁷ 0.0017	⁴ 0.0023	⁴ 0.0028	⁹ 0.0034	¹¹ 0.0039	¹⁵ 0.0046	¹⁷ 0.0056	¹⁸ 0.0047	¹⁶ 0.0066	¹⁸ 0.0121	¹⁸ 0.0194	¹⁹ 0.0287	¹⁹ 0.0385	²⁵ 0.0493	²⁶ 0.0662	²⁶ 0.0873	
12	CLOUDWALK-HR-000	⁸ 0.0019	⁷ 0.0024	⁸ 0.0029	⁶ 0.0032	⁵ 0.0032	⁴ 0.0036	³ 0.0041	¹ 0.0020	¹ 0.0029	¹ 0.0041	¹ 0.0054	¹ 0.0064	² 0.0073	³ 0.0085	³ 0.0102	³ 0.0112	
13	COGENT-000	⁹ 0.0128	⁹ 0.0184	⁹⁵ 0.0250	⁹² 0.0327	⁹³ 0.0407	⁹⁸ 0.0488	⁹⁸ 0.0611	⁹⁷ 0.0794	⁷⁷ 0.0559	⁷⁸ 0.0923	⁷⁶ 0.1342	⁷⁸ 0.2243	⁸² 0.2675	⁸¹ 0.3240	⁸⁶ 0.3992		
14	COGENT-001	⁹ 0.0128	⁹ 0.0184	⁹² 0.0250	⁹³ 0.0327	⁹² 0.0407	¹⁰⁸ 0.0488	⁹⁹ 0.0611	⁹⁸ 0.0794	⁷⁸ 0.0559	⁷⁹ 0.0923	⁷⁷ 0.1342	⁷⁸ 0.2243	⁸³ 0.2675	⁸² 0.3240	⁸⁵ 0.3992		
15	COGENT-002	⁶ 0.0081	⁶ 0.0105	⁶³ 0.0123	⁶⁴ 0.0137	⁶² 0.0157	⁷⁰ 0.0175	⁶⁸ 0.0215	⁶⁹ 0.0280	⁶⁹ 0.0499	⁶⁸ 0.0827	⁶⁷ 0.1207	⁶⁷ 0.1639	⁶⁹ 0.2037	⁷⁴ 0.2432	⁷⁵ 0.2972	⁷⁶ 0.3638	
16	COGENT-003	⁷ 0.0082	⁶ 0.0108	⁶⁵ 0.0128	⁶⁷ 0.0145	⁶⁶ 0.0168	⁷⁶ 0.0191	⁷⁷ 0.0239	⁷⁴ 0.0312	⁸⁰ 0.0582	⁸⁰ 0.0971	⁸⁰ 0.1417	⁸⁰ 0.1918	⁸⁰ 0.2380	⁸⁹ 0.2836	⁹¹ 0.3440	⁹² 0.4207	
17	COGENT-004	⁵⁹ 0.0066	⁵³ 0.0080	⁴³ 0.0085	³⁹ 0.0080	³¹ 0.0083	³⁹ 0.092	⁴⁰ 0.0106	⁴³ 0.0130	⁶³ 0.0410	⁶⁵ 0.0720	⁶⁵ 0.1099	⁶⁵ 0.1539	⁶⁴ 0.1974	⁷³ 0.2443	⁷⁸ 0.3043	⁷⁸ 0.3757	
18	COGNITEC-000	¹⁰⁵ 0.0265	¹⁰³ 0.0423	¹⁰⁵ 0.0588	¹⁰⁵ 0.0757	¹⁰⁵ 0.0894	¹¹⁰ 0.1014	¹¹⁰ 0.1169	¹⁰⁹ 0.1381	¹⁰⁸ 0.1522	⁹⁹ 0.2330	⁹⁹ 0.3051	⁹⁹ 0.3751	⁹⁹ 0.4300	¹⁰⁷ 0.4779	¹⁰⁸ 0.5307	¹⁰⁹ 0.5913	
19	COGNITEC-001	⁹³ 0.0149	⁹⁴ 0.0228	⁹⁴ 0.0312	⁹⁴ 0.0399	⁹⁴ 0.0479	¹⁰² 0.0546	¹⁰¹ 0.0656	⁹⁹ 0.0806	⁹³ 0.0963	⁹³ 0.1562	⁹³ 0.2157	⁹³ 0.2771	⁹³ 0.3287	¹⁰¹ 0.3771	¹⁰¹ 0.4343	⁹⁹ 0.4959	
20	COGNITEC-002	⁷ 0.0101	⁸⁰ 0.0138	⁸¹ 0.0170	⁸¹ 0.0201	⁸¹ 0.0237	⁸⁸ 0.0264	⁸⁶ 0.0309	⁸⁸ 0.0389	⁷² 0.0517	⁷¹ 0.0879	⁷¹ 0.1269	⁷¹ 0.1707	⁷¹ 0.2098	⁷⁶ 0.2463	⁷⁴ 0.2919	⁷⁴ 0.3535	
21	COGNITEC-003	⁷⁸ 0.0104	⁸¹ 0.0140	⁸² 0.0174	⁸² 0.0205	⁸² 0.0238	⁸² 0.0266	⁸⁷ 0.0311	⁸⁷ 0.0401	⁷¹ 0.0504	⁷⁰ 0.0855	⁶⁹ 0.1235	⁶⁹ 0.1662	⁶⁸ 0.2045	⁷³ 0.2403	⁷³ 0.2854	⁷² 0.3451	
22	COGNITEC-004	⁶ 0.0073	⁶⁵ 0.0099	⁶² 0.0118	⁵⁹ 0.0130	⁵⁹ 0.0147	⁶⁹ 0.0163	⁶⁵ 0.0189	⁶⁵ 0.0239	⁵³ 0.0325	⁵³ 0.0548	⁵² 0.0798	⁵¹ 0.1074	⁵⁶ 0.1325	⁵⁹ 0.1591	⁵⁶ 0.1952	⁵⁵ 0.2414	
23	CUBOX-000	⁷ 0.0019	⁵ 0.0024	⁵ 0.0028	⁴ 0.0031	⁴ 0.0032	⁵ 0.0037	⁶ 0.0044	⁶ 0.0044	⁶ 0.0027	⁶ 0.0039	⁶ 0.0059	⁷ 0.0083	⁸ 0.0111	⁸ 0.0141	¹⁰ 0.0185	¹⁰ 0.0252	¹⁰ 0.0339
24	CYBERLINK-002	⁵ 0.0055	⁴⁸ 0.0068	⁴¹ 0.0075	³⁵ 0.0078	³² 0.0084	⁴⁰ 0.0094	⁴¹ 0.0107	³⁹ 0.0114	³² 0.0180	³³ 0.0302	³⁵ 0.0460	³⁴ 0.0643	³⁴ 0.0837	⁴¹ 0.1058	⁴⁰ 0.1370	⁴⁰ 0.1787	
25	CYBERLINK-003	³⁵ 0.0041	³⁴ 0.0052	²⁷ 0.0057	²⁵ 0.0058	²⁵ 0.0061	³² 0.0068	²⁹ 0.0078	³¹ 0.0078	¹⁹ 0.0109	¹⁹ 0.0175	²⁰ 0.0259	²¹ 0.0356	²¹ 0.0594	²⁷ 0.0787	²⁸ 0.1072		
26	DAHUA-002	³ 0.0035	²⁸ 0.0047	²⁸ 0.0058	²⁷ 0.0067	²⁸ 0.0074	³⁵ 0.0082	³⁰ 0.0100	³⁰ 0.0108	³⁰ 0.0169	³² 0.0294	³¹ 0.0449	³⁰ 0.0635	³⁰ 0.0817	³⁸ 0.1013	³⁷ 0.1291	³⁶ 0.1638	
27	DAHUA-003	¹⁹ 0.0026	¹⁹ 0.0036	¹⁹ 0.0043	²⁰ 0.0050	²⁰ 0.0055	²⁵ 0.0062	³¹ 0.0080	²⁶ 0.0073	²⁹ 0.0160	³⁰ 0.0280	²⁹ 0.0432	²⁹ 0.0615	²⁹ 0.0794	³⁶ 0.0987	³⁶ 0.1270	³⁴ 0.1587	
28	DEEPLIGHT-001	¹ 0.0024	¹⁶ 0.0032	¹⁴ 0.0037	¹³ 0.0040	¹³ 0.0043	¹⁸ 0.0049	¹⁹ 0.0060	¹⁹ 0.0052	¹² 0.0058	¹¹ 0.0087	¹¹ 0.0119	¹¹ 0.0155	¹¹ 0.0199	¹³ 0.0249	¹³ 0.0338	¹³ 0.0463	
29	DEEPSA-001	⁷⁰ 0.0081	⁷⁰ 0.0116	⁷³ 0.0149	⁷⁶ 0.0182	⁷⁶ 0.0216	⁸⁷ 0.0260	⁸⁹ 0.0332	⁸⁹ 0.0432	⁶⁶ 0.0458	⁶⁶ 0.0752	⁶⁴ 0.1086	⁶³ 0.1460	⁶³ 0.1812	⁷¹ 0.2186	⁷⁰ 0.3213		
30	DERMALOG-006	⁸ 0.0113	⁸² 0.0142	⁷⁸ 0.0163	⁷⁷ 0.0183	⁷⁴ 0.0200	⁸¹ 0.0218	⁷⁰ 0.0251	⁷⁵ 0.0354	⁷⁵ 0.0545	⁷³ 0.0889	⁷³ 0.1271	⁷² 0.2090	⁷⁸ 0.2498	⁷⁷ 0.3028	⁷⁷ 0.3670		
31	DERMALOG-007	⁸ 0.0125	⁸⁹ 0.0170	⁸⁸ 0.0214	⁸⁸ 0.0264	⁸⁷ 0.0309	⁹¹ 0.0356	⁹⁵ 0.0432	⁹⁵ 0.0579	⁹² 0.0910	⁹² 0.1453	⁹² 0.2009	⁹² 0.3134	⁹⁹ 0.3649	⁹⁹ 0.4289	¹⁰⁰ 0.5007		
32	DERMALOG-008	⁵² 0.0057	⁵² 0.0077	⁵⁴ 0.0095	⁵⁴ 0.0110	⁵³ 0.0128	⁶³ 0.0148	⁶² 0.0180	⁶³ 0.0223	⁷⁰ 0.0501	⁶⁹ 0.0850	⁷⁰ 0.1247	⁷¹ 0.1692	⁷² 0.2105	⁷⁹ 0.2541	⁷⁹ 0.3762		
33	GORILLA-002	¹⁰⁰ 0.0213	¹⁰⁰ 0.0359	¹⁰¹ 0.0528	¹⁰² 0.0716	¹⁰¹ 0.0895	¹¹¹ 0.1088	¹¹¹ 0.1367	¹¹¹ 0.1765	¹⁰³ 0.1828	¹⁰⁴ 0.2787	¹⁰⁴ 0.3654	¹⁰⁴ 0.4485	¹⁰⁴ 0.5168	¹¹⁰ 0.5823	¹¹⁰ 0.6508	¹¹⁰ 0.7180	
34	GORILLA-005	³⁸ 0.0044	⁴⁷ 0.0070	⁵⁸ 0.0102	⁶² 0.0136	⁶⁷ 0.0170	⁷⁹ 0.0204	⁸² 0.0272	⁸⁴ 0.0373	⁷⁹ 0.0566	⁸¹ 0.0973	⁸² 0.1432	⁸¹ 0.1937	⁸¹ 0.2398	⁹¹ 0.2862	⁹⁰ 0.3437	⁹⁰ 0.4150	
35	IDEORIA-003	⁸ 0.0110	⁸⁶ 0.0151	⁸⁶ 0.0196	⁸⁵ 0.0238	⁸⁴ 0.0281	⁹² 0.0313	⁹² 0.0368	⁹² 0.0504	⁸⁷ 0.0717	⁸⁶ 0.1147	⁸⁶ 0.161						

MISS RATES		INVESTIGATION, FNIR(N, R = 1, T = 0)								IDENTIFICATION, FNIR(N, R = L, T ≥ 0) FOR FPIR = 0.001							
#	ALGORITHM	(0, 2]	(2, 4]	(4, 6]	(6, 8]	(8, 10]	(10, 12]	(12, 14]	(14, 18]	(0, 2]	(2, 4]	(4, 6]	(6, 8]	(8, 10]	(10, 12]	(12, 14]	(14, 18]
45	INNOVATRICS-004	¹¹⁴ 0.3594	¹¹³ 0.3629	¹¹⁵ 0.3688	¹¹⁵ 0.3754	¹¹⁵ 0.3813	¹²⁰ 0.3870	¹²⁰ 0.3960	¹²⁰ 0.4135	¹⁰⁵ 0.4234	¹⁰⁶ 0.4642	¹⁰⁶ 0.5073	¹⁰⁶ 0.5522	¹⁰⁵ 0.5902	¹¹³ 0.6274	¹¹¹ 0.6736	¹¹¹ 0.7253
46	INNOVATRICS-005	⁴¹ 0.0046	⁴¹ 0.0063	⁴² 0.0078	⁴⁵ 0.0092	⁴⁵ 0.0106	⁵¹ 0.0124	⁵¹ 0.0149	⁵¹ 0.0178	³⁵ 0.0343	³⁶ 0.0590	³⁸ 0.0886	³⁸ 0.1222	⁵⁹ 0.1544	⁶⁸ 0.1881	⁶⁷ 0.2321	⁶⁵ 0.2874
47	IREX-000	²⁴ 0.0031	²⁴ 0.0042	²⁵ 0.0051	²⁶ 0.0060	³⁶ 0.0068	³⁴ 0.0080	³⁵ 0.0095	³⁶ 0.0107	⁵² 0.0313	⁵² 0.0539	³⁵ 0.0815	³⁶ 0.1137	⁵¹ 0.1442	⁶³ 0.1755	⁶⁴ 0.2181	⁶¹ 0.2718
48	ISYSTEMS-002	⁷⁶ 0.0101	⁷⁹ 0.0135	⁸⁰ 0.0169	⁷⁹ 0.0197	⁸⁰ 0.0228	⁸⁵ 0.0256	⁸⁵ 0.0304	⁸⁶ 0.0398	⁹⁰ 0.0779	⁹⁸ 0.1258	⁹¹ 0.1759	⁹⁰ 0.2299	⁹⁰ 0.2758	⁹⁷ 0.3204	⁹⁷ 0.3763	⁹⁵ 0.4401
49	ISYSTEMS-003	⁷⁵ 0.0089	⁶⁹ 0.0115	⁶⁹ 0.0139	⁶⁹ 0.0158	⁷⁰ 0.0177	⁷⁸ 0.0198	⁷⁴ 0.0234	⁷¹ 0.0303	⁸⁴ 0.0647	⁸⁴ 0.1056	⁸⁴ 0.1502	⁸¹ 0.1986	⁸¹ 0.2402	⁸⁷ 0.2819	⁸⁶ 0.3351	⁸⁴ 0.3976
50	KEDACOM-001	⁸³ 0.0116	⁷⁵ 0.0130	⁶² 0.0135	⁶⁰ 0.0133	⁵⁷ 0.0135	⁵⁸ 0.0141	⁵² 0.0151	⁴⁹ 0.0176	⁴¹ 0.0241	⁴¹ 0.0360	³⁹ 0.0513	³⁴ 0.0689	³⁴ 0.0866	⁴² 0.1060	³⁸ 0.1327	³⁸ 0.1694
51	LOOKMAN-003	⁸⁸ 0.0123	⁸³ 0.0144	⁷⁷ 0.0158	⁷⁰ 0.0168	⁷¹ 0.0178	⁷⁴ 0.0188	⁶⁷ 0.0212	⁶⁷ 0.0260	⁶⁴ 0.0438	⁶² 0.0687	⁶¹ 0.0978	⁶¹ 0.1296	⁶⁷ 0.1581	⁶⁷ 0.1879	⁶⁶ 0.2294	⁶³ 0.2756
52	LOOKMAN-005	⁸⁵ 0.0118	⁷⁷ 0.0134	⁷⁰ 0.0142	⁶⁶ 0.0144	⁶¹ 0.0150	⁶⁸ 0.0160	⁶⁰ 0.0176	⁵⁸ 0.0213	⁵¹ 0.0310	⁴⁹ 0.0480	⁴⁶ 0.0698	⁴⁶ 0.0954	⁴⁶ 0.1216	⁵⁴ 0.1491	⁵⁴ 0.1890	⁵⁴ 0.2381
53	MICROFOCUS-005	¹¹⁵ 0.4269	¹¹⁵ 0.5527	¹¹⁵ 0.6355	¹¹⁵ 0.7024	¹¹⁵ 0.7503	¹²⁴ 0.7876	¹²⁴ 0.8234	¹²⁵ 0.8601	¹¹¹ 0.8338	¹¹² 0.9113	¹¹² 0.9468	¹¹² 0.9667	¹¹² 0.9771	¹¹⁵ 0.9836	¹¹⁵ 0.9880	¹¹⁵ 0.9924
54	MICROSOFT-003	²⁸ 0.0034	³² 0.0050	³³ 0.0064	³⁶ 0.0078	³⁸ 0.0092	⁴⁶ 0.0107	⁴⁷ 0.0135	⁴⁸ 0.0166	⁵⁰ 0.0288	⁵⁰ 0.0503	⁵⁰ 0.0763	⁵⁰ 0.1067	⁵¹ 0.1359	⁶¹ 0.1680	⁶⁰ 0.2116	⁵⁸ 0.2644
55	MICROSOFT-004	²⁵ 0.0032	²⁷ 0.0047	²⁹ 0.0060	³² 0.0075	³⁵ 0.0087	⁴³ 0.0103	⁴⁶ 0.0131	⁴⁶ 0.0159	⁴⁷ 0.0268	⁴⁸ 0.0470	⁴⁷ 0.0716	⁴⁸ 0.1007	⁴⁸ 0.1291	⁶⁰ 0.1610	⁵⁸ 0.2052	⁵⁷ 0.2590
56	MICROSOFT-005	²² 0.0031	²⁹ 0.0047	³⁸ 0.0066	⁴³ 0.0084	⁴³ 0.0103	⁵⁵ 0.0131	⁵⁷ 0.0164	⁵³ 0.0185	⁴³ 0.0243	⁴⁴ 0.0432	⁴⁴ 0.0658	⁴⁴ 0.0913	⁴¹ 0.1172	⁵¹ 0.1476	⁵³ 0.1874	⁵¹ 0.2272
57	MICROSOFT-006	²⁶ 0.0032	³¹ 0.0049	³⁴ 0.0065	⁴² 0.0081	⁴² 0.0096	⁵⁰ 0.0117	⁴⁹ 0.0144	⁴⁷ 0.0160	²⁴ 0.0134	²⁴ 0.0233	²⁵ 0.0346	²³ 0.0462	²³ 0.0578	²⁹ 0.0713	²⁹ 0.0903	²⁹ 0.1156
58	NEC-000	⁹ 0.0195	⁹⁹ 0.0316	⁹⁹ 0.0445	⁹⁹ 0.0581	⁹⁸ 0.0699	¹⁰² 0.0817	¹⁰⁷ 0.0998	¹⁰⁷ 0.1237	⁸⁹ 0.0759	⁸⁹ 0.1245	⁸⁹ 0.1729	⁸⁹ 0.2240	⁸⁹ 0.2671	⁹⁹ 0.3117	⁹⁴ 0.3639	⁹⁴ 0.4348
59	NEC-001	¹⁰⁴ 0.0246	¹⁰² 0.0382	¹⁰³ 0.0524	¹⁰⁷ 0.0672	¹⁰¹ 0.0793	¹⁰⁸ 0.0904	¹⁰⁸ 0.1076	¹⁰⁸ 0.1317	⁹⁴ 0.1019	⁹⁴ 0.1623	⁹⁴ 0.2214	⁹⁴ 0.2834	⁹⁴ 0.3341	¹⁰² 0.3844	¹⁰⁴ 0.4440	¹⁰¹ 0.5183
60	NEC-002	²⁹ 0.0033	²² 0.0041	¹⁸ 0.0043	¹⁶ 0.0044	¹⁵ 0.0045	¹⁷ 0.0049	¹⁶ 0.0056	¹⁵ 0.0041	¹⁵ 0.0066	¹¹ 0.0090	¹⁰ 0.0111	¹⁰ 0.0131	⁹ 0.0149	⁸ 0.0171	⁹ 0.0207	⁹ 0.0267
61	NEC-003	³¹ 0.0036	²⁶ 0.0046	²⁴ 0.0051	²⁴ 0.0055	²⁴ 0.0059	²⁷ 0.0067	²⁷ 0.0077	²⁹ 0.0073	⁹ 0.0056	⁹ 0.0076	⁹ 0.0091	⁷ 0.0105	⁶ 0.0119	⁷ 0.0137	⁶ 0.0162	⁶ 0.0209
62	NEC-004	³⁰ 0.0039	²⁵ 0.0045	²² 0.0047	¹⁸ 0.0046	¹⁴ 0.0044	¹⁶ 0.0046	¹⁵ 0.0052	¹² 0.0036	⁷ 0.0046	⁵ 0.0057	⁵ 0.0063	⁵ 0.0066	¹⁰ 0.0069	¹⁰ 0.0076	¹⁰ 0.0090	¹⁰ 0.0105
63	NEC-005								⁶ 0.0037	² 0.0041	² 0.0020				² 0.0080	² 0.0091	² 0.0107
64	NEUROTECHNOLOGY-003	¹⁰¹ 0.0234	¹⁰¹ 0.0379	¹⁰² 0.0549	¹⁰¹ 0.0682	¹⁰⁰ 0.0720	¹⁰⁶ 0.0747	¹⁰⁶ 0.0886	¹⁰⁴ 0.1066	¹⁰⁸ 0.6802	¹⁰⁹ 0.8187	¹¹⁰ 0.8920	¹¹⁰ 0.9355	¹¹⁰ 0.9738	¹¹⁸ 0.9826	¹¹⁸ 0.9885	
65	NEUROTECHNOLOGY-004	⁷⁹ 0.0104	⁷⁸ 0.0134	⁷⁶ 0.0156	⁷³ 0.0173	⁷² 0.0195	⁸⁰ 0.0212	⁷⁸ 0.0245	⁷⁵ 0.0320	⁸³ 0.0642	⁸² 0.1015	⁸¹ 0.1426	⁷⁸ 0.1881	⁸⁸ 0.2299	⁸⁸ 0.2722	⁸⁴ 0.3269	⁸³ 0.3943
66	NEUROTECHNOLOGY-005	⁷⁷ 0.0089	⁷¹ 0.0116	⁶⁸ 0.0136	⁶⁸ 0.0152	⁶⁹ 0.0173	⁷⁷ 0.0196	⁷³ 0.0233	⁷⁰ 0.0306	⁷⁶ 0.0556	⁷⁶ 0.0913	⁷⁴ 0.1315	⁷¹ 0.1766	⁷¹ 0.2192	⁸¹ 0.2617	⁸⁰ 0.3174	⁸⁰ 0.3843
67	NEUROTECHNOLOGY-007	⁶⁶ 0.0078	⁶⁹ 0.0103	⁶⁴ 0.0124	⁶³ 0.0140	⁶³ 0.0161	⁷¹ 0.0185	⁷⁰ 0.0225	⁶⁹ 0.0290	⁸² 0.0641	⁸⁵ 0.1069	⁸⁵ 0.1546	⁸⁸ 0.2075	⁸⁸ 0.2572	⁹³ 0.3081	⁹⁶ 0.3713	⁹⁶ 0.4421
68	NEUROTECHNOLOGY-010								²⁰ 0.0053	²⁰ 0.0061	²¹ 0.0053				³¹ 0.0863	³¹ 0.1050	³¹ 0.1333
69	NOBLIS-002	¹¹² 0.1520	¹¹² 0.2419	¹¹² 0.3296	¹¹³ 0.4114	¹¹² 0.4856	¹²¹ 0.5528	¹²¹ 0.6061	¹²¹ 0.6532	¹¹³ 0.9984	¹¹³ 0.9996	¹¹³ 0.9998	¹¹³ 0.9999	¹²¹ 1.0000	¹²² 1.0000		
70	NTECHLAB-003	⁶⁵ 0.0078	⁷⁶ 0.0131	⁸⁷ 0.0202	⁹⁰ 0.0295	⁹¹ 0.0405	¹⁰¹ 0.0543	¹⁰² 0.0761	¹⁰³ 0.1035	⁶⁸ 0.0491	⁷² 0.0881	⁷⁹ 0.1384	⁸³ 0.1985	⁸⁷ 0.2594	⁹⁸ 0.3270	⁹⁸ 0.4065	⁹⁸ 0.4891
71	NTECHLAB-004	⁶⁷ 0.0068	⁶⁸ 0.0110	⁷⁹ 0.0167	⁸⁶ 0.0239	⁸⁹ 0.0330	⁹⁸ 0.0447	¹⁰⁰ 0.0641	¹⁰¹ 0.0891	⁶⁰ 0.0379	⁶³ 0.0688	⁶⁹ 0.1108	⁶⁹ 0.1629	⁷⁷ 0.2192	⁹⁶ 0.2846	⁹⁵ 0.3657	⁹⁷ 0.4524
72	NTECHLAB-006	⁵¹ 0.0056	⁶² 0.0095	⁷² 0.0148	⁸³ 0.0218	⁸⁵ 0.0301	⁹⁶ 0.0413	⁹⁷ 0.0741	¹⁰⁰ 0.0814	⁵⁶ 0.0349	⁶⁰ 0.0636	⁶³ 0.1023	⁶⁴ 0.1506	⁶⁶ 0.2024	⁸⁰ 0.2617	⁸⁷ 0.3374	⁹¹ 0.4185
73	NTECHLAB-007	³⁷ 0.0044	⁴³ 0.0066	⁴⁹ 0.0089	⁵⁷ 0.0118	⁶⁰ 0.0150	⁷⁵ 0.0189	⁸⁰ 0.0255	⁸⁰ 0.0342	⁴⁵ 0.0256	⁴⁶ 0.0450	⁴⁸ 0.0705	⁴⁹ 0.1012	⁵¹ 0.1334	⁶² 0.1692	⁶¹ 0.2170	⁶² 0.2752
74	NTECHLAB-008	¹⁸ 0.0025	²¹ 0.0038	²⁶ 0.0052	³¹ 0.0074	⁴⁴ 0.0104	⁶⁰ 0.0146	⁷⁶ 0.0236	⁸¹ 0.0348	²⁶ 0.0143	²⁸ 0.0267	³² 0.0459	³⁷ 0.0733	⁴¹ 0.1062	⁵⁰ 0.1469	⁵⁷ 0.2044	⁵⁹ 0.2698
75	NTECHLAB-009	¹⁵ 0.0022	¹⁵ 0.0031	¹⁶ 0.0038	¹⁷ 0.0045	¹⁹ 0.0055	²⁹ 0.0067	³³ 0.0088	³⁰ 0.0100	¹⁸ 0.0073	¹⁷ 0.0117	¹⁷ 0.0170	¹⁷ 0.0238	¹⁸ 0.0319	²² 0.0419	²⁵ 0.0577	²⁵ 0.0833
76	NTECHLAB-011								²² 0.0056	²¹ 0.0066	²⁰ 0.0073				¹⁷ 0.0351	¹⁷ 0.0475	²¹ 0.0724
77	PARAVISION-002	⁵³ 0.0058	⁵⁸ 0.0083	⁶⁰ 0.0111	⁶³ 0.0137	⁶⁵ 0.0162	⁷³ 0.0187	⁷² 0.0229	⁷⁰ 0.0295								
78	PARAVISION-003	⁴¹ 0.0048	⁴⁴ 0.0067	⁵¹ 0.0090	⁵² 0.0109	⁵⁴ 0.0128	⁶¹ 0.0148	⁶¹ 0.0178	⁵⁹ 0.0219	⁵⁷ 0.0354	⁵⁸ 0.0618	⁵⁹ 0.0931	⁶⁰ 0.1290	⁶¹ 0.1625	⁶⁹ 0.1964	⁶⁹ 0.2408	⁶⁶ 0.2924
79	PARAVISION-004	¹⁶ 0.0024	¹⁷ 0.0032	¹⁷ 0.0040	¹⁹ 0.0047	¹⁸ 0.0053	²⁴ 0.0061	²⁵ 0.0073	²³ 0.0072	²⁰ 0.0118	²³ 0.0209	²⁴ 0.0327	²⁴ 0.0465	²⁴ 0.0613	³⁰ 0.0779	^{30</}	

MISS RATES		INVESTIGATION, FNIR(N, R = 1, T = 0)								IDENTIFICATION, FNIR(N, R = L, T ≥ 0) FOR FPIR = 0.001							
#	ALGORITHM	(0, 2]	(2, 4]	(4, 6]	(6, 8]	(8, 10]	(10, 12]	(12, 14]	(14, 18]	(0, 2]	(2, 4]	(4, 6]	(6, 8]	(8, 10]	(10, 12]	(12, 14]	(14, 18]
89	RANKONE-005	⁹² 0.0136	⁹³ 0.0192	⁹¹ 0.0246	⁹¹ 0.0303	⁹⁴ 0.0362	⁹⁷ 0.0422	⁹⁶ 0.0521	⁹⁶ 0.0694	⁸¹ 0.0582	⁷⁵ 0.0910	⁷¹ 0.1260	⁶⁸ 0.1645	⁶⁵ 0.2005	⁷² 0.2353	⁷² 0.2816	⁷³ 0.3522
90	RANKONE-007	⁶⁷ 0.0078	⁶⁹ 0.0099	⁶¹ 0.0113	⁵⁸ 0.0123	⁵⁸ 0.0139	⁶⁷ 0.0156	⁶⁶ 0.0191	⁶⁵ 0.0242	⁴² 0.0242	⁴² 0.0376	⁴¹ 0.0542	³⁸ 0.0737	³⁷ 0.0935	⁴¹ 0.1130	⁴⁵ 0.1416	⁴² 0.1811
91	RANKONE-009	⁴⁸ 0.0054	⁴⁹ 0.0072	⁴⁶ 0.0085	⁴⁷ 0.0098	⁴⁷ 0.0113	⁵³ 0.0130	⁵⁸ 0.0169	⁶² 0.0220	³⁷ 0.0208	³⁸ 0.0345	³⁷ 0.0504	³⁶ 0.0706	³⁶ 0.0930	⁴⁵ 0.1174	⁴⁶ 0.1504	⁴⁵ 0.2002
92	RANKONE-010	⁴² 0.0047	³⁹ 0.0061	³⁶ 0.0070	³³ 0.0076	³⁴ 0.0087	⁴² 0.0098	⁴³ 0.0113	⁴¹ 0.0120	³¹ 0.0177	²⁹ 0.0269	²⁶ 0.0368	²⁶ 0.0479	²⁷ 0.0590	²⁸ 0.0688	²⁸ 0.0803	²⁷ 0.0991
93	RANKONE-011	²³ 0.0031	²³ 0.0041	²³ 0.0047	²³ 0.0053	²² 0.0058	³⁰ 0.0067	²⁶ 0.0077	²⁸ 0.0073	²³ 0.0127	²⁰ 0.0194	²¹ 0.0265	²⁰ 0.0345	²⁰ 0.0422	²⁶ 0.0499	²⁹ 0.0611	²³ 0.0756
94	RANKONE-012						²⁶ 0.0065	²⁴ 0.0069	²⁰ 0.0053						²⁹ 0.0460	²¹ 0.0540	¹⁸ 0.0672
95	REALNETWORKS-002	¹⁰⁷ 0.0381	¹⁰⁸ 0.0687	¹⁰⁸ 0.1062	¹⁰⁸ 0.1495	¹⁰⁷ 0.1963	¹¹⁷ 0.2513	¹¹⁹ 0.3206	¹¹⁹ 0.3927	¹⁰⁵ 0.2153	¹⁰⁵ 0.3323	¹⁰⁵ 0.4444	¹⁰⁵ 0.5485	¹⁰⁶ 0.6355	¹¹⁴ 0.7132	¹¹⁵ 0.7855	¹¹⁵ 0.8437
96	REALNETWORKS-003	¹⁰³ 0.0245	¹⁰⁵ 0.0437	¹⁰⁵ 0.0686	¹⁰⁵ 0.0975	¹⁰⁶ 0.1312	¹¹⁵ 0.1719	¹¹⁵ 0.2294	¹¹⁶ 0.2907	⁹⁸ 0.1468	¹⁰³ 0.2370	¹⁰¹ 0.3313	¹⁰² 0.4269	¹⁰³ 0.5142	¹¹² 0.5979	¹¹³ 0.6815	¹¹³ 0.7567
97	REALNETWORKS-004	¹⁰² 0.0244	¹⁰⁴ 0.0428	¹⁰⁴ 0.0663	¹⁰⁵ 0.0939	¹⁰⁵ 0.1251	¹¹⁴ 0.1634	¹¹⁴ 0.2170	¹¹⁵ 0.2785	⁹⁹ 0.1484	¹⁰¹ 0.2377	¹⁰⁰ 0.3303	¹⁰² 0.4249	¹⁰² 0.5106	¹¹¹ 0.5924	¹¹² 0.6758	¹¹¹ 0.7534
98	REALNETWORKS-006						³³ 0.0069	²⁸ 0.0077	³² 0.0080						³⁹ 0.1022	³⁵ 0.1253	³⁵ 0.1622
99	SCANOVATE-001	⁶⁸ 0.0079	⁷² 0.0117	⁷⁸ 0.0151	⁷⁸ 0.0185	⁷⁸ 0.0221	⁸⁶ 0.0259	⁸⁸ 0.0321	⁸⁸ 0.0427	⁸⁸ 0.0727	⁸⁸ 0.1169	⁸⁷ 0.1650	⁸⁷ 0.2115	⁸⁴ 0.2528	⁹² 0.2925	⁸⁹ 0.3437	⁸⁸ 0.4084
100	SENSETIME-002	⁹⁶ 0.0186	⁹² 0.0191	⁸⁴ 0.0183	⁷³ 0.0179	⁶⁸ 0.0173	⁵⁶ 0.0133	³⁴ 0.0089	²² 0.0059	⁴⁰ 0.0220	²⁵ 0.0236	¹⁹ 0.0237	¹⁸ 0.0240	¹² 0.0245	¹¹ 0.0219	⁸ 0.0195	⁷ 0.0222
101	SENSETIME-003	¹¹ 0.0021	¹² 0.0028	¹¹ 0.0031	⁶ 0.0035	⁸ 0.0040	¹⁰ 0.0047	⁹ 0.0033	⁸ 0.0046	⁸ 0.0064	⁶ 0.0076	⁸ 0.0086	⁴ 0.0101	⁴ 0.0122	⁵ 0.0155	⁵ 0.0196	
102	SENSETIME-004	³ 0.0016	³ 0.0022	³ 0.0025	³ 0.0028	³ 0.0030	³ 0.0035	⁵ 0.0043	⁴ 0.0025	⁴ 0.0036	⁴ 0.0052	³ 0.0066	³ 0.0081	³ 0.0099	⁶ 0.0126	⁷ 0.0169	⁸ 0.0230
103	SENSETIME-005	⁰ 0.0015	⁰ 0.0020	⁰ 0.0024	² 0.0026	² 0.0029	² 0.0035	⁴ 0.0043	⁰ 0.0028	⁵ 0.0036	⁷ 0.0059	⁷ 0.0089	⁷ 0.0128	¹⁰ 0.0177	¹² 0.0240	¹⁴ 0.0345	¹⁴ 0.0493
104	SENSETIME-006	¹ 0.0015	¹ 0.0019	¹ 0.0022	¹ 0.0025	¹ 0.0027	¹ 0.0033	¹ 0.0040	¹ 0.0021	² 0.0031	² 0.0049	⁴ 0.0068	⁶ 0.0097	⁷ 0.0132	⁹ 0.0184	¹¹ 0.0262	¹¹ 0.0359
105	SIAT-002	¹¹⁷ 0.8309	¹¹⁷ 0.8310	¹¹⁷ 0.8311	¹¹⁷ 0.8306	¹¹⁷ 0.8296	¹²⁵ 0.8302	¹²⁵ 0.8300	¹²⁴ 0.8301	¹¹² 0.8340	¹¹⁶ 0.8368	¹⁰⁵ 0.8404	¹⁰⁹ 0.8445	¹⁰⁹ 0.8480	¹¹⁷ 0.8532	¹¹⁷ 0.8595	¹¹⁸ 0.8691
106	SYNESIS-003	⁸⁹ 0.0125	⁸⁵ 0.0151	⁸⁰ 0.0174	⁸⁰ 0.0199	⁷⁹ 0.0223	⁸³ 0.0240	⁸³ 0.0279	⁷⁸ 0.0331	⁸⁵ 0.0658	⁸³ 0.1052	⁸³ 0.1483	⁸² 0.1968	⁸² 0.2399	⁸⁸ 0.2834	⁸⁸ 0.3405	⁸⁷ 0.4046
107	SYNESIS-005	⁴⁰ 0.0044	³⁷ 0.0058	³⁷ 0.0070	⁴⁶ 0.0080	³⁷ 0.0091	⁴⁴ 0.0103	⁴⁴ 0.0125	⁴⁵ 0.0152	⁴⁶ 0.0262	⁴⁵ 0.0444	⁴⁵ 0.0666	⁴⁵ 0.0923	⁴¹ 0.1156	⁴⁹ 0.1399	⁴⁸ 0.2185	
108	TECH5-001	³⁷ 0.0061	⁶¹ 0.0093	⁶⁰ 0.0128	⁷¹ 0.0171	⁷⁷ 0.0221	⁹⁰ 0.0289	⁹³ 0.0412	⁹³ 0.0560	⁸⁶ 0.0660	⁸⁷ 0.1156	⁹¹ 0.1733	⁹¹ 0.2385	⁹¹ 0.2998	⁹² 0.3629	¹⁰¹ 0.4424	¹⁰² 0.5284
109	TOSHIBA-001	⁷³ 0.0086	⁷² 0.0119	⁷¹ 0.0150	⁷⁴ 0.0178	⁷⁵ 0.0209	⁸⁴ 0.0241	⁸⁴ 0.0292	⁸³ 0.0365								
110	TRUEFACE-000	³⁶ 0.0043	³⁶ 0.0057	³⁰ 0.0061	²⁹ 0.0067	²⁷ 0.0073	³⁶ 0.0084	³⁶ 0.0097	³⁴ 0.0099	³⁵ 0.0200	³⁷ 0.0338	³⁸ 0.0504	³⁵ 0.0705	³⁸ 0.0904	⁴³ 0.1112	⁴¹ 0.1401	⁴¹ 0.1792
111	VERIDAS-001	⁵⁸ 0.0063	⁵⁶ 0.0083	⁵⁶ 0.0099	⁵⁶ 0.0113	⁵⁶ 0.0132	⁶² 0.0148	⁶³ 0.0184	⁶⁰ 0.0219	⁶¹ 0.0403	⁶¹ 0.0684	⁶² 0.1012	⁶² 0.1386	⁶² 0.1741	⁷⁰ 0.2113	⁷⁰ 0.2611	⁷¹ 0.3233
112	VISIONLABS-004	⁴⁵ 0.0048	⁴⁶ 0.0069	⁵² 0.0091	⁵¹ 0.0111	⁵⁵ 0.0130	⁶⁵ 0.0152	⁶⁴ 0.0187	⁶⁶ 0.0242	⁷⁴ 0.0540	⁷⁷ 0.0916	⁷⁸ 0.1855	⁷⁸ 0.2303	⁸⁰ 0.2745	⁸⁰ 0.3312	⁸¹ 0.3913	
113	VISIONLABS-005	³⁹ 0.0044	³⁹ 0.0063	⁴³ 0.0081	⁴⁶ 0.0095	⁴⁶ 0.0109	⁵² 0.0125	⁵³ 0.0151	⁵⁴ 0.0187	⁶⁷ 0.0479	⁶⁸ 0.0812	⁶⁸ 0.1212	⁷⁰ 0.1664	⁶⁹ 0.2078	⁷⁷ 0.2473	⁷⁶ 0.2999	⁷⁵ 0.3577
114	VISIONLABS-006	²⁰ 0.0035	³⁰ 0.0048	³⁰ 0.0061	³⁶ 0.0069	²⁹ 0.0077	³⁷ 0.0087	³⁹ 0.0105	⁴² 0.0120	⁴⁸ 0.0273	⁴⁷ 0.0465	⁴⁷ 0.0702	⁴⁷ 0.0970	⁴⁷ 0.1228	⁵⁰ 0.1486	⁵² 0.1847	⁵² 0.2295
115	VISIONLABS-008	²¹ 0.0028	²⁰ 0.0037	²¹ 0.0047	²² 0.0053	²³ 0.0058	²⁸ 0.0067	³² 0.0081	³³ 0.0085	²⁷ 0.0143	²⁷ 0.0241	²⁸ 0.0373	²⁷ 0.0519	³¹ 0.0677	³² 0.0850	³² 0.1104	³² 0.1444
116	VISIONLABS-009	¹⁰ 0.0020	¹⁰ 0.0026	¹⁰ 0.0030	¹⁰ 0.0034	¹³ 0.0044	¹⁴ 0.0052	¹⁶ 0.0046	¹⁴ 0.0065	¹⁵ 0.0105	¹⁵ 0.0156	¹⁵ 0.0217	¹⁶ 0.0289	²⁰ 0.0368	¹⁹ 0.0499	¹⁹ 0.0681	
117	VISIONLABS-010	⁹ 0.0020	⁹ 0.0025	⁹ 0.0030	¹¹ 0.0034	⁹ 0.0036	¹² 0.0043	¹² 0.0051	¹⁷ 0.0047	¹⁷ 0.0069	¹⁶ 0.0113	¹⁶ 0.0170	¹⁶ 0.0238	¹⁷ 0.0316	²¹ 0.0411	²² 0.0557	²² 0.0740
118	VISIONLABS-011						¹⁰ 0.0042	⁸ 0.0046	¹¹ 0.0036					¹⁴ 0.0270	¹² 0.0337	¹² 0.0432	
119	VTS-000	¹¹⁶ 0.5878	¹¹⁶ 0.6312	¹¹⁶ 0.6602	¹¹⁵ 0.6863	¹¹⁵ 0.7073	¹²³ 0.7246	¹²³ 0.7458	¹²² 0.7747	¹⁰⁸ 0.5929	¹⁰⁸ 0.6397	¹⁰⁸ 0.6729	¹⁰⁸ 0.7034	¹⁰⁷ 0.7279	¹¹⁵ 0.7493	¹¹⁴ 0.7739	¹¹⁴ 0.8076
120	XFORWARDAI-000	²⁰ 0.0027	¹⁸ 0.0034	²¹ 0.0044	²¹ 0.0052	²¹ 0.0058	³¹ 0.0067	³⁰ 0.0079	³⁰ 0.0076	²⁸ 0.0157	³¹ 0.0281	³⁰ 0.0443	³¹ 0.0635	³² 0.0834	⁴⁰ 0.1050	³⁹ 0.1330	³⁹ 0.1714
121	XFORWARDAI-001	¹⁵ 0.0023	¹⁴ 0.0028	¹² 0.0034	¹² 0.0037	¹² 0.0039	¹⁴ 0.0045	¹³ 0.0052	¹⁵ 0.0043	¹³ 0.0060	¹⁴ 0.0096	¹³ 0.0144	¹² 0.0200	¹³ 0.0260	¹⁰ 0.0334	¹⁶ 0.0435	¹⁶ 0.0586
122	YITU-002	⁶⁰ 0.0066	⁵⁷ 0.0083	⁵³ 0.0094	⁴⁸ 0.0101	⁵⁰ 0.0121	⁶⁴ 0.0150	⁶⁹ 0.0223	⁷⁶ 0.0328	³³ 0.0189	³⁴ 0.0317	³⁵ 0.0494	³⁹ 0.0750	⁴¹ 0.1066	⁵³ 0.1494	⁶² 0.2171	⁶⁸ 0.2958
123	YITU-003	⁶⁵ 0.0072	⁶⁹ 0.0089	⁵⁹ 0.0100	⁵¹ 0.0107	⁵² 0.0125	⁶⁶ 0.0153	⁷¹ 0.0226	⁷⁹ 0.0334	³⁴ 0.0194	³⁵ 0.0321	³⁶ 0.0500	⁴¹ 0.0756	⁴² 0.1071	⁵⁰ 0.1500	⁶³ 0.2177	⁶⁹ 0.2964
124	YITU-004	⁵⁵ 0.0061	⁵¹ 0														

#	ALGORITHM	INVESTIGATION MODE						IDENTIFICATION MODE						FAILURE TO EXTRACT FEATURES																					
		RANK ONE MISS RATE, FNIR(N, 0, 1)						HIGH T → FPIR = 0.001, FNIR(N, T, L)						N=1.6M																					
		GALLERY		MUGSHOT	MUGSHOT	MUGSHOT	VISA	BORDER	BOR _L 10YR	KIOSK	MUGSHOT	MUGSHOT	MUGSHOT	VISA	BORDER	BOR _L 10YR	KIOSK	MUGSHOT	MUGSHOT	MUGSHOT	VISA	BORDER	BOR _L 10YR	KIOSK											
1	20FACE-000	239	0.055	239	0.085	140	0.736	167	0.056	90	0.239	159	0.243	233	0.348	231	0.450	205	1.000	167	0.424	87	0.772	16	0.938	0.000	0.000	0.000	0.000						
2	3DIVI-003	248	0.083	244	0.206	176	0.141	182	0.474	244	0.400	244	0.626	178	0.605	146	0.821	0.002	0.005																
3	3DIVI-004	208	0.018	217	0.062	150	0.035	163	0.279	219	0.169	222	0.343	150	0.277	12	0.607	0.002	0.005																
4	3DIVI-005	209	0.018	216	0.062	186	0.930	194	0.821	164	0.279	213	0.166	220	0.339	132	0.996	183	0.864	124	0.597	0.002	0.005	0.442											
5	3DIVI-006	217	0.024	224	0.074	166	0.047	172	0.312	216	0.168	234	0.342	159	0.283	12	0.615	0.002	0.005																
6	ACER-000	186	0.011	180	0.036	167	0.827	148	0.025	147	0.209	206	0.246	88	0.981	153	0.201	112	0.490	0.000	0.000	0.042													
7	ACER-001	14	0.005	132	0.020	87	0.422	111	0.008	79	0.050	99	0.098	146	0.056	131	0.109	165	0.999	116	0.068	83	0.406	11	0.479	0.001	0.001	0.041	0.000						
8	AIZE-001	147	0.006	145	0.022	130	0.683	134	0.016	81	0.050	131	0.165	168	0.077	158	0.143	113	0.994	129	0.101	27	0.364	93	0.387	0.001	0.001	0.047	0.000						
9	ALCHERA-000	204	0.016	204	0.047	174	0.870	159	0.046	169	0.292	203	0.138	185	0.216	148	0.999	146	0.176	142	0.803	0.006	0.014	0.328											
10	ALCHERA-001	274	0.987	270	1.000	196	1.000			225	1.000	27	0.999	269	1.000			23	1.000	234	1.000	0.006	0.013	0.324											
11	ALCHERA-002	249	0.095	241	0.166	199	0.954	191	0.668	180	0.446	251	0.486	241	0.591	172	1.000	182	0.827	143	0.811	0.001	0.002	0.106											
12	ALCHERA-003	18	0.010	178	0.035	141	0.741	135	0.016	145	0.206	20	0.155	196	0.239	138	0.999	147	0.172	10	0.464	0.001	0.002	0.106											
13	ALCHERA-004	188	0.011	183	0.038	79	0.345	136	0.017	87	0.088	120	0.144	243	0.394	237	0.529	108	0.991	168	0.424	86	0.708	121	0.546	0.001	0.001	0.046	0.000						
14	ALLGOVISION-000	19	0.011	174	0.033	177	0.894	141	0.021	166	0.282	188	0.088	174	0.166	105	0.990	135	0.117	118	0.526	0.002	0.003	0.122											
15	ALLGOVISION-001	174	0.009	189	0.038	126	0.661	140	0.021	157	0.241	188	0.102	189	0.221	95	0.986	142	0.150	113	0.491	0.001	0.001	0.042											
16	ANKE-000	19	0.013	184	0.038	189	0.931	231	1.000	221	1.000	196	0.117	187	0.220	112	0.994	259	1.000	21	1.000	0.000	0.001	0.080											
17	ANKE-001	200	0.013	185	0.038	194	0.946	254	1.000	198	1.000	199	0.119	188	0.220	118	0.994	259	1.000	192	1.000	0.000	0.001	0.080											
18	ANKE-002	16	0.003	106	0.016	104	0.522	71	0.005	96	0.119	10	0.032	7	0.079	63	0.948	81	0.034	6	0.245	0.001	0.001	0.049											
19	AWARE-003	226	0.031	230	0.090	211	0.966	188	0.316	168	0.290	198	0.128	214	0.298	92	0.984	169	0.428	119	0.530	0.004	0.003	0.874											
20	AWARE-004	243	0.068	243	0.176	218	0.976	171	0.122	178	0.414	229	0.269	236	0.509	176	1.000	167	0.397	14	0.816	0.003	0.003	0.776											
21	AWARE-005	22	0.031	218	0.067	219	0.978	167	0.048	171	0.308	239	0.364	201	0.253	180	1.000	157	0.255	156	0.916	0.001	0.002	0.189											
22	AWARE-006	245	0.070	237	0.128	221	0.983	173	0.111	179	0.421	230	0.276	225	0.398	168	0.999	162	0.368	136	0.749	0.001	0.002	0.189											
23	AYONIX-000	26	0.450	265	0.685	230	0.996	199	0.607	193	0.867	268	0.811	259	0.939	138	0.998	185	0.954	169	0.982	0.010	0.031	0.939											
24	AYONIX-001	263	0.341	258	0.527	226	0.993	195	0.994	191	0.778	262	0.824	254	0.920	164	0.999	191	0.999	166	0.969	0.010	0.031	0.939											
25	AYONIX-002	26	0.341	259	0.527	225	0.993	188	0.464	190	0.778	261	0.824	255	0.920	166	0.999	185	0.915	168	0.969	0.010	0.031	0.939											
26	CAMVI-003	238	0.052	231	0.090	179	0.911	170	0.093	178	0.360	163	0.071	158	0.132	71	0.970	131	0.114	96	0.402	0.006	0.013	0.675											
27	CAMVI-004	23	0.047	225	0.077	143	0.744	167	0.072	170	0.296	161	0.072	152	0.136	162	0.999	129	0.100	14	0.787	0.000	0.000												
28	CAMVI-005	242	0.065	235	0.103	145	0.746	177	0.098	174	0.341	184	0.099	181	0.179	174	1.000	145	0.156	177	0.999	0.000	0.000												
29	CANON-001	1	0.001	4	0.006	23	0.088	11	0.001	11	0.007	10	0.062	29	0.005	22	0.023	12	0.365	17	0.008	21	0.068	28	0.139	0.001	0.000	0.042	0.000						
30	CIB-000	37	0.002	18	0.008	27	0.100	22	0.002	30	0.011	17	0.069	51	0.012	49	0.045	188	1.000	41	0.017	39	0.141	153	0.894	0.000	0.000	0.000	0.000						
31	CLEARVIEWAI-000	1	0.001	10	0.007	7	0.062	16	0.001	8	0.006	5	0.056	30	0.006	25	0.025	76	0.974	18	0.008	19	0.057	20	0.268	0.000	0.000	0.037	0.000						
32	CLOUDWALK-HR-000	35	0.001	35	0.010	9	0.064	19	0.002	10	0.006	6	0.057	9	0.002	8	0.013	2	0.133	10	0.005	6	0.033	11	0.099	0.001	0.000	0.042	0.000						
33	CLOUDWALK-MT-000	52	0.002	52	0.011	3	0.057	3	0.001	3	0.004	2	0.051	8	0.002	8	0.013	1	0.109	1	0.002	1	0.018	1	0.072	0.001	0.000	0.042	0.000						
34	COGENT-000	184	0.010	201	0.046	209	0.965							138	0.053	154	0.140	124	0.995							0.000	0.000	0.000							
35	COGENT-001	18	0.010	202	0.046	210	0.965							139	0.053	155	0.140	125	0.995							0.000	0.000	0.000							
36	COGENT-002	118	0.004	134	0.020	184	0.925							132	0.044	122	0.098	137	0.998							0.000	0.000	0.000							
37	COGENT-003	120	0.004	138	0.021	193	0.939							130	0.046	116	0.095	140	0.998							0.000	0.000	0.000							
38	COGENT-004	70	0.002	76	0.013	183	0.922	67	0.004	81	0.019	90	0.113	119	0.033	85	0.051	135	0.997	51	0.022	36	0.126	105	0.456	0.000	0.000	0.000	0.000						
39	COGENT-005	47	0.002	43	0.010	32	0.126	23	0.002	28	0.010	97</																							

#	ALGORITHM	INVESTIGATION MODE						IDENTIFICATION MODE						FAILURE TO EXTRACT FEATURES					
		RANK ONE MISS RATE, FNIR(N, 0, 1)						HIGH T → FPIR = 0.001, FNIR(N, T, L)											
		N=1.6M						N=1.6M											
GALLERY	MUGSHOT	MUGSHOT	MUGSHOT	VISA	BORDER	VISA		MUGSHOT	MUGSHOT	MUGSHOT	VISA	BORDER	VISA	MUGSHOT	MUGSHOT	MUGSHOT	VISA	BORDER	KIOSK
PROBE	MUGSHOT	WEBCAM	PROFILE	BORDER	BOR _L 10YR	KIOSK		MUGSHOT	WEBCAM	PROFILE	BORDER	BOR _L 10YR	KIOSK	MUGSHOT	WEBCAM	PROFILE	BORDER	BOR _L 10YR	KIOSK
47	CUBOX-000	²⁸ 0.001	³⁸ 0.010	⁴ 0.058	¹⁰ 0.002	⁵ 0.004	¹ 0.049	¹⁵ 0.003	¹⁶ 0.019	³ 0.168	⁸ 0.004	⁵ 0.028	² 0.073	0.001	0.000	0.042	0.000		
48	CYBERLINK-000	¹²² 0.004	¹³¹ 0.020	¹³⁸ 0.717	¹⁰⁶ 0.007		¹¹² 0.134	¹⁴⁹ 0.056	¹³⁵ 0.116	¹²⁷ 0.995	¹¹³ 0.063	⁸⁸ 0.339	0.001	0.001	0.063				
49	CYBERLINK-001	¹¹⁶ 0.004	¹¹⁹ 0.018	¹³⁹ 0.731	⁹⁹ 0.007		¹¹¹ 0.133	¹⁴² 0.054	¹³² 0.109	¹²² 0.995	¹¹⁸ 0.062	¹²⁹ 0.652	0.000	0.000	0.040				
50	CYBERLINK-002	⁹⁶ 0.003	⁶⁴ 0.012	¹¹⁸ 0.577	⁶¹ 0.004		⁷⁸ 0.107	⁶⁰ 0.015	⁶³ 0.053	¹⁰⁰ 0.988	⁵⁸ 0.024	⁷⁵ 0.288	0.001	0.000	0.042				
51	CYBERLINK-003	⁴¹ 0.002	²⁵ 0.009	⁹⁵ 0.474	⁴⁰ 0.003	³¹ 0.012	⁴¹ 0.082	³⁸ 0.008	³⁶ 0.035	⁷⁴ 0.972	³⁸ 0.012	³¹ 0.100	⁹⁰ 0.368	0.000	0.000	0.039	0.000		
52	CYBERLINK-004	⁴⁶ 0.002	⁶⁰ 0.011	⁸⁸ 0.423	⁴⁰ 0.003	²⁹ 0.011	⁷⁰ 0.104	³² 0.007	³⁷ 0.036	¹⁹⁴ 1.000	³⁰ 0.013	³² 0.109	¹⁶⁴ 0.954	0.000	0.000	0.011	0.000		
53	CYBERLINK-005	⁵⁶ 0.002	⁴⁷ 0.011	⁴⁹ 0.209	²⁹ 0.002	²⁵ 0.010	⁶⁰ 0.098	⁴² 0.010	⁴³ 0.041	¹⁷⁸ 1.000	³⁶ 0.014	²⁷ 0.089	¹⁶⁰ 0.926	0.000	0.000	0.034			
54	DAHUA-000	¹⁷⁸ 0.009	¹⁶³ 0.026					¹⁷⁶ 0.086	¹⁵¹ 0.135					0.004	0.003				
55	DAHUA-001	¹⁵⁶ 0.007	¹⁵⁵ 0.024	¹³⁸ 0.703				¹⁶⁶ 0.073	¹⁴³ 0.122	⁸⁵ 0.980				0.002	0.002	0.346			
56	DAHUA-002	⁶¹ 0.002	⁶³ 0.012	⁶⁹ 0.304	³⁹ 0.003		⁴³ 0.084	⁶¹ 0.015	³¹ 0.046	³¹ 0.638	⁴¹ 0.017		³⁶ 0.159	0.001	0.000	0.099			
57	DAHUA-003	¹⁹ 0.001	¹¹ 0.007	⁴² 0.206	²⁰ 0.002	²³ 0.009	²¹ 0.073	⁵⁶ 0.014	⁴⁵ 0.041	²⁶ 0.579	³⁴ 0.013	²⁵ 0.081	²⁵ 0.134	0.000	0.000	0.000	0.000		
58	DAHUA-004	¹⁰ 0.001	¹⁴ 0.008	³⁶ 0.144	¹³ 0.002	¹⁴ 0.007	¹⁵ 0.069	³ 0.007	²⁷ 0.026	²¹ 0.485	²⁹ 0.008	¹³ 0.051	¹⁹ 0.113	0.000	0.000	0.000	0.000		
59	DAON-000	¹²⁵ 0.004	¹¹³ 0.017	¹⁰⁷ 0.530	⁷⁷ 0.005	⁵³ 0.020	¹⁰¹ 0.125	⁸⁷ 0.023	⁷⁵ 0.061	¹⁷⁹ 1.000	⁵⁹ 0.025	⁵⁶ 0.173	¹⁴⁹ 0.846	0.002	0.002	0.108	0.001		
60	DECATUR-000	⁷⁶ 0.002	⁶² 0.011	⁵⁸ 0.229	⁶⁹ 0.004	⁵⁰ 0.019	⁸¹ 0.109	⁹⁰ 0.023	⁸¹ 0.066	³⁵ 0.675	⁶² 0.027	⁵⁵ 0.173	⁶¹ 0.239	0.001	0.000	0.044			
61	DEEPLINT-001	³¹ 0.001	⁹ 0.007	⁴⁸ 0.200	³⁵ 0.002		²² 0.073	¹⁹ 0.003	¹⁰ 0.014	¹⁷¹ 1.000	¹³ 0.006		³⁵ 0.159	0.000	0.000	0.038			
62	DEEPMIA-001	¹³⁰ 0.004	¹⁰³ 0.016	¹⁶³ 0.814	¹¹⁴ 0.010		¹¹⁸ 0.140	¹² 0.046	¹²⁴ 0.101	⁹³ 0.985	¹² 0.077	⁸⁵ 0.326	0.000	0.001	0.047				
63	DERMALOG-003	²⁵³ 0.126	²⁴⁶ 0.217		¹⁹¹ 0.296		¹⁸⁵ 0.560	²⁵⁰ 0.482	²⁴⁶ 0.655		¹⁸¹ 0.677		¹⁵¹ 0.870	0.002	0.002	0.103			
64	DERMALOG-004	²⁵² 0.125	²⁴⁵ 0.215	¹⁸⁷ 0.930	¹⁷⁰ 0.135		¹⁸¹ 0.467	²⁴⁹ 0.480	²⁴⁷ 0.657	¹²⁸ 0.995	¹⁷ 0.603	¹⁸⁰ 0.856	0.001	0.002	0.107				
65	DERMALOG-005	²⁰³ 0.015	¹⁸² 0.037	¹³³ 0.701	¹⁸⁰ 0.242		¹⁷⁷ 0.384	¹⁷⁹ 0.088	¹⁶⁵ 0.154	¹⁰³ 0.990	¹⁶⁰ 0.300	¹²⁷ 0.614	0.001	0.002	0.102				
66	DERMALOG-006	¹⁶⁹ 0.008	¹⁵⁹ 0.024	¹²⁴ 0.619	¹¹⁰ 0.010		¹²⁷ 0.155	¹³⁶ 0.052	¹²⁷ 0.105	⁸⁷ 0.981	¹⁰⁸ 0.059	⁸⁴ 0.318	0.003	0.006	0.181				
67	DERMALOG-007	¹⁷⁷ 0.009	¹⁶⁴ 0.027	¹²⁸ 0.675	¹³⁰ 0.014		¹³³ 0.170	¹⁷⁷ 0.086	¹⁶³ 0.152	¹⁰⁴ 0.990	¹² 0.099	¹²³ 0.557	0.001	0.002	0.102				
68	DERMALOG-008	¹⁰⁴ 0.003	⁹⁶ 0.015	¹⁰² 0.516	⁹⁶ 0.007	⁷² 0.029	¹¹⁷ 0.139	¹²⁷ 0.045	¹¹³ 0.094	¹⁹⁷ 1.000	¹⁰⁵ 0.057	⁸¹ 0.382	¹⁶² 0.940	0.000	0.000	0.002	0.000		
69	DERMALOG-009	¹⁰² 0.003	⁹² 0.014	⁴² 0.167	¹⁰ 0.007	⁹² 0.999	⁷³ 0.106	⁸⁰ 0.021	⁸² 0.066	¹⁹¹ 1.000	⁷¹ 0.031	⁹⁰ 0.999	¹⁴⁸ 0.840	0.001	0.001	0.018	^{0.003}		
70	EYEDEA-003	²⁴⁷ 0.080	²³⁹ 0.148	²⁰³ 0.960	¹⁷² 0.101		¹⁷⁶ 0.379	²⁴⁸ 0.388	²³⁹ 0.543	¹¹⁹ 0.994	¹⁷⁸ 0.570	¹⁴¹ 0.792	0.001	0.003	0.161				
71	F8-001	¹⁹⁶ 0.012	¹² 0.669	²⁶ 1.000			¹⁰⁸ 1.000	²¹² 0.166	¹⁴⁷ 0.998				0.004	1.000	0.158				
72	FINCORE-000	¹⁸⁷ 0.011	¹⁷⁷ 0.034	¹⁵¹ 0.767	¹⁵² 0.032	⁸⁸ 0.117	¹⁴² 0.191	²⁰² 0.134	¹⁸⁶ 0.217	¹⁸³ 1.000	¹⁴⁹ 0.187	⁸⁵ 0.598	¹⁰⁶ 0.458	0.000	0.001	0.043	0.000		
73	FUJITSULAB-000	⁷⁹ 0.002	⁸⁵ 0.014	⁹¹ 0.440	⁶⁵ 0.004	⁵⁶ 0.023	⁶¹ 0.098	⁸¹ 0.021	⁶⁹ 0.056	⁵⁷ 0.024	⁵⁷ 0.177	⁶² 0.240	0.000	0.001	0.016	0.000			
74	GLORY-000	²⁵⁷ 0.178	²⁵² 0.320	²²⁹ 0.994	¹²⁹ 0.228		¹⁸⁷ 0.678	²³⁹ 0.367	²⁴⁰ 0.547	¹²¹ 0.995	¹⁷ 0.453	¹⁴⁷ 0.839	0.011	0.013	0.985				
75	GLORY-001	²⁵⁴ 0.127	²⁴⁹ 0.267	²²⁴ 0.992	¹⁷⁸ 0.178		¹⁸⁶ 0.594	²³¹ 0.305	¹¹⁰ 0.993	¹⁶ 0.408	¹⁴⁵ 0.819	0.011	0.013	0.988					
76	GORILLA-001	²⁴⁰ 0.060	²³² 0.095	¹⁹¹ 0.936	¹⁶⁷ 0.069		¹⁷³ 0.329	²⁴⁵ 0.406	²³² 0.453	²⁰¹ 1.000	¹⁷² 0.468	²⁴⁷ 1.000	0.001	0.001	0.069				
77	GORILLA-002	²¹⁵ 0.020	¹⁹⁸ 0.044	¹⁴⁷ 0.753	¹⁴⁶ 0.027		¹⁵² 0.214	²¹⁹ 0.188	²⁰⁸ 0.268	²⁰⁷ 1.000	¹⁵⁰ 0.250	¹⁸¹ 1.000	0.001	0.001	0.069				
78	GORILLA-003	²²⁸ 0.036	²²⁰ 0.070	¹⁶⁶ 0.821	¹⁶¹ 0.048		¹⁶¹ 0.265	²³³ 0.318	²²⁹ 0.434	²⁴⁵ 1.000	¹⁶⁸ 0.407	²²² 1.000	0.001	0.001	0.069				
79	GORILLA-004	¹⁵³ 0.006	¹⁵⁶ 0.024	¹³² 0.697	¹¹⁷ 0.012		¹³⁰ 0.162	¹⁸² 0.089	¹⁷¹ 0.160	⁶⁵ 0.959	¹³⁷ 0.135	¹⁰² 0.438	0.000	0.001	0.042				
80	GORILLA-005	¹¹⁰ 0.003	¹²⁰ 0.018	⁴⁸ 0.209	⁸⁰ 0.006		⁹⁹ 0.124	¹⁵³ 0.058	¹³⁷ 0.142	³⁷ 0.700	¹²² 0.088	⁸² 0.315	0.000	0.000	0.040				
81	GORILLA-006	⁵¹ 0.002	⁶⁶ 0.012	³⁰ 0.122	⁵⁰ 0.003	⁴⁶ 0.018	⁷² 0.105	¹⁰⁰ 0.027	¹⁰⁷ 0.089	²⁵ 0.531	⁶³ 0.028	⁵² 0.166	³⁵ 0.218	0.000	0.000	0.041	^{0.000}		
82	GRIAULE-000	⁹⁴ 0.002	⁷⁹ 0.014	⁷⁴ 0.327	¹¹⁸ 0.011	⁷⁴ 0.031	¹⁰² 0.126	²⁷⁸ 0.020	⁷⁸ 0.063	¹²³ 0.995	⁷⁹ 0.033	⁶¹ 0.185	³¹ 0.198	0.000	0.002	0.090			
83	HIK-003	¹⁹³ 0.012	¹⁶⁷ 0.027	¹³¹ 0.689	¹²² 0.012		¹²⁴ 0.151	¹⁸⁷ 0.103	¹⁶² 0.158	⁶⁹ 0.969	¹⁴⁰ 0.142	¹⁰⁴ 0.445	0.000	0.000	0.048				
84	HIK-004	¹⁹⁰ 0.011	¹⁶⁵ 0.027	¹⁴² 0.743	¹²² 0.012		¹²⁶ 0.152	¹⁸⁵ 0.099	¹⁶⁴ 0.153	⁷⁷ 0.976	¹³⁸ 0.137	¹⁰¹ 0.434	0.000	0.000	0.048				
85	HIK-005	¹³⁵ 0.005	¹⁰⁸ 0.017	¹⁰⁹ 0.535	¹⁰¹ 0.007		⁸⁴ 0.111	¹²² 0.044	⁹⁶ 0.077	¹⁶⁹ 0.999	¹¹¹ 0.068	¹²⁰ 0.541	0.000	0.000	0.000				
86	HIK-006	¹³⁴ 0.005	¹⁰⁷ 0.017	¹¹⁶ 0.535			¹³ 0.047	¹⁰⁴ 0.086	²⁰³ 1.000				0.000	0.000	0				

#	ALGORITHM	INVESTIGATION MODE						IDENTIFICATION MODE						FAILURE TO EXTRACT FEATURES					
		RANK ONE MISS RATE, FNIR(N, 0, 1)						HIGH T → FPIR = 0.001, FNIR(N, T, L)											
		N=1.6M						N=1.6M											
	GALLERY	MUGSHOT	MUGSHOT	MUGSHOT	VISA	BORDER	VISA	MUGSHOT	MUGSHOT	MUGSHOT	VISA	BORDER	VISA	MUGSHOT	MUGSHOT	MUGSHOT	VISA	BORDER	KIOSK
93	PROBE	MUGSHOT	WEBCAM	PROFILE	BORDER	BOR ₂ 10YR	KIOSK	MUGSHOT	WEBCAM	PROFILE	BORDER	BOR ₂ 10YR	KIOSK	MUGSHOT	WEBCAM	PROFILE	BORDER	BOR ₂ 10YR	KIOSK
94	IDEMLA-008	⁹ 0.001	⁵ 0.007	²⁰ 0.079	¹² 0.001	¹⁵ 0.007	²⁷ 0.075	⁷ 0.002	⁷ 0.013	³ 0.024	⁹ 0.005	¹⁰ 0.036	¹⁵ 0.106	0.000	0.000	0.040	0.000	0.000	0.000
95	IMAGUS-002	²⁶ 0.220	²⁵⁰ 0.301	²²³ 0.988				²⁵⁸ 0.749	²⁵¹ 0.816	¹⁹⁷ 1.000					0.004	0.008	0.550		
96	IMAGUS-003	²⁶ 0.356	²⁵⁶ 0.513	²²⁷ 0.993				²⁵⁹ 0.807	²⁵³ 0.909	¹⁹⁸ 1.000					0.004	0.008	0.550		
97	IMAGUS-005	⁶⁷ 0.002	⁶⁵ 0.012	⁷¹ 0.319	⁸⁸ 0.006	⁵⁴ 0.022	¹¹⁰ 0.132	⁷⁵ 0.018	⁸⁰ 0.066	⁵⁰ 0.838	⁶⁵ 0.029	⁵¹ 0.161	⁵⁸ 0.231	0.000	0.000	0.000	0.000	0.000	0.000
98	IMAGUS-006	⁷¹ 0.002	⁸² 0.014	⁶⁷ 0.293	⁶⁶ 0.004	⁵² 0.019	⁸⁷ 0.112	⁷⁷ 0.019	⁸⁵ 0.069	⁵⁸ 0.897	⁶⁴ 0.028	⁵⁰ 0.161	⁶⁷ 0.260	0.000	0.000	0.000	0.000	0.000	0.000
99	IMPERIAL-000	⁷³ 0.002	⁷⁷ 0.013	⁷² 0.321	⁶² 0.004	⁵⁵ 0.022	⁹⁴ 0.117	⁸⁹ 0.023	⁹¹ 0.073	⁵⁶ 0.893	⁷² 0.031	⁵³ 0.169	⁷² 0.265	0.000	0.000	0.000	0.000	0.000	0.000
100	INCODE-000	²³⁷ 0.049	²³⁴ 0.100	¹⁹⁷ 0.951				²³² 0.310	²²⁷ 0.420	¹⁴⁴ 0.998					0.001	0.004	0.173		
101	INCODE-001	²⁰ 0.017	²⁰ 0.046	¹⁴⁸ 0.762				²² 0.212	²¹¹ 0.296	²⁰⁴ 1.000					0.001	0.004	0.173		
102	INCODE-002	²¹⁹ 0.018	²⁰⁵ 0.048	¹⁶⁹ 0.843				²¹⁸ 0.184	²⁰⁹ 0.269	¹¹¹ 0.993					0.000	0.001	0.066		
103	INCODE-003	¹⁹⁸ 0.013	¹⁹² 0.040	¹⁴⁹ 0.764				²¹⁴ 0.167	²⁰⁵ 0.264	¹⁶⁷ 0.999					0.000	0.001	0.066		
104	INCODE-004	¹¹⁷ 0.004	¹¹⁷ 0.017	⁹⁶ 0.475	¹¹² 0.008			¹¹⁴ 0.135	¹⁴⁵ 0.054	¹⁴² 0.120	¹²⁰ 0.995	¹¹² 0.063	⁸⁰ 0.313	0.000	0.001	0.066			
105	INCODE-005	⁴⁵ 0.002	³⁸ 0.011	³⁸ 0.147	³² 0.002	³⁶ 0.013	³⁶ 0.079	⁴⁶ 0.011	⁴⁸ 0.043	²³ 0.528	⁴³ 0.017	⁴² 0.145	³³ 0.155	0.000	0.000	0.042	0.000	0.000	0.000
106	INNOVATRICS-002	²³ 0.045	²²³ 0.074	¹⁷² 0.853				²² 0.234	²¹⁶ 0.310	¹⁹⁸ 1.000					0.000	0.001	0.046		
107	INNOVATRICS-003	²² 0.026	²⁰⁸ 0.055	¹⁷¹ 0.845				²²³ 0.221	²¹² 0.297	¹⁷⁷ 1.000					0.000	0.001	0.046		
108	INNOVATRICS-004	¹⁹ 0.012	¹⁹⁴ 0.040	²⁰¹ 0.958				²⁰ 0.132	¹⁹⁰ 0.222	⁸³ 0.980					0.000	0.001	0.046		
109	INNOVATRICS-005	⁹² 0.002	⁹¹ 0.014	⁸⁶ 0.407	⁷⁸ 0.005			⁸⁰ 0.109	¹¹¹ 0.034	¹⁰⁸ 0.089	⁵¹ 0.846	⁹⁷ 0.047	⁶⁵ 0.251	0.000	0.001	0.041			
110	INNOVATRICS-007	⁴⁸ 0.002	⁵⁷ 0.011	⁵⁹ 0.248	³⁶ 0.002	³⁸ 0.013	³⁰ 0.077	⁵³ 0.013	⁵⁶ 0.051	³⁹ 0.743	⁴² 0.017	²⁹ 0.093	³¹ 0.154	0.000	0.001	0.041	0.000	0.000	0.000
111	INTSYSMSU-000	²⁵ 0.146	¹⁵⁴ 0.023	¹¹⁷ 0.562	¹⁶⁰ 0.072			¹⁰⁹ 0.132	²⁶⁹ 0.998	²⁶⁴ 1.000	¹⁷⁹ 1.000	¹⁹⁰ 0.999	¹⁷⁸ 0.999	0.000	0.000	0.050			
112	IREX-000	¹³¹ 0.004	²⁸ 0.010	¹²⁹ 0.681	³¹ 0.002	³² 0.012	³⁹ 0.082	¹⁰⁴ 0.028	⁷⁴ 0.060	⁶⁴ 0.957	⁹³ 0.044	⁷⁴ 0.302	⁴¹ 0.170	0.000	0.000	0.042	0.000	0.000	0.000
113	ISYSTEMS-002	¹⁵ 0.006	¹⁶² 0.026	¹⁷⁰ 0.844				¹⁷⁰ 0.078	¹⁴⁶ 0.126	¹³⁶ 0.998					0.002	0.002	0.142		
114	ISYSTEMS-003	¹⁴² 0.005	¹⁵¹ 0.023	¹⁵⁴ 0.791				¹⁵⁴ 0.059	¹³⁰ 0.107	¹⁸¹ 1.000					0.002	0.002	0.142		
115	KAKAO-000	³⁷ 0.001	⁴⁶ 0.011	²⁹ 0.119	³⁴ 0.002	³⁵ 0.013	³² 0.078	⁶³ 0.015	⁶⁸ 0.056	¹⁸ 0.468	⁴⁷ 0.019	³⁸ 0.141	³⁴ 0.158	0.000	0.000	0.041	0.000	0.000	0.000
116	KEDACOM-001	¹⁶⁴ 0.008	¹⁷⁹ 0.036	²¹⁵ 0.972	¹⁵⁴ 0.034			¹⁵⁴ 0.237	⁸⁸ 0.023	⁸⁹ 0.072	⁹⁷ 0.986	¹⁰⁴ 0.055	⁷⁸ 0.305	0.000	0.000	0.000	0.000	0.000	0.000
117	KNERON-000	¹⁴ 0.006	¹⁶⁶ 0.027	¹¹⁵ 0.552	¹⁴⁷ 0.028			¹⁴³ 0.195							0.000	0.000	0.000		
118	KNERON-001	²²⁵ 0.030	²⁶⁴ 0.621	³⁸ 0.237	¹⁷⁷ 0.144	⁸⁹ 0.207	¹⁶⁵ 0.280								0.000	0.000	0.000		
119	LINE-000	⁸ 0.002	⁸³ 0.014	⁵⁴ 0.223	⁸¹ 0.005	⁷⁰ 0.029	⁷⁵ 0.107	¹⁰⁷ 0.031	¹¹⁷ 0.095	⁹⁵ 0.046	⁷² 0.278	²⁷⁴ 1.000	0.000	0.000	0.000	0.000	0.000	0.000	
120	LINE-001	¹⁴ 0.001	¹³ 0.007	⁸ 0.063	¹⁸ 0.002	²¹ 0.008	⁴⁷ 0.085	²⁴ 0.005	²⁸ 0.027	¹⁹⁶ 1.000	²⁸ 0.009	²² 0.072	²⁵² 1.000	0.000	0.000	0.000	0.000	0.000	0.000
121	LOOKMAN-003	¹⁷ 0.009	¹⁸⁸ 0.038		¹⁵ 0.035			¹⁵⁶ 0.239	¹² 0.044	¹³⁴ 0.112	¹²⁴ 0.084	⁸⁹ 0.355	0.000	0.000					
122	LOOKMAN-004	¹⁷⁵ 0.009	¹⁹¹ 0.039	²¹⁷ 0.973				¹²⁶ 0.045	¹²⁹ 0.105	⁷⁸ 0.977					0.000	0.000	0.000		
123	LOOKMAN-005	¹⁶ 0.008	¹⁸¹ 0.036	²¹⁶ 0.972	¹⁵⁶ 0.035			¹³⁵ 0.237	¹⁶ 0.030	¹⁰³ 0.086	⁸¹ 0.978	¹¹¹ 0.062	⁷⁹ 0.308	0.000	0.000	0.000	0.000	0.000	0.000
124	MANTRA-000	³⁹ 0.002	³⁹ 0.010	¹³⁶ 0.709	⁹⁷ 0.007	⁶¹ 0.024	⁸⁶ 0.112	⁴⁵ 0.010	⁴⁴ 0.041	²⁴⁸ 1.000	⁶⁶ 0.029	⁴⁶ 0.152	¹⁸⁰ 1.000	0.002	0.001	0.591	0.003		
125	MEGVII-001	¹⁹⁴ 0.012	¹¹⁶ 0.017		²⁴ 1.000			¹⁶⁵ 0.072	¹²¹ 0.097						0.002	0.000			
126	MEGVII-002	¹⁹ 0.012	¹¹⁸ 0.017	⁹² 0.450	²⁰³ 1.000			¹⁶⁹ 0.077	¹¹⁹ 0.096	¹⁴⁶ 0.998					0.002	0.000	0.033		
127	MICROFOCUS-003	²⁷ 0.594	²⁸⁸ 0.781		¹⁹ 0.708			¹⁹⁸ 0.907	²⁶⁵ 0.931	²⁶³ 0.979	¹⁸⁹ 0.982	¹⁷³ 0.991	0.001	0.005					
128	MICROFOCUS-004	²⁷ 0.576	²⁶⁷ 0.758		¹⁹ 0.701			¹⁹⁴ 0.904	²⁷⁰ 0.999	²⁶¹ 0.975	¹⁸⁸ 0.974	¹⁷¹ 0.989	0.001	0.005					
129	MICROFOCUS-005	²⁶ 0.424	²⁶² 0.601		¹⁸⁸ 0.494			¹⁸⁹ 0.777	²⁶³ 0.835	²⁵⁷ 0.928	¹⁸⁶ 0.935	¹⁷⁰ 0.985	0.001	0.005					
130	MICROFOCUS-006	²⁶ 0.427	²⁶¹ 0.583		¹⁸⁷ 0.490			¹⁹² 0.782	²⁶⁷ 0.978	²⁵⁶ 0.923	¹⁸⁵ 0.923	¹⁶⁷ 0.971	0.001	0.005					
131	MICROSOFT-003	⁴² 0.002	⁶⁹ 0.012		⁵⁹ 0.004			⁸² 0.109	¹⁰² 0.028	¹¹¹ 0.091	⁸³ 0.036	⁶⁴ 0.233	0.000	0.001					
132	MICROSOFT-004	³⁶ 0.001		⁵¹ 0.011	³⁷ 0.144	⁴⁷ 0.003		⁸³ 0.109	⁹⁸ 0.026	¹⁰⁵ 0.087	⁷⁹ 0.033	⁵⁶ 0.222	0.000	0.001					
133	MICROSOFT-005	⁶³ 0.002		⁵¹ 0.011	³⁷ 0.144	⁴⁷ 0.003		⁶² 0.099	⁹³ 0.026	⁸⁷ 0.070	²⁷ 0.587	⁶⁰ 0.027	⁴⁶ 0.180	0.000	0.001	0.049			
134	MICROSOFT-006	⁶⁹ 0.002		⁶¹ 0.011	⁴⁰ 0.150	⁵⁶ 0.004		⁶⁴ 0.100	⁴⁷ 0.012	³⁸ 0.037	²³ 0.386	²⁰ 0.032	⁴³ 0.178	0.000	0.001	0.049			
135	NEC-000	²⁰ 0.017	¹⁹⁶ 0.041	²⁰⁴ 0.959	¹⁴⁴ 0.025			¹⁵⁸ 0.243	¹⁷² 0.079	¹⁵⁶ 0.140	⁸² 0.979			¹¹⁰ 0.474	0.001	0.002	0.890		
136	NEC-001	²¹⁶ 0.021	²⁰⁹ 0.056	²¹² 0.967	¹⁵³ 0.033			¹⁶² 0.277	¹⁸⁹ 0.106	¹⁸³ 0.197	⁹⁶ 0.986	¹³⁶ 0.133	¹⁰⁹ 0.468	0.005	0.003	0.934			
137	NEC-002	⁸ 0.001	²³ 0.009	⁸² 0.363	⁵² 0.003			⁹³ 0.117	¹⁵ 0.003	¹⁹ 0.020	¹⁶³ 0.999	²⁰ 0.008	¹³¹ 0.676	0.000	0.001	0.041			
138	NEC-003	²³ 0.001	³⁷ 0.010	⁸¹ 0.352	⁵⁶ 0.004	³⁴ 0.013	⁹⁸ 0.120	¹¹ 0.002	¹⁵ 0.017	⁴⁷ 0.824	²³ 0.008	¹¹⁰ 0.036	¹³⁰ 0.668	0.000	0.001	0.041	^{0.001}		

Table 12: **Miss rates by dataset**: At left, rank 1 miss rates relevant to investigations; at right, with threshold set to target FPIR = 0.01 for higher volume, low prior, uses. Yellow indicates most accurate algorithm. Throughout blue superscripts indicate the rank of the algorithm for that column.

2022/02/23
14:06:29

$\text{FNIR}(N, R, T) = \text{False neg. identification rate}$
 $\text{FPIR}(N, T) = \text{False pos. identification rate}$

N = Num. enrolled subjects
R = Num. candidates examined

= Threshold

$T = 0 \rightarrow$ Investigation
 $T > 0 \rightarrow$ Identification

#	ALGORITHM	INVESTIGATION MODE						IDENTIFICATION MODE						FAILURE TO EXTRACT FEATURES										
		RANK ONE MISS RATE, FNIR(N, 0, 1)						HIGH T → FPIR = 0.001, FNIR(N, T, L)						N=1.6M										
		GALLERY		MUGSHOT	MUGSHOT	MUGSHOT	VISA	BORDER	VISA	MUGSHOT	MUGSHOT	MUGSHOT	VISA	BORDER	VISA	MUGSHOT	MUGSHOT	MUGSHOT	VISA	BORDER	KIOSK			
PROBE		MUGSHOT	WEBCAM	PROFILE	BORDER	BOR ₁ 10YR	KIOSK			MUGSHOT	WEBCAM	PROFILE	BORDER	BOR ₁ 10YR	KIOSK	MUGSHOT	WEBCAM	PROFILE	BORDER	BOR ₁ 10YR	KIOSK			
139	NEC-004	29.001	22.009	111.058	45.003	18.007	26.075	5.002	6.013	30.622	7.004	3.019	12.100	0.000	0.001	0.041	0.000	0.001	0.001	0.001	0.001			
140	NEC-005	17.001	15.008	21.081	17.002	7.005	23.073	2.002	2.012	34.673	4.003	2.019	9.099	0.000	0.001	0.040	0.000	0.001	0.000	0.001	0.001			
141	NEUROTECHNOLOGY-003	217.022	197.042	208.961				256.036	207.266	236.1.000						0.000	0.001	0.131						
142	NEUROTECHNOLOGY-004	144.006	130.020	217.070				159.063	136.0117	116.0994						0.000	0.001	0.131						
143	NEUROTECHNOLOGY-005	129.004	158.024	178.093				146.054	148.0130	139.0998						0.000	0.000	0.030						
144	NEUROTECHNOLOGY-006	211.018	200.045	122.060				228.0249	226.0418						0.000	0.000								
145	NEUROTECHNOLOGY-007	121.004	137.021	157.076	115.009			139.180	158.062	177.0173	184.1.000	16.0339	265.1.000		0.001	0.001	0.041							
146	NEUROTECHNOLOGY-008	78.002	90.014	93.0457	64.004	58.0023	66.0101	140.053	99.080	202.1.000	82.035	73.293	52.0203	0.000	0.001	0.052	0.001							
147	NEUROTECHNOLOGY-009	30.001	49.011	41.0179	26.002	37.013	35.079	64.015	60.052	28.0588	40.020	47.153	38.0165	0.001	0.000	0.046	0.000							
148	NEUROTECHNOLOGY-010	20.001	22.009	16.070	7.001	17.007	14.068	41.010	40.037	10.0277	30.010	24.075	22.0126	0.000	0.000	0.041	0.000							
149	NEWLAND-002	246.079	236.117	196.093				247.0438	233.0466	155.0999					0.007	0.012	0.200							
150	NOBLIS-001	262.0249	257.0522	228.0993				272.0000	268.0000	201.0000					0.000	0.000	0.000							
151	NOBLIS-002	258.0179	254.0392	229.0982				268.0097	272.0000	206.0000					0.000	0.000	0.000							
152	NOTIONTAG-000	92.002	70.012	46.0204	66.0004	43.016	54.0095	67.0017	73.0599	29.611	52.021	45.150	42.176	0.000	0.000	0.000	0.000	0.000	0.000	0.000	0.000			
153	NTECHLAB-003	150.006	148.023	95.054				144.054	137.0118	49.0837					0.000	0.000	0.040							
154	NTECHLAB-004	138.005	125.019	99.0506	108.0008			105.0129	119.041	128.0105	48.0833	103.053	69.0263	0.000	0.000	0.040								
155	NTECHLAB-005	136.005	121.018	81.0367	110.0008			95.0118	120.042	126.0102	42.0771	118.0073	76.0294	0.000	0.000	0.040								
156	NTECHLAB-006	126.004	112.017	80.0347	105.0007			91.0113	114.037	114.094	41.0754	106.057	68.0260	0.000	0.000	0.040								
157	NTECHLAB-007	97.003	71.012	73.0326	72.0004			76.107	92.026	83.067	46.0750	70.032	57.0223	0.000	0.000	0.042								
158	NTECHLAB-008	49.002	29.010	41.0157	31.0003			44.0084	37.014	50.045	29.0529	30.0033	47.0183	0.000	0.000	0.044								
159	NTECHLAB-009	21.001	16.008	34.0138	24.0002	39.013	25.074	26.0005	21.022	15.0430	37.015	33.109	27.0142	0.000	0.000	0.041	0.001	0.001	0.000	0.000	0.000			
160	NTECHLAB-010	13.001	19.008	21.085	16.0002	20.008	7.057	12.0003	13.015	9.0252	18.0007	18.059	8.098	0.001	0.001	0.043	0.000							
161	NTECHLAB-011	7.001	7.007	17.072	9.0001	19.0007	3.0051	16.0003	12.015	7.228	27.009	23.074	6.091	0.000	0.000	0.040								
162	PARAVISION-000	212.019	187.038	105.0534	185.0423			184.0529	181.089	175.0170	157.0999	17.0470	159.0926	0.000	0.000	0.000								
163	PARAVISION-001	119.004	135.020	75.0329	184.0414			183.0484	133.049	147.0128	149.0999	170.0444	135.0739	0.000	0.000	0.000								
164	PARAVISION-002	124.004	141.022	77.0335	13.0015			135.0175	136.050	140.0119	96.0983	12.0080	114.0497	0.000	0.000	0.032								
165	PARAVISION-003	109.003	127.019	60.0252	133.0015			132.0167	112.035	118.0096	117.0994	107.058	77.0296	0.000	0.000	0.032								
166	PARAVISION-004	43.002	42.010	21.0104	86.0006			88.0112	45.0010	41.038	195.1.000	45.018	155.0908	0.000	0.000	0.032								
167	PARAVISION-005	38.002	32.010	19.079	100.0007			74.0106	21.0004	23.024	84.0980	31.011	23.0132	0.000	0.000	0.038								
168	PARAVISION-007	16.001	17.008	11.066	29.0005	26.010	65.0101	20.0004	24.025	193.1.000	26.009	34.0113	267.1.000	0.000	0.000	0.000	0.000	0.000	0.000	0.000	0.000			
169	PARAVISION-009	6.001	12.007	12.067	6.0001	4.0004	4.054	14.0003	17.019	38.0735	3.0003	7.003	3.0073	0.000	0.001	0.025								
170	PIXELALL-002	133.005	144.022	162.0810	117.0011			140.0187	188.0105	224.0388	209.1.000	176.0602	201.1.000	0.000	0.000	0.000								
171	PIXELALL-003	77.002	89.014	107.0515	95.0006			123.0151	84.022	90.073	173.1.000	88.037	122.0554	0.000	0.000	0.000								
172	PIXELALL-004	74.002	94.015	107.0523	83.0005			125.0152	74.018	98.079	188.1.000	99.051	174.0994	0.000	0.000	0.000								
173	PIXELALL-005	64.002	50.011	62.0264	121.0012	67.0028	121.0146	49.012	54.0050	208.1.000	6.0027	83.0203	179.1.000	0.000	0.000	0.000								
174	PTAKURATSATU-000	107.003	111.017	121.0605	82.0005	65.027	71.0105	113.0037	145.0124	60.0924	96.046	65.0206	59.0232	0.000	0.001	0.039	0.000							
175	QNAP-000	165.008	169.027	105.0522	128.0013	82.054	128.0158	197.0129	195.0238	211.000	158.0191	84.0539	176.0998	0.001	0.000	0.054	0.000							
176	QNAP-001	127.004	142.022	97.0498	94.0006	78.041	89.0112	143.0054	153.0137	61.0928	122.081	79.0368	87.0331	0.000	0.000	0.004	0.000							
177	QUANTASOFT-001	259.0218	266.0272					257.0639						0.000	0.000									
178	RANKONE-002	214.019	221.071					193.0118	203.0261					0.000	0.000									
179	RANKONE-003	213.019	219.068					192.0118	202.0255					0.000	0.000									
180	RANKONE-004	234.041	238.0141					220.0193	228.0426					0.000	0.000									
181	RANKONE-005	179.009	195.041	222.0986				155.0059	178.0173	141.0998				0.000	0.000	0.489								
182	RANKONE-006	140.005	149.0797					115.0037		79.0977				0.000	0.002	0.167								
183	RANKONE-007	113.003	124.019	150.0796	85.0006		113.0134	70.018	84.096	68.0967	70.076	109.062	86.0328	0.000	0.001	0.102								
184	RANKONE-009	87.002	73.013	112.0549	85.0006									0.000	0.000	0.000								

Table 13: **Miss rates by dataset:** At left, rank 1 miss rates relevant to investigations; at right, with threshold set to target FPIR = 0.01 for higher volume, low prior, uses. Yellow indicates most accurate algorithm. Throughout blue superscripts indicate the rank of the algorithm for that column.

2022/02/23

FNIR(N, R, T) =

False neg. identification rate

N = Num. enrolled subjects

R = Num. candidates examined

T = Threshold

T = 0 → Investigation
T > 0 → Identification

#	ALGORITHM	INVESTIGATION MODE										IDENTIFICATION MODE										FAILURE TO EXTRACT FEATURES														
		RANK ONE MISS RATE, FNIR(N, 0, 1)					HIGH T → FPIR = 0.001, FNIR(N, T, L)					N=1.6M					N=1.6M																			
		GALLERY	MUGSHOT	MUGSHOT	MUGSHOT	VISA	BORDER	BOR _{10YR}	KIOSK	MUGSHOT	MUGSHOT	MUGSHOT	VISA	BORDER	VISA	MUGSHOT	MUGSHOT	MUGSHOT	VISA	BORDER	BOR _{10YR}	KIOSK	MUGSHOT	MUGSHOT	MUGSHOT	VISA	BORDER	BOR _{10YR}	KIOSK							
185	RANKONE-010	⁸¹ 0.002	³³ 0.010	⁸¹ 0.374	⁷⁸ 0.005	⁶³ 0.027	¹⁰³ 0.126	⁵⁵ 0.014	⁷¹ 0.058	⁴⁵ 0.802	¹⁰² 0.052	⁷⁶ 0.208	⁶⁶ 0.259	0.000	0.000	0.000	0.000	0.000	0.000	0.000	0.000	0.000	0.000	0.000	0.000	0.000	0.000	0.000	0.000	0.000						
186	RANKONE-011	³⁵ 0.002	⁵⁹ 0.011	⁵⁰ 0.223	⁵⁶ 0.004	⁴⁹ 0.019	⁴² 0.082	³⁶ 0.009	⁵² 0.048	⁸ 0.037	⁸⁸ 0.182	¹⁶⁸ 0.977	0.000	0.000	0.000	0.000	0.000	0.000	0.000	0.000	0.000	0.000	0.000	0.000	0.000	0.000	0.000	0.000	0.000	0.000						
187	RANKONE-012	²⁴ 0.001	⁴⁵ 0.010	³³ 0.127	⁴⁶ 0.003	⁴¹ 0.014	¹⁶ 0.069	³³ 0.008	⁶⁴ 0.053	⁶⁷ 0.029	⁴¹ 0.144	¹⁰⁸ 0.465	0.000	0.000	0.000	0.000	0.000	0.000	0.000	0.000	0.000	0.000	0.000	0.000	0.000	0.000	0.000	0.000	0.000	0.000						
188	REALNETWORKS-000	²³² 0.040	²²⁷ 0.078							²² 0.234	²¹⁸ 0.319										0.001	0.000														
189	REALNETWORKS-001	²³³ 0.040	²²⁸ 0.078							²²⁶ 0.234	²¹⁹ 0.319										0.001	0.000														
190	REALNETWORKS-002	²²⁹ 0.039	²²⁶ 0.078							²²⁴ 0.231	²¹⁷ 0.315										0.001	0.000														
191	REALNETWORKS-003	²²⁰ 0.024	²¹⁵ 0.062	¹⁵³ 0.771	¹⁵¹ 0.031					²¹⁰ 0.159	²⁰⁶ 0.266	¹⁴⁵ 0.998	¹⁴⁴ 0.164	¹¹⁵ 0.500	0.001	0.000	0.009																			
192	REALNETWORKS-004	²¹⁸ 0.024	²¹³ 0.059	¹⁵⁹ 0.797	¹⁵⁰ 0.031					²⁰⁹ 0.158	²⁰⁴ 0.263	¹⁵⁹ 0.999	¹⁴⁶ 0.170	¹²⁶ 0.613	0.001	0.000	0.009																			
193	REALNETWORKS-005	⁸³ 0.002	⁷⁸ 0.013	⁹⁶ 0.433	⁷⁰ 0.004	⁵⁷ 0.023	⁶⁸ 0.102	¹⁰¹ 0.028	⁹² 0.074	⁷² 0.971	⁸ 0.037	⁶⁷ 0.223	⁵⁴ 0.215	0.000	0.000	0.006	0.000	0.000	0.000	0.000	0.000	0.000	0.000	0.000	0.000	0.000	0.000	0.000	0.000	0.000						
194	REALNETWORKS-006	²⁶ 0.001	³⁴ 0.010	⁶⁶ 0.287	³⁷ 0.002	²⁷ 0.010	³³ 0.078	⁵⁸ 0.015	⁶² 0.053	⁸⁶ 0.980	³⁸ 0.016	³⁵ 0.120	³² 0.154	0.000	0.000	0.009	0.000	0.000	0.000	0.000	0.000	0.000	0.000	0.000	0.000	0.000	0.000	0.000	0.000	0.000						
195	REMARKAI-000	¹¹⁵ 0.003	¹²² 0.018	¹²⁵ 0.660	¹⁰⁷ 0.008					¹²² 0.148	¹⁴ 0.055	¹⁴¹ 0.120	¹⁵⁶ 0.999	¹¹⁷ 0.069	¹³³ 0.717	0.000	0.000	0.000	0.000	0.000	0.000	0.000	0.000	0.000	0.000	0.000	0.000	0.000	0.000	0.000	0.000					
196	REMARKAI-000	¹⁷² 0.009	¹⁷² 0.030							¹⁹⁷ 0.128	¹⁸⁴ 0.203									0.000	0.001	0.017														
197	REMARKAI-002	¹⁷⁰ 0.008	¹⁷¹ 0.029	¹⁶⁰ 0.802						¹⁹⁶ 0.124	¹⁸² 0.196	¹⁰⁷ 0.991								0.000	0.001	0.017														
198	RENDIP-000	³⁹ 0.002	⁹⁵ 0.015	⁸⁹ 0.424	⁹¹ 0.006	⁶⁶ 0.028	⁴⁵ 0.084	⁴⁸ 0.012	⁷² 0.059	⁵⁷ 0.894	⁵³ 0.022	⁶⁰ 0.185	³⁹ 0.167	0.000	0.000	0.041	0.000	0.000	0.000	0.000	0.000	0.000	0.000	0.000	0.000	0.000	0.000	0.000	0.000	0.000						
199	REVEALMEDIA-000	⁶² 0.002	⁵⁰ 0.010	⁶³ 0.275	²⁹ 0.002	³³ 0.012	²⁴ 0.074	³⁰ 0.012	⁴⁷ 0.042	³⁶ 0.680	⁵ 0.021	²⁰ 0.093	²⁸ 0.143	0.000	0.000	0.041	0.000	0.000	0.000	0.000	0.000	0.000	0.000	0.000	0.000	0.000	0.000	0.000	0.000	0.000						
200	S1-000	⁸⁹ 0.002	¹¹⁰ 0.017	⁶¹ 0.258	⁸⁴ 0.005	⁶² 0.025	⁴⁹ 0.090	¹⁰³ 0.028	¹⁰² 0.085	²¹² 1.000	⁹⁸ 0.047	¹⁶⁴ 1.000	²³⁰ 1.000	0.000	0.000	0.040	0.000	0.000	0.000	0.000	0.000	0.000	0.000	0.000	0.000	0.000	0.000	0.000	0.000	0.000	0.000					
201	S1-001	¹⁰⁸ 0.003	⁸⁶ 0.014	⁵² 0.215	⁴⁵ 0.003	⁴⁷ 0.018	²⁸ 0.077	⁶⁵ 0.016	⁵⁹ 0.052	⁹⁴ 0.985	⁴ 0.019	³⁷ 0.136	²⁹ 0.148	0.001	0.000	0.035	0.000	0.000	0.000	0.000	0.000	0.000	0.000	0.000	0.000	0.000	0.000	0.000	0.000	0.000						
202	SCANOVATE-000	¹³⁹ 0.005	¹⁹⁹ 0.045	¹¹⁸ 0.560	¹⁵⁵ 0.035					¹⁵⁰ 0.211	¹⁶² 0.067	¹⁹⁸ 0.240	⁵⁵ 0.893	¹⁵⁴ 0.215	⁹⁵ 0.400	0.000	0.001	0.057																		
203	SCANOVATE-001	¹⁴³ 0.005	¹⁹³ 0.040	¹²⁰ 0.585	¹⁴⁹ 0.031					¹³⁸ 0.178	¹⁷³ 0.081	¹⁹² 0.227	⁵⁹ 0.911	¹⁵¹ 0.192	⁹⁸ 0.404	0.000	0.001	0.044																		
204	SENSETIME-000	⁸⁵ 0.002	¹⁰² 0.016	¹⁰⁸ 0.528						⁸² 0.021	⁷⁷ 0.063	²⁶¹ 1.000								0.004	0.000	0.042														
205	SENSETIME-001	⁸⁶ 0.002	¹⁰¹ 0.016							⁸⁵ 0.022	⁷⁹ 0.064									0.004	0.000															
206	SENSETIME-002	²⁰¹ 0.014	¹²⁸ 0.020	⁸⁹ 0.384	¹¹⁶ 0.011					⁶⁹ 0.104	³⁹ 0.015	³¹ 0.028	¹¹⁵ 0.994	⁷⁴ 0.032	¹¹⁷ 0.523	0.009	0.000	0.040																		
207	SENSETIME-003	⁵ 0.001	⁶ 0.007	³⁹ 0.150	³⁸ 0.003					⁵⁰ 0.091	⁶ 0.002	³ 0.012	¹⁹ 0.477	²¹ 0.008	²⁴ 0.133	0.000	0.000	0.041																		
208	SENSETIME-004	⁴ 0.001	⁸ 0.007	¹⁸ 0.072	³⁶ 0.002					⁴⁶ 0.084	³ 0.002	⁵ 0.013	⁸ 0.229	¹⁸ 0.006	¹⁸ 0.113	0.000	0.000	0.041																		
209	SENSETIME-005	³ 0.001	³ 0.006	⁶ 0.059	²⁹ 0.002	¹⁶ 0.007	³⁸ 0.082	¹⁰ 0.002	¹¹ 0.014	⁴ 0.173	¹⁵ 0.007	¹⁴ 0.051	¹⁴ 0.104	0.000	0.000	0.041	0.000	0.000	0.000	0.000	0.000	0.000	0.000	0.000	0.000	0.000	0.000	0.000	0.000	0.000	0.000					
210	SENSETIME-006	² 0.001	² 0.006	² 0.055	¹ 0.001	² 0.004	¹² 0.064	¹ 0.002	¹⁴ 0.012	¹⁴⁵ 0.998	⁰ 0.004	⁸ 0.034	⁰ 0.093	0.000	0.000	0.025	0.000	0.000	0.000	0.000	0.000	0.000	0.000	0.000	0.000	0.000	0.000	0.000	0.000	0.000	0.000					
211	SENSETIME-007	¹ 0.001	¹ 0.006	¹ 0.052	¹ 0.001	¹ 0.003	²⁶ 0.062	⁹ 0.062	¹ 0.001	¹ 0.009	¹⁶¹ 0.999	² 0.003	⁴ 0.024	⁴ 0.085	0.000	0.000	0.025	0.000	0.000	0.000	0.000	0.000	0.000	0.000	0.000	0.000	0.000	0.000	0.000	0.000	0.000	0.000				
212	SHAMAN-003	²⁵⁰ 0.124	²⁴² 0.172							²⁴⁸ 0.451	²⁴² 0.597								0.020	0.011																
213	SHAMAN-004	²⁶¹ 0.222	²⁵¹ 0.319							²⁵⁵ 0.615	²⁴⁹ 0.754								0.020	0.011																
214	SHAMAN-006	²³¹ 0.040	²¹¹ 0.058	¹⁹² 0.938						²⁰⁴ 0.141	¹⁹⁴ 0.237	⁷³ 0.972							0.020	0.011	^{0.869}															
215	SHAMAN-007	²³⁰ 0.040	²¹⁰ 0.057							²⁰⁵ 0.141	¹⁹⁷ 0.240								0.020	0.010																
216	SIAT-001	³⁵ 0.002	²⁵³ 0.333																																	

#	ALGORITHM	INVESTIGATION MODE										IDENTIFICATION MODE										FAILURE TO EXTRACT FEATURES												
		RANK ONE MISS RATE, FNIR(N, 0, 1)										HIGH T → FPIR = 0.001, FNIR(N, T, L)										N=1.6M												
		MUGSHOT	MUGSHOT	WEBCAM	PROFILE	BORDER	BOR ₁ 10YR	KIOSK	MUGSHOT	MUGSHOT	WEBCAM	PROFILE	BORDER	BOR ₁ 10YR	KIOSK	MUGSHOT	MUGSHOT	WEBCAM	PROFILE	BORDER	BOR ₁ 10YR	KIOSK												
231	TEVIAN-007	34.002	26.009	26.093	21.002	24.009	13.067	28.005	20.022	11.301	29.009	20.065	20.0122	0.000	0.000	0.062	0.000	0.000	0.000	0.000	0.000	0.000	0.000	0.000	0.000	0.000	0.000	0.000	0.000					
232	TIGER-000	241.062	233.095					242.0390	235.0500							0.000	0.000																	
233	TIGER-002	146.006	150.023	100.514				175.086	169.158	153.999						0.000	0.000	0.056																
234	TIGER-003	145.006	149.023					174.086	168.158							0.000	0.000																	
235	TONGYITRANS-000	158.007	147.022					167.074	133.112							0.003	0.001																	
236	TONGYITRANS-001	157.007	146.022					161.066	125.101							0.003	0.001																	
237	TOSHIBA-000	132.004	139.022	153.766				157.062	138.118	128.995						0.000	0.000	0.070																
238	TOSHIBA-001	137.005	143.022					152.058	112.092							0.000	0.000																	
239	TRUEFACE-000	112.003	80.014	56.230	102.007	59.024	52.092	73.018	76.062	52.082	68.030	62.0194	49.188		0.001	0.001	0.047		0.003															
240	VD-000	269.474	260.551					264.917	260.946							0.011	0.013																	
241	VD-001	224.028	207.053					221.201	210.281							0.005	0.001																	
242	VD-002	180.010	168.027	175.0893	127.013	80.050	136.0176	171.079	161.148	129.0996	126.095	78.367	91.372		0.004	0.003	0.156		0.002															
243	VD-003	163.008	140.022	150.773	109.008	73.030	116.137	128.046	123.100	154.0999	100.051	69.244	83.315		0.003	0.003	0.144		0.002															
244	VERIDAS-001	101.003	88.014	113.0550	93.006	68.028	106.131	117.037	101.082	99.987	92.044	70.266	70.264		0.000	0.002	0.093		0.001															
245	VERIDAS-002	100.003	87.014	111.0550	92.006	69.028	107.0131	116.037	100.082	98.987	91.044	71.266	71.264		0.000	0.002	0.093		0.001															
246	VERIDAS-003	57.002	54.011	68.0297	63.004	44.016	79.108	66.017	67.055	133.997	48.020	44.150	44.178		0.000	0.002	0.093		0.001															
247	VIGILANTSOLUTIONS-003	244.069	240.151	207.0958				246.4048	248.660	150.999						0.000	0.001	0.127																
248	VIGILANTSOLUTIONS-004	251.125	248.244	208.965				252.0549	252.817	131.996						0.000	0.001	0.127																
249	VIGILANTSOLUTIONS-005	176.009	180.920					241.388		210.1000						0.000	0.001	0.127																
250	VIGILANTSOLUTIONS-006	182.010	182.921					236.0353		192.1000						0.000	0.001	0.127																
251	VIGILANTSOLUTIONS-007	114.003	114.017	180.925	125.013	85.068	134.0175	105.028	106.088	130.096	123.081	80.371	94.391		0.000	0.001	0.127		0.001															
252	VIGILANTSOLUTIONS-008	106.003	115.017	180.913	129.014	86.072	137.0178	79.021	95.077	152.0999	130.104	82.398	116.511		0.000	0.001	0.127		0.001															
253	VISIONBOX-000	65.002	56.011	146.0752	74.005	45.017	34.078	71.018	70.057	108.0990	56.023	43.146	37.0162		0.000	0.001	0.043		0.001															
254	VISIONLABS-004	99.003	129.020	70.343				151.058	170.159	54.890						0.001	0.001	0.046																
255	VISIONLABS-005	88.002	123.019	76.334				135.050	160.147	53.888						0.001	0.001	0.046																
256	VISIONLABS-006	59.002	99.015	51.211	50.004			56.096	98.027	110.090	32.672					0.001	0.001	0.051																
257	VISIONLABS-007	53.002	98.015	50.211	54.004			55.095	97.027	109.090	33.672	73.031				0.001	0.001	0.051																
258	VISIONLABS-008	72.002	81.014	37.141	28.002			37.081	53.013	58.051	26.0481	40.017	30.151		0.001	0.000	0.075																	
259	VISIONLABS-009	15.001	21.008	25.091	8.001			19.071	23.005	26.025	44.0799	25.008				0.000	0.000	0.060																
260	VISIONLABS-010	27.001	44.010	17.069	5.001	9.006	18.069	0.069	27.005	30.027		17.0088	16.055	16.109		0.000	0.000	0.040		0.000														
261	VISIONLABS-011	18.001	24.009	17.064	4.001	6.004	11.063	18.003	18.020		8.004	9.034	5.090		0.000	0.000	0.032		0.000															
262	VOCORD-003	151.006	157.024	161.804	166.061			141.188	195.122	166.155	142.0998	141.157				0.001	0.011	0.425																
263	VOCORD-004	166.008	136.021	150.792	123.012			104.127	237.0355	176.173	181.1000	154.193	172.0991		0.000	0.000	0.000																	
264	VOCORD-005	160.007	153.023	163.012	163.055			144.206	208.0158	149.130	134.0997	139.0138	92.0381		0.001	0.009	0.554																	
265	VOCORD-006	275.1000	272.1000	271.1000	234.1000			224.1000	276.1000	273.1000	259.1000	231.1000				0.001	0.009	0.554																
266	VTS-000	271.0594	263.0608	178.0909	189.0607	91.724	178.0739	254.0598	243.0619	160.0999	179.0613	87.0760	132.0761		0.000	0.001	0.047																	
267	VTS-001	36.002	36.010	41.067	36.006	48.018	31.007	57.051	54.022	40.141	50.192	0.000	0.000		0.040																			
268	VTS-002	66.002	75.013	57.023	131.014	77.038	100.125	94.026	93.075	170.1000	94.045	68.0231	99.0417		0.000	0.000	0.029																	
269	XFORWARDAI-000	82.002	84.014	27.089	60.004	42.015	53.0094	62.015	65.0053	16.0440	58.021	49.159	40.169		0.000	0.000	0.000																	
270	XFORWARDAI-001	75.002	72.013	114.067	44.0003	22.009	40.082	25.005	32.028	17.0448	22.008	19.062	21.123		0.000	0.000	0.000																	
271	XFORWARDAI-002	68.002	67.012	30.059	35.002	13.007	29.077	17.0003	14.016	22.0525	11.005	12.041	10.099		0.000	0.000	0.000																	
272	YISHENG-001	223.027	214.060			165.058		167.0287	234.0346	250.0808	180.0666	157.0919				0.002	0.005																	

#	ALGORITHM	MISSES BELOW THRESHOLD, T	ENROL, MOST RECENT				
		DATASET: FRVT 2018 MUGSHOTS					
		N=0.64M	N=1.6M	N=3.0M	N=6.0M	N=12.0M	
1	3DIVI-005	²¹³ 0.1358	²¹³ 0.1664	¹⁸⁸ 0.1915	¹⁷⁷ 0.2370	¹⁶⁹ 0.3054	
2	ACER-000	²⁰⁷ 0.1185	²⁰⁶ 0.1455	¹⁸⁰ 0.1714	¹⁷⁰ 0.2074	¹⁶² 0.2537	
3	ALCHERA-003	²⁰⁹ 0.1176	²⁰⁷ 0.1553	¹⁸⁸ 0.1853	¹⁷⁸ 0.2409	¹⁷⁷ 0.3553	
4	ALLGOVISION-000	¹⁷⁹ 0.0688	¹⁸⁰ 0.0881	¹⁶³ 0.1084	¹⁵⁸ 0.1389	¹⁴² 0.2129	
5	ALLGOVISION-001	¹⁸⁵ 0.0785	¹⁸⁵ 0.1017	¹⁷⁰ 0.1218	¹⁶² 0.1584	¹⁴⁸ 0.2273	
6	ANKE-000	¹⁹² 0.0942	¹⁹⁰ 0.1169	¹⁷⁸ 0.1404	¹⁶⁷ 0.1776	¹⁶³ 0.2559	
7	ANKE-002	¹⁰⁹ 0.0229	¹⁰⁹ 0.0318	¹¹⁰ 0.0406	¹⁰⁵ 0.0605	⁹¹ 0.1466	
8	AWARE-003	²⁰² 0.1098	¹⁹⁸ 0.1283	¹⁷⁶ 0.1447	¹⁶⁵ 0.1768	¹⁵⁴ 0.2364	
9	AWARE-005	²⁴⁸ 0.3389	²³⁸ 0.3643	¹⁹⁷ 0.3993	¹⁸⁶ 0.4526	¹⁶¹ 0.2531	
10	AYONIX-002	²⁶¹ 0.7862	²⁶¹ 0.8242	¹⁹⁹ 0.8508	¹⁹¹ 0.8704	¹⁸⁵ 0.8939	
11	CAMVI-004	¹³⁵ 0.0367	¹⁶⁴ 0.0716	¹⁵⁸ 0.0983	¹⁸⁰ 0.2508	¹⁶⁶ 0.2701	
12	CANON-001	²⁹ 0.0039	²⁹ 0.0054	²⁹ 0.0074	²⁶ 0.0158	³² 0.0924	
13	CIB-000	⁴⁸ 0.0086	⁵¹ 0.0125	⁵¹ 0.0160	⁵⁴ 0.0303	⁷¹ 0.1251	
14	CLEARVIEWAI-000	³⁰ 0.0040	³⁰ 0.0058	³⁰ 0.0078	²⁷ 0.0159	³⁵ 0.0971	
15	CLOUDWALK-HR-000	⁷ 0.0019	⁹ 0.0020	⁷ 0.0023	¹¹ 0.0072	¹³ 0.0701	
16	CLOUDWALK-MT-000	¹⁰ 0.0019	⁸ 0.0020	⁶ 0.0022	⁵ 0.0049	⁸ 0.0466	
17	COGENT-000	¹⁵³ 0.0430	¹³⁸ 0.0527	¹³⁹ 0.0695	¹⁴¹ 0.1133	¹³¹ 0.1960	
18	COGENT-001	¹⁵⁴ 0.0430	¹³⁹ 0.0527	¹⁴⁰ 0.0695	¹⁴⁰ 0.1133	¹³² 0.1960	
19	COGENT-002	¹² 0.0322	¹²⁵ 0.0444	¹²² 0.0610	¹³⁸ 0.1116	¹⁴ 0.2180	
20	COGENT-003	¹²² 0.0328	¹³⁰ 0.0463	¹³⁷ 0.0683	¹⁴⁸ 0.1294	¹⁵⁶ 0.2445	
21	COGENT-004	¹⁰⁶ 0.0210	¹¹⁰ 0.0331	¹²⁰ 0.0527	¹⁴³ 0.1138	¹⁴¹ 0.2119	
22	COGENT-005	³⁸ 0.0064	³⁷ 0.0091	³⁷ 0.0123	³⁵ 0.0303	⁶⁷ 0.1233	
23	COGNITEC-000	²¹⁵ 0.1377	²¹¹ 0.1606	¹⁸⁵ 0.1870	¹⁷² 0.2176	¹⁶⁸ 0.2831	
24	COGNITEC-001	¹⁸ 0.0807	¹⁸⁶ 0.1017	¹⁶⁹ 0.1214	¹⁵⁸ 0.1513	¹⁴ 0.2238	
25	COGNITEC-002	¹⁴⁶ 0.0406	¹⁴¹ 0.0531	¹³³ 0.0666	¹²⁶ 0.0935	¹²⁷ 0.1874	
26	COGNITEC-003	¹⁴ 0.0400	¹³⁷ 0.0526	¹²⁸ 0.0650	¹²¹ 0.0895	¹² 0.1772	
27	COGNITEC-004	¹⁰⁸ 0.0222	¹⁰⁸ 0.0313	¹⁰⁸ 0.0388	⁹⁸ 0.0540	³¹ 0.1103	
28	COGNITEC-005	³⁷ 0.0063	³⁹ 0.0096	⁴¹ 0.0144	⁴⁹ 0.0287	⁴⁵ 0.0967	
29	COGNITEC-006	³³ 0.0053	³⁴ 0.0077	³⁶ 0.0117	³⁹ 0.0254	²⁸ 0.0919	
30	CYBERLINK-000	¹⁴⁸ 0.0414	¹⁴⁹ 0.0565	¹⁴⁴ 0.0707	¹³⁴ 0.1031	¹³⁸ 0.2050	
31	CYBERLINK-001	¹³⁹ 0.0392	¹⁴² 0.0536	¹³⁸ 0.0695	¹³¹ 0.0973	¹² 0.1794	
32	CYBERLINK-002	⁵⁷ 0.0105	⁶⁰ 0.0148	⁶⁵ 0.0202	⁷⁶ 0.0399	⁷² 0.1255	
33	CYBERLINK-003	³⁴ 0.0056	³⁵ 0.0077	³⁶ 0.0100	³⁵ 0.0235	⁶⁸ 0.1237	
34	CYBERLINK-004	³² 0.0051	³² 0.0071	³⁴ 0.0102	³⁰ 0.0199	²⁵ 0.1269	
35	CYBERLINK-005	⁴⁰ 0.0067	⁴² 0.0099	⁴⁰ 0.0138	³³ 0.0394	¹⁰ 0.1566	
36	DAIHUA-001	¹⁶⁸ 0.0569	¹⁶⁶ 0.0727	¹⁵⁸ 0.0878	¹⁴⁴ 0.1148	¹²⁶ 0.1867	
37	DAIHUA-002	⁶² 0.0108	⁶¹ 0.0151	⁶⁰ 0.0191	⁵¹ 0.0291	⁶¹ 0.1153	
38	DAIHUA-003	⁵⁵ 0.0100	⁵⁶ 0.0139	⁵⁷ 0.0180	⁵² 0.0296	⁵⁵ 0.1130	
39	DAIHUA-004	³¹ 0.0048	³¹ 0.0069	³¹ 0.0090	²⁸ 0.0164	²³ 0.0853	
40	DAON-000	⁸ 0.0161	⁸⁷ 0.0226	⁸⁷ 0.0293	¹⁰⁴ 0.0562	¹¹⁴ 0.1702	
41	DECATUR-000	⁸⁹ 0.0173	⁹⁰ 0.0229	⁹⁰ 0.0305	⁸⁸ 0.0464	⁸⁸ 0.1433	
42	DEEPLINT-001	¹⁹ 0.0027	¹⁹ 0.0033	¹⁸ 0.0043	²⁰ 0.0121	³¹ 0.0922	
43	DEEPSEA-001	¹³¹ 0.0347	¹²⁹ 0.0462	¹²⁴ 0.0586	¹¹⁹ 0.0802	¹¹⁶ 0.1708	
44	DERMALOG-005	¹⁸³ 0.0700	¹⁷⁹ 0.0880	¹⁶⁸ 0.1144	¹⁶¹ 0.1578	¹⁵⁹ 0.2451	
45	DERMALOG-006	¹⁴⁰ 0.0395	¹³⁶ 0.0517	¹²⁹ 0.0659	¹³⁰ 0.0973	¹¹⁹ 0.1745	
46	DERMALOG-007	¹⁸ 0.0691	¹⁷⁷ 0.0863	¹⁶⁴ 0.1107	¹⁵⁷ 0.1504	¹⁵ 0.2299	
47	DERMALOG-008	¹²⁷ 0.0338	¹²⁷ 0.0455	¹²⁷ 0.0626	¹³⁵ 0.1060	¹⁵⁰ 0.2276	
48	DERMALOG-009	⁸⁰ 0.0148	⁸⁰ 0.0206	⁸¹ 0.0268	⁷⁷ 0.0416	⁸¹ 0.1374	
49	FUJITSULAB-000	⁸¹ 0.0148	⁸¹ 0.0206	⁸⁸ 0.0277	¹⁰⁰ 0.0541	¹¹⁸ 0.1739	
50	GORILLA-002	²¹ 0.1539	²¹⁹ 0.1880	¹⁸⁹ 0.2184	¹⁸¹ 0.2596	¹⁷ 0.3398	
51	GORILLA-004	¹⁸² 0.0699	¹⁸² 0.0892	¹⁶¹ 0.1048	¹⁵³ 0.1370	¹³⁵ 0.1969	
52	GORILLA-005	¹⁵⁸ 0.0453	¹⁵³ 0.0583	¹⁴⁷ 0.0704	¹³² 0.0974	⁹² 0.1474	
53	GORILLA-006	¹⁰¹ 0.0196	¹⁰⁰ 0.0275	⁹¹ 0.0331	⁹² 0.0516	⁹¹ 0.1113	
54	GRIAULE-000	⁷⁷ 0.0145	⁷⁸ 0.0201	⁷⁸ 0.0253	⁷⁸ 0.0407	⁸⁹ 0.1440	
55	HIK-003	¹⁸⁸ 0.0828	¹⁸⁷ 0.1028	¹⁶⁸ 0.1202	¹⁶⁰ 0.1525	¹⁵⁹ 0.2480	
56	HIK-004	¹⁸⁶ 0.0796	¹⁸³ 0.0988	¹⁶⁶ 0.1147	¹⁵⁶ 0.1474	¹⁶⁰ 0.2483	
57	HIK-005	¹¹⁹ 0.0312	¹²² 0.0436	¹²³ 0.0560	¹²³ 0.0911	¹⁴ 0.2129	
58	HYPERVERGE-001	²³ 0.0033	²² 0.0045	²² 0.0059	¹⁷ 0.0117	²⁵ 0.0872	
59	IDEMIA-003	¹² 0.0346	¹³² 0.0471	¹⁵⁷ 0.0892	¹⁸³ 0.2789	¹⁸ 0.4311	
60	IDEMIA-004	¹¹⁸ 0.0300	¹¹⁸ 0.0373	¹¹² 0.0447	¹⁰⁶ 0.0617	¹¹³ 0.1635	
61	IDEMIA-005	¹³ 0.0360	¹²⁴ 0.0440	¹²¹ 0.0537	¹¹⁸ 0.0764	¹² 0.1915	
62	IDEMIA-006	¹³² 0.0351	¹²¹ 0.0433	¹¹⁸ 0.0525	¹¹⁵ 0.0734	¹⁴⁵ 0.2201	
63	IDEMIA-007	²⁸ 0.0136	⁷² 0.0181	⁶⁹ 0.0228	⁶⁶ 0.0357	⁸⁰ 0.1402	
64	IDEMIA-008	⁷ 0.0016	⁷ 0.0019	⁹ 0.0024	⁶ 0.0053	⁹ 0.0470	
65	IMAGUS-005	⁷⁴ 0.0137	⁷⁵ 0.0185	⁷³ 0.0237	⁶⁸ 0.0368	⁴⁷ 0.1067	
66	IMAGUS-006	⁷² 0.0137	⁷⁷ 0.0190	⁷⁹ 0.0244	⁷⁴ 0.0396	⁶² 0.1159	
67	IMAGUS-007	⁸⁵ 0.0160	⁸⁹ 0.0228	⁸⁷ 0.0284	⁸² 0.0444	⁶⁴ 0.1179	
68	IMPERIAL-000	⁹ 0.0187	⁹⁵ 0.0259	¹⁰¹ 0.0358	¹¹⁴ 0.0733	¹² 0.1794	
69	INCODE-003	²¹² 0.1324	²¹⁴ 0.1672	¹⁸⁷ 0.1961	¹⁷⁵ 0.2345	¹⁷¹ 0.3123	
70	INCODE-004	¹⁴⁴ 0.0403	¹⁴⁵ 0.0538	¹³⁸ 0.0662	¹²⁵ 0.0917	¹¹¹ 0.1619	
71	INCODE-005	⁴⁶ 0.0083	⁴⁶ 0.0113	⁴⁵ 0.0145	³⁶ 0.0247	²⁷ 0.0912	
72	INNOVATRICS-007	⁵² 0.0093	⁵² 0.0125	⁵⁰ 0.0159	⁴¹ 0.0259	⁴⁸ 0.1092	

Table 16: **Identification-mode: Effect of N on FNIR at high threshold.** Values are threshold-based miss rates i.e. FNIR at FPIR = 0.001 for five enrollment population sizes, N. The right six columns apply for enrollment of one image. Missing entries usually apply because another algorithm from the same developer was run instead. Some developers are missing because less accurate algorithms were not run on galleries with $N \geq 3\,000\,000$. Throughout blue superscripts indicate the rank of the algorithm for that column.

#	ALGORITHM	MISSES BELOW THRESHOLD, T		ENROL MOST RECENT				
		FNIR(N, T > 0, R > L)		DATASET: FRVT 2018 MUGSHOTS				
		N=0.64M	N=1.6M	N=3.0M	N=6.0M	N=12.0M		
73	INTSYSMSU-000	²⁷ 0.9982	²⁶ 0.9984	²⁰ 0.9985	¹⁹ 0.9987	¹⁸ 0.9988		
74	IREX-000	⁹⁹ 0.0190	¹⁰⁴ 0.0280	¹⁰⁷ 0.0391	¹¹⁰ 0.0677	⁹⁵ 0.1479		
75	ISYSTEMS-002	¹⁷⁰ 0.0584	¹⁷⁰ 0.0783	¹⁵⁷ 0.0973	¹⁵⁴ 0.1373	¹⁵¹ 0.2295		
76	ISYSTEMS-003	¹⁵⁶ 0.0438	¹⁵⁴ 0.0590	¹⁵⁰ 0.0807	¹⁴⁶ 0.1259	¹⁵³ 0.2357		
77	KAKAO-000	⁶³ 0.0109	⁶³ 0.0151	⁶⁶ 0.0196	⁶¹ 0.0324	³⁸ 0.1010		
78	KEDACOM-001	⁹¹ 0.0181	⁸⁸ 0.0227	⁷⁹ 0.0265	⁸¹ 0.0422	⁸² 0.1340		
79	LOOKMAN-003	¹³ 0.0346	¹²³ 0.0437	¹¹⁷ 0.0514	¹¹³ 0.0724	¹¹¹ 0.1620		
80	LOOKMAN-005	¹¹⁰ 0.0240	¹⁰⁶ 0.0301	¹⁰² 0.0356	⁹¹ 0.0512	⁸¹ 0.1334		
81	MANTRA-000	³⁹ 0.0065	⁴³ 0.0101	⁴⁶ 0.0151	⁵⁶ 0.0308	⁴¹ 0.1035		
82	MEGVII-001	¹⁶⁶ 0.0562	¹⁶³ 0.0722	¹⁵¹ 0.0872	¹⁵⁰ 0.1309	¹⁶⁷ 0.2713		
83	MICROFOCUS-005	²⁶ 0.9732	²⁶ 0.8354	²⁰ 0.8555	¹⁹ 0.8755	¹⁸ 0.8954		
84	MICROSOFT-003	¹⁰² 0.0198	¹⁰² 0.0278	¹⁰¹ 0.0356	⁹⁷ 0.0538	¹⁰¹ 0.1539		
85	MICROSOFT-004	⁹⁴ 0.0185	⁹⁶ 0.0259	⁹⁷ 0.0333	⁹³ 0.0517	⁹⁹ 0.1510		
86	MICROSOFT-005	⁹² 0.0181	⁹³ 0.0256	⁹² 0.0320	⁹⁰ 0.0512	⁹⁷ 0.1491		
87	MICROSOFT-006	⁵¹ 0.0091	⁴⁷ 0.0120	⁵² 0.0162	⁵³ 0.0301	⁹⁶ 0.1482		
88	NEC-000	¹⁷⁴ 0.0637	¹⁷² 0.0789	¹⁵⁶ 0.0933	¹⁴⁵ 0.1163	¹³⁹ 0.1941		
89	NEC-001	¹⁸⁹ 0.0863	¹⁸⁹ 0.1055	¹⁷¹ 0.1249	¹⁵⁹ 0.1519	¹⁴⁸ 0.2253		
90	NEC-002	¹³ 0.0020	¹³ 0.0026	¹⁵ 0.0033	²² 0.0135	¹³ 0.0653		
91	NEC-003	¹⁴ 0.0021	¹¹ 0.0024	¹⁰ 0.0028	⁸ 0.0059	¹¹ 0.0540		
92	NEC-004	³ 0.0017	⁵ 0.0018	² 0.0020	² 0.0037	³ 0.0329		
93	NEC-005	³ 0.0015	² 0.0017	² 0.0019	⁹ 0.0065	¹ 0.0307		
94	NEUROTECHNOLOGY-003	²⁵ 0.5698	²⁵ 0.6362	¹⁹ 0.7035	¹⁹ 0.7602	¹⁸ 0.8224		
95	NEUROTECHNOLOGY-004	¹⁶⁰ 0.0466	¹⁵⁹ 0.0629	¹⁴⁸ 0.0779	¹⁴² 0.1135	¹⁴⁰ 0.2102		
96	NEUROTECHNOLOGY-005	¹⁴¹ 0.0396	¹⁴⁶ 0.0538	¹³⁹ 0.0675	¹²⁹ 0.0950	¹³⁴ 0.1966		
97	NEUROTECHNOLOGY-007	¹⁵⁵ 0.0436	¹⁵⁸ 0.0623	¹⁴⁷ 0.0802	¹³¹ 0.1320	¹⁵¹ 0.2393		
98	NEUROTECHNOLOGY-008	¹²⁸ 0.0339	¹⁴⁰ 0.0530	¹⁵¹ 0.0893	¹⁶⁶ 0.1769	¹⁷⁴ 0.3288		
99	NEUROTECHNOLOGY-009	⁶¹ 0.0108	⁶⁴ 0.0152	⁶⁶ 0.0196	⁵⁹ 0.0324	⁵⁶ 0.1102		
100	NEUROTECHNOLOGY-010	⁴² 0.0069	⁴¹ 0.0099	⁴³ 0.0138	⁸⁴ 0.0449	¹¹⁷ 0.1727		
101	NOTIONTAG-000	⁶ 0.0128	⁶⁷ 0.0175	⁶⁶ 0.0228	⁶⁷ 0.0357	²⁶ 0.1270		
102	NTECHLAB-003	¹⁵⁰ 0.0421	¹⁴⁴ 0.0537	¹³⁴ 0.0674	¹²² 0.0907	¹⁰⁷ 0.1582		
103	NTECHLAB-004	¹² 0.0312	¹⁹ 0.0405	¹¹⁸ 0.0519	¹¹² 0.0722	⁹⁶ 0.1503		
104	NTECHLAB-005	¹²⁴ 0.0334	¹²⁰ 0.0424	¹²² 0.0537	¹¹⁷ 0.0760	¹⁰⁴ 0.1543		
105	NTECHLAB-006	¹¹⁶ 0.0288	¹¹⁴ 0.0367	¹¹³ 0.0471	¹⁰⁹ 0.0670	¹⁰⁰ 0.1523		
106	NTECHLAB-007	⁹⁶ 0.0188	⁹² 0.0256	⁹¹ 0.0317	⁸⁹ 0.0495	⁸⁶ 0.1306		
107	NTECHLAB-008	⁵⁹ 0.0107	⁵⁷ 0.0145	⁵⁹ 0.0187	⁴⁸ 0.0286	³⁷ 0.0995		
108	NTECHLAB-009	²⁶ 0.0037	²⁶ 0.0049	²⁵ 0.0062	²¹ 0.0125	¹⁸ 0.0735		
109	NTECHLAB-010	¹¹ 0.0020	¹² 0.0025	¹¹ 0.0030	¹³ 0.0077	¹⁷ 0.0710		
110	NTECHLAB-011	¹² 0.0022	¹⁶ 0.0030	¹⁷ 0.0038	¹² 0.0075	¹² 0.0625		
111	PARAVISION-003	¹¹² 0.0260	¹¹² 0.0351	¹¹² 0.0447	¹¹⁸ 0.0657	¹¹² 0.1630		
112	PARAVISION-004	⁴ 0.0074	⁴⁵ 0.0101	⁴¹ 0.0136	⁴⁴ 0.0267	²⁶ 0.1256		
113	PARAVISION-005	²¹ 0.0032	²¹ 0.0041	²¹ 0.0057	²⁹ 0.0174	⁴² 0.1037		
114	PARAVISION-007	²⁰ 0.0030	²⁰ 0.0040	²⁰ 0.0055	³¹ 0.0211	⁴⁹ 0.1097		
115	PARAVISION-009	¹² 0.0020	¹⁴ 0.0026	¹⁶ 0.0038	¹⁶ 0.0098	²⁴ 0.0857		
116	PIXELALL-002	¹⁸⁴ 0.0716	¹⁸⁸ 0.1052	¹⁷⁸ 0.1475	¹⁷⁹ 0.2489	¹⁷⁹ 0.3904		
117	PIXELALL-003	⁸ 0.0158	⁸⁴ 0.0218	⁸⁶ 0.0288	⁸⁶ 0.0474	⁵⁶ 0.1138		
118	PIXELALL-004	⁶⁹ 0.0129	⁷⁴ 0.0183	⁷⁷ 0.0245	⁶⁹ 0.0378	⁸⁴ 0.1375		
119	PIXELALL-005	⁴⁹ 0.0087	⁴⁹ 0.0121	⁵⁴ 0.0171	³⁸ 0.0250	⁴¹ 0.1052		
120	PTAKURATSATU-000	¹¹³ 0.0275	¹¹³ 0.0366	¹¹⁴ 0.0458	⁹⁵ 0.0523	¹⁰ 0.1523		
121	QNAP-001	¹⁴ 0.00404	¹⁴³ 0.0536	¹³¹ 0.0661	¹²⁴ 0.0916	¹⁰⁸ 0.1595		
122	QUANTASOFT-001	²⁵ 0.6387	²⁵ 0.6387	¹⁹ 0.6387		¹⁸² 0.6387		
123	RANKONE-002	¹⁹⁸ 0.0973	¹⁹³ 0.1175	¹⁷⁸ 0.1359	¹⁶⁴ 0.1718	¹⁶⁵ 0.2613		
124	RANKONE-003	¹⁹⁷ 0.0973	¹⁹² 0.1175	¹⁷³ 0.1359	¹⁶³ 0.1718	¹⁶⁴ 0.2613		
125	RANKONE-005	¹⁶ 0.0473	¹⁵⁵ 0.0592	¹⁴¹ 0.0700	¹²⁷ 0.0944	¹³⁸ 0.1998		
126	RANKONE-007	⁸⁸ 0.0168	⁸⁶ 0.0222	⁸⁰ 0.0266	⁷¹ 0.0381	⁵⁶ 0.1132		
127	RANKONE-009	²⁰ 0.0132	⁷⁰ 0.0177	⁷⁹ 0.0230	⁶³ 0.0344	³⁰ 0.0921		
128	RANKONE-010	⁵⁸ 0.0106	⁵⁵ 0.0136	⁵⁶ 0.0174	⁴⁵ 0.0265	²¹ 0.0785		
129	RANKONE-011	³⁶ 0.0063	³⁶ 0.0087	³⁵ 0.0115	⁴⁵ 0.0269	⁵⁸ 0.1135		
130	RANKONE-012	³⁰ 0.0058	³³ 0.0077	³¹ 0.0100	³² 0.0220	⁵⁶ 0.1111		
131	REALNETWORKS-002	²²⁵ 0.1943	²²⁴ 0.2314	¹⁹² 0.2656	¹⁸⁵ 0.3134	¹⁷³ 0.3208		
132	REALNETWORKS-003	²¹ 0.1300	²¹⁰ 0.1594	¹⁸⁴ 0.1858	¹⁷³ 0.2246	¹⁷¹ 0.3076		
133	REALNETWORKS-004	²¹⁰ 0.1279	²⁰⁹ 0.1581	¹⁸³ 0.1857	¹⁷⁴ 0.2329	¹⁷² 0.3179		
134	REALNETWORKS-005	¹⁸ 0.0202	¹⁰¹ 0.0277	¹⁰⁸ 0.0355	¹⁰³ 0.0560	⁸⁷ 0.1431		
135	REALNETWORKS-006	³⁴ 0.0097	³⁸ 0.0145	³⁶ 0.0182	³⁷ 0.0308	³⁶ 0.0991		
136	REMARKAI-000	¹⁴⁷ 0.0406	¹⁴⁷ 0.0552	¹³⁶ 0.0676	¹³³ 0.1028	¹³⁷ 0.2003		
137	RENDIP-000	⁴⁷ 0.0085	⁴⁸ 0.0121	⁴⁸ 0.0156	⁴⁷ 0.0277	⁶⁵ 0.1182		
138	REVEALMEDIA-000	⁵⁰ 0.0090	⁵⁰ 0.0122	⁴⁹ 0.0158	⁴⁶ 0.0277	³⁹ 0.1019		
139	S1-000	¹⁰⁵ 0.0204	¹⁰³ 0.0279	¹⁰⁸ 0.0382	¹⁰⁷ 0.0630	¹¹¹ 0.1707		
140	S1-001	⁶⁴ 0.0115	⁶⁵ 0.0156	⁶⁴ 0.0199	⁷² 0.0392	⁷⁴ 0.1256		
141	SCANOVATE-000	¹⁶² 0.0498	¹⁶² 0.0667	¹⁴⁸ 0.0804	¹³⁷ 0.1097	⁵⁴ 0.1109		
142	SCANOVATE-001	¹⁷³ 0.0630	¹⁷³ 0.0815	¹⁵⁹ 0.0993	¹⁴⁷ 0.1292	¹³³ 0.1960		
143	SENSETIME-000	⁸³ 0.0158	⁸² 0.0208	⁸¹ 0.0270	⁷⁵ 0.0398	⁶⁶ 0.1232		
144	SENSETIME-001	⁸⁶ 0.0161	⁸⁵ 0.0219	⁸⁶ 0.0277	⁸⁰ 0.0420	⁷⁸ 0.1304		

Table 17: Identification-mode: Effect of N on FNIR at high threshold. Values are threshold-based miss rates i.e. FNIR at FPIR = 0.001 for five enrollment population sizes, N. The right six columns apply for enrollment of one image. Missing entries usually apply because another algorithm from the same developer was run instead. Some developers are missing because less accurate algorithms were not run on galleries with $N \geq 3\ 000\ 000$. Throughout blue superscripts indicate the rank of the algorithm for that column.

#	ALGORITHM	MISSES BELOW THRESHOLD, T FNIR(N, T > 0, R > L)					ENROL MOST RECENT DATASET: FRVT 2018 MUGSHOTS				
		N=0.64M		N=1.6M		N=3.0M		N=6.0M		N=12.0M	
		FNIR	RANK	FNIR	RANK	FNIR	RANK	FNIR	RANK	FNIR	RANK
145	SENSETIME-002	⁷⁸ 0.0146		⁵⁹ 0.0148	⁴⁷ 0.0153	³⁴ 0.0234	¹⁴ 0.0657				
146	SENSETIME-003	⁷ 0.0016		⁶ 0.0018	⁷ 0.0021	⁷ 0.0054	⁷ 0.0451				
147	SENSETIME-004	⁴ 0.0015		³ 0.0018	⁴ 0.0021	³ 0.0040	⁴ 0.0354				
148	SENSETIME-005	⁶ 0.0016		¹⁰ 0.0022	¹² 0.0031	¹⁵ 0.0089	⁷ 0.0454				
149	SENSETIME-006	⁷ 0.0014		⁴ 0.0018	⁸ 0.0023	⁴ 0.0047	⁷ 0.0372				
150	SENSETIME-007	¹ 0.0012		¹ 0.0014	¹ 0.0016	¹ 0.0036	² 0.0316				
151	SHAMAN-007	²⁰⁹ 0.1212		²⁰⁵ 0.1413	¹⁷ 0.1587	¹⁶⁸ 0.1879	¹⁵⁸ 0.2460				
152	SIAT-001	⁷² 0.0136		⁶⁸ 0.0176	⁷¹ 0.0230	⁶² 0.0344	⁴⁰ 0.1035				
153	SIAT-002	⁸² 0.0154		⁸³ 0.0216	⁸ 0.0273	⁷⁷ 0.0404	⁷ 0.1283				
154	SQISOFT-001	¹⁹⁰ 0.0921		²⁰¹ 0.1322	¹⁸¹ 0.1781	¹⁷⁶ 0.2348	¹⁸⁷ 0.9271				
155	SYNESIS-003	²⁵ 0.5341		²⁵³ 0.5821	¹⁹ 0.6113	¹⁸⁹ 0.6479	¹⁸³ 0.6822				
156	SYNESIS-003	¹⁶³ 0.0499		¹⁶⁰ 0.0652	¹⁴⁹ 0.0804	¹³⁶ 0.1095	¹²⁹ 0.1916				
157	SYNESIS-005	⁹⁰ 0.0181		⁹¹ 0.0248	⁹² 0.0319	⁹⁴ 0.0518	¹⁰⁶ 0.1580				
158	TECH5-001	¹⁴⁹ 0.0420		¹⁵⁰ 0.0574	¹⁵⁸ 0.0911	¹⁷¹ 0.2106	¹⁷⁸ 0.3725				
159	TECH5-002	¹⁰⁰ 0.0194		⁹⁹ 0.0269	⁹⁸ 0.0346	⁹⁶ 0.0537	¹⁰⁹ 0.1607				
160	TEVIAN-005	¹⁸¹ 0.0692		¹⁷⁸ 0.0873	¹⁶⁵ 0.1066	¹⁴⁹ 0.1301	¹²⁴ 0.1840				
161	TEVIAN-006	⁴⁵ 0.0078		⁴⁰ 0.0098	³⁹ 0.0130	⁴² 0.0261	⁷⁹ 0.1305				
162	TEVIAN-007	²⁹ 0.0038		²⁸ 0.0052	²⁹ 0.0065	²⁵ 0.0154	³³ 0.0957				
163	TIGER-002	¹⁷⁶ 0.0647		¹⁷⁵ 0.0861	¹⁶⁰ 0.1036	¹⁵² 0.1332	¹⁴⁶ 0.2231				
164	TOSHIBA-000	¹⁵⁹ 0.0460		¹⁵⁷ 0.0620	¹⁴⁶ 0.0780	¹³⁹ 0.1117	¹³⁹ 0.2082				
165	TRUEFACE-000	⁷¹ 0.0134		⁷³ 0.0182	⁷⁴ 0.0238	⁷⁰ 0.0380	⁸⁵ 0.1385				
166	VD-001	²² 0.1642		²²¹ 0.2015	¹⁹ 0.2351	¹⁸² 0.2736	¹⁷ 0.3293				
167	VERIDAS-001	¹¹⁴ 0.0278		¹¹⁷ 0.0373	¹¹⁶ 0.0491	¹¹⁶ 0.0753	¹⁰² 0.1541				
168	VERIDAS-002	¹¹⁵ 0.0278		¹¹⁶ 0.0373	¹⁰⁸ 0.0373	⁸⁸ 0.0491	¹⁹ 0.0753				
169	VERIDAS-003	⁶⁵ 0.0117		⁶⁶ 0.0166	⁶⁶ 0.0219	⁸³ 0.0446	¹⁰³ 0.1543				
170	VIGILANTSOLUTIONS-008	⁷⁰ 0.0146		⁷⁹ 0.0205	⁸ 0.0269	⁸⁷ 0.0489	⁶³ 0.1164				
171	VISIONBOX-000	⁶⁶ 0.0122		⁷¹ 0.0177	⁷⁵ 0.0239		¹⁸⁸ 0.9538				
172	VISIONLABS-004	¹⁵² 0.0427		¹⁵¹ 0.0578	¹⁴ 0.0703	¹²⁸ 0.0949	¹²⁵ 0.1853				
173	VISIONLABS-005	¹³⁷ 0.0369		¹³⁵ 0.0502	¹²⁶ 0.0626	¹²⁰ 0.0847	¹²³ 0.1815				
174	VISIONLABS-006	⁹⁰ 0.0188		⁹⁸ 0.0267	⁹⁷ 0.0336	¹⁰¹ 0.0542	⁹³ 0.1478				
175	VISIONLABS-007	⁹⁷ 0.0188		⁹⁷ 0.0266	⁹⁶ 0.0335	⁹⁹ 0.0540	⁹⁴ 0.1479				
176	VISIONLABS-008	⁵³ 0.0096		⁵³ 0.0131	⁵⁸ 0.0166	⁵⁰ 0.0291	²⁰ 0.1247				
177	VISIONLABS-009	²⁴ 0.0034		²³ 0.0046	²⁵ 0.0060	²³ 0.0140	²⁶ 0.0881				
178	VISIONLABS-010	²⁷ 0.0038		²⁷ 0.0051	²⁸ 0.0070	²⁴ 0.0149	²⁹ 0.0920				
179	VISIONLABS-011	⁷ 0.0025		¹⁸ 0.0033	¹⁸ 0.0044	¹⁹ 0.0120	²² 0.0825				
180	VOCORD-005	²⁰⁶ 0.1179		²⁰⁸ 0.1577	¹⁸⁸ 0.2183	¹⁸⁴ 0.3122	¹⁸¹ 0.4490				
181	VTS-001	⁵⁶ 0.0102		⁵⁴ 0.0133	⁵⁶ 0.0175	⁵⁸ 0.0322	⁶⁹ 0.1243				
182	VTS-002	⁹³ 0.0185		⁹⁴ 0.0259	⁹⁸ 0.0344	¹⁰² 0.0549	⁹⁰ 0.1447				
183	XFORWARDAI-000	⁶⁰ 0.0107		⁶² 0.0151	⁶¹ 0.0195	⁶⁰ 0.0324	⁴⁵ 0.1057				
184	XFORWARDAI-001	²⁵ 0.0037		²⁵ 0.0049	²⁴ 0.0060	¹⁸ 0.0120	²¹ 0.0800				
185	XFORWARDAI-002	¹⁸ 0.0026		¹⁷ 0.0030	¹⁸ 0.0035	¹⁴ 0.0078	¹⁵ 0.0706				
186	YITU-002	⁶⁸ 0.0129		⁶⁹ 0.0177	⁶⁹ 0.0228	⁶⁴ 0.0345	⁵⁷ 0.1133				
187	YITU-003	⁷⁶ 0.0138		⁷⁶ 0.0185	⁷⁵ 0.0236	⁶⁵ 0.0353	⁶⁰ 0.1148				
188	YITU-004	⁴¹ 0.0067		³⁸ 0.0096	³⁸ 0.0129	³³ 0.0232	⁴³ 0.1046				
189	YITU-005	⁴⁴ 0.0074		⁴⁴ 0.0101	⁴⁰ 0.0135	⁴⁰ 0.0255	⁴⁶ 0.1057				

Table 18: Identification-mode: Effect of N on FNIR at high threshold. Values are threshold-based miss rates i.e. FNIR at FPIR = 0.001 for five enrollment population sizes, N. The right six columns apply for enrollment of one image. Missing entries usually apply because another algorithm from the same developer was run instead. Some developers are missing because less accurate algorithms were not run on galleries with $N \geq 3\,000\,000$. Throughout blue superscripts indicate the rank of the algorithm for that column.

MISSES AT GIVEN RANK FNIR(N, T = 0, r)		ENROL MOST RECENT																							
#	ALGORITHM	RANK 1					RANK 50																		
		N=0.64M	N=1.6M	N=3.0M	N=6.0M	N=12.0M	aN ^b	N=0.64M	N=1.6M	N=3.0M	N=6.0M	N=12.0M	aN ^b												
1	3DIVI-005	211	0.0137	209	0.0176	179	0.0210	173	0.0253	168	0.0302	136	0.0004 N ^{0.271} 150	193	0.0040	192	0.0049	169	0.0057	165	0.0068	160	0.0081	48	0.0002 N ^{0.240} 155
2	ACER-000	180	0.0081	186	0.0106	167	0.0128	165	0.0157	161	0.0195	60	0.0001 N ^{0.299} 174	139	0.0020	157	0.0026	147	0.0031	147	0.0037	142	0.0045	19	0.0000 N ^{0.284} 168
3	ALCHERA-003	176	0.0079	181	0.0104	167	0.0123	164	0.0147	159	0.0180	88	0.0002 N ^{0.278} 161	174	0.0027	173	0.0032	158	0.0035	158	0.0042	143	0.0048	58	0.0002 N ^{0.199} 145
4	ALLGOVISION-000	194	0.0101	191	0.0114	166	0.0127	163	0.0145	158	0.0166	166	0.0010 N ^{0.171} 89	212	0.0063	208	0.0067	174	0.0071	168	0.0075	159	0.0081	172	0.0020 N ^{0.086} 103
5	ALLGOVISION-001	168	0.0069	174	0.0096	166	0.0107	158	0.0128	159	0.0157	74	0.0002 N ^{0.277} 159	161	0.0023	162	0.0027	148	0.0031	146	0.0036	139	0.0043	41	0.0001 N ^{0.211} 150
6	ANKE-000	197	0.0102	190	0.0132	173	0.0155	170	0.0188	167	0.0225	119	0.0003 N ^{0.270} 149	183	0.0032	185	0.0040	165	0.0046	158	0.0056	151	0.0066	40	0.0001 N ^{0.247} 157
7	ANKE-002	102	0.0024	103	0.0028	103	0.0032	99	0.0037	94	0.0043	68	0.0002 N ^{0.203} 104	113	0.0016	113	0.0017	105	0.0017	98	0.0018	93	0.0019	103	0.0006 N ^{0.167} 91
8	AWARE-003	228	0.0238	226	0.0306	196	0.0361	184	0.0431	181	0.0506	163	0.0008 N ^{0.258} 144	206	0.0055	214	0.0075	184	0.0092	179	0.0113	178	0.0143	39	0.0001 N ^{0.323} 178
9	AWARE-005	229	0.0245	227	0.0311	191	0.0366	185	0.0434	172	0.0312	182	0.0056 N ^{0.118} 49	210	0.0062	220	0.0082	186	0.0101	182	0.0128	162	0.0089	125	0.0007 N ^{0.169} 140
10	AYONIX-002	263	0.2935	267	0.3414	201	0.3736	193	0.4101	187	0.4465	187	0.0440 N ^{0.143} 63	262	0.0590	264	0.1274	201	0.1524	193	0.1828	186	0.2150	177	0.0233 N ^{0.29} 166
11	CAMVI-004	204	0.0124	226	0.0468	198	0.0719	192	0.2363	186	0.2367	34	0.0000 N ^{0.155} 188	235	0.0117	197	0.0715	183	0.2361	187	0.2364	3	0.0000 N ^{0.107} 188		
12	CANON-001	13	0.0011	12	0.0011	12	0.0012	14	0.0013	12	0.0014	100	0.0002 N ^{0.113} 42	17	0.0009	16	0.0009	19	0.0009	15	0.0010	102	0.0006 N ^{0.26} 42		
13	CIB-000	39	0.0014	37	0.0015	36	0.0017	39	0.0019	44	0.0131	4	0.0000 N ^{0.635} 187	50	0.0012	45	0.0012	43	0.0012	42	0.0012	174	0.0122	4	0.0000 N ^{0.647} 187
14	CLEARVIEWAI-000	10	0.0010	11	0.0011	15	0.0012	15	0.0013	15	0.0015	79	0.0002 N ^{0.129} 56	19	0.0009	15	0.0009	15	0.0009	14	0.0010	116	0.0007 N ^{0.119} 33		
15	CLOUDWALK-HR-000	44	0.0015	43	0.0015	38	0.0015	25	0.0016	20	0.0017	159	0.0007 N ^{0.054} 10	99	0.0014	86	0.0014	76	0.0014	70	0.0014	53	0.0012 N ^{0.012} 14		
16	CLOUDWALK-MT-000	70	0.0018	52	0.0018	48	0.0018	35	0.0019	29	0.0020	167	0.0011 N ^{0.058} 5	126	0.0018	121	0.0018	110	0.0018	89	0.0018	169	0.0017 N ^{0.002} 4		
17	COGENT-000	195	0.0101	184	0.0105	161	0.0109	154	0.0115	146	0.0125	180	0.0038 N ^{0.071} 16	149	0.0021	151	0.0024	142	0.0028	145	0.0036	165	0.0095	9	0.0000 N ^{0.466} 183
18	COGENT-001	196	0.0101	188	0.0105	162	0.0109	153	0.0115	147	0.0125	170	0.0038 N ^{0.071} 17	150	0.0021	180	0.0024	145	0.0028	144	0.0036	166	0.0095	8	0.0000 N ^{0.466} 184
19	COGENT-002	115	0.0029	118	0.0036	116	0.0041	114	0.0049	110	0.0059	42	0.0001 N ^{0.244} 136	96	0.0014	104	0.0015	100	0.0017	102	0.0021	53	0.0002 N ^{0.144} 134		
20	COGENT-003	121	0.0031	120	0.0034	121	0.0043	117	0.0051	117	0.0060	56	0.0001 N ^{0.230} 126	107	0.0015	114	0.0017	118	0.0018	110	0.0020	56	0.0002 N ^{0.143} 133		
21	COGENT-004	71	0.0018	70	0.0020	68	0.0022	66	0.0025	59	0.0028	94	0.0002 N ^{0.159} 78	89	0.0013	83	0.0014	81	0.0014	74	0.0015	64	0.0015	110	0.0007 N ^{0.050} 72
22	COGENT-005	51	0.0016	47	0.0017	46	0.0018	43	0.0020	37	0.0021	138	0.0004 N ^{0.108} 37	90	0.0013	78	0.0013	61	0.0014	52	0.0014	157	0.0017 N ^{0.017} 26		
23	COGNITEC-000	222	0.0252	187	0.0297	182	0.0352	176	0.0417	156	0.0606 N ^{0.259} 148	202	0.0050	206	0.0065	181	0.0077	178	0.0097	173	0.0122	37	0.0001 N ^{0.305} 172		
24	COGNITEC-001	190	0.0090	191	0.0117	172	0.0139	168	0.0166	167	0.0199	110	0.0002 N ^{0.271} 152	179	0.0030	178	0.0034	162	0.0040	157	0.0046	51	0.0002 N ^{0.207} 149		
25	COGNITEC-002	150	0.0048	148	0.0057	146	0.0067	134	0.0079	131	0.0094	96	0.0002 N ^{0.232} 128	163	0.0024	159	0.0026	145	0.0028	139	0.0030	87	0.0005 N ^{0.117} 120		
26	COGNITEC-003	153	0.0053	152	0.0062	143	0.0072	140	0.0085	136	0.0100	130	0.0003 N ^{0.222} 117	176	0.0028	170	0.0030	150	0.0034	140	0.0037	132	0.0008 N ^{0.097} 111		
27	COGNITEC-004	110	0.0027	111	0.0032	107	0.0047	107	0.0056	92	0.0031	32	0.0001 N ^{0.233} 142	87	0.0013	87	0.0014	88	0.0015	81	0.0017	62	0.0002 N ^{0.123} 125		
28	COGNITEC-005	41	0.0014	44	0.0016	49	0.0018	46	0.0021	47	0.0024	61	0.0001 N ^{0.169} 86	41	0.0011	42	0.0011	39	0.0012	31	0.0012	108	0.0007 N ^{0.037} 94		
29	COGNITEC-006	36	0.0014	36	0.0017	37	0.0022	36	0.0022	77	0.0002 N ^{0.154} 70	43	0.0011	40	0.0011	38	0.0012	36	0.0012	30	0.0007 N ^{0.036} 53				
30	CYBERLINK-000	127	0.0034	124	0.0046	120	0.0054	118	0.0063	90	0.0002 N ^{0.209} 110	146	0.0021	141	0.0022	134	0.0023	130	0.0025	121	0.0027	99	0.0006 N ^{0.092} 108		
31	CYBERLINK-001	118	0.0030	118	0.0035	118	0.0042	116	0.0050	112	0.0060	43	0.0001 N ^{0.243} 135	115	0.0016	120	0.0017	111	0.0018	108	0.0020	105	0.0022	78	0.0004 N ^{0.109} 115
32	CYBERLINK-002	103	0.0024	96	0.0028	88	0.0031	79	0.0035	130	0.0005 N ^{0.121} 50	142	0.0020	136	0.0021	129	0.0022	122	0.0022	107	0.0022	160	0.0012 N ^{0.036} 52		
33	CYBERLINK-003	42	0.0015	41	0.0016	39	0.0017	32	0.0018	29	0.0020	124	0.0003 N ^{0.110} 39	46	0.0011	44	0.0012	42	0.0012	36	0.0013	35	0.0008 N ^{0.047} 68		
34	CYBERLINK-004	35	0.0016	44	0.0017	44	0.0018	36	0.0019	35	0.0021	135	0.0005 N ^{0.088} 27	97	0.0014	99	0.0015	78	0.0014	71	0.0015	154	0.0010 N ^{0.022} 36		
35	CYBERLINK-005	64	0.0017	56	0.0018	51	0.0019	48	0.0021	42	0.0023	143	0.0004 N ^{0.099} 34	102	0.0014	90	0.0015	86	0.0015	77	0.0015	144	0.0009 N ^{0.132} 50		
36	DAHUA-001	154	0.0053	154	0.0067	147	0.0079	145	0.0093	140	0.0112	76	0.0002 N ^{0.256} 143	173	0.0027	165	0.0029	149	0.0031	139	0.0038	92	0.0005 N ^{0.121} 123		
37	DAHUA-002	62	0.0017	61	0.0018	62	0.0021	57	0.0023	53	0.0027	89	0.0002 N ^{0.156} 72	80	0.0013	75	0.0013	73	0.0014	58	0.0015	121	0.0007 N ^{0.043} 65		
38	DAHUA-003	12	0.0010	19	0.0012	21	0.0014	21	0.0016	25	0.0018	23	0.0001 N ^{0.199} 101	13	0.0009	11	0.0009	10	0.0009	11	0.0009	97	0.0006 N ^{0.027} 43		
39	DAHUA-004	11	0.0010	10	0.0012	10	0.0013	13	0.0014	10	0.0015	100	0.0002 N ^{0.113} 45	15	0.0009	14	0.0009	12	0.0009	14	0.0009	105	0.0006 N ^{0.023} 37		
40	DAON-000	138	0.0039	128	0.0041	118	0.0043																		

MISSES AT GIVEN RANK			ENROL MOST RECENT											
#	ALGORITHM	FNIR(N, T= 0, R)	RANK 1					aN^b	RANK 50					aN^b
			N=0.64M	N=1.6M	N=3.0M	N=6.0M	N=12.0M		N=0.64M	N=1.6M	N=3.0M	N=6.0M	N=12.0M	
73	INTSYSMU-000	²⁵⁵ 0.1395	²⁵⁵ 0.1457	¹⁹⁷ 0.1498	¹⁸⁹ 0.1544	¹⁸³ 0.1591	¹⁸⁹ 0.0768 N ^{0.045} 7	²⁶⁴ 0.1098	²⁶² 0.1163	²⁰⁰ 0.1206	¹⁹¹ 0.1252	¹⁸⁵ 0.1296	¹⁸⁹ 0.0519 N ^{0.056} 79	
74	IREX-000	¹⁴² 0.0043	¹³¹ 0.0044	¹²² 0.0044	¹¹⁰ 0.0046	¹⁰¹ 0.0048	¹⁷⁶ 0.0028 N ^{0.032} 4	¹⁹⁷ 0.0043	¹⁸⁸ 0.0043	¹⁶³ 0.0043	¹⁵³ 0.0043	¹³⁸ 0.0043	¹⁷⁹ 0.0042 N ^{0.002} 5	
75	ISYSTEMS-002	¹⁵⁵ 0.0053	¹⁵⁴ 0.0064	¹⁴⁶ 0.0072	¹³⁸ 0.0083	¹³² 0.0096	¹³² 0.0003 N ^{0.204} 108	¹⁸¹ 0.0033	¹⁷⁹ 0.0034	¹⁴⁸ 0.0036	¹⁴⁸ 0.0038	¹³⁶ 0.0041	¹⁶¹ 0.0013 N ^{0.017} 93	
76	ISYSTEMS-003	¹⁴⁶ 0.0046	¹⁴² 0.0052	¹³³ 0.0057	¹²⁸ 0.0066	¹²² 0.0076	¹⁴² 0.0004 N ^{0.174} 91	¹⁸¹ 0.0031	¹⁷⁵ 0.0033	¹⁵¹ 0.0034	¹⁴¹ 0.0035	¹³⁴ 0.0037	¹⁶² 0.0013 N ^{0.063} 87	
77	KAKAO-000	²⁶ 0.0013	³² 0.0015	³⁶ 0.0016	³⁸ 0.0019	⁴¹ 0.0022	³⁶ 0.0001 N ^{0.192} 100	²⁵ 0.0009	²² 0.0010	²¹ 0.0010	²² 0.0011	⁸³ 0.0005 N ^{0.050} 73		
78	KEDACOM-001	¹⁷³ 0.0076	¹⁶⁴ 0.0077	¹⁴⁹ 0.0079	¹³⁷ 0.0083	¹²⁷ 0.0087	¹⁸¹ 0.0040 N ^{0.047} 8	²¹⁶ 0.0071	²¹⁰ 0.0072	¹⁷⁸ 0.0072	¹⁶⁶ 0.0073	¹⁵³ 0.0073	¹⁸⁴ 0.0063 N ^{0.009} 12	
79	KNERON-000	¹⁴⁹ 0.0048	¹⁴⁹ 0.0059	¹⁴⁰ 0.0067	¹³⁵ 0.0079	¹³² 0.0093	¹⁰⁸ 0.0002 N ^{0.226} 122	¹⁹⁷ 0.0048	²⁰¹ 0.0059	¹⁷³ 0.0067	¹⁷¹ 0.0079	¹⁶⁴ 0.0093	⁶¹ 0.0002 N ^{0.265} 133	
80	LOOKMAN-003	¹⁸³ 0.0083	¹⁷³ 0.0088	¹⁵⁶ 0.0091	¹⁴⁸ 0.0096	¹³⁸ 0.0104	¹⁷⁷ 0.0030 N ^{0.076} 19	²²⁰ 0.0072	²¹³ 0.0074	¹⁸⁰ 0.0075	¹⁶⁹ 0.0076	¹⁵⁷ 0.0077	¹⁸² 0.0054 N ^{0.022} 35	
81	LOOKMAN-005	¹⁷⁵ 0.0078	¹⁶⁷ 0.0080	¹⁵¹ 0.0083	¹⁴¹ 0.0086	¹³⁰ 0.0092	¹⁷⁸ 0.0038 N ^{0.035} 9	²¹⁶ 0.0072	²¹¹ 0.0072	¹⁷⁹ 0.0073	¹⁶⁶ 0.0073	¹⁵⁴ 0.0074	¹⁸³ 0.0060 N ^{0.013} 19	
82	MANTRA-000	⁴⁸ 0.0015	⁸⁰ 0.0017	⁹² 0.0019	⁹² 0.0022	⁹⁰ 0.0025	⁶⁴ 0.0002 N ^{0.171} 88	⁵⁷ 0.0012	⁴⁹ 0.0012	⁴⁸ 0.0012	³⁹ 0.0013	¹⁰⁷ 0.0007 N ^{0.042} 62		
83	MEGVII-001	¹⁹⁹ 0.0105	¹⁹⁴ 0.0118	¹⁶¹ 0.0128	¹⁶¹ 0.0142	¹⁵⁰ 0.0161	¹⁷² 0.0015 N ^{0.143} 64	²²² 0.0077	²¹⁹ 0.0080	¹⁸² 0.0082	¹⁷⁶ 0.0086	¹⁷⁸ 0.0040 N ^{0.048} 70		
84	MICROFOCUS-005	²⁶⁶ 0.3700	²⁶⁶ 0.4242	²⁰² 0.4610	¹⁹¹ 0.5000	¹⁸⁸ 0.5391	¹⁸⁸ 0.0674 N ^{0.128} 55	²⁶ 0.1300	²⁶⁷ 0.1724	²⁰² 0.2046	¹⁹⁴ 0.2425	¹⁸⁸ 0.2810	¹⁷⁷ 0.0040 N ^{0.265} 163	
85	MICROSOFT-003	²⁴ 0.0013	⁴² 0.0016	⁴⁸ 0.0018	⁵⁶ 0.0022	⁵⁶ 0.0028	¹⁴ 0.0000 N ^{0.271} 153	² 0.0006	² 0.0006	⁴ 0.0007	⁸ 0.0008	²⁸ 0.0001 N ^{0.158} 139		
86	MICROSOFT-004	²³ 0.0012	³⁴ 0.0015	⁴² 0.0018	⁵¹ 0.0021	⁵⁶ 0.0028	¹³ 0.0000 N ^{0.281} 162	¹ 0.0006	¹ 0.0006	¹ 0.0007	¹ 0.0007	³⁸ 0.0001 N ^{0.139} 131		
87	MICROSOFT-005	⁴⁶ 0.0015	⁶³ 0.0019	⁷¹ 0.0023	⁸⁴ 0.0030	⁸⁴ 0.0037	⁷⁰ 0.0000 N ^{0.320} 179	³ 0.0006	³ 0.0006	⁷ 0.0008	⁶ 0.0009	³⁹ 0.0001 N ^{0.136} 130		
88	MICROSOFT-006	⁵⁰ 0.0016	⁶⁹ 0.0020	⁸¹ 0.0025	⁸⁸ 0.0030	⁸⁸ 0.0038	¹² 0.0000 N ^{0.305} 175	⁴ 0.0006	⁴ 0.0007	³ 0.0007	⁸ 0.0009	²² 0.0000 N ^{0.184} 142		
89	NEC-000	²⁰⁷ 0.0131	²⁰⁷ 0.0170	¹⁷⁸ 0.0203	¹⁷² 0.0244	¹⁶⁷ 0.0294	¹²⁸ 0.0003 N ^{0.276} 158	¹⁷⁸ 0.0029	¹⁸⁴ 0.0038	¹⁶⁶ 0.0048	¹⁶¹ 0.0059	¹⁵⁵ 0.0074	¹⁶ 0.0000 N ^{0.319} 176	
90	NEC-001	²¹⁹ 0.0180	²¹⁶ 0.0209	¹⁸² 0.0233	¹⁷⁶ 0.0266	¹⁶⁹ 0.0304	¹⁷³ 0.0016 N ^{0.179} 93	²²⁶ 0.0109	²²⁶ 0.0113	¹⁸⁷ 0.0116	¹⁸⁰ 0.0121	¹⁷⁵ 0.0129	¹⁸¹ 0.0051 N ^{0.056} 77	
91	NEC-002	⁴ 0.0009	⁸ 0.0010	⁷ 0.0012	⁶ 0.0013	⁹² 0.0002 N ^{0.113} 44	⁵ 0.0008	⁵ 0.0008	⁴ 0.0008	⁴ 0.0008	⁸² 0.0005 N ^{0.038} 56			
92	NEC-003	²⁸ 0.0013	²³ 0.0014	²³ 0.0015	²⁵ 0.0016	¹⁹ 0.0016	¹⁴⁴ 0.0005 N ^{0.079} 21	⁵⁴ 0.0012	⁴⁷ 0.0012	⁴⁵ 0.0012	⁴⁰ 0.0012	¹⁴³ 0.0009 N ^{0.019} 32		
93	NEC-004	³⁴ 0.0014	²⁹ 0.0014	²⁵ 0.0015	²¹ 0.0016	¹⁸ 0.0017	¹⁵⁵ 0.0006 N ^{0.059} 12	⁷⁷ 0.0013	⁶⁵ 0.0013	⁶¹ 0.0013	⁵⁸ 0.0013	¹⁵³ 0.0010 N ^{0.016} 24		
94	NEC-005	²¹ 0.0011	¹⁷ 0.0012	¹⁷ 0.0013	¹² 0.0013	¹⁰ 0.0014	¹⁴⁵ 0.0005 N ^{0.065} 14	³⁶ 0.0011	³⁵ 0.0011	³⁰ 0.0011	²⁸ 0.0011	¹⁴² 0.0009 N ^{0.013} 18		
95	NEUROTECHNOLOGY-003	²¹⁸ 0.0179	²¹⁷ 0.0225	¹⁸⁴ 0.0263	¹⁷³ 0.0306	¹⁷⁴ 0.0361	¹⁶² 0.0007 N ^{0.239} 134	¹⁹⁶ 0.0042	²⁰⁰ 0.0057	¹⁷⁷ 0.0072	¹⁷² 0.0090	¹⁷² 0.0012	²¹ 0.0000 N ^{0.334} 179	
96	NEUROTECHNOLOGY-004	¹⁴⁷ 0.0046	¹⁴⁴ 0.0056	¹³⁵ 0.0074	¹²⁸ 0.0088	¹¹¹ 0.0092	¹⁵² 0.0002 N ^{0.220} 116	¹⁵⁷ 0.0022	¹⁵² 0.0025	¹⁴⁴ 0.0028	¹³⁸ 0.0031	¹²⁹ 0.0034	⁶⁵ 0.0003 N ^{0.154} 136	
97	NEUROTECHNOLOGY-005	¹³¹ 0.0035	¹²⁹ 0.0043	¹²⁷ 0.0049	¹²² 0.0057	¹¹⁷ 0.0068	⁸⁹ 0.0002 N ^{0.223} 119	¹⁴⁸ 0.0021	¹⁴⁶ 0.0023	¹³⁶ 0.0024	¹³¹ 0.0025	¹²³ 0.0028	¹⁰⁰ 0.0006 N ^{0.092} 109	
98	NEUROTECHNOLOGY-007	¹²⁴ 0.0032	¹²¹ 0.0039	¹²³ 0.0044	¹¹⁸ 0.0052	¹¹⁴ 0.0062	⁷⁰ 0.0002 N ^{0.222} 118	¹⁴³ 0.0020	¹³⁹ 0.0022	¹³³ 0.0023	¹²⁵ 0.0024	¹¹⁶ 0.0026	¹²⁴ 0.0007 N ^{0.076} 97	
99	NEUROTECHNOLOGY-008	⁷⁵ 0.0019	⁷⁸ 0.0022	⁷⁰ 0.0025	⁸⁰ 0.0029	⁷⁹ 0.0034	⁴⁴ 0.0001 N ^{0.205} 108	⁸⁴ 0.0013	⁷³ 0.0013	⁶⁹ 0.0013	⁶⁴ 0.0014	⁵⁷ 0.0015	¹²² 0.0007 N ^{0.043} 63	
100	NEUROTECHNOLOGY-009	²⁹ 0.0013	³⁰ 0.0014	³² 0.0016	³³ 0.0018	³³ 0.0021	⁵⁹ 0.0001 N ^{0.162} 80	³⁹ 0.0011	³⁷ 0.0011	³⁵ 0.0011	³¹ 0.0012	²⁸ 0.0012	¹²⁸ 0.0007 N ^{0.029} 47	
101	NEUROTECHNOLOGY-010	²⁰ 0.0011	²⁰ 0.0012	¹⁷ 0.0013	¹⁶ 0.0015	¹⁰ 0.0016	⁹⁵ 0.0002 N ^{0.125} 83	³¹ 0.0010	³⁰ 0.0010	²² 0.0010	²¹ 0.0010	¹⁹ 0.0011	¹³⁶ 0.0008 N ^{0.014} 20	
102	NOTIONTAG-000	¹⁰⁰ 0.0023	⁹² 0.0024	⁸⁶ 0.0026	⁷⁸ 0.0029	⁷⁰ 0.0032	¹⁴⁵ 0.0005 N ^{0.117} 47	¹⁵⁶ 0.0019	¹⁵² 0.0019	¹²⁷ 0.0020	¹¹⁵ 0.0020	¹⁰¹ 0.0021	¹⁶³ 0.0013 N ^{0.027} 44	
103	NTechLab-003	¹⁴⁸ 0.0046	¹⁵⁰ 0.0062	¹⁴⁶ 0.0076	¹⁴⁷ 0.0094	¹⁴⁴ 0.0114	²⁵ 0.0001 N ^{0.310} 176	⁸³ 0.0013	¹⁰⁷ 0.0016	¹¹⁷ 0.0018	¹²⁰ 0.0022	¹¹⁷ 0.0026	²⁴ 0.0001 N ^{0.237} 154	
104	NTechLab-004	¹³⁴ 0.0037	¹³⁸ 0.0048	¹³⁴ 0.0058	¹³⁰ 0.0071	¹²⁶ 0.0085	²⁷ 0.0001 N ^{0.291} 167	⁴⁷ 0.0011	⁴⁷ 0.0011	⁴⁷ 0.0012	⁴⁹ 0.0012	⁴⁴ 0.0012	³⁴ 0.0001 N ^{0.198} 144	
105	NTechLab-005	¹²⁸ 0.0035	¹³⁶ 0.0047	¹³⁰ 0.0054	¹²⁷ 0.0073	¹²⁰ 0.0092	¹⁶ 0.0000 N ^{0.334} 182	¹⁸ 0.0008	³³ 0.0011	⁴⁷ 0.0012	⁴⁸ 0.0015	⁴⁰ 0.0016	³² 0.0007 N ^{0.285} 167	
106	NTechLab-006	¹¹⁷ 0.0030	¹²⁶ 0.0041	¹²⁵ 0.0050	¹²² 0.0062	¹²² 0.0078	⁶³ 0.0000 N ^{0.228} 181	¹²⁴ 0.0017	¹³¹ 0.0019	¹²⁸ 0.0021	¹²⁶ 0.0024	¹¹⁸ 0.0027	³⁷ 0.0002 N ^{0.154} 137	
107	PIXELALL-002	¹³⁶ 0.0037	¹³³ 0.0045	¹³⁰ 0.0052	¹²⁶ 0.0062	¹²⁷ 0.0075	⁶³ 0.0002 N ^{0.228} 132	¹²⁴ 0.0017	¹³¹ 0.0019	¹²⁸ 0.0021	¹²⁵ 0.0024	¹¹⁸ 0.0027	³⁷ 0.0002 N ^{0.154} 137	
108	PIXELALL-003	⁷⁷ 0.0019	⁷⁷ 0.0021	⁷⁶ 0.0024	⁷⁴ 0.0028	⁷² 0.0032	⁷ 0.0002 N ^{0.182} 95	⁹¹ 0.0014	⁸⁸ 0.0014	⁸⁰ 0.0014	⁷⁶ 0.0015	⁷⁰ 0.0016	¹³⁰ 0.0007 N ^{0.045} 66	
109	PIXELALL-004	⁶³ 0.0017	⁷⁴ 0.0020	⁷⁰ 0.0023	⁶⁹ 0.0026	⁶⁵ 0.0030	⁸³ 0.0001 N ^{0.192} 99	⁷⁹ 0.0013	⁷⁹ 0.0013	⁷⁴ 0.0014	⁶⁹ 0.0014	⁶⁰ 0.0015	¹¹² 0.0007 N ^{0.046} 67	
110	PIXELALL-005	⁶⁸ 0.0018	⁶⁴ 0.0019	⁵⁶ 0.0020	⁵⁰ 0.0021	⁴⁶ 0.0024	¹⁴⁸ 0.0005 N ^{0.098} 33	¹¹⁰ 0.0015	¹⁰⁶ 0.0016	⁹⁶ 0.0016	⁸⁴ 0.0016	⁷⁴ 0.0016	¹⁵⁸ 0.0012 N ^{0.018} 28	
111	PTAKURATSATU-000	¹⁰⁵ 0.0025	¹⁰⁷ 0.0											

MISSES AT GIVEN RANK		ENROL MOST RECENT											
FNIR(N, T = 0, R)		RANK 1					RANK 50						
#	ALGORITHM	N=0.64M	N=1.6M	N=3.0M	N=6.0M	N=12.0M	aN ^b	N=0.64M	N=1.6M	N=3.0M	N=6.0M	N=12.0M	aN ^b
145	SENSETIME-001	⁹⁰ 0.0022	⁸⁶ 0.0023	⁸² 0.0025	⁸¹ 0.0029	⁸³ 0.0037	⁸⁶ 0.0002 N ^{0.177} 92	¹¹⁸ 0.0016	¹⁰⁸ 0.0016	¹⁰³ 0.0017	⁹⁷ 0.0018	¹¹² 0.0024	⁶⁶ 0.0003 N ^{0.125} 126
146	SENSETIME-002	²¹⁰ 0.0136	²⁰¹ 0.0137	¹⁷¹ 0.0137	¹⁶¹ 0.0138	¹⁵⁰ 0.0139	¹⁸³ 0.0124 N ^{0.007} 2	²³⁹ 0.0136	²³² 0.0136	¹⁸⁹ 0.0136	¹⁸³ 0.0136	¹⁷⁷ 0.0136	¹⁸⁸ 0.0135 N ^{0.001} 3
147	SENSETIME-003	⁶ 0.0010	⁵ 0.0010	⁵ 0.0010	⁵ 0.0011	⁵ 0.0012	¹²³ 0.0003 N ^{0.085} 26	²² 0.0009	²⁰ 0.0009	¹⁸ 0.0009	¹⁷ 0.0010	¹³ 0.0010	¹³³ 0.0008 N ^{0.013} 16
148	SENSETIME-004	⁵ 0.0010	⁴ 0.0010	⁴ 0.0010	⁴ 0.0011	⁴ 0.0012	¹²⁵ 0.0003 N ^{0.081} 22	¹¹ 0.0008	⁹ 0.0009	⁹ 0.0009	⁹ 0.0009	⁷ 0.0009	¹⁰⁶ 0.0007 N ^{0.018} 31
149	SENSETIME-005	³ 0.0008	³ 0.0009	³ 0.0009	³ 0.0010	³ 0.0011	¹¹⁴ 0.0003 N ^{0.085} 25	⁷ 0.0008	⁶ 0.0008	⁶ 0.0008	⁵ 0.0008	⁵ 0.0008	¹³⁵ 0.0008 N ^{0.002} 6
150	SENSETIME-006	² 0.0008	² 0.0009	² 0.0009	² 0.0010	² 0.0010	¹² 0.0003 N ^{0.069} 15	⁸ 0.0008	⁷ 0.0008	⁷ 0.0008	⁸ 0.0008	⁵ 0.0008	¹¹⁷ 0.0007 N ^{0.011} 13
151	SENSETIME-007	¹ 0.0008	¹ 0.0008	¹ 0.0009	¹ 0.0009	¹ 0.0010	¹³⁴ 0.0004 N ^{0.061} 13	⁷ 0.0008	⁸ 0.0008	⁸ 0.0008	⁵ 0.0008	² 0.0008	¹²⁸ 0.0007 N ^{0.008} 11
152	SHAMAN-007	²³⁷ 0.0371	²³⁰ 0.0396	¹⁹² 0.0416	¹⁸⁶ 0.0443	¹⁸⁰ 0.0473	¹⁸⁴ 0.0122 N ^{0.083} 23	²⁵² 0.0308	²⁴⁶ 0.0314	¹⁹⁵ 0.0319	¹⁸⁷ 0.0326	¹⁸¹ 0.0337	¹⁸⁷ 0.0207 N ^{0.029} 48
153	SIAT-001	⁵⁸ 0.0017	⁵⁵ 0.0018	⁵⁸ 0.0020	⁵⁹ 0.0023	⁵⁵ 0.0027	⁶⁷ 0.0002 N ^{0.173} 90	³⁸ 0.0010	³⁸ 0.0011	⁴⁰ 0.0012	⁴³ 0.0013	⁴¹ 0.0013	⁷⁰ 0.0003 N ^{0.085} 102
154	SIAT-002	⁵⁷ 0.0016	⁵⁸ 0.0018	⁶⁰ 0.0020	⁵⁸ 0.0023	⁵² 0.0027	⁶⁹ 0.0002 N ^{0.171} 87	⁴⁷ 0.0011	⁵² 0.0012	⁵³ 0.0013	⁵¹ 0.0013	⁴⁹ 0.0014	⁸⁹ 0.0005 N ^{0.062} 86
155	SQISOFT-001	¹¹³ 0.0028	¹²⁸ 0.0042	¹³⁶ 0.0059	¹³⁹ 0.0084	¹⁸⁹ 0.9207	² 0.0000 N ^{1.674} 189	²⁹ 0.0010	³² 0.0010	³³ 0.0011	³⁸ 0.0012	¹⁸⁹ 0.9198	² 0.0000 N ^{0.883} 189
156	SYNEIS-003	²⁵⁶ 0.1456	²⁵⁶ 0.1700	¹⁸⁶ 0.1876	¹⁹⁶ 0.2088	¹⁸⁵ 0.2317	¹⁸⁶ 0.0177 N ^{0.158} 76	²⁵⁸ 0.0828	¹⁹⁶ 0.0869	¹⁹⁶ 0.0920	¹⁸⁹ 0.0998	¹⁸³ 0.1104	¹⁸⁸ 0.0218 N ^{0.098} 112
157	SYNEIS-003	²¹⁶ 0.0161	²⁰⁵ 0.0162	¹⁷⁶ 0.0163	¹⁶⁷ 0.0165	¹⁶⁶ 0.0254	¹⁷⁵ 0.0027 N ^{0.127} 34	²⁴² 0.0160	²³⁷ 0.0160	¹⁹¹ 0.0160	¹⁸⁵ 0.0160	¹⁸⁰ 0.0245	¹⁴⁸ 0.0009 N ^{0.192} 143
158	SYNEIS-005	¹⁸⁵ 0.0085	¹⁷¹ 0.0085	¹⁵⁴ 0.0085	¹⁴² 0.0086	¹²⁹ 0.0088	¹⁸³ 0.0072 N ^{0.012} 3	²²⁶ 0.0085	²²¹ 0.0085	¹⁸³ 0.0085	¹⁷³ 0.0085	¹⁶¹ 0.0085	¹⁸⁵ 0.0085 N ^{0.000} 2
159	TECH5-001	¹²³ 0.0032	¹²³ 0.0040	¹²⁶ 0.0047	¹²¹ 0.0057	¹¹⁷ 0.0071	³⁶ 0.0001 N ^{0.271} 151	¹¹⁷ 0.0016	¹¹⁵ 0.0017	¹¹⁵ 0.0018	¹⁰⁷ 0.0020	¹⁰⁹ 0.0023	⁶⁸ 0.0003 N ^{0.119} 121
160	TECH5-002	⁸⁴ 0.0020	⁹⁸ 0.0027	¹⁰¹ 0.0031	⁹⁷ 0.0037	⁹⁷ 0.0047	¹⁷ 0.0000 N ^{0.285} 165	¹⁸ 0.0009	²⁴ 0.0010	³¹ 0.0011	³³ 0.0012	⁴⁰ 0.0013	⁴⁹ 0.0002 N ^{0.122} 128
161	TEVIAN-005	¹⁶⁰ 0.0056	¹⁶² 0.0073	¹⁵³ 0.0084	¹⁵⁰ 0.0105	¹⁴⁸ 0.0130	⁵⁶ 0.0001 N ^{0.283} 164	¹⁴⁶ 0.0020	¹⁴⁵ 0.0023	¹⁴⁶ 0.0025	¹³⁴ 0.0028	¹²⁷ 0.0034	⁸⁰ 0.0002 N ^{0.178} 141
162	TEVIAN-006	⁹⁹ 0.0023	⁹⁰ 0.0024	⁸⁸ 0.0026	⁷⁴ 0.0028	⁶⁸ 0.0031	¹⁵³ 0.0005 N ^{0.106} 36	¹¹⁴ 0.0016	¹¹⁰ 0.0017	¹⁰² 0.0017	⁹² 0.0017	⁸² 0.0018	¹⁴⁵ 0.0009 N ^{0.041} 60
163	TEVIAN-007	⁶⁵ 0.0017	⁵⁴ 0.0018	⁴⁷ 0.0018	⁴⁰ 0.0020	³⁶ 0.0021	¹⁵⁷ 0.0006 N ^{0.073} 18	⁷⁰ 0.0013	⁶⁰ 0.0013	⁵³ 0.0013	⁴⁶ 0.0013	⁴⁰ 0.0009 N ^{0.026} 41	
164	TIGER-002	¹⁴³ 0.0044	¹⁴⁶ 0.0056	¹⁴² 0.0068	¹⁴⁸ 0.0086	¹⁵⁹ 0.0105	²⁸ 0.0001 N ^{0.299} 173	⁷⁶ 0.0013	⁹⁸ 0.0015	¹⁰⁹ 0.0018	¹¹⁸ 0.0021	¹¹⁹ 0.0027	¹⁸ 0.0000 N ^{0.253} 159
165	TOSHIBA-000	¹³⁰ 0.0035	¹³² 0.0045	¹³¹ 0.0052	¹²² 0.0061	¹³⁹ 0.0154	⁸ 0.0000 N ^{0.449} 185	¹¹⁵ 0.0016	¹²⁴ 0.0018	¹²⁰ 0.0019	¹²¹ 0.0021	¹⁷¹ 0.0105	⁵ 0.0000 N ^{0.539} 186
166	TRUEFACE-000	¹²⁰ 0.0031	¹¹² 0.0033	¹⁰⁸ 0.0035	¹⁰¹ 0.0039	⁹³ 0.0043	¹⁵⁸ 0.0006 N ^{0.115} 46	¹⁸⁸ 0.0025	¹⁵⁵ 0.0026	¹⁴¹ 0.0026	¹⁵³ 0.0027	¹²⁴ 0.0028	¹⁶⁶ 0.0015 N ^{0.038} 57
167	VD-001	²²⁷ 0.0230	²²⁴ 0.0276	¹⁸⁶ 0.0315	¹⁸³ 0.0363	¹⁷⁷ 0.0418	¹⁷¹ 0.0015 N ^{0.204} 107	²³⁰ 0.0120	²³¹ 0.0130	¹⁹⁰ 0.0140	¹⁸⁴ 0.0154	¹⁷⁹ 0.0170	¹⁷⁵ 0.0024 N ^{0.120} 122
168	VERIDAS-001	⁹⁸ 0.0023	¹⁰¹ 0.0028	¹⁰² 0.0032	¹⁰⁰ 0.0037	⁹⁷ 0.0045	³⁹ 0.0001 N ^{0.231} 127	¹⁰¹ 0.0014	⁹⁵ 0.0015	⁹⁰ 0.0015	⁸⁷ 0.0016	⁸¹ 0.0018	⁸¹ 0.0005 N ^{0.083} 101
169	VERIDAS-002	⁹⁷ 0.0023	¹⁰⁰ 0.0028	⁹² 0.0028	⁸⁹ 0.0032	⁸⁸ 0.0037	¹¹⁸ 0.0003 N ^{0.158} 74	⁹⁶ 0.0014	⁹⁴ 0.0015	⁸³ 0.0015	⁷⁹ 0.0015	⁷² 0.0016	¹²⁹ 0.0007 N ^{0.047} 69
170	VERIDAS-003	⁵⁹ 0.0017	⁵⁷ 0.0018	⁵³ 0.0020	⁶⁰ 0.0023	⁷² 0.0034	¹⁵ 0.0001 N ^{0.248} 139	⁵⁶ 0.0012	⁵² 0.0013	⁵⁰ 0.0013	⁵³ 0.0012	⁴⁹ 0.0014	¹¹⁵ 0.0007 N ^{0.043} 64
171	VIGILANTSOLUTIONS-008	¹⁰⁴ 0.0025	¹⁰⁶ 0.0029	¹⁰⁷ 0.0034	¹⁰⁴ 0.0040	⁹⁸ 0.0047	⁵⁰ 0.0001 N ^{0.224} 120	⁵³ 0.0012	⁶² 0.0013	⁷⁹ 0.0014	⁸¹ 0.0015	⁷⁷ 0.0017	⁸⁴ 0.0002 N ^{0.130} 129
172	VISIONBOX-000	⁶⁷ 0.0017	⁶⁵ 0.0019	⁶⁹ 0.0022	²⁷⁸ 1.0000	¹⁹⁰ 0.9526	¹ 0.0000 N ^{2.570} 190	⁶⁹ 0.0012	⁶¹ 0.0013	⁶⁵ 0.0013	¹⁹⁶ 1.0000	¹⁹⁰ 0.9525	¹ 0.0000 N ^{2.710} 190
173	VISIONLABS-004	⁹³ 0.0022	⁹⁹ 0.0027	¹⁰⁴ 0.0032	¹⁰⁴ 0.0044	¹¹⁸ 0.0070	⁷ 0.0000 N ^{0.387} 183	⁶⁷ 0.0012	⁸⁴ 0.0014	¹⁰¹ 0.0017	¹²⁹ 0.0025	¹⁴¹ 0.0045	⁶ 0.0005 N ^{0.435} 182
174	VISIONLABS-005	⁸⁰ 0.0020	⁸⁸ 0.0024	⁹⁶ 0.0029	⁹⁶ 0.0037	¹⁰⁵ 0.0051	¹¹ 0.0000 N ^{0.322} 180	⁶³ 0.0012	⁶⁹ 0.0013	⁹⁴ 0.0016	¹⁰⁶ 0.0019	¹²⁵ 0.0029	¹² 0.0000 N ^{0.298} 170
175	VISIONLABS-006	⁵⁶ 0.0016	⁵⁹ 0.0018	⁷⁰ 0.0022	⁷⁶ 0.0028	⁹² 0.0041	¹⁰ 0.0000 N ^{0.314} 178	⁶⁰ 0.0012	⁶² 0.0013	⁸⁵ 0.0015	¹⁰⁰ 0.0019	¹²⁰ 0.0027	¹⁴ 0.0000 N ^{0.275} 164
176	VISIONLABS-007	⁵⁴ 0.0016	⁵³ 0.0018	³⁹ 0.0020	⁶⁰ 0.0023	⁷⁷ 0.0034	¹⁵ 0.0001 N ^{0.248} 139	⁵⁶ 0.0012	⁵² 0.0013	⁵⁰ 0.0013	⁵³ 0.0012	⁴⁵ 0.0013	⁴⁵ 0.0001 N ^{0.152} 135
177	VISIONLABS-008	⁷⁴ 0.0019	⁷² 0.0020	⁶⁵ 0.0021	⁶⁷ 0.0025	⁶⁶ 0.0030	⁸³ 0.0002 N ^{0.169} 85	¹²² 0.0016	¹¹⁹ 0.0017	¹⁰⁸ 0.0017	¹¹¹ 0.0020	¹¹⁰ 0.0023	⁷¹ 0.0003 N ^{0.114} 118
178	VISIONLABS-009	¹⁶ 0.0011	¹⁵ 0.0011	¹³ 0.0012	¹⁶ 0.0014	²¹ 0.0017	⁴⁶ 0.0001 N ^{0.160} 79	²⁹ 0.0010	²³ 0.0010	²⁵ 0.0010	²⁸ 0.0011	⁵¹ 0.0014	³⁹ 0.0002 N ^{0.109} 114
179	VISIONLABS-010	³² 0.0014	²⁷ 0.0014	²⁶ 0.0015	²⁸ 0.0017	³¹ 0.0021	⁹¹ 0.0002 N ^{0.137} 59	⁷³ 0.0013	⁵⁷ 0.0013	⁶⁶ 0.0013	⁶⁸ 0.0014	⁷⁵ 0.0017	⁷³ 0.0004 N ^{0.090} 107
180	VISIONLABS-011	¹⁷ 0.0011	¹⁸ 0.0012	¹⁸ 0.0013	¹⁷ 0.0014	²³ 0.0018	⁴⁵ 0.0001 N ^{0.162} 81	³⁴ 0.0010	³⁴ 0.0011	³⁴ 0.0011	³⁶ 0.0012	⁶¹ 0.0015	⁵⁶ 0.0002 N ^{0.114} 119
181	VOCORD-005	¹⁶¹ 0.0060	¹⁶⁰ 0.0070	¹⁵⁰ 0.0082	¹⁴⁹ 0.0097	¹⁴³ 0.0117	¹¹² 0.0003 N ^{0.232} 129	¹⁸⁰ 0.0033	¹⁸⁰ 0.0035	¹⁶¹ 0.0037	¹⁴⁹ 0.0040	¹⁴⁹ 0.0043	¹⁴⁹ 0.0010 N ^{0.090} 106
182	VTS-001	⁵¹ 0.0014	⁵⁶ 0.0015	⁵³ 0.0017	⁴⁹ 0.0019	⁴³ 0.0023	⁴⁷ 0.0001 N ^{0.179} 94	²⁷ 0.0010	<sup				

#	ALGORITHM	MISSES OUTSIDE RANK R		RESOURCE USAGE		ENROL MOST RECENT, N = 1.6M					
		FNIR(N, T=0, R)		TEMPLATE		FRVT 2018 MUGSHOTS					
		BYTES	MSEC	R=1	R=5	R=10	R=20	R=50	WORK-10		
1	20FACE-000	16 ⁷ 2048	40 ²⁴⁷	23 ^{0.0552}	23 ^{0.0269}	23 ^{0.0198}	23 ^{0.0146}	22 ^{0.0099}	23 ^{1.275}		
2	3DIVI-003	37 ⁵¹²	141 ⁶²⁵	248 ^{0.0833}	243 ^{0.0444}	243 ^{0.0349}	239 ^{0.0270}	239 ^{0.0191}	244 ^{1.447}		
3	3DIVI-004	25 ⁴⁰⁹⁶	142 ⁶²⁸	20 ^{0.0175}	20 ^{0.0091}	19 ^{0.0075}	19 ^{0.0061}	19 ^{0.0049}	20 ^{1.092}		
4	3DIVI-005	25 ⁴⁰⁹⁶	151 ⁶⁵³	20 ^{0.0176}	20 ^{0.0091}	19 ^{0.0074}	19 ^{0.0061}	19 ^{0.0049}	20 ^{1.092}		
5	3DIVI-006	54 ⁵²⁸	150 ⁶⁵³	21 ^{0.0240}	22 ^{0.0171}	22 ^{0.0160}	23 ^{0.0154}	23 ^{0.0148}	22 ^{1.162}		
6	ACER-000	40 ⁵¹²	30 ²⁰¹	18 ^{0.0106}	17 ^{0.0051}	16 ^{0.0041}	16 ^{0.0034}	15 ^{0.0026}	17 ^{1.053}		
7	ACER-001	128 ²⁰⁴⁸	21 ¹⁸⁴	14 ^{0.0051}	14 ^{0.0032}	14 ^{0.0028}	14 ^{0.0025}	14 ^{0.0022}	14 ^{1.031}		
8	AIZE-001	18 ²⁰⁴⁸	80 ⁴⁰³	14 ^{0.0056}	14 ^{0.0037}	15 ^{0.0033}	15 ^{0.0030}	16 ^{0.0027}	14 ^{1.035}		
9	ALCHERA-000	141 ²⁰⁴⁸	44 ²⁶³	20 ^{0.0161}	21 ^{0.0124}	21 ^{0.0117}	22 ^{0.0111}	22 ^{0.0105}	21 ^{1.116}		
10	ALCHERA-001	16 ²⁰⁴⁸	7 ⁶⁶	27 ^{0.9869}	27 ^{0.9782}	27 ^{0.9735}	27 ^{0.9679}	27 ^{0.9590}	27 ^{9.811}		
11	ALCHERA-002	135 ²⁰⁴⁸	14 ¹¹⁵	24 ^{0.0949}	24 ^{0.0555}	24 ^{0.0443}	24 ^{0.0354}	24 ^{0.0254}	24 ^{1.544}		
12	ALCHERA-003	12 ²⁰⁴⁸	125 ⁵⁴⁸	18 ^{0.0104}	17 ^{0.0054}	17 ^{0.0045}	17 ^{0.0038}	17 ^{0.0032}	17 ^{1.055}		
13	ALCHERA-004	165 ²⁰⁴⁸	233 ⁸⁵⁴	18 ^{0.0110}	16 ^{0.0049}	16 ^{0.0038}	15 ^{0.0032}	15 ^{0.0025}	16 ^{1.051}		
14	ALLGOVISION-000	140 ²⁰⁴⁸	90 ⁴²⁵	19 ^{0.0114}	19 ^{0.0084}	20 ^{0.0078}	20 ^{0.0073}	20 ^{0.0067}	19 ^{1.079}		
15	ALLGOVISION-001	180 ²⁰⁴⁸	212 ⁷⁹²	17 ^{0.0090}	16 ^{0.0048}	16 ^{0.0040}	16 ^{0.0033}	16 ^{0.0027}	16 ^{1.048}		
16	ANKE-000	22 ²⁰⁷²	43 ⁴³¹	19 ^{0.0132}	18 ^{0.0073}	18 ^{0.0060}	18 ^{0.0050}	18 ^{0.0040}	19 ^{1.072}		
17	ANKE-001	22 ²⁰⁷²	93 ⁴³³	20 ^{0.0132}	18 ^{0.0073}	18 ^{0.0061}	18 ^{0.0050}	18 ^{0.0040}	19 ^{1.073}		
18	ANKE-002	217 ²⁰⁵⁶	145 ⁶⁴¹	10 ^{0.0028}	10 ^{0.0020}	10 ^{0.0018}	10 ^{0.0018}	11 ^{0.0017}	10 ^{1.019}		
19	AWARE-003	228 ²⁰⁷⁶	186 ⁷¹⁶	22 ^{0.0306}	22 ^{0.0162}	22 ^{0.0127}	21 ^{0.0100}	21 ^{0.0075}	22 ^{1.163}		
20	AWARE-004	2 ⁹²	182 ⁷¹²	243 ^{0.0679}	240 ^{0.0348}	237 ^{0.0274}	237 ^{0.0208}	234 ^{0.0145}	240 ^{1.354}		
21	AWARE-005	240 ³¹⁰⁰	220 ⁸²⁷	22 ^{0.0311}	22 ^{0.0167}	22 ^{0.0134}	21 ^{0.0107}	22 ^{0.0082}	22 ^{1.167}		
22	AWARE-006	3 ¹²⁴	216 ⁸¹⁸	245 ^{0.0697}	242 ^{0.0369}	238 ^{0.0288}	238 ^{0.0223}	236 ^{0.0158}	242 ^{1.371}		
23	AYONIX-000	8 ¹⁰³⁶	1 ¹⁰	26 ^{0.4505}	26 ^{0.3540}	26 ^{0.3176}	26 ^{0.2834}	26 ^{0.2381}	26 ^{4.288}		
24	AYONIX-001	83 ¹⁰³⁶	3 ¹²	263 ^{0.3414}	263 ^{0.2338}	263 ^{0.1977}	264 ^{0.1652}	263 ^{0.1274}	263 ^{3.226}		
25	AYONIX-002	84 ¹⁰³⁶	2 ¹¹	26 ^{0.3414}	26 ^{0.2338}	26 ^{0.1977}	26 ^{0.1652}	26 ^{0.1274}	26 ^{3.226}		
26	CAMVI-003	71 ¹⁰²⁴	179 ⁷⁰⁷	238 ^{0.0520}	237 ^{0.0517}	248 ^{0.0517}	251 ^{0.0517}	251 ^{0.0517}	248 ^{1.466}		
27	CAMVI-004	71 ¹⁰²⁴	188 ⁷¹⁸	23 ^{0.0468}	24 ^{0.0465}	24 ^{0.0465}	24 ^{0.0464}	250 ^{0.0464}	247 ^{1.419}		
28	CAMVI-005	72 ¹⁰²⁴	203 ⁷⁶⁹	242 ^{0.0652}	249 ^{0.0648}	250 ^{0.0648}	253 ^{0.0648}	253 ^{0.0647}	249 ^{1.584}		
29	CANON-001	258 ⁴⁰⁹⁶	249 ⁸⁹³	12 ^{0.0011}	18 ^{0.0010}	15 ^{0.0010}	16 ^{0.0009}	16 ^{0.0009}	14 ^{1.009}		
30	CIB-000	274 ⁸¹⁹⁶	158 ⁶⁷⁴	37 ^{0.0015}	43 ^{0.0013}	40 ^{0.0012}	42 ^{0.0012}	45 ^{0.0012}	41 ^{1.012}		
31	CLEARVIEWAI-000	25 ⁴⁰⁹⁶	200 ⁷⁶⁵	11 ^{0.0011}	16 ^{0.0010}	18 ^{0.0010}	15 ^{0.0009}	15 ^{0.0009}	12 ^{1.009}		
32	CLOUDWALK-HR-000	119 ²⁰⁴⁸	256 ⁹⁰⁸	33 ^{0.0015}	61 ^{0.0014}	67 ^{0.0014}	76 ^{0.0014}	86 ^{0.0014}	59 ^{1.013}		
33	CLOUDWALK-MT-000	17 ²⁰⁴⁸	241 ⁸⁷⁰	32 ^{0.0018}	85 ^{0.0018}	97 ^{0.0018}	105 ^{0.0018}	121 ^{0.0018}	81 ^{1.016}		
34	COGENT-000	50 ⁵²⁵	126 ⁵⁵¹	184 ^{0.0105}	207 ^{0.0096}	219 ^{0.0095}	158 ^{0.0032}	151 ^{0.0024}	205 ^{1.088}		
35	COGENT-001	51 ⁵²⁵	127 ⁵⁵²	185 ^{0.0105}	206 ^{0.0096}	211 ^{0.0095}	159 ^{0.0032}	150 ^{0.0024}	203 ^{1.088}		
36	COGENT-002	80 ¹⁰⁴³	274 ⁹⁸⁷	118 ^{0.0036}	113 ^{0.0022}	111 ^{0.0020}	107 ^{0.0018}	104 ^{0.0015}	111 ^{1.021}		
37	COGENT-003	87 ¹⁰⁴³	271 ⁹⁶⁰	120 ^{0.0038}	124 ^{0.0024}	119 ^{0.0021}	122 ^{0.0019}	114 ^{0.0017}	122 ^{1.023}		
38	COGENT-004	21 ²⁰⁵³	268 ⁹⁵²	20 ^{0.0200}	72 ^{0.0116}	74 ^{0.0115}	82 ^{0.0015}	83 ^{0.0014}	71 ^{1.015}		
39	COGENT-005	88 ¹⁰⁶²	206 ⁷⁷⁴	47 ^{0.0017}	59 ^{0.0014}	60 ^{0.0014}	69 ^{0.0014}	78 ^{0.0013}	58 ^{1.013}		
40	COGNITEC-000	19 ²⁰⁵²	19 ¹⁷⁶	22 ^{0.0252}	219 ^{0.0136}	217 ^{0.0107}	216 ^{0.0085}	206 ^{0.0065}	22 ^{1.136}		
41	COGNITEC-001	210 ²⁰⁵²	31 ²⁰²	192 ^{0.0117}	180 ^{0.0062}	179 ^{0.0051}	181 ^{0.0042}	178 ^{0.0034}	180 ^{1.062}		
42	COGNITEC-002	20 ²⁰⁵²	36 ²²⁷	14 ^{0.0057}	147 ^{0.0037}	144 ^{0.0032}	150 ^{0.0029}	159 ^{0.0026}	148 ^{1.035}		
43	COGNITEC-003	19 ²⁰⁵²	54 ²⁹⁷	152 ^{0.0062}	156 ^{0.0040}	157 ^{0.0036}	163 ^{0.0033}	170 ^{0.0030}	159 ^{1.039}		
44	COGNITEC-004	208 ²⁰⁵²	27 ¹⁹²	111 ^{0.0032}	106 ^{0.0020}	95 ^{0.0018}	99 ^{0.0015}	87 ^{0.0014}	108 ^{1.020}		
45	COGNITEC-005	20 ²⁰⁵²	68 ³⁶⁷	4 ^{0.0016}	38 ^{0.0013}	37 ^{0.0012}	38 ^{0.0012}	42 ^{0.0011}	37 ^{1.012}		
46	COGNITEC-006	193 ²⁰⁵²	102 ⁴⁶³	40 ^{0.0016}	37 ^{0.0013}	35 ^{0.0012}	37 ^{0.0012}	40 ^{0.0011}	38 ^{1.012}		
47	CUBOX-000	15 ²⁰⁴⁸	260 ⁹¹⁸	29 ^{0.0014}	50 ^{0.0014}	61 ^{0.0014}	70 ^{0.0014}	80 ^{0.0014}	46 ^{1.012}		
48	CYBERLINK-000	198 ²⁰⁵²	174 ⁶⁹⁹	123 ^{0.0040}	134 ^{0.0028}	138 ^{0.0026}	141 ^{0.0024}	141 ^{0.0022}	133 ^{1.027}		
49	CYBERLINK-001	19 ²⁰⁵²	44 ⁴³³	110 ^{0.0035}	119 ^{0.0023}	118 ^{0.0021}	112 ^{0.0018}	120 ^{0.0017}	117 ^{1.022}		
50	CYBERLINK-002	268 ⁴¹⁴⁰	195 ⁷³⁸	96 ^{0.0026}	102 ^{0.0023}	122 ^{0.0022}	132 ^{0.0021}	136 ^{0.0021}	112 ^{1.021}		
51	CYBERLINK-003	27 ⁶²¹²	172 ⁶⁹⁶	4 ^{0.0016}	41 ^{0.0013}	43 ^{0.0013}	44 ^{0.0012}	44 ^{0.0012}	43 ^{1.012}		
52	CYBERLINK-004	27 ⁶²¹²	196 ⁷³⁸	46 ^{0.0017}	65 ^{0.0015}	73 ^{0.0015}	78 ^{0.0014}	89 ^{0.0014}	62 ^{1.014}		
53	CYBERLINK-005	27 ⁶²¹²	197 ⁷³⁹	56 ^{0.0018}	73 ^{0.0016}	79 ^{0.0015}	86 ^{0.0015}	90 ^{0.0014}	68 ^{1.015}		
54	DAHUA-000	159 ²⁰⁴⁸	74 ³⁷⁸	178 ^{0.0093}	183 ^{0.0066}	187 ^{0.0061}	193 ^{0.0057}	196 ^{0.0054}	181 ^{1.062}		
55	DAHUA-001	150 ²⁰⁴⁸	70 ³⁷¹	156 ^{0.0067}	157 ^{0.0040}	156 ^{0.0036}	161 ^{0.0033}	165 ^{0.0029}	157 ^{1.040}		
56	DAHUA-002	180 ²⁰⁴⁸	173 ⁶⁹⁹	6 ^{0.0018}	63 ^{0.0015}	69 ^{0.0014}	74 ^{0.0014}	75 ^{0.0013}	63 ^{1.014}		
57	DAHUA-003	126 ²⁰⁴⁸	191 ⁷²⁵	19 ^{0.0012}	13 ^{0.0010}	12 ^{0.0009}	11 ^{0.0009}	11 ^{0.0009}	11 ^{1.009}		
58	DAHUA-004	180 ²⁰⁴⁸	199 ⁷⁵⁹	10 ^{0.0011}	11 ^{0.0010}	13 ^{0.0009}	15 ^{0.0009}	14 ^{0.0009}	16 ^{1.009}		
59	DAON-000	221 ²⁰⁶⁹	132 ⁵⁸⁴	125 ^{0.0041}	149 ^{0.0038}	160 ^{0.0037}	170 ^{0.0037}	181 ^{0.0036}	148 ^{1.034}		
60	DECATAR-000	19 ²⁰⁵²	243 ⁸⁷⁴	7 ^{0.0021}	74 ^{0.0016}	77 ^{0.0015}	75 ^{0.0014}	70 ^{0.0013}	74 ^{1.015}		
61	DEEPLINT-001	25 ⁴⁰⁹⁶	163 ⁶⁸⁷	31 ^{0.0014}	48 ^{0.0014}	51 ^{0.0013}	58 ^{0.0013}	64 ^{0.0013}	49 ^{1.012}		
62	DEEPSA-001	14 ²⁰⁴⁸	209 ⁷⁸⁰	130 ^{0.0043}	114 ^{0.0022}	108 ^{0.0018}	95 ^{0.0016}	82 ^{0.0014}	118 ^{1.022}		
63	DERMALOG-003	5 ¹²⁸	33 ²¹¹	253 ^{0.1259}	252 ^{0.0744}	251 ^{0.0603}	250 ^{0.0480}	249 ^{0.0347}	2		

#	ALGORITHM	MISSES OUTSIDE RANK R		RESOURCE USAGE		ENROL MOST RECENT, N = 1.6M					
		FNIR(N, T=0, R)		TEMPLATE		R=1		R=5		R=10	
		BYTES	MSEC	BYTES	MSEC	R=1	R=5	R=10	R=20	R=50	WORK-10
73	FUJITSULAB-000	771032	26950	790.0022	780.0016	800.0015	800.0015	800.0014	780.0014	780.0014	780.0015
74	GLORY-000	32418	15160	250.1781	2590.1391	2590.1266	2590.1154	2590.1007	2580.2298	2580.2298	2580.2298
75	GLORY-001	111726	89405	2540.1268	2590.0967	2540.0869	2590.0778	2590.0673	2540.1903	2540.1903	2540.1903
76	GORILLA-001	2302156	17169	2400.0603	2350.0304	2340.0230	2340.0174	2270.0117	2350.1309	2350.1309	2350.1309
77	GORILLA-002	921132	69341	2150.0197	2000.0092	1930.0070	1880.0054	1800.0041	2070.1096	2070.1096	2070.1096
78	GORILLA-003	2312156	130563	2280.0361	2200.0146	2160.0106	2100.0078	1980.0054	2230.1158	2230.1158	2230.1158
79	GORILLA-004	2352192	78395	1530.0063	1480.0032	1390.0026	1360.0023	1220.0018	1440.1033	1440.1033	1440.1033
80	GORILLA-005	2776288	110483	1100.0032	900.0019	900.0017	840.0015	660.0013	1010.1018	1010.1018	1010.1018
81	GORILLA-006	2758336	201768	510.0017	360.0013	340.0012	350.0012	360.0011	400.1012	400.1012	400.1012
82	GRIAULE-000	1912052	89419	940.0025	1000.0020	1040.0019	1100.0018	1120.0017	980.1018	980.1018	980.1018
83	HIK-003	991408	143633	1930.0117	1780.0060	1770.0048	1780.0039	1690.0030	1790.1061	1790.1061	1790.1061
84	HIK-004	911152	115510	1900.0113	1770.0059	1760.0047	1710.0037	1660.0030	1780.1060	1780.1060	1780.1060
85	HIK-005	1001408	140619	1350.0046	1260.0025	1140.0020	1020.0017	960.0015	1280.1025	1280.1025	1280.1025
86	HIK-006	961408	139610	1340.0046	1220.0025	1150.0020	1060.0017	970.0015	1270.1025	1270.1025	1270.1025
87	HYPERVERGE-001	701024	231846	250.0014	390.0013	480.0013	540.0013	680.0013	360.0012	360.0012	360.0012
88	IDEMIA-003	52528	16689	1590.0069	1600.0045	1640.0039	1660.0034	1630.0027	1600.1043	1600.1043	1600.1043
89	IDEMIA-004	53528	15669	1550.0066	1530.0038	1490.0032	1480.0027	1570.0021	1510.1038	1510.1038	1510.1038
90	IDEMIA-005	30352	78374	1680.0081	1600.0044	1580.0036	1600.0032	1600.0030	1630.1044	1630.1044	1630.1044
91	IDEMIA-006	31352	71373	1810.0096	1770.0052	1700.0042	1770.0039	1820.0037	1700.1052	1700.1052	1700.1052
92	IDEMIA-007	63860	214807	950.0026	750.0016	660.0014	530.0013	480.0012	790.1015	790.1015	790.1015
93	IDEMIA-008	29300	97451	90.0011	80.0009	110.0009	140.0009	130.0009	70.1009	70.1009	70.1009
94	IMAGUS-002	38512	776	2600.2203	2580.1342	2570.1090	2560.0871	2540.0632	2590.2308	2590.2308	2590.2308
95	IMAGUS-003	36512	557	2650.3559	2670.2491	2650.2132	2650.1791	2650.1397	2650.3363	2650.3363	2650.3363
96	IMAGUS-005	1752048	211788	670.0019	760.0016	750.0015	730.0014	720.1015	720.1015	720.1015	720.1015
97	IMAGUS-006	1252048	25905	710.0020	800.0016	830.0015	830.0015	750.1015	750.1015	750.1015	750.1015
98	IMAGUS-007	1422048	133590	730.0020	660.0015	630.0014	550.0013	590.0013	640.1014	640.1014	640.1014
99	IMPERIAL-000	1392048	15654	910.0024	900.0019	1010.0018	1080.0018	1100.0017	930.1018	930.1018	930.1018
100	INCODE-000	691024	259190	2370.0489	2300.0261	2330.0204	2310.0160	2280.0117	2320.1262	2320.1262	2320.1262
101	INCODE-001	1602048	166690	2060.0166	1970.0084	1910.0067	1900.0055	1890.0043	1980.1086	1980.1086	1980.1086
102	INCODE-002	1312048	51291	2100.0178	2090.0090	1940.0070	1910.0056	1900.0043	2040.1092	2040.1092	2040.1092
103	INCODE-003	1692048	176704	1980.0129	1820.0064	1800.0051	1790.0040	1710.0031	1860.1066	1860.1066	1860.1066
104	INCODE-004	1152048	115508	1170.0035	1200.0024	1220.0021	1250.0020	1200.0019	1190.1023	1190.1023	1190.1023
105	INCODE-005	1612048	113500	450.0017	490.0014	380.0014	520.0013	580.0013	500.1013	500.1013	500.1013
106	INNOVATRICS-002	55530	42255	2350.0451	2390.0342	2400.0322	2420.0308	2400.0297	2390.1321	2390.1321	2390.1321
107	INNOVATRICS-003	56530	41255	2220.0263	2140.0126	2100.0095	2080.0074	1950.0053	2170.1129	2170.1129	2170.1129
108	INNOVATRICS-004	891076	84046	1970.0123	1810.0063	1780.0050	1800.0040	1700.0032	1850.1064	1850.1064	1850.1064
109	INNOVATRICS-005	59538	228542	930.0024	880.0018	890.0017	930.0016	910.0014	880.1017	880.1017	880.1017
110	INNOVATRICS-007	58538	210785	480.0017	540.0014	520.0013	510.0013	560.0012	530.1013	530.1013	530.1013
111	INTSYSMSU-000	1592048	160675	2550.0145	2590.1320	2600.1272	2600.1225	2600.1163	2570.2203	2570.2203	2570.2203
112	IREX-000	2393080	2762379	1310.0044	1590.0043	1720.0043	1820.0043	1880.0043	1560.1039	1560.1039	1560.1039
113	ISYSTEMS-002	1392048	59316	1540.0064	1590.0043	1650.0039	1660.0037	1590.0034	1590.1041	1590.1041	1590.1041
114	ISYSTEMS-003	1542048	234856	1420.0052	1540.0039	1590.0036	1680.0034	1750.0033	1500.1037	1500.1037	1500.1037
115	KAKAO-000	1952052	228840	320.0015	250.0011	250.0011	210.0010	210.0009	260.1010	260.1010	260.1010
116	KEDACOM-001	28292	121537	1640.0077	1890.0074	1950.0073	2020.0072	2100.0072	1870.1067	1870.1067	1870.1067
117	KNERON-000	1592048	115530	1490.0059	1700.0059	1840.0059	1940.0059	1940.0059	2010.1053	2010.1053	2010.1053
118	KNERON-001	1342048	106468	2250.0295	2340.0295	2390.0295	2410.0295	2430.0295	2330.1266	2330.1266	2330.1266
119	LINE-000	1252048	108482	800.0022	790.0015	620.0014	480.0013	460.0012	700.1015	700.1015	700.1015
120	LINE-001	1442048	258910	1440.0011	1770.0010	1900.0010	1700.0009	1800.0009	1500.1009	1500.1009	1500.1009
121	LOOKMAN-003	27292	61342	1730.0088	1970.0078	2010.0076	2070.0075	2120.0073	1910.1072	1910.1072	1910.1072
122	LOOKMAN-004	61548	60525	1750.0091	1940.0079	2000.0076	2080.0075	2120.0073	1880.1068	1880.1068	1880.1068
123	LOOKMAN-005	60548	115514	1670.0080	1900.0075	1980.0074	2040.0073	2100.0072	2180.1068	2180.1068	2180.1068
124	MANTRA-000	2022052	85412	500.0017	4500.0013	4700.0013	4700.0012	4900.0012	4800.1013	4800.1013	4800.1013
125	MEGVII-001	2514096	146652	1940.0118	2080.0093	2040.0087	2140.0084	2190.0080	1990.1086	1990.1086	1990.1086
126	MEGVII-002	2494096	154656	1950.0118	2050.0093	2060.0088	2130.0084	2180.0080	2000.1087	2000.1087	2000.1087
127	MICROFOCUS-003	22256	47269	2720.05942	2710.04692	2710.04204	2710.03724	2710.03095	2710.5361	2710.5361	2710.5361
128	MICROFOCUS-004	16256	48270	2700.05763	2790.04519	2700.04026	2700.03560	2700.02957	2700.5199	2700.5199	2700.5199
129	MICROFOCUS-005	21256	46266	2660.04242	2660.03028	2660.02606	2660.02209	2660.01724	2660.3861	2660.3861	2660.3861
130	MICROFOCUS-006	17256	47265	2670.04268	2670.03049	2670.02623	2680.02233	2680.01746	2670.3880	2670.3880	2670.3880
131	MICROSOFT-003	671024	81404	420.0016	150.0010	70.0009	30.0008	20.0008	180.1009	180.1009	180.1009
132	MICROSOFT-004	1412048	207773	340.0015	70.0009	10.0008	1.0007	1.0006	160.1009	160.1009	160.1009
133	MICROSOFT-005	661024	157673	630.0019	120.0010	60.0008	40.0008	30.0008	220.1010	220.1010	220.1010
134	MICROSOFT-006	691024	176695	690.0020	20.0011	160.0010	40.0008	40.0008	30.0007	30.0007	30.0007
135	NEC-000	2372592	8282	2070.0170	1990.0086	1900.0066	1800.0052	1840.0038	2010.1087	2010.1087	2010.1087
136	NEC-001	2392592	9888	2160.0209	2280.0141	2210.0128	2240.0119	2260.0113	2160.1135	2160.1135	2160.1135
137	NEC-002	1091616	149653	800.0010	40.0009	50.0008	50.0008	50.0008	40.0008	40.0008	40.0008
138	NEC-003	1101712	169690	230.0014	30.0012	38.0012	38.0012	45.00012	47.00012	32.00112	32.00112
139	NEC-004	901104	27967	290.0014	40.0013	25.0011	27.00011	30.0011	35.00011	44.00112	44.00112
140	NEC-005	911104	272964	170.0012	25.0011	27.00011	27.00011	30.0011	35.00011	25.00110	25.00110</td

MISSES OUTSIDE RANK R		RESOURCE USAGE		ENROL MOST RECENT, N = 1.6M					
#	ALGORITHM	BYTES	MSEC	R=1	R=5	R=10	R=20	R=50	WORK-10
145	NEUROTECHNOLOGY-007	¹⁵ 256	¹⁸ 169	121.0039	¹³ 0.0027	¹⁶ 0.0025	¹⁵ 0.0023	¹³ 0.0022	¹² 0.1026
146	NEUROTECHNOLOGY-008	⁴⁹ 514	²¹³ 804	78.0022	⁶⁷ 0.0015	⁷⁰ 0.0014	⁷¹ 0.0014	⁷³ 0.0013	⁶⁹ 1.015
147	NEUROTECHNOLOGY-009	⁴⁸ 513	¹⁶ 686	30.0014	³⁶ 0.0012	³³ 0.0012	³⁴ 0.0011	³⁶ 0.0011	³¹ 1.011
148	NEUROTECHNOLOGY-010	²⁰ 256	¹⁵ 663	20.0012	²⁰ 0.0011	²² 0.0010	²² 0.0010	³⁰ 0.0010	²¹ 1.010
149	NEWLAND-002	¹⁸⁷ 2048	²³⁹ 868	246.0786	²⁴⁶ 0.0480	²⁴⁵ 0.0397	²⁴⁵ 0.0332	²⁴² 0.0263	²⁴⁷ 1.468
150	NOBLIS-001	¹⁵ 2048	³⁴ 211	²⁶² 0.1111	²⁶² 0.1772	²⁶² 0.1542	²⁶² 0.1339	²⁶⁰ 0.1112	²⁶² 2.679
151	NOBLIS-002	²⁶ 6144	¹²⁰ 535	280.1794	²⁵⁸ 0.1108	²⁵⁸ 0.0903	²⁵⁸ 0.0722	²⁵³ 0.0535	²⁵⁵ 2.077
152	NOTIONTAG-000	²²⁹ 2120	¹⁰ 461	92.0024	¹¹⁹ 0.0021	¹¹⁷ 0.0021	¹²⁸ 0.0020	¹³² 0.0019	¹⁰⁶ 1.019
153	NTECHLAB-003	²⁴³ 3484	²²² 831	150.0062	¹³⁹ 0.0029	¹³² 0.0023	¹²³ 0.0019	¹⁰⁷ 0.0016	¹⁴² 1.030
154	NTECHLAB-004	²⁴⁴ 3484	²⁶ 929	138.0048	¹¹⁷ 0.0023	¹⁰⁶ 0.0019	⁹⁷ 0.0016	⁷⁶ 0.0013	¹²⁵ 1.024
155	NTECHLAB-005	¹¹⁴ 1940	¹⁸⁷ 717	136.0047	¹¹² 0.0022	⁹⁴ 0.0017	⁶⁰ 0.0013	³³ 0.0011	¹²⁰ 1.023
156	NTECHLAB-006	¹¹⁵ 1940	²² 841	126.0041	⁹ 0.0019	⁷⁶ 0.0015	⁴¹ 0.0012	⁷ 0.0009	¹⁰⁷ 1.019
157	NTECHLAB-007	²⁴¹ 3348	²²⁵ 834	⁹⁷ 0.0027	⁸¹ 0.0017	⁶⁸ 0.0014	⁶⁵ 0.0013	⁵¹ 0.0012	⁸³ 1.016
158	NTECHLAB-008	⁹⁶ 1300	¹²⁶ 562	49.0007	³¹ 0.0012	³² 0.0012	³¹ 0.0011	³¹ 0.0010	³⁴ 1.012
159	NTECHLAB-009	⁹⁷ 1300	²⁵² 900	210.0013	²⁹ 0.0011	²³ 0.0010	²⁰ 0.0010	²¹ 0.0009	²³ 1.010
160	NTECHLAB-010	⁹⁸ 1280	²⁴⁴ 875	130.0011	¹⁹ 0.0010	²⁰ 0.0010	²³ 0.0010	²⁹ 0.0010	¹⁷ 1.009
161	NTECHLAB-011	⁹⁹ 1280	²³⁹ 865	70.0010	⁸ 0.0009	¹⁰ 0.0009	¹² 0.0009	¹² 0.0009	⁶ 1.008
162	PARAVISION-000	¹⁸⁸ 2048	⁹⁶ 438	212.0188	²²⁵ 0.0171	²³⁰ 0.0167	²³¹ 0.0165	²³⁸ 0.0164	²²² 1.156
163	PARAVISION-001	¹² 2048	¹³ 590	119.0038	¹²² 0.0024	¹²³ 0.0022	¹²⁵ 0.0020	¹²³ 0.0019	¹²³ 1.023
164	PARAVISION-002	¹⁴⁵ 2048	⁷³ 377	124.0040	¹²⁸ 0.0025	¹²⁹ 0.0022	¹³¹ 0.0021	¹²⁸ 0.0019	¹²⁶ 1.025
165	PARAVISION-003	¹³ 2048	¹⁹ 735	109.0031	¹¹¹ 0.0022	¹¹⁶ 0.0020	¹¹⁷ 0.0019	¹¹⁸ 0.0017	¹¹¹ 1.021
166	PARAVISION-004	²⁴⁸ 4096	¹⁹⁰ 720	43.0016	⁵³ 0.0014	⁵⁷ 0.0013	⁶³ 0.0013	⁷¹ 0.0013	⁵² 1.013
167	PARAVISION-005	²⁴⁹ 4096	²⁵ 858	38.0015	⁵¹ 0.0014	⁵⁶ 0.0013	⁶⁴ 0.0013	⁷⁰ 0.0013	⁴⁷ 1.013
168	PARAVISION-007	²⁴ 4096	¹⁷⁸ 706	16.0012	²³ 0.0011	²⁴ 0.0010	²⁵ 0.0010	²⁵ 0.0010	²⁰ 1.010
169	PARAVISION-009	²⁶⁰ 4100	¹⁴⁴ 638	6.0010	¹⁰ 0.0010	¹⁴ 0.0010	¹⁹ 0.0009	¹⁹ 0.0009	⁹ 1.009
170	PIXELALL-002	²³⁹ 2560	²⁸ 198	133.0045	¹³⁸ 0.0029	¹³⁷ 0.0025	¹³⁴ 0.0022	¹³¹ 0.0019	¹³⁸ 1.028
171	PIXELALL-003	²³⁴ 2560	¹⁸⁹ 719	77.0021	⁷⁷ 0.0016	⁸¹ 0.0015	⁷⁹ 0.0014	⁸⁸ 0.0014	⁷⁷ 1.015
172	PIXELALL-004	²³⁵ 2560	⁹⁸ 453	74.0020	⁶⁹ 0.0015	⁷² 0.0015	⁷⁷ 0.0014	⁷⁹ 0.0013	⁶⁷ 1.014
173	PIXELALL-005	²³⁵ 2560	²³⁰ 845	64.0019	⁸² 0.0017	⁸⁴ 0.0016	⁹⁶ 0.0016	¹⁰⁶ 0.0016	⁷⁶ 1.015
174	PTAKURATSATU-000	⁵⁷ 538	²⁵ 910	107.0030	¹⁰⁸ 0.0021	¹¹⁰ 0.0019	¹⁰⁵ 0.0018	¹⁰⁷ 0.0016	¹⁰⁹ 1.020
175	QNAP-000	¹⁴⁹ 2048	⁹⁹ 457	165.0078	¹⁶¹ 0.0044	¹⁶¹ 0.0037	¹⁶² 0.0033	¹⁶⁴ 0.0028	¹⁶¹ 1.043
176	QNAP-001	¹⁵ 2048	¹³ 615	127.0041	¹³⁷ 0.0029	¹⁴¹ 0.0027	¹⁴⁵ 0.0025	¹⁴⁹ 0.0023	¹³⁵ 1.028
177	QUANTASOFT-001	¹³² 2048	⁷⁹ 396	259.02177	²⁶¹ 0.1643	²⁶¹ 0.1468	²⁶¹ 0.1312	²⁶¹ 0.1116	²⁶¹ 2.539
178	RANKONE-002	⁹ 133	¹³ 113	214.0194	²⁰ 0.0112	²⁰⁸ 0.0093	²⁰⁹ 0.0077	²⁰³ 0.0060	²¹⁰ 1.111
179	RANKONE-003	⁸ 133	¹³ 114	213.0194	²¹⁰ 0.0112	²⁰⁹ 0.0093	²⁰⁸ 0.0077	²⁰⁴ 0.0060	²⁰⁹ 1.111
180	RANKONE-004	⁸⁵	⁴³⁶	234.00415	²³ 0.0226	²³¹ 0.0177	²²⁷ 0.0141	²²² 0.0102	²³¹ 1.225
181	RANKONE-005	¹⁰ 133	¹⁰ 94	179.0094	¹⁷¹ 0.0054	¹⁷⁴ 0.0046	¹⁷⁶ 0.0039	¹⁷² 0.0032	¹⁷⁴ 1.054
182	RANKONE-006	¹² 165	⁴³ 261	140.0050	¹⁴² 0.030	¹⁴² 0.0207	¹³⁹ 0.024	¹³⁴ 0.021	¹⁴¹ 1.030
183	RANKONE-007	¹¹ 165	⁵⁰ 278	113.0034	¹¹⁹ 0.0023	¹²⁰ 0.0021	¹¹⁴ 0.0018	¹¹¹ 0.0017	¹¹⁵ 1.022
184	RANKONE-009	²³ 260	²⁸ 191	87.0024	⁷⁹ 0.0016	⁸² 0.0015	⁸⁵ 0.0015	⁸⁵ 0.0014	⁸⁰ 1.015
185	RANKONE-010	²⁴ 261	²⁹ 200	81.0022	⁸⁸ 0.0018	⁸⁷ 0.0016	⁹¹ 0.0015	⁸⁵ 0.0015	⁸⁵ 1.016
186	RANKONE-011	²⁶ 261	¹³¹ 567	35.0015	³⁴ 0.0012	³⁶ 0.0012	³⁹ 0.0012	⁴³ 0.0012	³³ 1.011
187	RANKONE-012	²⁵ 261	¹² 563	24.0014	²⁹ 0.0012	³⁰ 0.0011	³³ 0.0011	³⁶ 0.0011	²⁷ 1.011
188	REALNETWORKS-000	²⁵⁹ 4100	³⁸ 244	232.0402	²²⁹ 0.0195	²²⁶ 0.0149	²²² 0.0111	²¹⁷ 0.0077	²³⁰ 1.201
189	REALNETWORKS-001	²⁶ 4104	³⁷ 243	233.0402	²³⁹ 0.0195	²²⁵ 0.0149	²²¹ 0.0111	²¹⁷ 0.0077	²⁹ 1.201
190	REALNETWORKS-002	²⁶ 4104	³⁹ 245	229.0393	²²⁹ 0.0189	²²⁴ 0.0142	²²⁰ 0.0108	²¹⁵ 0.0076	²²⁸ 1.195
191	REALNETWORKS-003	¹¹² 1848	²⁰ 178	220.0242	²¹² 0.0117	²⁰⁷ 0.0090	²⁰¹ 0.0070	¹⁹⁷ 0.0054	²¹⁴ 1.120
192	REALNETWORKS-004	¹¹ 1848	²¹ 185	218.0236	²¹¹ 0.0112	²⁰⁵ 0.0087	¹⁹⁹ 0.0068	¹⁹³ 0.0050	²¹¹ 1.116
193	REALNETWORKS-005	²¹³ 2056	⁶² 337	83.0023	⁷¹ 0.0016	⁶⁴ 0.0014	⁶⁶ 0.0013	⁵⁴ 0.0012	⁷³ 1.015
194	REALNETWORKS-006	²¹ 2056	⁶⁹ 350	26.0014	³⁶ 0.0012	²⁹ 0.0011	²⁷ 0.0011	²⁶ 0.0010	²⁸ 1.011
195	REMARKAI-000	¹²³ 2048	¹⁶⁸ 691	115.0034	¹⁰⁸ 0.0021	¹⁰³ 0.0019	⁹⁹ 0.0017	¹⁰⁵ 0.0015	¹¹⁰ 1.020
196	REMARKAI-000	¹⁷ 2048	¹⁵ 615	172.0086	¹⁶⁴ 0.0044	¹⁵⁴ 0.0036	¹⁵⁶ 0.0031	¹⁵³ 0.0025	¹⁶⁴ 1.045
197	REMARKAI-002	¹³⁰ 2048	⁹⁵ 434	170.0081	¹⁵⁵ 0.0040	¹⁴⁷ 0.0031	¹⁴⁴ 0.0026	¹³⁵ 0.0021	¹⁵⁸ 1.041
198	RENDIP-000	¹² 2048	²⁵ 894	39.0015	⁴ 0.0013	⁴¹ 0.0012	⁴³ 0.0012	³⁸ 0.0012	⁴² 1.012
199	REVEALMEDIA-000	²⁰¹ 2052	⁷⁵ 385	62.0019	⁴⁴ 0.0013	⁵⁰ 0.0013	⁵⁰ 0.0013	⁵⁵ 0.0012	⁵¹ 1.013
200	S1-000	²⁵ 4096	²³ 865	89.0024	⁸⁹ 0.0018	⁸⁸ 0.0017	⁹⁴ 0.0016	¹⁰³ 0.0015	⁸⁷ 1.017
201	S1-001	¹⁷⁹ 2048	²¹ 814	108.0031	¹²⁰ 0.0025	¹³⁵ 0.0024	¹³⁸ 0.0024	¹⁴⁸ 0.0023	¹²¹ 1.023
202	SCANOVATE-000	¹⁵³ 2048	¹⁸³ 712	139.0050	¹³⁰ 0.0026	¹²⁸ 0.0022	¹¹⁵ 0.0018	¹⁰³ 0.0015	¹³² 1.026
203	SCANOVATE-001	¹⁶⁸ 2048	¹⁵ 675	143.0053	¹³⁷ 0.0027	¹²⁸ 0.0022	¹¹⁵ 0.0018	¹⁰² 0.0015	¹³⁶ 1.028
204	SENSETIME-000	²⁶⁵ 4104	¹⁸³ 715	85.0023	¹⁰⁴ 0.0020	¹⁰⁸ 0.0019	¹¹¹ 0.0018	¹¹⁷ 0.0017	⁹⁹ 1.018
205	SENSETIME-001	²⁶ 4104	¹⁵ 656	86.0023	¹⁰⁰ 0.0020	¹⁰⁵ 0.0019	¹⁰⁵ 0.0017	¹⁰⁸ 0.0016	⁹⁶ 1.018
206	SENSETIME-002	²¹⁸ 2056	¹⁴⁷ 650	201.0137	²¹⁸ 0.0136	²²³ 0.0136	²²⁶ 0.0136	²³² 0.0136	²¹⁵ 1.122
207	SENSETIME-003	²¹ 2056	²⁶ 940	50.0010	¹⁸ 0.0010	¹⁷ 0.0010	¹⁸ 0.0009	²⁰ 0.0009	⁸ 1.009
208	SENSETIME-004	⁷⁸ 1032	¹⁸¹ 710	44.0010	⁵ 0.0009	⁸ 0.0009	⁹ 0.0009	⁹ 0.0009	⁵ 1.008
209	SENSETIME-005	⁸⁰ 1032	²⁷⁵ 1007	30.0009	² 0.0008	² 0.0008	⁶ 0.0008	⁷ 0.0008	² 1.008
210	SENSETIME-006	⁷⁵ 1032	²⁶ 956	20.0009	³ 0.0008	⁴ 0.0008	⁸ 0.0008	⁷ 0.0008	³ 1.008
211	SENSETIME-007	⁷⁶ 1032	²⁷⁰ 958	10.0008	¹ 0.0008	³ 0.0008	⁷ 0.0008	⁸ 0.0008	¹ 1.007
212	SHAMAN-003	¹⁸ 2048	¹⁷ 704	250.01243	²⁵⁹ 0.08				

MISSES OUTSIDE RANK R		RESOURCE USAGE		ENROL MOST RECENT, N = 1.6M					
#	ALGORITHM	BYTES	MSEC	R=1	R=5	R=10	R=20	R=50	WORK-10
217	SIAT-002	²⁰⁹ 2052	²⁵⁵ 906	⁵⁸ 0.0018	⁵² 0.0014	³⁴ 0.0013	⁵⁶ 0.0013	³² 0.0012	³⁷ 1.013
218	SMILART-004	⁴¹ 512	¹⁶ 167	²⁷ 0.9648	²⁷ 0.9641	²⁷ 0.9640	²⁷ 0.9639	²⁷ 0.9638	²⁷ 9.678
219	SMILART-005	¹⁶⁰ 2048	¹⁰⁴ 464						²⁷ 10.000
220	SQISOFT-001	²¹⁶ 2056	¹⁰⁸ 460	¹²⁸ 0.0042	⁶⁰ 0.0014	⁴² 0.0013	³⁶ 0.0012	³² 0.0010	⁸⁴ 1.016
221	STAQU-000	²⁴⁶ 4096	²¹⁹ 827	¹⁶¹ 0.0071	¹⁷⁹ 0.0060	¹⁸¹ 0.0057	¹⁸⁹ 0.0055	¹⁹⁴ 0.0053	¹⁷⁶ 1.056
222	SYNESIS-003	²⁴⁷ 4096	¹¹³ 103	²⁵⁶ 0.1700	²⁵⁸ 0.1172	²⁵⁶ 0.1047	²⁵⁷ 0.0953	²⁵⁸ 0.0869	²⁵⁶ 2.120
223	SYNESIS-003	¹⁸³ 2048	²¹⁵ 215	²⁰⁵ 0.0162	²²² 0.0160	²²⁷ 0.0160	²³² 0.0160	²³⁷ 0.0160	²²¹ 1.144
224	SYNESIS-005	²⁶¹ 4104	²⁰¹ 772	¹⁷¹ 0.0085	¹⁹⁸ 0.0085	²⁰³ 0.0085	²¹⁵ 0.0085	²²¹ 0.0085	¹⁹⁵ 1.076
225	TECH5-001	¹⁰¹ 1536	²⁵¹ 898	¹²³ 0.0040	¹²¹ 0.0024	¹²¹ 0.0021	¹¹⁶ 0.0018	¹¹⁵ 0.0017	¹²⁴ 1.024
226	TECH5-002	⁴⁷ 513	²⁶⁶ 941	⁹⁸ 0.0027	⁵⁸ 0.0014	³⁹ 0.0012	³² 0.0011	²⁴ 0.0010	⁶⁶ 1.014
227	TEVIAN-003	¹⁷⁴ 2048	⁵⁶ 300	²⁰² 0.0147	¹⁹⁰ 0.0074	¹⁸² 0.0059	¹⁸⁴ 0.0047	¹⁸³ 0.0037	¹⁹⁴ 1.075
228	TEVIAN-004	¹³⁶ 2048	⁵³ 299	¹⁸⁹ 0.0113	¹⁷⁸ 0.0057	¹⁷⁸ 0.0047	¹⁷² 0.0037	¹⁶⁷ 0.0030	¹⁷⁷ 1.058
229	TEVIAN-005	¹⁶⁶ 2048	⁸⁸ 416	¹⁶² 0.0073	¹⁵⁷ 0.0038	¹⁴⁶ 0.0031	¹⁴⁷ 0.0027	¹⁴³ 0.0023	¹⁵⁴ 1.038
230	TEVIAN-006	⁸¹ 1032	¹³⁵ 599	⁹⁰ 0.0024	⁸⁸ 0.0018	⁹⁶ 0.0018	¹⁰¹ 0.0017	¹¹⁰ 0.0017	⁸⁹ 1.017
231	TEVIAN-007	⁷⁹ 1032	²⁰⁸ 779	⁵⁴ 0.0018	⁴⁷ 0.0014	⁵³ 0.0013	⁶² 0.0013	⁶⁰ 0.0013	⁴⁹ 1.013
232	TIGER-000	²⁰⁷ 2052	⁹¹ 428	²⁴¹ 0.0161	²³⁶ 0.0310	²³⁵ 0.0236	²³⁸ 0.0178	²²⁹ 0.0120	²³⁷ 1.315
233	TIGER-002	²¹¹ 2052	¹⁰⁸ 464	¹⁴⁶ 0.0056	¹⁴⁹ 0.0029	¹³⁴ 0.0024	¹¹⁵ 0.0019	⁹⁹ 0.0015	¹⁴⁹ 1.030
234	TIGER-003	¹⁹⁶ 2052	¹⁰⁵ 464	¹⁴⁵ 0.0056	¹⁴¹ 0.0029	¹³³ 0.0024	¹¹⁸ 0.0019	⁹⁹ 0.0015	¹⁴⁰ 1.030
235	TONGYITRANS-000	²²⁴ 2070	²¹ 190	¹⁵⁸ 0.0069	¹⁵⁹ 0.0038	¹⁵¹ 0.0032	¹⁵² 0.0029	¹⁵⁹ 0.0026	¹⁵² 1.038
236	TONGYITRANS-001	²²² 2070	²³ 189	¹⁵⁷ 0.0069	¹⁵¹ 0.0038	¹⁵⁰ 0.0032	¹⁵¹ 0.0029	¹⁵⁸ 0.0026	¹⁵³ 1.038
237	TOSHIBA-000	¹⁰⁸ 1548	²⁶² 930	¹³² 0.0045	¹²⁹ 0.0026	¹²⁷ 0.0022	¹²⁸ 0.0020	¹²⁴ 0.0018	¹³⁰ 1.026
238	TOSHIBA-001	²²⁰ 2060	²⁶³ 931	¹³⁷ 0.0048	¹³³ 0.0027	¹³⁰ 0.0023	¹²⁵ 0.0020	¹²⁵ 0.0018	¹³⁴ 1.027
239	TRUEFACE-000	¹¹⁶ 2000	⁶⁷ 365	¹¹² 0.0033	¹³⁹ 0.0028	¹⁴⁴ 0.0028	¹⁴⁶ 0.0026	¹⁵⁵ 0.0026	¹³¹ 1.026
240	VD-000	⁷⁴ 1028	⁶¹ 337	²⁶⁹ 0.4737	²⁶⁹ 0.3204	²⁶⁸ 0.2695	²⁶⁶ 0.2215	²⁶⁶ 0.1678	²⁶⁸ 4.058
241	VD-001	²⁰⁰ 2052	¹⁷⁰ 695	²²⁴ 0.0276	²²⁷ 0.0181	²²⁹ 0.0162	²²⁸ 0.0146	²³¹ 0.0130	²²⁷ 1.174
242	VD-002	²⁰⁴ 2052	¹⁶¹ 689	¹⁸⁰ 0.0095	¹⁹² 0.0077	¹⁹⁶ 0.0073	²⁰⁰ 0.0070	²⁰⁹ 0.0068	¹⁸⁹ 1.071
243	VD-003	²⁰³ 2052	¹⁶⁹ 693	¹⁶³ 0.0076	¹⁸⁵ 0.0069	¹⁹² 0.0067	¹⁹⁸ 0.0066	²⁰⁷ 0.0066	¹⁸³ 1.063
244	VERIDAS-001	¹⁴⁰ 2048	²⁴⁸ 885	¹⁰¹ 0.0028	⁹⁷ 0.0019	⁹³ 0.0017	⁹² 0.0015	⁹⁵ 0.0015	⁹⁷ 1.018
245	VERIDAS-002	¹¹⁷ 2048	²⁴⁷ 888	¹⁰⁰ 0.0028	⁹⁶ 0.0019	⁹¹ 0.0017	⁸⁹ 0.0015	⁹⁴ 0.0015	⁹⁵ 1.018
246	VERIDAS-003	¹⁸¹ 2048	²⁴⁷ 877	⁵⁷ 0.0018	⁶⁹ 0.0015	⁶⁵ 0.0014	⁶⁷ 0.0013	⁶¹ 0.0013	⁶¹ 1.014
247	VIGILANTSOLUTIONS-003	¹⁰⁵ 1544	²²³ 832	²⁴⁴ 0.0694	²⁴¹ 0.0349	²³⁶ 0.0262	²³⁸ 0.0201	²³³ 0.0140	²⁴¹ 1.355
248	VIGILANTSOLUTIONS-004	¹⁰⁷ 1544	²²³ 830	²⁵¹ 0.1249	²⁵⁹ 0.0706	²⁴⁹ 0.0557	²⁴⁷ 0.0434	²⁵⁰ 1.699	
249	VIGILANTSOLUTIONS-005	¹⁰⁴ 1544	²⁰⁷ 778	¹⁷⁶ 0.0092	¹⁶⁴ 0.0045	¹³⁵ 0.0036	¹⁴⁹ 0.0029	¹⁴⁰ 0.0022	¹⁶⁵ 1.046
250	VIGILANTSOLUTIONS-006	¹⁰² 1544	²²⁴ 834	¹⁸² 0.0099	¹⁶⁹ 0.0048	¹⁶³ 0.0038	¹⁵⁹ 0.0030	¹⁴⁴ 0.0022	¹⁶⁸ 1.049
251	VIGILANTSOLUTIONS-007	¹⁰³ 1544	¹⁵⁷ 618	¹¹⁴ 0.0034	⁹⁹ 0.0020	⁹² 0.0017	⁸⁹ 0.0015	⁷² 0.0013	¹⁰⁵ 1.019
252	VIGILANTSOLUTIONS-008	¹⁰⁶ 1544	⁸² 405	¹⁰⁶ 0.0029	⁹¹ 0.0018	⁸⁵ 0.0016	⁸¹ 0.0015	⁶³ 0.0013	⁹⁴ 1.018
253	VISIONBOX-000	²¹⁹ 2059	¹⁰⁹ 482	⁶⁵ 0.0019	⁶⁹ 0.0015	⁷¹ 0.0014	⁶⁸ 0.0013	⁶¹ 0.0013	⁶⁵ 1.014
254	VISIONLABS-004	¹⁹ 256	⁵⁸ 315	⁹⁹ 0.0027	⁸⁷ 0.0018	⁸⁶ 0.0016	⁸⁷ 0.0015	⁸⁴ 0.0014	⁹¹ 1.017
255	VISIONLABS-005	³¹ 512	⁵⁷ 300	⁸⁸ 0.0024	⁸⁴ 0.0017	⁷⁸ 0.0015	⁷⁷ 0.0014	⁶⁹ 0.0013	⁸² 1.016
256	VISIONLABS-006	⁴⁵ 512	⁵² 292	⁵⁹ 0.0018	⁶² 0.0015	⁵⁹ 0.0014	⁶¹ 0.0013	⁶² 0.0013	⁶⁰ 1.014
257	VISIONLABS-007	⁴⁶ 512	⁵⁸ 293	⁵³ 0.0018	⁵⁷ 0.0014	⁴⁹ 0.0013	⁴⁵ 0.0013	⁵⁶ 0.0012	⁵⁶ 1.013
258	VISIONLABS-008	³⁵ 512	⁴⁹ 277	⁷² 0.0020	⁹⁹ 0.0018	⁹⁸ 0.0018	¹⁰⁸ 0.0018	¹¹⁹ 0.0017	⁸⁶ 1.017
259	VISIONLABS-009	⁴³ 512	¹¹² 494	¹⁵ 0.0020	²¹ 0.0011	²¹ 0.0010	²⁴ 0.0010	²³ 0.0010	¹⁹ 1.010
260	VISIONLABS-010	⁴² 512	¹⁹² 732	²⁷ 0.0014	⁴⁰ 0.0013	⁴⁶ 0.0013	⁵² 0.0013	³⁷ 0.0013	³⁹ 1.012
261	VISIONLABS-011	⁴⁶ 512	¹⁹⁴ 736	¹⁸⁰ 0.0012	²⁴ 0.0011	²⁸ 0.0011	²⁹ 0.0011	³⁴ 0.0011	²⁴ 1.010
262	VOCORD-003	⁶ 896	¹⁸⁴ 714	¹⁵¹ 0.0062	¹⁴⁸ 0.0035	¹⁴⁵ 0.0030	¹⁴⁸ 0.0026	¹⁴⁶ 0.0023	¹⁴⁶ 1.035
263	VOCORD-004	⁶⁸ 896	¹²² 538	¹⁶⁶ 0.0079	¹⁶⁸ 0.0049	¹⁷¹ 0.0043	¹⁷³ 0.0038	¹⁷⁷ 0.0034	¹⁶⁶ 1.048
264	VOCORD-005	⁶ 768	²¹ 822	¹⁶⁰ 0.0070	¹⁶⁸ 0.0046	¹⁶⁸ 0.0041	¹⁷⁴ 0.0038	¹⁸⁰ 0.0035	¹⁶² 1.044
265	VOCORD-006	²⁷⁶ 10240	²¹⁸ 825	²⁷³ 1.0000	²⁷⁶ 1.0000	²⁷⁶ 1.0000	²⁷⁵ 1.0000	²⁷⁵ 1.0000	²⁷⁶ 10.000
266	VTS-000	¹⁷⁰ 2048	¹¹ 492	²⁷¹ 0.5937	²⁷⁸ 0.5936	²⁷² 0.5936	²⁷⁷ 0.5936	²⁷⁷ 0.5936	²⁷² 6.343
267	VTS-001	¹³³ 2048	²⁴⁸ 891	³⁶ 0.0015	²⁸ 0.0012	²⁶ 0.0011	²⁶ 0.0011	²⁷ 0.0010	²⁹ 1.011
268	VTS-002	¹⁵² 2048	²⁵³ 903	⁶⁶ 0.0019	⁵⁶ 0.0014	⁴⁴ 0.0013	⁴⁶ 0.0012	⁴¹ 0.0011	⁵⁹ 1.013
269	XFORWARDAI-000	¹⁷² 2048	²⁰² 768	⁸² 0.0023	¹⁰⁸ 0.0020	¹¹² 0.0020	¹²⁴ 0.0019	¹³⁰ 0.0019	¹⁰⁰ 1.018
270	XFORWARDAI-001	¹²⁰ 2048	¹⁶¹ 681	⁷⁵ 0.0020	⁹⁸ 0.0019	¹⁰⁹ 0.0019	¹²¹ 0.0019	¹²⁹ 0.0019	⁹² 1.018
271	XFORWARDAI-002	²⁵² 4096	²⁰¹ 935	⁶⁸ 0.0020	⁹⁹ 0.0019	¹⁰⁷ 0.0019	¹²⁰ 0.0019	¹²² 0.0019	⁹⁰ 1.017
272	YISHENG-001	²⁴⁴ 3704	⁷⁷ 387	²²³ 0.0265	²¹⁷ 0.0130	²¹⁴ 0.0102	²¹² 0.0080	²⁰² 0.0059	²¹⁸ 1.134
273	YITU-002	²⁶⁷ 4138	²⁴¹ 870	⁶⁰ 0.0018	³¹ 0.0012	³¹ 0.0011	²⁸ 0.0011	²⁶ 0.0010	³⁸ 1.012
274	YITU-003	²⁶⁶ 4138	²⁴² 871	¹⁰⁵ 0.0029	¹¹⁶ 0.0023	¹²⁶ 0.0022	¹³³ 0.0021	¹³⁸ 0.0021	¹¹³ 1.021
275	YITU-004	²²³ 2070	²⁵ 910	²² 0.0013	⁷ 0.0009	⁹ 0.0009	¹⁶ 0.0009	¹⁰ 0.0009	¹³ 1.009
276	YITU-005	²²⁵ 2070	²⁵⁶ 861	⁸⁴ 0.0023	¹⁰⁷ 0.0021	¹¹³ 0.0020	¹²² 0.0020	¹³³ 0.0020	¹⁰² 1.019

Table 25: Rank-based accuracy for the FRVT 2018 mugshot sets. In columns 3 and 4 are template size and template generation duration. Thereafter values are rank-based FNIR with $T = 0$ and FPIR = 1. This is appropriate to investigational uses but not those with higher volumes where candidates from all searches would need review. The next column is a workload statistic, a small value shows an algorithm front-loads mates into the first 10 candidates. Throughout, blue superscripts indicate the rank of the algorithm for that column, and the best value is highlighted in yellow.

MISSES BELOW THRESHOLD, T		ENROL RECENT MUGSHOT, N = 1.6M												ENROL APPLICATION PORTRAIT, N = 1.6M																		
#	ALGORITHM	ENROL: MUGSHOT			ENROL: MUGSHOT			ENROL: WEBCAM			ENROL: PROFILE			ENROL: VISA			ENROL: BORDER			PROBE: BORDER			PROBE: BORDER 10+YR			PROBE: KIOSK						
		FPIR=0.0003	FPIR=0.001	FPIR=0.01	FPIR=0.0003	FPIR=0.001	FPIR=0.01	FPIR=0.0003	FPIR=0.001	FPIR=0.01	FPIR=0.0003	FPIR=0.001	FPIR=0.01	FPIR=0.0001	FPIR=0.001	FPIR=0.01	FPIR=0.0001	FPIR=0.001	FPIR=0.01	FPIR=0.0001	FPIR=0.001	FPIR=0.01	FPIR=0.0001	FPIR=0.001	FPIR=0.01							
1	20FACE-000	228	0.462	235	0.348	242	0.230	237	0.763	231	0.450	231	0.301	201	1.000	205	1.000	209	1.000	167	0.424	166	0.255	88	0.772	89	0.599	161	0.938	173	0.836	
2	3DIVI-003	230	0.482	244	0.400	248	0.282	232	0.685	244	0.626	246	0.497					178	0.605	177	0.445			146	0.821	163	0.717					
3	3DIVI-004	201	0.256	216	0.169	220	0.093	204	0.400	222	0.343	226	0.237					158	0.277	161	0.172			125	0.607	143	0.485					
4	3DIVI-005	200	0.255	213	0.166	217	0.093	201	0.395	223	0.339	225	0.234	130	0.998	132	0.996	143	0.990	183	0.864	188	0.846			124	0.597	144	0.484			
5	3DIVI-006	199	0.253	215	0.168	222	0.096	207	0.403	221	0.342	227	0.238					159	0.283	162	0.174			128	0.615	146	0.490					
6	ACER-000	188	0.208	206	0.146	209	0.074	184	0.300	190	0.246	201	0.157	81	0.987	88	0.981	109	0.955	153	0.201	157	0.114			112	0.490	130	0.363			
7	ACER-001	131	0.109	148	0.056	152	0.026	126	0.136	131	0.109	134	0.069	157	1.000	165	0.999	189	0.998	116	0.068	116	0.036	83	0.406	84	0.250	111	0.479	86	0.206	
8	AIZE-001	142	0.127	168	0.077	166	0.034	154	0.187	158	0.143	157	0.087	104	0.995	113	0.994	132	0.983	129	0.101	13	0.052	77	0.364	80	0.216	93	0.387	114	0.289	
9	ALCHERA-000	192	0.231	203	0.138	204	0.070	197	0.259	185	0.216	195	0.146	146	0.999	148	0.999	172	0.996	148	0.176	158	0.111			142	0.803	140	0.456			
10	ALCHERA-001	271	1.000	271	0.999	277	0.999	261	1.000	271	1.000					237	1.000	26	1.000					234	1.000	227	1.000					
11	ALCHERA-002	250	0.807	251	0.486	251	0.302	231	0.685	241	0.591	241	0.442	175	1.000	172	1.000	194	0.999	182	0.827	182	0.770			143	0.811	168	0.705			
12	ALCHERA-003	224	0.450	207	0.155	205	0.070	189	0.304	196	0.239	200	0.152	167	1.000	158	0.999	177	0.997	147	0.172	146	0.097			107	0.464	129	0.362			
13	ALCHERA-004	234	0.520	243	0.394	241	0.211	228	0.642	237	0.529	235	0.327	105	0.995	108	0.991	76	0.813	168	0.424	164	0.232	86	0.708	88	0.515	121	0.546	138	0.398	
14	ALLGOVISION-000	151	0.138	180	0.088	186	0.045	165	0.202	174	0.166	181	0.106	90	0.993	105	0.990	132	0.982	132	0.117	139	0.066			116	0.526	137	0.396			
15	ALLGOVISION-001	160	0.155	185	0.102	192	0.053	182	0.275	180	0.221	194	0.141	95	0.993	95	0.986	97	0.933	142	0.150	141	0.081			113	0.491	136	0.389			
16	ANKE-000	171	0.184	190	0.117	201	0.063	175	0.256	187	0.220	198	0.151	101	0.995	112	0.994	142	0.990	229	1.000	275	1.000			211	1.000	217	1.000			
17	ANKE-001	169	0.183	194	0.119	202	0.063	176	0.256	188	0.220	199	0.151	102	0.995	118	0.994	155	0.992	254	1.000	249	1.000			192	1.000	193	1.000			
18	ANKE-002	96	0.062	108	0.032	108	0.014	93	0.103	97	0.079	99	0.050	61	0.975	63	0.948	71	0.795	81	0.034	83	0.018			63	0.245	80	0.190			
19	AWARE-003	168	0.174	198	0.128	210	0.082	197	0.351	217	0.298	219	0.204	78	0.987	92	0.984	122	0.977	169	0.428	177	0.378			119	0.530	139	0.443			
20	AWARE-004	216	0.355	229	0.269	237	0.175	224	0.619	236	0.509	239	0.375	171	1.000	176	1.000	197	0.999	164	0.397	168	0.279			144	0.816	159	0.631			
21	AWARE-005	240	0.608	248	0.364	211	0.085	194	0.342	207	0.253	203	0.163	168	1.000	180	1.000	199	0.999	157	0.255	159	0.122			136	0.916	162	0.714			
22	AWARE-006	229	0.475	230	0.276	238	0.175	215	0.466	225	0.398	230	0.283	154	1.000	168	0.999	160	0.999	162	0.368	168	0.254			136	0.749	152	0.623			
23	AYONIX-000	253	0.846	260	0.811	261	0.724	250	0.956	259	0.939	261	0.892	131	0.998	138	0.998	170	0.995	187	0.954	181	0.891			169	0.982	179	0.959			
24	AYONIX-001	254	0.875	262	0.824	263	0.701	245	0.946	254	0.920	257	0.845	166	1.000	164	0.999	173	0.996	191	0.999	191	0.998			166	0.969	176	0.926			
25	AYONIX-002	876	0.876	261	0.824	264	0.702	246	0.946	255	0.920	256	0.845	164	1.000	166	0.999	174	0.996	184	0.915	183	0.821			165	0.969	175	0.926			
26	CAMVI-003	120	0.094	163	0.071	19	0.058	135	0.152	150	0.132	182	0.108	67	0.979	71	0.970	10	0.940	131	0.114	147	0.100			96	0.402	133	0.377			
27	CAMVI-004	129	0.107	164	0.072	197	0.054	172	0.240	152	0.136	171	0.100	156	1.000	162	0.999	180	0.998	128	0.100	143	0.081			140	0.787	147	0.507			
28	CAMVI-005	152	0.139	184	0.099	217	0.076	181	0.451	187	0.179	189	0.132	162	1.000	174	1.000	188	0.998	143	0.156	159	0.112			177	0.999	187	0.983			
29	CANON-001	23	0.012	29	0.005	27	0.002	22	0.031	22	0.023	22	0.015	22	0.633	12	0.365	20	0.217	17	0.008	18	0.004	21	0.068	22	0.034	26	0.139	17	0.092	
30	CIB-000	70	0.044	51	0.012	40	0.005	67	0.077	49	0.045	46	0.025	181	1.000	186	1.000	203	1.000	44	0.017	36	0.008	39	0.141	37	0.068	133	0.894	148	0.521	
31	CLEARVIEWAI-000	25	0.013	30	0.006	26	0.002	29	0.036	25	0.025	25	0.016	143	0.999	76	0.974	9	0.149	18	0.008	13	0.004	17	0.057	17	0.027	73	0.268	10	0.080	
32	CLOUDWALK-HR-000	7	0.004	9	0.002	13	0.002	7	0.015	7	0.013	12	0.012	208	1.000	208	1.000	105	0.005	10	0.003	6	0.033	7	0.018	11	0.099	9	0.075			
33	CLOUDWALK-MT-000	4	0.003	8	0.002	16	0.002	4	0.015	8	0.013	14	0.012	10	0.169	1	0.109	1	0.077	1	0.002	3	0.002	1	0.018	1	0.009	1	0.072	3	0.063	
34	COGENT-000	159	0.143	138	0.053	158	0.029	146	0.175	154	0.140	173	0.100	111	0.996	125	0.995	148	0.991													
35	COGENT-001	156	0.143	139	0.053	157	0.029	145	0.175	155	0.140	174	0.100	133	0.998	137	0.998	159	0.994													
36	COGENT-002	165	0.159	125	0.044	117	0.017	112	0.124	122	0.098	126	0.063	135	0.998	137	0.998	159	0.994													
37	COGENT-003	183	0.203	130	0.046	113	0.016	110	0.121	116	0.095	123	0.061	136	0.999	140	0.998	168	0.995													

MISSES BELOW THRESHOLD, T		ENROL RECENT MUGSHOT, N = 1.6M												ENROL APPLICATION PORTRAIT, N = 1.6M																					
#	ALGORITHM	ENROL: MUGSHOT			ENROL: MUGSHOT			ENROL: MUGSHOT			ENROL: VISA			ENROL: BORDER			ENROL: BORDER 10+YR			ENROL: KIOSK															
		FPIR=0.0003	FPIR=0.001	FPIR=0.01	FPIR=0.0003	FPIR=0.001	FPIR=0.01	FPIR=0.0003	FPIR=0.001	FPIR=0.01	FPIR=0.0001	FPIR=0.001	FPIR=0.01	FPIR=0.0001	FPIR=0.001	FPIR=0.01	FPIR=0.0001	FPIR=0.001	FPIR=0.01	FPIR=0.0001	FPIR=0.001	FPIR=0.01													
47	CUBOX-000	10	0.005	15	0.003	18	0.002	16	0.022	16	0.019	18	0.014	5	0.276	3	0.168	5	0.104	6	0.004	7	0.003	5	0.028	5	0.014	2	0.073	2	0.062				
48	CYBERLINK-000	150	0.137	149	0.056	139	0.023	140	0.162	135	0.116	137	0.070	122	0.997	127	0.995	132	0.981	113	0.063	111	0.032			88	0.339	99	0.232						
49	CYBERLINK-001	121	0.096	142	0.054	137	0.022	128	0.138	132	0.109	131	0.067	121	0.997	122	0.995	135	0.984	110	0.062	107	0.031			129	0.652	101	0.239						
50	CYBERLINK-002	62	0.038	60	0.015	61	0.006	59	0.068	63	0.053	62	0.032	97	0.994	106	0.988	111	0.957	58	0.024	59	0.013			75	0.288	66	0.157						
51	CYBERLINK-003	73	0.045	35	0.008	35	0.004	33	0.045	36	0.035	33	0.021	98	0.995	74	0.972	79	0.845	33	0.012	34	0.007	31	0.100	31	0.051	90	0.368	36	0.120				
52	CYBERLINK-004	179	0.188	32	0.007	30	0.003	40	0.063	39	0.036	37	0.022	205	1.000	194	1.000	199	0.999	35	0.013	36	0.007	32	0.109	29	0.050	164	0.954	117	0.291				
53	CYBERLINK-005	186	0.208	42	0.010	41	0.004	39	0.054	45	0.041	48	0.026	177	1.000	178	1.000	85	0.888	36	0.014	35	0.007	27	0.089	26	0.043	160	0.926	108	0.266				
54	DAHUA-000	144	0.128	176	0.086	18	0.045	149	0.179	15	0.135	155	0.083																						
55	DAHUA-001	128	0.106	166	0.073	170	0.037	134	0.151	143	0.122	146	0.075	80	0.987	85	0.980	96	0.933																
56	DAHUA-002	44	0.026	61	0.015	59	0.006	41	0.060	51	0.046	52	0.029	27	0.681	31	0.638	42	0.522	41	0.017	40	0.008			36	0.159	39	0.125						
57	DAHUA-003	43	0.025	56	0.014	50	0.005	38	0.054	45	0.041	44	0.024	23	0.647	26	0.579	34	0.447	34	0.013	36	0.006	25	0.081	27	0.043	25	0.134	26	0.109				
58	DAHUA-004	26	0.014	31	0.007	31	0.003	25	0.033	27	0.026	26	0.016	15	0.552	21	0.485	29	0.345	24	0.008	21	0.004	13	0.051	15	0.027	19	0.113	20	0.094				
59	DAON-000	148	0.135	87	0.023	88	0.009	71	0.079	75	0.061	77	0.039	174	1.000	179	1.000	186	0.998	59	0.025	58	0.013	56	0.173	51	0.091	49	0.846	68	0.172				
60	DECATUR-000	67	0.043	90	0.023	90	0.010	76	0.085	81	0.066	79	0.040	30	0.757	35	0.675	39	0.509	62	0.027	67	0.014	55	0.173	60	0.098	61	0.239	58	0.156				
61	DEEPLINT-001	18	0.010	19	0.003	19	0.002	10	0.018	10	0.014	70	0.010	197	1.000	171	1.000	30	0.503	13	0.006	20	0.004			35	0.159	21	0.097						
62	DEEPSA-001	108	0.073	129	0.046	135	0.022	118	0.129	124	0.101	118	0.059	84	0.988	92	0.985	122	0.973	120	0.077	122	0.041			88	0.326	103	0.251						
63	DERMALOG-003	236	0.550	250	0.482	254	0.360	235	0.715	246	0.655	250	0.526																						
64	DERMALOG-004	238	0.554	249	0.480	253	0.358	234	0.711	247	0.657	248	0.526	115	0.997	128	0.995	157	0.991	177	0.603	179	0.458			150	0.856	166	0.751						
65	DERMALOG-005	180	0.189	179	0.088	170	0.043	16	0.201	165	0.154	168	0.096	113	0.996	103	0.990	10	0.950	160	0.300	16	0.267			127	0.614	141	0.459						
66	DERMALOG-006	123	0.098	136	0.052	151	0.026	127	0.137	127	0.105	130	0.067	85	0.989	87	0.981	97	0.933	108	0.059	109	0.031			84	0.318	97	0.230						
67	DERMALOG-007	17	0.188	177	0.086	170	0.040	16	0.200	16	0.152	165	0.093	112	0.996	104	0.990	10	0.950	127	0.099	13	0.052			125	0.557	121	0.299						
68	DERMALOG-008	204	0.268	127	0.045	118	0.017	170	0.231	113	0.094	110	0.054	184	1.000	197	1.000	206	1.000	105	0.057	99	0.025	81	0.382	77	0.158	162	0.940	158	0.678				
69	DERMALOG-009	66	0.041	80	0.021	82	0.009	77	0.086	82	0.066	82	0.040	176	1.000	191	1.000	203	1.000	71	0.031	74	0.016	90	0.999	91	0.999	148	0.840	93	0.222				
70	EYEDEA-003	233	0.509	240	0.388	246	0.265	226	0.625	239	0.543	240	0.404	116	0.997	119	0.994	141	0.990	175	0.570	174	0.392			141	0.792	157	0.658						
71	F-001	226	0.458	212	0.166	167	0.036							142	0.999	147	0.998	171	0.995																
72	FINCORE-000	176	0.187	202	0.071	181	0.026	186	0.217	192	0.140	170	1.000	183	1.000	164	0.995	149	0.187	154	0.108	85	0.598	87	0.418	106	0.458	126	0.349						
73	FUJITSULAB-000	196	0.246	81	0.021	29	0.008	60	0.070	69	0.056	71	0.035					57	0.024	62	0.013	57	0.177	58	0.093	62	0.240	59	0.156						
74	GLORY-000	223	0.441	239	0.367	250	0.295	222	0.586	240	0.547	244	0.470	100	0.995	121	0.995	156	0.993	171	0.453	177	0.381			147	0.839	177	0.795						
75	GLORY-001	215	0.355	231	0.305	243	0.236	221	0.582	238	0.537	242	0.448	96	0.994	110	0.993	146	0.991	166	0.408	170	0.336			145	0.819	167	0.753						
76	GORILLA-001	248	0.747	245	0.406	232	0.246	222	0.590	232	0.453	233	0.314	188	1.000	200	1.000	219	1.000	172	0.468	169	0.299			247	1.000	161	0.710						
77	GORILLA-002	203	0.266	219	0.188	226	0.106	196	0.342	208	0.268	209	0.170	203	1.000	207	1.000	157	0.993	156	0.250	160	0.137			181	1.000	143	0.466						
78	GORILLA-003	246	0.694	233	0.318	239	0.157	227	0.684	222	0.434	228	0.247	269	1.000	245	1.000	219	1.000	165	0.407	167	0.213			222	1.000	150	0.562						
79	GORILLA-004	147	0.135	182	0.089	179	0.043	162	0.202	171	0.160	176	0.101	88	0.972	65	0.959	87	0.903	137	0.135	140	0.072			102	0.438	123	0.309						
80	GORILLA-005	118	0.086	153	0.058	150	0.026	148	0.179	15	0.142	159	0.088	33	0.770	37	0.700	47	0.553	125	0.088	12	0.040			82	0.315	94	0.223						
81	GORILLA-006	76	0.046	106	0.027	96	0.011	105	0.118	107	0.089	106	0.053	19	0.602	25	0.531	31	0.369	63	0.028	60	0.013	52	0.166	57	0.093	55	0.218	57	0.154				
82	GRIAULE-000	69	0.044	78	0.020	81	0.009	74	0.082	76	0.063	76	0.038	124	0.997	123	0.995	105	0.952	78	0.033	91	0.020	61	0.185	62	0.107	51	0.198	64	0.166				
83	HIK-003	166	0.159	187	0.103	196	0.057	157	0.190	167	0.158	180	0.105	69	0.980	69	0.969	92	0.925	140	0.142	142	0.080			104	0.445	128	0.359						
84	HIK-004</																																		

MISSES BELOW THRESHOLD, T		ENROL RECENT MUGSHOT, N = 1.6M												ENROL APPLICATION PORTRAIT, N = 1.6M															
		ENROL: MUGSHOT				ENROL: MUGSHOT				ENROL: WEBCAM				ENROL: MUGSHOT				ENROL: BORDER				ENROL: BORDER 10+YR				ENROL: VISA			
#	ALGORITHM	FPIR=0.0003	FPIR=0.001	FPIR=0.01	FPIR=0.0003	FPIR=0.001	FPIR=0.01	FPIR=0.0003	FPIR=0.001	FPIR=0.01	FPIR=0.0003	FPIR=0.001	FPIR=0.01	FPIR=0.0003	FPIR=0.001	FPIR=0.01	FPIR=0.0003	FPIR=0.001	FPIR=0.01	FPIR=0.0003	FPIR=0.001	FPIR=0.01	FPIR=0.0003	FPIR=0.001	FPIR=0.01	FPIR=0.0003	FPIR=0.001	FPIR=0.01	
93	IDEMIA-008	⁵ 0.004	⁷ 0.002	⁸ 0.001	²⁵ 0.908	²⁵ 0.749	²⁶ 0.564	²⁴ 0.944	²³ 0.816	²³ 0.645	¹⁸ 1.000	¹⁹ 1.000	²¹ 1.000	⁹ 0.005	⁸ 0.003	¹⁰ 0.036	¹¹ 0.019	¹⁵ 0.106	¹⁶ 0.092										
94	IMAGUS-002	²⁵ 0.908	²⁵ 0.807	²⁶ 0.669	²⁴ 0.954	²⁵ 0.816	²⁵ 0.645	¹⁸ 1.000	¹⁹ 1.000	²⁰ 1.000	¹⁸ 1.000	¹⁹ 1.000	²¹ 1.000																
95	IMAGUS-003	⁵⁶ 0.898	⁷⁵ 0.018	⁷⁵ 0.008	⁷⁸ 0.088	⁸⁰ 0.066	⁸⁰ 0.040	⁴⁷ 0.926	⁵⁰ 0.838	⁵⁷ 0.647	⁶⁵ 0.029	⁷⁵ 0.016	⁵¹ 0.161	⁵⁹ 0.094	⁵⁸ 0.231	⁷⁸ 0.189													
96	IMAGUS-005	⁶³ 0.039	⁷⁷ 0.019	⁷⁰ 0.008	⁸² 0.093	⁸³ 0.069	⁸⁸ 0.042	⁷¹ 0.980	⁵⁸ 0.897	⁵² 0.621	⁶⁴ 0.028	⁶⁹ 0.015	⁵⁰ 0.161	⁵⁶ 0.092	⁶⁷ 0.260	⁷⁴ 0.181													
97	IMAGUS-006	⁶⁸ 0.044	⁸⁹ 0.023	⁸⁹ 0.010	⁹¹ 0.073	⁹² 0.045	⁹⁹ 0.973	⁵⁶ 0.893	⁵⁸ 0.651	⁷² 0.031	⁵³ 0.169	⁶¹ 0.098	⁷² 0.265	⁷³ 0.181															
98	IMAGUS-007	¹⁵⁹ 0.154	⁹⁵ 0.026	⁸⁸ 0.009	⁸⁴ 0.089	⁸⁵ 0.041	¹⁸³ 1.000	¹⁵¹ 0.999	¹⁶ 0.995	⁹⁰ 0.042	⁹² 0.020	⁶⁴ 0.245	⁶⁵ 0.168																
99	IMPERIAL-000	²² 0.423	²³ 0.310	²³ 0.199	²¹ 0.486	²² 0.420	²³ 0.304	¹⁶³ 1.000	¹⁴⁴ 0.998	¹⁶¹ 0.994																			
100	INCODE-000	²¹ 0.319	²² 0.212	²² 0.112	¹⁹ 0.348	²¹ 0.296	²¹ 0.198	²⁰⁰ 1.000	²⁰⁴ 1.000	²⁰ 1.000																			
101	INCODE-001	²⁰ 0.285	²¹ 0.184	²⁰ 0.100	¹⁹ 0.333	²⁰ 0.269	²¹ 0.176	¹²⁶ 0.998	¹¹¹ 0.993	¹²⁷ 0.976																			
102	INCODE-002	²⁰ 0.286	²¹ 0.167	²¹ 0.084	²⁰ 0.372	²⁰ 0.264	²⁰ 0.164	¹⁷³ 1.000	¹⁶⁷ 0.999	¹⁷ 0.996																			
103	INCODE-003	¹²⁵ 0.099	¹⁴⁵ 0.054	¹⁴¹ 0.023	¹⁴² 0.167	¹⁴² 0.120	¹³⁸ 0.070	¹²³ 0.997	¹²⁰ 0.995	⁹⁴ 0.929	¹¹² 0.063	¹⁰⁸ 0.031	⁸⁰ 0.313	⁹⁵ 0.226															
104	INCODE-004	³² 0.021	⁴⁶ 0.011	⁴⁴ 0.005	⁴¹ 0.055	⁴⁸ 0.043	⁴⁹ 0.026	²¹ 0.614	²² 0.528	³² 0.372	⁴³ 0.017	⁴³ 0.009	⁴² 0.145	⁴¹ 0.073	³³ 0.155	³⁰ 0.116													
105	INCODE-005																												
106	INNOVATRICS-002	²² 0.379	²² 0.234	²³ 0.139	²⁰ 0.403	²¹ 0.310	²² 0.209	¹⁸³ 1.000	¹⁹⁸ 1.000	²⁰² 0.999																			
107	INNOVATRICS-003	²¹⁰ 0.297	²²³ 0.221	²³¹ 0.132	²⁰⁰ 0.351	²¹² 0.297	²¹⁸ 0.203	¹⁷² 1.000	¹⁷⁷ 1.000	¹⁸⁵ 0.998																			
108	INNOVATRICS-004	¹⁷⁴ 0.184	²⁰⁰ 0.132	²¹⁷ 0.074	¹⁷⁸ 0.262	¹⁹ 0.222	¹⁹⁶ 0.149	⁷⁶ 0.984	⁸³ 0.980	¹¹⁷ 0.973	⁶⁵ 0.251	⁷⁸ 0.182																	
109	INNOVATRICS-005	⁹³ 0.057	¹¹¹ 0.034	¹¹⁰ 0.014	¹⁰¹ 0.114	¹⁰⁸ 0.089	¹⁰⁵ 0.052	⁴³ 0.890	⁵¹ 0.846	⁶³ 0.723	⁹⁷ 0.047	⁹⁵ 0.022	⁸⁵ 0.355	³¹ 0.154	³⁶ 0.120														
110	INNOVATRICS-007	³⁷ 0.024	⁵² 0.013	⁵¹ 0.005	⁴⁹ 0.065	⁵⁸ 0.051	⁵⁸ 0.032	³⁷ 0.806	³⁹ 0.743	⁴⁸ 0.567	⁴² 0.017	⁴⁴ 0.009	²⁹ 0.093	³² 0.053	³¹ 0.154	³⁶ 0.120													
111	INTSYSMSU-000	²⁶ 0.999	²⁶ 0.998	²⁷ 0.990	²⁶ 1.000	²⁶ 1.000	²⁶ 0.998	¹⁶⁹ 1.000	¹⁷⁵ 1.000	¹⁸¹ 0.998	¹⁹⁰ 0.999	¹⁹⁰ 0.989	¹⁷⁸ 0.999	¹⁸⁷ 0.988															
112	IREX-000	¹⁰⁵ 0.068	¹⁰⁴ 0.028	⁷³ 0.008	⁸⁰ 0.099	⁷⁴ 0.060	⁶⁰ 0.032	⁸³ 0.988	⁶⁴ 0.957	⁶² 0.680	⁹³ 0.044	⁵⁶ 0.011	⁷⁴ 0.302	³⁵ 0.062	⁴¹ 0.170	⁴⁷ 0.135													
113	ISYSTEMS-002	¹⁶¹ 0.155	¹⁷⁰ 0.078	¹⁶³ 0.032	¹⁵⁸ 0.161	¹⁴⁶ 0.126	¹⁵² 0.080	¹³³ 0.998	¹³⁶ 0.998	¹⁵⁵ 0.993																			
114	ISYSTEMS-003	¹⁸⁴ 0.204	¹⁵⁴ 0.059	¹⁴⁴ 0.024	¹²⁵ 0.135	¹³⁰ 0.107	¹³³ 0.068	¹⁷⁹ 1.000	¹⁸¹ 1.000	¹⁷⁷ 0.997																			
115	KAKAO-000	⁴⁷ 0.028	⁶³ 0.015	⁶² 0.006	⁶³ 0.071	⁶⁸ 0.056	⁶⁹ 0.034	¹⁴ 0.539	¹⁸ 0.468	²⁸ 0.327	⁴⁷ 0.019	⁴⁸ 0.010	³⁸ 0.141	⁴² 0.075	³⁴ 0.158	³⁷ 0.120													
116	KEDACOM-001	⁶⁵ 0.041	⁸⁸ 0.023	¹⁰ 0.013	⁸³ 0.096	⁸⁷ 0.072	¹⁰ 0.054	⁸⁶ 0.989	⁹⁷ 0.986	¹² 0.973	¹⁰⁴ 0.055	¹² 0.943																	
117	KNERON-000							¹⁶⁵ 0.033		¹⁷⁰ 0.099																			
118	KNERON-001							¹⁹ 0.052																					
119	LINE-000	⁹⁷ 0.062	¹⁰⁷ 0.031	¹⁰⁶ 0.012	¹²² 0.132	¹¹⁷ 0.095	¹¹¹ 0.054			²¹⁶ 1.000	⁹⁵ 0.046	⁹³ 0.021	⁷² 0.278	⁷⁶ 0.151	²⁴ 1.000	¹⁰⁸ 0.268													
120	LINE-001	⁵⁰ 0.030	²⁴ 0.005	²¹ 0.002	³⁰ 0.066	²⁸ 0.027	²⁴ 0.015	¹⁸⁰ 1.000	¹⁹⁶ 1.000	²²² 1.000	²⁸ 0.009	¹⁸ 0.004	²² 0.072	²³ 0.034	²⁵ 1.000	¹⁷⁴ 0.858													
121	LOOKMAN-003	¹⁰² 0.066	¹²³ 0.044	¹⁴⁶ 0.025	¹²¹ 0.131	¹³⁴ 0.112	¹⁵³ 0.082			¹²⁴ 0.084	¹³⁰ 0.061																		
122	LOOKMAN-004	¹⁰⁹ 0.074	¹²⁶ 0.045	¹⁴² 0.024	¹¹¹ 0.123	¹²⁹ 0.105	¹⁴⁴ 0.075	⁶⁶ 0.979	⁷⁸ 0.977	¹²⁵ 0.974																			
123	LOOKMAN-005	⁸² 0.050	¹⁰⁶ 0.030	¹¹⁶ 0.017	⁹¹ 0.102	¹⁰³ 0.086	¹²⁷ 0.063	⁷⁰ 0.980	⁸¹ 0.978	¹²⁰ 0.973	¹¹¹ 0.062	¹²⁸ 0.047																	
124	MANTRA-000	¹⁰⁴ 0.066	⁴³ 0.010	³⁷ 0.004	⁴⁵ 0.063	⁴⁴ 0.041	³⁶ 0.022	²⁶⁴ 1.000	²⁴⁸ 1.000	¹⁹⁶ 0.999	⁶⁶ 0.029	⁶⁴ 0.014	⁴⁶ 0.152	⁴⁸ 0.081	¹⁸⁰ 1.000	⁵⁵ 0.151													
125	MEGVII-001	¹⁸⁸ 0.210	¹⁶³ 0.072	¹⁷¹ 0.037	¹⁶⁸ 0.120	¹¹⁹ 0.096	¹¹⁷ 0.059	¹⁴¹ 0.999	¹⁴⁶ 0.998	⁸³ 0.872																			
126	MEGVII-002	²⁰² 0.258	¹⁶⁹ 0.077	¹⁷¹ 0.037	¹⁶⁸ 0.120	¹¹⁹ 0.096	¹¹⁷ 0.059	¹⁴¹ 0.999	¹⁴⁶ 0.998	⁸³ 0.872																			
127	MICROFOCUS-003	²⁶¹ 0.958	²⁶⁵ 0.931	²⁶ 0.866	²⁵ 0.988	²⁶ 0.979	²⁶³ 0.948			¹⁸⁸ 0.982	¹⁸⁹ 0.945																		
128	MICROFOCUS-004	²⁶⁹ 0.999	²⁷⁰																										

MISSES BELOW THRESHOLD, T		ENROL RECENT MUGSHOT, N = 1.6M												ENROL APPLICATION PORTRAIT, N = 1.6M							
#	ALGORITHM	ENROL: MUGSHOT			ENROL: MUGSHOT			ENROL: WEBCAM			PROBE: PROFILE			ENROL: VISA		ENROL: BORDER		ENROL: KIOSK			
		FPIR=0.0003	FPIR=0.001	FPIR=0.01	FPIR=0.0003	FPIR=0.001	FPIR=0.01	FPIR=0.0003	FPIR=0.001	FPIR=0.01	FPIR=0.0003	FPIR=0.001	FPIR=0.01	FPIR=0.001	FPIR=0.01	FPIR=0.001	FPIR=0.01	FPIR=0.001	FPIR=0.01		
139	NEC-004	¹ 0.003	⁵ 0.002	¹⁰ 0.002	⁶ 0.015	⁹ 0.013	⁸ 0.010	²⁴ 0.654	³⁰ 0.622	⁴⁹ 0.575	⁷ 0.004	¹¹ 0.004	³ 0.019	⁴ 0.012	¹² 0.100	¹³ 0.088					
140	NEC-005	¹⁴ 0.007	² 0.002	⁷ 0.001	² 0.014	¹ 0.012	⁵ 0.009	⁴⁴ 0.901	³⁴ 0.673	¹⁵ 0.177	⁴ 0.003	⁵ 0.002	² 0.019	³ 0.011	⁹ 0.099	¹² 0.087					
141	NEUROTECHNOLOGY-003	²⁶⁸ 0.999	²⁵⁶ 0.636	²²⁴ 0.099	²³⁸ 0.773	²⁰⁷ 0.266	²⁰⁴ 0.164	²¹⁹ 1.000	²³⁶ 1.000	²⁶⁹ 1.000											
142	NEUROTECHNOLOGY-004	¹³⁶ 0.120	¹⁵⁹ 0.063	¹⁵⁸ 0.028	¹³¹ 0.146	¹³⁶ 0.117	¹⁴⁰ 0.073	¹¹⁴ 0.996	¹¹⁶ 0.994	¹⁴³ 0.990											
143	NEUROTECHNOLOGY-005	¹³⁵ 0.117	¹⁴⁶ 0.054	¹³⁶ 0.022	¹⁷⁴ 0.252	¹⁴⁸ 0.130	¹⁴³ 0.074	¹³⁹ 0.999	¹³⁹ 0.998	¹⁴⁶ 0.989											
144	NEUROTECHNOLOGY-006	²⁶⁶ 0.987	²²⁸ 0.249	²²⁹ 0.121	²⁷⁴ 1.000	²²⁶ 0.418	²²⁰ 0.206														
145	NEUROTECHNOLOGY-007	¹⁹⁸ 0.252	¹⁵⁸ 0.062	¹³³ 0.021	²⁵⁹ 0.996	¹⁷⁷ 0.173	¹³² 0.068	¹⁹³ 1.000	¹⁸⁴ 1.000	¹⁷⁸ 0.997	¹⁶¹ 0.339	¹¹⁵ 0.036									
146	NEUROTECHNOLOGY-008	²⁴⁹ 0.797	¹⁴⁰ 0.053	¹⁰⁸ 0.012	⁹⁷ 0.110	⁹⁹ 0.080	⁹⁶ 0.047	¹⁸⁹ 1.000	²⁰² 1.000	²²¹ 1.000	⁸² 0.035	⁸⁰ 0.017	⁷⁵ 0.293	⁷⁴ 0.149	⁵² 0.203	⁵⁶ 0.152					
147	NEUROTECHNOLOGY-009	⁴⁵ 0.027	⁶⁴ 0.015	⁵⁷ 0.006	⁵² 0.066	⁶⁹ 0.052	⁵⁹ 0.032	²⁵ 0.661	²⁸ 0.588	³⁴ 0.436	⁴⁹ 0.020	⁴⁷ 0.010	⁴⁷ 0.153	⁵⁰ 0.082	³⁸ 0.165	⁴³ 0.129					
148	NEUROTECHNOLOGY-010	²¹³ 0.346	⁴¹ 0.010	³⁴ 0.003	³⁴ 0.047	⁴⁰ 0.037	⁴² 0.023	¹⁰ 0.377	¹⁰ 0.277	¹⁴ 0.170	³⁰ 0.010	²⁴ 0.005	²⁴ 0.075	²⁵ 0.039	²² 0.126	²² 0.097					
149	NEWLAND-002	²³⁸ 0.523	²⁴⁷ 0.438	²⁴⁹ 0.294	²¹⁸ 0.535	²³³ 0.466	²³⁶ 0.335	¹⁴⁷ 0.999	¹⁵⁸ 0.999	¹⁸⁴ 0.998											
150	NOBLIS-001	²⁷² 1.000	²⁷² 1.000	²⁷⁷ 0.991	²⁷⁶ 1.000	²⁶⁹ 1.000	¹⁸⁶ 1.000	²⁰¹ 1.000	²¹⁸ 1.000												
151	NOBLIS-002	²⁷⁰ 1.000	²⁶⁸ 0.997	²⁵⁸ 0.488	²⁶⁷ 1.000	²⁷² 1.000	²⁰² 1.000	²⁰⁶ 1.000	²¹³ 1.000												
152	NOTIONTAG-000	⁵⁴ 0.032	⁶⁷ 0.017	⁷¹ 0.007	⁶⁶ 0.076	⁷³ 0.059	⁷⁴ 0.036	²⁶ 0.671	²⁹ 0.611	³⁶ 0.467	⁸² 0.021	⁵³ 0.011	⁴⁵ 0.150	⁵¹ 0.084	⁴² 0.176	⁴⁹ 0.140					
153	NTechLab-003	¹¹² 0.080	¹⁴⁴ 0.054	¹⁵⁶ 0.028	¹³² 0.148	¹³⁷ 0.118	¹⁴⁵ 0.075	⁴¹ 0.873	⁴⁹ 0.837	⁷⁰ 0.752											
154	NTechLab-004	⁹⁹ 0.063	¹¹⁹ 0.041	¹³¹ 0.021	¹²⁰ 0.131	¹²⁵ 0.105	¹²⁹ 0.065	⁴⁰ 0.868	⁴⁸ 0.833	⁶⁸ 0.746	¹⁰³ 0.053	¹⁰⁶ 0.030									
155	NTechLab-005	⁹⁸ 0.062	¹²⁰ 0.042	¹³² 0.021	¹¹⁹ 0.130	¹²⁶ 0.102	¹²⁶ 0.063	³⁸ 0.816	⁴² 0.771	⁶⁹ 0.661	¹¹⁸ 0.073	¹¹⁹ 0.039									
156	NTechLab-006	⁹² 0.056	¹¹⁴ 0.037	¹²¹ 0.018	¹⁰⁸ 0.121	¹¹⁴ 0.094	¹¹⁶ 0.059	³⁶ 0.802	⁴¹ 0.754	⁵⁵ 0.635	¹⁰⁶ 0.057	¹¹⁰ 0.032									
157	NTechLab-007	⁶⁴ 0.040	⁹² 0.026	¹⁰² 0.012	⁷⁹ 0.085	⁸³ 0.067	⁸⁴ 0.041	³⁵ 0.796	⁴⁰ 0.750	⁵⁶ 0.642	⁷⁶ 0.032	⁸¹ 0.017									
158	NTechLab-008	³⁹ 0.024	⁵⁷ 0.014	⁶⁴ 0.007	⁴² 0.057	⁵⁶ 0.045	⁵³ 0.029	¹⁸ 0.601	²⁴ 0.529	³³ 0.391	⁸⁰ 0.033	⁸⁵ 0.018									
159	NTechLab-009	¹⁷ 0.010	²⁶ 0.005	²⁸ 0.003	²⁰ 0.028	²¹ 0.022	²⁰ 0.014	¹³ 0.522	¹⁵ 0.430	²⁴ 0.311	³⁷ 0.015	³⁸ 0.008	³⁵ 0.109	³⁴ 0.061	²⁷ 0.142	²⁷ 0.114					
160	PARAVISION-010	¹¹ 0.005	¹² 0.003	⁹ 0.002	¹² 0.018	¹³ 0.015	¹¹ 0.011	⁹ 0.334	⁹ 0.252	¹³ 0.169	¹⁴ 0.007	¹⁶ 0.004	¹⁸ 0.059	²⁰ 0.031	⁸ 0.098	⁷ 0.077					
161	PARAVISION-011	¹² 0.006	¹⁶ 0.003	¹² 0.002	¹¹ 0.018	¹² 0.015	¹⁰ 0.010	⁷ 0.291	⁷ 0.228	¹¹ 0.150	²⁷ 0.009	²³ 0.004	²⁵ 0.074	²⁴ 0.038	⁶ 0.091	⁵ 0.075					
162	PARAVISION-000	²⁰² 0.278	¹⁸¹ 0.089	¹⁸⁸ 0.045	²¹² 0.447	¹⁷⁶ 0.170	¹⁷⁵ 0.100	¹⁹⁹ 1.000	¹⁵⁷ 0.999	¹⁷⁶ 0.997	¹⁷³ 0.470	¹⁷⁷ 0.443									
163	PARAVISION-001	¹⁵³ 0.140	¹³³ 0.049	¹²⁸ 0.020	¹⁶⁶ 0.207	¹⁴⁷ 0.128	¹⁴² 0.074	¹⁹⁵ 1.000	¹⁴⁹ 0.999	¹⁶⁸ 0.994	¹⁷⁰ 0.444	¹⁷⁶ 0.428									
164	PARAVISION-002	¹¹⁷ 0.085	¹³⁴ 0.050	¹³⁸ 0.022	¹³⁶ 0.152	¹⁴⁰ 0.119	¹⁴⁷ 0.076	⁸⁹ 0.992	⁹⁰ 0.983	⁶⁹ 0.748	¹²¹ 0.080	¹²² 0.043									
165	PARAVISION-003	¹⁰⁰ 0.063	¹¹² 0.035	¹¹² 0.016	¹¹⁴ 0.124	¹¹⁸ 0.096	¹¹⁹ 0.060	¹²⁰ 0.997	¹¹⁷ 0.994	⁶⁴ 0.733	¹⁰⁷ 0.058	¹¹³ 0.034									
166	PARAVISION-004	⁴⁰ 0.025	⁴⁵ 0.010	⁴³ 0.004	³⁶ 0.049	⁴¹ 0.038	⁴³ 0.024	¹⁹⁴ 1.000	¹⁹⁵ 1.000	⁷⁴ 0.797	⁴⁵ 0.018	⁵⁰ 0.011									
167	PARAVISION-005	²⁸ 0.014	²¹ 0.004	²³ 0.002	²⁵ 0.031	²⁵ 0.024	²⁷ 0.016	¹¹⁸ 0.997	⁸⁴ 0.980	¹⁶ 0.181	³¹ 0.011	³⁹ 0.008									
168	PARAVISION-007	⁷⁸ 0.048	²⁰ 0.004	¹⁷ 0.002	²¹⁹ 0.560	²⁴ 0.025	²³ 0.015	¹⁹² 1.000	¹⁹³ 1.000	²¹⁷ 1.000	²⁶ 0.009	³¹ 0.006	³⁴ 0.113	¹⁴ 0.024	²⁶⁷ 1.000	²⁷⁴ 1.000					
169	PARAVISION-009	¹⁵ 0.007	¹⁴ 0.003	⁶ 0.001	¹⁸ 0.026	¹⁷ 0.019	¹⁵ 0.012	³⁴ 0.778	³⁸ 0.735	⁴⁶ 0.550	³ 0.003	² 0.002	⁷ 0.033	⁶ 0.015	² 0.073	¹ 0.061					
170	PIXELALL-002	²⁴³ 0.664	¹⁸⁸ 0.105	¹⁵⁹ 0.030	²⁵² 0.974	²²² 0.388	¹⁵⁴ 0.083			²⁰⁹ 1.000	²¹¹ 1.000	¹⁷⁶ 0.602	¹²⁸ 0.047								
171	PIXELALL-003	⁷⁹ 0.049	⁸⁴ 0.022	⁸³ 0.009	⁹² 0.102	⁹⁰ 0.073	⁸⁹ 0.043			¹⁷³ 1.000	¹⁸³ 0.998	⁸⁶ 0.037	⁹⁰ 0.020								
172	PIXELALL-004	¹³⁷ 0.120	⁷⁴ 0.018	⁶⁸ 0.007	²³⁹ 0.783	⁹⁹ 0.079	⁷⁵ 0.037			¹⁸⁸ 1.000	¹⁹³ 0.999	⁹⁹ 0.051	⁷¹ 0.015								
173	PIXELALL-005	¹¹¹ 0.079	⁴⁹ 0.012	⁴⁵ 0.005	²¹⁴ 0.456	⁵¹ 0.050	⁵⁰ 0.027			²⁰⁸ 1.000	²⁰¹ 0.999	⁶¹ 0.027	⁷⁷ 0.017	⁶³ 0.203	³⁸ 0.071	¹⁷⁹ 1.000	¹⁸⁴ 0.983				
174	PTAKURATSATU-000	⁹⁴ 0.057	¹¹³ 0.037	¹¹¹ 0.017	¹⁴¹ 0.165	¹⁴⁵ 0.124	¹³⁹ 0.071	⁵⁵ 0.947	⁶⁰ 0.924	⁸¹ 0.868	⁹⁶ 0.046	⁹⁴ 0.022	⁶² 0.206	⁶⁷ 0.120	⁵⁹ 0.232	⁷² 0.179					
175	QNAP-000	²⁶⁴ 0.972	¹⁹⁹ 0.129	¹⁹¹ 0.052	²⁶¹ 0.998	¹⁹⁵ 0.238	¹⁸⁸ 0.117	²⁰⁴ 1.000	²¹¹ 1.000	²²⁰ 1.000	¹⁵⁰ 0.191	¹³⁸ 0.068	⁸⁴ 0.539	⁸⁶ 0.263	¹⁷⁶ 0.998	¹⁸⁶ 0.985					
176	QNAP-001	¹¹⁶ 0.083	¹⁴³ 0.054	¹⁴⁵ 0.024	¹⁴⁷ 0.176	¹⁵⁷ 0.137	¹⁵⁶ 0.085	⁵¹ 0.943	⁶¹ 0.928	⁸² 0.870	¹²² 0.081	¹²³ 0.041	⁷⁹ 0.368	⁸² 0.							

MISSES BELOW THRESHOLD, T		ENROL RECENT MUGSHOT, N = 1.6M												ENROL APPLICATION PORTRAIT, N = 1.6M												
#	ALGORITHM	ENROL: MUGSHOT			ENROL: MUGSHOT			ENROL: WEBCAM			ENROL: MUGSHOT			ENROL: PROFILE			ENROL: VISA		ENROL: BORDER		ENROL: BORDER 10+YR		ENROL: VISA			
		FPIR=0.0003	FPIR=0.001	FPIR=0.01	FPIR=0.0003	FPIR=0.001	FPIR=0.01	FPIR=0.0003	FPIR=0.001	FPIR=0.01	FPIR=0.0003	FPIR=0.001	FPIR=0.01	FPIR=0.0003	FPIR=0.001	FPIR=0.01	FPIR=0.001	FPIR=0.01	FPIR=0.001	FPIR=0.01	FPIR=0.001	FPIR=0.01	FPIR=0.001	FPIR=0.01		
185	RANKONE-010	³⁴ 0.023	³⁵ 0.014	⁶⁹ 0.007	⁶⁸ 0.077	⁷¹ 0.058	⁷³ 0.036	⁴⁶ 0.905	⁴⁵ 0.802	⁵⁹ 0.652	¹⁰² 0.052	¹⁰³ 0.027	⁶⁶ 0.208	⁶⁹ 0.119	⁶⁶ 0.259	⁸¹ 0.194										
186	RANKONE-011	¹³² 0.109	³⁶ 0.009	⁴⁰ 0.004	⁷² 0.079	⁵³ 0.048	⁵⁴ 0.029				⁸⁵ 0.037	⁸² 0.017	⁵⁸ 0.182	⁵⁶ 0.092	¹⁶⁸ 0.977	¹⁴² 0.465										
187	RANKONE-012	³¹ 0.020	³³ 0.008	³⁸ 0.004	⁶⁴ 0.072	⁶⁴ 0.053	⁵⁵ 0.030				⁶⁷ 0.029	⁶⁶ 0.014	⁴¹ 0.144	³⁹ 0.072	¹⁰⁸ 0.465	⁴³ 0.128										
188	REALNETWORKS-000	²¹⁹ 0.374	²²³ 0.234	²³⁴ 0.138	²⁰⁹ 0.433	²¹⁸ 0.319	²²² 0.209																			
189	REALNETWORKS-001	²¹⁸ 0.374	²²⁶ 0.234	²³³ 0.138	²¹⁰ 0.433	²¹⁷ 0.319	²²³ 0.209																			
190	REALNETWORKS-002	²¹⁷ 0.370	²²⁴ 0.231	²³² 0.137	²⁰⁸ 0.416	²¹⁷ 0.315	²²⁴ 0.209																			
191	REALNETWORKS-003	²⁰⁵ 0.273	²¹⁰ 0.159	²¹⁶ 0.090	¹⁹⁰ 0.342	²⁰⁶ 0.266	²¹⁰ 0.172	¹⁴⁵ 0.999	¹⁴⁵ 0.998	¹³⁷ 0.987	¹⁴⁵ 0.164	¹⁵⁰ 0.103											¹¹⁵ 0.500	¹³¹ 0.364		
192	REALNETWORKS-004	¹⁹⁵ 0.242	²⁰⁹ 0.158	²¹⁵ 0.090	²⁰¹ 0.353	²⁰⁴ 0.263	²⁰⁷ 0.169	¹⁵⁹ 1.000	¹⁵⁹ 0.999	¹⁵⁴ 0.992	¹⁴⁶ 0.170	¹⁵¹ 0.103											¹²⁶ 0.613	¹³² 0.370		
193	REALNETWORKS-005	⁸⁵ 0.052	¹⁰¹ 0.028	¹⁰⁴ 0.012	⁸² 0.094	⁹² 0.074	⁹⁵ 0.047	⁷⁵ 0.984	⁷² 0.971	⁸⁸ 0.896	⁸⁴ 0.037	⁷⁹ 0.017	⁶⁷ 0.223	⁶⁹ 0.123	⁵⁴ 0.215	⁶⁷ 0.165										
194	REALNETWORKS-006	⁴² 0.025	⁵⁸ 0.015	⁵⁴ 0.006	⁶² 0.053	⁶³ 0.032	⁹¹ 0.993	⁸⁶ 0.980	⁷⁸ 0.838	³⁸ 0.016	⁴¹ 0.008	³⁵ 0.120	³⁶ 0.063	³² 0.154	²⁹ 0.116											
195	REMARKAI-000	¹⁴¹ 0.125	¹⁴⁷ 0.055	¹⁴⁰ 0.023	¹⁴⁴ 0.173	¹⁴¹ 0.120	¹³⁶ 0.070	¹⁵² 0.999	¹⁵⁶ 0.999	¹⁶⁶ 0.995	¹¹⁷ 0.069	¹¹² 0.033											¹³³ 0.717	¹²⁴ 0.315		
196	REMARKAI-000	¹⁸² 0.197	¹⁹² 0.128	¹⁹⁹ 0.059	¹⁷⁷ 0.263	¹⁸⁶ 0.203	¹⁸⁸ 0.123																			
197	REMARKAI-002	¹⁷⁸ 0.188	¹⁹⁶ 0.124	¹⁹⁸ 0.059	¹⁷³ 0.248	¹⁸² 0.196	¹⁸⁷ 0.122	⁹⁴ 0.993	¹⁰⁷ 0.991	¹³⁰ 0.980																
198	RENDIP-000	³⁵ 0.023	⁴⁸ 0.012	⁴⁹ 0.005	¹⁵⁶ 0.189	⁷² 0.059	⁶⁸ 0.034	⁵⁴ 0.945	⁵⁷ 0.894	⁶⁷ 0.744	⁵³ 0.022	⁵⁹ 0.013	⁶⁰ 0.185	⁵² 0.089	³⁹ 0.167	⁴⁴ 0.130										
199	REVEALMEDIA-000	³⁶ 0.024	⁵⁰ 0.012	⁵³ 0.006	⁴⁰ 0.054	⁴⁷ 0.042	⁴⁷ 0.025	²⁹ 0.755	³⁶ 0.680	⁴⁵ 0.539	⁵¹ 0.021	⁵¹ 0.011	³⁰ 0.093	³² 0.051	²⁸ 0.143	³² 0.118										
200	S1-000	¹⁴⁹ 0.137	¹⁰³ 0.028	⁹⁷ 0.011	¹¹⁷ 0.129	¹⁰² 0.085	⁹⁷ 0.048	²⁰⁶ 1.000	²¹² 1.000	⁹⁵ 0.596	⁹⁸ 0.047	⁸⁸ 0.018	¹⁶⁴ 1.000	⁶⁹ 0.123	²³⁰ 1.000	¹⁵⁶ 0.632										
201	S1-001	⁸⁸ 0.054	⁶⁵ 0.016	⁶⁶ 0.007	⁵¹ 0.066	⁵⁹ 0.052	⁶⁷ 0.033	⁸⁸ 0.992	⁹⁴ 0.985	¹⁰⁷ 0.952	⁴⁶ 0.019	⁴⁶ 0.010	³⁷ 0.136	⁴³ 0.075												
202	SCANOVATE-000	¹²⁷ 0.103	¹⁶² 0.067	¹⁶⁰ 0.030	¹⁸⁶ 0.296	¹⁹⁶ 0.240	¹⁹⁷ 0.150	⁴⁹ 0.931	⁵⁵ 0.893	⁷⁰ 0.803	¹⁵⁴ 0.215	¹⁵⁸ 0.118										⁹⁵ 0.400	¹²⁸ 0.299			
203	SCANOVATE-001	¹⁴³ 0.128	¹⁷³ 0.081	¹⁷² 0.037	¹⁸⁵ 0.281	¹⁹² 0.227	¹⁹³ 0.140	⁵⁰ 0.935	⁵⁹ 0.911	⁷⁷ 0.834	¹⁵¹ 0.192	¹⁵² 0.103										⁹⁸ 0.404	¹¹⁶ 0.290			
204	SENSETIME-000	⁵⁹ 0.036	⁸² 0.021	⁸⁰ 0.009	⁶⁹ 0.078	⁷⁷ 0.063	⁸¹ 0.040	²³⁶ 1.000	²⁶¹ 1.000	¹³⁸ 0.988																
205	SENSETIME-001	⁶⁰ 0.036	⁸⁵ 0.022	⁸⁸ 0.010	⁷⁵ 0.080	⁷⁹ 0.064	⁸⁷ 0.041																			
206	SENSETIME-002	⁶¹ 0.037	⁵⁹ 0.015	¹¹¹ 0.014	¹¹³ 0.124	³¹ 0.028	⁴⁰ 0.023	¹¹⁷ 0.997	¹¹⁵ 0.994	¹²⁸ 0.979	⁷⁴ 0.032	⁷⁹ 0.017										¹¹⁷ 0.523	⁶² 0.160			
207	SENSETIME-003	⁶ 0.004	⁶ 0.002	¹ 0.001	³ 0.014	³ 0.012	³ 0.009	²⁰ 0.607	¹⁹ 0.477	² 0.311	²¹ 0.008	² 0.005	²⁴ 0.133	²⁹ 0.115												
208	SENSETIME-004	³ 0.003	³ 0.002	⁴ 0.001	⁵ 0.015	⁵ 0.013	⁸ 0.010	³⁰ 0.301	⁸ 0.229	¹⁰ 0.149	¹² 0.006	¹² 0.004	¹⁸ 0.113	²¹ 0.100												
209	SENSETIME-005	²⁰ 0.011	¹⁰ 0.002	³ 0.001	¹⁴ 0.018	¹¹ 0.014	⁶ 0.010	³⁰ 0.259	⁴ 0.173	³ 0.103	¹⁵ 0.007	¹⁴ 0.004	¹⁴ 0.051	¹³ 0.023	¹⁴ 0.104	¹⁸ 0.093										
210	SENSETIME-006	⁸ 0.005	⁴ 0.002	² 0.001	⁸ 0.016	⁴ 0.012	²⁴³ 0.009	¹³⁷ 0.999	¹⁴³ 0.998	⁶¹ 0.680	⁵ 0.004	⁴ 0.002	⁸ 0.034	⁷ 0.016	⁷ 0.093	⁹ 0.079										
211	SENSETIME-007	² 0.003	¹ 0.001	¹ 0.001	¹ 0.012	¹ 0.009	¹⁰ 0.007	¹⁶⁰ 1.000	¹⁶¹ 0.999	⁴¹ 0.538	² 0.003	¹ 0.001	⁴ 0.024	³ 0.011	⁴ 0.085	⁴ 0.074										
212	SHAMAN-003	²³² 0.506	²⁴⁸ 0.451	²⁵² 0.347	²²⁹ 0.650	²⁴² 0.597	²⁴⁵ 0.472																			
213	SHAMAN-004	²⁴⁴ 0.679	²⁵⁵ 0.615	²⁵⁸ 0.488	²⁴⁸ 0.812	²⁴⁷ 0.754	²⁵² 0.639																			
214	SHAMAN-006	¹⁷⁸ 0.185	²⁰⁴ 0.141	²¹⁸ 0.092	¹⁸³ 0.278	¹⁹⁴ 0.237	²⁰⁶ 0.168	⁶⁵ 0.978	⁷³ 0.972	¹¹² 0.960																
215	SHAMAN-007	¹⁷⁰ 0.183	²⁰⁵ 0.141	²¹⁷ 0.092	¹⁸⁴ 0.280	¹⁹⁷ 0.240	²⁰⁸ 0.169																			
216	SIAT-001	¹⁴⁶ 0.132	⁶⁸ 0.018	⁶⁵ 0.007	²² 0.641	²²³ 0.365	²³⁷ 0.348				⁷⁰ 0.031	⁶⁸ 0.014														
217	SIAT-002	²²¹ 0.417	⁸³ 0.022	²⁰ 0.007	²⁴³ 0.942	²³⁴ 0.478	²⁴³ 0.460				¹⁶³ 0.372	¹⁷¹ 0.356										¹⁵⁸ 0.923	⁶⁶ 0.169			
218	SMILART-004	²⁶³ 0.970	²⁶⁶ 0.968	²⁷⁰ 0.965	²⁵³ 0.977	²⁶² 0.976	²⁶⁴ 0.973																			
219	SMILART-005																									
220	SQISOFT-001	¹⁹¹ 0.226	²⁰¹ 0.132	¹⁸² 0.044	¹⁹³ 0.340	²⁰⁰ 0.252	¹⁸³ 0.111	⁵⁷ 0.956	⁴³ 0.797	⁵¹ 0.608	⁸⁸ 0.040	⁸⁸ 0.019	⁷⁶ 0.317	⁷⁵ 0.150	¹⁰⁰ 0.420	⁷⁹ 0.189										
221	STAQU-000	²¹² 0.334	¹⁵⁶ 0.062	¹³⁴ 0.022	²⁴¹ 0.848	²³⁰ 0.443	¹²¹ 0.061	¹⁷⁸ 1.000</td																		

MISSES BELOW THRESHOLD, T		ENROL RECENT MUGSHOT, N = 1.6M												ENROL APPLICATION PORTRAIT, N = 1.6M								
#	ALGORITHM	ENROL: MUGSHOT			ENROL: MUGSHOT			ENROL: WEBCAM			PROBE: PROFILE			ENROL: VISA		ENROL: BORDER		ENROL: KIOSK				
		FPIR=0.0003	FPIR=0.001	FPIR=0.01	FPIR=0.0003	FPIR=0.001	FPIR=0.01	FPIR=0.0003	FPIR=0.001	FPIR=0.01	FPIR=0.0003	FPIR=0.001	FPIR=0.01	FPIR=0.001	FPIR=0.01	FPIR=0.001	FPIR=0.01	FPIR=0.001	FPIR=0.01	FPIR=0.001	FPIR=0.01	
231	TEVIAN-007	²¹ 0.011	²⁸ 0.005	²⁹ 0.003	¹⁹ 0.028	²⁰ 0.022	²¹ 0.015	¹² 0.504	¹¹ 0.301	¹⁷ 0.183	²⁹ 0.009	²⁵ 0.005	²⁰ 0.065	²¹ 0.033	²⁰ 0.122	²⁵ 0.102						
232	TIGER-000	²² 0.462	²⁴ 0.390	²⁴ 0.261	²³ 0.565	²³ 0.500	²³ 0.366															
233	TIGER-002	¹⁶⁴ 0.158	¹⁷⁵ 0.086	¹⁷⁷ 0.039	¹⁶⁷ 0.202	¹⁶⁷ 0.158	¹⁶⁷ 0.095	¹⁵³ 0.999	¹⁵³ 0.999	¹²⁶ 0.975												
234	TIGER-003	¹⁶³ 0.158	¹⁷⁴ 0.086	¹⁷⁴ 0.039	¹⁶⁴ 0.202	¹⁶⁸ 0.158	¹⁶⁶ 0.095															
235	TONGYITRANS-000	¹³⁰ 0.107	¹⁶⁷ 0.074	¹⁷⁷ 0.038	¹²⁷ 0.141	¹³³ 0.112	¹³⁵ 0.069															
236	TONGYITRANS-001	¹⁴⁰ 0.124	¹⁶¹ 0.066	¹⁶² 0.032	¹¹⁶ 0.128	¹²⁵ 0.101	¹²⁵ 0.062															
237	TOSHIBA-000	¹³⁹ 0.123	¹⁵⁷ 0.062	¹⁵⁷ 0.027	¹³³ 0.150	¹³⁵ 0.118	¹⁴¹ 0.074	¹¹⁹ 0.997	¹²⁶ 0.995	¹³⁹ 0.988												
238	TOSHIBA-001	¹⁸⁹ 0.225	¹⁵² 0.058	¹²³ 0.019	¹²⁴ 0.133	¹¹² 0.092	¹¹² 0.054															
239	TRUEFACE-000	⁷⁴ 0.046	⁷³ 0.018	⁷⁸ 0.008	⁷⁰ 0.079	⁷⁸ 0.062	⁷⁸ 0.039	¹⁰⁶ 0.995	⁵² 0.882	³⁷ 0.499	⁶⁸ 0.030	⁷⁶ 0.016	⁶² 0.194	⁶⁵ 0.111	⁴⁹ 0.188	⁵³ 0.145						
240	VD-000	²⁶⁰ 0.950	²⁶⁴ 0.917	²⁶⁷ 0.827	²⁵¹ 0.968	²⁶⁰ 0.946	²⁶⁰ 0.871															
241	VD-001	²⁰⁶ 0.278	²²¹ 0.201	²²⁹ 0.116	¹⁹¹ 0.331	²¹⁰ 0.281	²¹⁵ 0.188															
242	VD-002	¹⁵⁷ 0.144	¹⁷¹ 0.079	¹⁶⁸ 0.036	¹⁵⁵ 0.188	¹⁶⁷ 0.148	¹⁶¹ 0.092	¹²⁸ 0.998	¹²⁹ 0.996	¹³⁶ 0.987	¹²⁶ 0.095	¹²⁹ 0.048	⁷⁸ 0.367	⁸¹ 0.220	⁹¹ 0.372	¹¹² 0.280						
243	VD-003	¹⁹³ 0.234	¹²⁸ 0.046	¹²⁵ 0.020	¹²³ 0.133	¹²² 0.100	¹²⁴ 0.061	¹⁵⁰ 0.999	¹⁵⁴ 0.999	¹⁵⁶ 0.994	¹⁰⁰ 0.051	¹⁰¹ 0.027	⁶⁷ 0.244	⁷⁰ 0.133	⁸⁰ 0.315	⁸³ 0.203						
244	VERIDAS-001	¹¹³ 0.080	¹¹⁷ 0.037	¹¹⁴ 0.016	⁹⁶ 0.106	¹⁰¹ 0.082	¹⁰¹ 0.051	⁹² 0.993	⁹⁹ 0.987	⁹⁹ 0.938	⁹² 0.044	⁹⁷ 0.023	⁷⁰ 0.266	⁷² 0.146	⁷⁰ 0.264	⁸⁴ 0.204						
245	VERIDAS-002	¹¹⁴ 0.080	¹¹⁶ 0.037	¹¹⁵ 0.016	⁹⁵ 0.106	¹⁰³ 0.082	¹⁰⁰ 0.051	⁹³ 0.993	⁹⁸ 0.987	¹⁰⁸ 0.938	⁹¹ 0.044	⁹⁸ 0.023	⁷¹ 0.266	⁷³ 0.146	⁷¹ 0.264	⁸⁵ 0.204						
246	VERIDAS-003	¹⁰⁶ 0.072	⁶⁶ 0.017	⁶⁹ 0.006	⁶¹ 0.071	⁶⁷ 0.055	⁶⁵ 0.033	¹³⁴ 0.998	¹³³ 0.997	⁹³ 0.927	⁴⁸ 0.020	⁴⁹ 0.011	⁴⁴ 0.150	⁴⁴ 0.078	⁴⁴ 0.178	⁵¹ 0.142						
247	VIGILANTSOLUTIONS-003	²³¹ 0.482	²⁴⁶ 0.408	²⁴⁷ 0.282	²³⁶ 0.730	²⁴⁸ 0.660	²⁴⁹ 0.526	¹⁴⁶ 0.999	¹⁵⁰ 0.999	¹⁶⁷ 0.995												
248	VIGILANTSOLUTIONS-004	²⁴¹ 0.624	²⁵² 0.549	²⁵⁹ 0.422	²⁴⁷ 0.858	²⁵⁷ 0.817	²⁵⁴ 0.709	¹³² 0.998	¹³¹ 0.996	¹⁴⁹ 0.991												
249	VIGILANTSOLUTIONS-005	²⁵⁹ 0.936	²⁴¹ 0.388	¹⁷⁷ 0.043				¹⁹⁶ 1.000	²¹⁰ 1.000	²¹⁴ 1.000												
250	VIGILANTSOLUTIONS-006	²⁶² 0.959	²³⁶ 0.353	¹⁸⁰ 0.043				¹⁹¹ 1.000	¹⁹² 1.000	²¹⁷ 1.000												
251	VIGILANTSOLUTIONS-007	¹¹⁰ 0.076	¹⁰⁵ 0.028	⁹⁹ 0.011	¹⁰⁰ 0.113	¹⁰⁶ 0.088	¹⁰⁷ 0.053	¹²⁵ 0.997	¹³⁰ 0.996	¹⁵¹ 0.991	¹²³ 0.081	¹²⁷ 0.047	⁸⁰ 0.371	⁸³ 0.242	⁹⁴ 0.391	¹¹⁹ 0.295						
252	VIGILANTSOLUTIONS-008	⁸⁴ 0.051	⁷⁹ 0.021	⁸⁷ 0.010	⁹⁴ 0.105	⁹⁵ 0.077	⁹³ 0.046	¹³⁵ 1.000	¹⁵² 0.999	¹⁴⁷ 0.991	¹³⁰ 0.104	¹³² 0.054	⁸² 0.398	⁸⁵ 0.259	¹¹⁶ 0.511	¹²⁵ 0.316						
253	VISIONBOX-000	¹⁰⁷ 0.073	⁷¹ 0.018	⁶⁷ 0.007	⁶² 0.071	⁷⁰ 0.057	⁷² 0.035	⁹⁹ 0.995	¹⁰⁶ 0.990	¹²³ 0.974	³⁶ 0.023	³⁹ 0.012	⁴³ 0.146	⁴⁶ 0.081	³⁷ 0.162	⁴⁰ 0.126						
254	VISIONLABS-004	¹¹⁹ 0.091	¹⁵¹ 0.058	¹⁴⁴ 0.024	¹⁵⁹ 0.199	¹⁷⁷ 0.159	¹⁶⁹ 0.097	³² 0.944	⁵⁴ 0.890	⁶⁶ 0.742												
255	VISIONLABS-005	¹¹⁵ 0.080	¹³⁵ 0.050	¹²⁷ 0.020	¹⁵³ 0.183	¹⁶⁸ 0.147	¹⁵⁸ 0.087	³³ 0.945	³³ 0.888	⁶⁵ 0.736												
256	VISIONLABS-006	⁷² 0.044	⁹⁸ 0.027	⁹² 0.010	¹⁰⁴ 0.117	¹¹⁰ 0.090	¹⁰³ 0.051	³¹ 0.764	³² 0.672	⁴² 0.511												
257	VISIONLABS-007	⁷¹ 0.044	⁹⁷ 0.027	⁹¹ 0.010	¹⁰³ 0.117	¹⁰⁹ 0.090	¹⁰² 0.051	³² 0.764	³³ 0.672	⁴¹ 0.511	⁷³ 0.031	⁶⁸ 0.014										
258	VISIONLABS-008	⁴⁶ 0.028	⁵³ 0.013	⁵³ 0.006	⁵⁶ 0.068	⁵⁸ 0.051	⁶¹ 0.032	¹⁷ 0.574	²⁰ 0.481	²⁶ 0.317	⁴⁰ 0.017	³⁷ 0.008										
259	VISIONLABS-009	²⁴ 0.012	²⁵ 0.005	²⁶ 0.002	²⁵ 0.032	²⁸ 0.025	²⁸ 0.017	⁴⁸ 0.930	⁴⁴ 0.799	¹⁹ 0.196	²⁵ 0.008	²² 0.004										
260	VISIONLABS-010	²⁷ 0.014	²⁷ 0.005	²⁵ 0.002	²⁶ 0.034	³⁰ 0.027	³⁰ 0.019				¹² 0.169	¹⁹ 0.008	¹⁴ 0.004	¹⁶ 0.055	¹⁶ 0.027	¹⁶ 0.109	¹⁵ 0.089					
261	VISIONLABS-011	²² 0.011	¹⁸ 0.003	¹⁴ 0.002	¹⁷ 0.024	¹⁸ 0.020	¹⁹ 0.014				¹⁸ 0.194	⁸ 0.004	⁹ 0.034	⁸ 0.017	⁷ 0.090	⁸ 0.079						
262	VOCORD-003	²¹⁴ 0.354	¹⁹⁵ 0.122	¹⁸⁸ 0.048	¹⁵⁸ 0.195	¹⁶⁶ 0.155	¹⁶⁴ 0.093	¹³⁸ 0.999	¹⁴² 0.998	¹⁴⁸ 0.991	¹⁴⁴ 0.157	¹⁵³ 0.105										
263	VOCORD-004	²⁵² 0.826	²³⁷ 0.355	¹⁸⁷ 0.051	²⁰⁹ 0.401	¹⁷⁸ 0.173	¹⁶² 0.093	¹⁹⁸ 1.000	¹⁸⁵ 1.000	¹⁹² 0.999	¹⁵² 0.193	¹³⁶ 0.065										
264	VOCORD-005	²⁴⁵ 0.689	²⁰⁸ 0.158	¹⁸¹ 0.044	¹³⁹ 0.161	¹⁴⁹ 0.130	¹³¹ 0.080	¹⁴⁴ 0.999	¹³⁴ 0.997	¹¹⁸ 0.968	¹³⁹ 0.138	¹⁴⁷ 0.090										
265	VOCORD-006	²⁷ 0.100	²⁷ 0.000	²⁵ 0.000	²⁶ 1.000	²⁷ 0.100	²⁷ 0.000	²⁵ 1.000	²⁸ 1.000	²² 1.000	²³ 1.000	²⁷ 0.100										
266	VTS-000	²³⁹ 0.605	²⁵⁴ 0.598	²⁶ 0.595	²² 0.624	²⁴ 0.619	²³ 0.613	¹⁵¹ 0.999	¹⁶⁰ 0.999	¹⁸⁸ 0.998	¹⁷⁹ 0.613	¹⁸¹ 0.609	⁸⁷ 0.760	⁹⁰ 0.739	¹³ 0.761	¹⁶ 0.749						
267	VTS-001	⁵⁷ 0.035	⁵⁴ 0.013	⁵⁵ 0.006	⁵⁸ 0.067	⁵⁷ 0.051	⁵⁶ 0.031	¹²⁷ 0.998	¹¹⁴ 0.994	⁴⁰ 0.510	⁵⁴ 0.022	⁵⁶ 0.012	⁴⁰ 0.141	⁴⁵ 0.079	⁵⁰ 0.192	⁴¹ 0.126						
268	VTS-002	⁸⁶ 0.053	⁹⁴ 0.026	⁹⁰ 0.010	⁸⁹ 0.098	⁹³ 0.075	⁹⁴ 0.046	¹⁶⁵ 1.000	¹⁷⁰ 1.000	¹⁰⁸ 0.953	⁹⁴ 0.045	¹⁰⁰ 0.026	⁶⁸ 0.231	⁷¹ 0.133	⁹⁹ 0.417	⁷⁷ 0.187						
269	XFORWARDAI-000	⁴⁸ 0.029	⁶² 0.015	⁶³ 0.006	⁵⁹ 0.070	⁶⁵ 0.053</td																

Appendices

Appendix A Accuracy on large-population FRVT 2018 mugshots

2022/02/23
14:06:29

$\text{FNIR(N, R, T)} =$ $\text{FPIR(N, T)} =$	False neg. identification rate False pos. identification rate	$N = \text{Num. enrolled subjects}$ $R = \text{Num. candidates examined}$	$T = \text{Threshold}$ $T = 0 \rightarrow \text{Investigation}$ $T > 0 \rightarrow \text{Identification}$
---	--	--	---

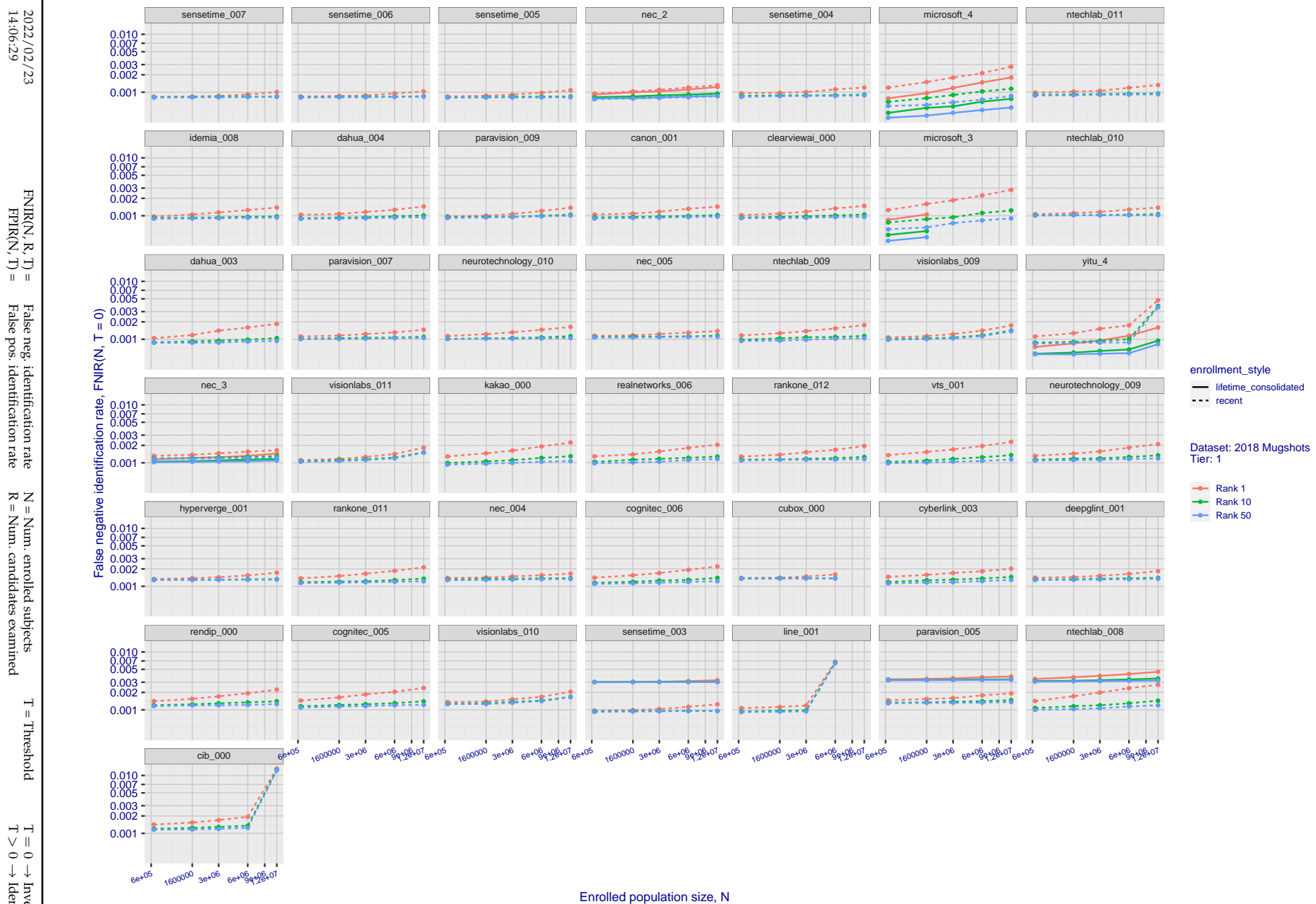


Figure 20: [FRVT-2018 Mugshot Dataset] Rank-based identification miss rates vs. number of enrolled subjects. The figure shows false negative identification rates, $\text{FNIR}(N, R)$, across various gallery sizes and ranks 1, 10 and 50. The threshold is set to zero, so this metric rewards even weak scoring rank 1 mates. This also means $\text{FPIR} = 1$, so any search without an enrolled mate will return non-mated candidates. For clarity, results are sorted and reported into tiers spanning multiple pages, the tiering criteria being rank 1 hit rate on a gallery size of 640 000.

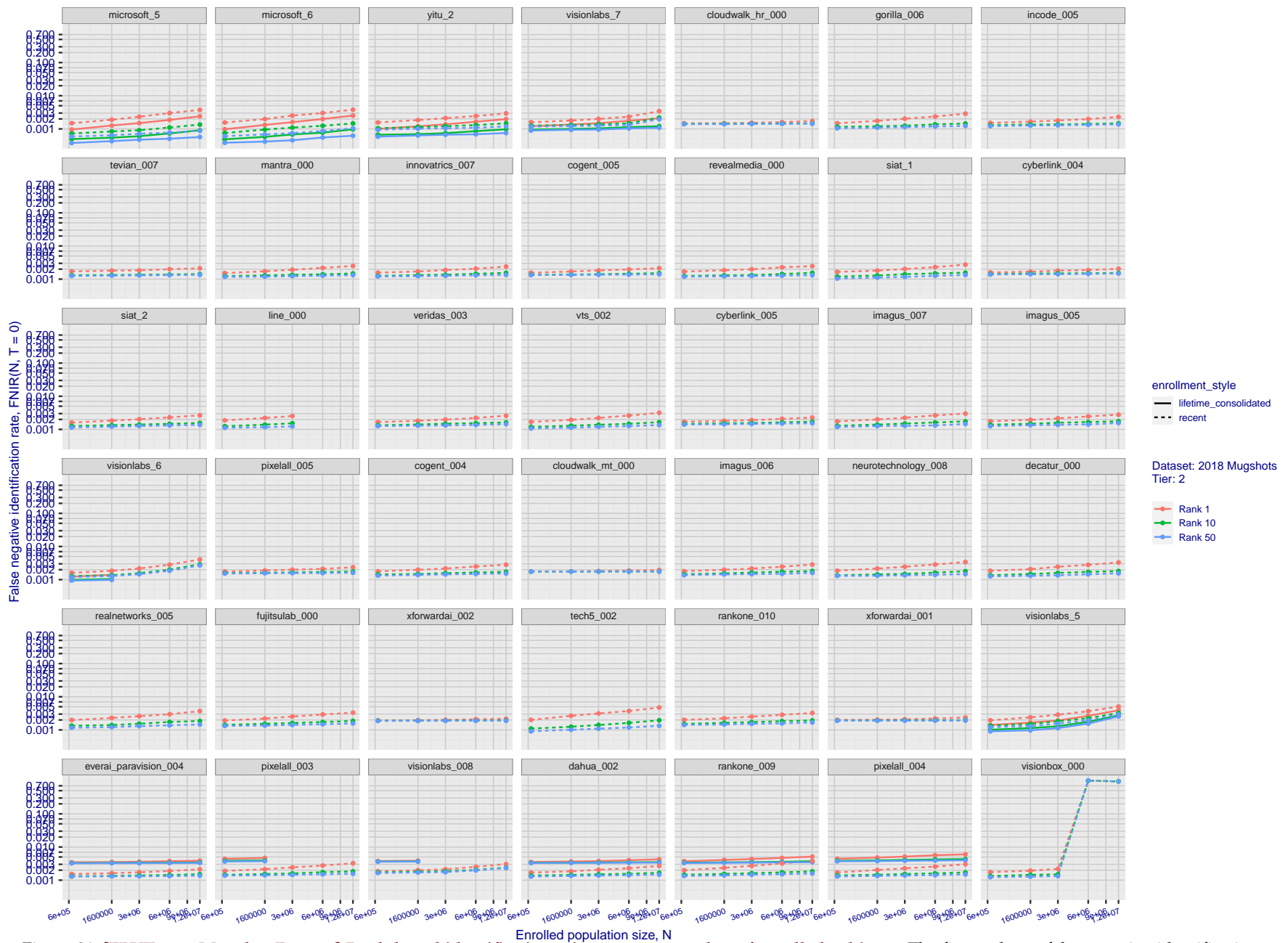


Figure 21: [FRVT-2018 Mugshot Dataset] Rank-based identification miss rates vs. number of enrolled subjects. The figure shows false negative identification rates, $\text{FNIR}(N, R)$, across various gallery sizes and ranks 1, 10 and 50. The threshold is set to zero, so this metric rewards even weak scoring rank 1 mates. This also means $\text{FPIR} = 1$, so any search without an enrolled mate will return non-mated candidates. For clarity, results are sorted and reported into tiers spanning multiple pages, the tiering criteria being rank 1 hit rate on a gallery size of 640 000.

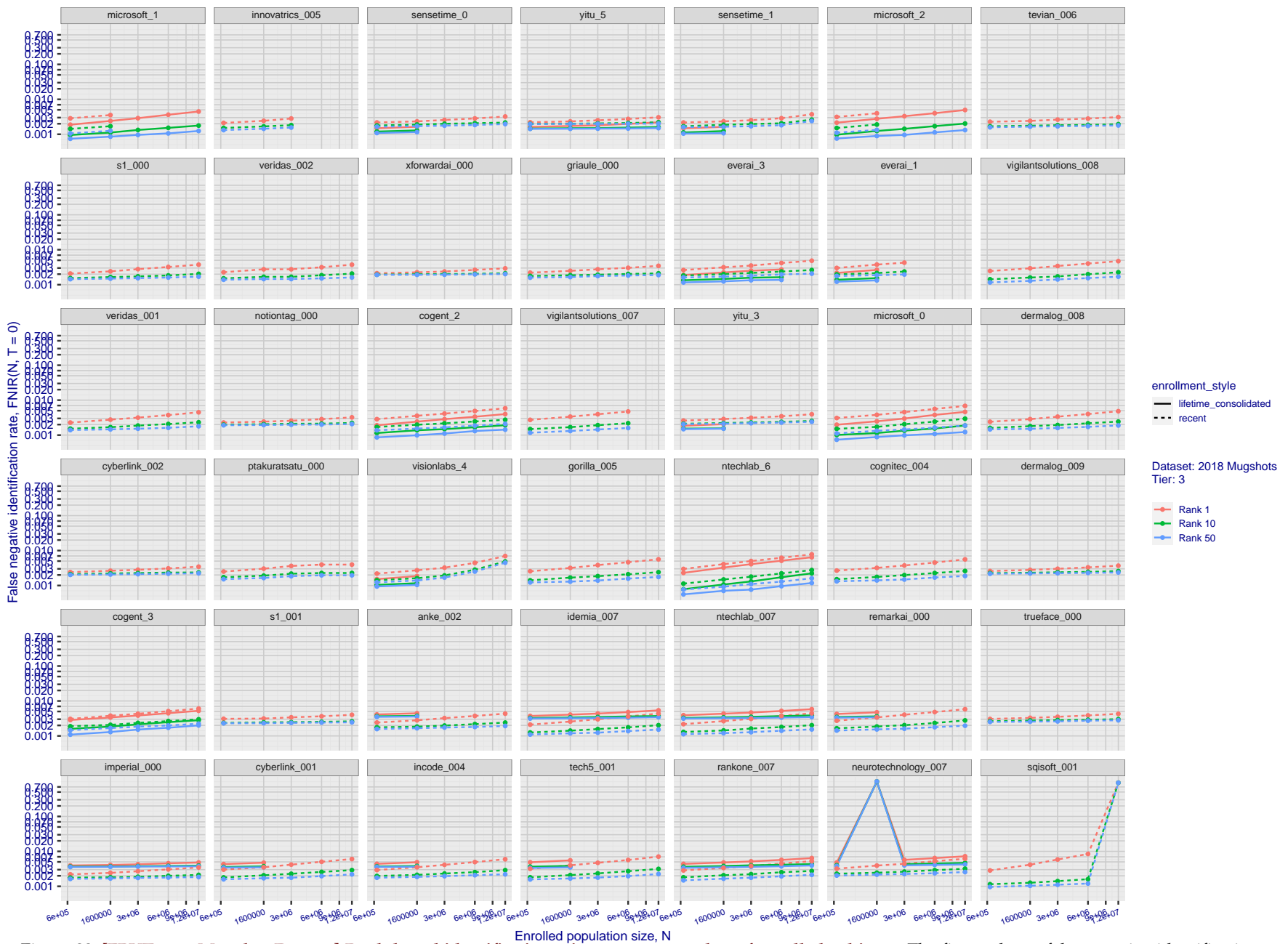


Figure 22: [FRVT-2018 Mugshot Dataset] Rank-based identification miss rates vs. number of enrolled subjects. The figure shows false negative identification rates, $\text{FNIR}(N, R)$, across various gallery sizes and ranks 1, 10 and 50. The threshold is set to zero, so this metric rewards even weak scoring rank 1 mates. This also means $\text{FPIR} = 1$, so any search without an enrolled mate will return non-mated candidates. For clarity, results are sorted and reported into tiers spanning multiple pages, the tiering criteria being rank 1 hit rate on a gallery size of 640 000.

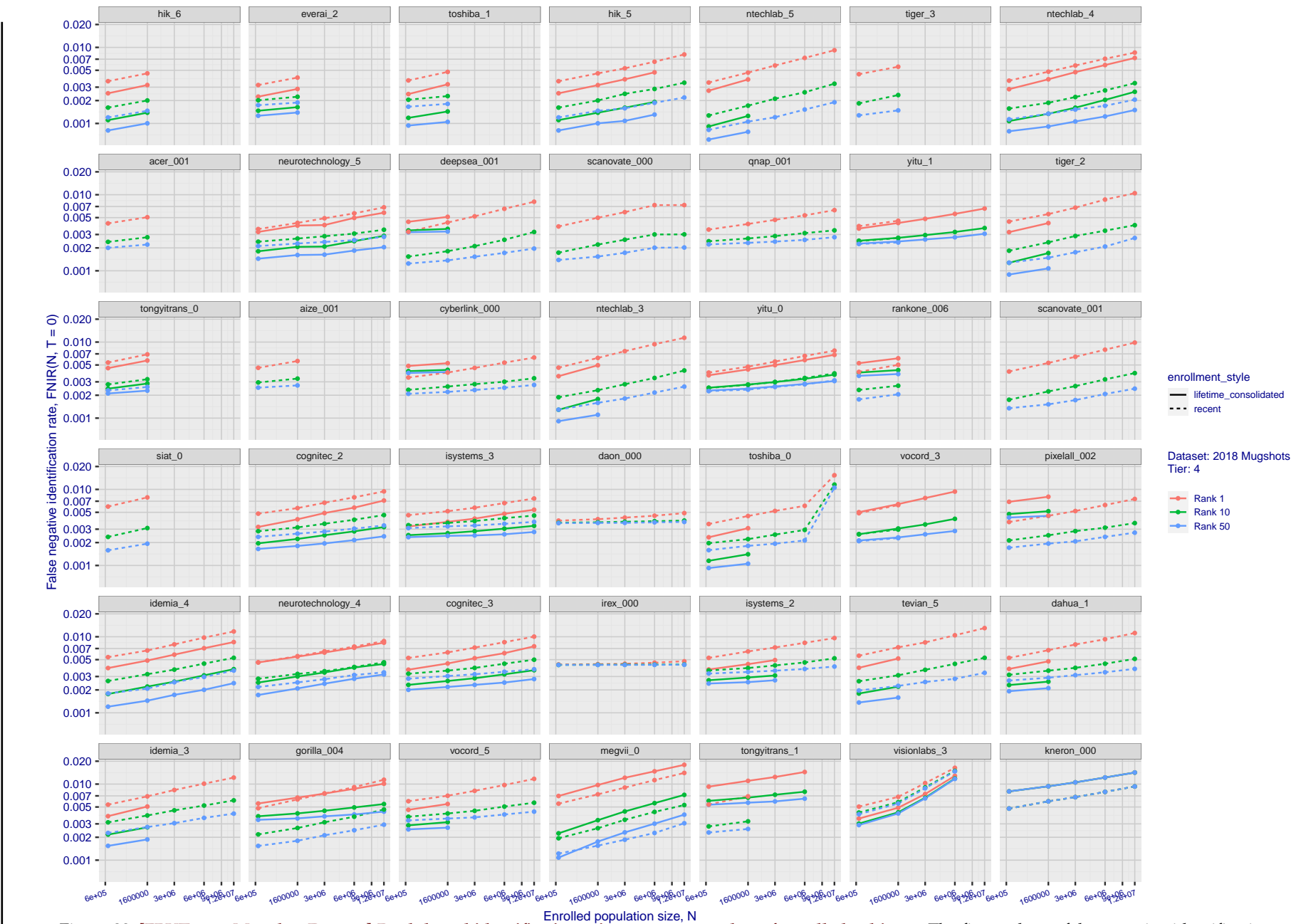


Figure 23: [FRVT-2018 Mugshot Dataset] Rank-based identification miss rates vs. number of enrolled subjects. The figure shows false negative identification rates, $\text{FNIR}(N, R)$, across various gallery sizes and ranks 1, 10 and 50. The threshold is set to zero, so this metric rewards even weak scoring rank 1 mates. This also means $\text{FPIR} = 1$, so any search without an enrolled mate will return non-mated candidates. For clarity, results are sorted and reported into tiers spanning multiple pages, the tiering criteria being rank 1 hit rate on a gallery size of 640 000.

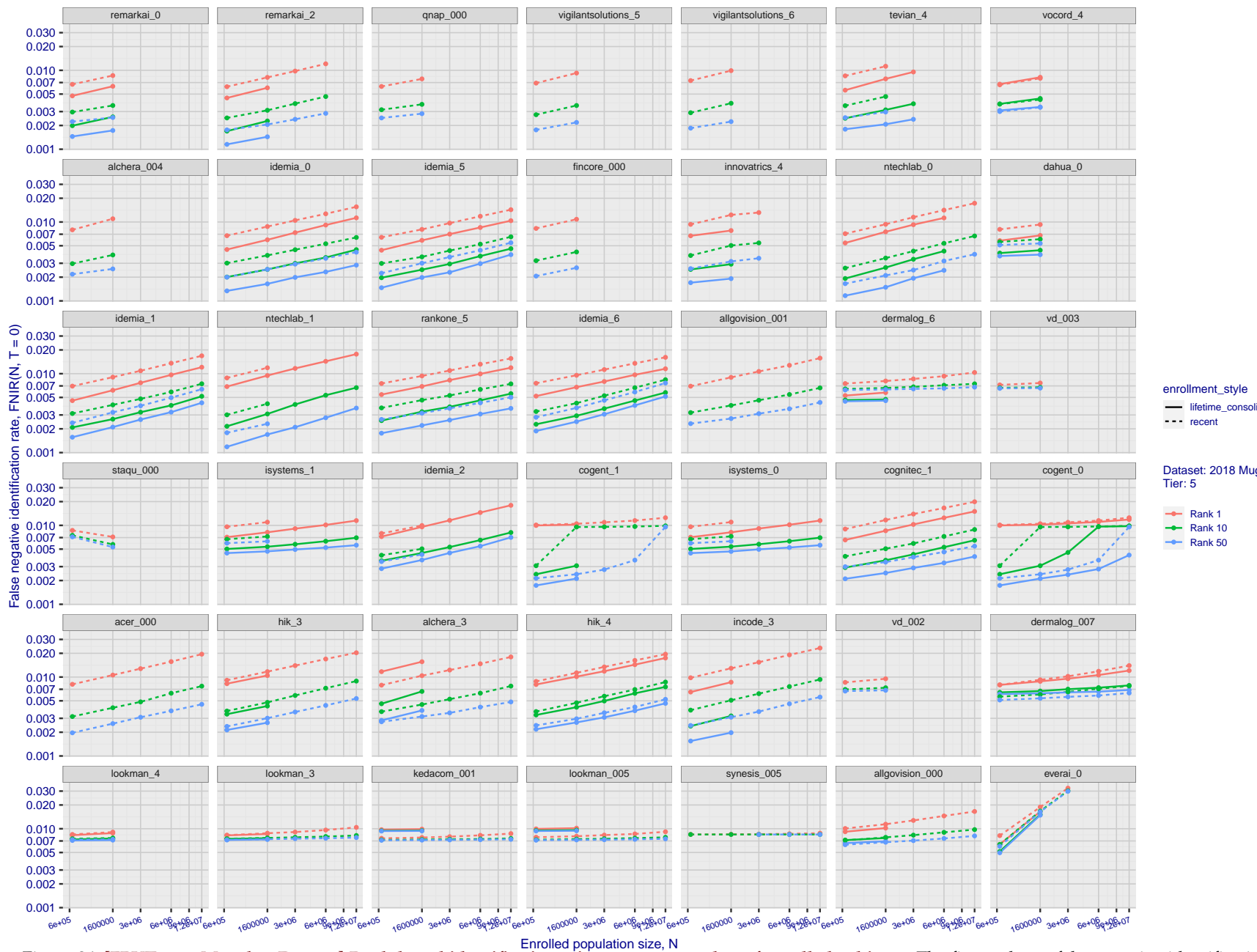


Figure 24: [FRVT-2018 Mugshot Dataset] Rank-based identification miss rates vs. number of enrolled subjects. The figure shows false negative identification rates, $\text{FNIR}(N, R)$, across various gallery sizes and ranks 1, 10 and 50. The threshold is set to zero, so this metric rewards even weak scoring rank 1 mates. This also means $\text{FPIR} = 1$, so any search without an enrolled mate will return non-mated candidates. For clarity, results are sorted and reported into tiers spanning multiple pages, the tiering criteria being rank 1 hit rate on a gallery size of 640 000.

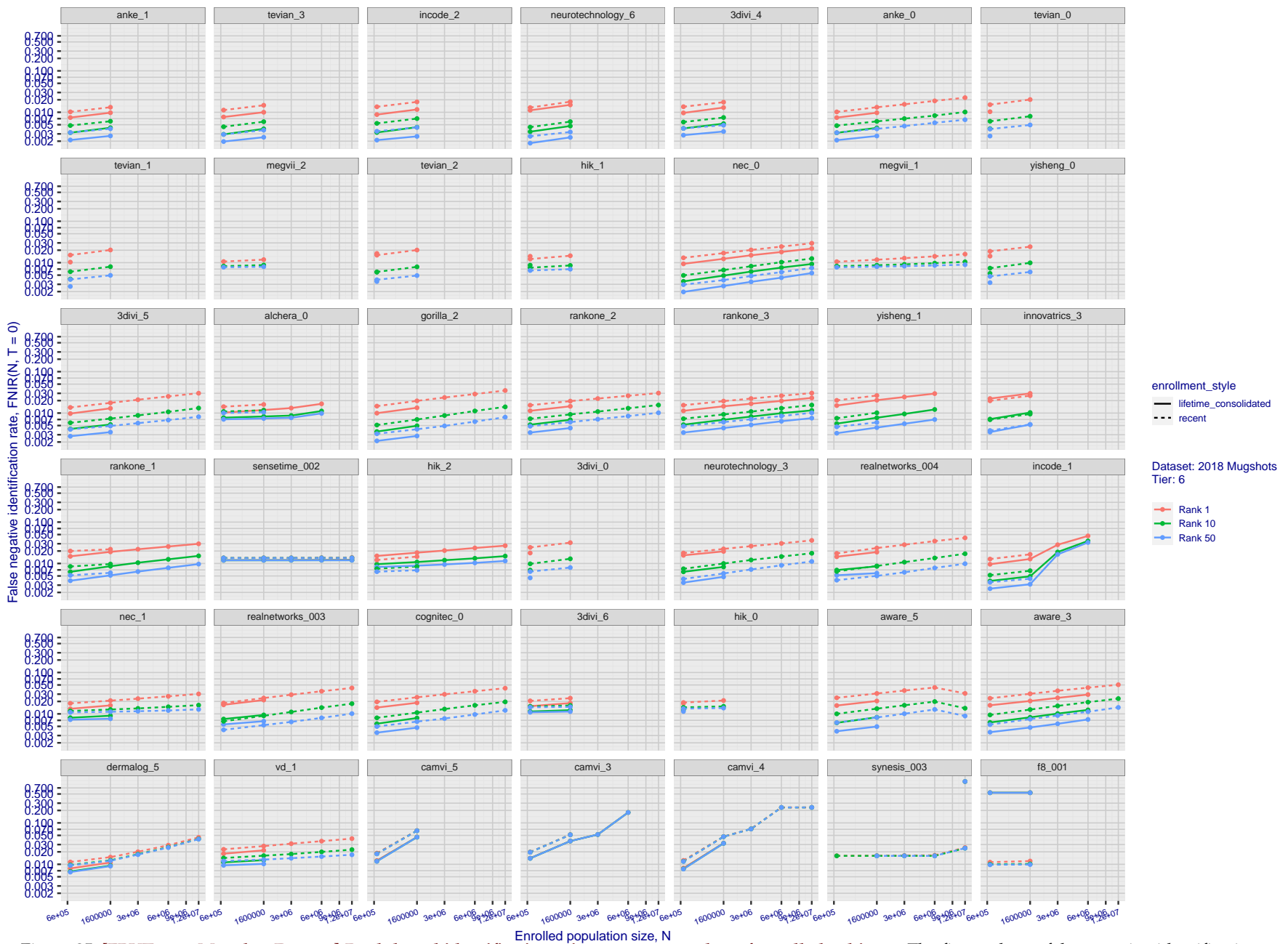


Figure 25: [FRVT-2018 Mugshot Dataset] Rank-based identification miss rates vs. number of enrolled subjects. The figure shows false negative identification rates, $\text{FNIR}(N, R)$, across various gallery sizes and ranks 1, 10 and 50. The threshold is set to zero, so this metric rewards even weak scoring rank 1 mates. This also means $\text{FPIR} = 1$, so any search without an enrolled mate will return non-mated candidates. For clarity, results are sorted and reported into tiers spanning multiple pages, the tiering criteria being rank 1 hit rate on a gallery size of 640 000.

2022/02/23

14:06:29

FNIR(N, R, T) =
False neg. identification rateN = Num. enrolled subjects
R = Num. candidates examined

T = Threshold

T = 0 → Investigation
T > 0 → Identification

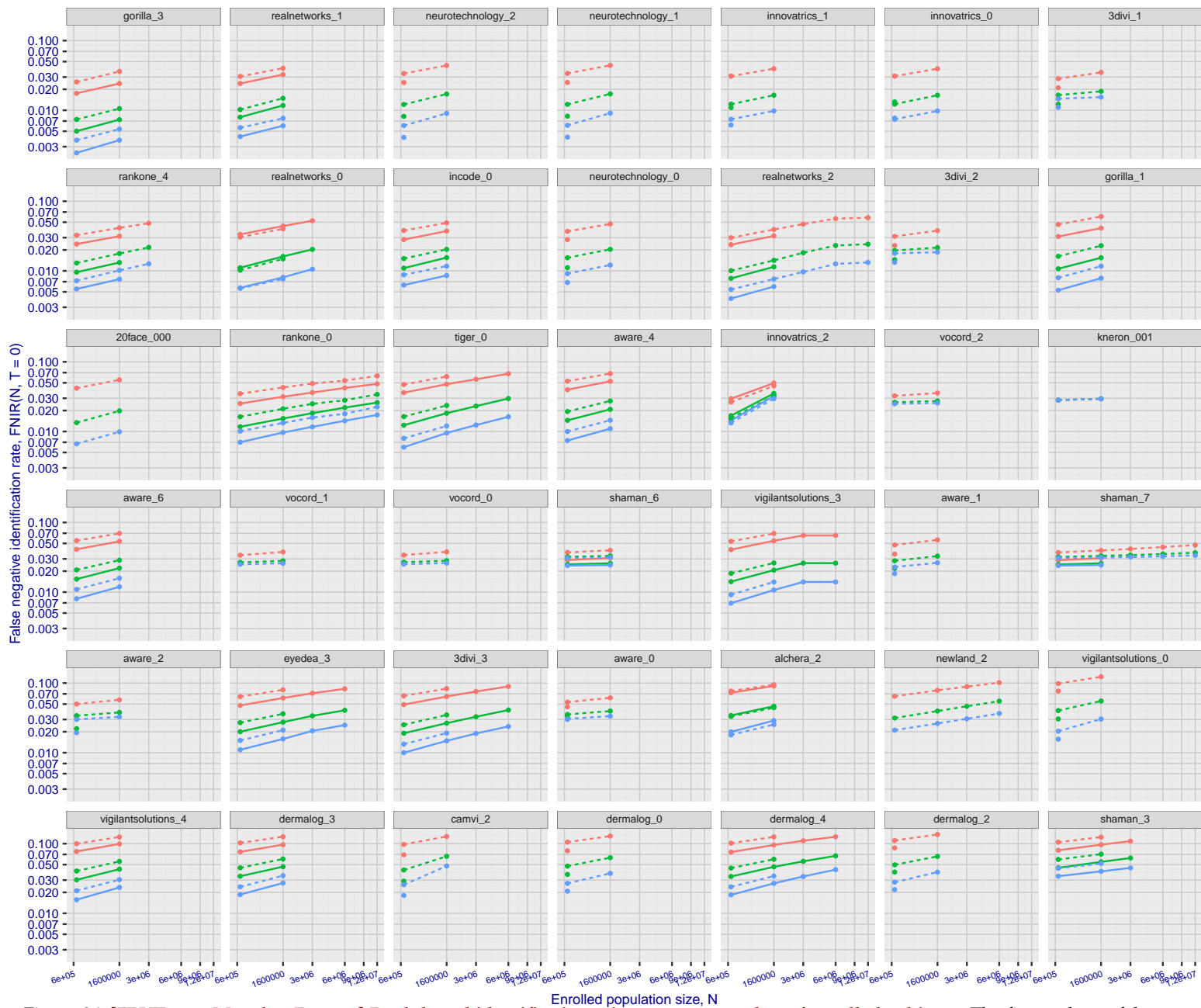


Figure 26: [FRVT-2018 Mugshot Dataset] Rank-based identification miss rates vs. number of enrolled subjects. The figure shows false negative identification rates, $\text{FNIR}(N, R)$, across various gallery sizes and ranks 1, 10 and 50. The threshold is set to zero, so this metric rewards even weak scoring rank 1 mates. This also means $\text{FPIR} = 1$, so any search without an enrolled mate will return non-mated candidates. For clarity, results are sorted and reported into tiers spanning multiple pages, the tiering criteria being rank 1 hit rate on a gallery size of 640 000.

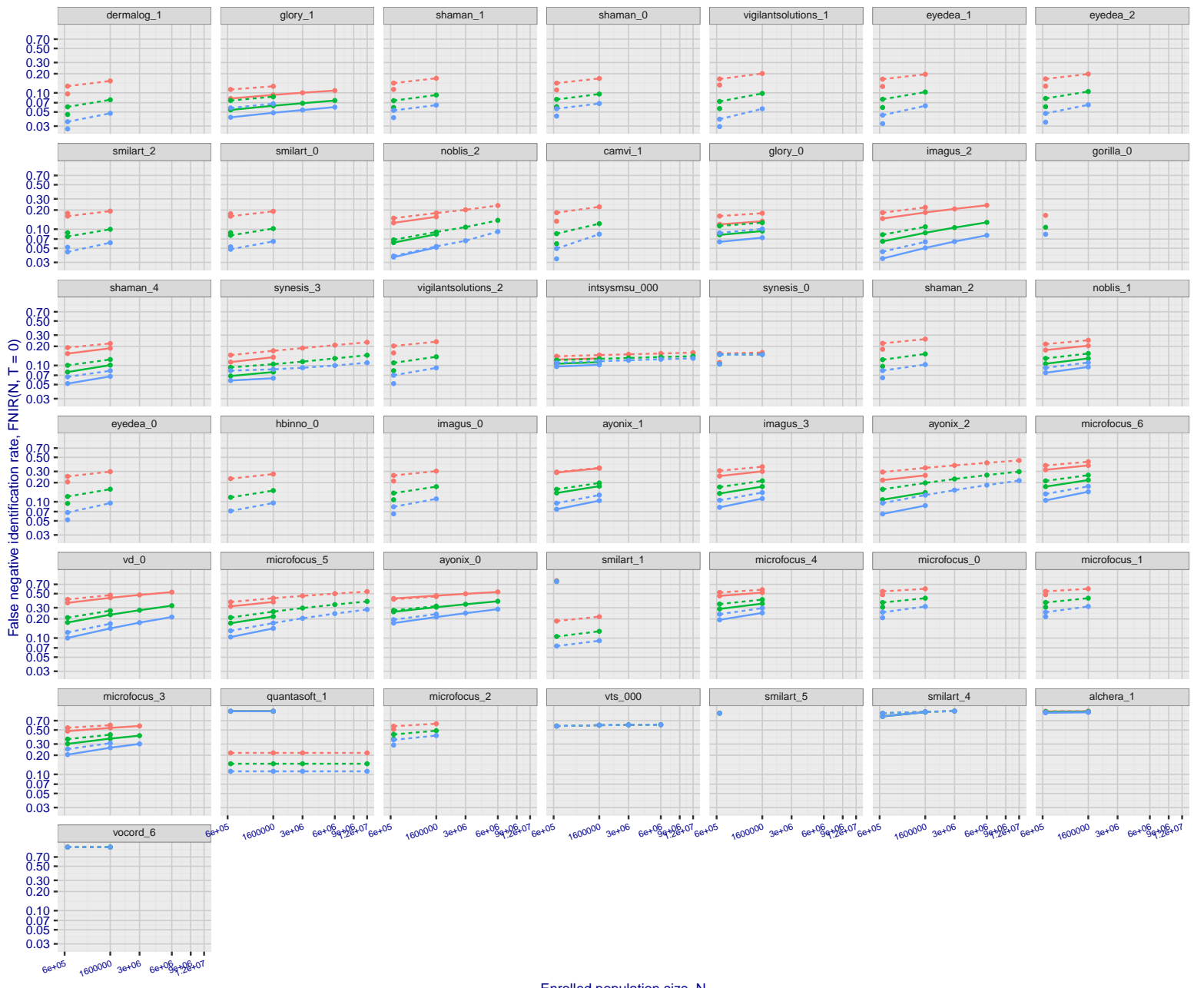


Figure 27: [FRVT-2018 Mugshot Dataset] Rank-based identification miss rates vs. number of enrolled subjects. The figure shows false negative identification rates, $\text{FNIR}(N, R)$, across various gallery sizes and ranks 1, 10 and 50. The threshold is set to zero, so this metric rewards even weak scoring rank 1 mates. This also means $\text{FPIR} = 1$, so any search without an enrolled mate will return non-mated candidates. For clarity, results are sorted and reported into tiers spanning multiple pages, the tiering criteria being rank 1 hit rate on a gallery size of 640 000.

2022/02/23
14:06:29 FNIR(N, R, T) = False neg. identification rate
FPIR(N, T) = False pos. identification rate
N = Num. enrolled subjects
R = Num. candidates examined
T = Threshold
 $T = 0 \rightarrow$ Investigation
 $T > 0 \rightarrow$ Identification

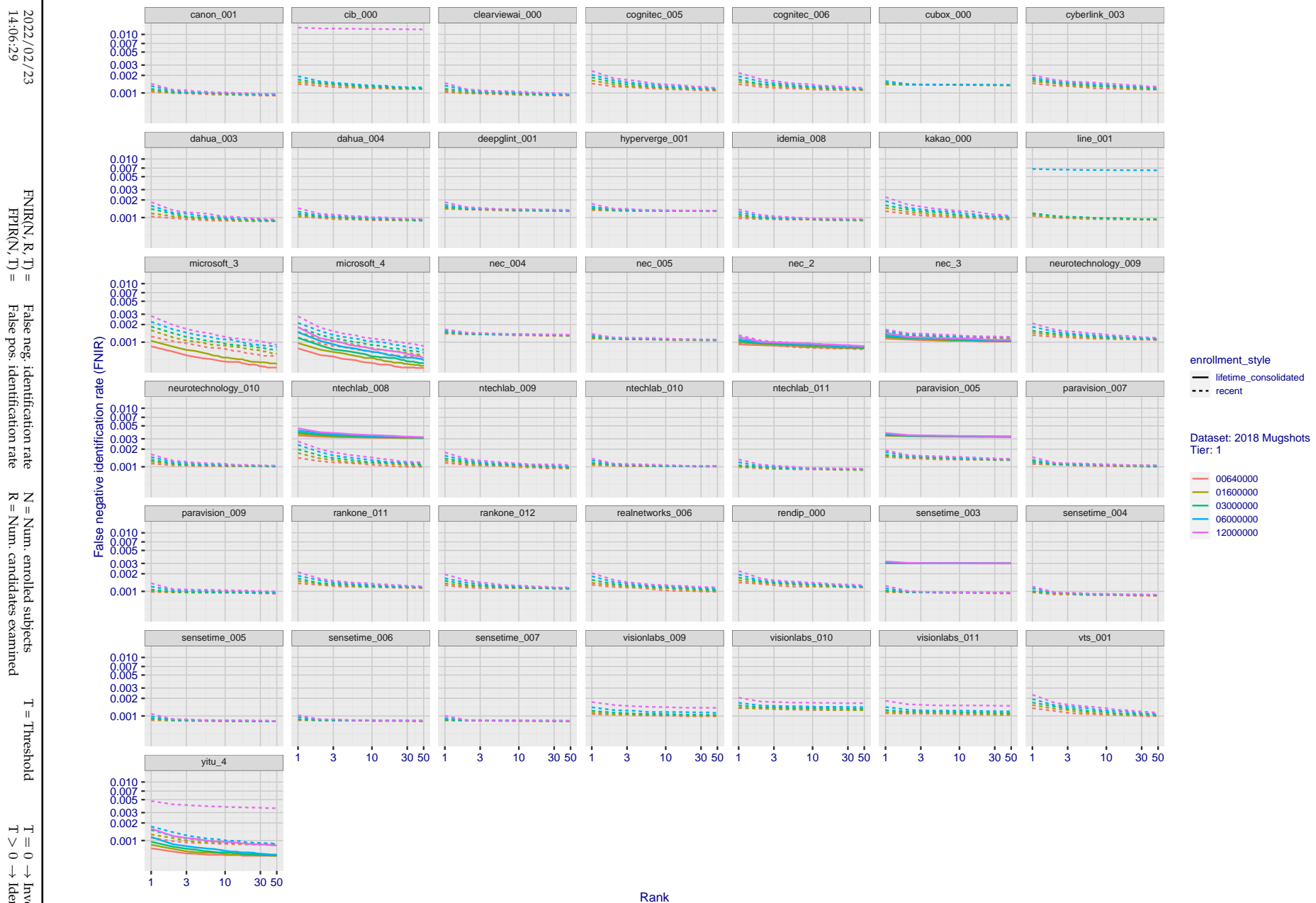


Figure 28: [FRVT-2018 Mugshot Dataset] Rank-based identification miss rates vs. rank. The figure shows false negative identification rates (FNIR) for ranks up to 50. This metric is appropriate to investigational applications where human reviewers will adjudicate sorted candidate lists. Note that with threshold set to zero, FPIR = 1, i.e. any search without an enrolled mate will return non-mated candidates. Results are sorted and reported into tiers for clarity, with the tiering criteria being rank 1 hit rate on a gallery size of $N = 640\,000$ subjects.

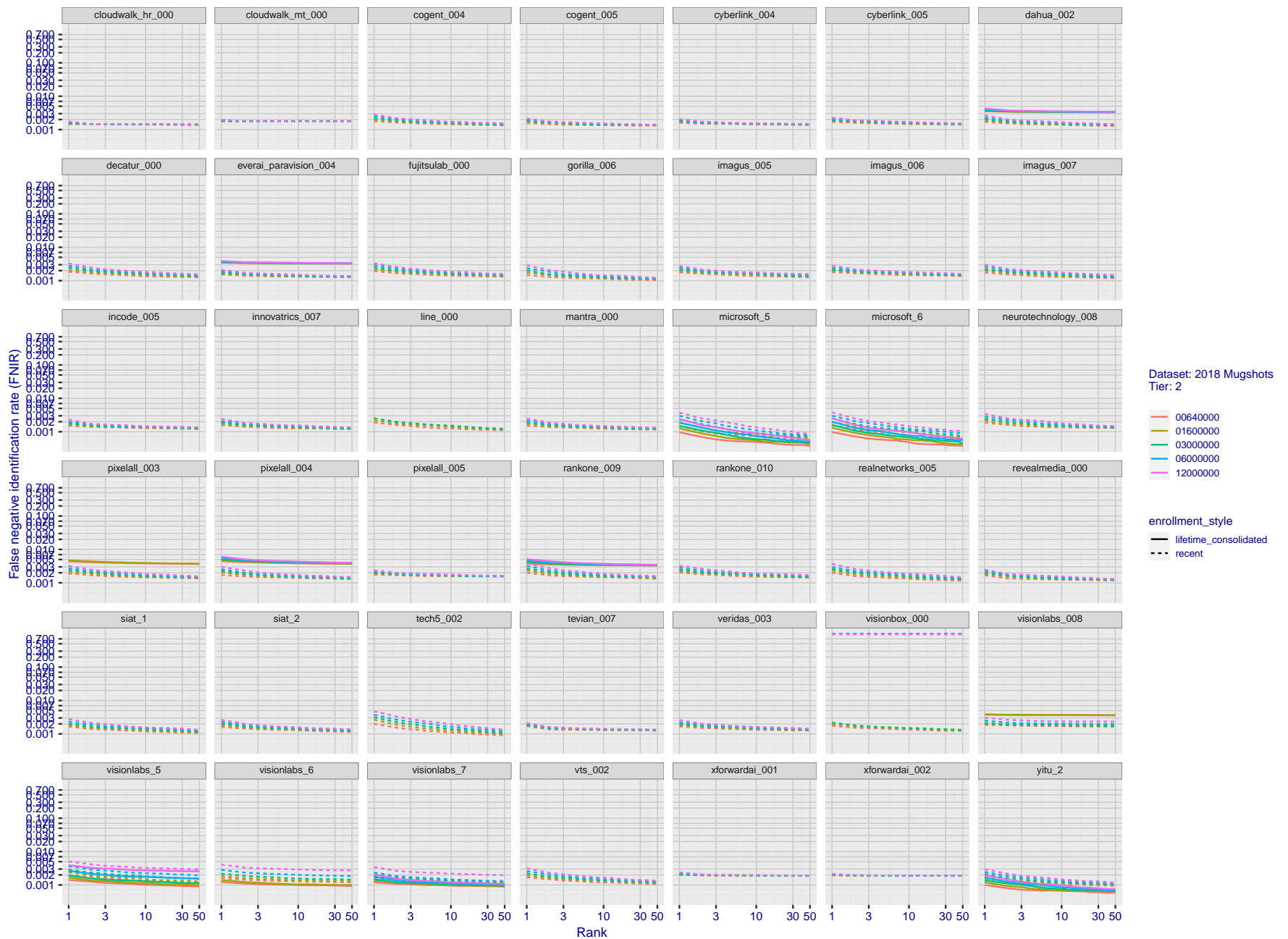


Figure 29: [FRVT-2018 Mugshot Dataset] Rank-based identification miss rates vs. rank. The figure shows false negative identification rates (FNIR) for ranks up to 50. This metric is appropriate to investigational applications where human reviewers will adjudicate sorted candidate lists. Note that with threshold set to zero, FPIR = 1, i.e. any search without an enrolled mate will return non-mated candidates. Results are sorted and reported into tiers for clarity, with the tiering criteria being rank 1 hit rate on a gallery size of N = 640 000 subjects.

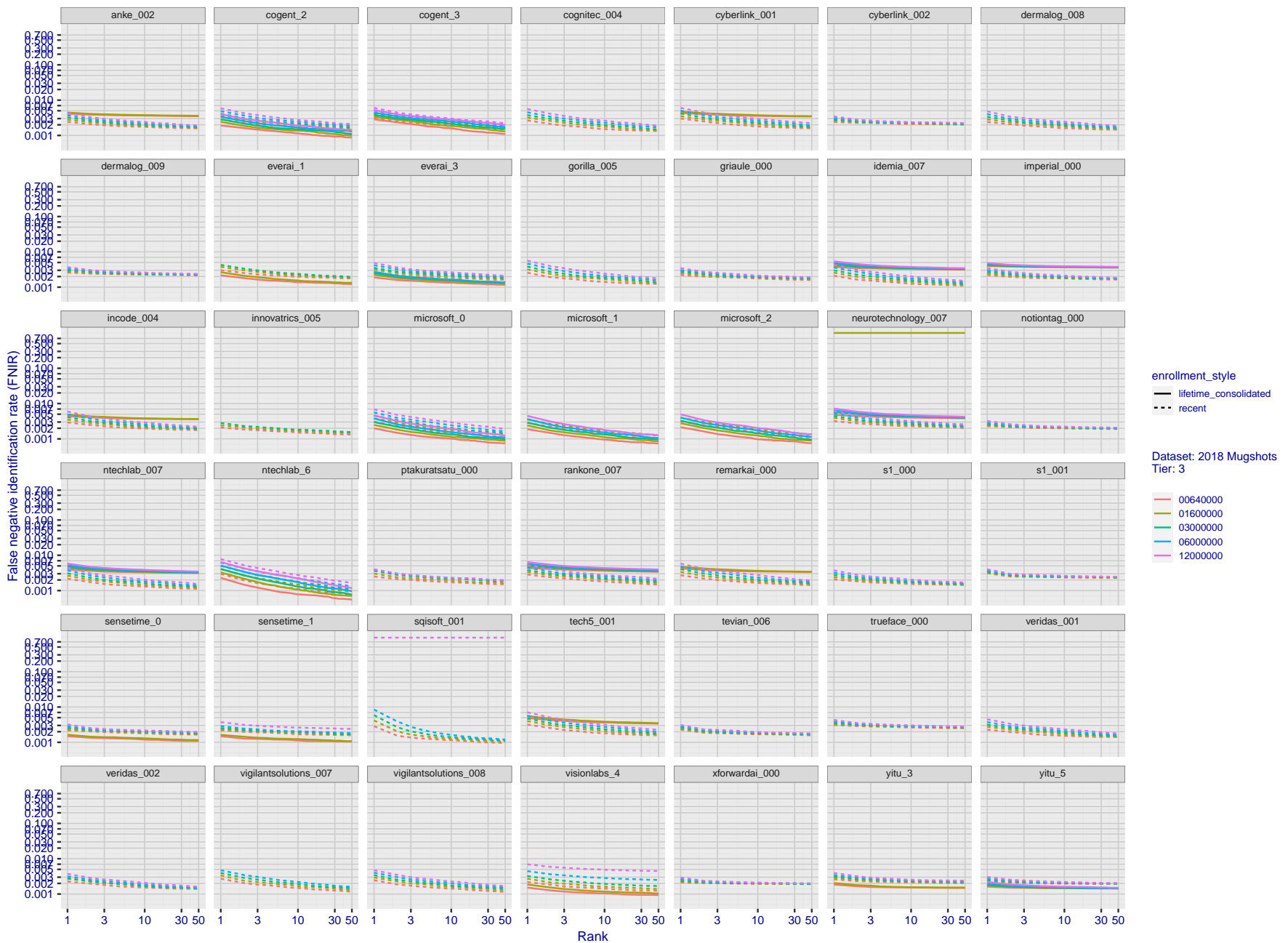


Figure 30: [FRVT-2018 Mugshot Dataset] Rank-based identification miss rates vs. rank. The figure shows false negative identification rates (FNIR) for ranks up to 50. This metric is appropriate to investigational applications where human reviewers will adjudicate sorted candidate lists. Note that with threshold set to zero, FPIR = 1, i.e. any search without an enrolled mate will return non-mated candidates. Results are sorted and reported into tiers for clarity, with the tiering criteria being rank 1 hit rate on a gallery size of N = 640 000 subjects.

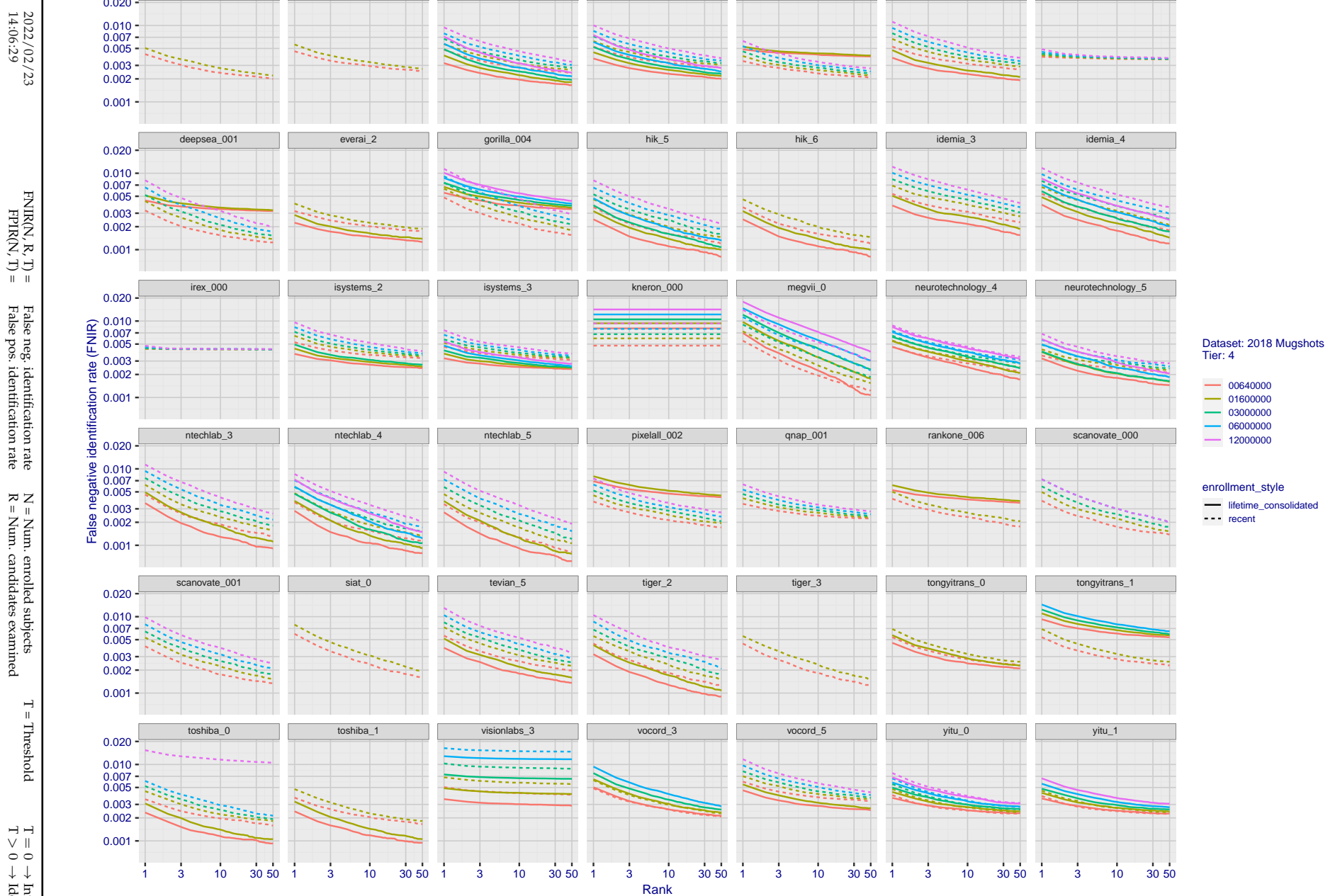


Figure 31: [FRVT-2018 Mugshot Dataset] Rank-based identification miss rates vs. rank. The figure shows false negative identification rates (FNIR) for ranks up to 50. This metric is appropriate to investigational applications where human reviewers will adjudicate sorted candidate lists. Note that with threshold set to zero, FPIR = 1, i.e. any search without an enrolled mate will return non-mated candidates. Results are sorted and reported into tiers for clarity, with the tiering criteria being rank 1 hit rate on a gallery size of $N = 640\,000$ subjects.

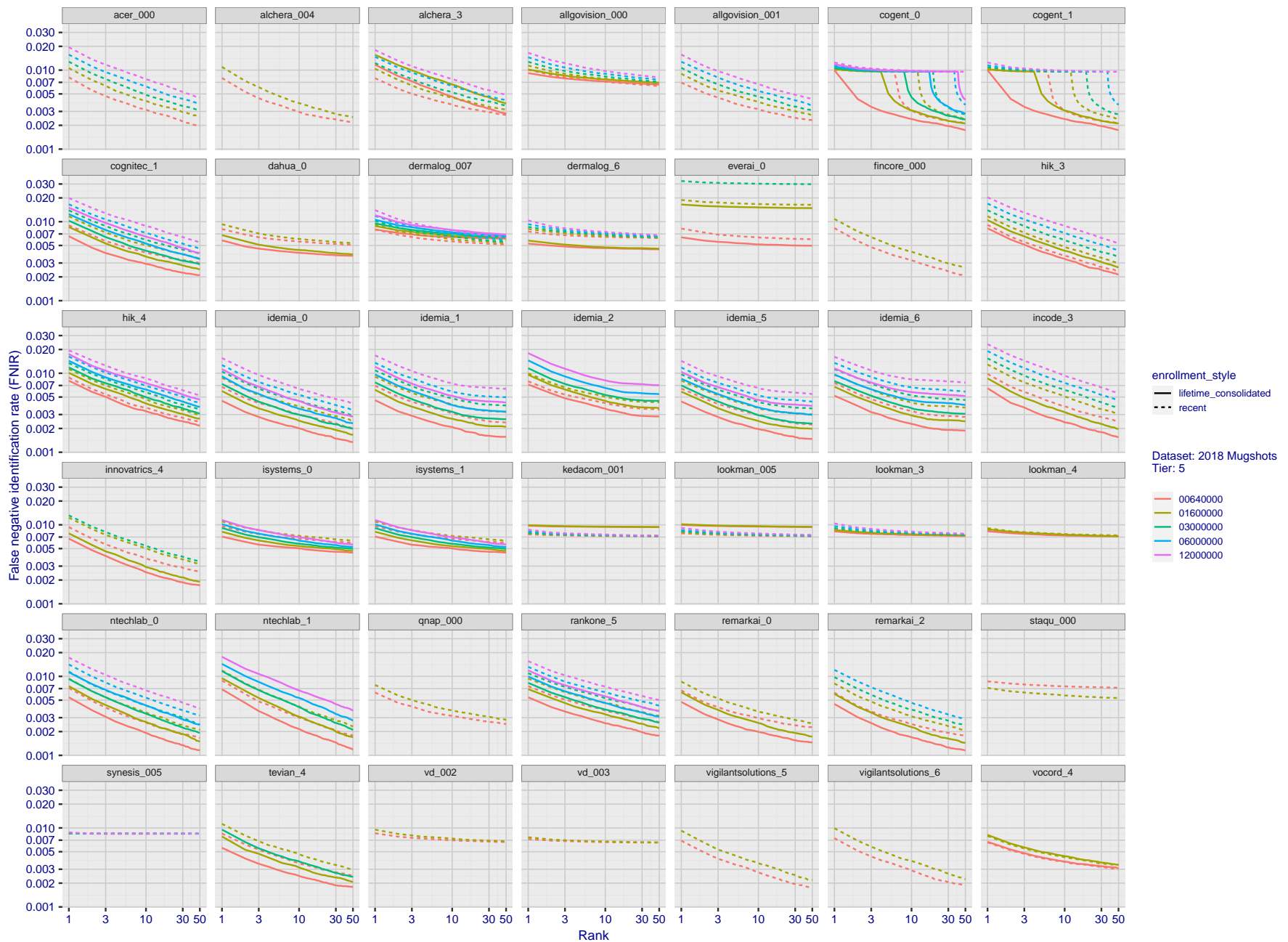


Figure 32: [FRVT-2018 Mugshot Dataset] Rank-based identification miss rates vs. rank. The figure shows false negative identification rates (FNIR) for ranks up to 50. This metric is appropriate to investigational applications where human reviewers will adjudicate sorted candidate lists. Note that with threshold set to zero, FPIR = 1, i.e. any search without an enrolled mate will return non-mated candidates. Results are sorted and reported into tiers for clarity, with the tiering criteria being rank 1 hit rate on a gallery size of $N = 640\,000$ subjects.

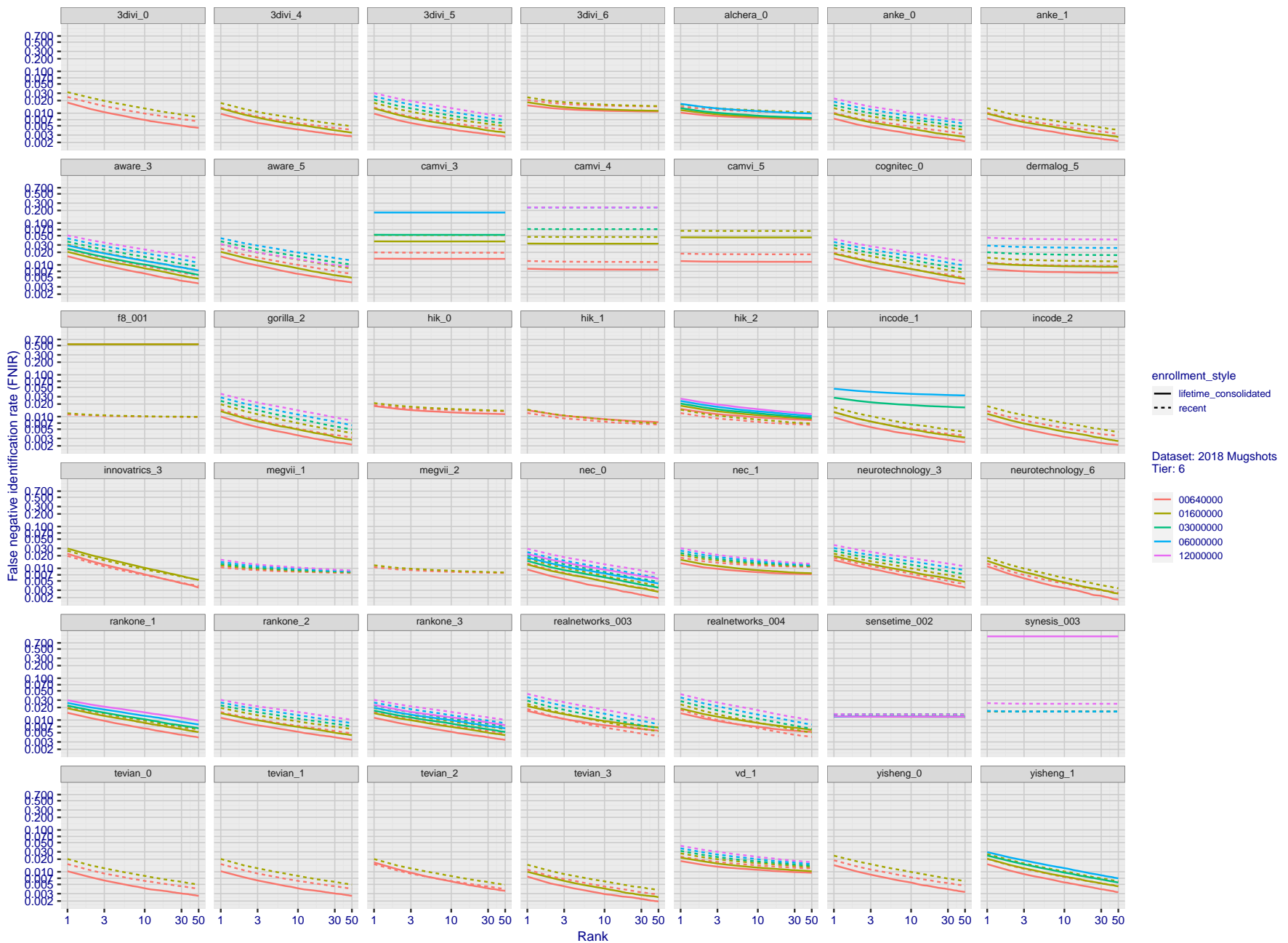


Figure 33: [FRVT-2018 Mugshot Dataset] Rank-based identification miss rates vs. rank. The figure shows false negative identification rates (FNIR) for ranks up to 50. This metric is appropriate to investigational applications where human reviewers will adjudicate sorted candidate lists. Note that with threshold set to zero, FPIR = 1, i.e. any search without an enrolled mate will return non-mated candidates. Results are sorted and reported into tiers for clarity, with the tiering criteria being rank 1 hit rate on a gallery size of $N = 640\,000$ subjects.

2022/02/23

14:06:29

FNIR(N, R, T) = False neg. identification rate

N = Num. enrolled subjects

T = Threshold

T = 0 → Investigation

T > 0 → Identification

FPIR(N, T) = False pos. identification rate

R = Num. candidates examined

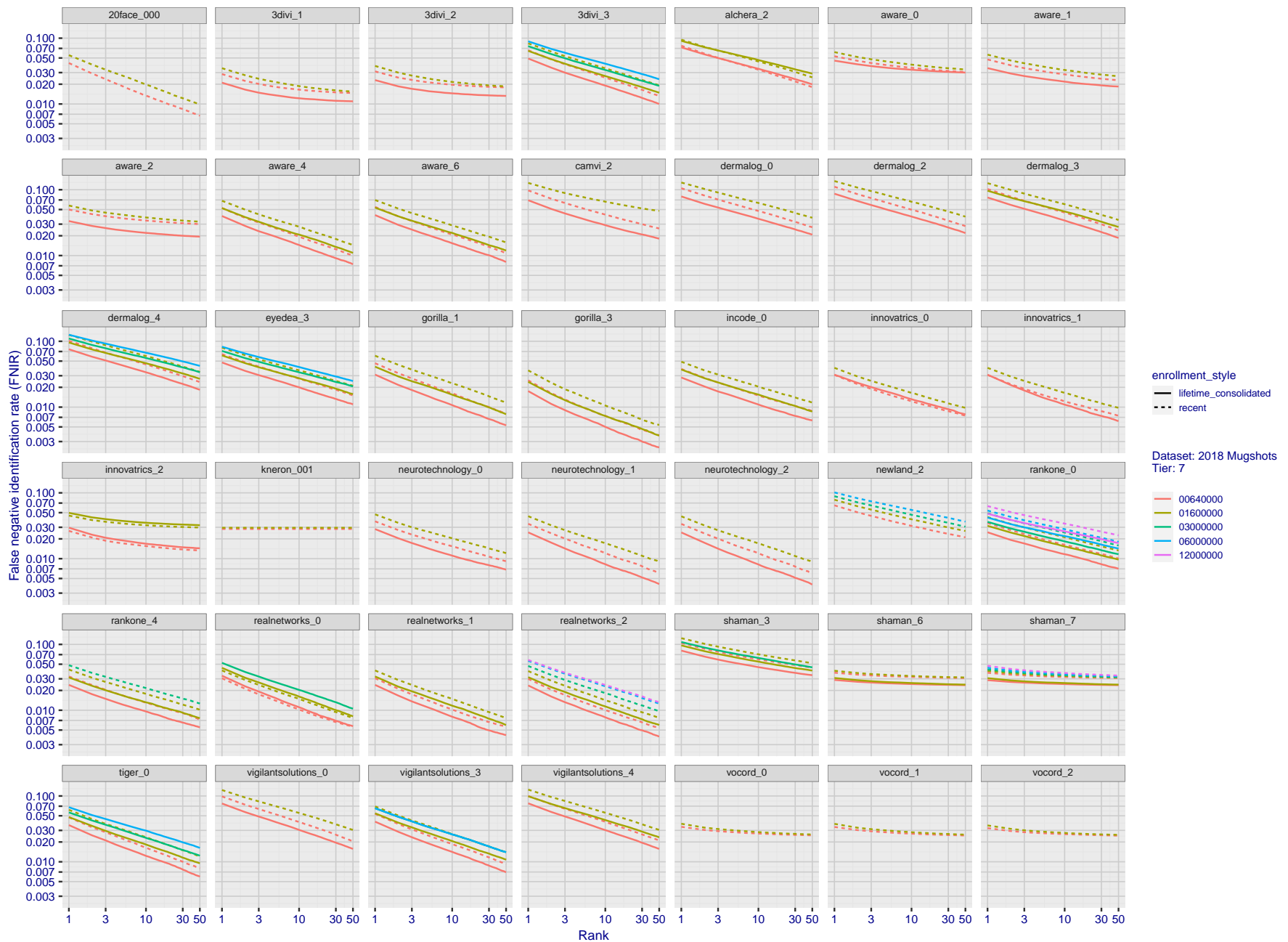


Figure 34: [FRVT-2018 Mugshot Dataset] Rank-based identification miss rates vs. rank. The figure shows false negative identification rates (FNIR) for ranks up to 50. This metric is appropriate to investigational applications where human reviewers will adjudicate sorted candidate lists. Note that with threshold set to zero, FPTR = 1, i.e. any search without an enrolled mate will return non-mated candidates. Results are sorted and reported into tiers for clarity, with the tiering criteria being rank 1 hit rate on a gallery size of $N = 640\,000$ subjects.

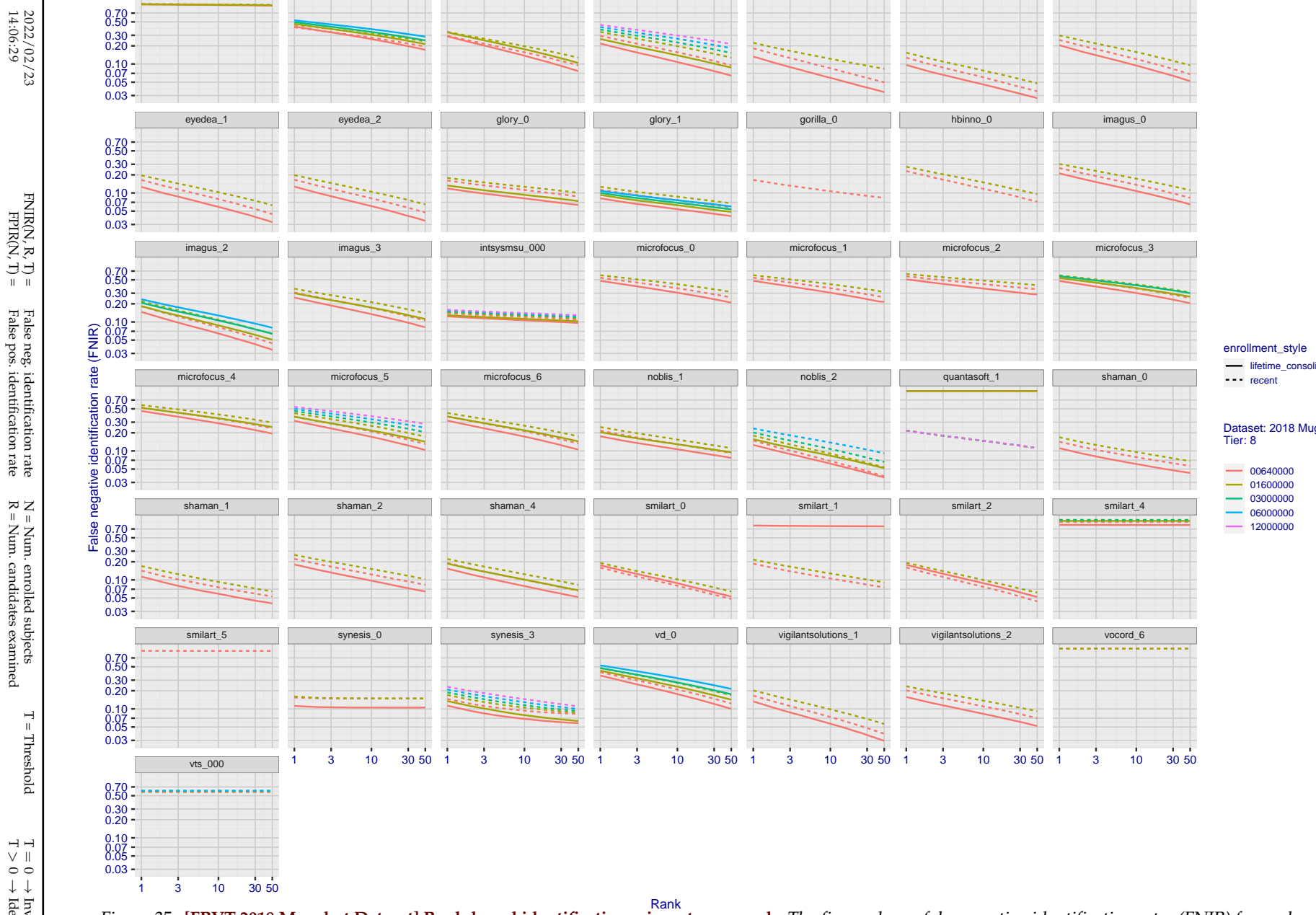


Figure 35: [FRVT-2018 Mugshot Dataset] Rank-based identification miss rates vs. rank. The figure shows false negative identification rates (FNIR) for ranks up to 50. This metric is appropriate to investigational applications where human reviewers will adjudicate sorted candidate lists. Note that with threshold set to zero, FPIR = 1, i.e. any search without an enrolled mate will return non-mated candidates. Results are sorted and reported into tiers for clarity, with the tiering criteria being rank 1 hit rate on a gallery size of N = 640 000 subjects.

2022/02/23
14:06:29 FNIR(N, R, T) = False neg. identification rate
FPIR(N, T) = False pos. identification rate
N = Num. enrolled subjects
R = Num. candidates examined
T = Threshold
 $T = 0 \rightarrow$ Investigation
 $T > 0 \rightarrow$ Identification

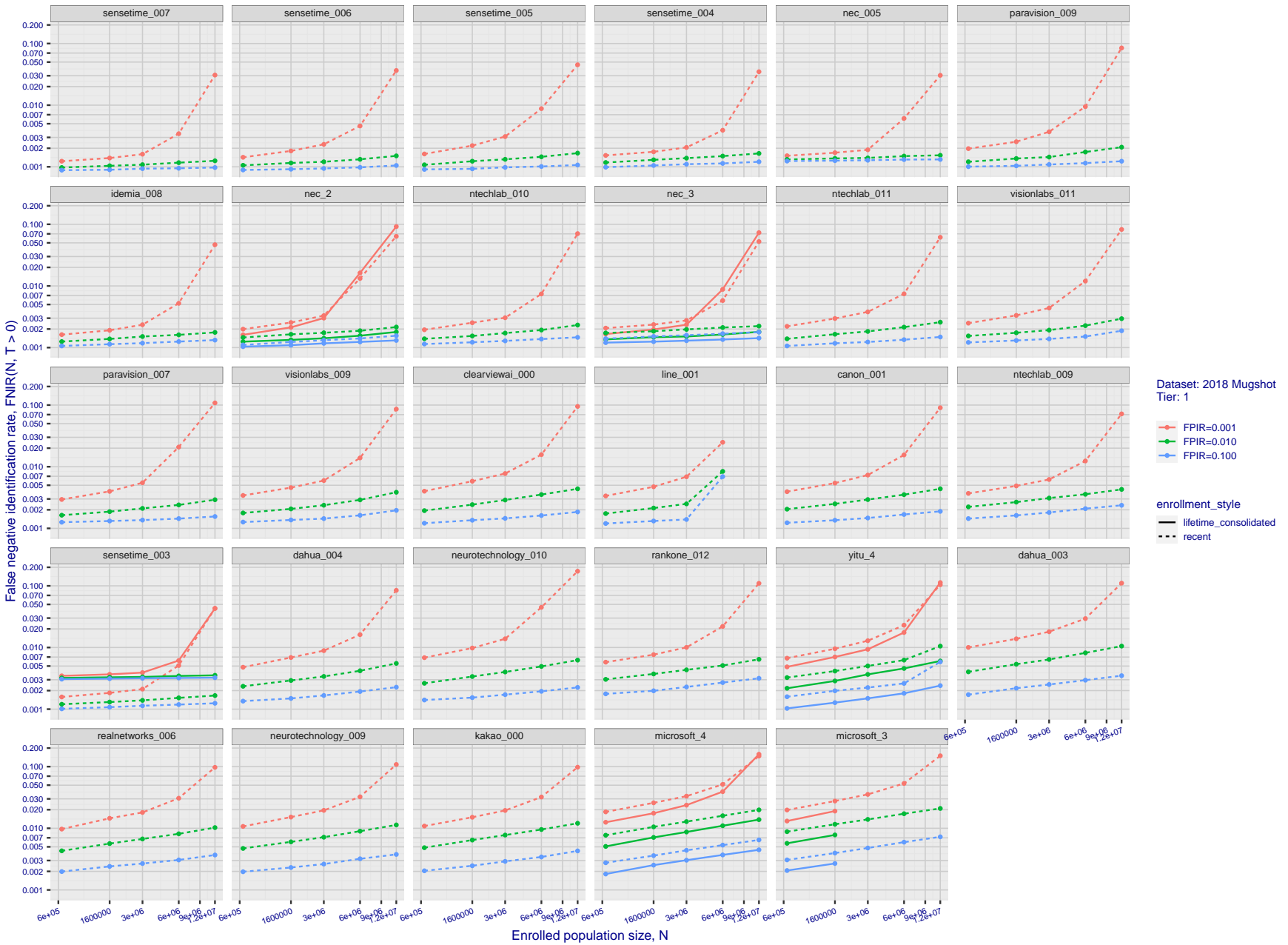


Figure 36: [FRVT-2018 Mugshot Dataset] Threshold-based identification miss rates vs. number of enrolled subjects. The figure shows $\text{FNIR}(N, T)$ across various gallery sizes when the threshold is set to achieve the given FPIRs. The rank criterion is irrelevant at high thresholds as mates are always at rank 1. The results are computed from the trials listed in rows 1-10 of Table 1. Less accurate algorithms were not run on large N , so results are missing. For clarity, results are sorted and reported into tiers spanning multiple pages. The tiering criteria is complicated: First paging by $\text{FNIR}(N_b, 1, 0)$, then sorting by median $\text{FNIR}(N_b, T)$, $N_b = 640\,000$.

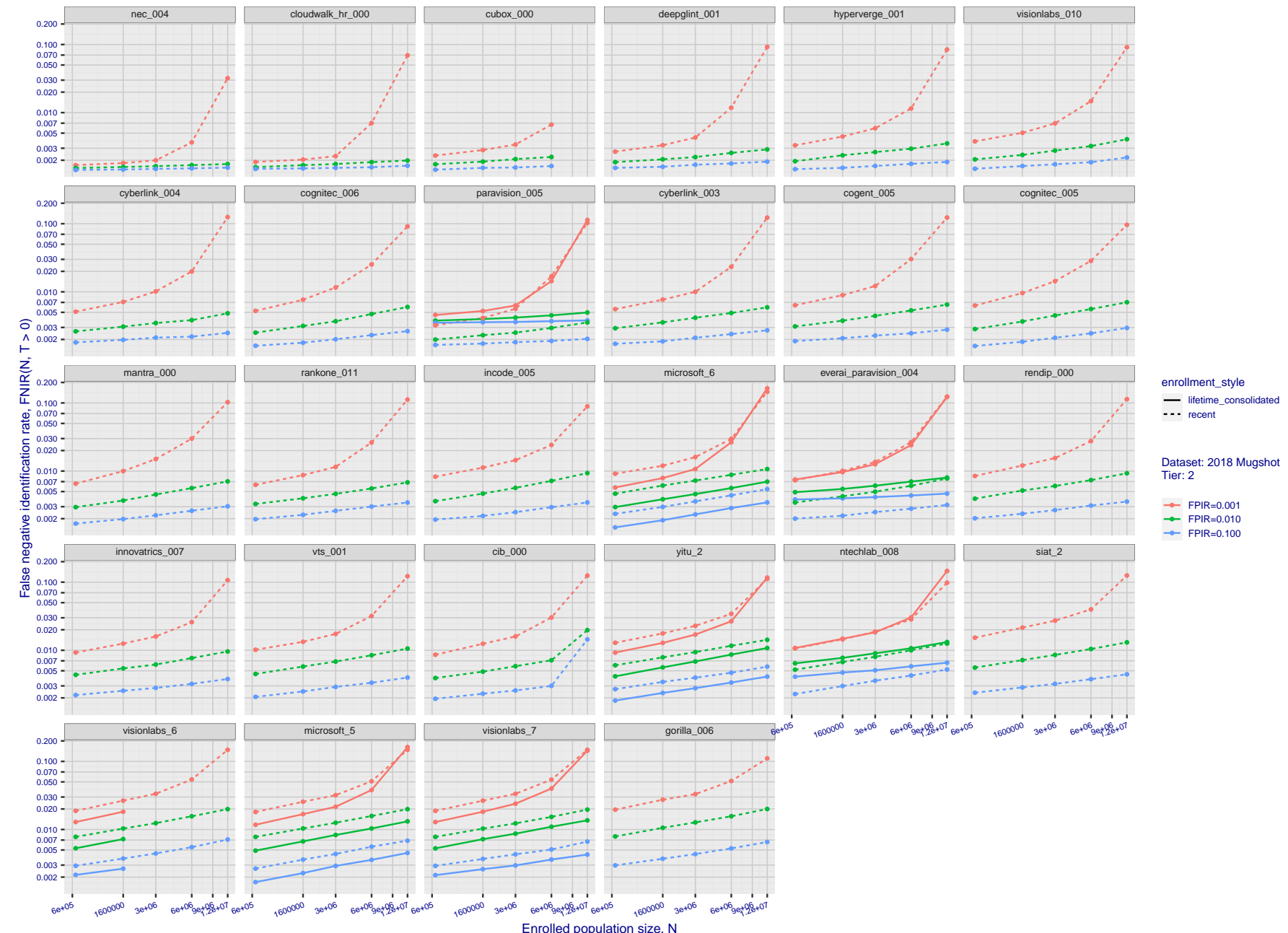


Figure 37: [FRVT-2018 Mugshot Dataset] Threshold-based identification miss rates vs. number of enrolled subjects. The figure shows $\text{FNIR}(N, T)$ across various gallery sizes when the threshold is set to achieve the given FPIRs. The rank criterion is irrelevant at high thresholds as mates are always at rank 1. The results are computed from the trials listed in rows 1-10 of Table 1. Less accurate algorithms were not run on large N , so results are missing. For clarity, results are sorted and reported into tiers spanning multiple pages. The tiering criteria is complicated: First paging by $\text{FNIR}(N_b, 1, 0)$, then sorting by median $\text{FNIR}(N_b, T)$, $N_b = 640\,000$.

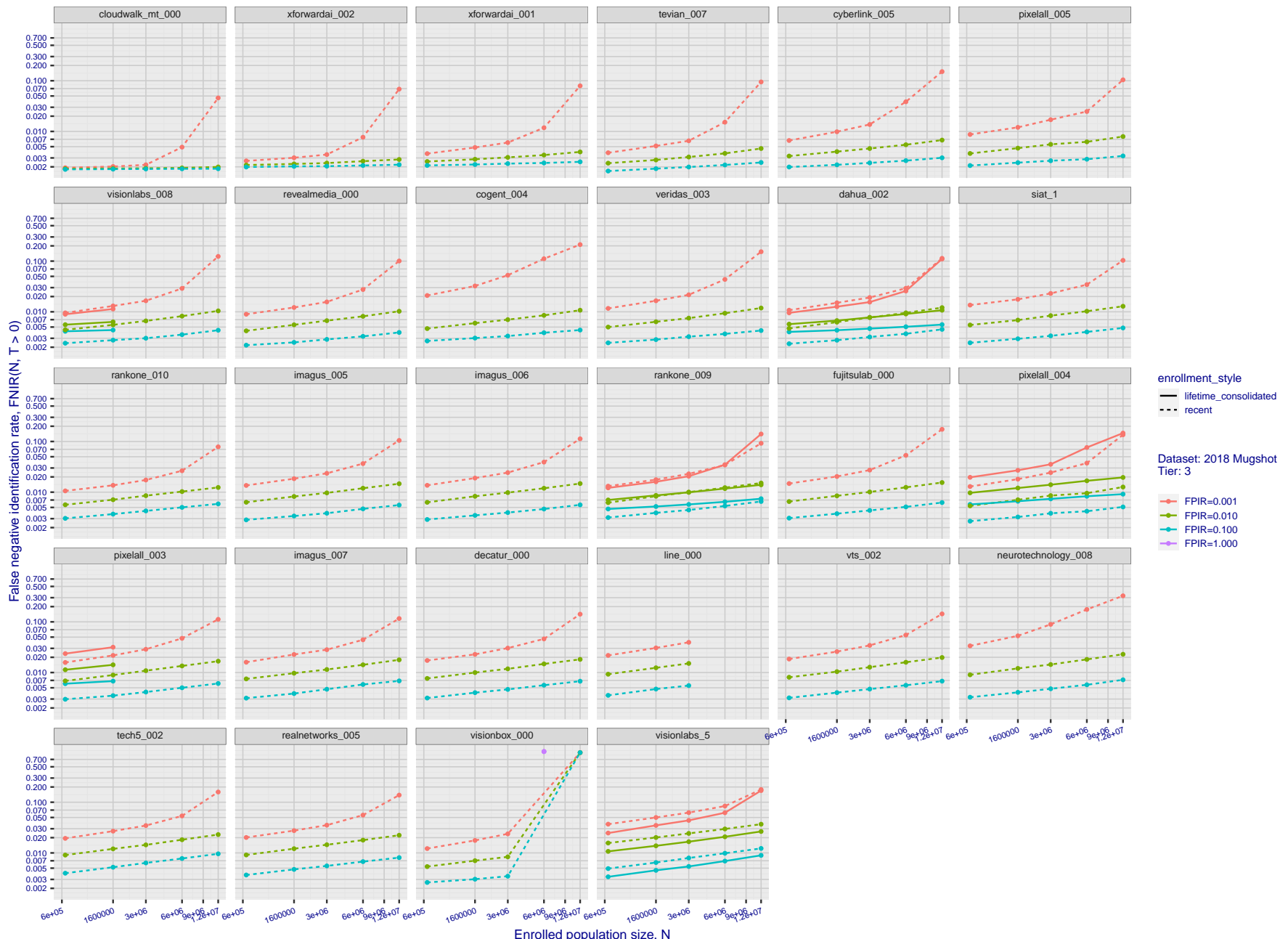


Figure 38: [FRVT-2018 Mugshot Dataset] Threshold-based identification miss rates vs. number of enrolled subjects. The figure shows $\text{FNIR}(N, T)$ across various gallery sizes when the threshold is set to achieve the given FPIRs. The rank criterion is irrelevant at high thresholds as mates are always at rank 1. The results are computed from the trials listed in rows 1-10 of Table 1. Less accurate algorithms were not run on large N , so results are missing. For clarity, results are sorted and reported into tiers spanning multiple pages. The tiering criteria is complicated: First paging by $\text{FNIR}(N_b, 1, 0)$, then sorting by median $\text{FNIR}(N_b, T)$, $N_b = 640\,000$.

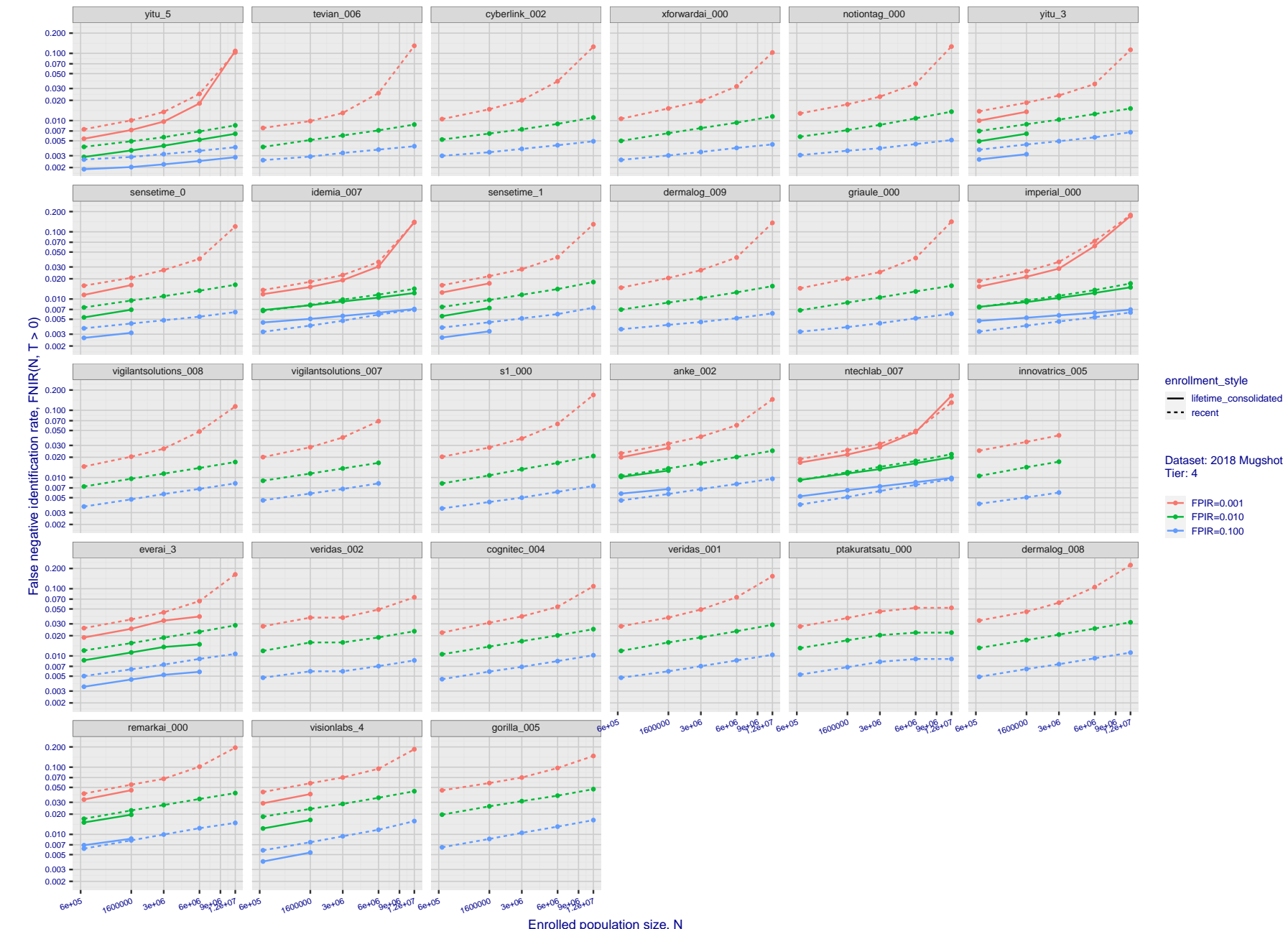


Figure 39: [FRVT-2018 Mugshot Dataset] Threshold-based identification miss rates vs. number of enrolled subjects. The figure shows $\text{FNIR}(N, T)$ across various gallery sizes when the threshold is set to achieve the given FPIRs. The rank criterion is irrelevant at high thresholds as mates are always at rank 1. The results are computed from the trials listed in rows 1-10 of Table 1. Less accurate algorithms were not run on large N , so results are missing. For clarity, results are sorted and reported into tiers spanning multiple pages. The tiering criteria is complicated: First paging by $\text{FNIR}(N_b, 1, 0)$, then sorting by median $\text{FNIR}(N_b, T)$, $N_b = 640\,000$.

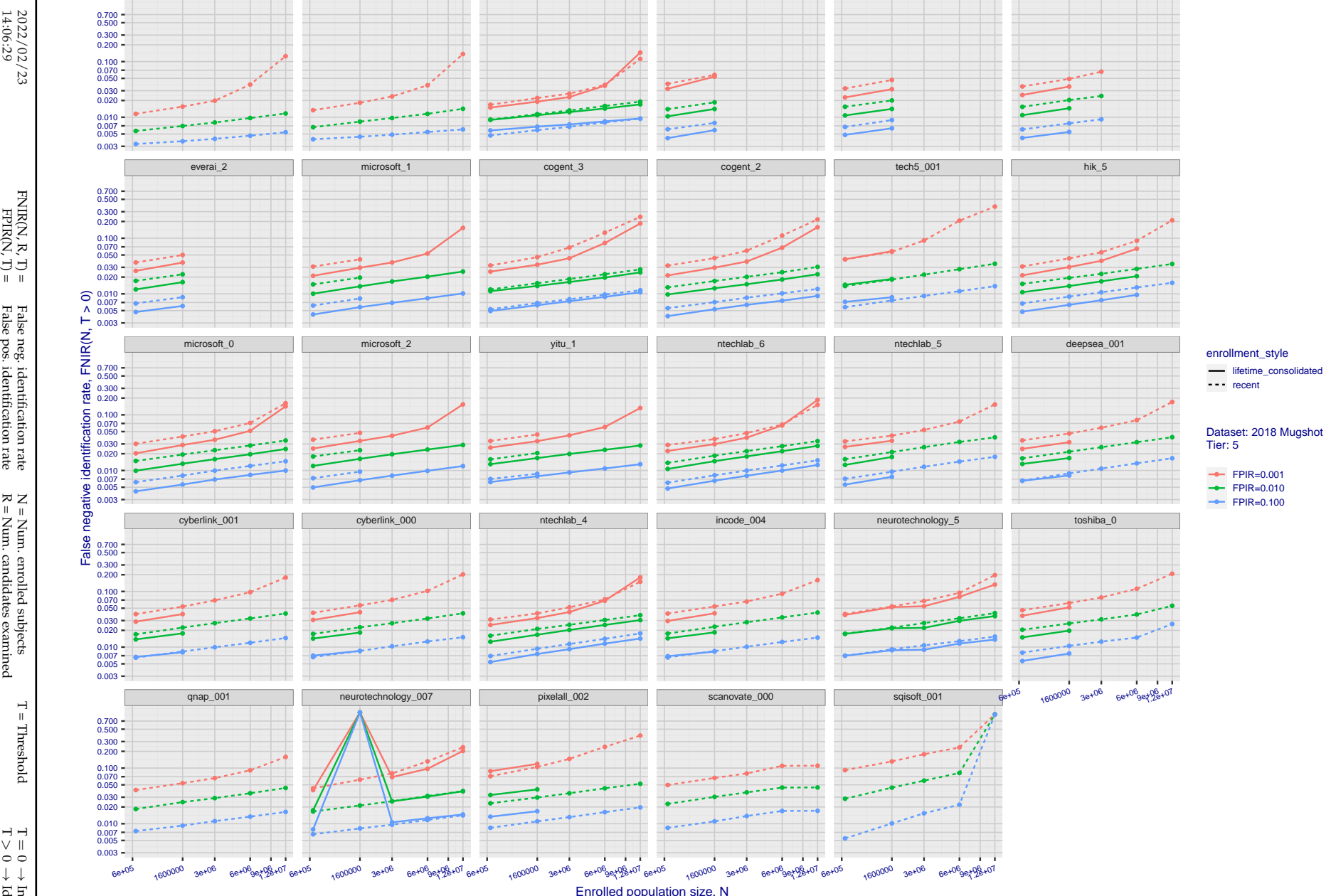


Figure 40: [FRVT-2018 Mugshot Dataset] Threshold-based identification miss rates vs. number of enrolled subjects. The figure shows $\text{FNIR}(N, T)$ across various gallery sizes when the threshold is set to achieve the given FPIRs. The rank criterion is irrelevant at high thresholds as mates are always at rank 1. The results are computed from the trials listed in rows 1-10 of Table 1. Less accurate algorithms were not run on large N , so results are missing. For clarity, results are sorted and reported into tiers spanning multiple pages. The tiering criteria is complicated: First paging by $\text{FNIR}(N_b, 1, 0)$, then sorting by median $\text{FNIR}(N_b, T)$, $N_b = 640\,000$.

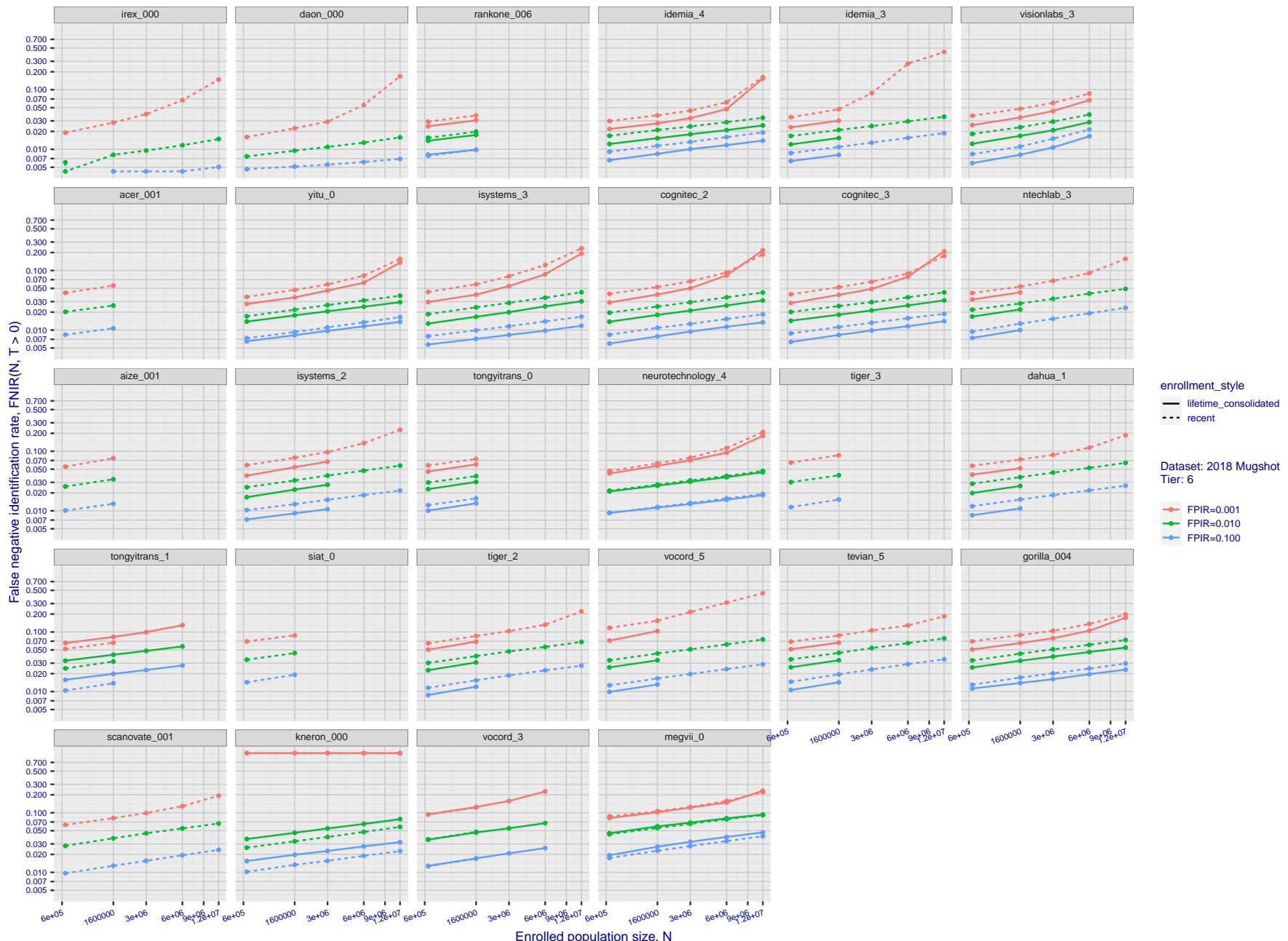


Figure 41: [FRVT-2018 Mugshot Dataset] Threshold-based identification miss rates vs. number of enrolled subjects. The figure shows FNIR(N, T) across various gallery sizes when the threshold is set to achieve the given FPIRs. The rank criterion is irrelevant at high thresholds as mates are always at rank 1. The results are computed from the trials listed in rows 1-10 of Table 1. Less accurate algorithms were not run on large N , so results are missing. For clarity, results are sorted and reported into tiers spanning multiple pages. The tiering criteria is complicated: First paging by FNIR($N_b, 1, 0$), then sorting by median FNIR(N_b, T), $N_b = 640\,000$.

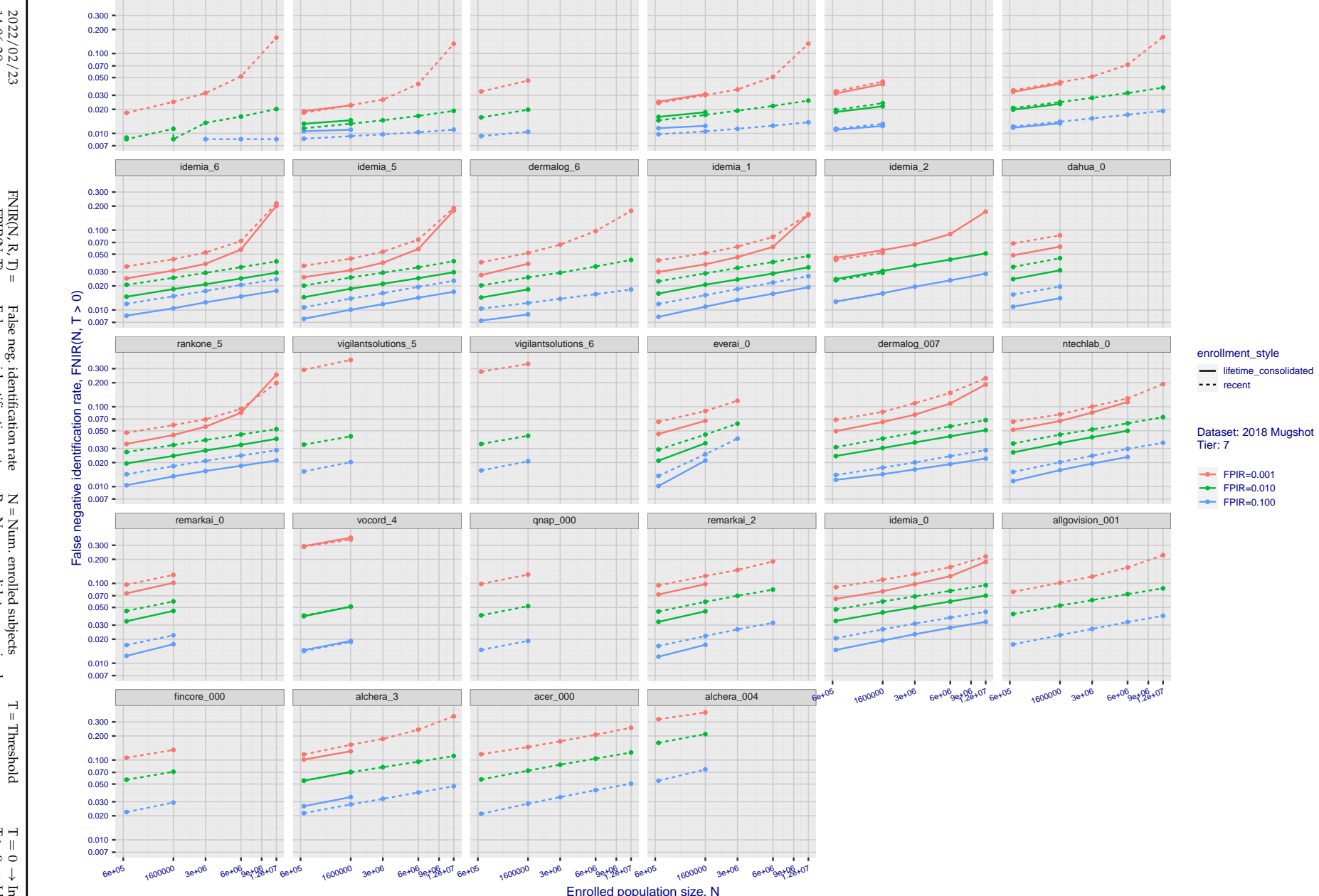


Figure 42: [FRVT-2018 Mugshot Dataset] Threshold-based identification miss rates vs. number of enrolled subjects. The figure shows $\text{FNIR}(N, T)$ across various gallery sizes when the threshold is set to achieve the given FPIRs. The rank criterion is irrelevant at high thresholds as mates are always at rank 1. The results are computed from the trials listed in rows 1-10 of Table 1. Less accurate algorithms were not run on large N , so results are missing. For clarity, results are sorted and reported into tiers spanning multiple pages. The tiering criteria is complicated: First paging by $\text{FNIR}(N_b, 1, 0)$, then sorting by median $\text{FNIR}(N_b, T)$, $N_b = 640\,000$.

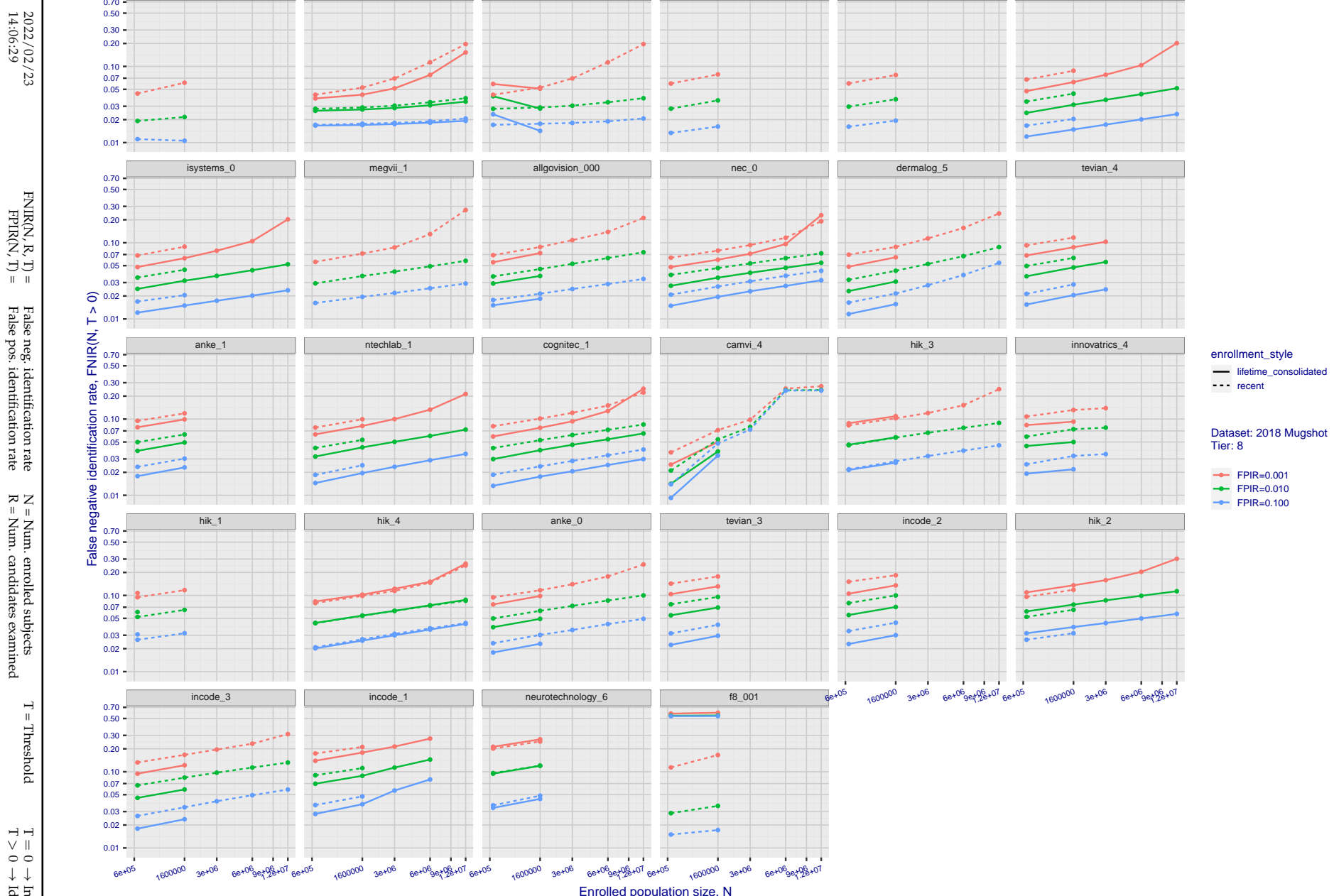


Figure 43: [FRVT-2018 Mugshot Dataset] Threshold-based identification miss rates vs. number of enrolled subjects. The figure shows $\text{FNIR}(N, T)$ across various gallery sizes when the threshold is set to achieve the given FPIRs. The rank criterion is irrelevant at high thresholds as mates are always at rank 1. The results are computed from the trials listed in rows 1-10 of Table 1. Less accurate algorithms were not run on large N , so results are missing. For clarity, results are sorted and reported into tiers spanning multiple pages. The tiering criteria is complicated: First paging by $\text{FNIR}(N_b, 1, 0)$, then sorting by median $\text{FNIR}(N_b, T)$, $N_b = 640\,000$.

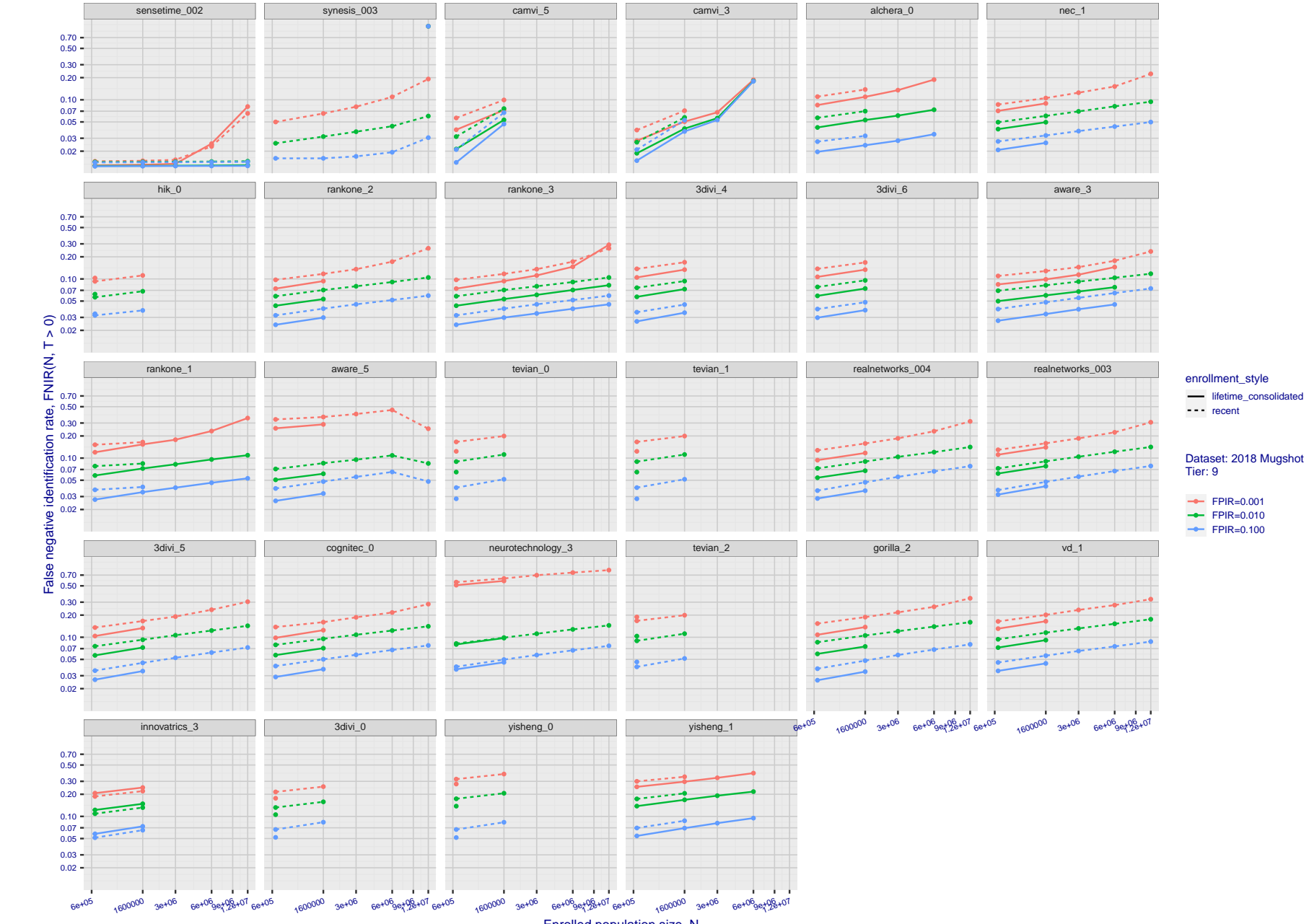


Figure 44: [FRVT-2018 Mugshot Dataset] Threshold-based identification miss rates vs. number of enrolled subjects. The figure shows FNIR(N, T) across various gallery sizes when the threshold is set to achieve the given FPIRs. The rank criterion is irrelevant at high thresholds as mates are always at rank 1. The results are computed from the trials listed in rows 1-10 of Table 1. Less accurate algorithms were not run on large N, so results are missing. For clarity, results are sorted and reported into tiers spanning multiple pages. The tiering criteria is complicated: First paging by $\text{FNIR}(N_b, 1, 0)$, then sorting by median $\text{FNIR}(N_b, T)$, $N_b = 640\,000$.

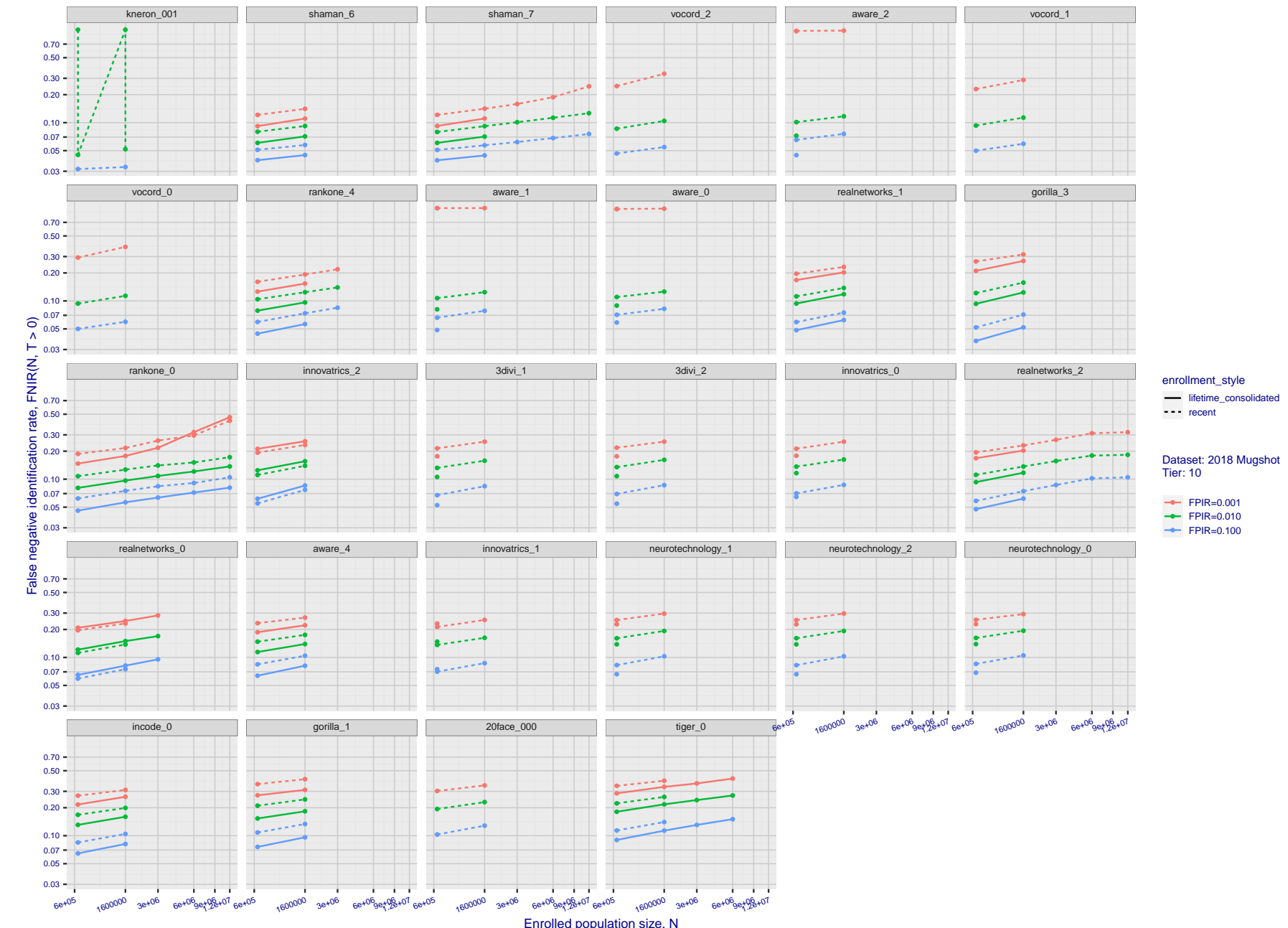


Figure 45: [FRVT-2018 Mugshot Dataset] Threshold-based identification miss rates vs. number of enrolled subjects. The figure shows $\text{FNIR}(N, T)$ across various gallery sizes when the threshold is set to achieve the given FPIRs. The rank criterion is irrelevant at high thresholds as mates are always at rank 1. The results are computed from the trials listed in rows 1-10 of Table 1. Less accurate algorithms were not run on large N , so results are missing. For clarity, results are sorted and reported into tiers spanning multiple pages. The tiering criteria is complicated: First paging by $\text{FNIR}(N_b, 1, 0)$, then sorting by median $\text{FNIR}(N_b, T)$, $N_b = 640\,000$.

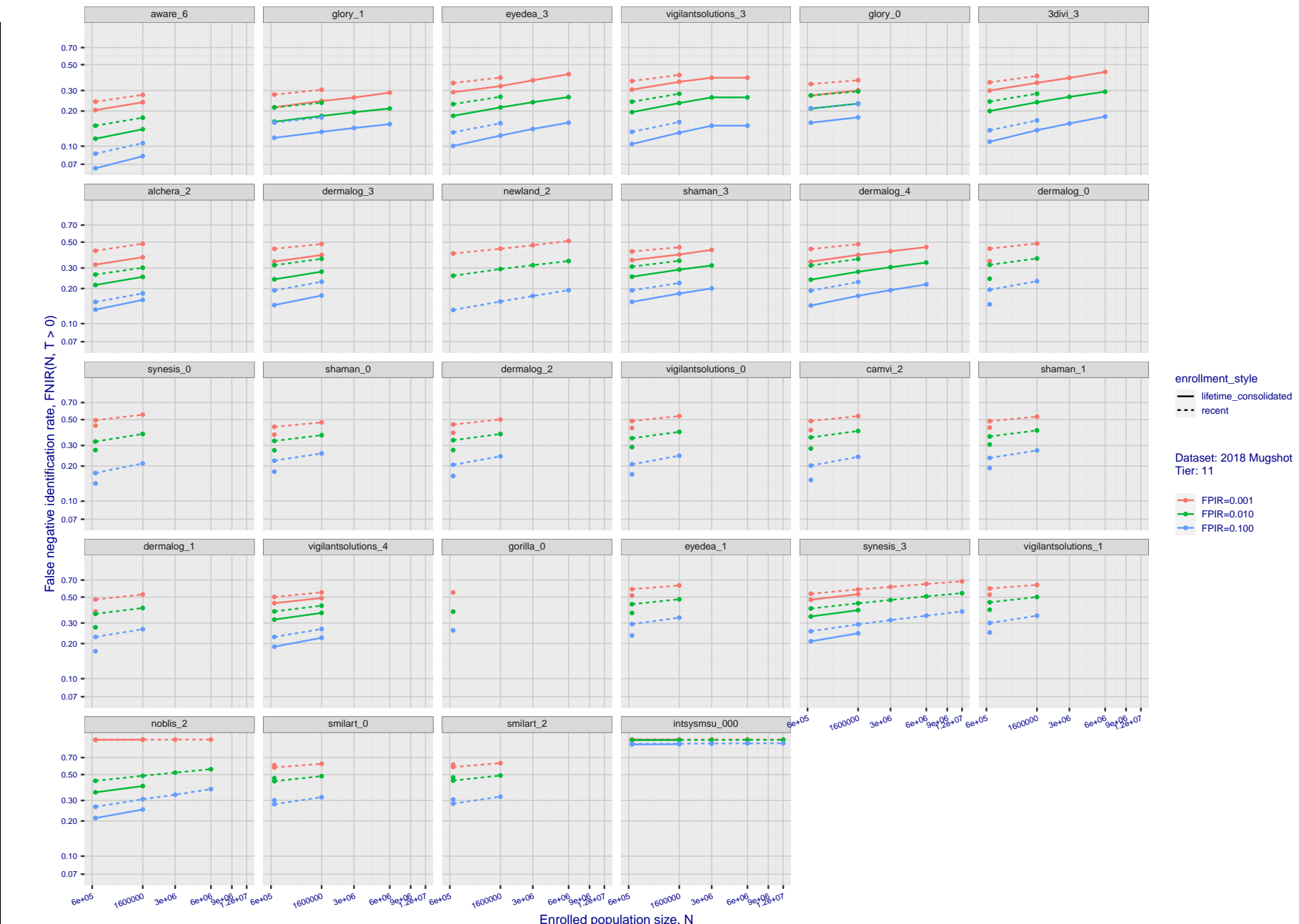
2022/02/23
14:06:29

Figure 46: [FRVT-2018 Mugshot Dataset] Threshold-based identification miss rates vs. number of enrolled subjects. The figure shows $\text{FNIR}(N, T)$ across various gallery sizes when the threshold is set to achieve the given FPIRs. The rank criterion is irrelevant at high thresholds as mates are always at rank 1. The results are computed from the trials listed in rows 1-10 of Table 1. Less accurate algorithms were not run on large N , so results are missing. For clarity, results are sorted and reported into tiers spanning multiple pages. The tiering criteria is complicated: First paging by $\text{FNIR}(N_b, 1, 0)$, then sorting by median $\text{FNIR}(N_b, T)$, $N_b = 640\,000$.

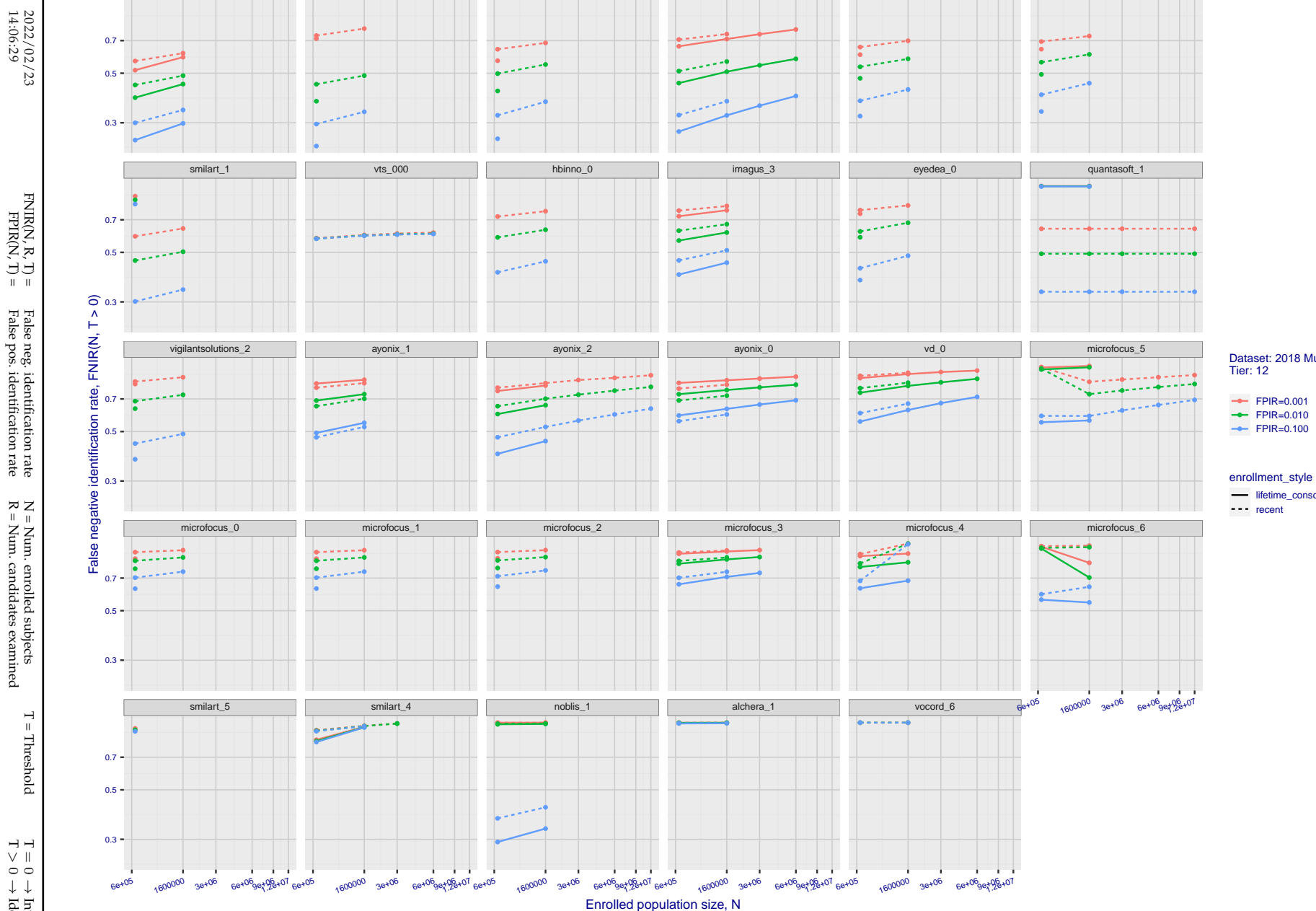


Figure 47: [FRVT-2018 Mugshot Dataset] Threshold-based identification miss rates vs. number of enrolled subjects. The figure shows FNIR(N, T) across various gallery sizes when the threshold is set to achieve the given FPIRs. The rank criterion is irrelevant at high thresholds as mates are always at rank 1. The results are computed from the trials listed in rows 1-10 of Table 1. Less accurate algorithms were not run on large N, so results are missing. For clarity, results are sorted and reported into tiers spanning multiple pages. The tiering criteria is complicated: First paging by FNIR(N_b , 1, 0), then sorting by median FNIR(N_b , T), $N_b = 640\,000$.

2022/02/23 FNIR(N, R, T) = False neg. identification rate
FPIR(N, T) = False pos. identification rate
N = Num. enrolled subjects
R = Num. candidates examined
T = Threshold
 $T = 0 \rightarrow$ Investigation
 $T > 0 \rightarrow$ Identification

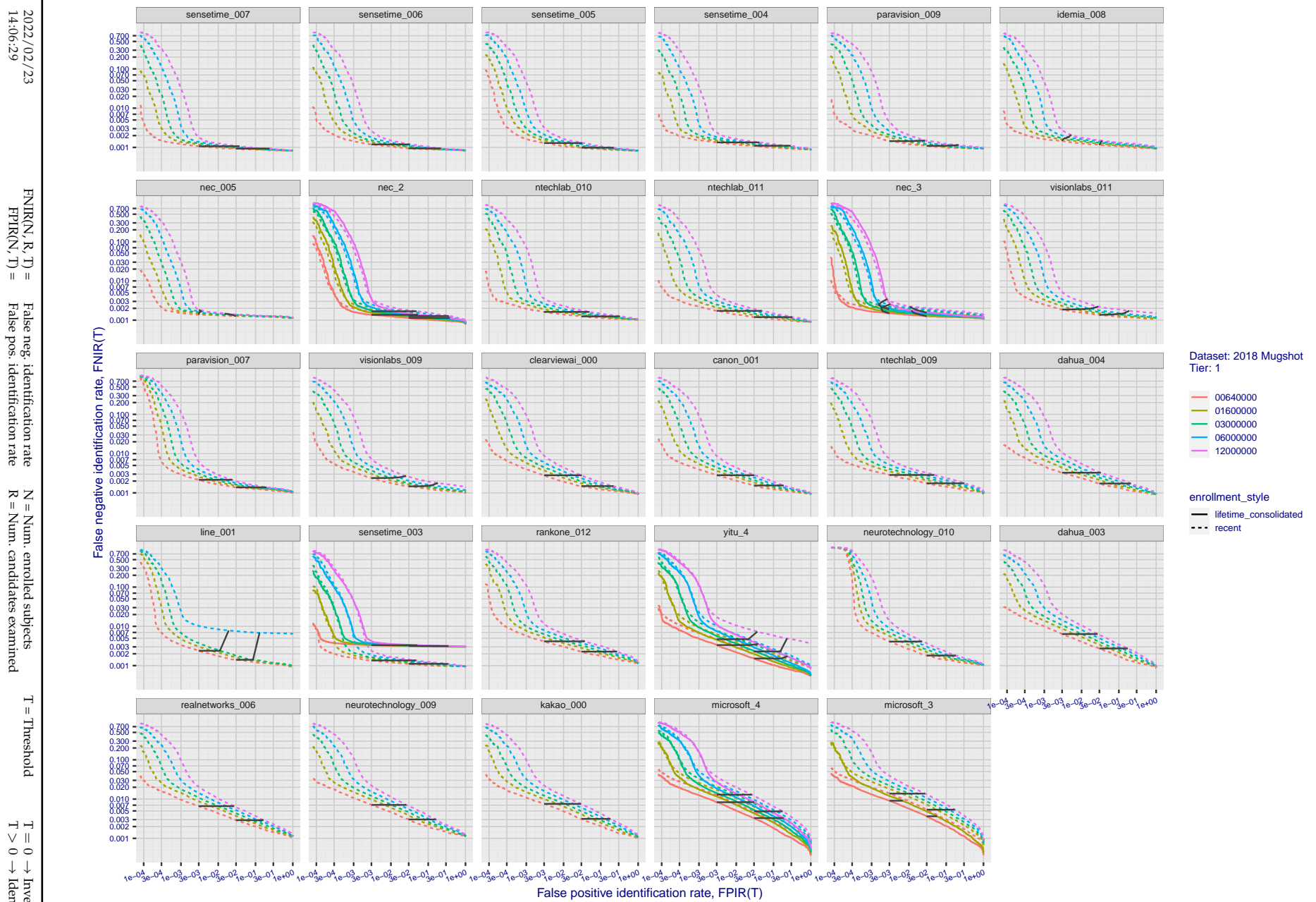


Figure 48: [FRVT-2018 Mugshot Dataset] Identification miss rates vs. false positive rates. The figure shows miss rates $\text{FNIR}(N, L, T)$ as a function of $\text{FPIR}(N, T)$, with N ranging from 640 000 to 12 000 000 as noted in rows 1-10 of Table 1. These error tradeoff characteristics are useful for applications where a threshold must be elevated to limit false positives, such as when human reviewer labor is not matched to the volume of searches. Dark lines join points of equal threshold: If horizontal, $\text{FPIR}(T)$ rises with N , and mate scores are independent of N . Other algorithms adjust scores in an attempt to make FPIR independent of N .

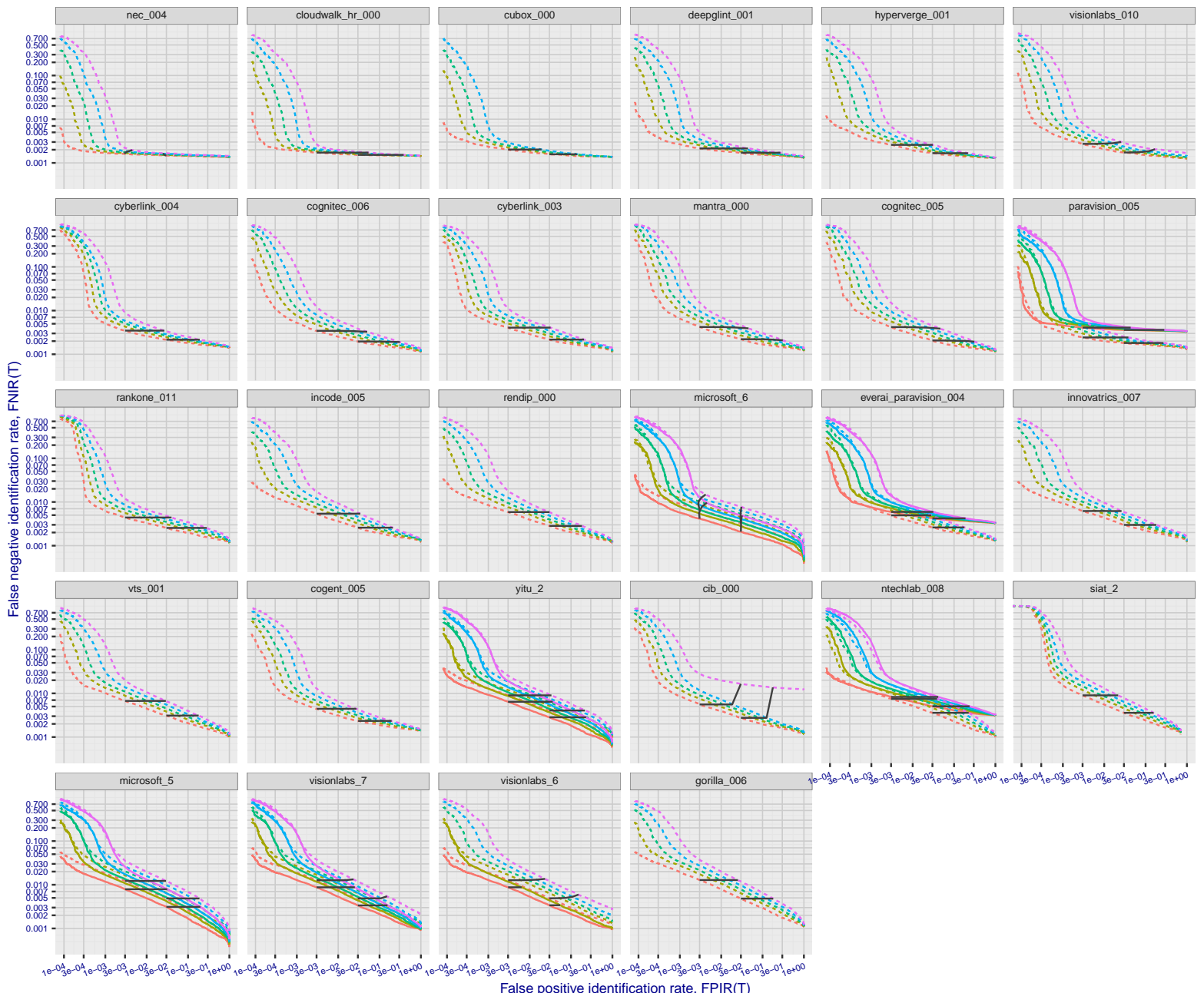


Figure 49: [FRVT-2018 Mugshot Dataset] Identification miss rates vs. false positive rates. The figure shows miss rates $\text{FNIR}(N, L, T)$ as a function of $\text{FPIR}(N, T)$, with N ranging from 640 000 to 12 000 000 as noted in rows 1-10 of Table 1. These error tradeoff characteristics are useful for applications where a threshold must be elevated to limit false positives, such as when human reviewer labor is not matched to the volume of searches. Dark lines join points of equal threshold: If horizontal, $\text{FPIR}(T)$ rises with N , and mate scores are independent of N . Other algorithms adjust scores in an attempt to make FPIR independent of N .

2022/02/23

14:06:29

 $\text{FNIR}(N, R, T) = \text{False neg. identification rate}$ $\text{FPIR}(N, T) = \text{False pos. identification rate}$ $N = \text{Num. enrolled subjects}$ $R = \text{Num. candidates examined}$ $T = \text{Threshold}$ $T = 0 \rightarrow \text{Investigation}$ $T > 0 \rightarrow \text{Identification}$

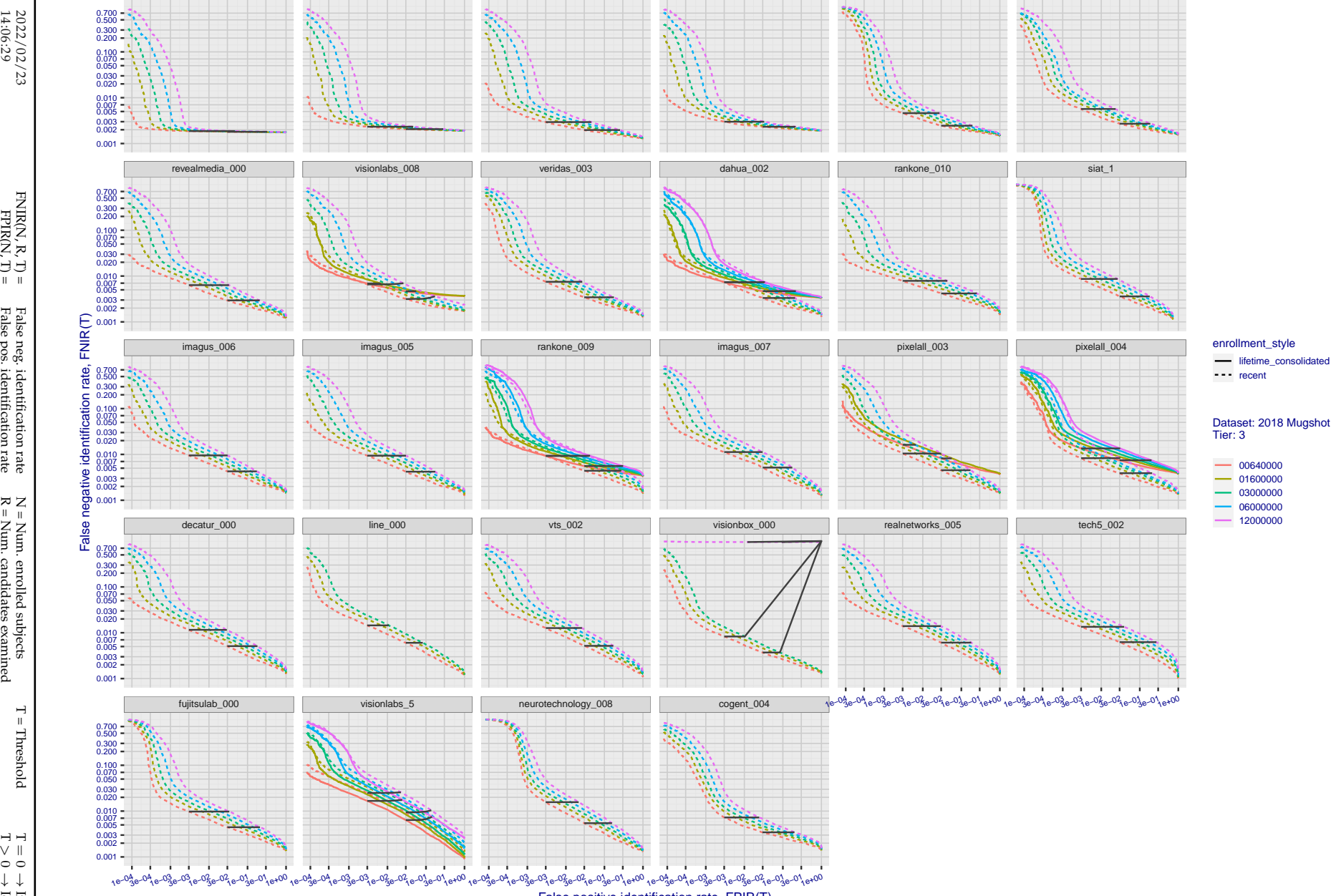


Figure 50: [FRVT-2018 Mugshot Dataset] Identification miss rates vs. false positive rates. The figure shows miss rates $\text{FNIR}(N, L, T)$ as a function of $\text{FPIR}(N, T)$, with N ranging from 640 000 to 12 000 000 as noted in rows 1-10 of Table 1. These error tradeoff characteristics are useful for applications where a threshold must be elevated to limit false positives, such as when human reviewer labor is not matched to the volume of searches. Dark lines join points of equal N . If horizontal, $\text{FPIR}(T)$ rises with N , and mate scores are independent of N . Other algorithms adjust scores in an attempt to make FPIR independent of N .

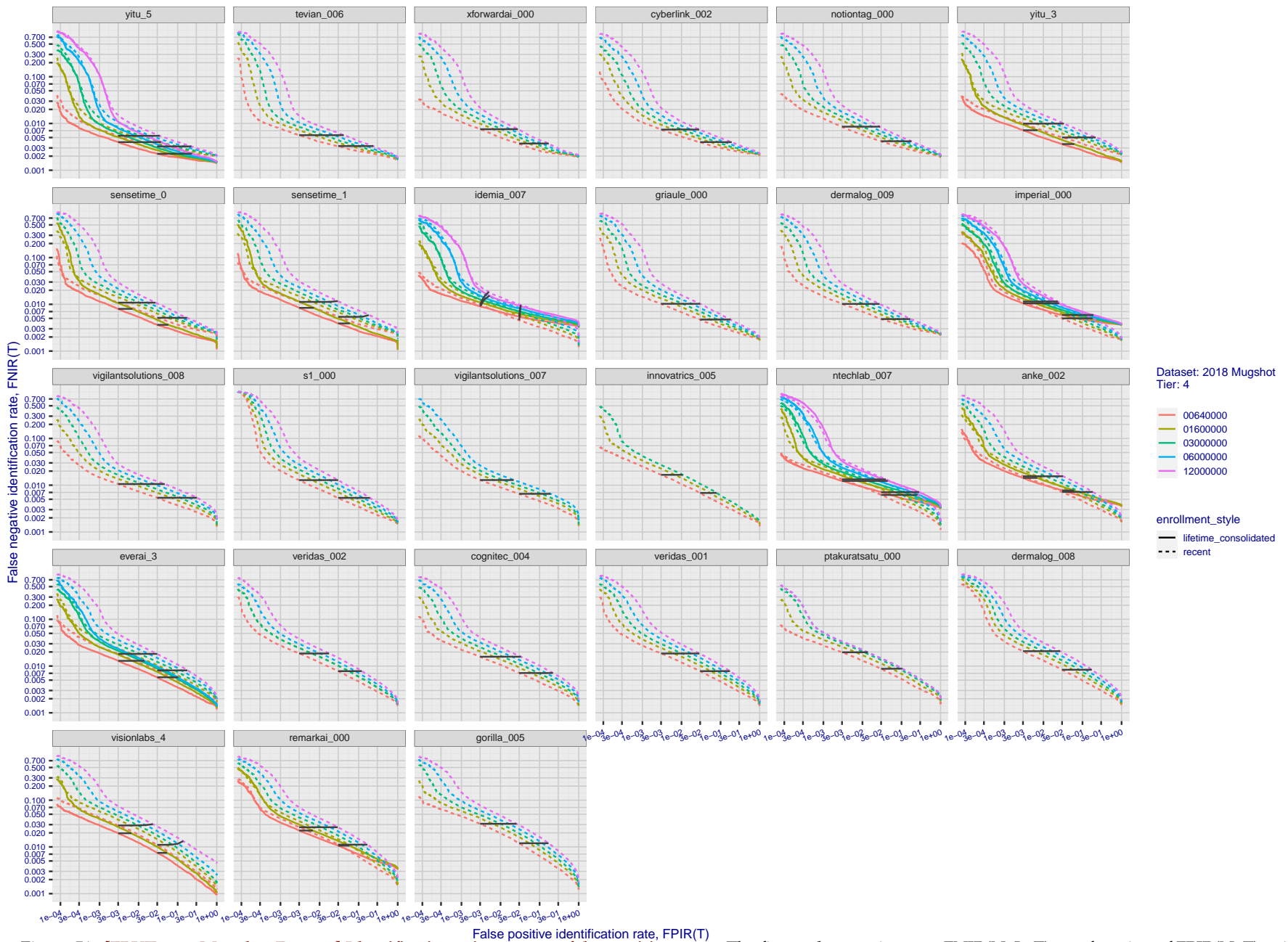


Figure 51: [FRVT-2018 Mugshot Dataset] Identification miss rates vs. false positive rates. The figure shows miss rates $\text{FNIR}(N, L, T)$ as a function of $\text{FPIR}(N, T)$, with N ranging from 640 000 to 12 000 000 as noted in rows 1-10 of Table 1. These error tradeoff characteristics are useful for applications where a threshold must be elevated to limit false positives, such as when human reviewer labor is not matched to the volume of searches. Dark lines join points of equal threshold: If horizontal, $\text{FPIR}(T)$ rises with N , and mate scores are independent of N . Other algorithms adjust scores in an attempt to make FPIR independent of N .

2022/02/23
14:06:29FNIR(N, R, T) = False neg. identification rate
FPIR(N, T) = False pos. identification rate
N = Num. enrolled subjects
R = Num. candidates examined

T = Threshold

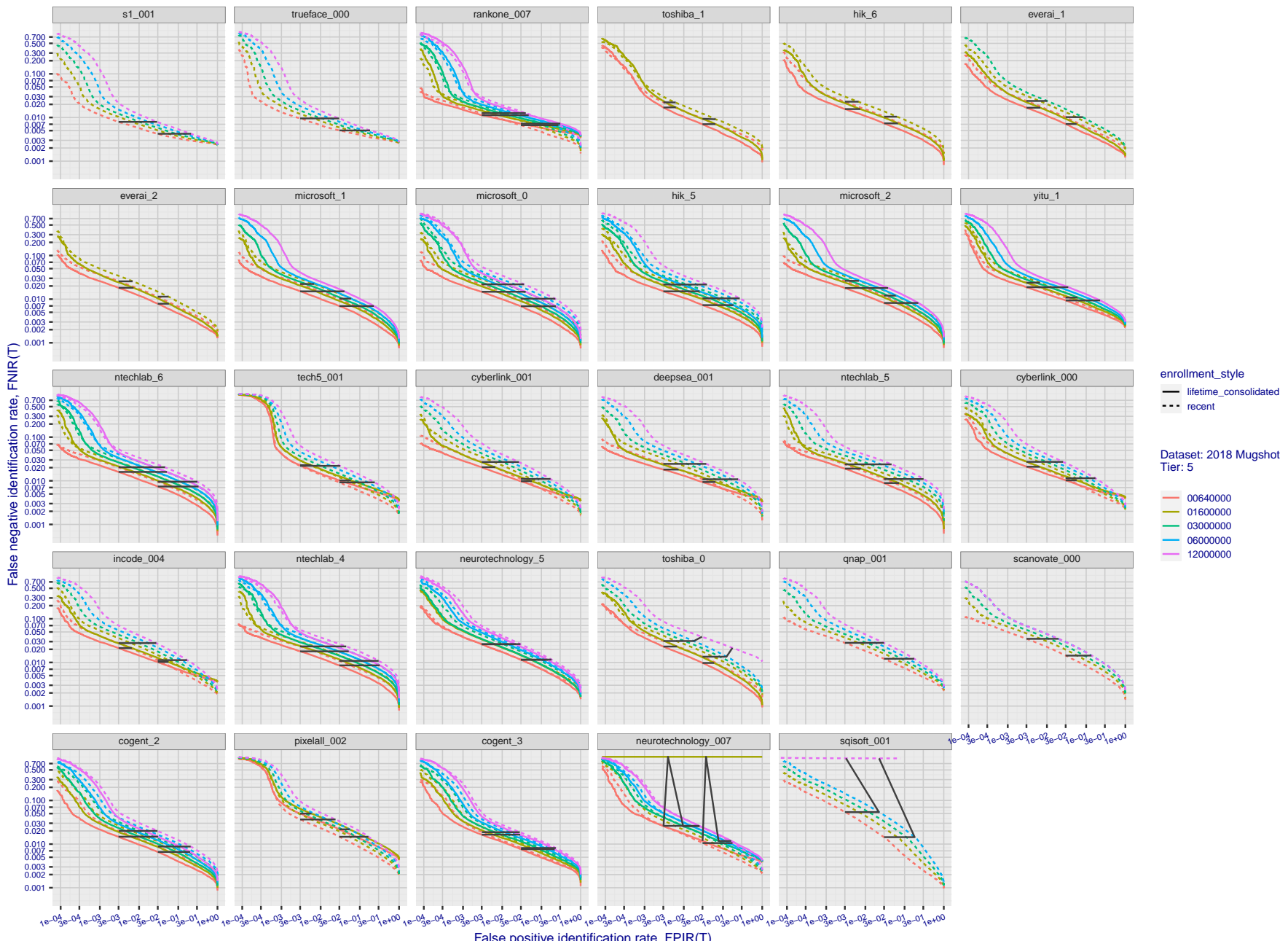
T = 0 → Investigation
 $T > 0 \rightarrow$ Identification

Figure 52: [FRVT-2018 Mugshot Dataset] Identification miss rates vs. false positive rates. The figure shows miss rates $\text{FNIR}(N, L, T)$ as a function of $\text{FPIR}(N, T)$, with N ranging from 640 000 to 12 000 000 as noted in rows 1-10 of Table 1. These error tradeoff characteristics are useful for applications where a threshold must be elevated to limit false positives, such as when human reviewer labor is not matched to the volume of searches. Dark lines join points of equal N . Other algorithms adjust scores in an attempt to make FPIR independent of N .

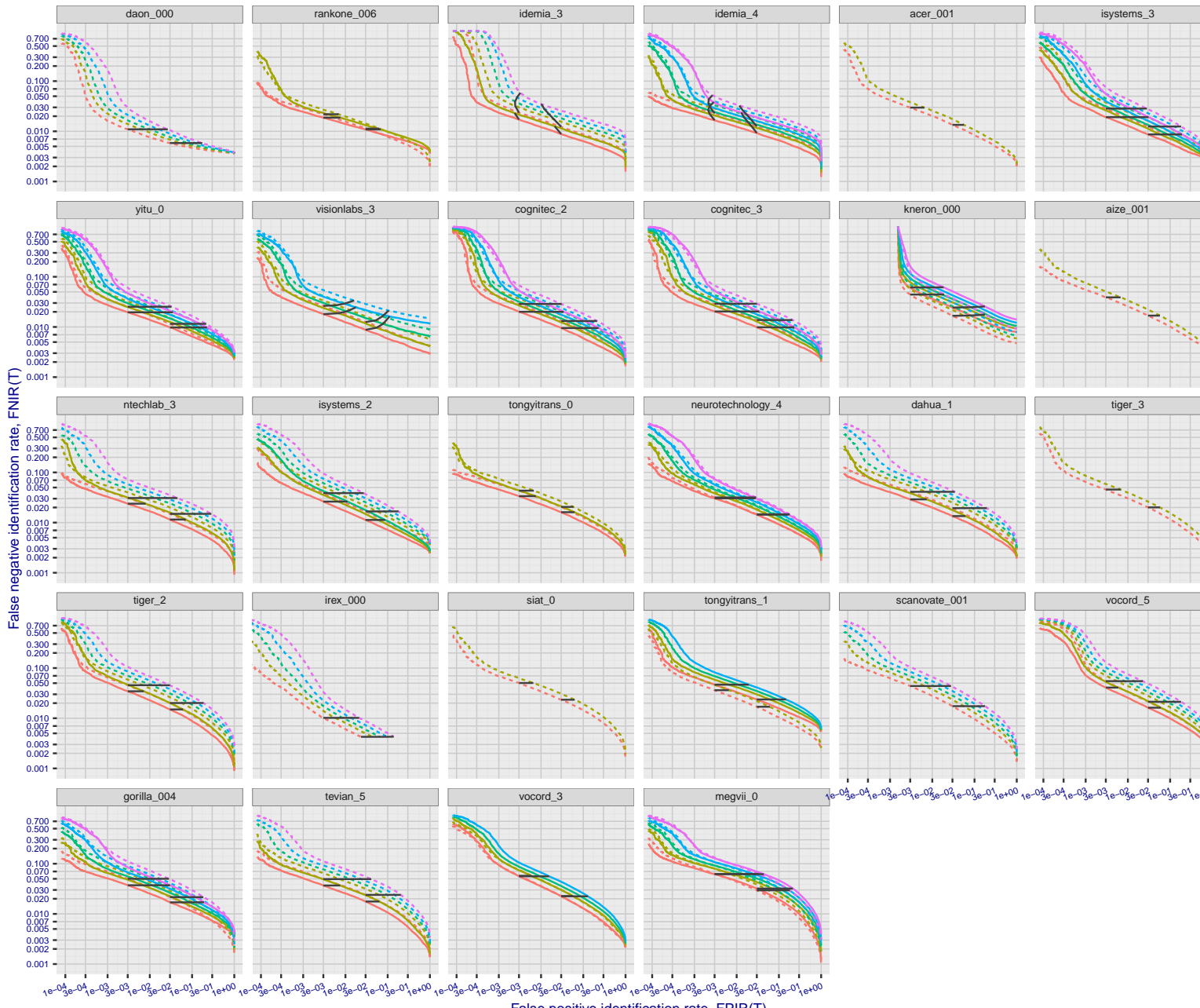
2022/02/23
14:06:29

$\text{FNIR}(N, R, T) =$ False neg. identification rate
 $\text{FPIR}(N, T) =$ False pos. identification rate

$N =$ Num. enrolled subjects
 $R =$ Num. candidates examined

$T =$ Threshold

$T = 0 \rightarrow$ Investigation
 $T > 0 \rightarrow$ Identification



Dataset: 2018 Mugshot
Tier: 6

00640000
01600000
03000000
06000000
12000000

enrollment_style
— lifetime Consolidated
- - recent

Figure 53: [FRVT-2018 Mugshot Dataset] Identification miss rates vs. false positive rates. The figure shows miss rates $\text{FNIR}(N, L, T)$ as a function of $\text{FPIR}(N, T)$, with N ranging from 640 000 to 12 000 000 as noted in rows 1-10 of Table 1. These error tradeoff characteristics are useful for applications where a threshold must be elevated to limit false positives, such as when human reviewer labor is not matched to the volume of searches. Dark lines join points of equal N . Other algorithms adjust scores in an attempt to make FPIR independent of N .

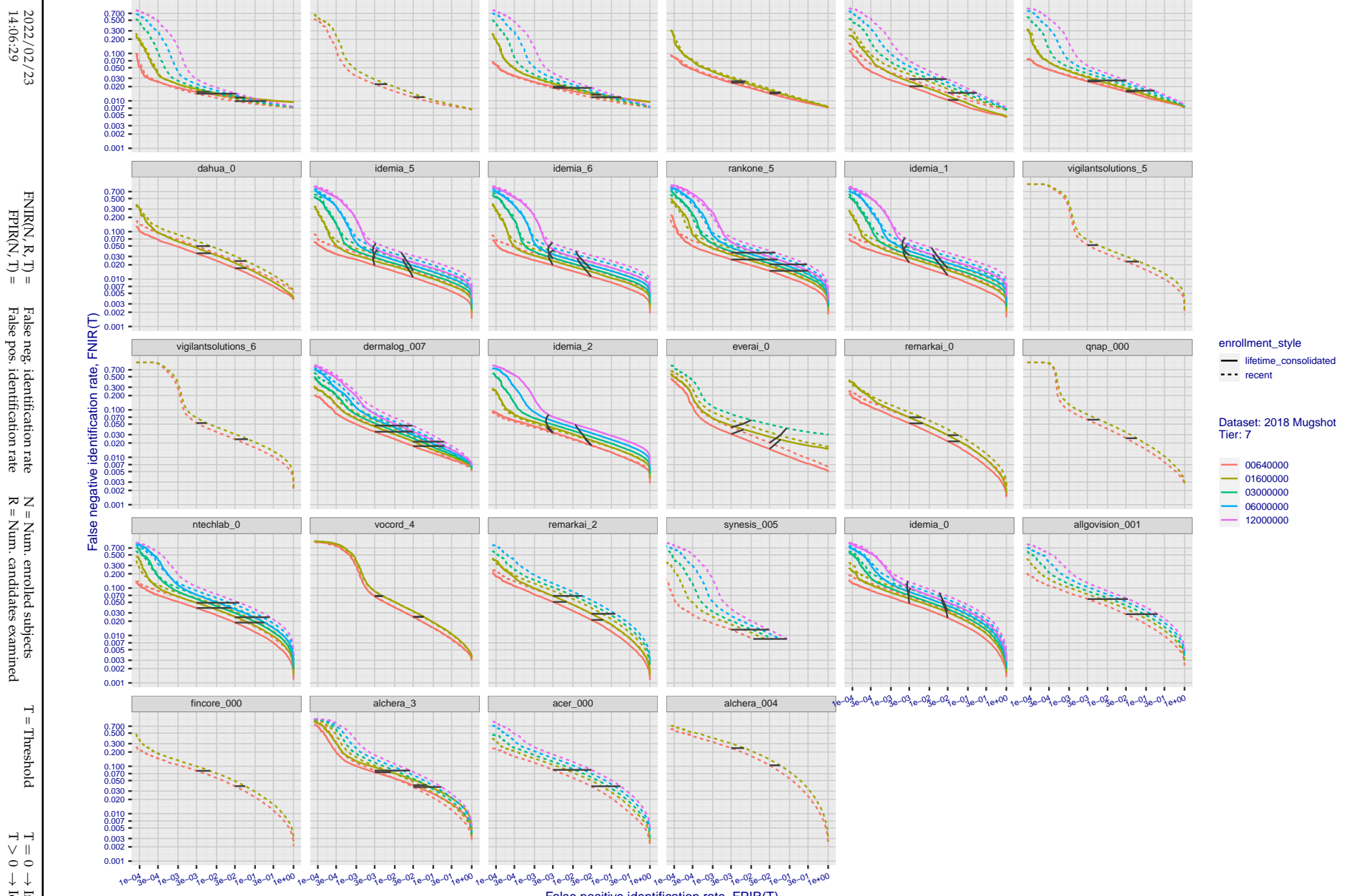


Figure 54: [FRVT-2018 Mugshot Dataset] Identification miss rates vs. false positive rates. The figure shows miss rates $\text{FNIR}(N, L, T)$ as a function of $\text{FPIR}(N, T)$, with N ranging from 640 000 to 12 000 000 as noted in rows 1-10 of Table 1. These error tradeoff characteristics are useful for applications where a threshold must be elevated to limit false positives, such as when human reviewer labor is not matched to the volume of searches. Dark lines join points of equal threshold: If horizontal, $\text{FPIR}(T)$ rises with N , and mate scores are independent of N . Other algorithms adjust scores in an attempt to make FPIR independent of N .

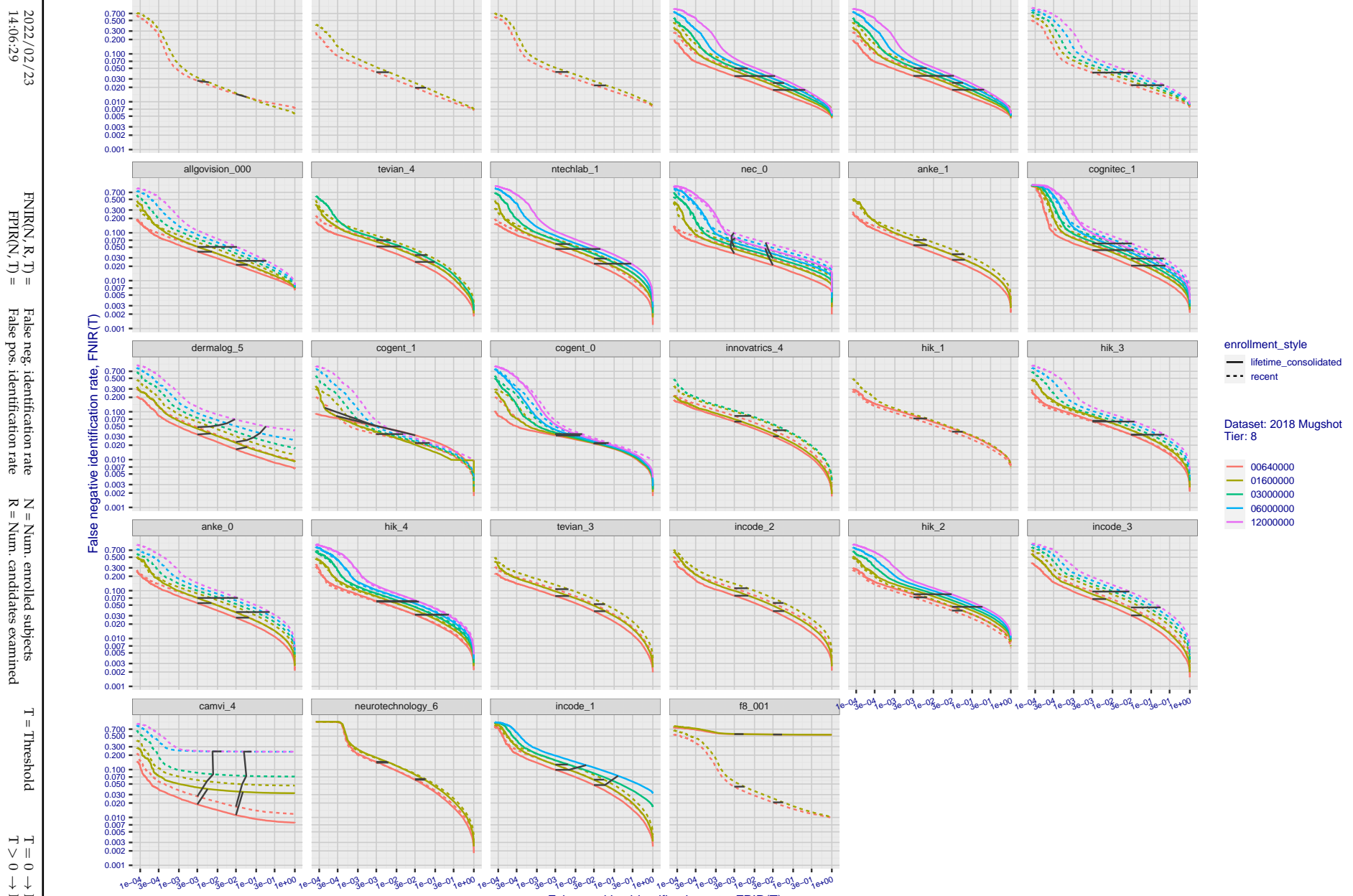


Figure 55: [FRVT-2018 Mugshot Dataset] Identification miss rates vs. false positive rates. The figure shows miss rates $\text{FNIR}(N, L, T)$ as a function of $\text{FPIR}(N, T)$, with N ranging from 640 000 to 12 000 000 as noted in rows 1-10 of Table 1. These error tradeoff characteristics are useful for applications where a threshold must be elevated to limit false positives, such as when human reviewer labor is not matched to the volume of searches. Dark lines join points of equal threshold: If horizontal, $\text{FPIR}(T)$ rises with N , and mate scores are independent of N . Other algorithms adjust scores in an attempt to make FPIR independent of N .

2022/02/23
14:06:29FNIR(N, R, T) = False neg. identification rate
FPIR(N, T) = False pos. identification rate
N = Num. enrolled subjects
R = Num. candidates examined

T = Threshold

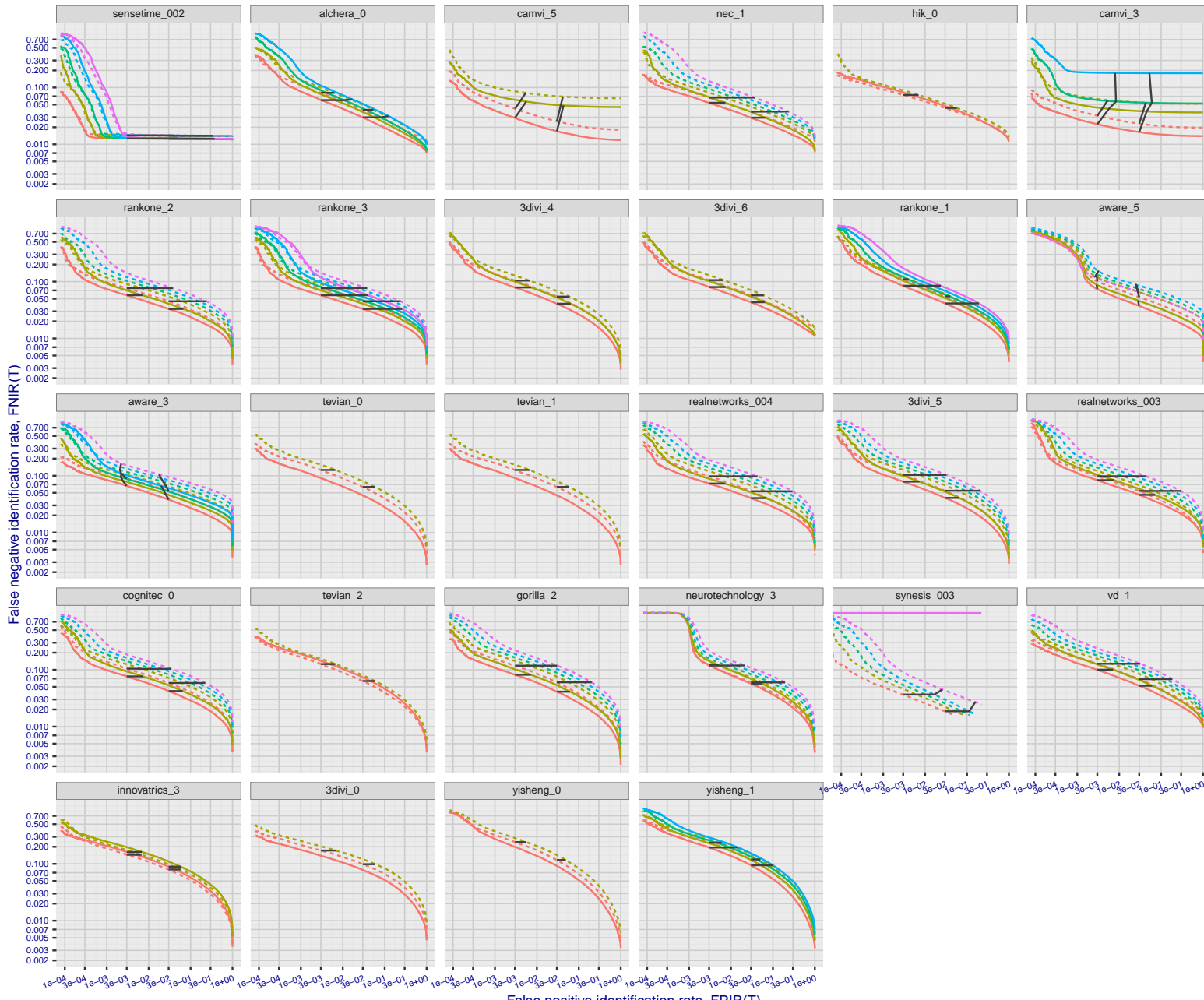
T = 0 → Investigation
 $T > 0 \rightarrow$ Identification

Figure 56: [FRVT-2018 Mugshot Dataset] Identification miss rates vs. false positive rates. The figure shows miss rates $\text{FNIR}(N, L, T)$ as a function of $\text{FPIR}(N, T)$, with N ranging from 640 000 to 12 000 000 as noted in rows 1-10 of Table 1. These error tradeoff characteristics are useful for applications where a threshold must be elevated to limit false positives, such as when human reviewer labor is not matched to the volume of searches. Dark lines join points of equal threshold: If horizontal, $\text{FPIR}(T)$ rises with N , and mate scores are independent of N . Other algorithms adjust scores in an attempt to make FPIR independent of N .

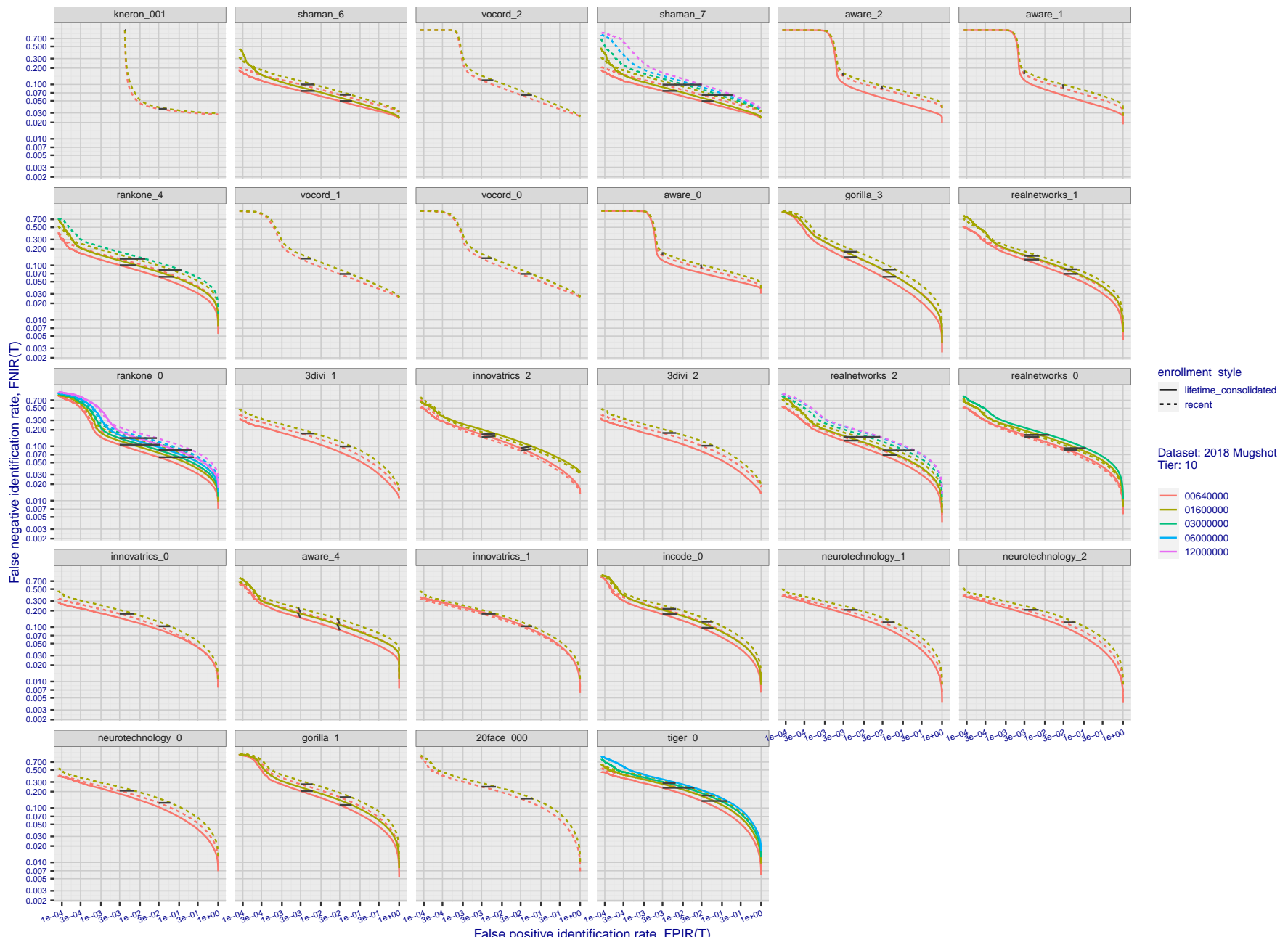


Figure 57: [FRVT-2018 Mugshot Dataset] Identification miss rates vs. false positive rates. The figure shows miss rates $\text{FNIR}(N, L, T)$ as a function of $\text{FPIR}(N, T)$, with N ranging from 640 000 to 12 000 000 as noted in rows 1-10 of Table 1. These error tradeoff characteristics are useful for applications where a threshold must be elevated to limit false positives, such as when human reviewer labor is not matched to the volume of searches. Dark lines join points of equal threshold: If horizontal, $\text{FPIR}(T)$ rises with N , and mate scores are independent of N . Other algorithms adjust scores in an attempt to make FPIR independent of N .

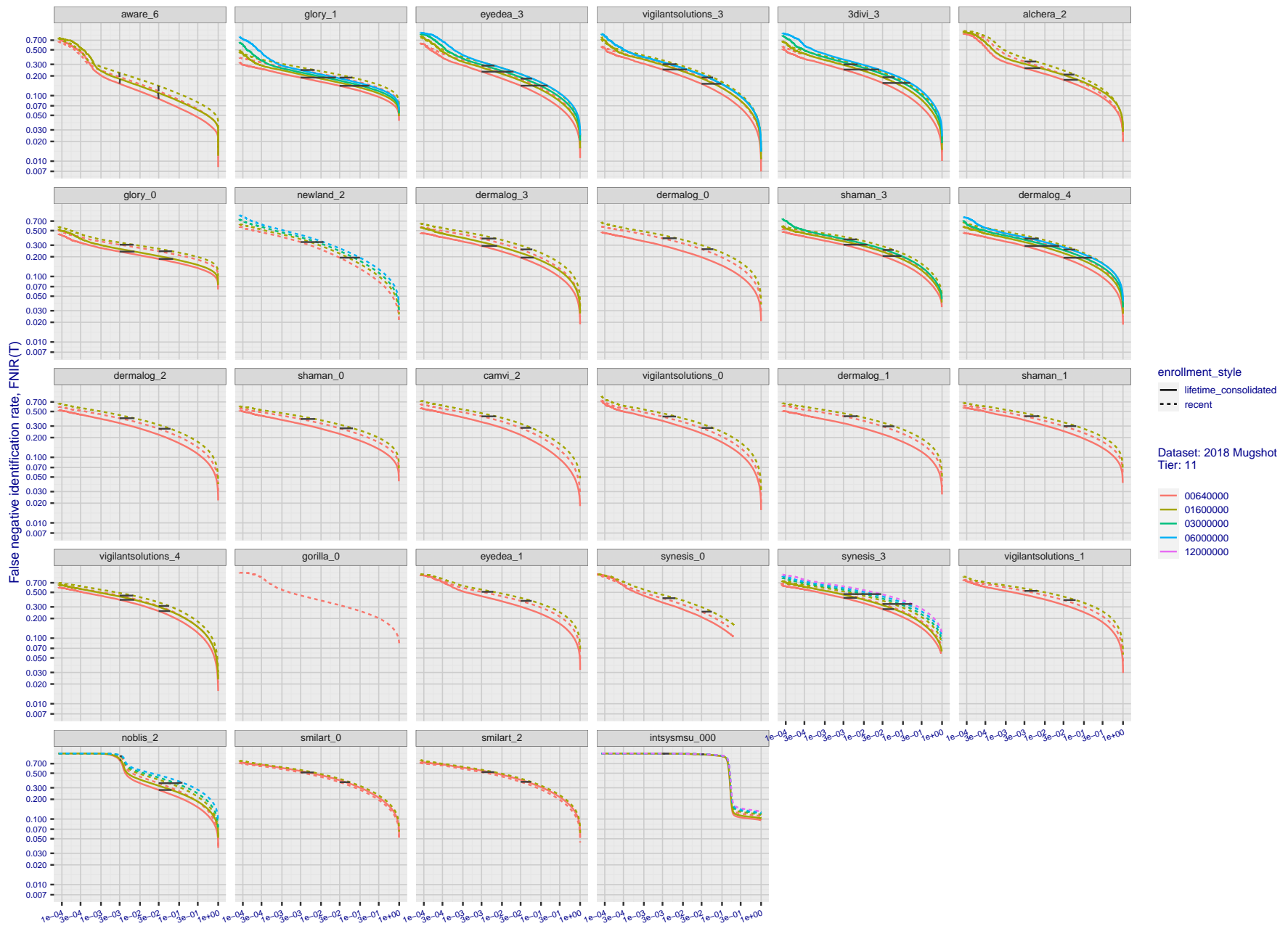


Figure 58: [FRVT-2018 Mugshot Dataset] Identification miss rates vs. false positive rates. The figure shows miss rates $\text{FNIR}(N, L, T)$ as a function of $\text{FPIR}(N, T)$, with N ranging from 640 000 to 12 000 000 as noted in rows 1-10 of Table 1. These error tradeoff characteristics are useful for applications where a threshold must be elevated to limit false positives, such as when human reviewer labor is not matched to the volume of searches. Dark lines join points of equal threshold: If horizontal, $\text{FPIR}(T)$ rises with N , and mate scores are independent of N . Other algorithms adjust scores in an attempt to make FPIR independent of N .

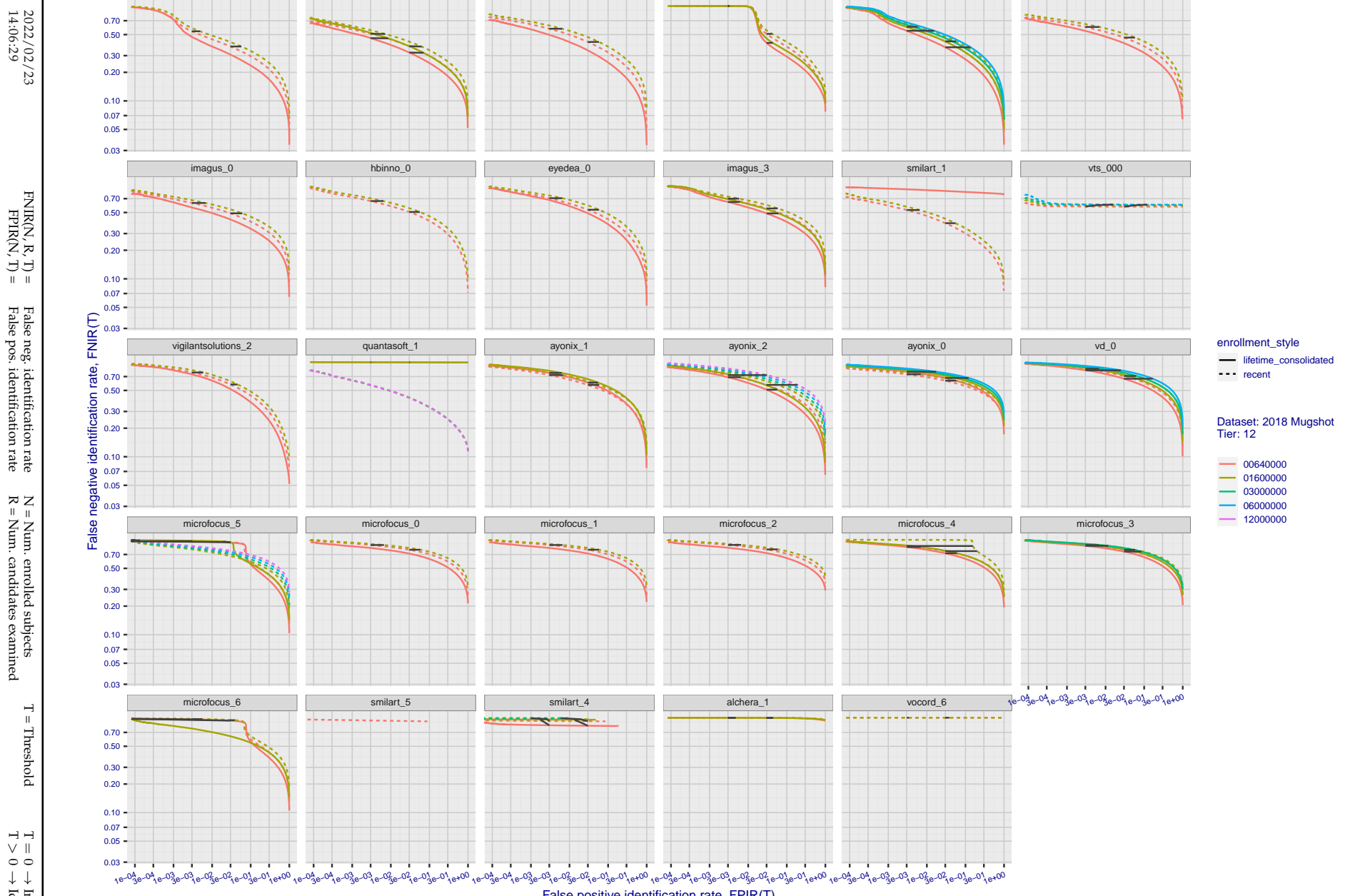


Figure 59: [FRVT-2018 Mugshot Dataset] Identification miss rates vs. false positive rates. The figure shows miss rates $\text{FNIR}(N, L, T)$ as a function of $\text{FPIR}(N, T)$, with N ranging from 640 000 to 12 000 000 as noted in rows 1-10 of Table 1. These error tradeoff characteristics are useful for applications where a threshold must be elevated to limit false positives, such as when human reviewer labor is not matched to the volume of searches. Dark lines join points of equal threshold: If horizontal, $\text{FPIR}(T)$ rises with N , and mate scores are independent of N . Other algorithms adjust scores in an attempt to make FPIR independent of N .

Appendix B Effect of time-lapse: Accuracy after face ageing

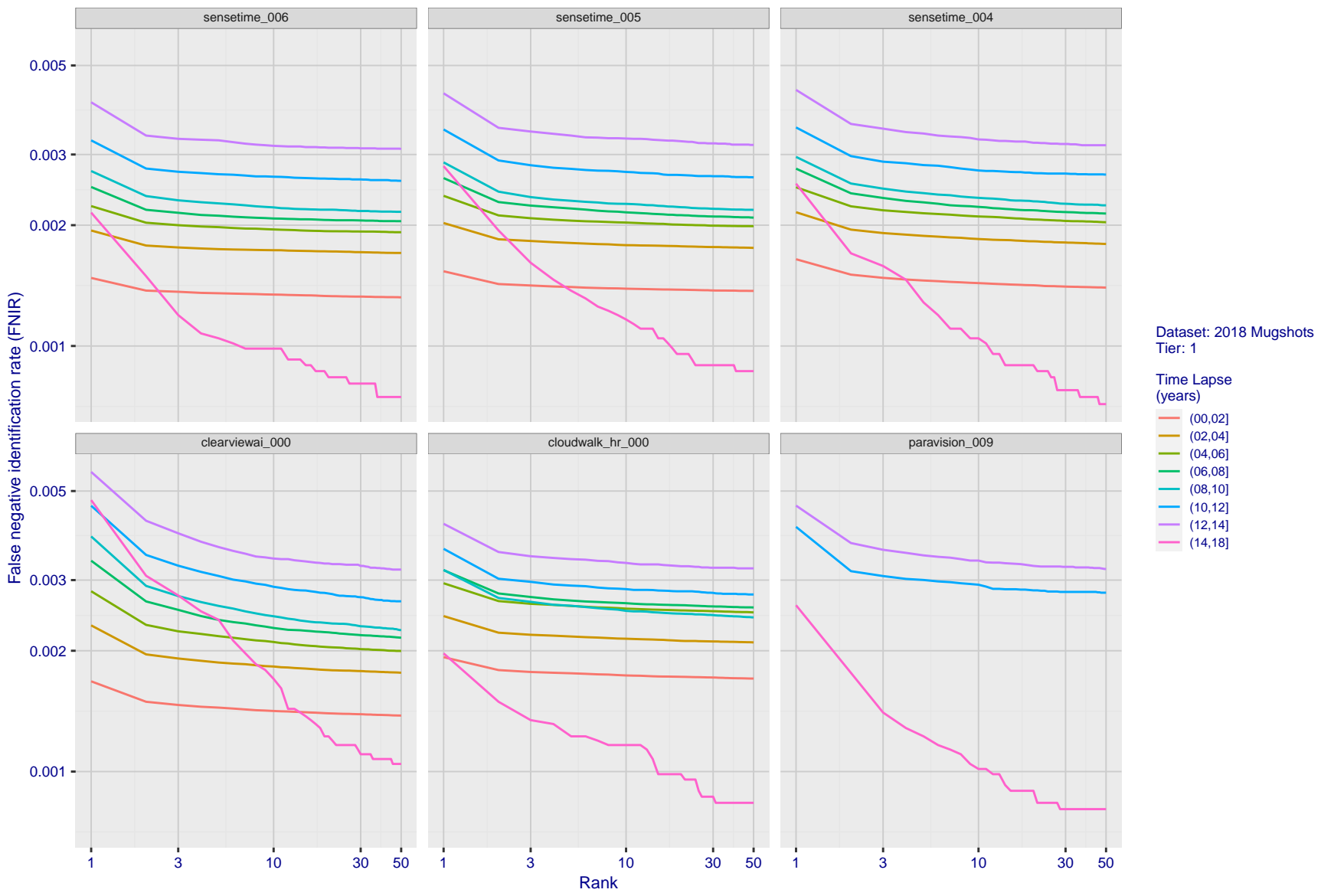


Figure 60: [FRVT-2018 Mugshot Ageing Dataset] Identification miss rates vs. rank by time-elapsed. The oldest image of each individual is enrolled. Thereafter, all more recent images are searched. Miss rates are computed over all searches noted in row 17 of Table 1 and binned by number of years between search and initial enrollment.

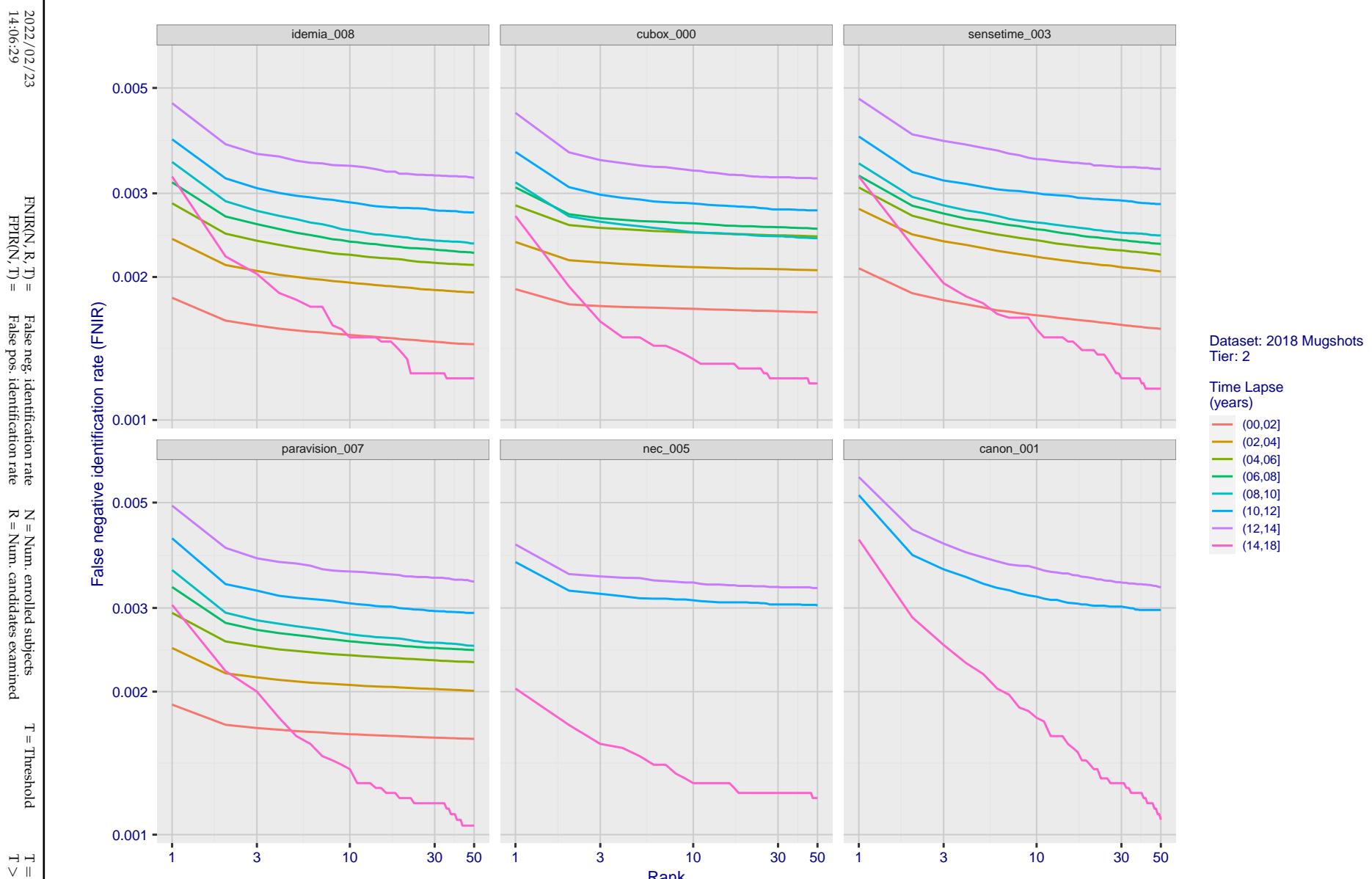


Figure 61: [FRVT-2018 Mugshot Ageing Dataset] Identification miss rates vs. rank by time elapsed. The oldest image of each individual is enrolled. Thereafter, all more recent images are searched. Miss rates are computed over all searches noted in row 17 of Table 1 and binned by number of years between search and initial enrollment.

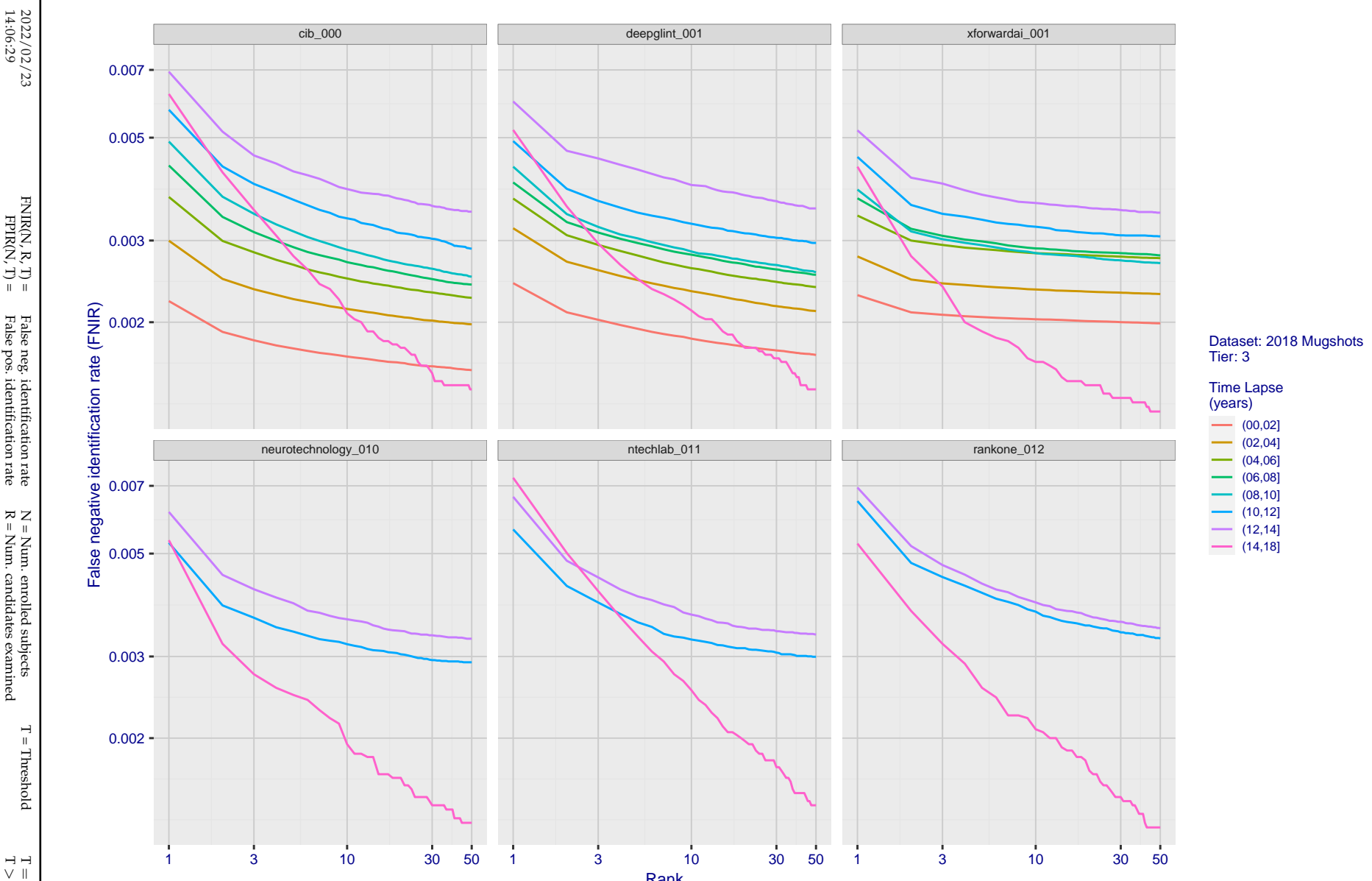


Figure 62: [FRVT-2018 Mugshot Ageing Dataset] Identification miss rates vs. rank by time-elapsed. The oldest image of each individual is enrolled. Thereafter, all more recent images are searched. Miss rates are computed over all searches noted in row 17 of Table 1 and binned by number of years between search and initial enrollment.

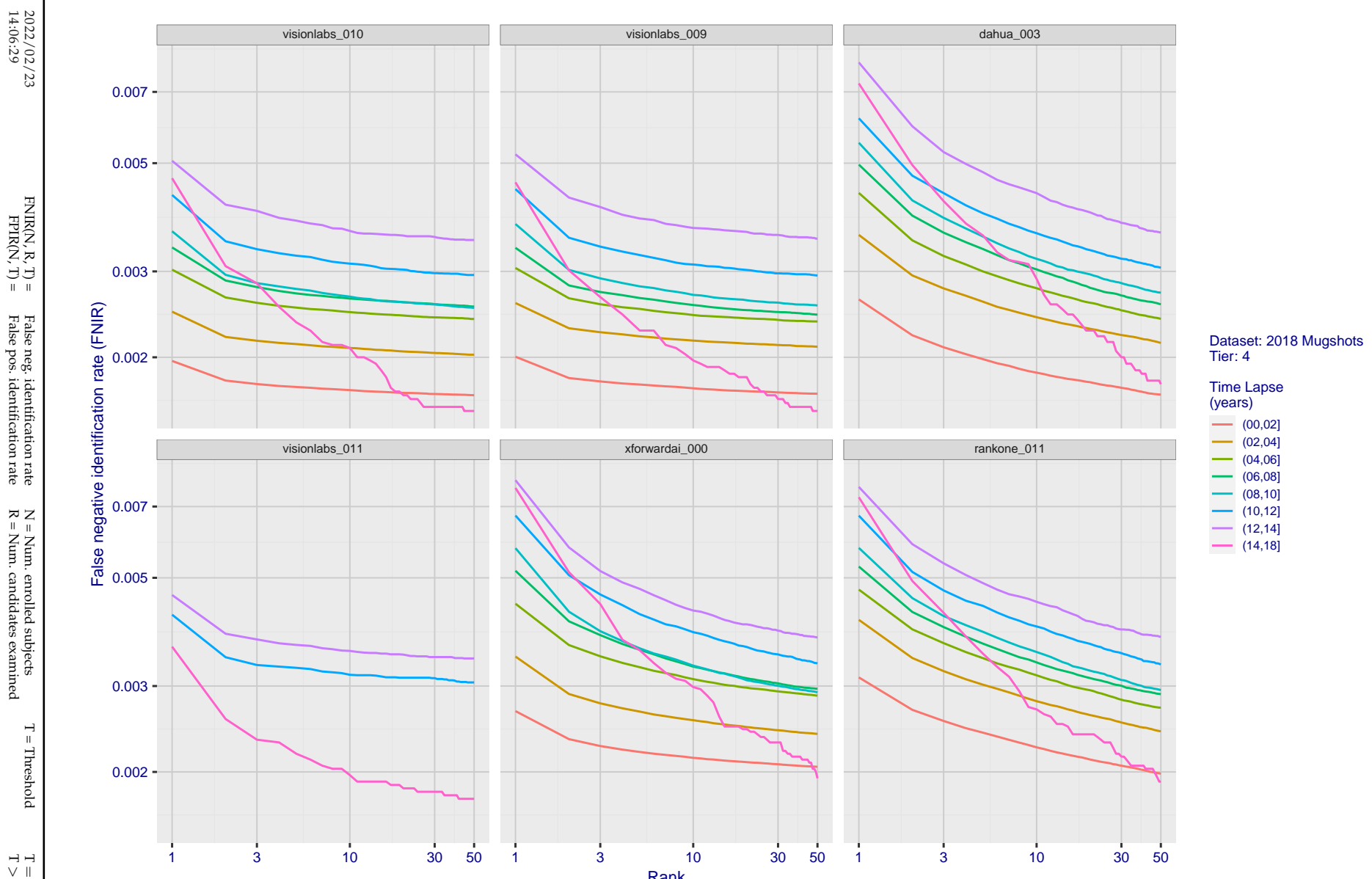


Figure 63: [FRVT-2018 Mugshot Ageing Dataset] Identification miss rates vs. rank by time-elapsed. The oldest image of each individual is enrolled. Thereafter, all more recent images are searched. Miss rates are computed over all searches noted in row 17 of Table 1 and binned by number of years between search and initial enrollment.

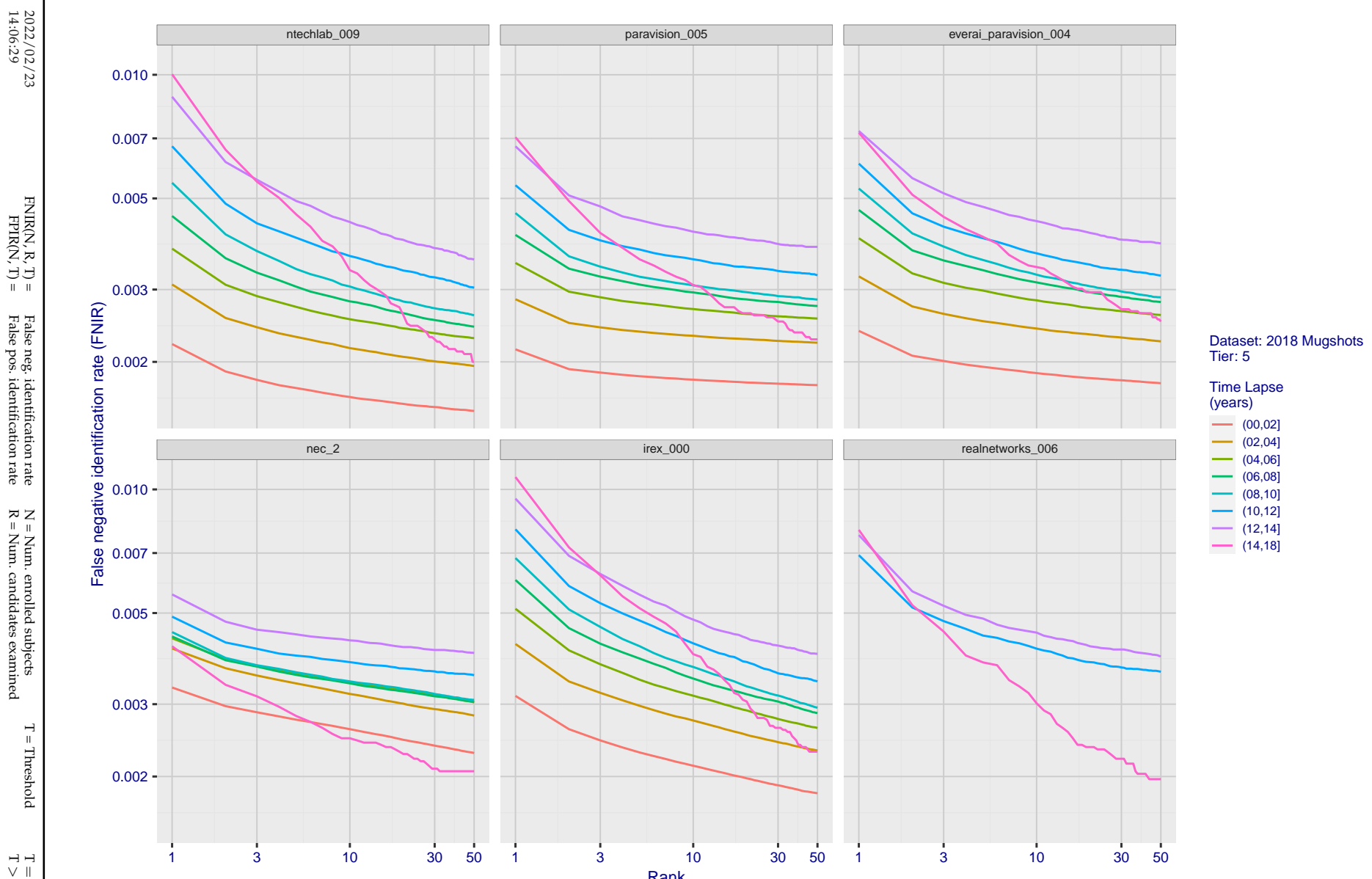


Figure 64: [FRVT-2018 Mugshot Ageing Dataset] Identification miss rates vs. rank by time-elapsed. The oldest image of each individual is enrolled. Thereafter, all more recent images are searched. Miss rates are computed over all searches noted in row 17 of Table 1 and binned by number of years between search and initial enrollment.

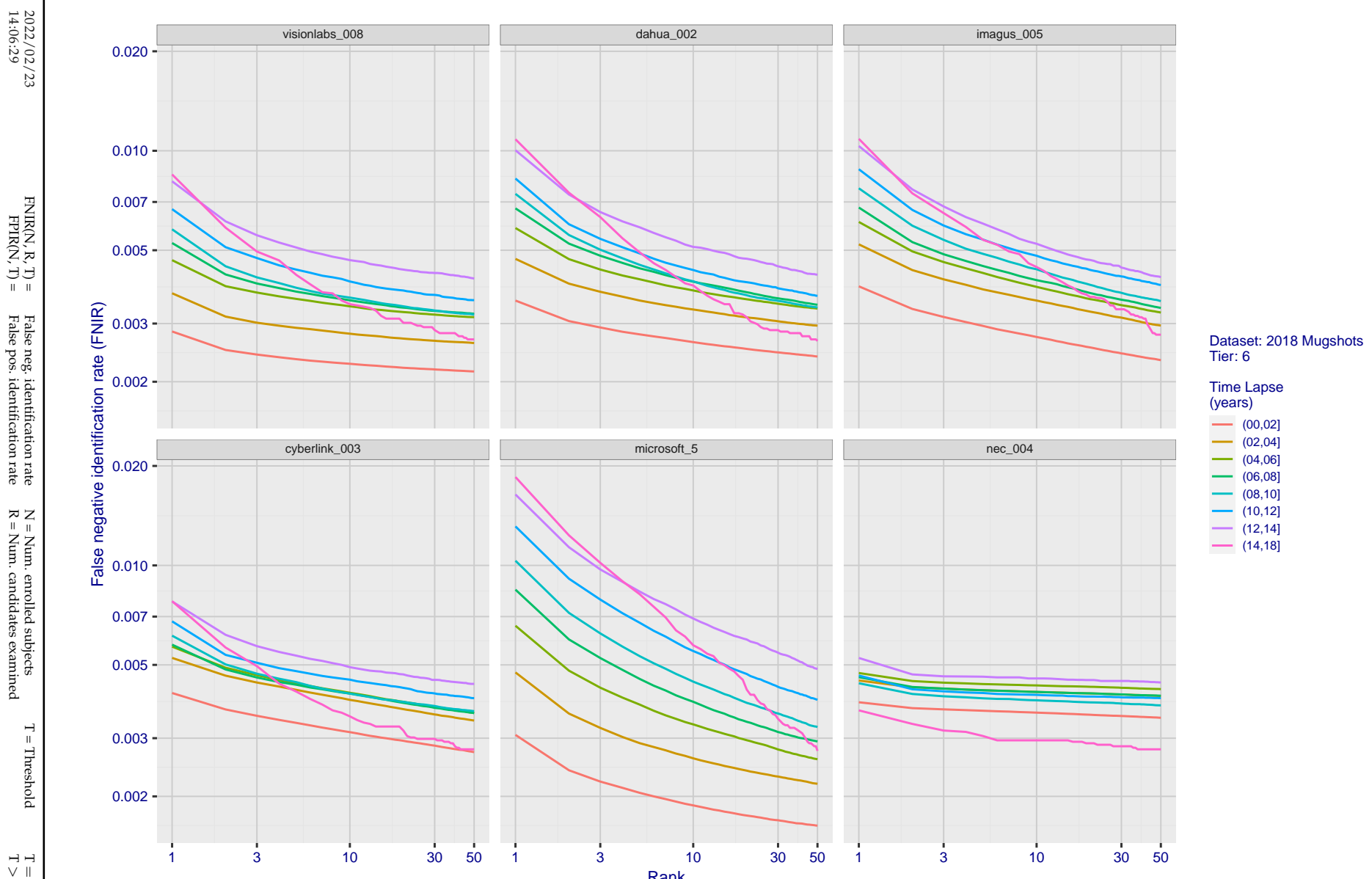


Figure 65: [FRVT-2018 Mugshot Ageing Dataset] Identification miss rates vs. rank by time-elapsed. The oldest image of each individual is enrolled. Thereafter, all more recent images are searched. Miss rates are computed over all searches noted in row 17 of Table 1 and binned by number of years between search and initial enrollment.

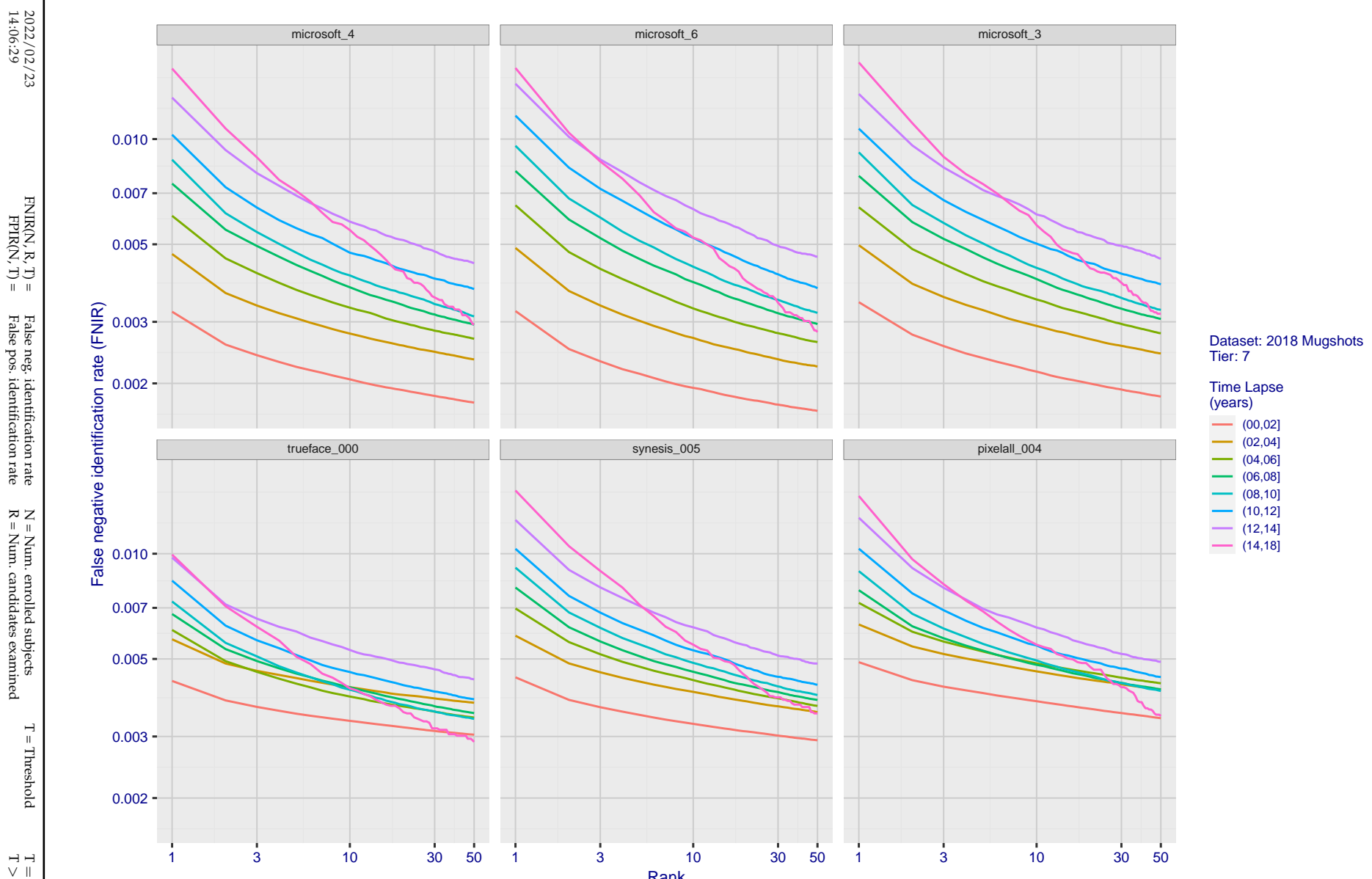


Figure 66: [FRVT-2018 Mugshot Ageing Dataset] Identification miss rates vs. rank by time-elapsed. The oldest image of each individual is enrolled. Thereafter, all more recent images are searched. Miss rates are computed over all searches noted in row 17 of Table 1 and binned by number of years between search and initial enrollment.

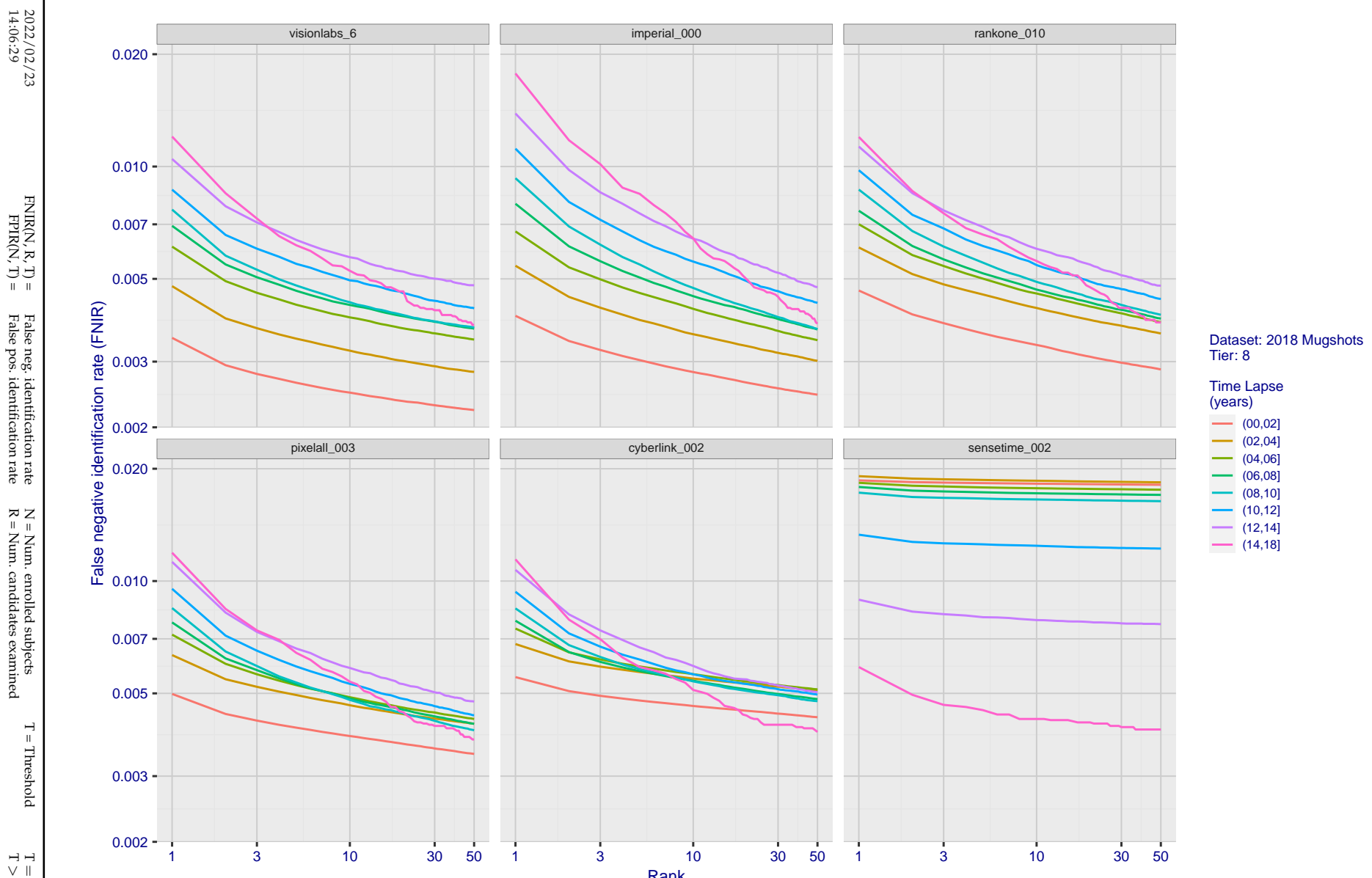


Figure 67: [FRVT-2018 Mugshot Ageing Dataset] Identification miss rates vs. rank by time-elapsed. The oldest image of each individual is enrolled. Thereafter, all more recent images are searched. Miss rates are computed over all searches noted in row 17 of Table 1 and binned by number of years between search and initial enrollment.

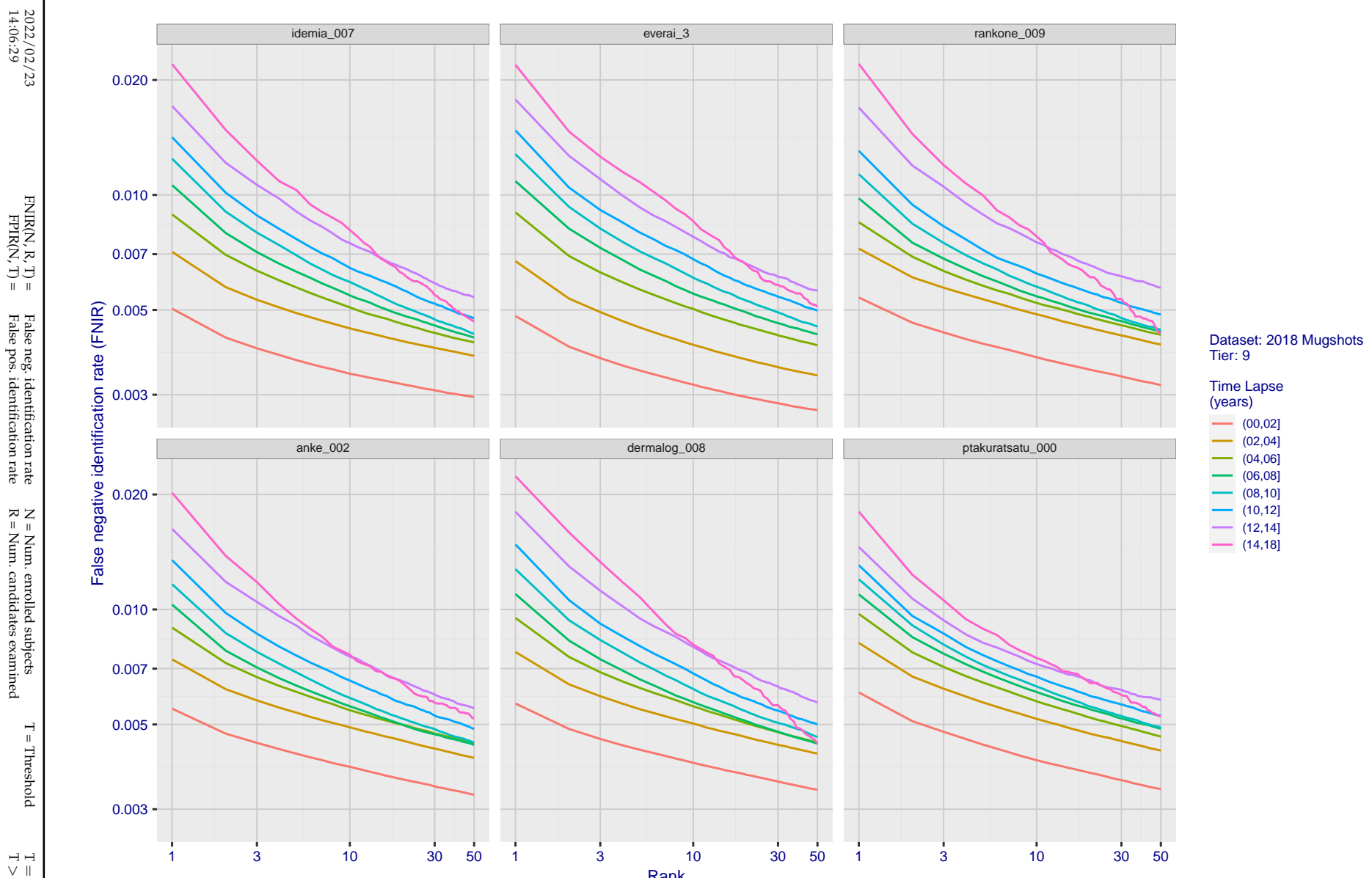


Figure 68: [FRVT-2018 Mugshot Ageing Dataset] Identification miss rates vs. rank by time-elapsed. The oldest image of each individual is enrolled. Thereafter, all more recent images are searched. Miss rates are computed over all searches noted in row 17 of Table 1 and binned by number of years between search and initial enrollment.

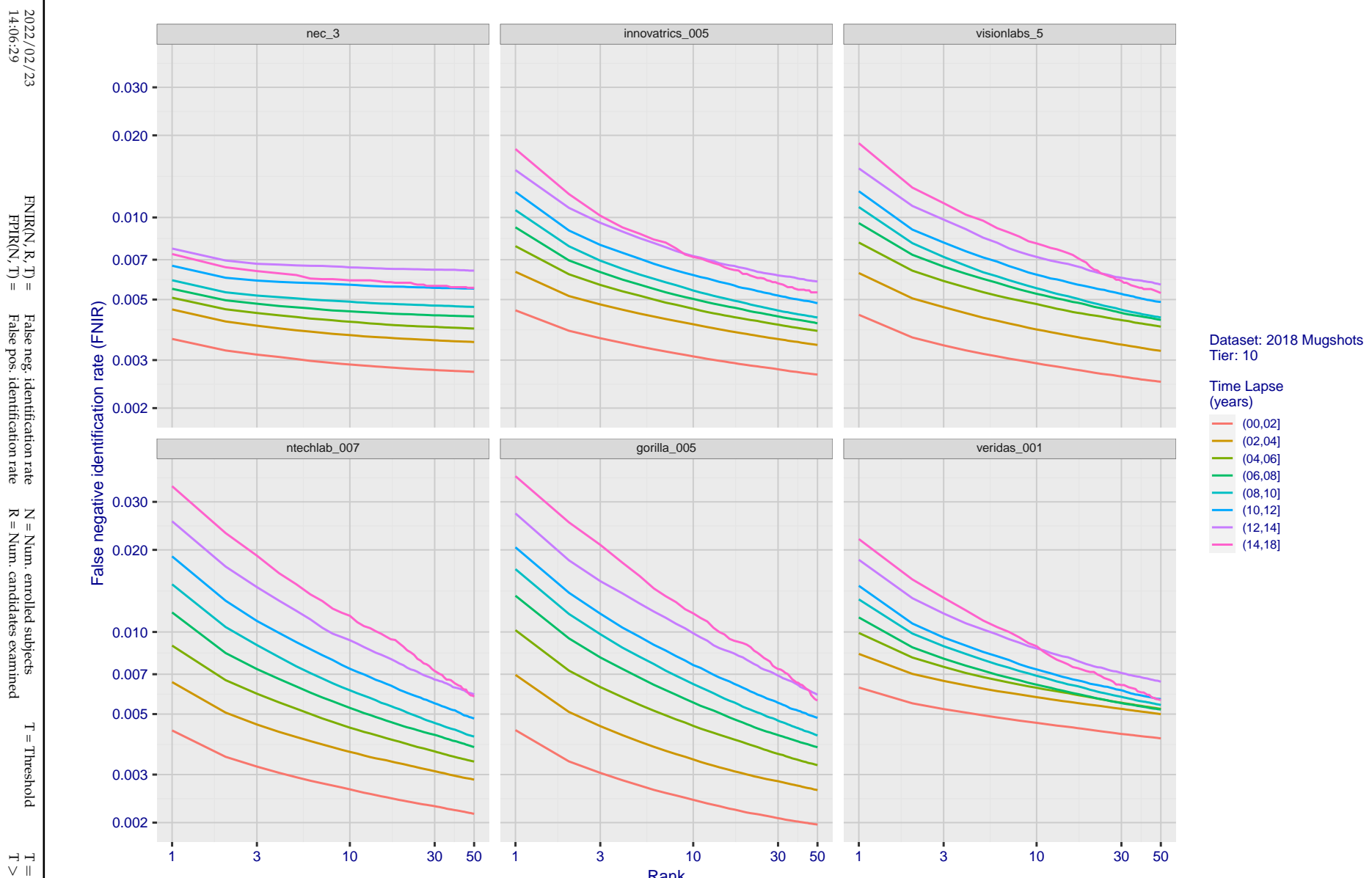


Figure 69: [FRVT-2018 Mugshot Ageing Dataset] Identification miss rates vs. rank by time-elapsed. The oldest image of each individual is enrolled. Thereafter, all more recent images are searched. Miss rates are computed over all searches noted in row 17 of Table 1 and binned by number of years between search and initial enrollment.

2022/02/23
14:06:29

 $FNIR(N, R, T)$ = False neg. identification rate
 $FPIR(N, T)$ = False pos. identification rate
 N = Num. enrolled subjects
 R = Num. candidates examined
 T = Threshold
 $T = 0 \rightarrow$ Investigation
 $T > 0 \rightarrow$ Identification

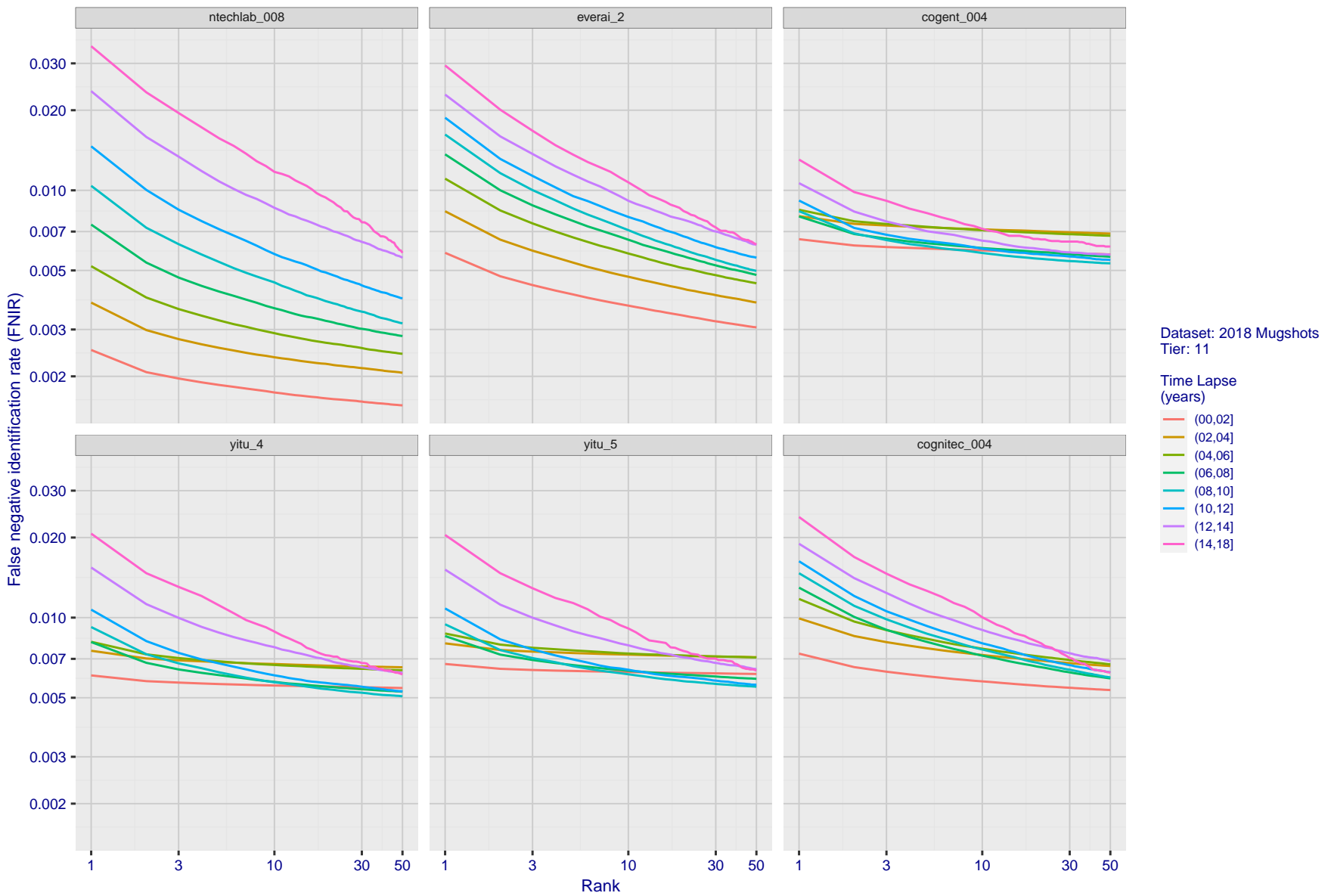


Figure 70: [FRVT-2018 Mugshot Ageing Dataset] Identification miss rates vs. rank by time-elapsed. The oldest image of each individual is enrolled. Thereafter, all more recent images are searched. Miss rates are computed over all searches noted in row 17 of Table 1 and binned by number of years between search and initial enrollment.

Dataset: 2018 Mugshots
Tier: 11

Time Lapse (years)
 (00,02]
 (02,04]
 (04,06]
 (06,08]
 (08,10]
 (10,12]
 (12,14]
 (14,18]

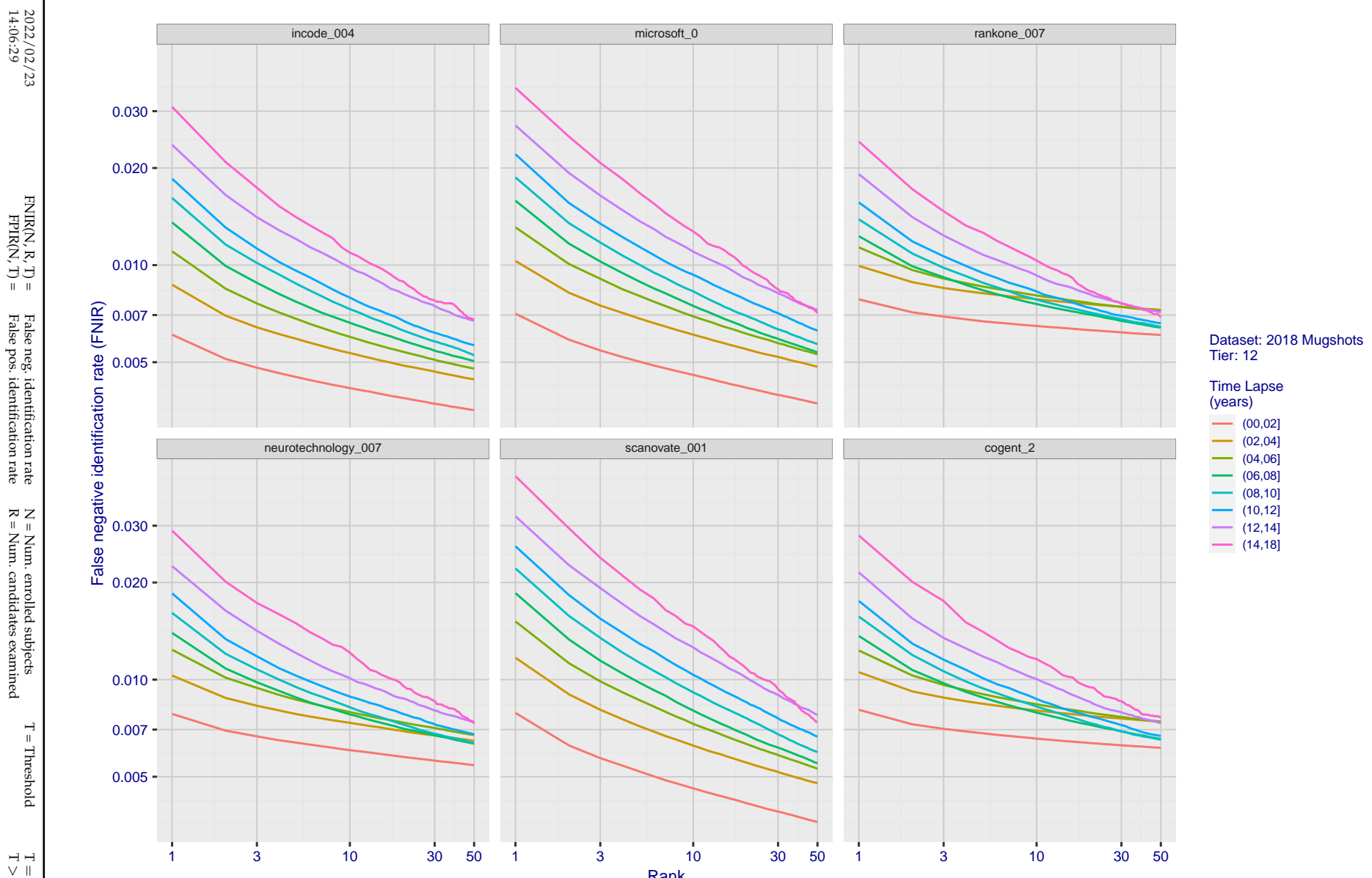


Figure 71: [FRVT-2018 Mugshot Ageing Dataset] Identification miss rates vs. rank by time-elapsed. The oldest image of each individual is enrolled. Thereafter, all more recent images are searched. Miss rates are computed over all searches noted in row 17 of Table 1 and binned by number of years between search and initial enrollment.

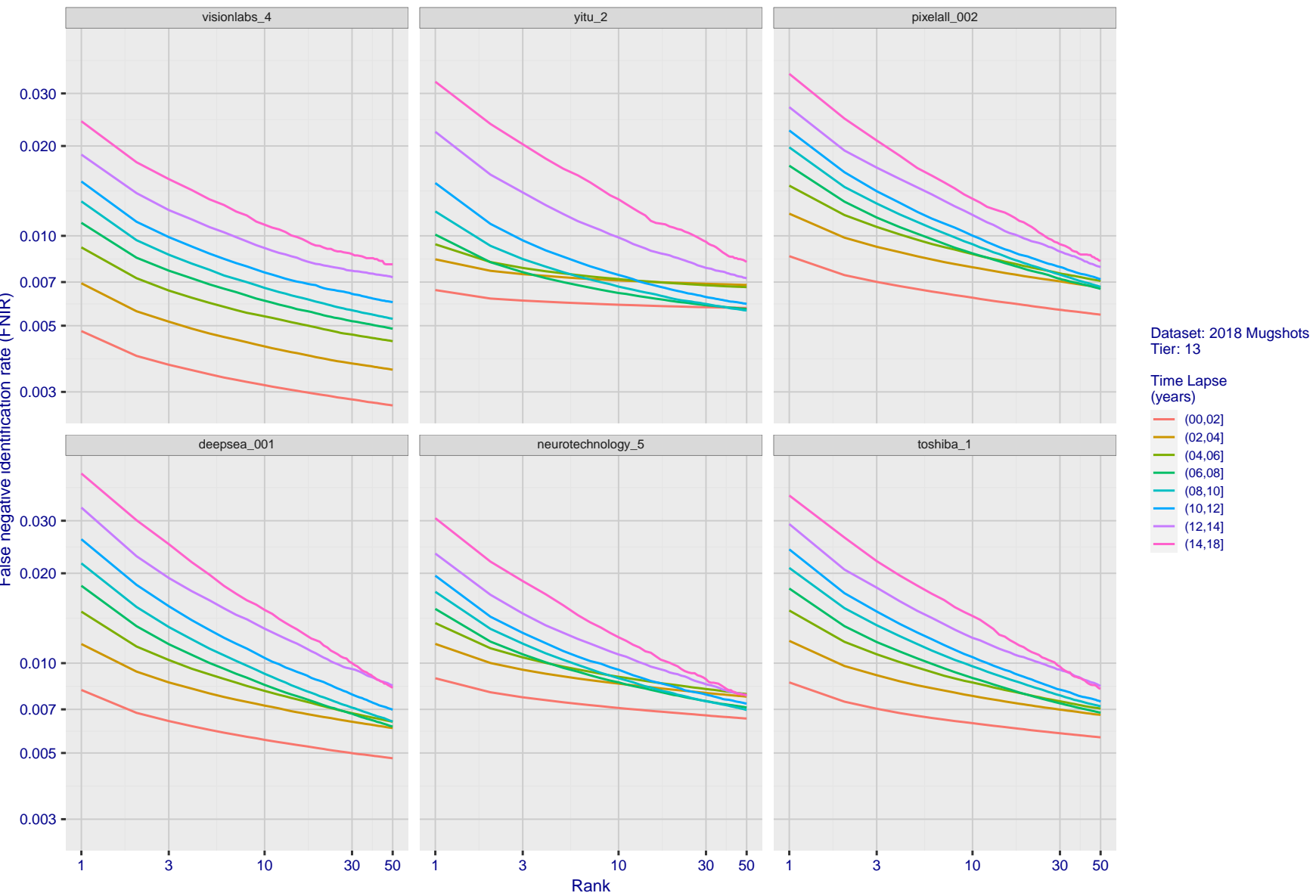
2022/02/23
14:06:29

Figure 72: [FRVT-2018 Mugshot Ageing Dataset] Identification miss rates vs. rank by time-elapsed. The oldest image of each individual is enrolled. Thereafter, all more recent images are searched. Miss rates are computed over all searches noted in row 17 of Table 1 and binned by number of years between search and initial enrollment.

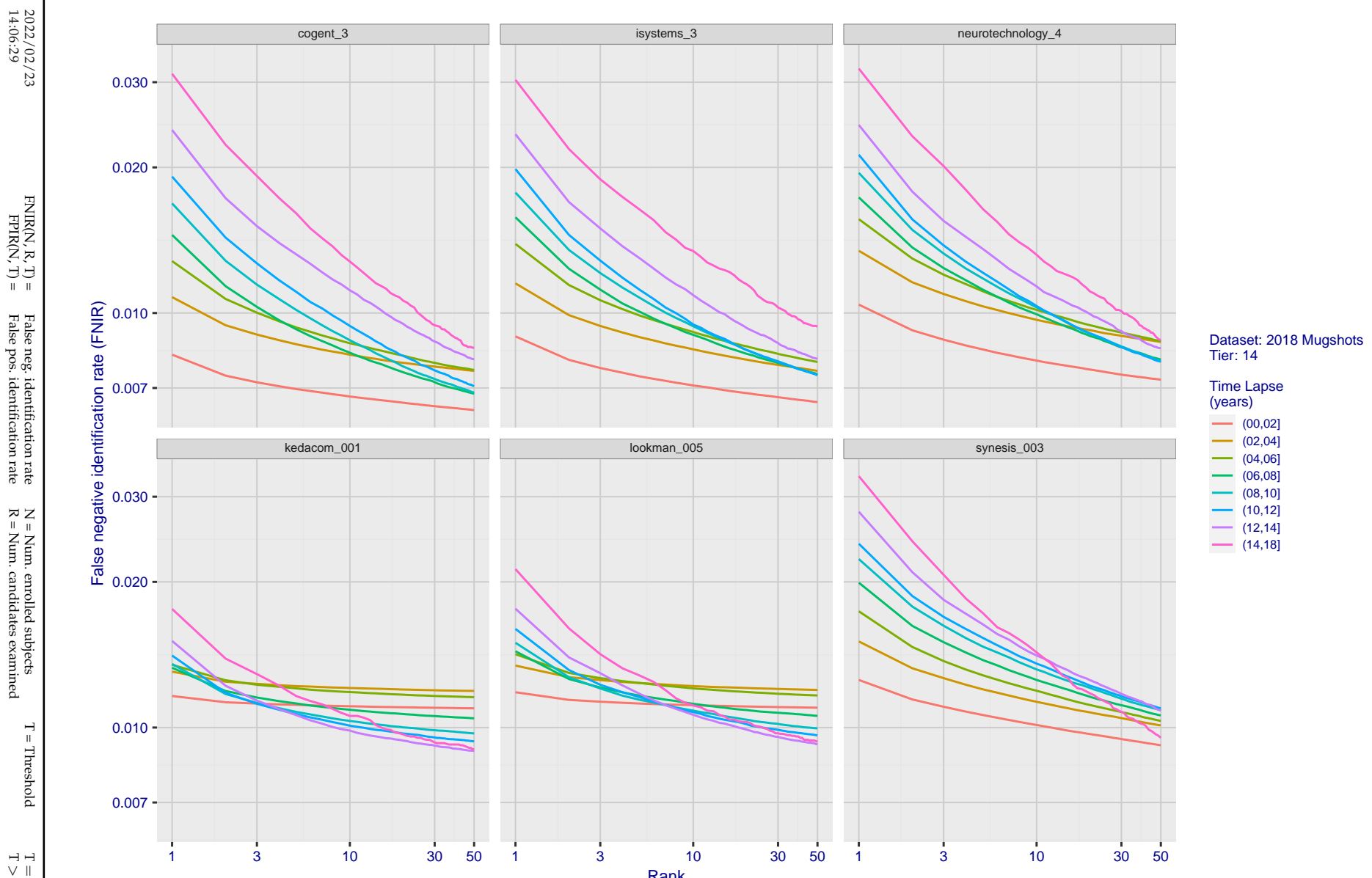


Figure 73: [FRVT-2018 Mugshot Ageing Dataset] Identification miss rates vs. rank by time-elapsed. The oldest image of each individual is enrolled. Thereafter, all more recent images are searched. Miss rates are computed over all searches noted in row 17 of Table 1 and binned by number of years between search and initial enrollment.

2022/02/23
14:06:29

$FNIR(N, k, l) =$ False neg. identification rate
 $FPIRN(T) =$ False pos. identification rate
 $N =$ Num. enrolled subjects
 $R =$ Num. candidates examined

T = Threshold

$T = 0 \rightarrow$ Investigation
 $T > 0 \rightarrow$ Identification

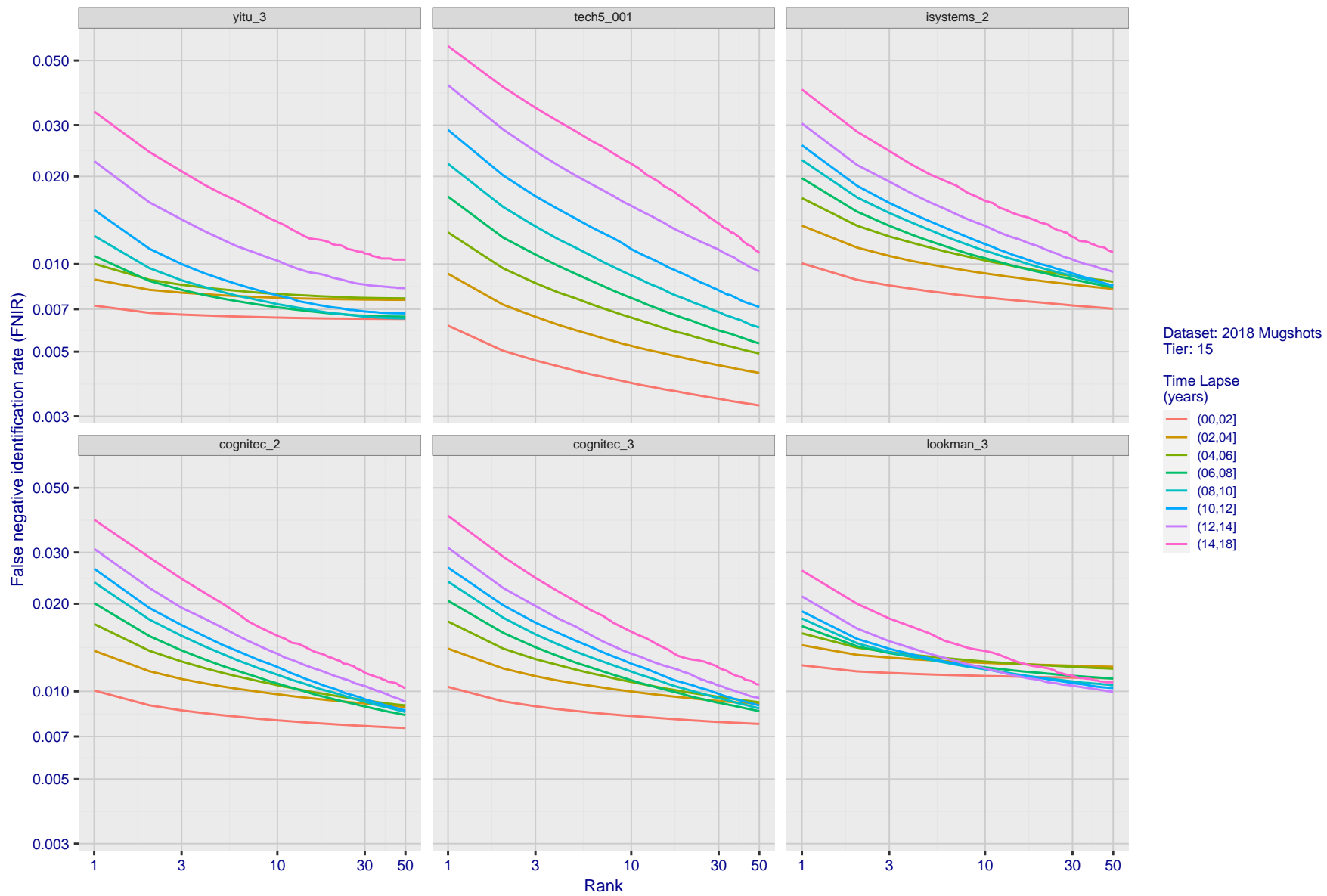


Figure 74: [FRVT-2018 Mugshot Ageing Dataset] Identification miss rates vs. rank by time-elapsed. The oldest image of each individual is enrolled. Thereafter, all more recent images are searched. Miss rates are computed over all searches noted in row 17 of Table 1 and binned by number of years between search and initial enrollment.

2022/02/23
14:06:29

 $\text{FNIR}(N, R, T) =$
False neg. identification rate
 $\text{FPIR}(N, T) =$
False pos. identification rate
 $N =$ Num. enrolled subjects
 $R =$ Num. candidates examined
 $T =$ Threshold
 $T = 0 \rightarrow$ Investigation
 $T > 0 \rightarrow$ Identification

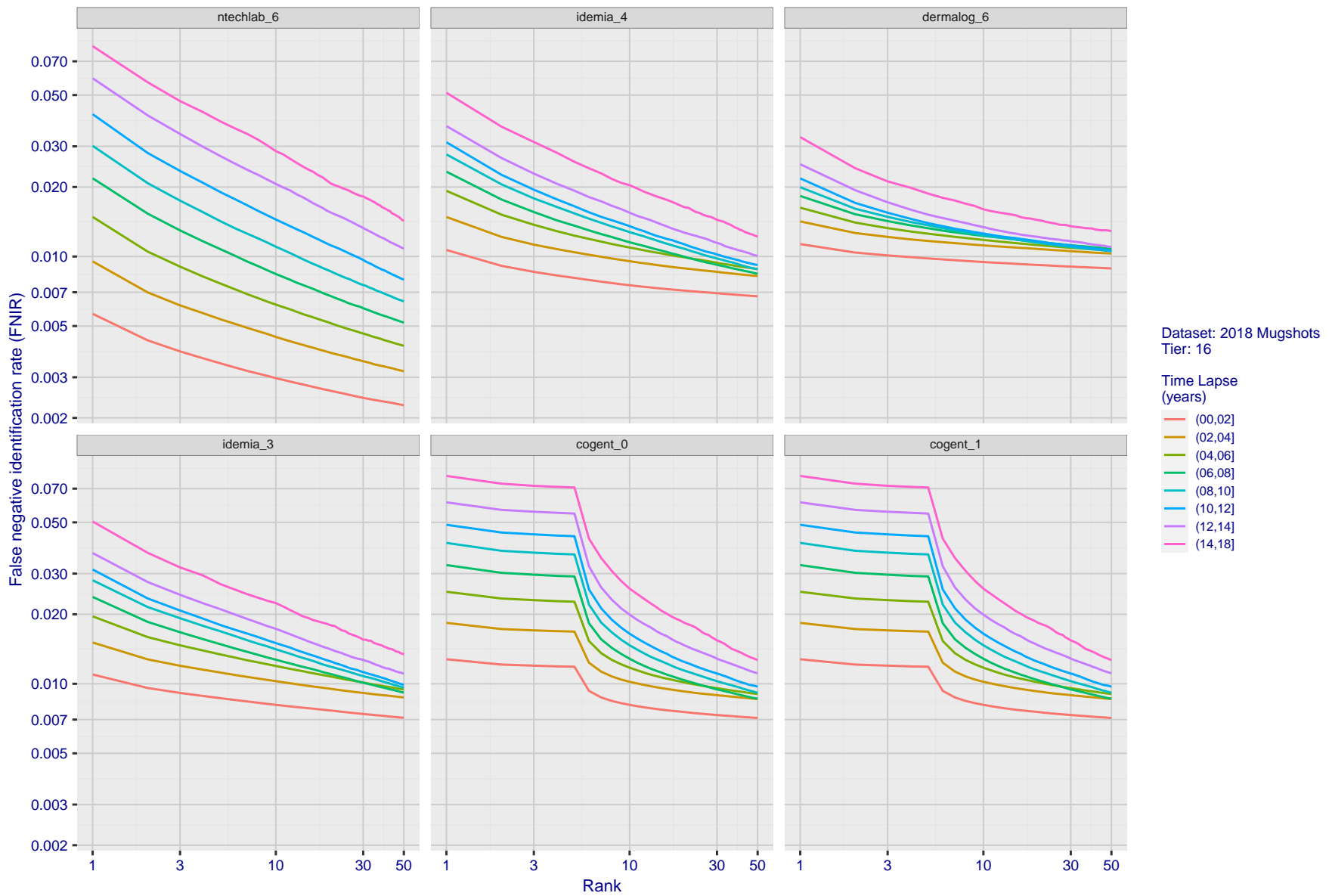


Figure 75: [FRVT-2018 Mugshot Ageing Dataset] Identification miss rates vs. rank by time elapsed. The oldest image of each individual is enrolled. Thereafter, all more recent images are searched. Miss rates are computed over all searches noted in row 17 of Table 1 and binned by number of years between search and initial enrollment.

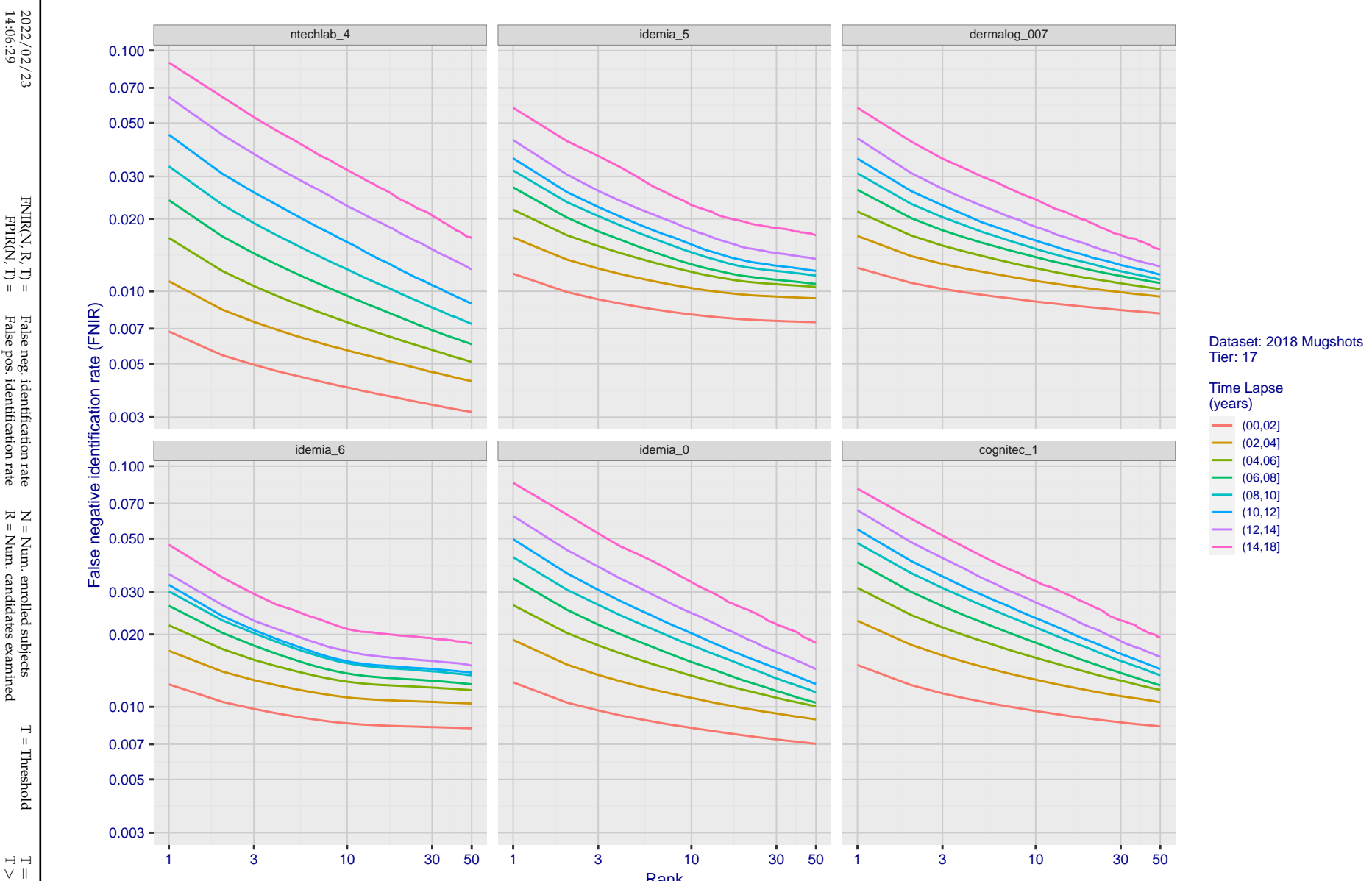


Figure 76: [FRVT-2018 Mugshot Ageing Dataset] Identification miss rates vs. rank by time elapsed. The oldest image of each individual is enrolled. Thereafter, all more recent images are searched. Miss rates are computed over all searches noted in row 17 of Table 1 and binned by number of years between search and initial enrollment.

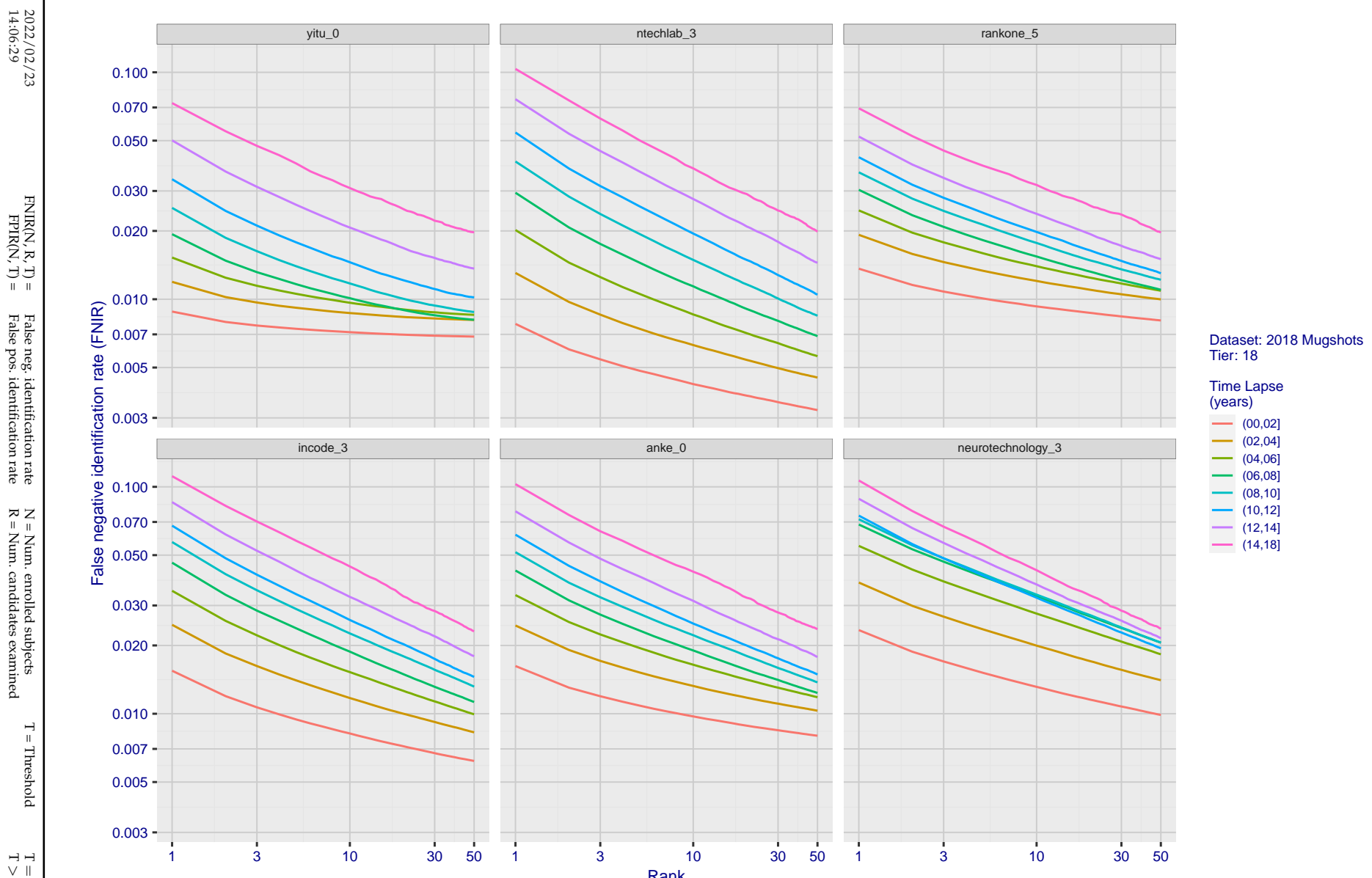


Figure 77: [FRVT-2018 Mugshot Ageing Dataset] Identification miss rates vs. rank by time-elapsed. The oldest image of each individual is enrolled. Thereafter, all more recent images are searched. Miss rates are computed over all searches noted in row 17 of Table 1 and binned by number of years between search and initial enrollment.

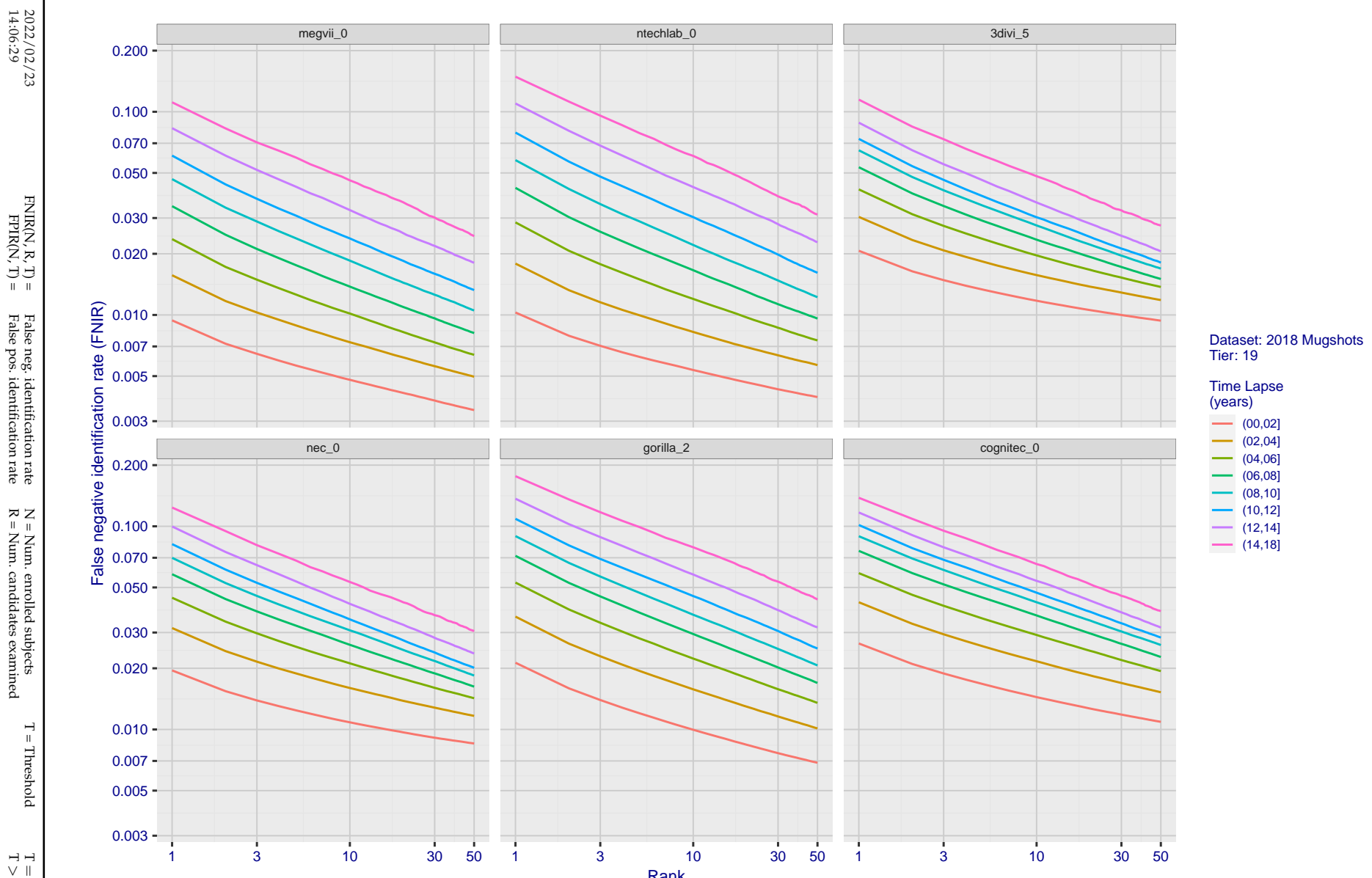


Figure 78: [FRVT-2018 Mugshot Ageing Dataset] Identification miss rates vs. rank by time-elapsed. The oldest image of each individual is enrolled. Thereafter, all more recent images are searched. Miss rates are computed over all searches noted in row 17 of Table 1 and binned by number of years between search and initial enrollment.

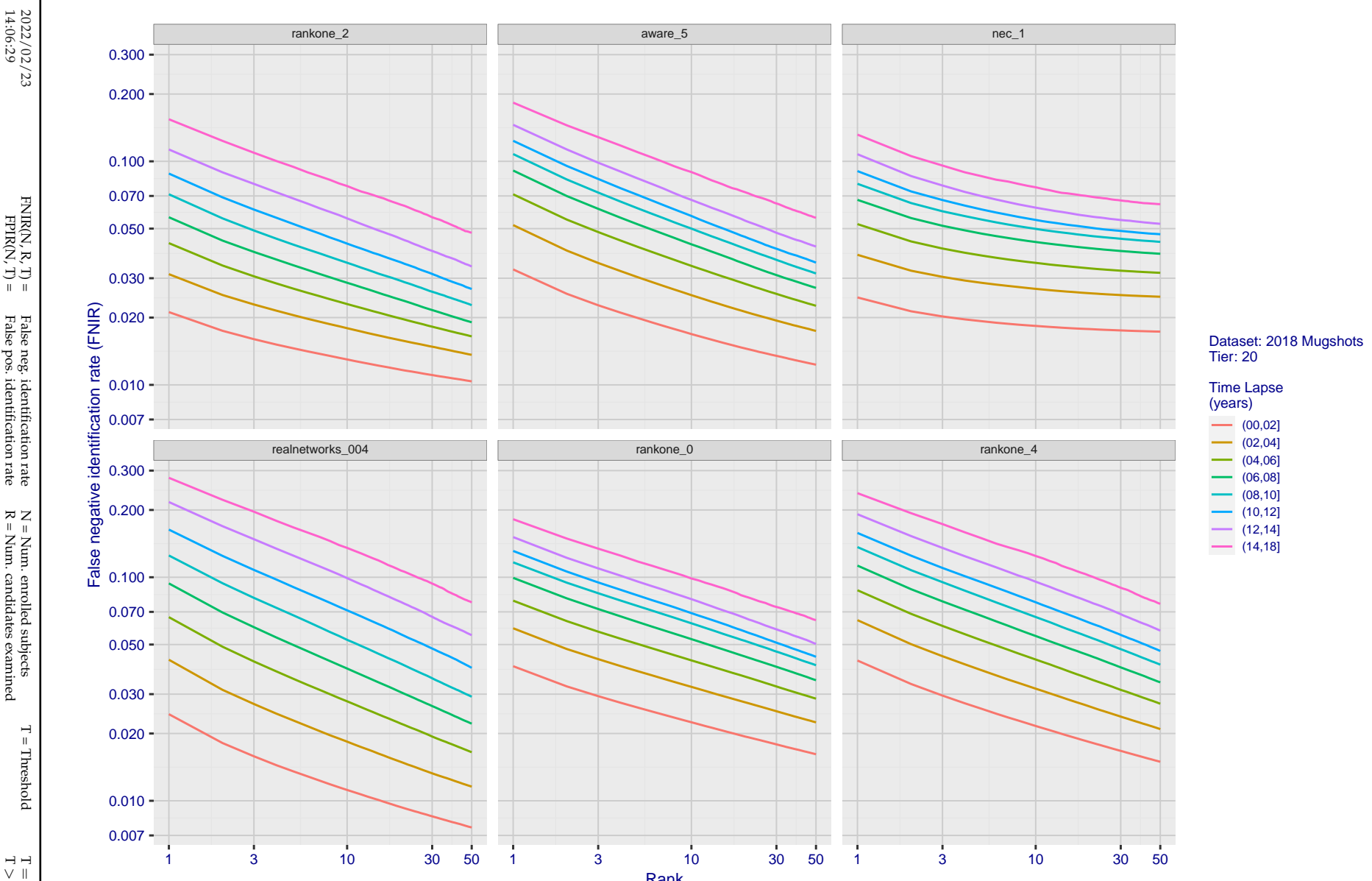


Figure 79: [FRVT-2018 Mugshot Ageing Dataset] Identification miss rates vs. rank by time-elapsed. The oldest image of each individual is enrolled. Thereafter, all more recent images are searched. Miss rates are computed over all searches noted in row 17 of Table 1 and binned by number of years between search and initial enrollment.

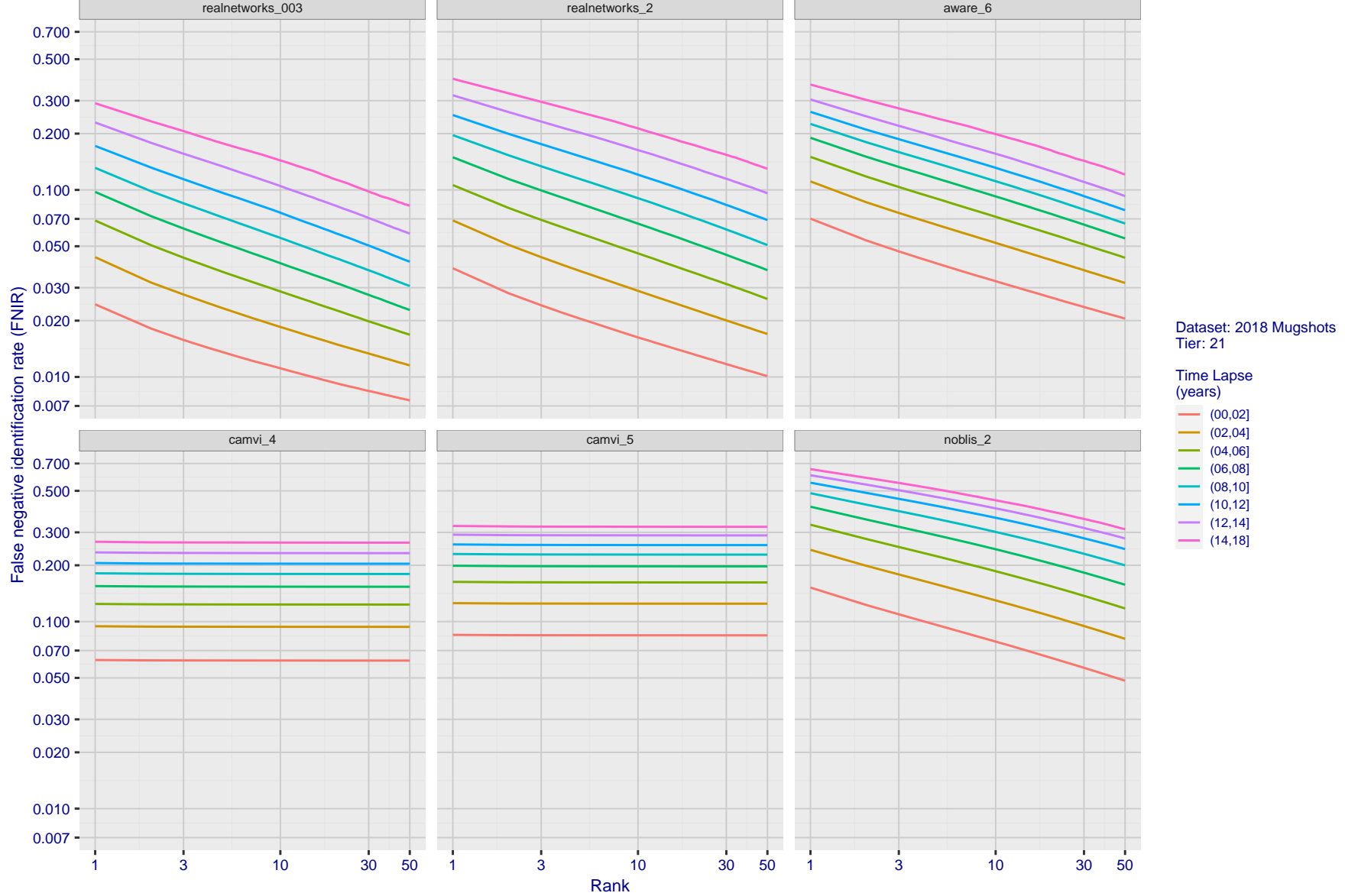


Figure 80: [FRVT-2018 Mugshot Ageing Dataset] Identification miss rates vs. rank by time-elapsed. The oldest image of each individual is enrolled. Thereafter, all more recent images are searched. Miss rates are computed over all searches noted in row 17 of Table 1 and binned by number of years between search and initial enrollment.

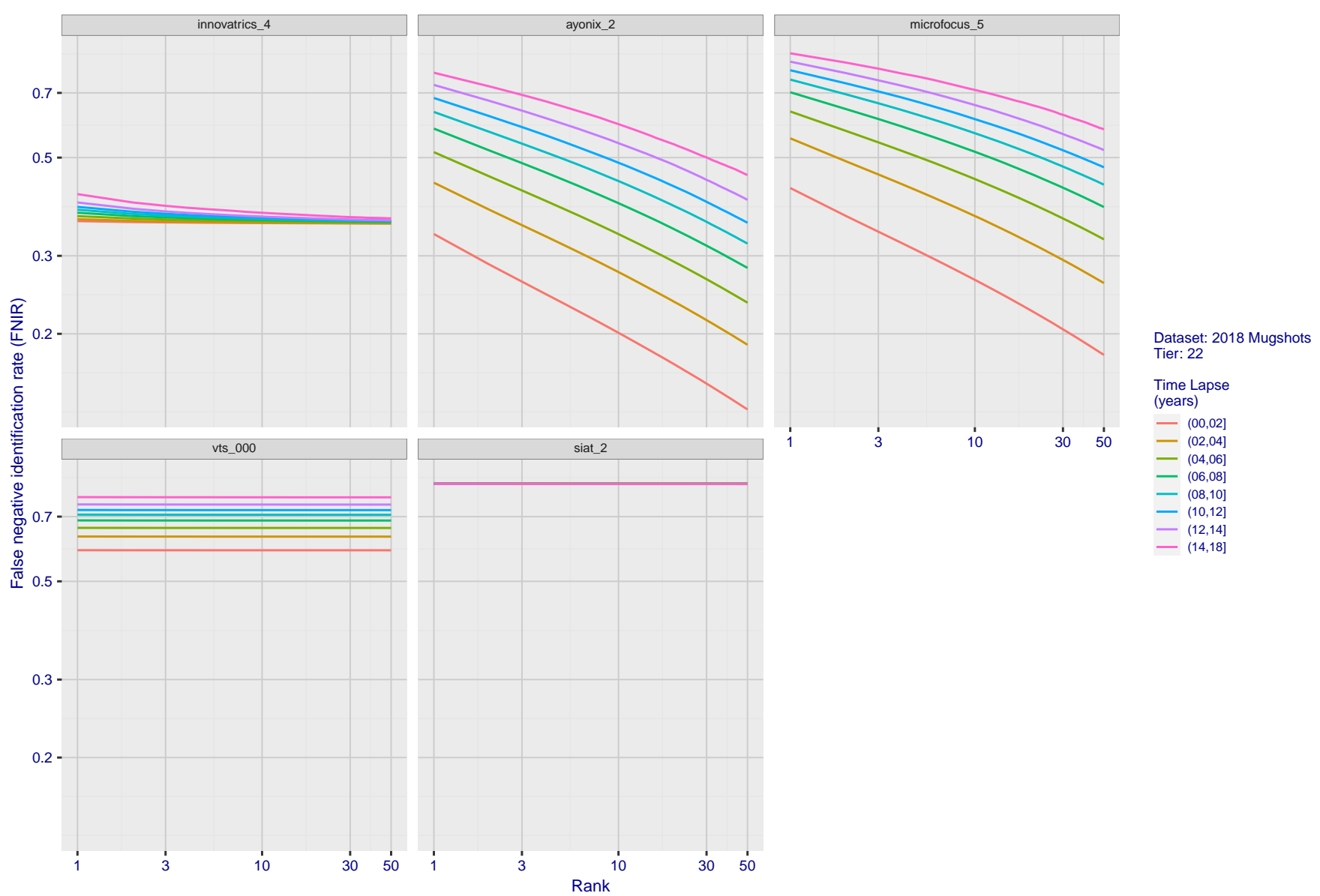


Figure 81: [FRVT-2018 Mugshot Ageing Dataset] Identification miss rates vs. rank by time elapsed. The oldest image of each individual is enrolled. Thereafter, all more recent images are searched. Miss rates are computed over all searches noted in row 17 of Table 1 and binned by number of years between search and initial enrollment.

2022/02/23	$\text{FNIR}(\text{N}, \text{R}, \text{T}) =$ $\text{FPIR}(\text{N}, \text{T}) =$	False neg. identification rate False pos. identification rate	$\text{N} = \text{Num. enrolled subjects}$ $\text{R} = \text{Num. candidates examined}$	$\text{T} = \text{Threshold}$	$\text{T} = 0 \rightarrow \text{Investigation}$ $\text{T} > 0 \rightarrow \text{Identification}$
14:06:29					

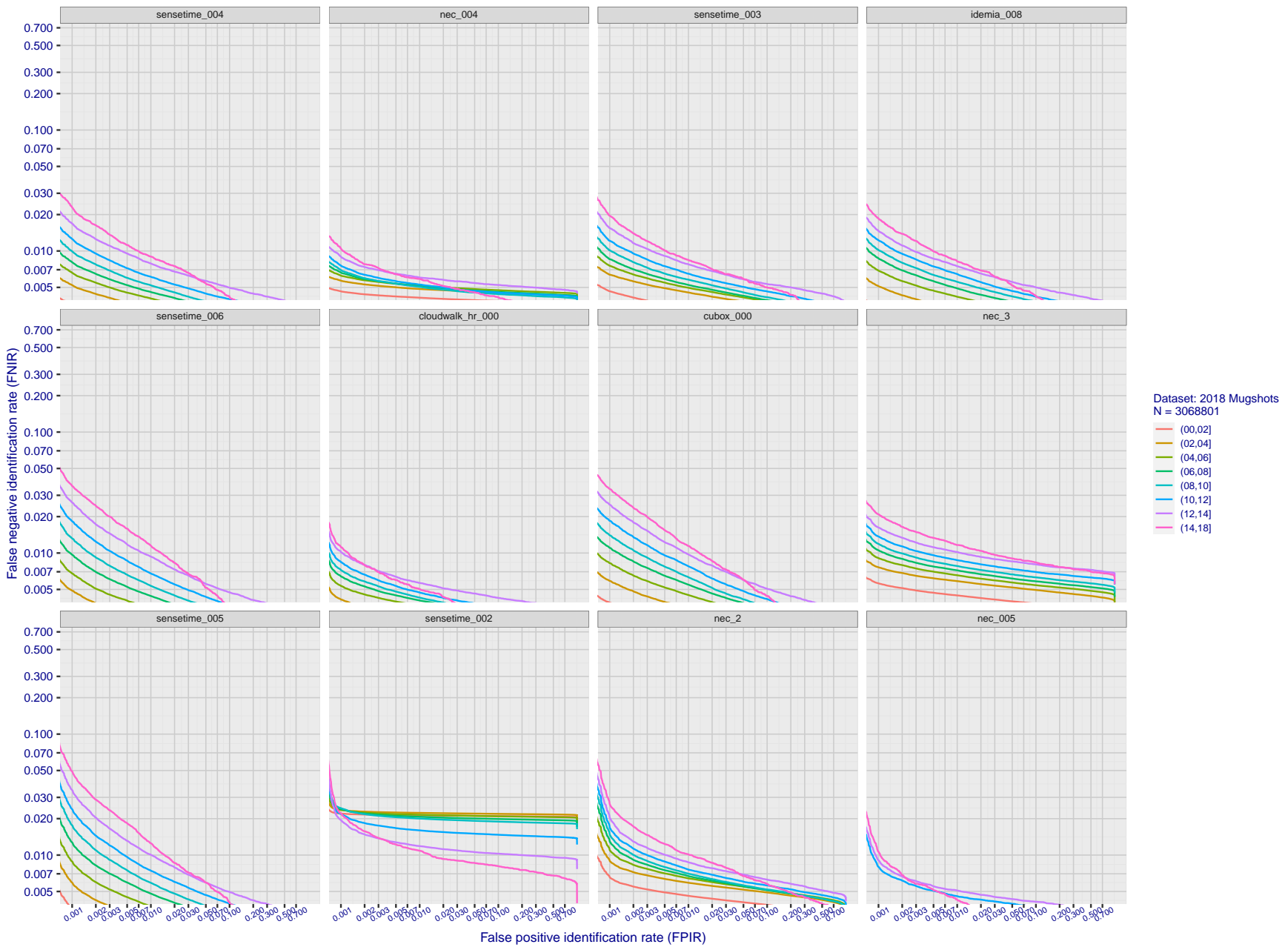


Figure 82: [FRVT-2018 Mugshot Ageing Dataset] Identification miss rates vs. FPIR by time-elapsed. The oldest image of each individual is enrolled. Thereafter, all more recent images are searched. Miss rates are computed over all searches noted in row 17 of Table 1 and binned by number of years between search and initial enrollment. FPIR is computed from the same FRVT 2018 non-mates noted in row 3 of Table 1 with $N = 3000\,000$.

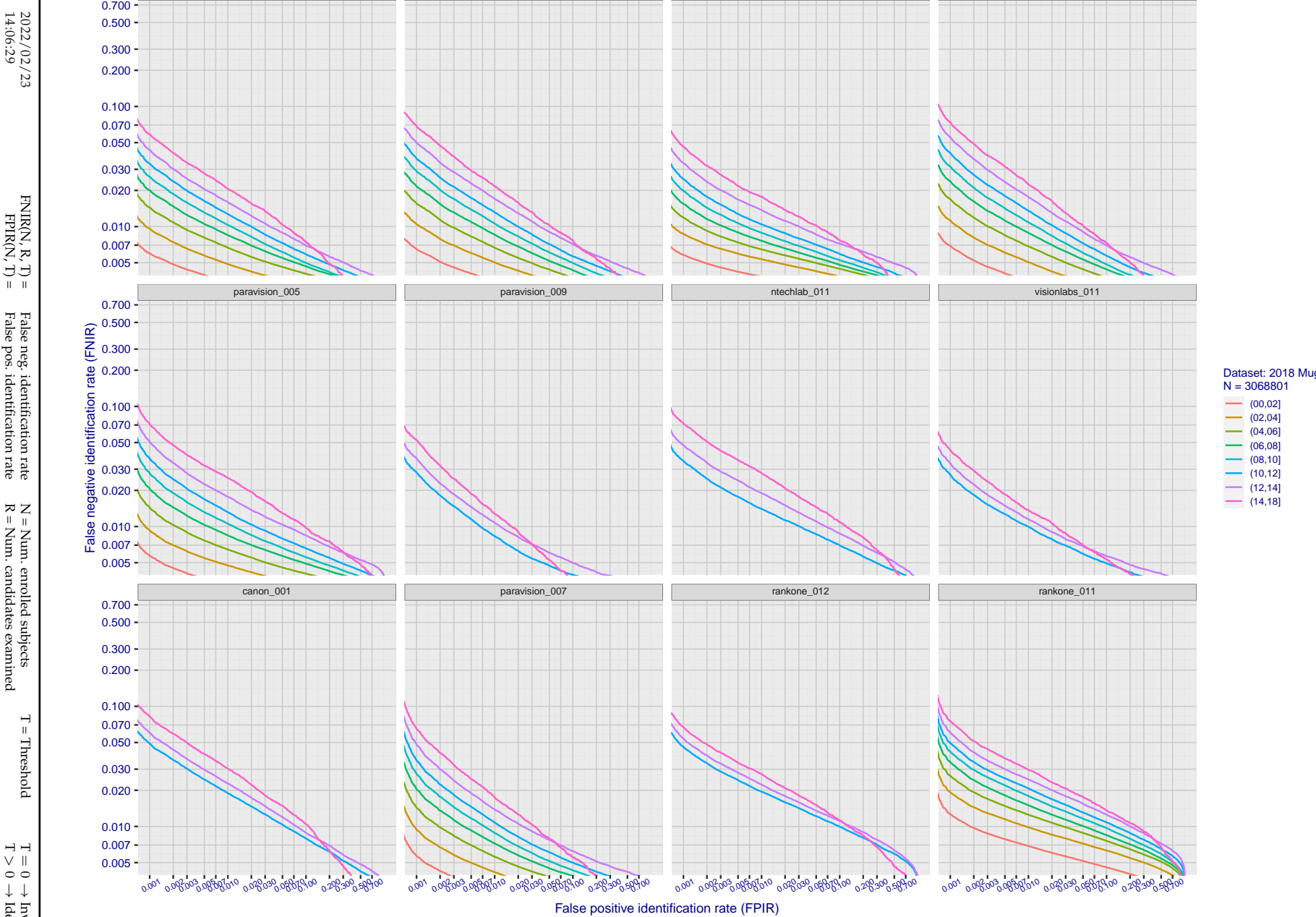


Figure 83: [FRVT-2018 Mugshot Ageing Dataset] Identification miss rates vs. FPIR by time-elapsed. The oldest image of each individual is enrolled. Thereafter, all more recent images are searched. Miss rates are computed over all searches noted in row 17 of Table 1 and binned by number of years between search and initial enrollment. FPIR is computed from the same FRVT 2018 non-mates noted in row 3 of Table 1 with $N = 3\,000\,000$.

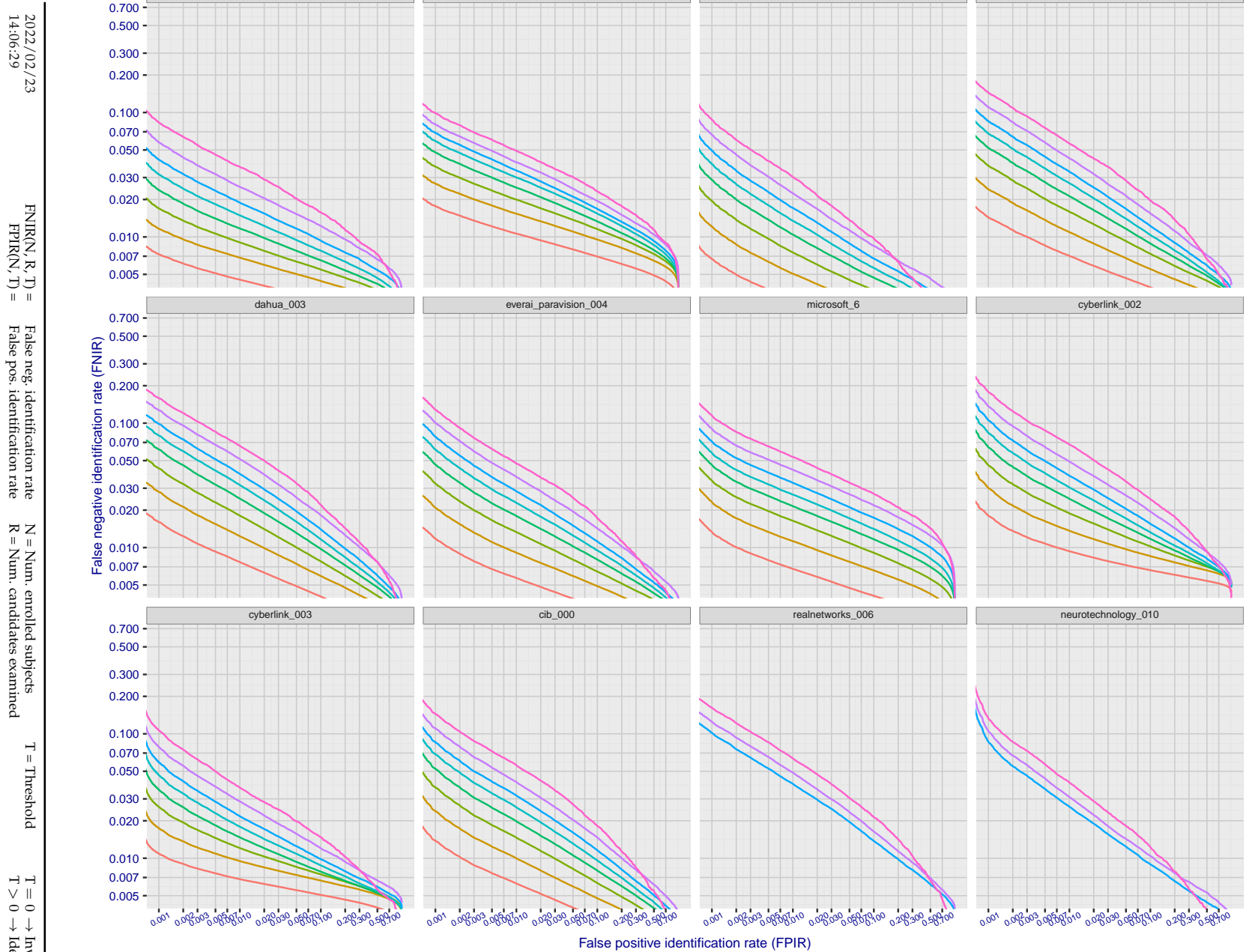


Figure 84: [FRVT-2018 Mugshot Ageing Dataset] Identification miss rates vs. FPIR by time-elapsed. The oldest image of each individual is enrolled. Thereafter, all more recent images are searched. Miss rates are computed over all searches noted in row 17 of Table 1 and binned by number of years between search and initial enrollment. FPIR is computed from the same FRVT 2018 non-mates noted in row 3 of Table 1 with $N = 3\,000\,000$.

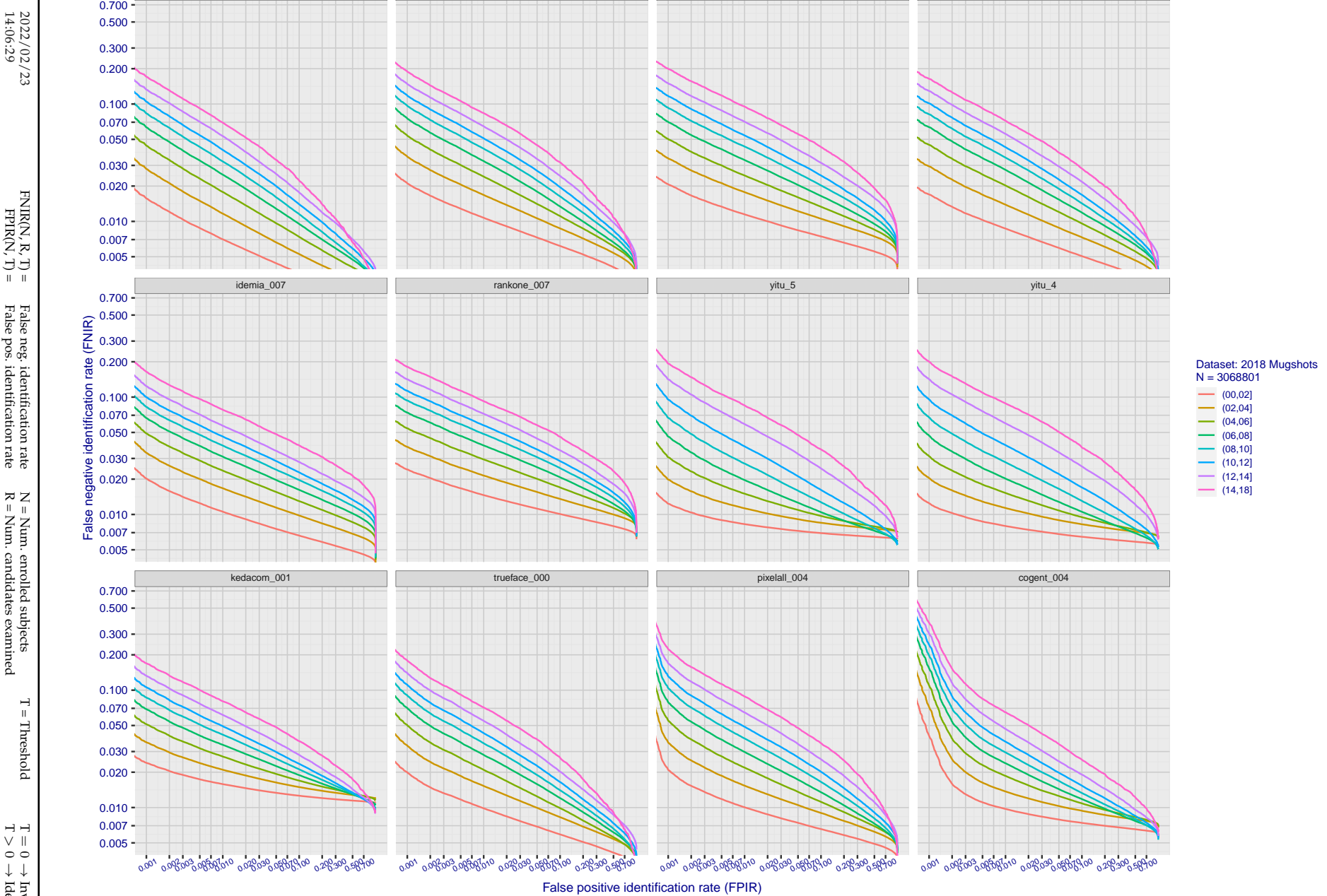


Figure 85: [FRVT-2018 Mugshot Ageing Dataset] Identification miss rates vs. FPIR by time-elapsed. The oldest image of each individual is enrolled. Thereafter, all more recent images are searched. Miss rates are computed over all searches noted in row 17 of Table 1 and binned by number of years between search and initial enrollment. FPIR is computed from the same FRVT 2018 non-mates noted in row 3 of Table 1 with $N = 3\,000\,000$.

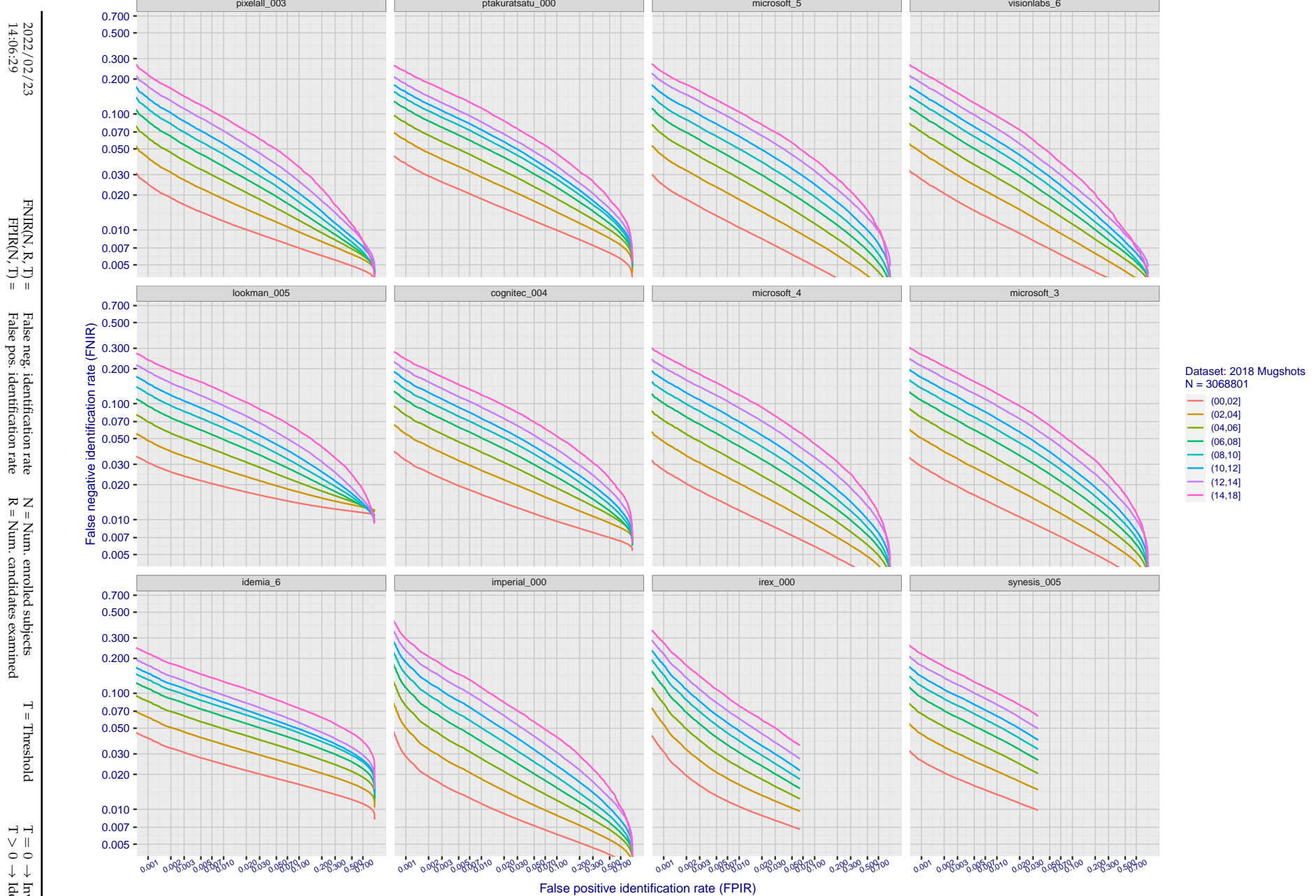


Figure 86: [FRVT-2018 Mugshot Ageing Dataset] Identification miss rates vs. FPIR by time-elapsed. The oldest image of each individual is enrolled. Thereafter, all more recent images are searched. Miss rates are computed over all searches noted in row 17 of Table 1 and binned by number of years between search and initial enrollment. FPIR is computed from the same FRVT 2018 non-mates noted in row 3 of Table 1 with $N = 3\,000\,000$.

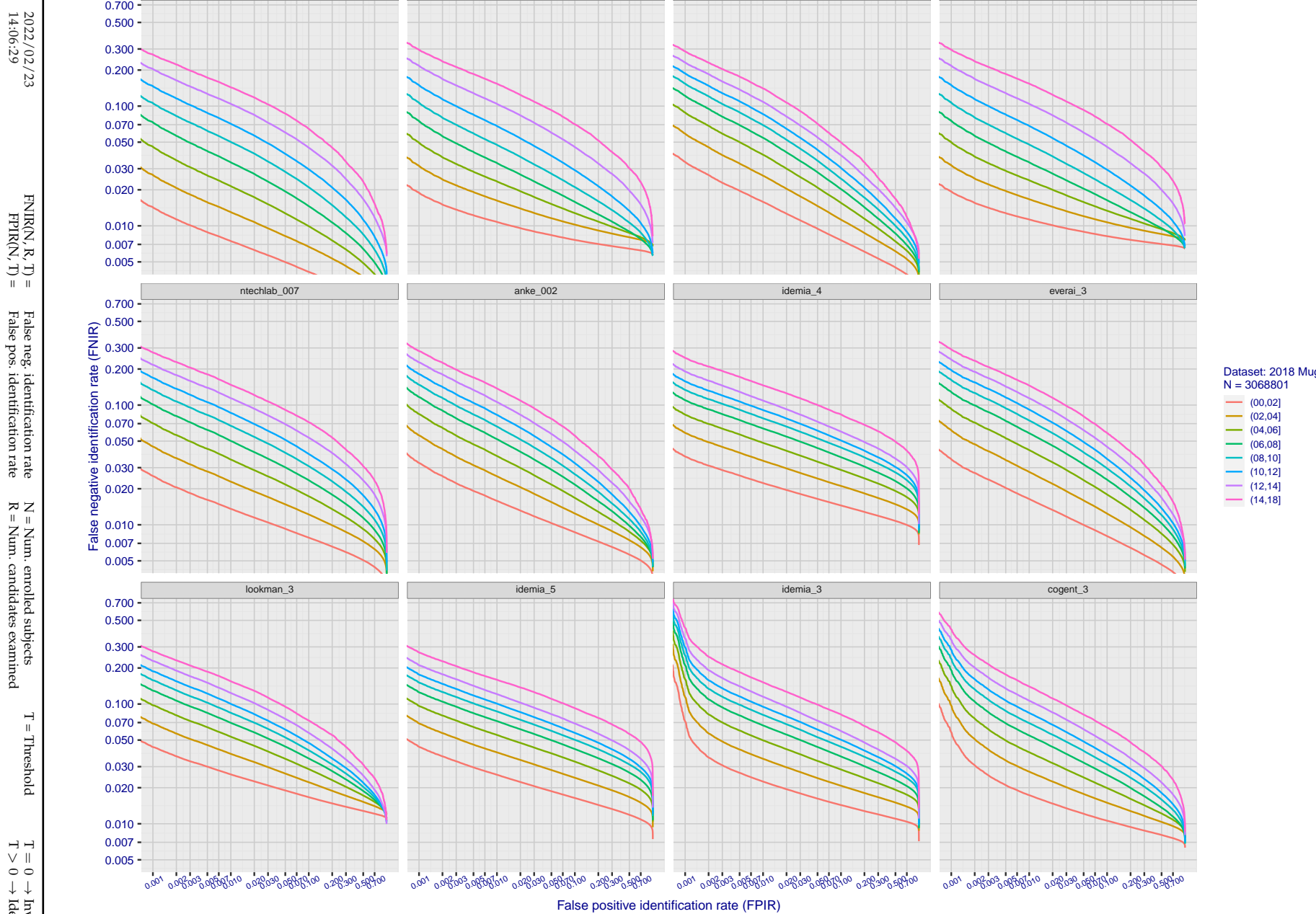


Figure 87: [FRVT-2018 Mugshot Ageing Dataset] Identification miss rates vs. FPIR by time-elapsed. The oldest image of each individual is enrolled. Thereafter, all more recent images are searched. Miss rates are computed over all searches noted in row 17 of Table 1 and binned by number of years between search and initial enrollment. FPIR is computed from the same FRVT 2018 non-mates noted in row 3 of Table 1 with N = 3 000 000.

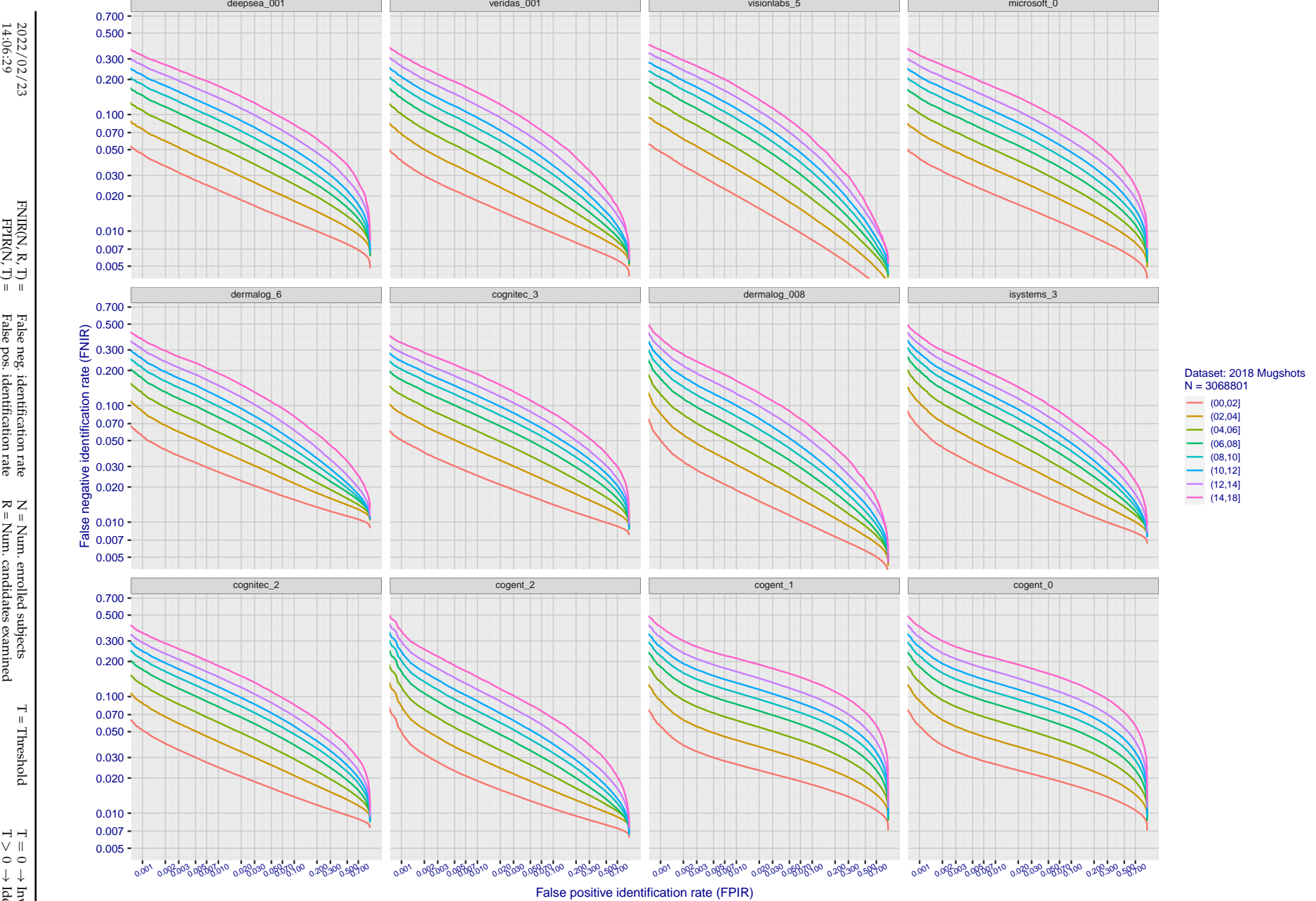


Figure 88: [FRVT-2018 Mugshot Ageing Dataset] Identification miss rates vs. FPIR by time-elapsed. The oldest image of each individual is enrolled. Thereafter, all more recent images are searched. Miss rates are computed over all searches noted in row 17 of Table 1 and binned by number of years between search and initial enrollment. FPIR is computed from the same FRVT 2018 non-mates noted in row 3 of Table 1 with $N = 3\,000\,000$.

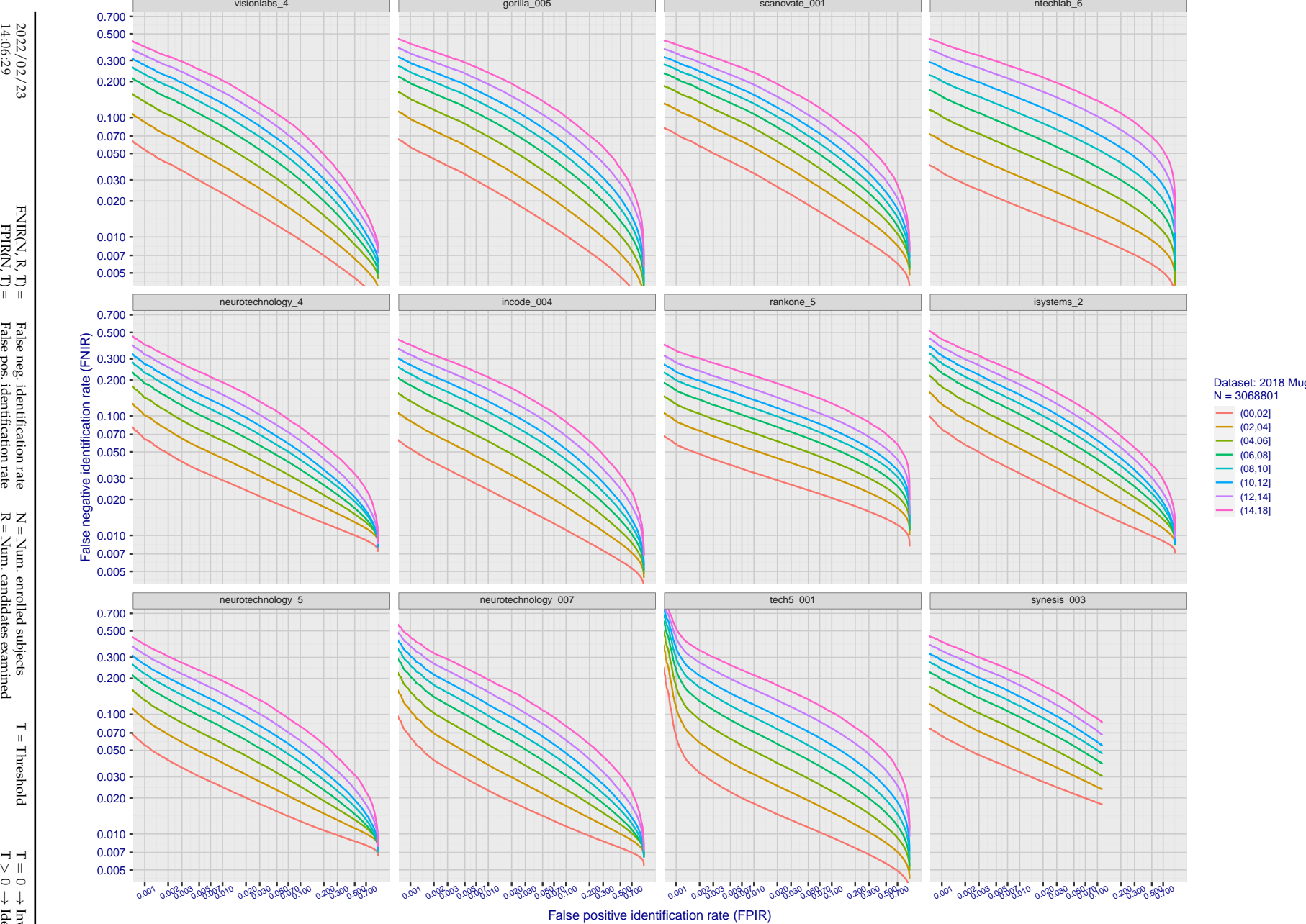


Figure 89: [FRVT-2018 Mugshot Ageing Dataset] Identification miss rates vs. FPIR by time-elapsed. The oldest image of each individual is enrolled. Thereafter, all more recent images are searched. Miss rates are computed over all searches noted in row 17 of Table 1 and binned by number of years between search and initial enrollment. FPIR is computed from the same FRVT 2018 non-mates noted in row 3 of Table 1 with $N = 3\,000\,000$.

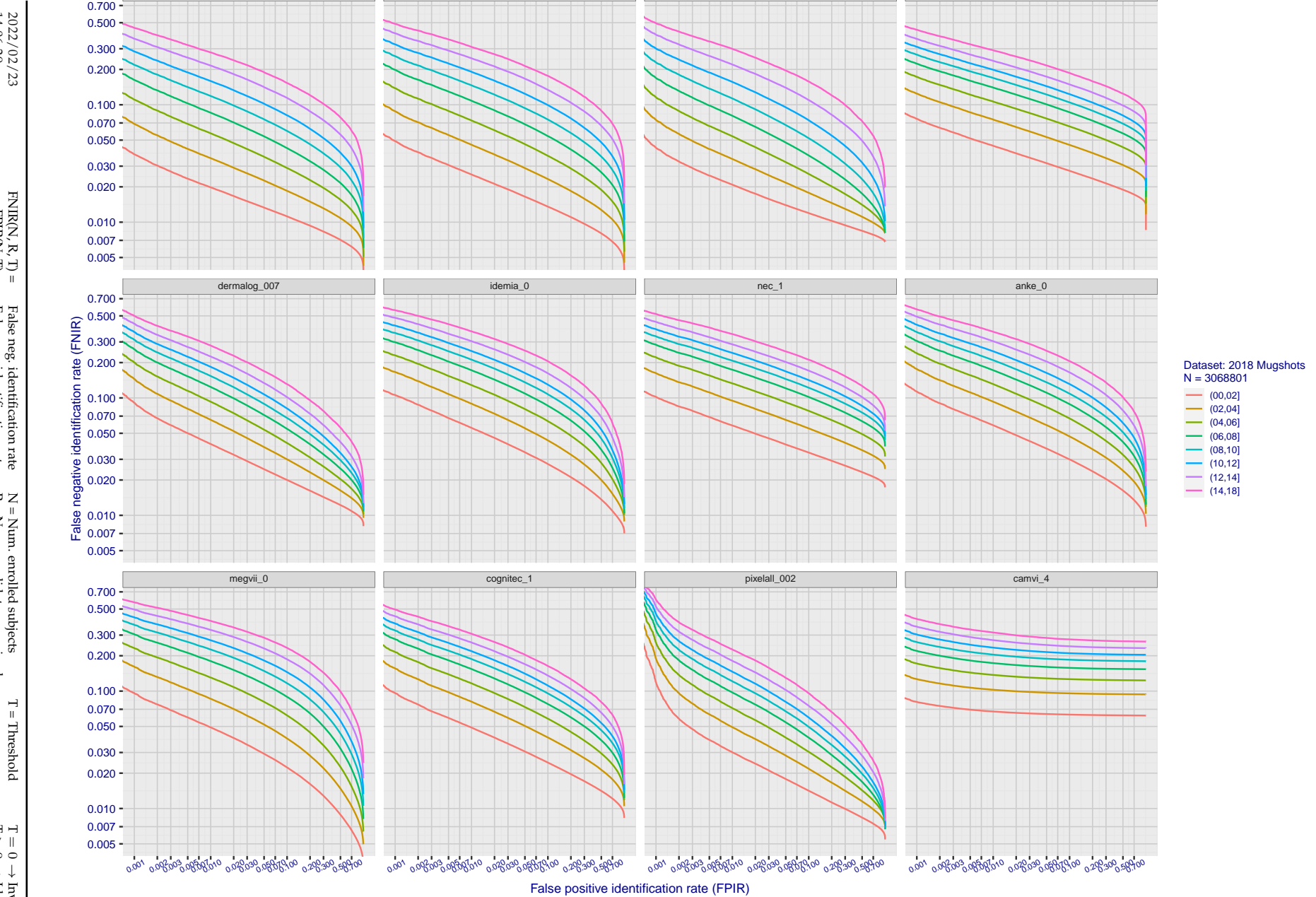


Figure 90: [FRVT-2018 Mugshot Ageing Dataset] Identification miss rates vs. FPIR by time-elapsed. The oldest image of each individual is enrolled. Thereafter, all more recent images are searched. Miss rates are computed over all searches noted in row 17 of Table 1 and binned by number of years between search and initial enrollment. FPIR is computed from the same FRVT 2018 non-mates noted in row 3 of Table 1 with $N = 3\,000\,000$.

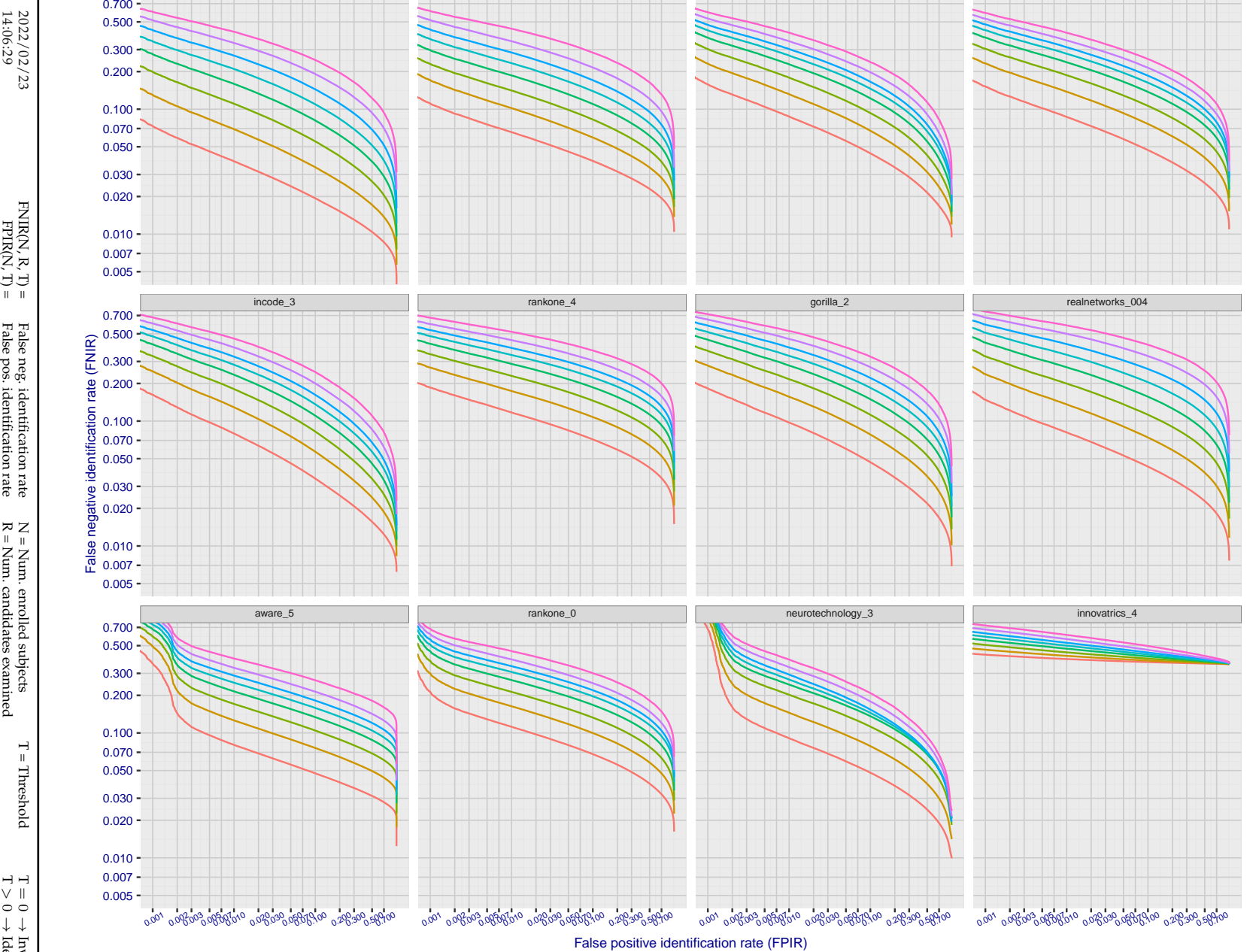


Figure 91: [FRVT-2018 Mugshot Ageing Dataset] Identification miss rates vs. FPIR by time elapsed. The oldest image of each individual is enrolled. Thereafter, all more recent images are searched. Miss rates are computed over all searches noted in row 17 of Table 1 and binned by number of years between search and initial enrollment. FPIR is computed from the same FRVT 2018 non-mates noted in row 3 of Table 1 with $N = 3\,000\,000$.

2022/02/23
14:06:29FNIR(N, R, T) = False neg. identification rate
FPIR(N, T) = False pos. identification rateN = Num. enrolled subjects
R = Num. candidates examined

T = Threshold

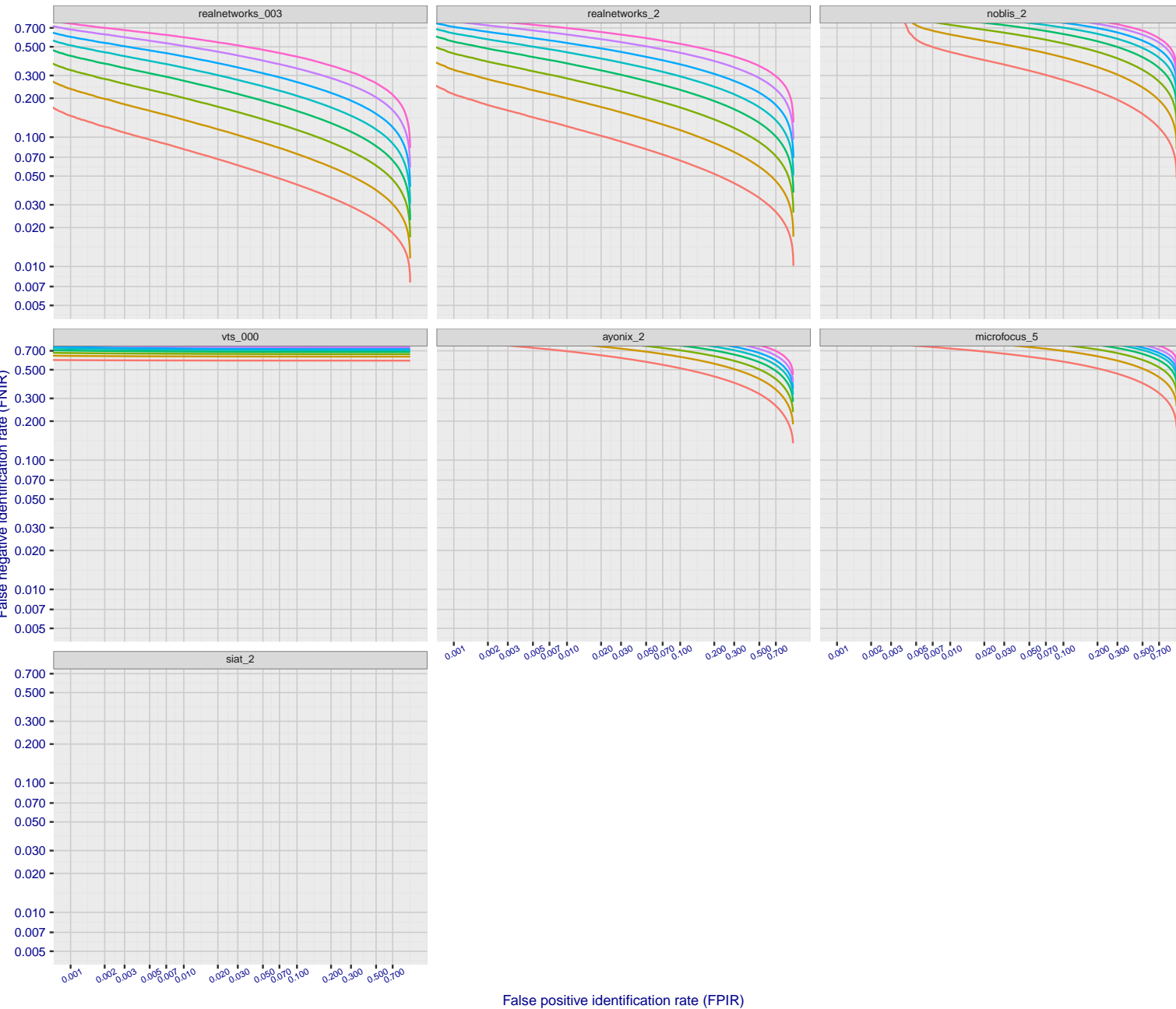
T = 0 → Investigation
T > 0 → Identification

Figure 92: [FRVT-2018 Mugshot Ageing Dataset] Identification miss rates vs. FPIR by time-elapsed. The oldest image of each individual is enrolled. Thereafter, all more recent images are searched. Miss rates are computed over all searches noted in row 17 of Table 1 and binned by number of years between search and initial enrollment. FPIR is computed from the same FRVT 2018 non-mates noted in row 3 of Table 1 with N = 3 000 000.

2022/02/23
14:06:29

$\text{FNIR}(\text{N}, \text{R}, \text{T}) =$	False neg. identification rate	$\text{N} =$ Num. enrolled subjects	$\text{T} =$ Threshold	$\text{T} = 0 \rightarrow$ Investigation
$\text{FPRI}(\text{N}, \text{T}) =$	False pos. identification rate	$\text{R} =$ Num. candidates examined	$\text{T} > 0$	\rightarrow Identification

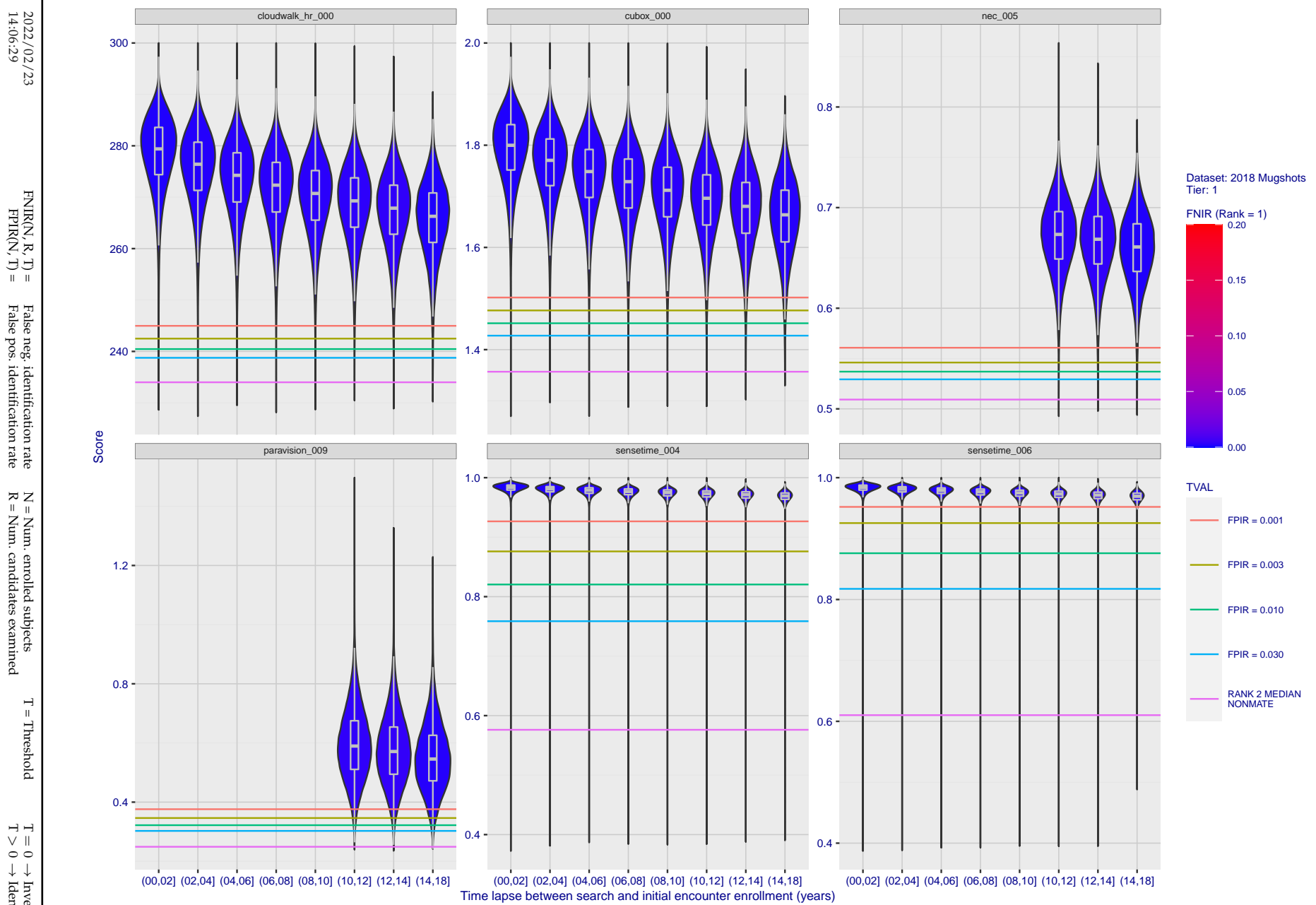


Figure 93: [FRVT-2018 Mugshot Ageing Dataset] Native mate scores vs. time-elapsed. The oldest image of each individual is enrolled. Thereafter, all more recent images are searched. Mated score distributions are computed over all searches noted in row 17 of Table 1 binned by number of years between search and initial enrollment.

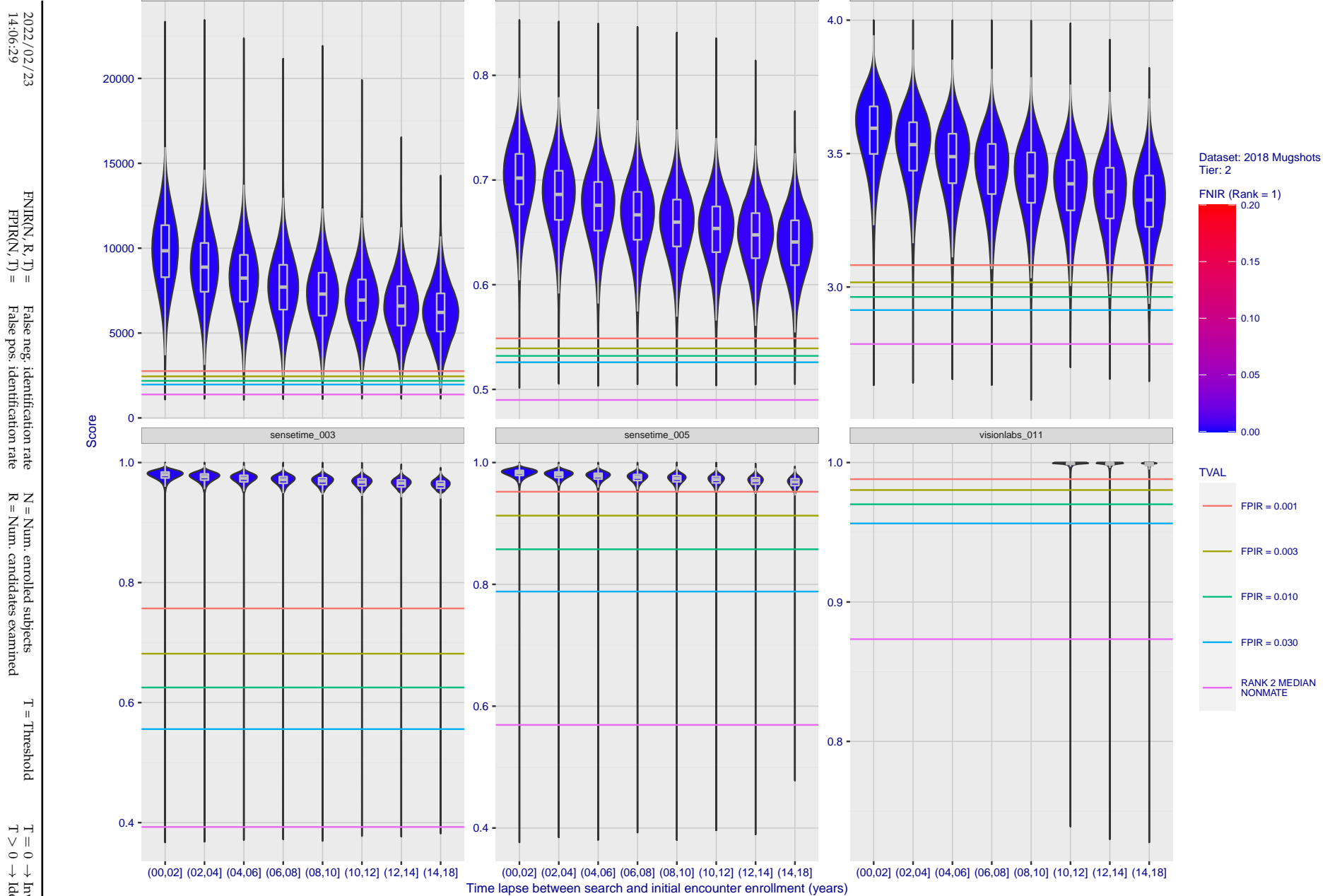


Figure 94: [FRVT-2018 Mugshot Ageing Dataset] Native mate scores vs. time-elapsed. The oldest image of each individual is enrolled. Thereafter, all more recent images are searched. Mated score distributions are computed over all searches noted in row 17 of Table 1 binned by number of years between search and initial enrollment.

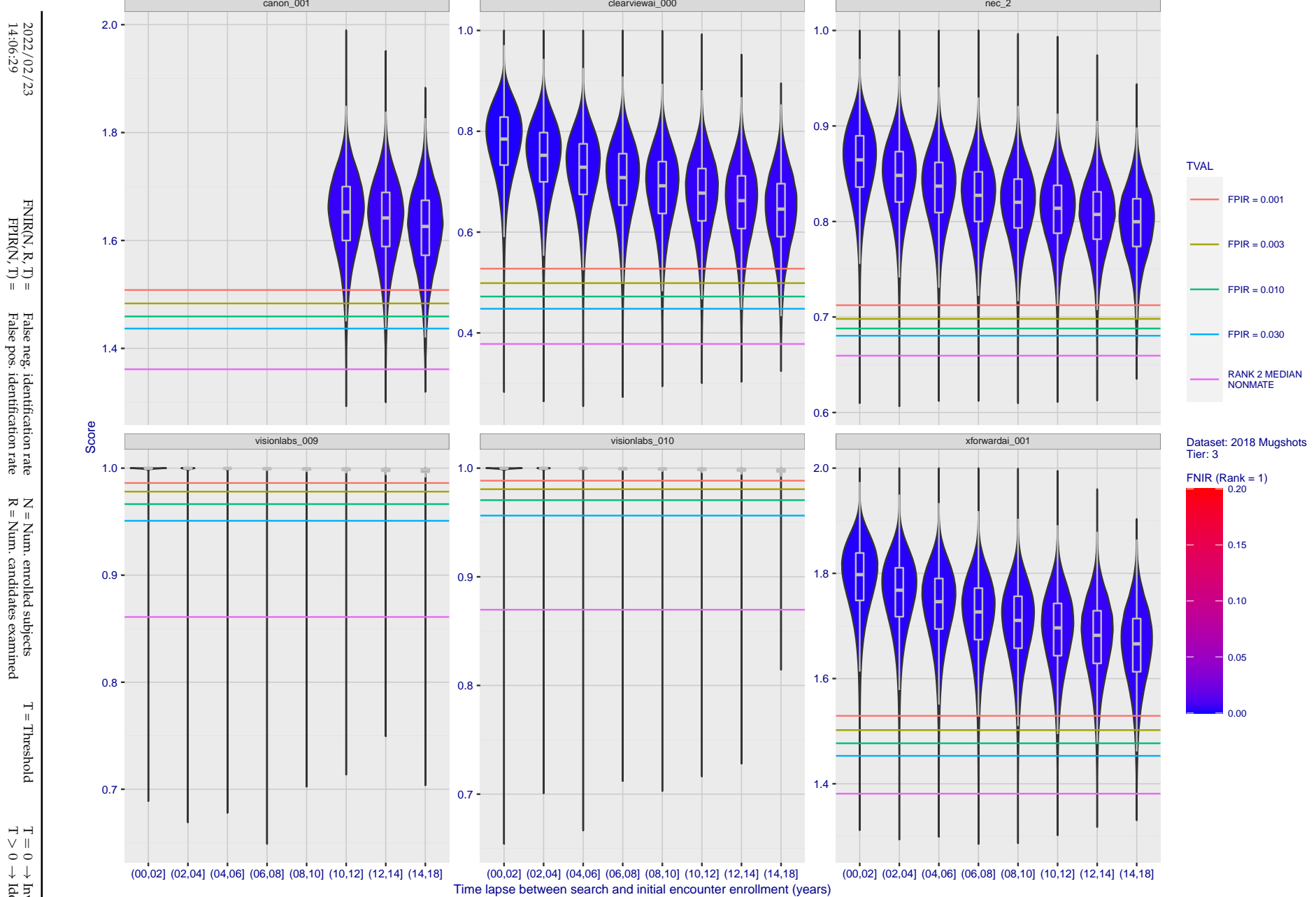


Figure 95: [FRVT-2018 Mugshot Ageing Dataset] Native mate scores vs. time-elapsed. The oldest image of each individual is enrolled. Thereafter, all more recent images are searched. Mated score distributions are computed over all searches noted in row 17 of Table 1 binned by number of years between search and initial enrollment.

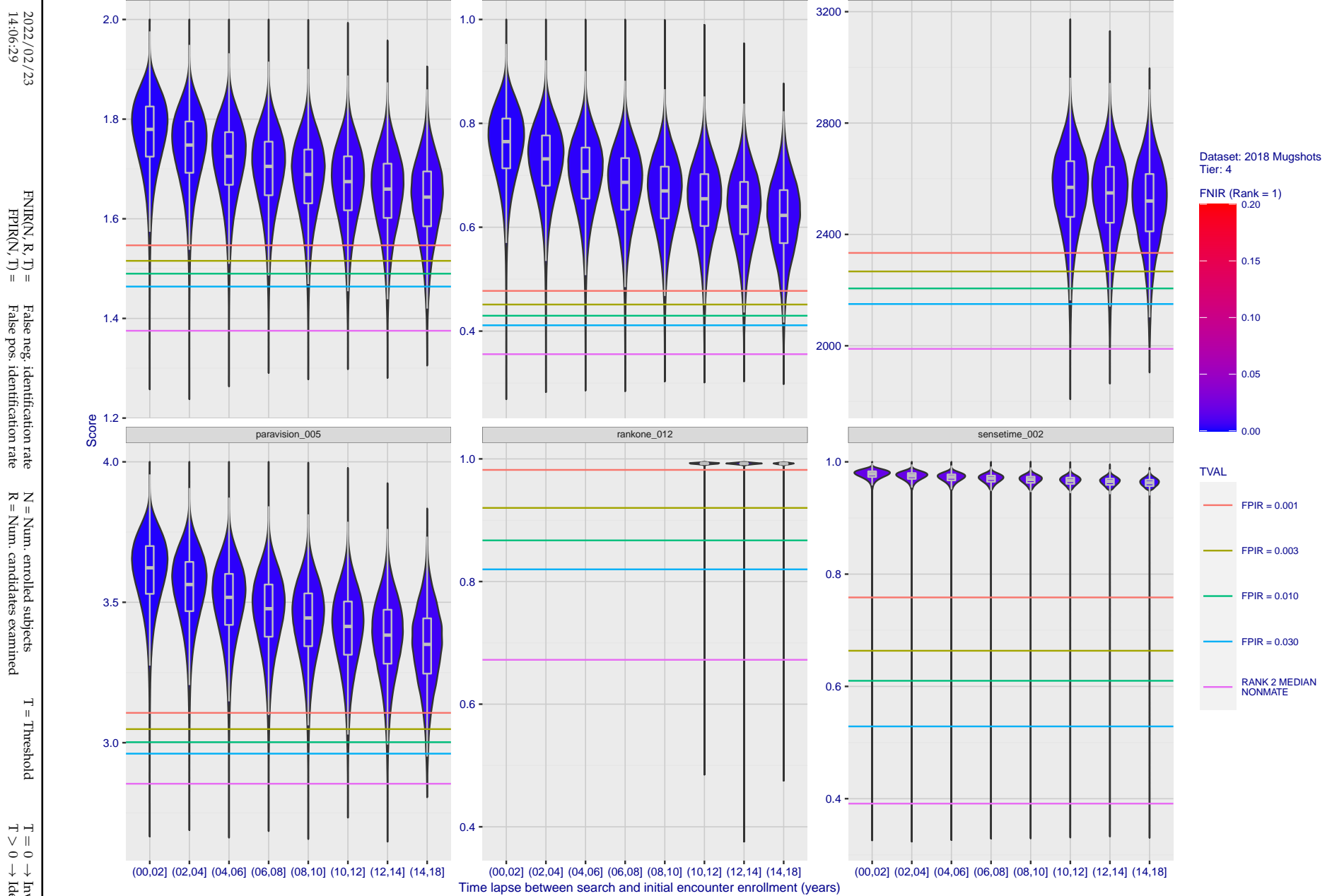


Figure 96: [FRVT-2018 Mugshot Ageing Dataset] Native mate scores vs. time-elapsed. The oldest image of each individual is enrolled. Thereafter, all more recent images are searched. Mated score distributions are computed over all searches noted in row 17 of Table 1 binned by number of years between search and initial enrollment.

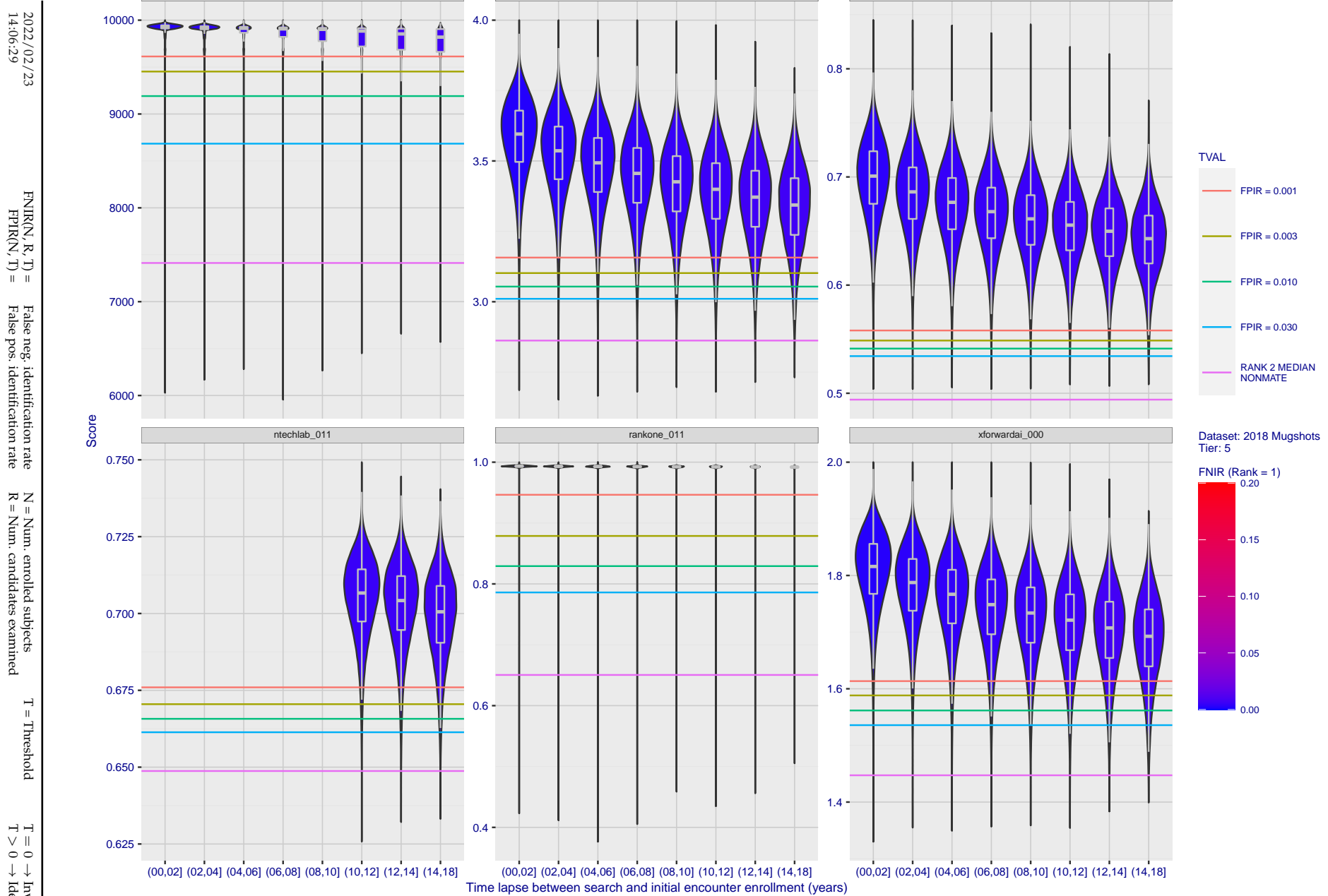


Figure 97: [FRVT-2018 Mugshot Ageing Dataset] Native mate scores vs. time-elapsed. The oldest image of each individual is enrolled. Thereafter, all more recent images are searched. Mated score distributions are computed over all searches noted in row 17 of Table 1 binned by number of years between search and initial enrollment.

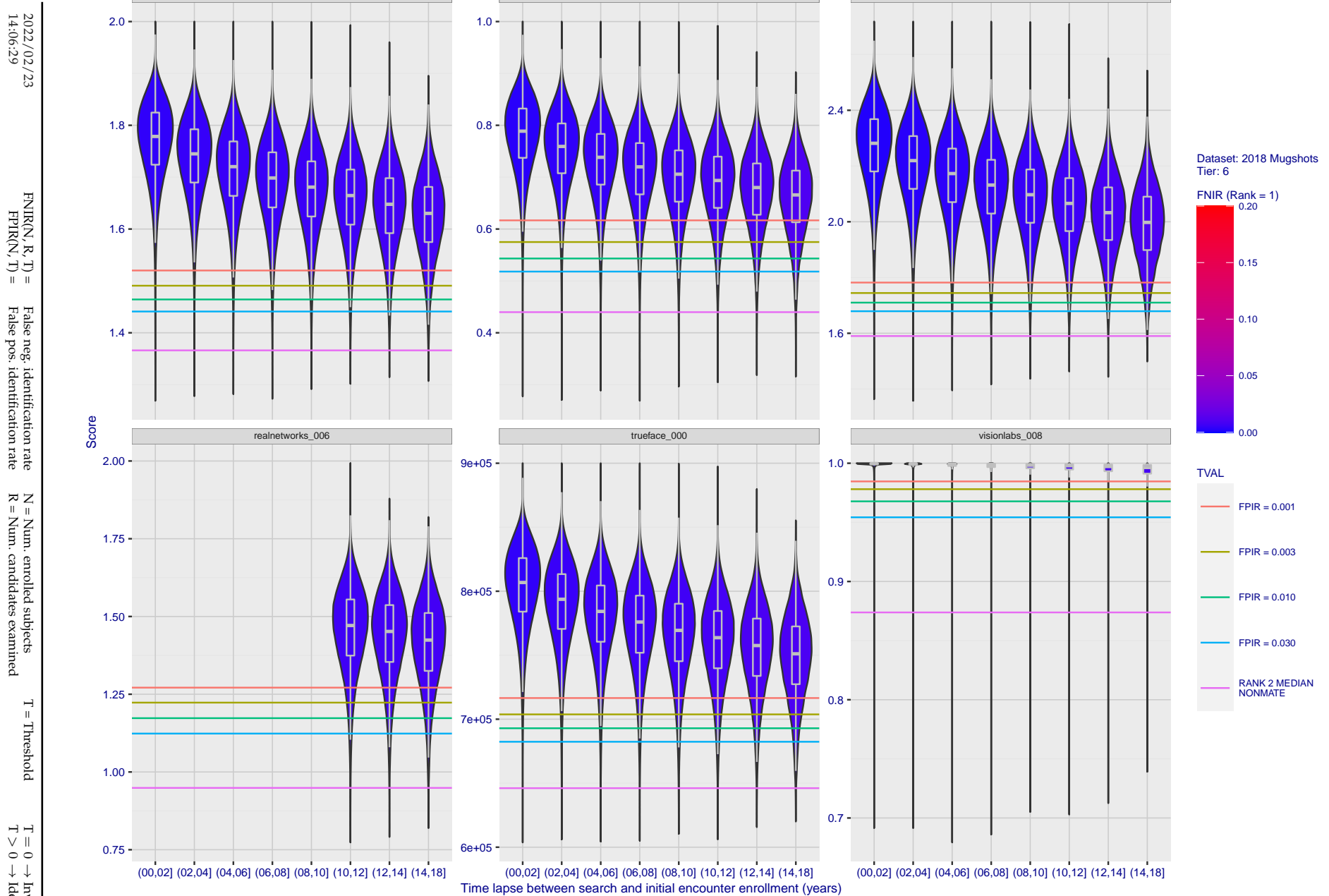


Figure 98: [FRVT-2018 Mugshot Ageing Dataset] Native mate scores vs. time-elapsed. The oldest image of each individual is enrolled. Thereafter, all more recent images are searched. Mated score distributions are computed over all searches noted in row 17 of Table 1 binned by number of years between search and initial enrollment.

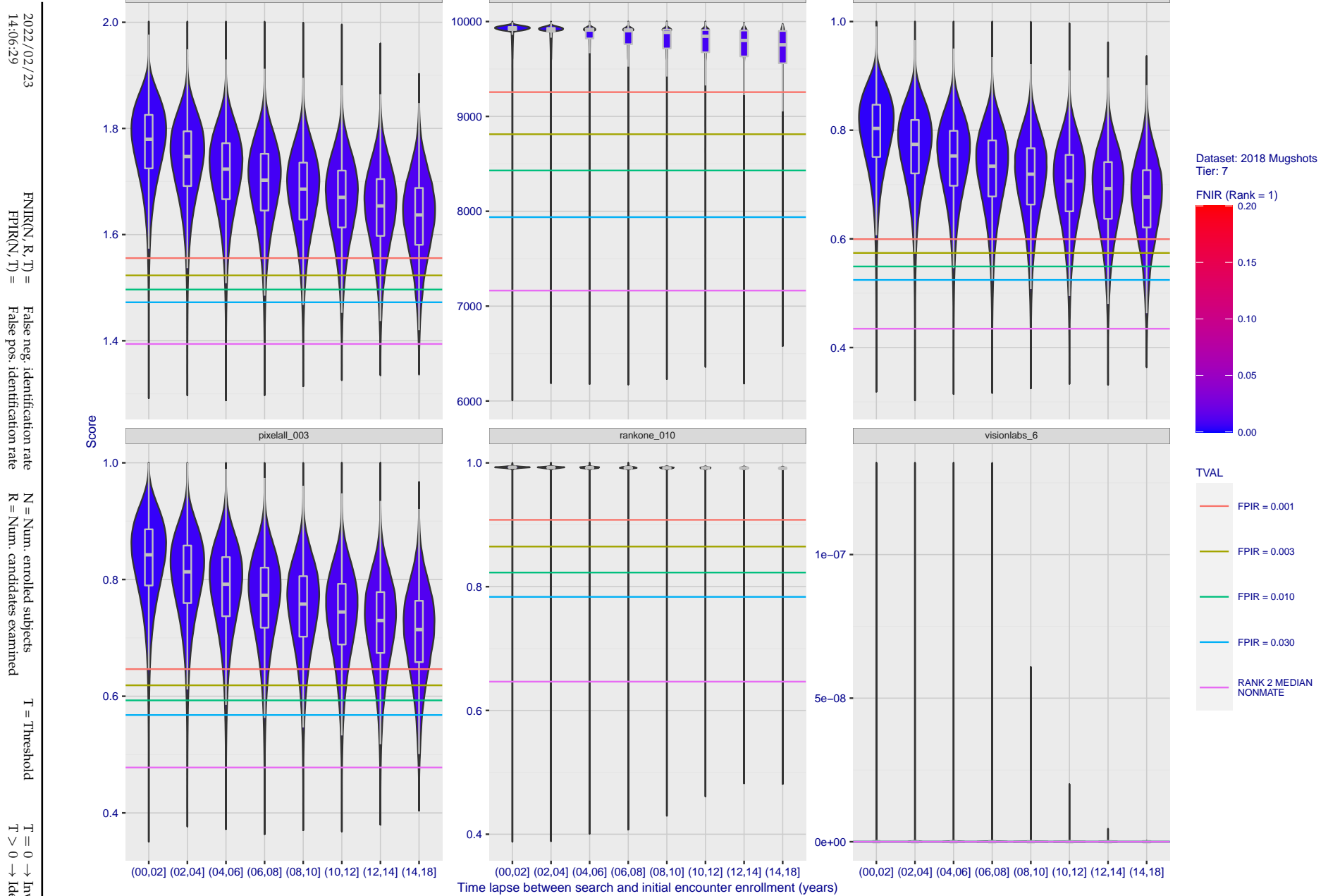


Figure 99: [FRVT-2018 Mugshot Ageing Dataset] Native mate scores vs. time-elapsed. The oldest image of each individual is enrolled. Thereafter, all more recent images are searched. Mated score distributions are computed over all searches noted in row 17 of Table 1 binned by number of years between search and initial enrollment.

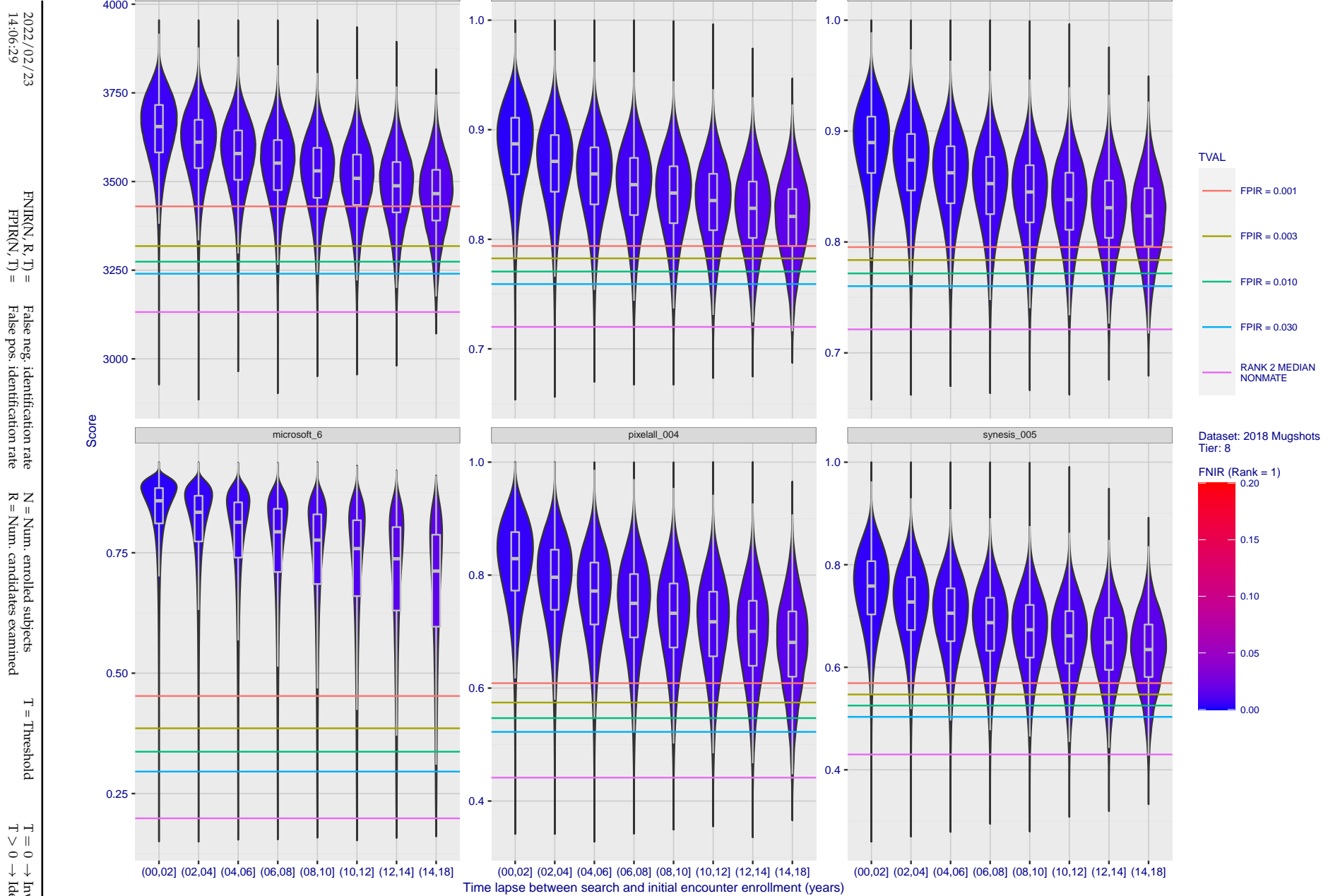


Figure 100: [FRVT-2018 Mugshot Ageing Dataset] Native mate scores vs. time-elapsed. The oldest image of each individual is enrolled. Thereafter, all more recent images are searched. Mated score distributions are computed over all searches noted in row 17 of Table 1 binned by number of years between search and initial enrollment.

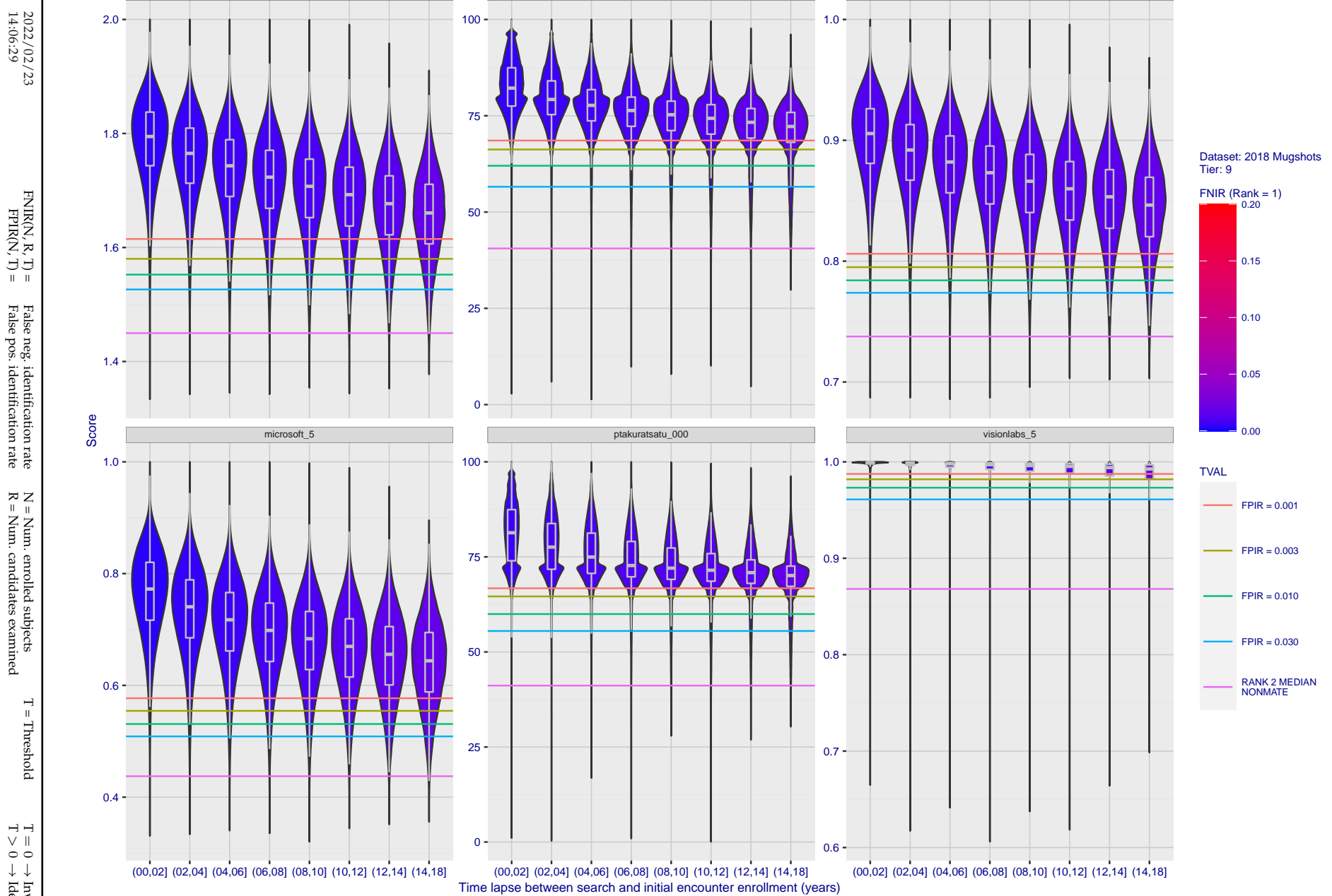


Figure 101: [FRVT-2018 Mugshot Ageing Dataset] Native mate scores vs. time-elapsed. The oldest image of each individual is enrolled. Thereafter, all more recent images are searched. Mated score distributions are computed over all searches noted in row 17 of Table 1 binned by number of years between search and initial enrollment.

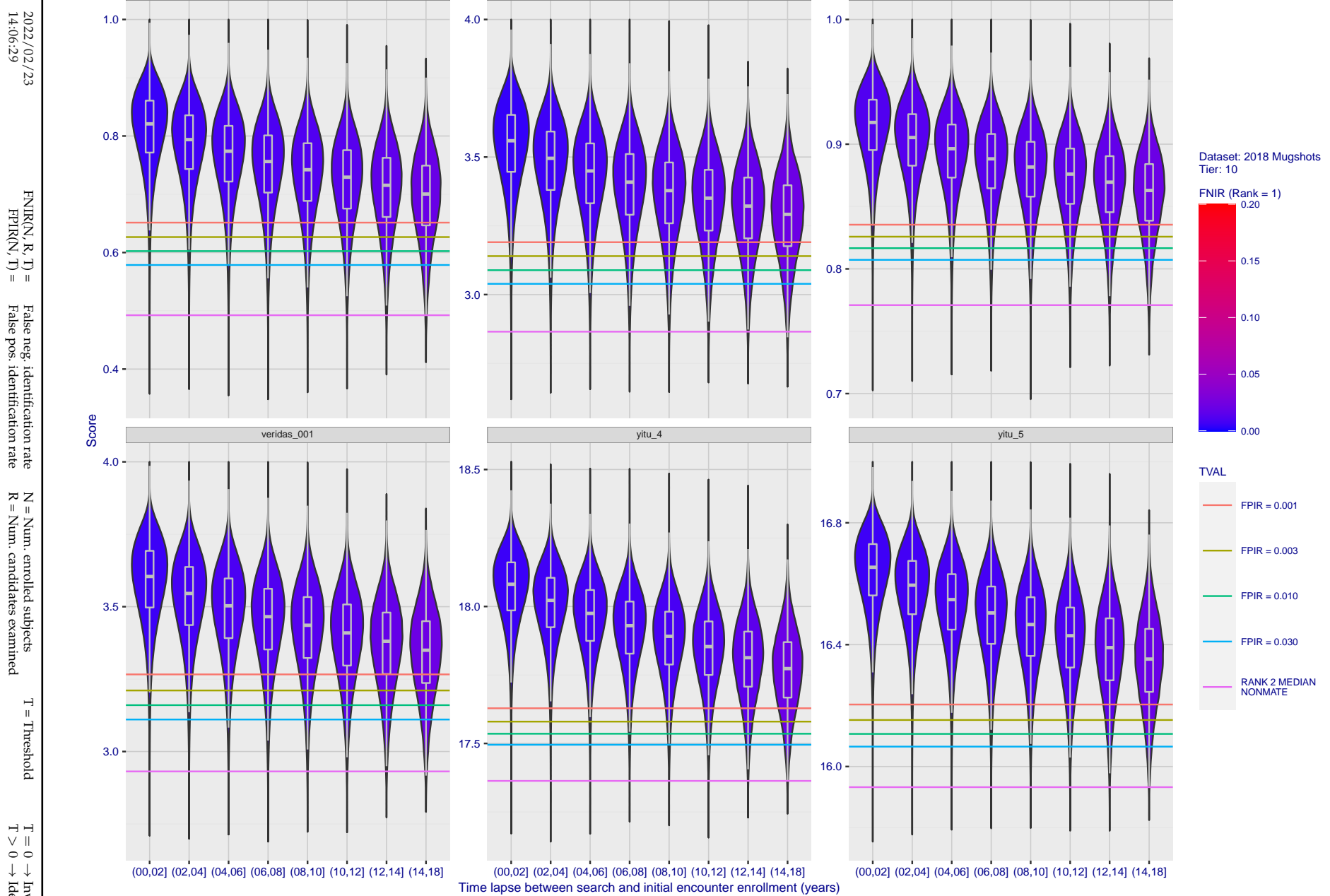


Figure 102: [FRVT-2018 Mugshot Ageing Dataset] Native mate scores vs. time-elapsed. The oldest image of each individual is enrolled. Thereafter, all more recent images are searched. Mated score distributions are computed over all searches noted in row 17 of Table 1 binned by number of years between search and initial enrollment.

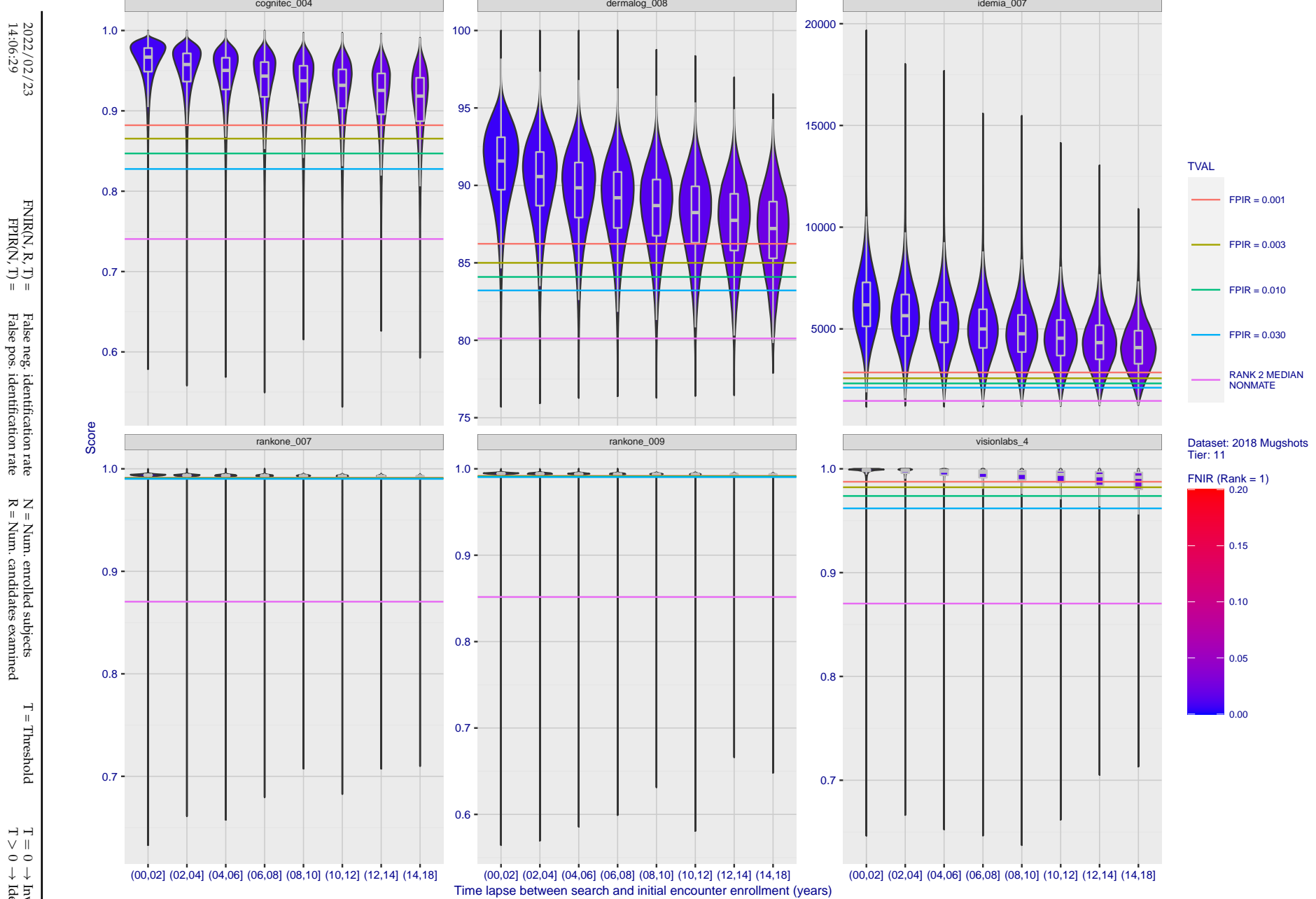


Figure 103: [FRVT-2018 Mugshot Ageing Dataset] Native mate scores vs. time-elapsed. The oldest image of each individual is enrolled. Thereafter, all more recent images are searched. Mated score distributions are computed over all searches noted in row 17 of Table 1 binned by number of years between search and initial enrollment.

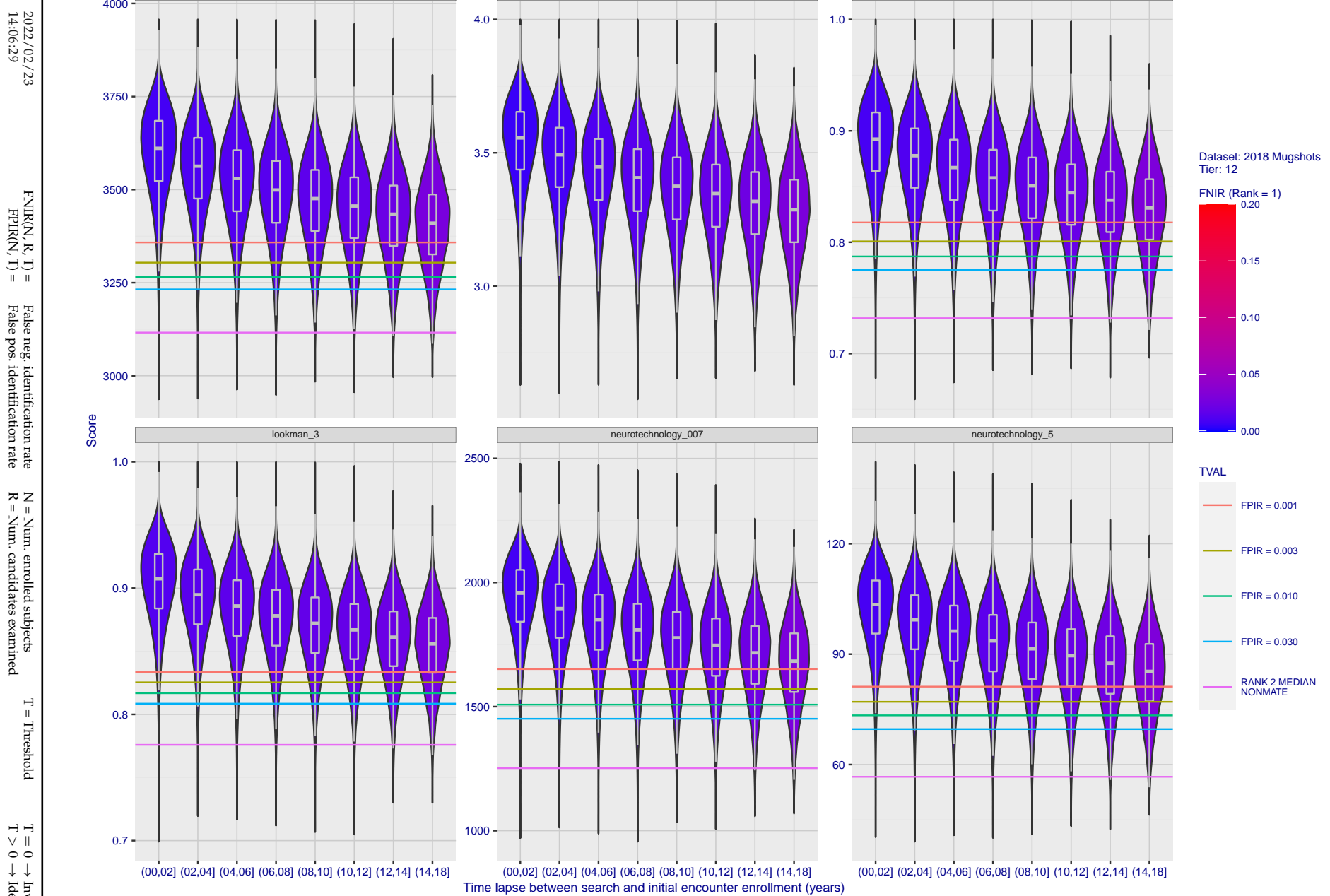


Figure 104: [FRVT-2018 Mugshot Ageing Dataset] Native mate scores vs. time-elapsed. The oldest image of each individual is enrolled. Thereafter, all more recent images are searched. Mated score distributions are computed over all searches noted in row 17 of Table 1 binned by number of years between search and initial enrollment.

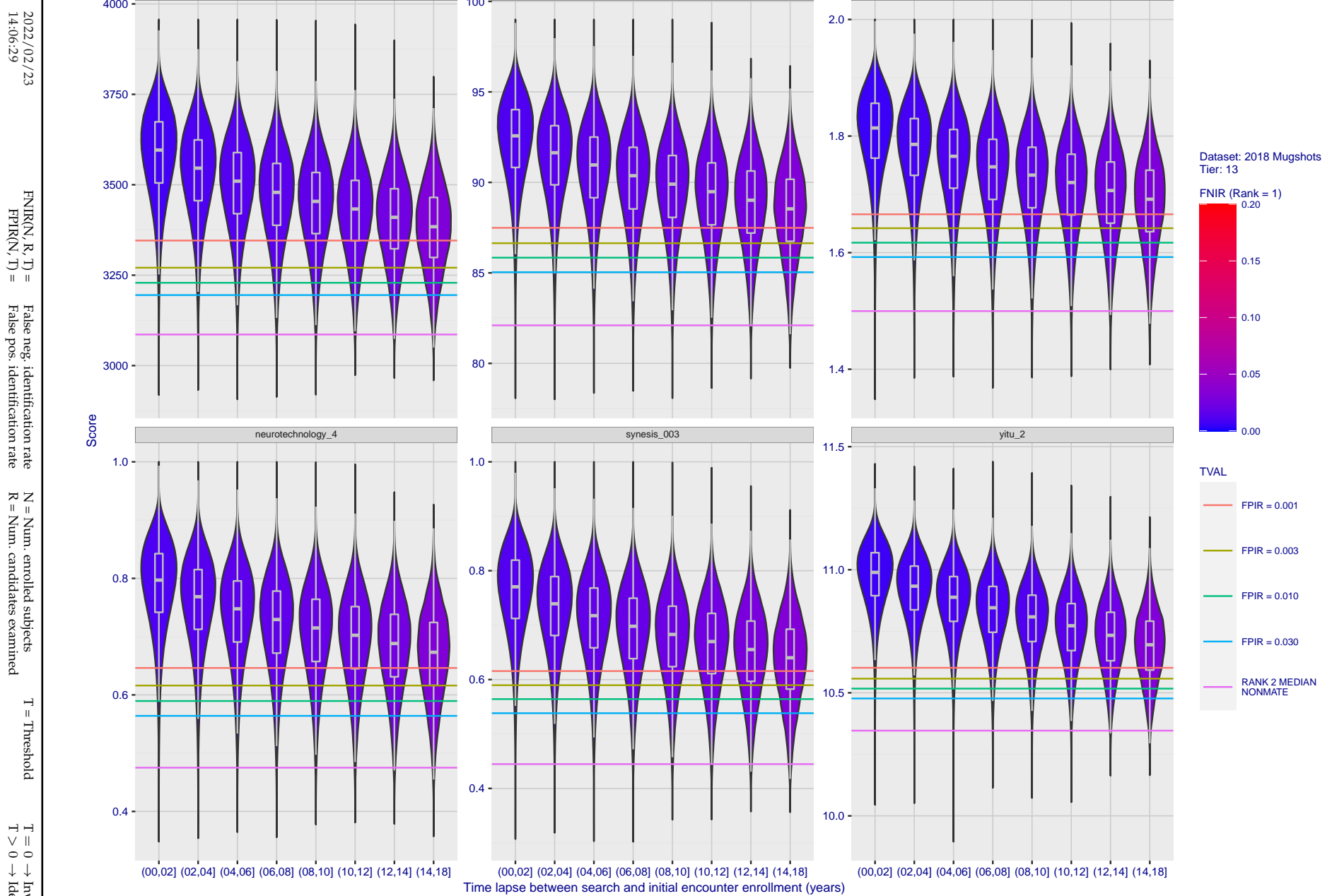


Figure 105: [FRVT-2018 Mugshot Ageing Dataset] Native mate scores vs. time-elapsed. The oldest image of each individual is enrolled. Thereafter, all more recent images are searched. Mated score distributions are computed over all searches noted in row 17 of Table 1 binned by number of years between search and initial enrollment.

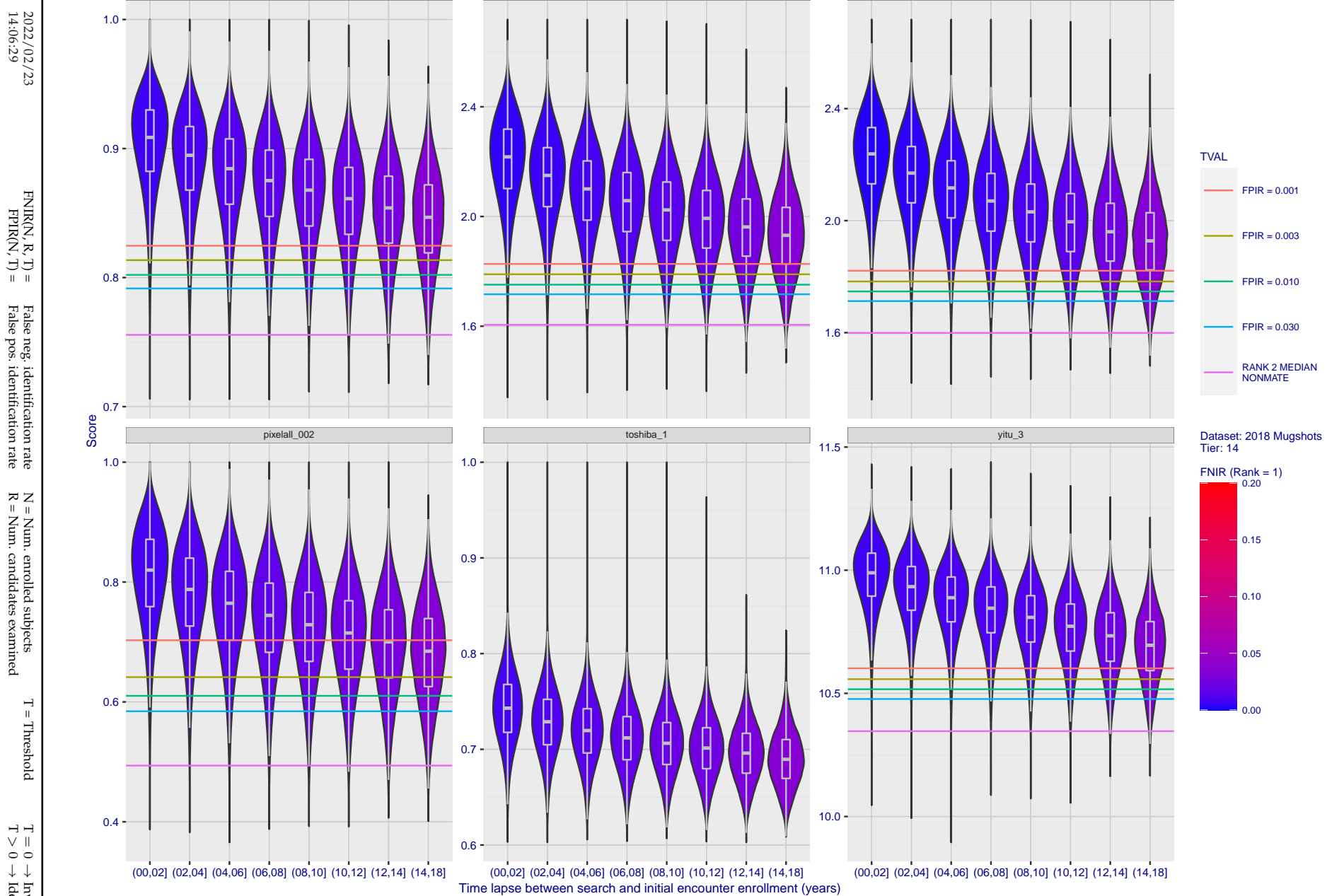


Figure 106: [FRVT-2018 Mugshot Ageing Dataset] Native mate scores vs. time-elapsed. The oldest image of each individual is enrolled. Thereafter, all more recent images are searched. Mated score distributions are computed over all searches noted in row 17 of Table 1 binned by number of years between search and initial enrollment.

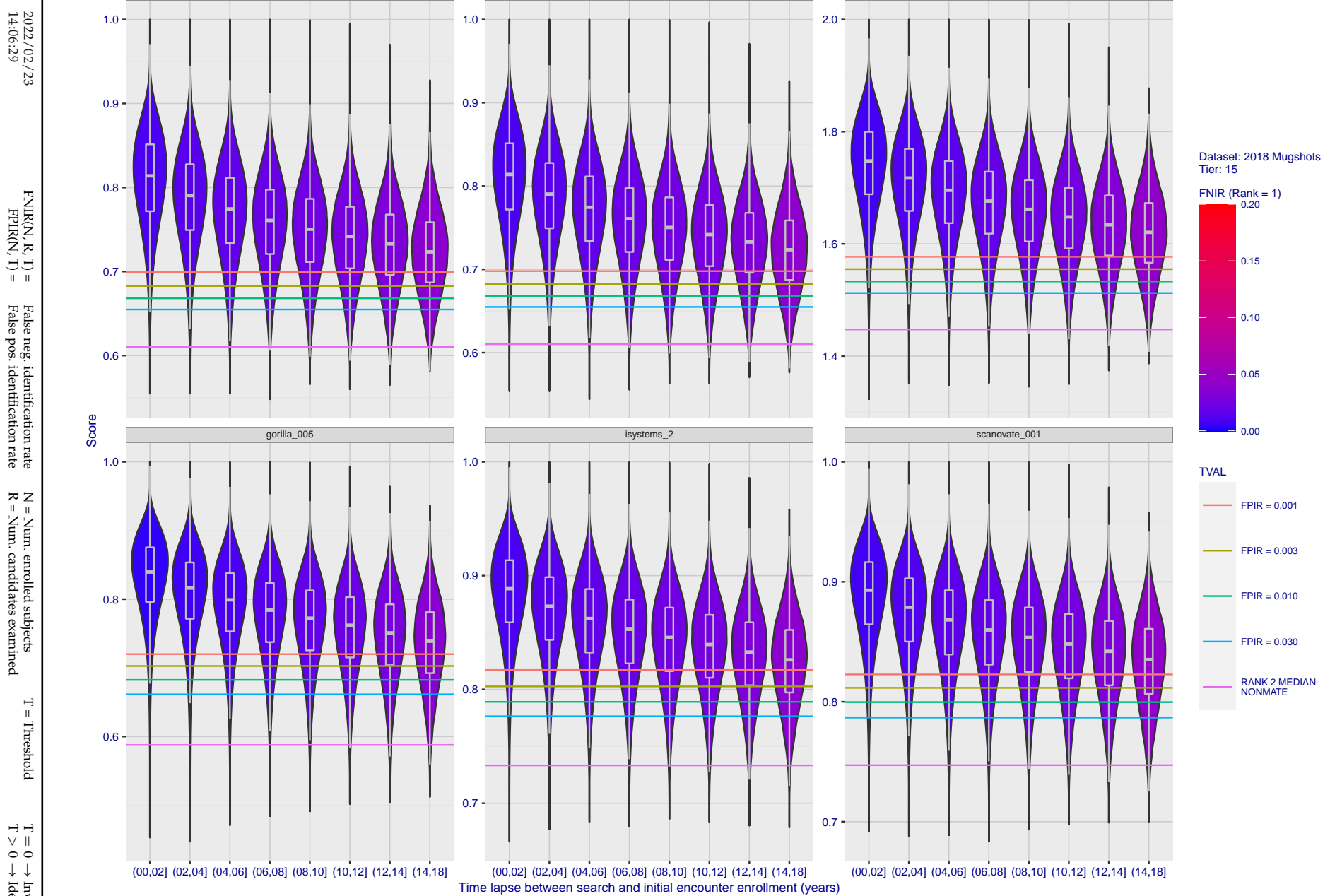


Figure 107: [FRVT-2018 Mugshot Ageing Dataset] Native mate scores vs. time-elapsed. The oldest image of each individual is enrolled. Thereafter, all more recent images are searched. Mated score distributions are computed over all searches noted in row 17 of Table 1 binned by number of years between search and initial enrollment.

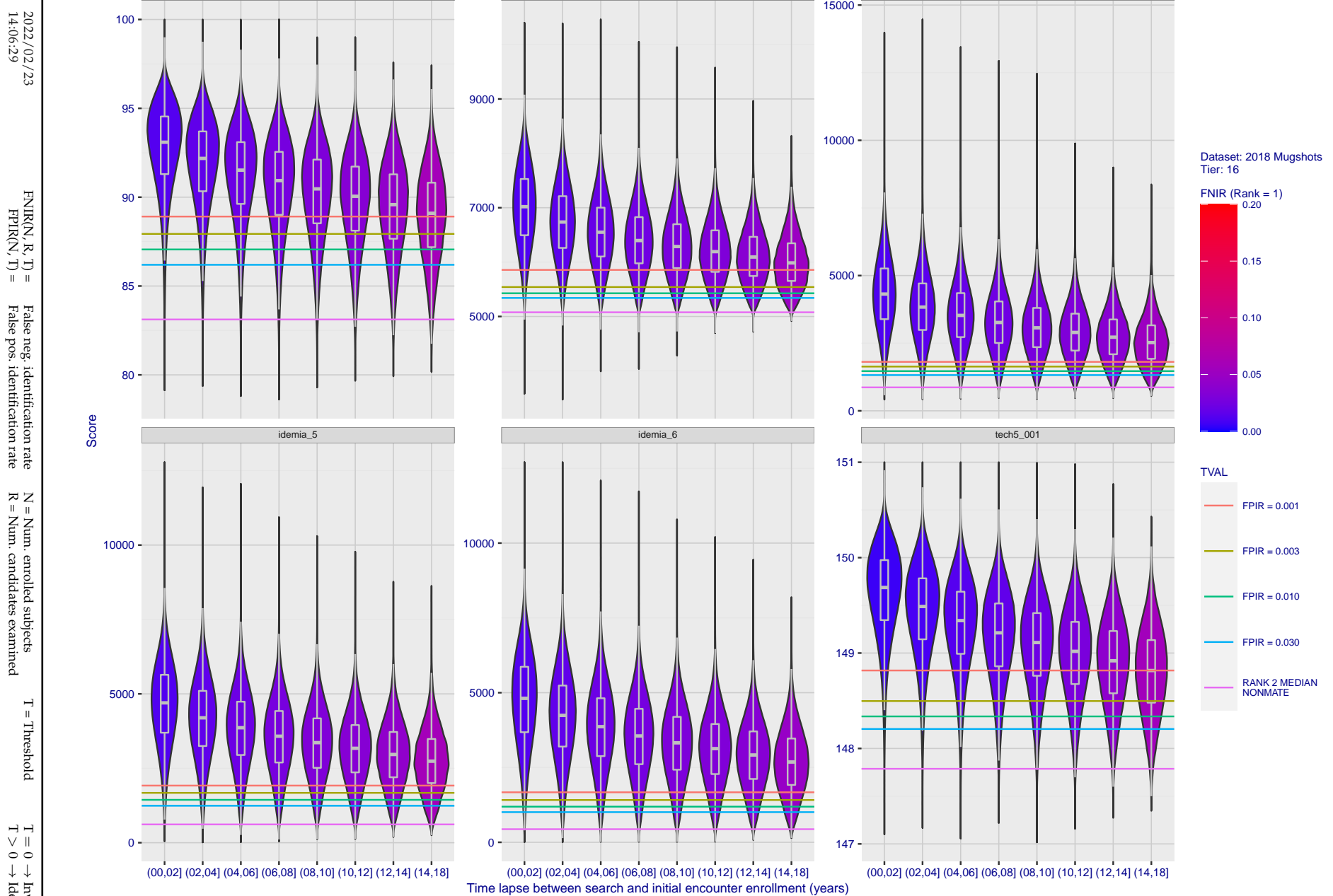


Figure 108: [FRVT-2018 Mugshot Ageing Dataset] Native mate scores vs. time-elapsed. The oldest image of each individual is enrolled. Thereafter, all more recent images are searched. Mated score distributions are computed over all searches noted in row 17 of Table 1 binned by number of years between search and initial enrollment.

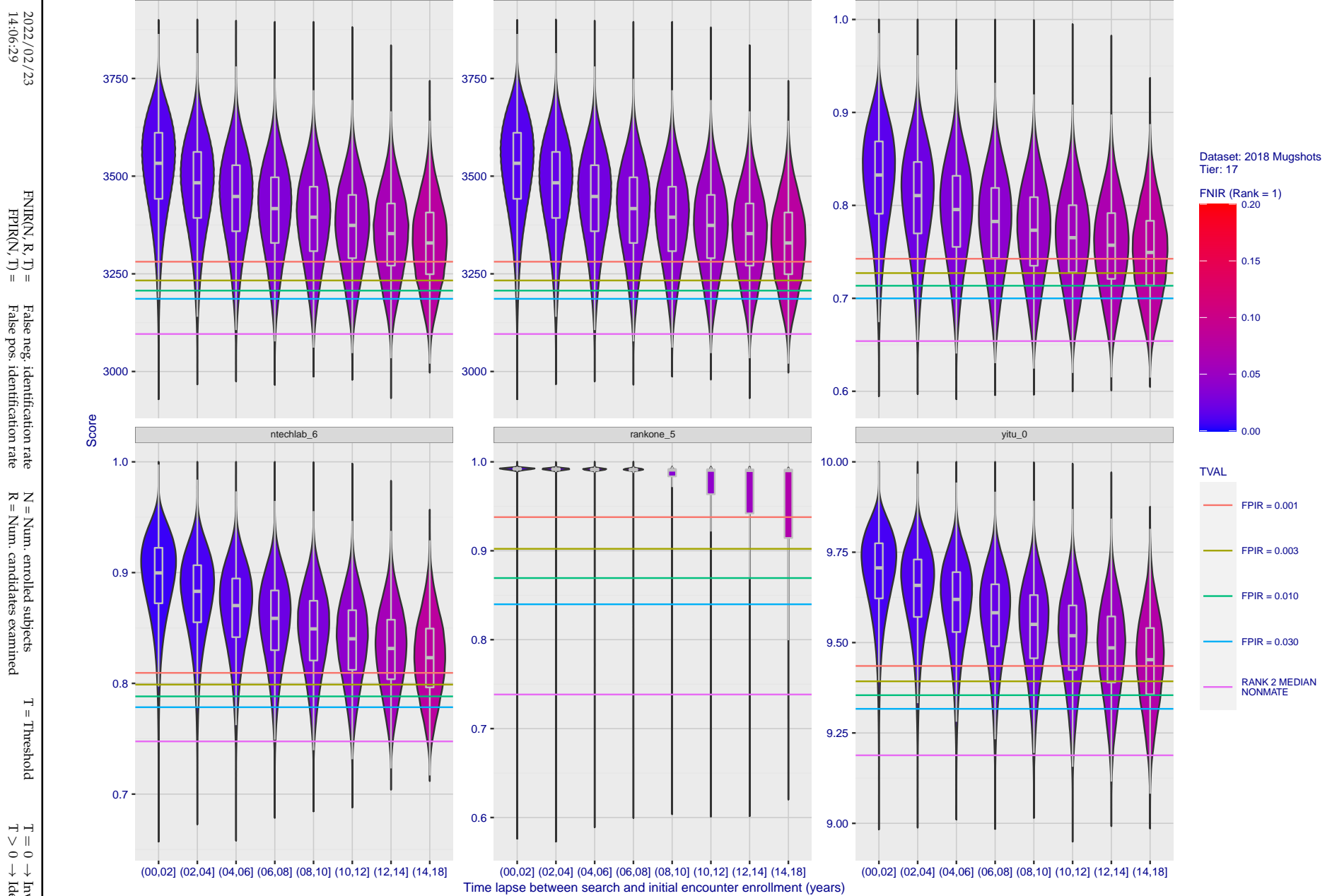


Figure 109: [FRVT-2018 Mugshot Ageing Dataset] Native mate scores vs. time-elapsed. The oldest image of each individual is enrolled. Thereafter, all more recent images are searched. Mated score distributions are computed over all searches noted in row 17 of Table 1 binned by number of years between search and initial enrollment.

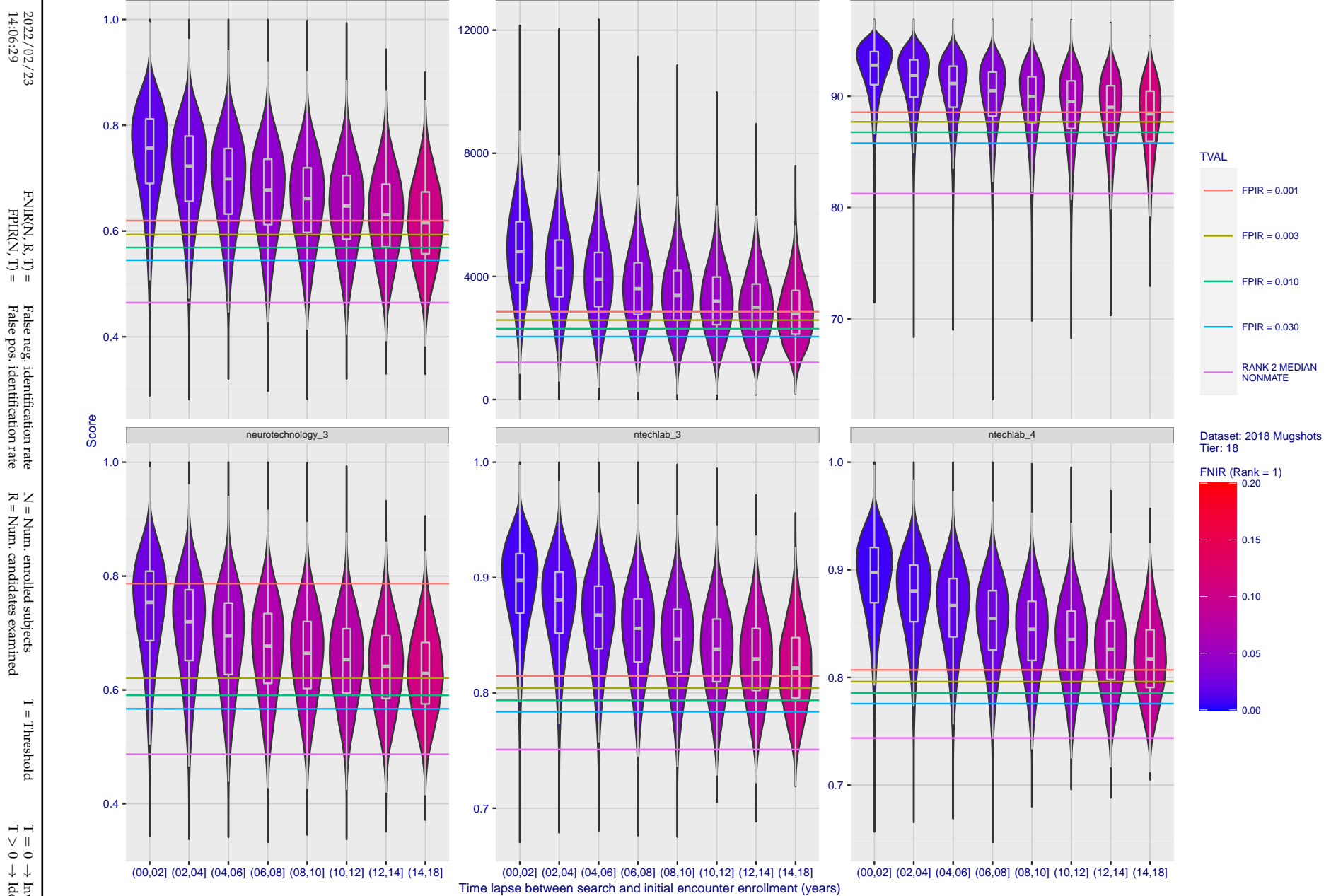


Figure 110: [FRVT-2018 Mugshot Ageing Dataset] Native mate scores vs. time-elapsed. The oldest image of each individual is enrolled. Thereafter, all more recent images are searched. Mated score distributions are computed over all searches noted in row 17 of Table 1 binned by number of years between search and initial enrollment.

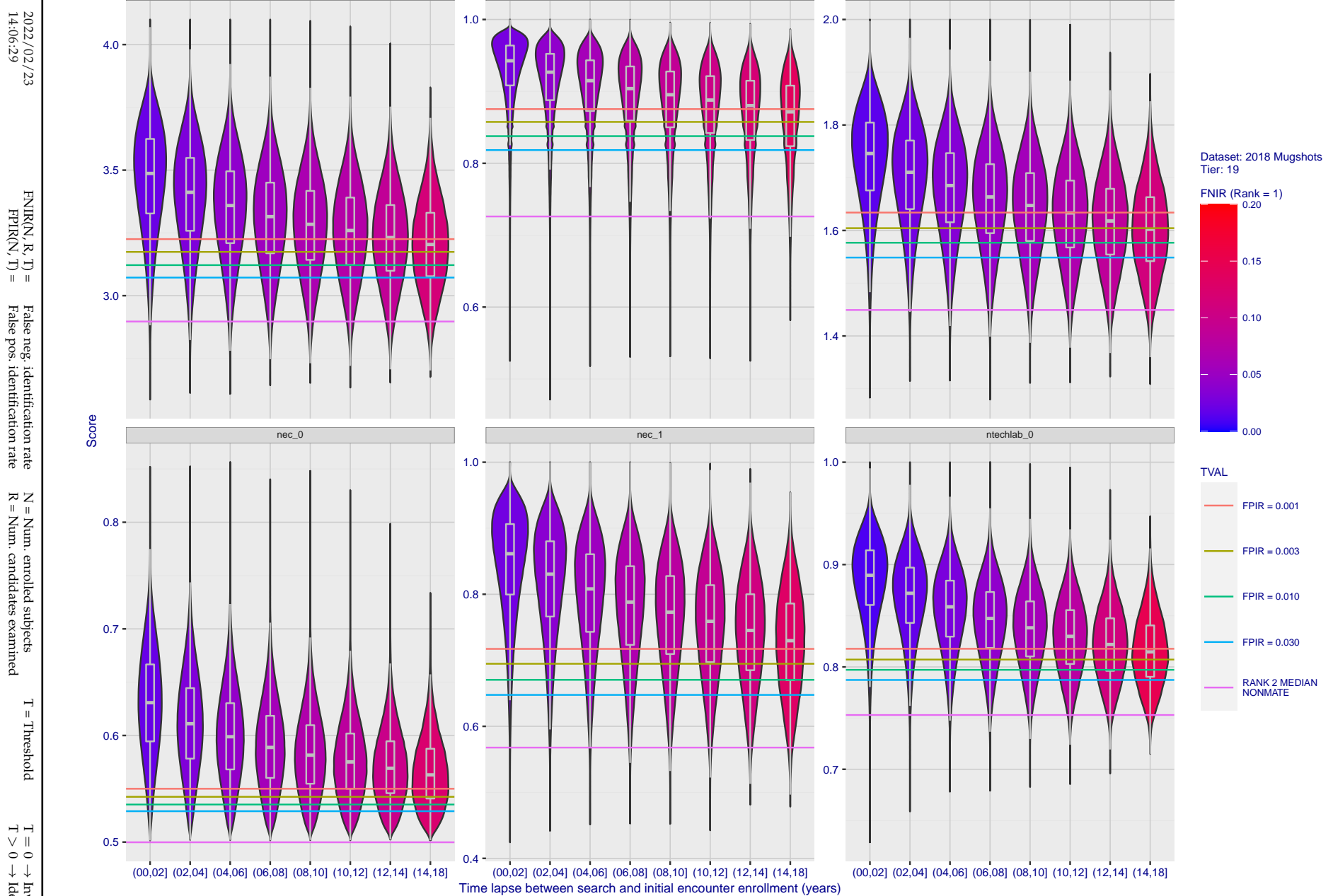


Figure 111: [FRVT-2018 Mugshot Ageing Dataset] Native mate scores vs. time-elapsed. The oldest image of each individual is enrolled. Thereafter, all more recent images are searched. Mated score distributions are computed over all searches noted in row 17 of Table 1 binned by number of years between search and initial enrollment.

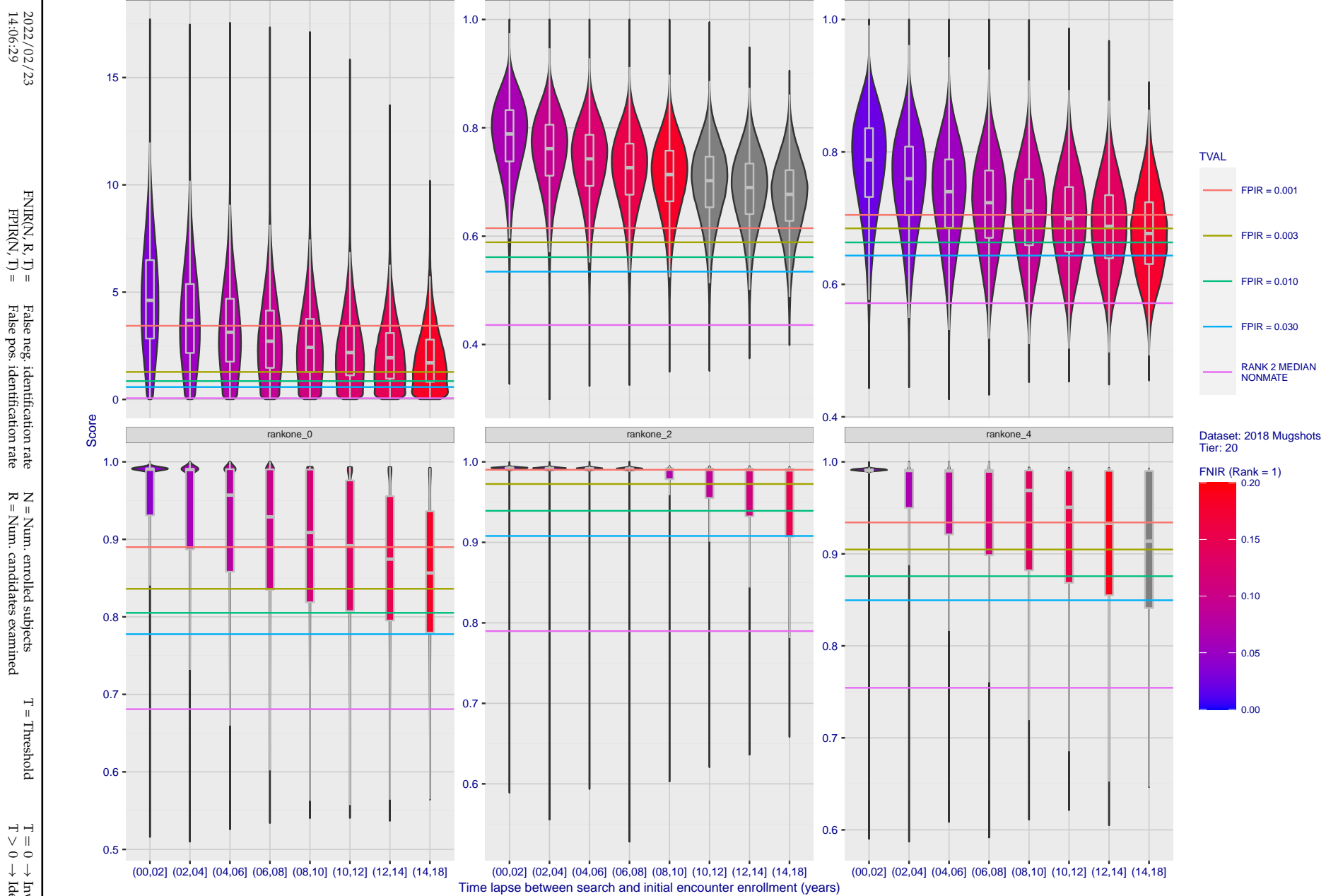


Figure 112: [FRVT-2018 Mugshot Ageing Dataset] Native mate scores vs. time-elapsed. The oldest image of each individual is enrolled. Thereafter, all more recent images are searched. Mated score distributions are computed over all searches noted in row 17 of Table 1 binned by number of years between search and initial enrollment.

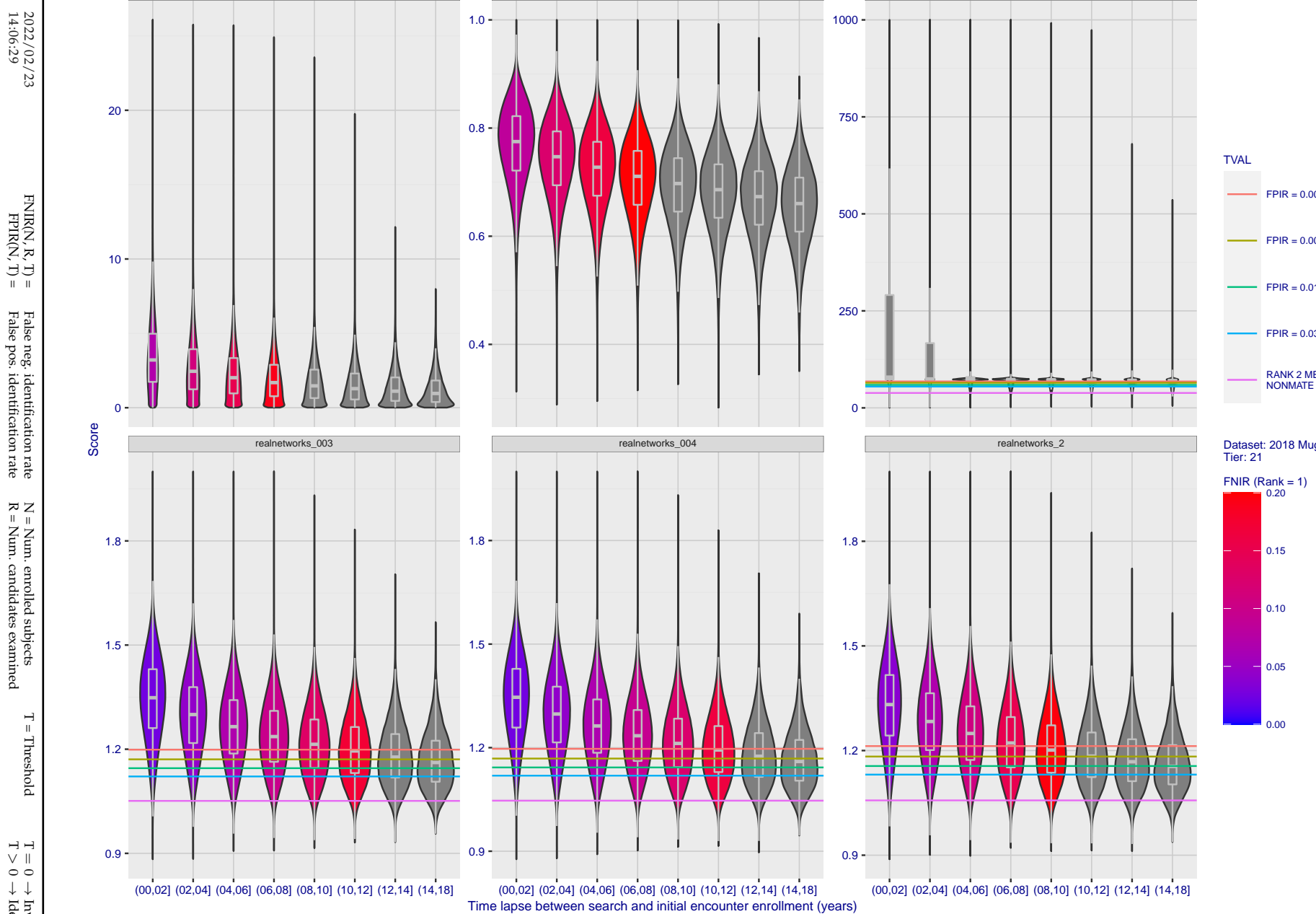


Figure 113: [FRVT-2018 Mugshot Ageing Dataset] Native mate scores vs. time-elapsed. The oldest image of each individual is enrolled. Thereafter, all more recent images are searched. Mated score distributions are computed over all searches noted in row 17 of Table 1 binned by number of years between search and initial enrollment.

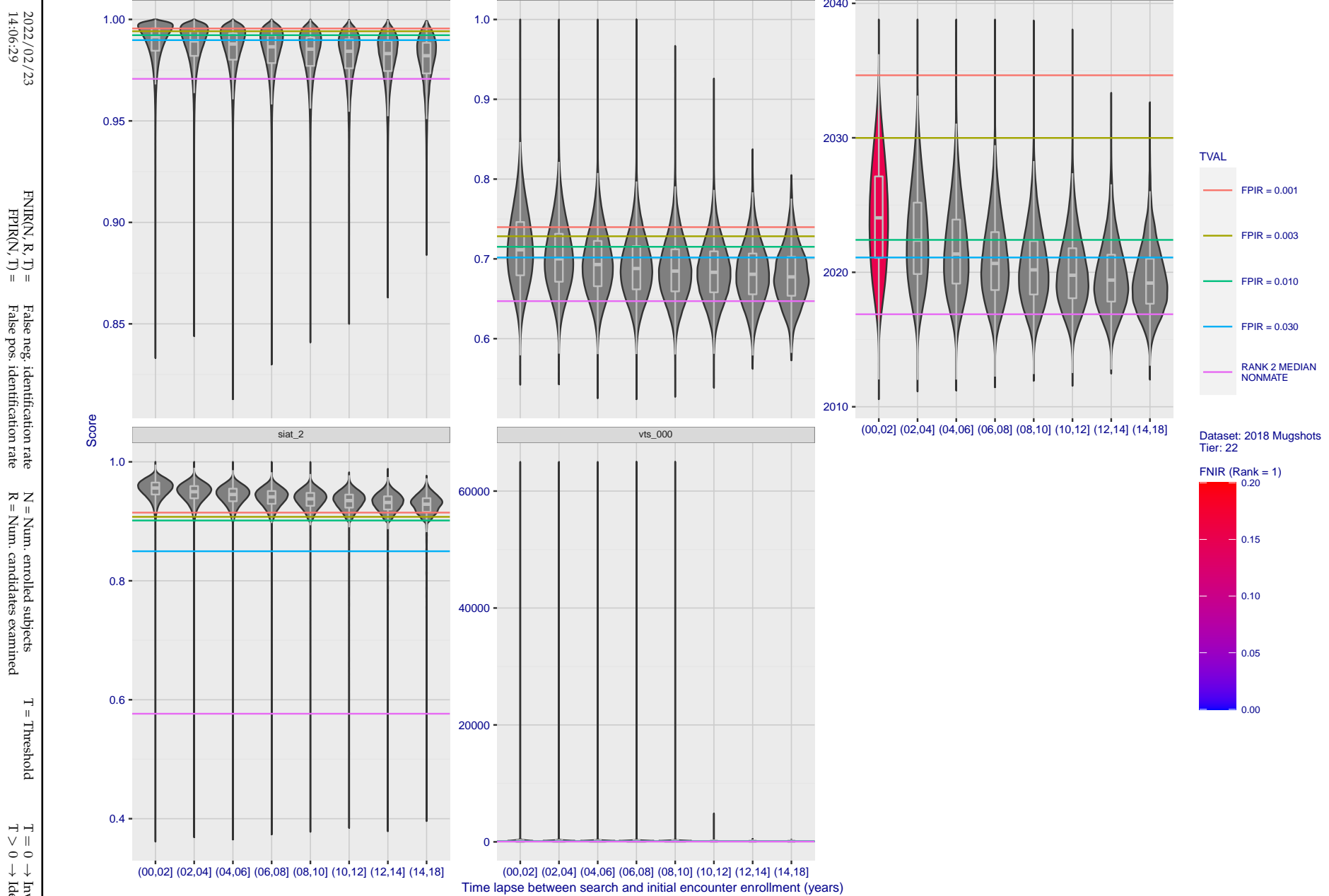


Figure 114: [FRVT-2018 Mugshot Ageing Dataset] Native mate scores vs. time-elapsed. The oldest image of each individual is enrolled. Thereafter, all more recent images are searched. Mated score distributions are computed over all searches noted in row 17 of Table 1 binned by number of years between search and initial enrollment.

Appendix C Effect of enrolling multiple images

2022/02/23
14:06:29FNIR(N, R, T) = False neg. identification rate
FPIR(N, T) = False pos. identification rateN = Num. enrolled subjects
R = Num. candidates examinedT = Threshold
T = 0 → Investigation

T > 0 → Identification

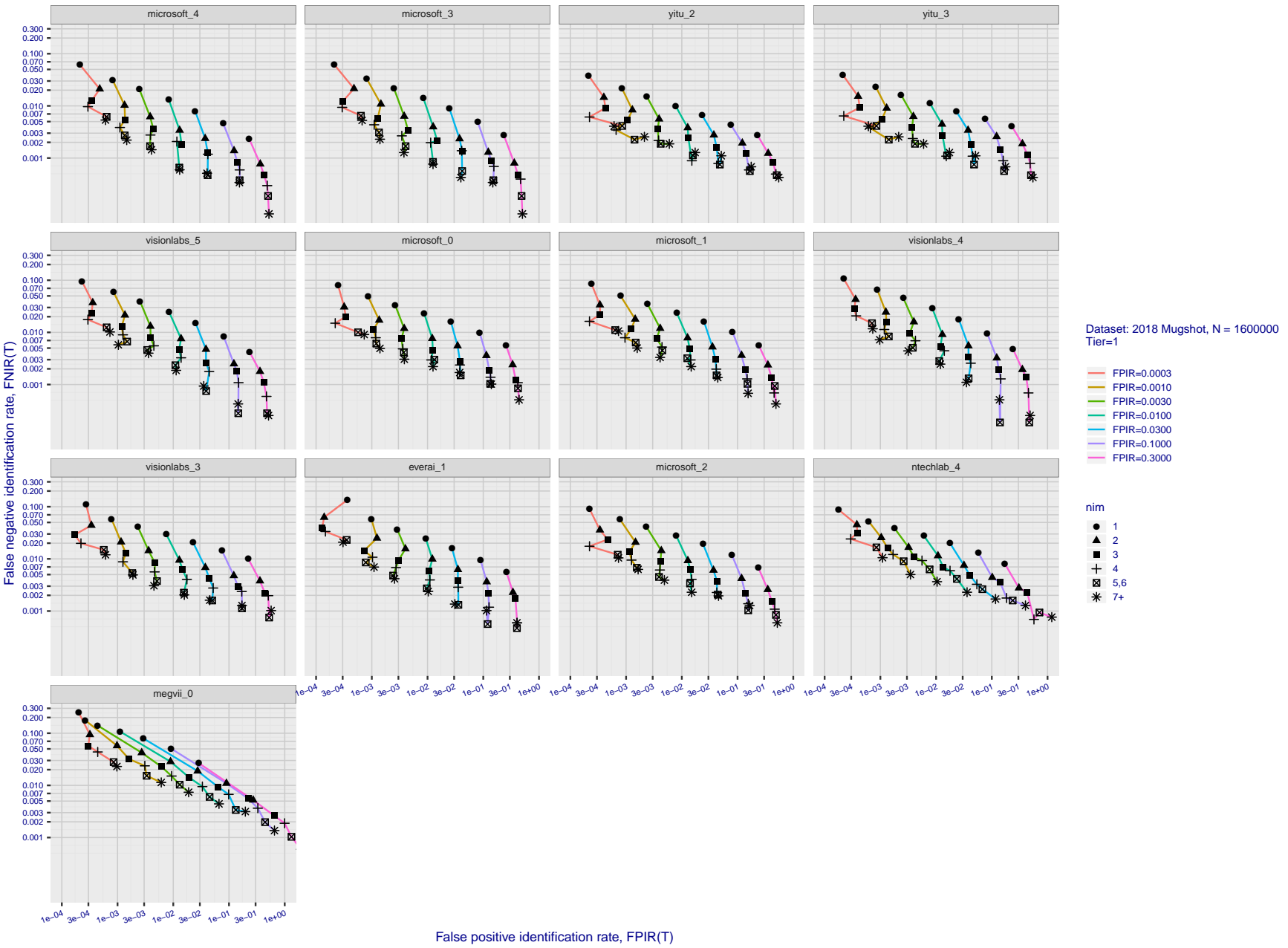


Figure 115: [FRVT-2018 Mugshot Dataset] Effect of enrolling multiple images for each identity. The plot shows an identification miss rates vs. false positive rates, at seven operating thresholds. The enrolled population size is fixed. The images are enrolled with lifetime-consolidation - see section 2.3.

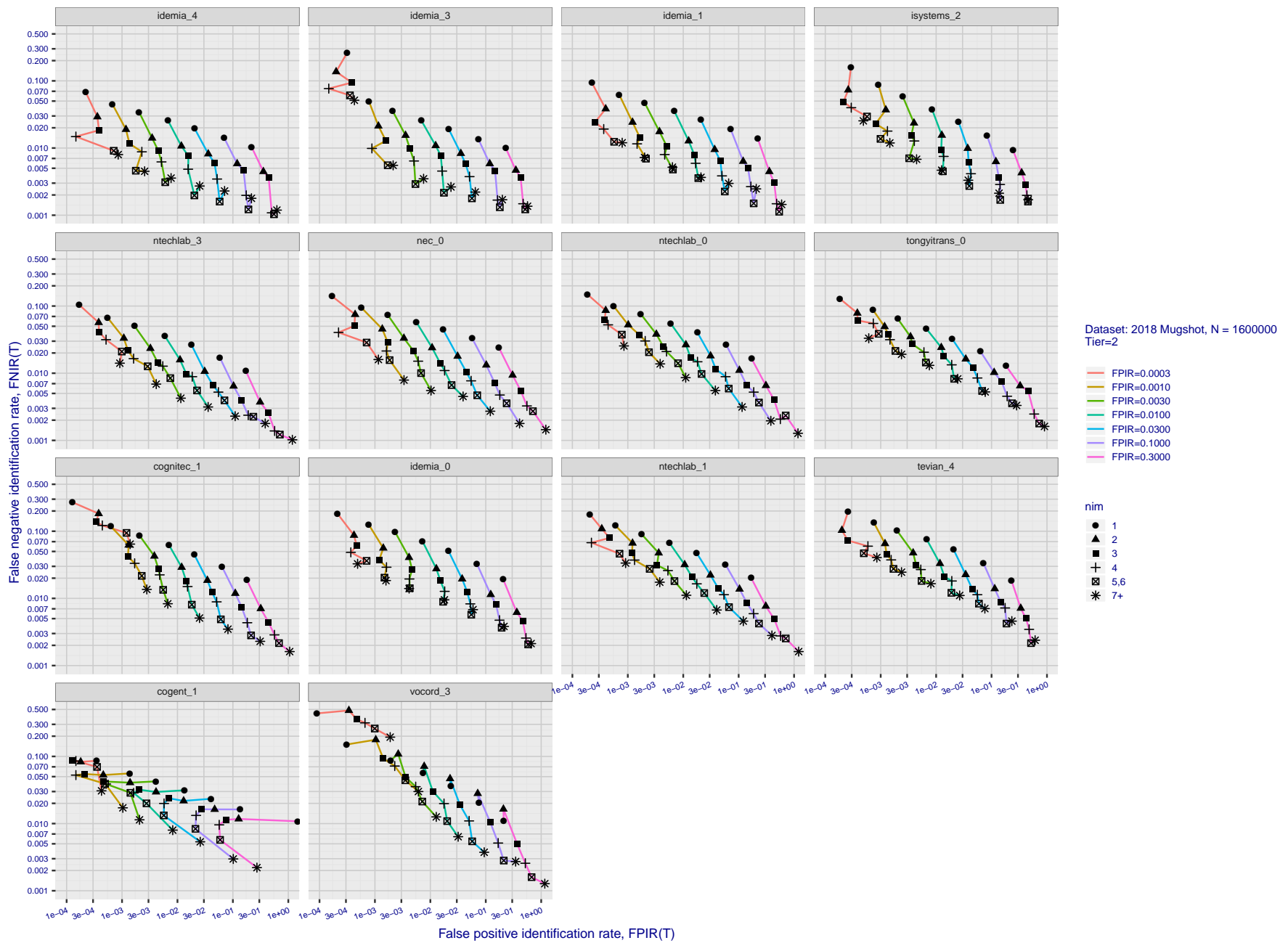


Figure 116: [FRVT-2018 Mugshot Dataset] Effect of enrolling multiple images for each identity. The plot shows an identification miss rates vs. false positive rates, at seven operating thresholds. The enrolled population size is fixed. The images are enrolled with lifetime-consolidation - see section 2.3.

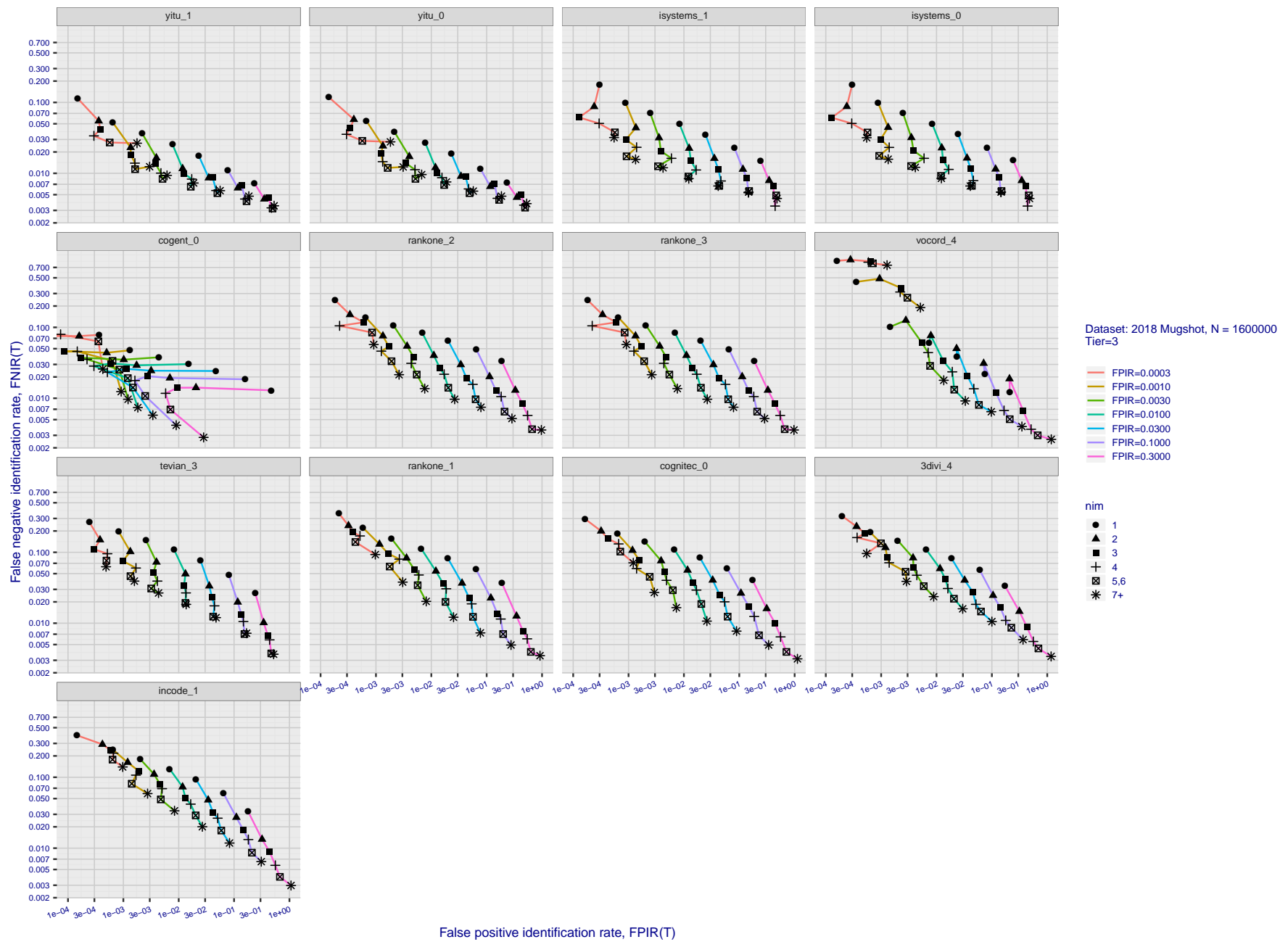


Figure 117: [FRVT-2018 Mugshot Dataset] Effect of enrolling multiple images for each identity. The plot shows an identification miss rates vs. false positive rates, at seven operating thresholds. The enrolled population size is fixed. The images are enrolled with lifetime-consolidation - see section 2.3.

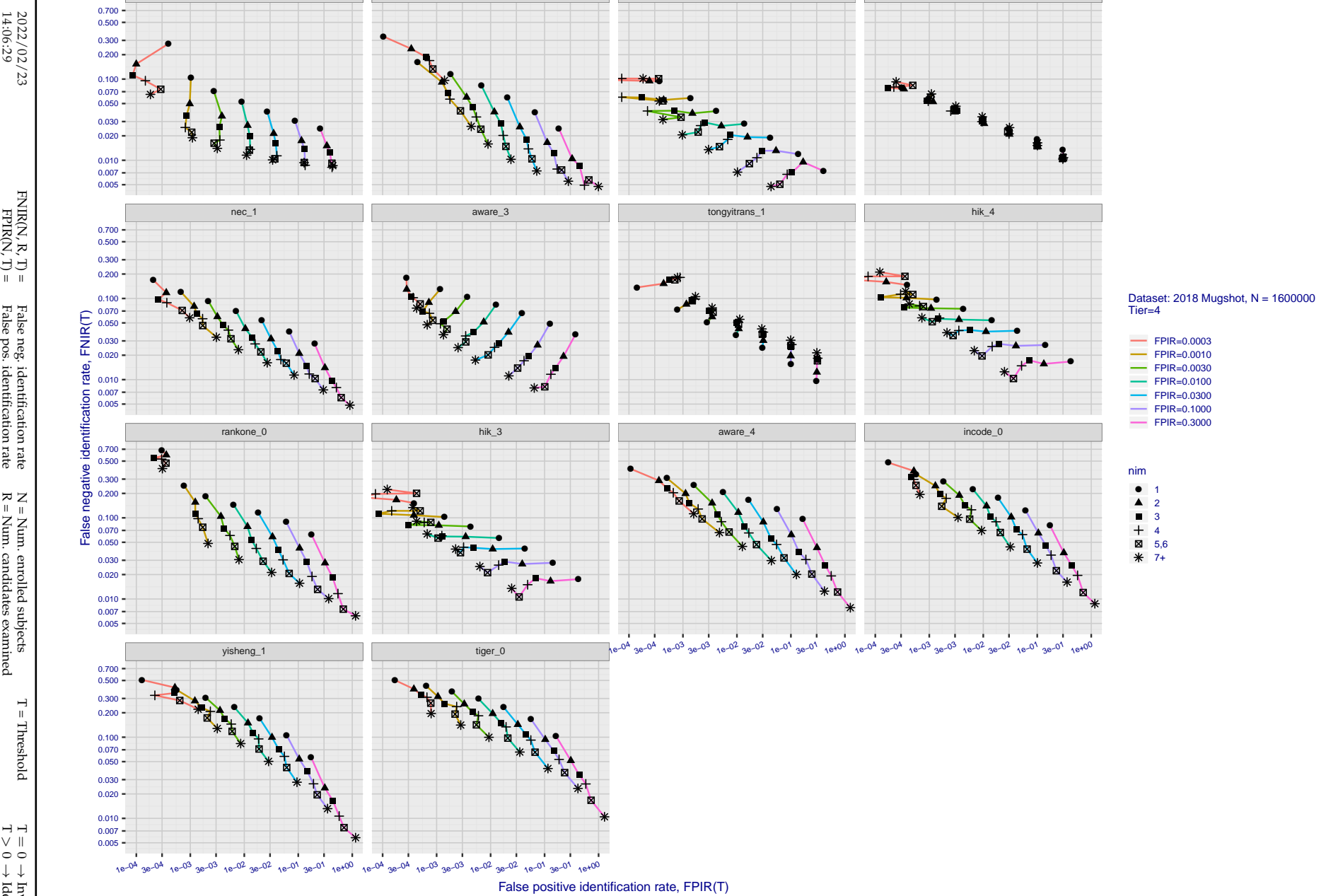


Figure 118: [FRVT-2018 Mugshot Dataset] Effect of enrolling multiple images for each identity. The plot shows an identification miss rates vs. false positive rates, at seven operating thresholds. The enrolled population size is fixed. The images are enrolled with lifetime-consolidation - see section 2.3.

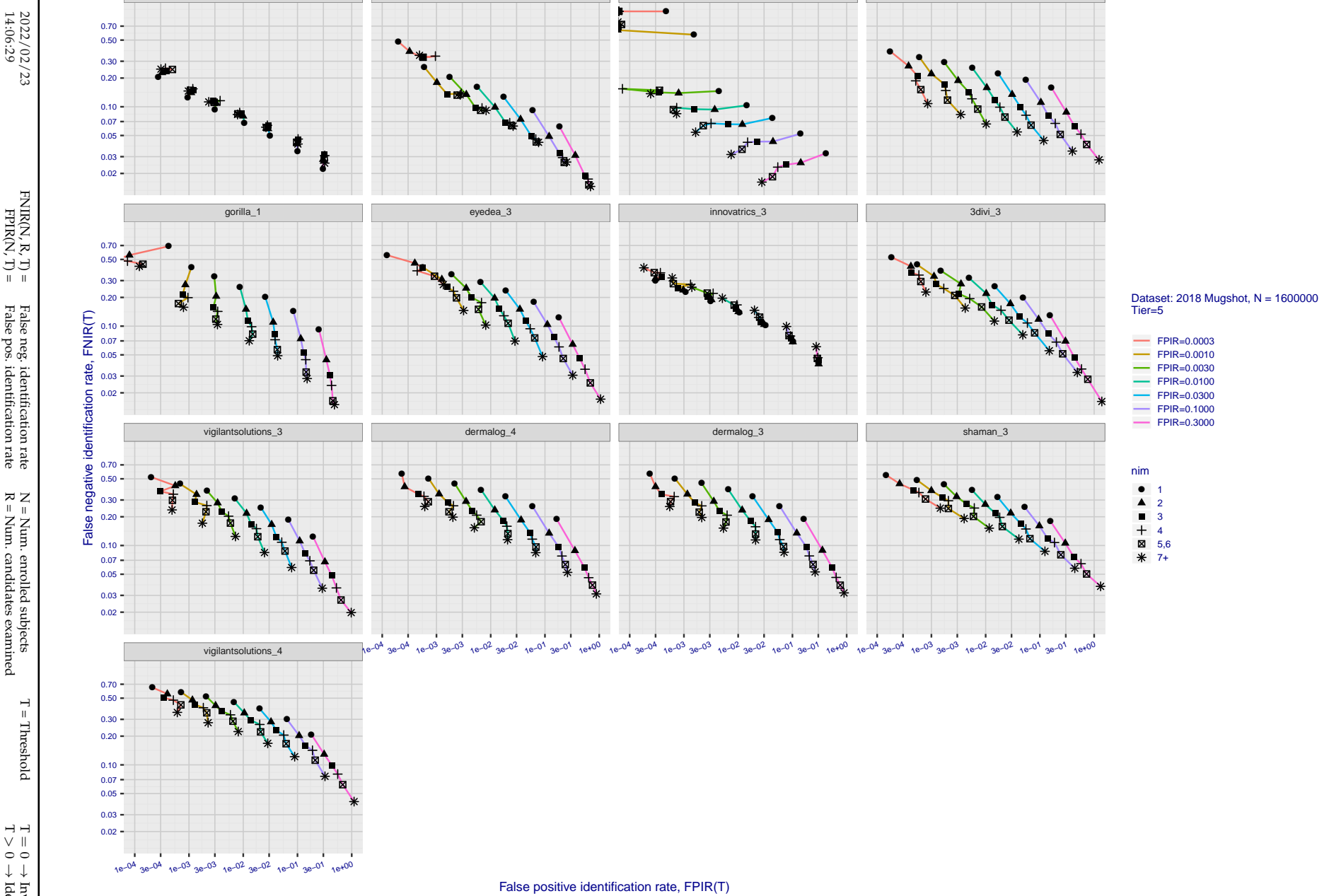


Figure 119: [FRVT-2018 Mugshot Dataset] Effect of enrolling multiple images for each identity. The plot shows an identification miss rates vs. false positive rates, at seven operating thresholds. The enrolled population size is fixed. The images are enrolled with lifetime-consolidation - see section 2.3.

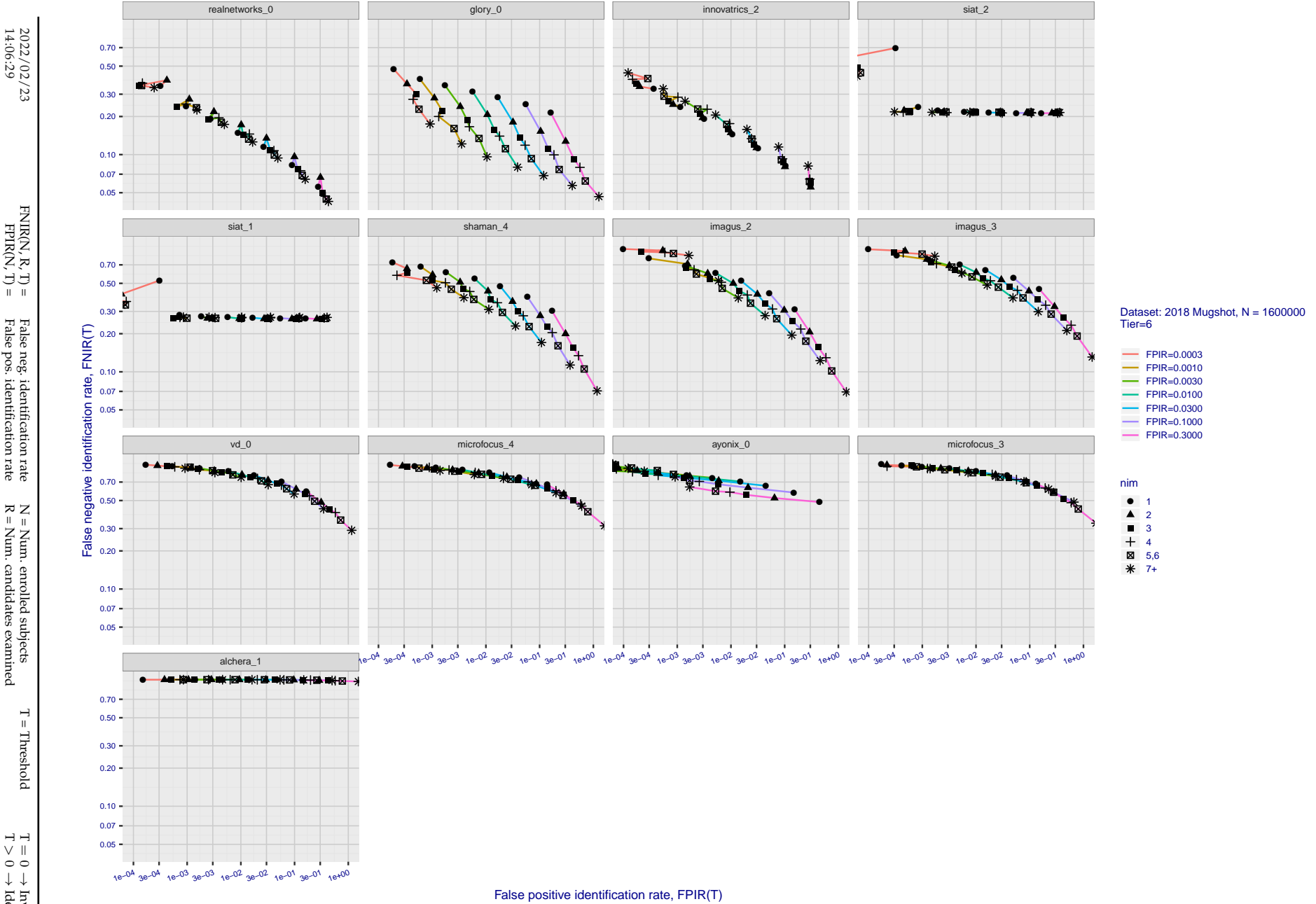


Figure 120: [FRVT-2018 Mugshot Dataset] Effect of enrolling multiple images for each identity. The plot shows an identification miss rates vs. false positive rates, at seven operating thresholds. The enrolled population size is fixed. The images are enrolled with lifetime-consolidation - see section 2.3.

Appendix D Accuracy with poor quality webcam images

2022/02/23 FNIR(N, R, T) = False neg. identification rate
FPIR(N, T) = False pos. identification rate
N = Num. enrolled subjects
R = Num. candidates examined
T = Threshold
 $T = 0 \rightarrow$ Investigation
 $T > 0 \rightarrow$ Identification

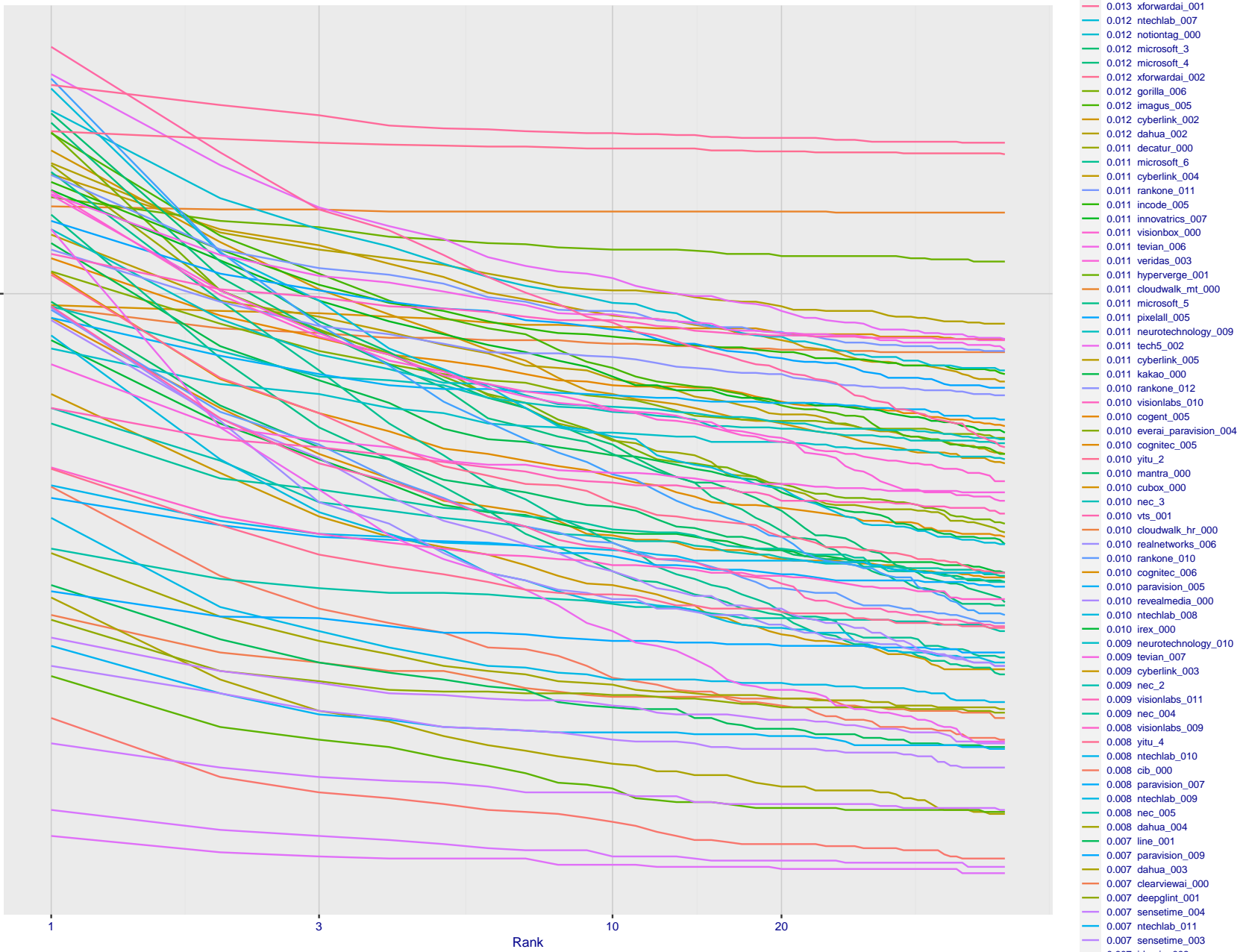


Figure 121: [Webcam Dataset] Identification miss rates vs. rank. The results apply to cross-domain recognition in which webcams are searched against enrolled mugshots. The FNIR values are higher than those for mugshot-mugshot identification due to low image resolution, lighting and less constrained subject pose in webcam images - see Figure 6.

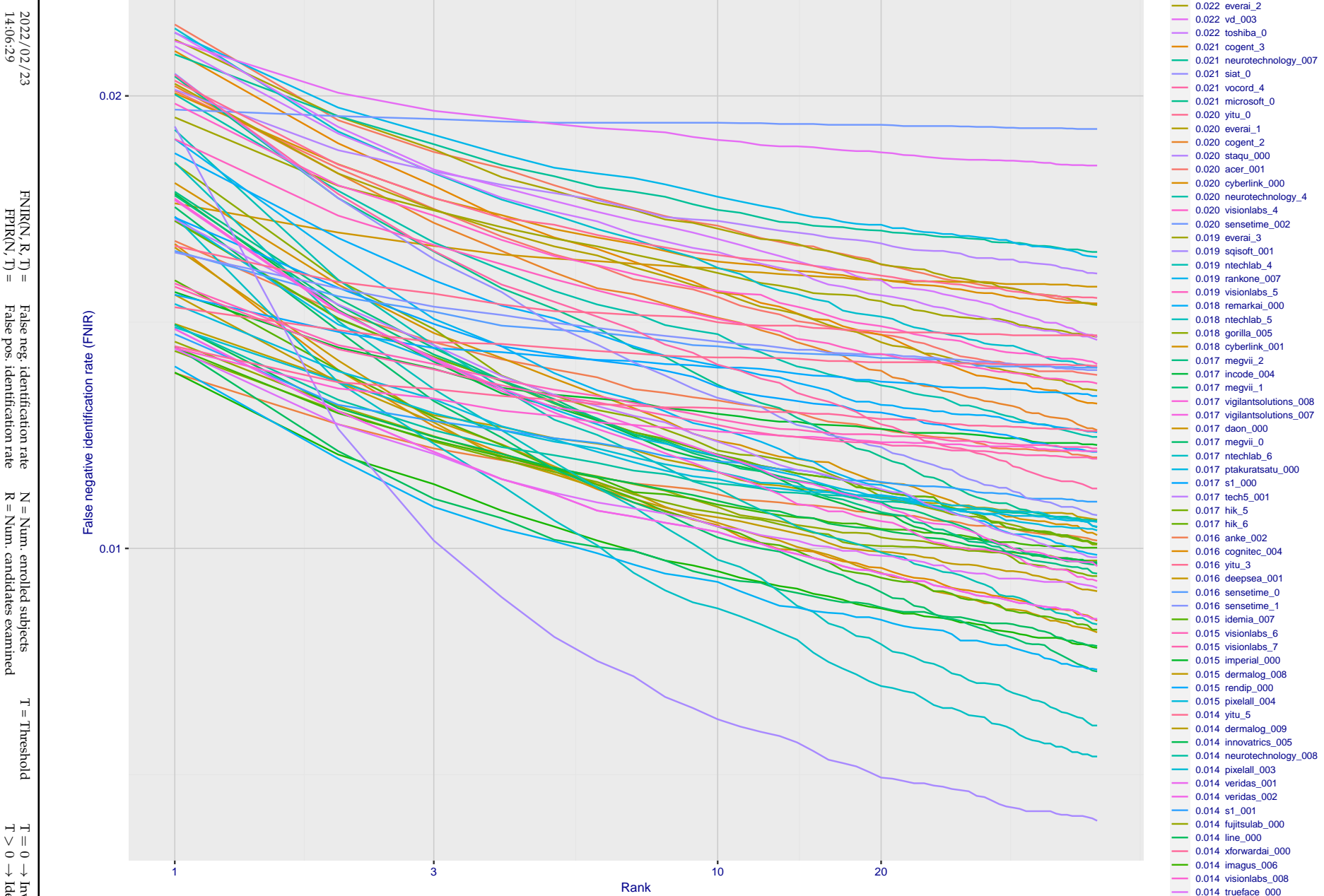


Figure 122: [Webcam Dataset] Identification miss rates vs. rank. The results apply to cross-domain recognition in which webcams are searched against enrolled mugshots. The FNIR values are higher than those for mugshot-mugshot identification due to low image resolution, lighting and less constrained subject pose in webcam images - see Figure 6.

2022/02/23

14:06:29

FNIR(N, R, T) = False neg. identification rate
FPFR(N, T) = False pos. identification rateN = Num. enrolled subjects
R = Num. candidates examinedT = Threshold
T = 0 → Investigation
T > 0 → Identification

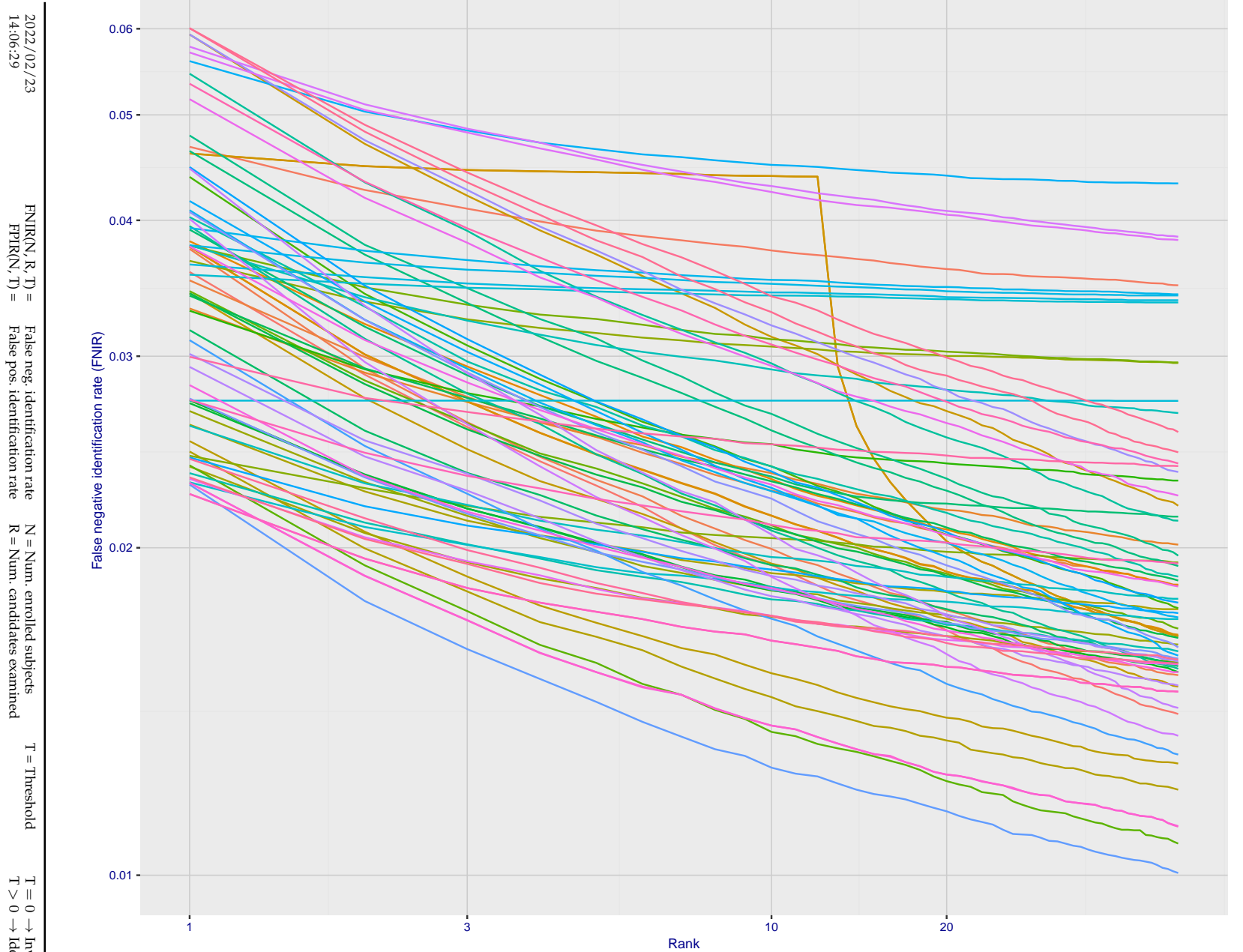


Figure 123: [Webcam Dataset] Identification miss rates vs. rank. The results apply to cross-domain recognition in which webcams are searched against enrolled mugshots. The FNIR values are higher than those for mugshot-mugshot identification due to low image resolution, lighting and less constrained subject pose in webcam images - see Figure 6.

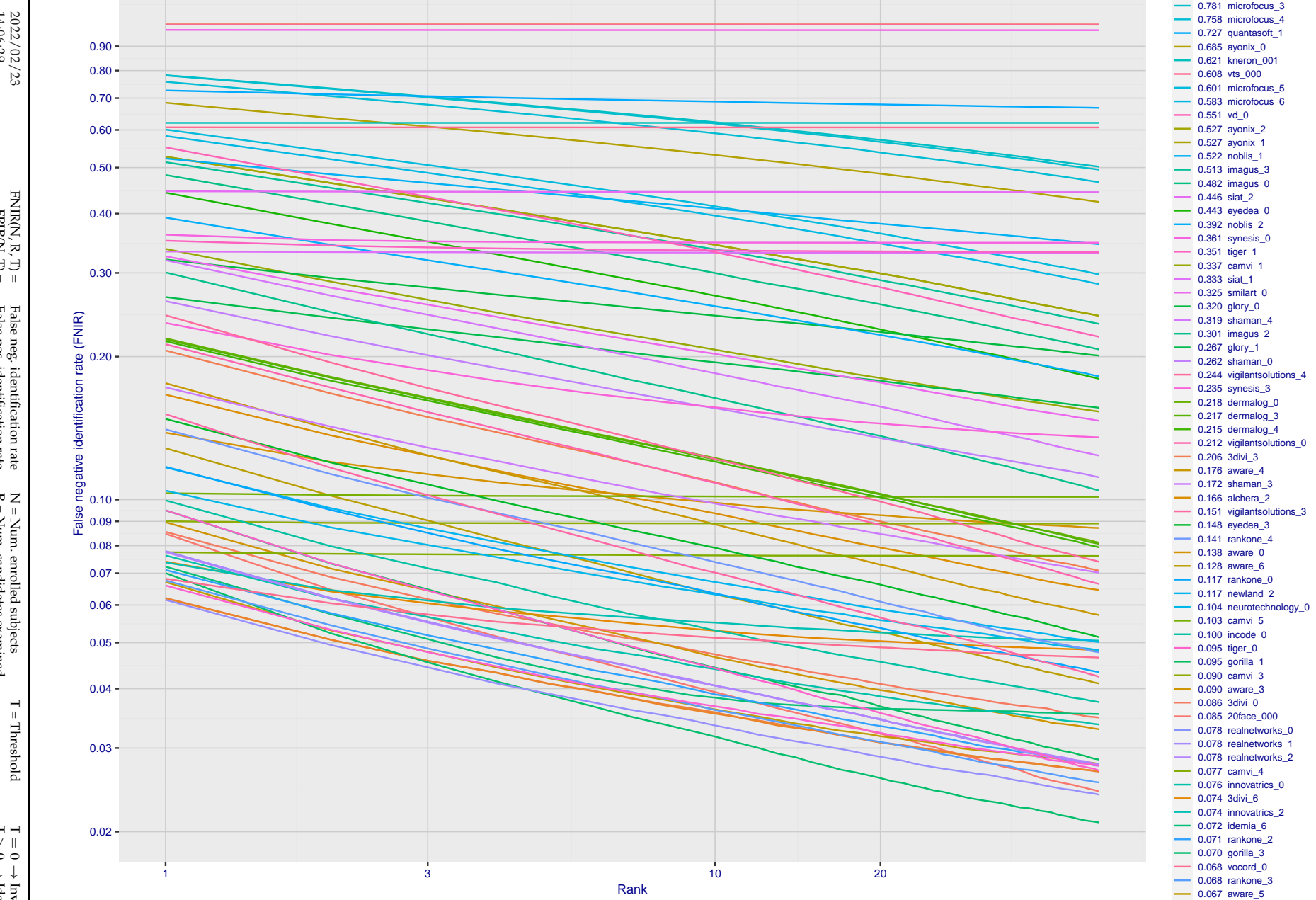


Figure 124: [Webcam Dataset] Identification miss rates vs. rank. The results apply to cross-domain recognition in which webcams are searched against enrolled mugshots. The FNIR values are higher than those for mugshot-mugshot identification due to low image resolution, lighting and less constrained subject pose in webcam images - see Figure 6.

2022/02/23 14:06:29	$\text{FNIR}(N, R, T) =$ $\text{FPTR}(N, T) =$	False neg. identification rate False pos. identification rate	$N =$ Num. enrolled subjects $R =$ Num. candidates examined	$T =$ Threshold $T > 0 \rightarrow$ Identification	$T = 0 \rightarrow$ Investigation
------------------------	---	--	--	---	-----------------------------------

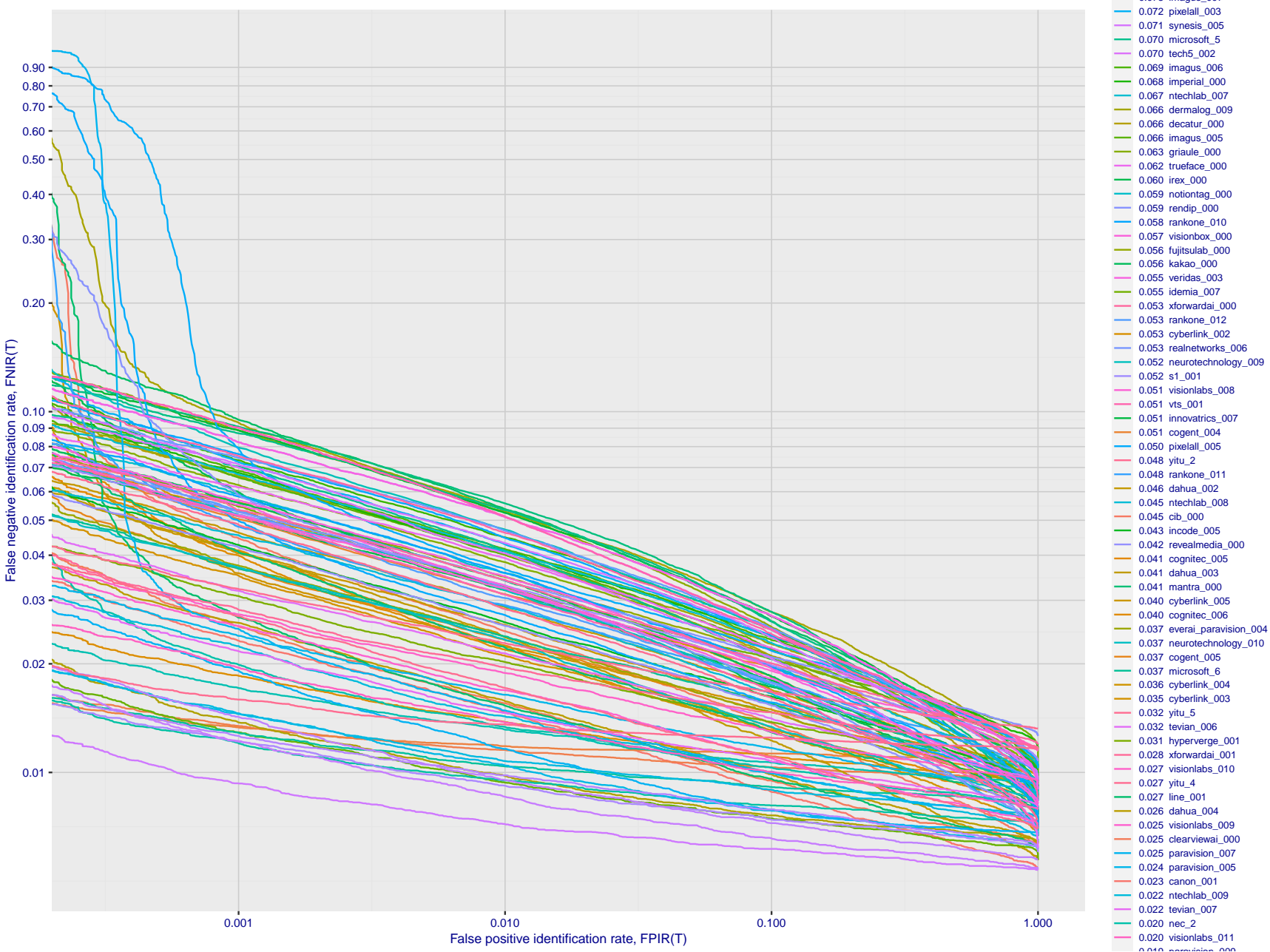


Figure 125: [Webcam Dataset] Identification miss rates vs. false positive rates. The results apply to cross-domain recognition in which webcams are searched against enrolled mugshots. The FNIR values are higher than those for mugshot-mugshot identification due to low image resolution, lighting and less constrained subject pose in webcam images - see Figure 6.

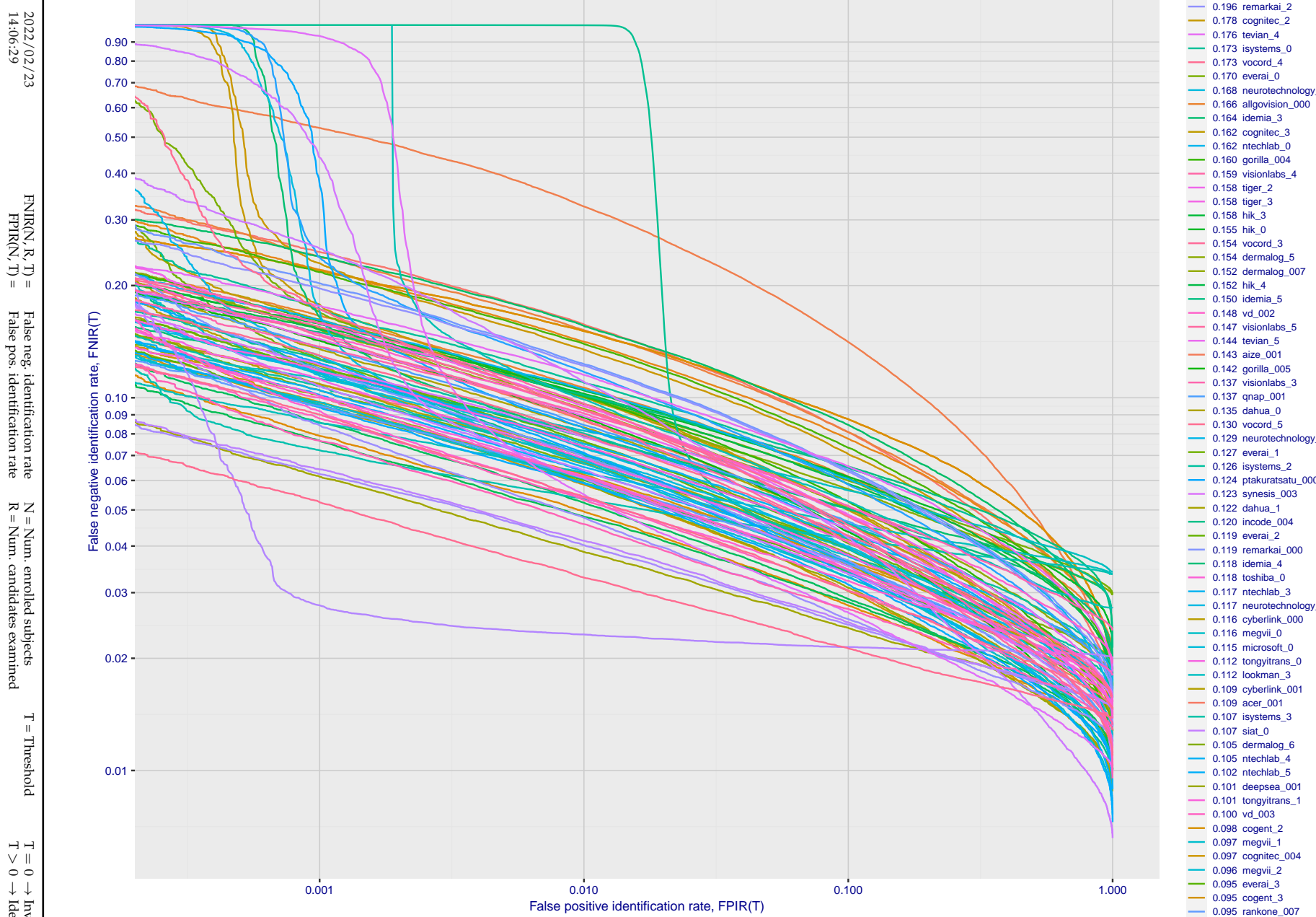


Figure 126: [Webcam Dataset] Identification miss rates vs. false positive rates. The results apply to cross-domain recognition in which webcams are searched against enrolled mugshots. The FNIR values are higher than those for mugshot-mugshot identification due to low image resolution, lighting and less constrained subject pose in webcam images - see Figure 6.

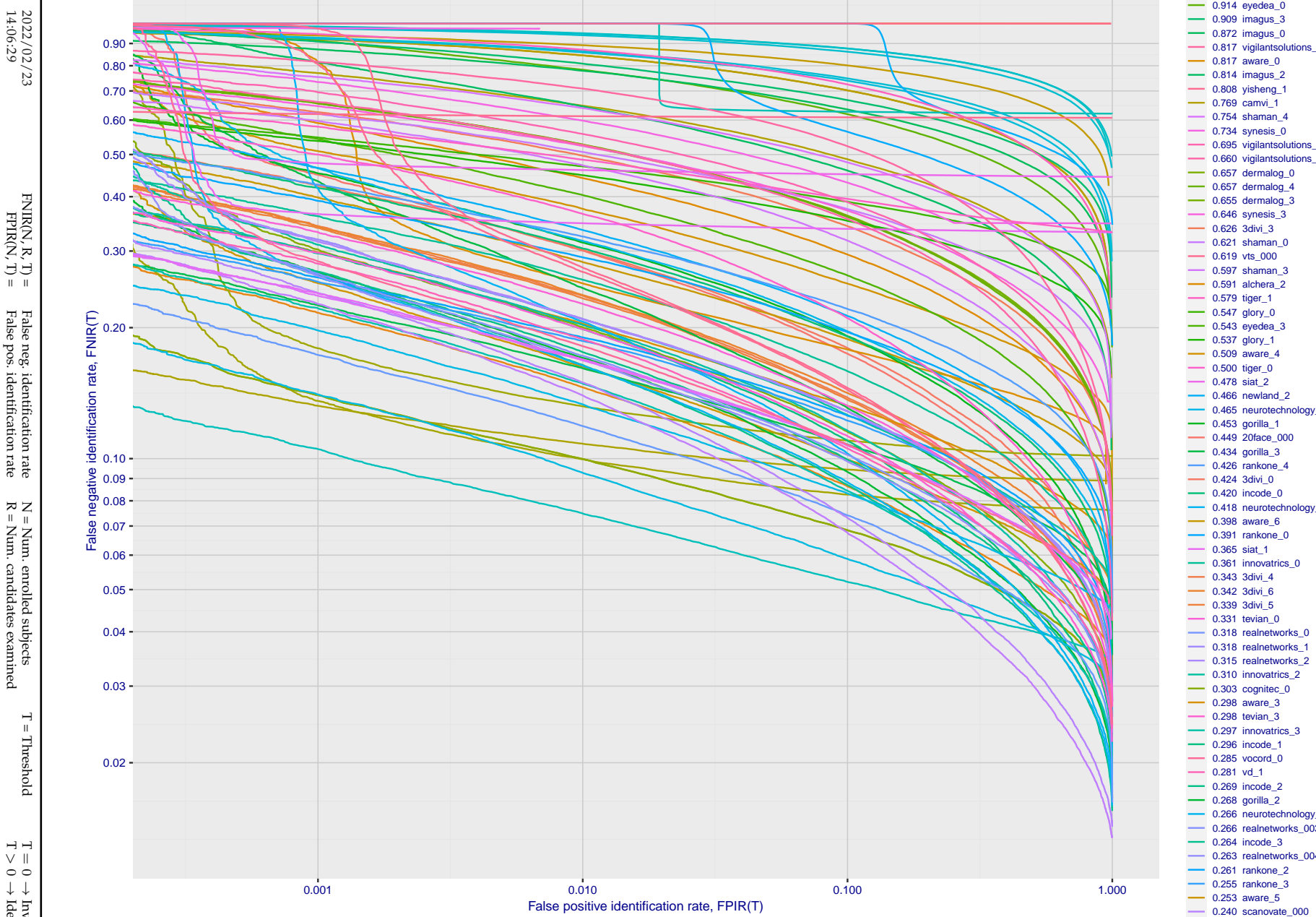


Figure 127: [Webcam Dataset] Identification miss rates vs. false positive rates. The results apply to cross-domain recognition in which webcams are searched against enrolled mugshots. The FNIR values are higher than those for mugshot-mugshot identification due to low image resolution, lighting and less constrained subject pose in webcam images - see Figure 6.

Appendix E Accuracy for profile-view to frontal recognition

Figures 128 - 130 gives accuracy results for searching 100 000 mated and 100 000 non-mated profile-view images against the same FRVT 2018 frontal enrollment dataset, $N = 1\,600\,000$, used in the main mugshot trials. This experiment corresponds to row-13 of Table 1. An example of profile-view image is given in Figure 7.

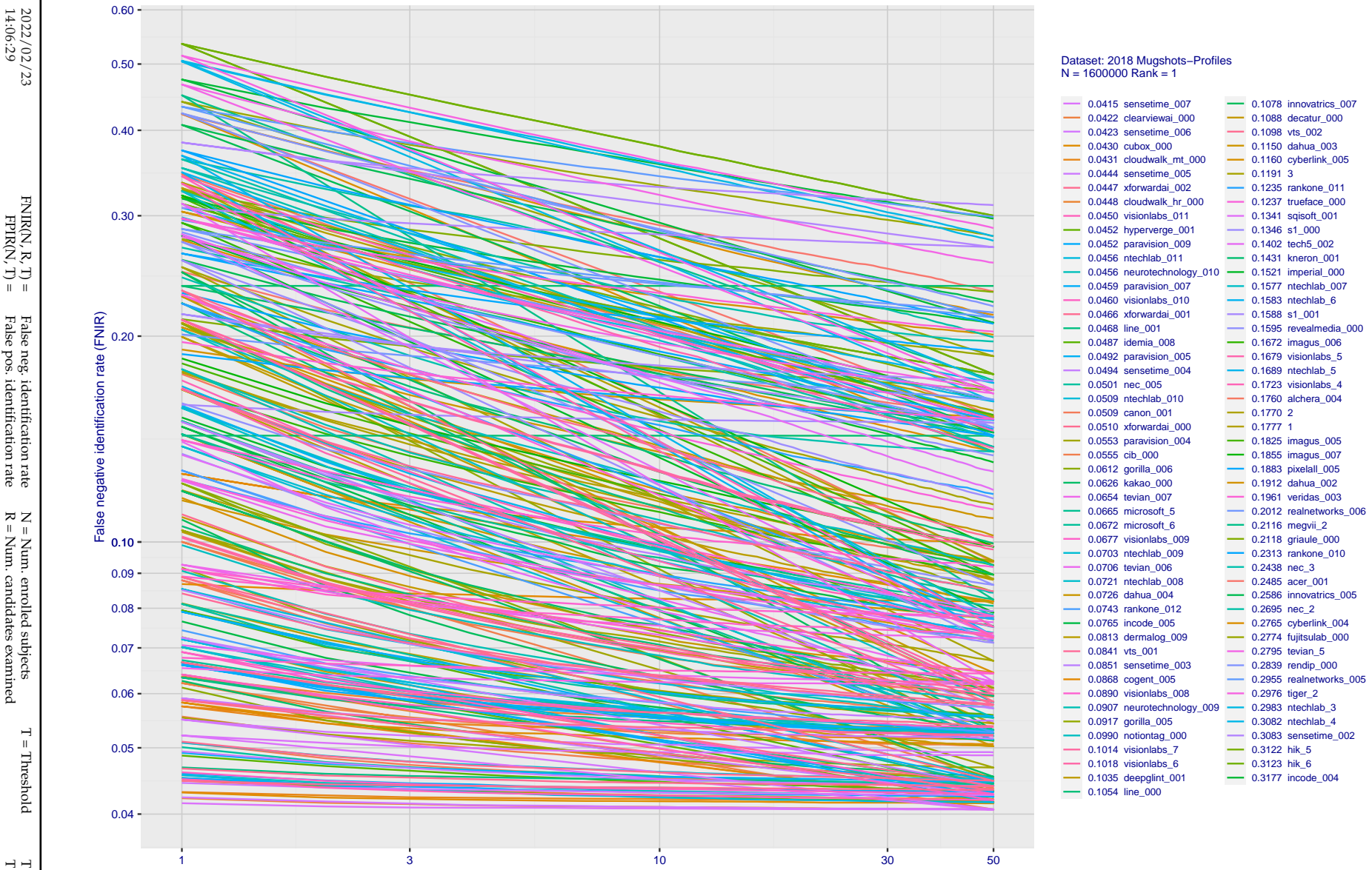


Figure 128: [Mugshot and profile-view dataset] Rank-based accuracy. For some of the more accurate Phase 3 algorithms the figure plots error tradeoff characteristics for frontal and profile-view searches into an enrolled set of $N = 1600\,000$ frontal images. Note that some algorithms fail on profile-view images with $\text{FNIR} \rightarrow 1$ - this evaluation did not ask developers to provide profile-view capability. Some algorithms, on the other hand, give FNIR approaching that for frontal-view searches using c. 2010 algorithms. The best result is that 91% of profile-view searches yield the correct mate at rank 1, and better than 94% in the top-50 candidates.

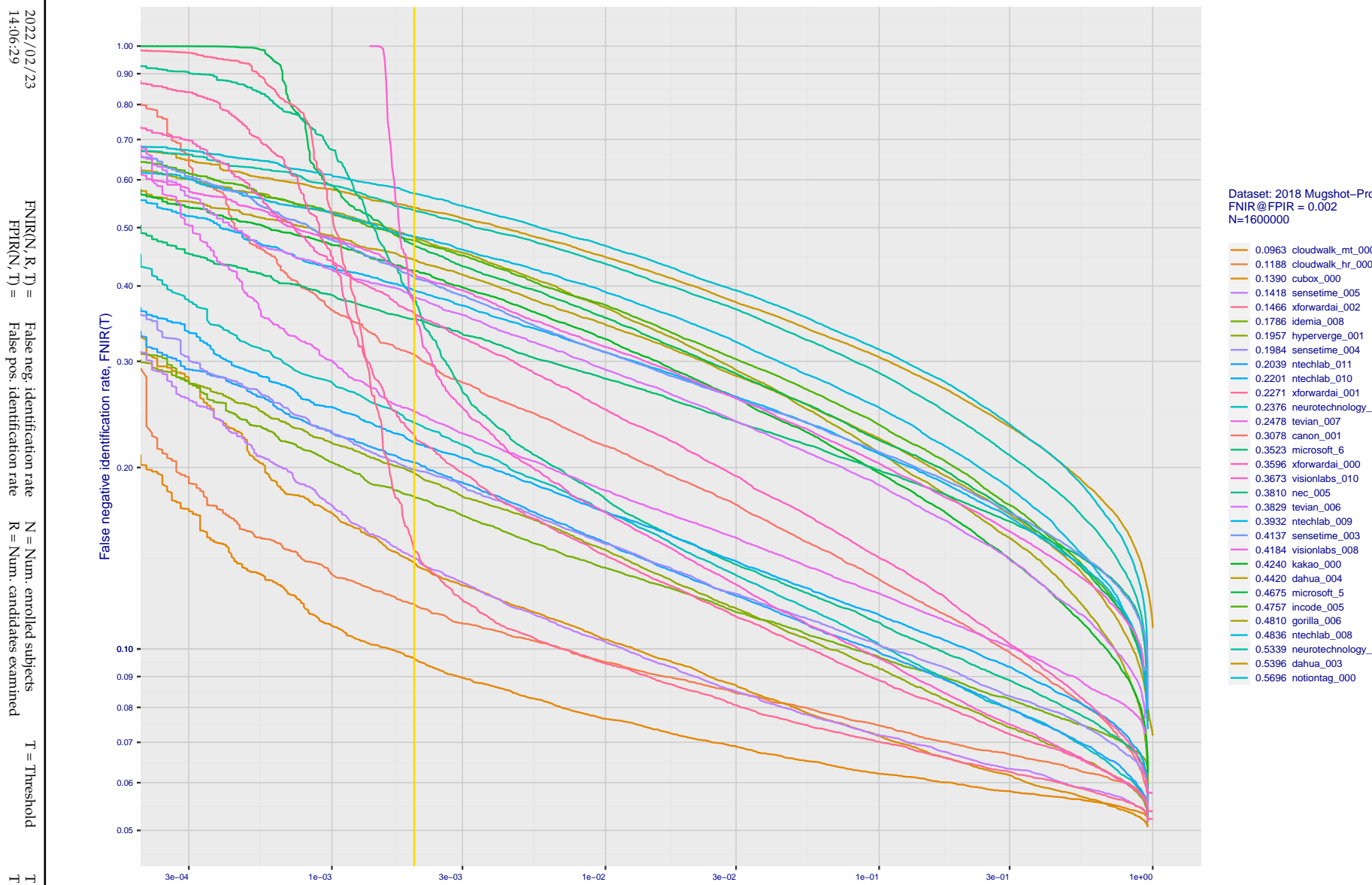


Figure 129: [Mugshot and profile-view dataset] Threshold-based accuracy. For some of the more accurate Phase 3 algorithms the figure plots error tradeoff characteristics for frontal and profile-view searches into an enrolled set of $N = 1\,600\,000$ frontal images. Note that some algorithms fail on profile-view images with $\text{FNIR} \rightarrow 1$ - this evaluation did not ask developers to provide profile-view capability. Some algorithms, on the other hand, give FNIR approaching that for frontal-view searches using c. 2010 algorithms.

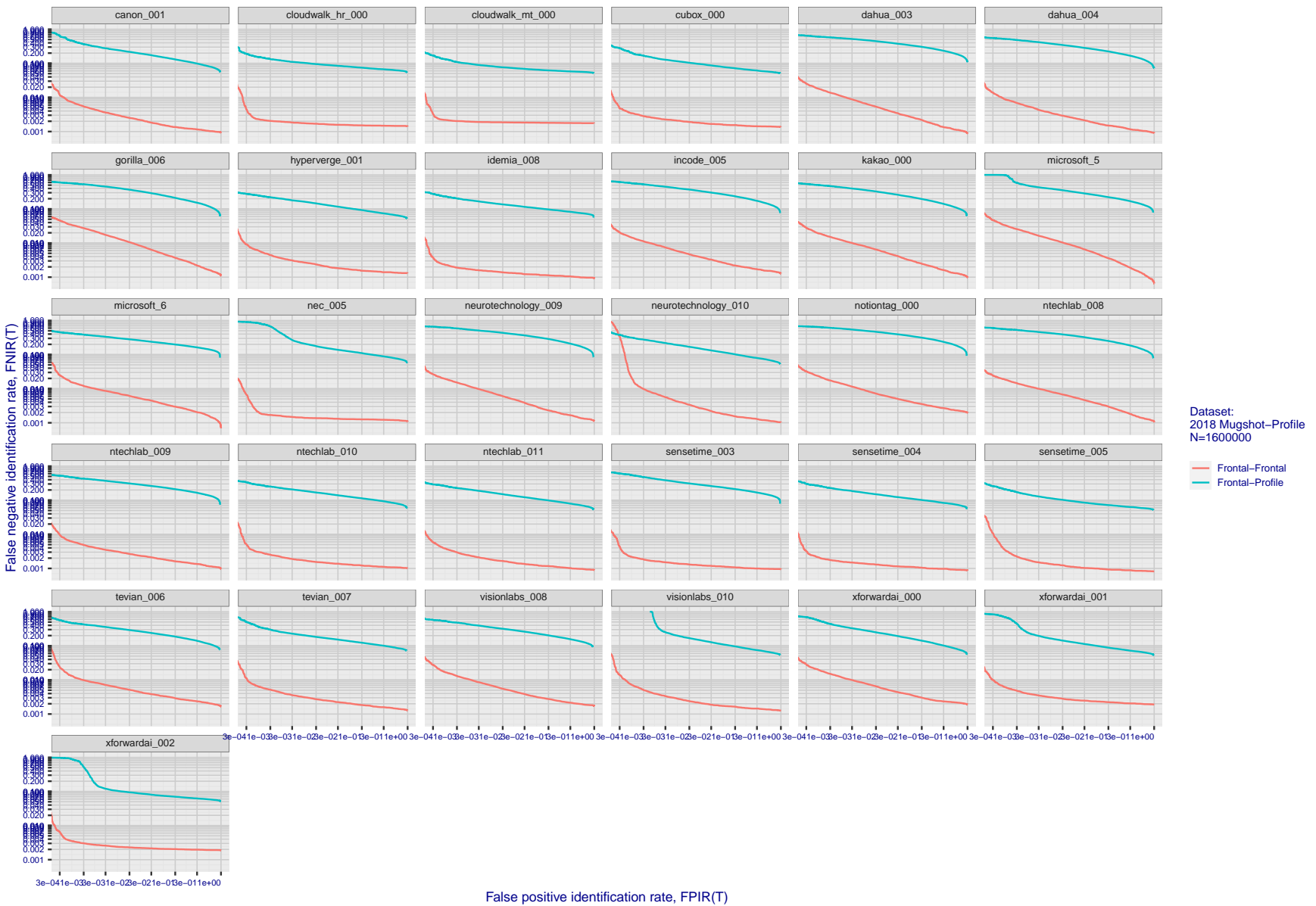


Figure 130: [Mugshot and profile-view dataset] Speed-accuracy tradeoff. For some of the more accurate Phase 3 algorithms the figure plots error tradeoff characteristics for frontal and profile-view searches into an enrolled set of $N = 1\,600\,000$ frontal images. Some algorithms fail on profile-view images with $\text{FNIR} \rightarrow 1$ - this evaluation did not ask developers to provide profile-view capability. Some algorithms, on the other hand, give FNIR approaching that for frontal-view searches using c. 2010 algorithms. Blue lines connect points of equal threshold from which it is evident that some algorithms would give markedly higher false positive outcomes if profile-view images were searched in a system configured for frontal searches. This would be a vulnerability in an access control system.

Appendix F Search duration

As in and prior tests, this section documents search speeds spanning three orders of magnitude. In applications where search volumes are high enough, this will have implications for hardware requirements especially for large N or when search duration is appreciably larger than the time it takes to prepare a template from the search image(s). Further, given very large (and growing) operational databases, the scalability of algorithms is important. It has been reported previously [8] that search duration can scale sublinearly with enrolled population size N. Further there has been considerable recent research on indexing, exact [13] and approximate nearest neighbor search [1,13] and fast-search [14,16].

Figure 131 charts the search duration measurements presented earlier in Tables 2 - 4.

- ▷ Most algorithms scale linearly. For those in that category, there is a wide range in speed with search durations ranging from 82 milliseconds for a 12 million gallery (for NEC-3) to more than 40 seconds (for Yitu-3, Toshiba-2) and even higher for less accurate algorithms.
- ▷ Some developers (Camvi, Dermalog, EverAI, Innovatrics, and Visionlabs) provide algorithms whose template search durations grow approximately logarithmically i.e. $T(N) \sim \log N$ with the constant a varying between implementations. In the figure this model is fit using the point $T(1) = 0$, and $T(640\,000)$. This very sublinear behaviour affords extremely fast search times in very large galleries. One caveat for the sublinear algorithms is that their fast-search data structures can require considerable computation time - on the order of hours - for N in the millions, and this scales mildly super-linearly, i.e. $O(N^b)$, $b > 1$. There are exceptions: the Camvi algorithms take minutes; and Innovatrics' scale sublinearly.

2022/02/23
14:06:29
 $\text{FNIR}(\text{N}, \text{R}, \text{T}) =$
 $\text{FPRI}(\text{N}, \text{T}) =$

False neg. identification rate
False pos. identification rate

$\text{N} = \text{Num. enrolled subjects}$
 $\text{R} = \text{Num. candidates examined}$

$\text{T} = \text{Threshold}$
 $\text{T} > 0 \rightarrow \text{Identification}$

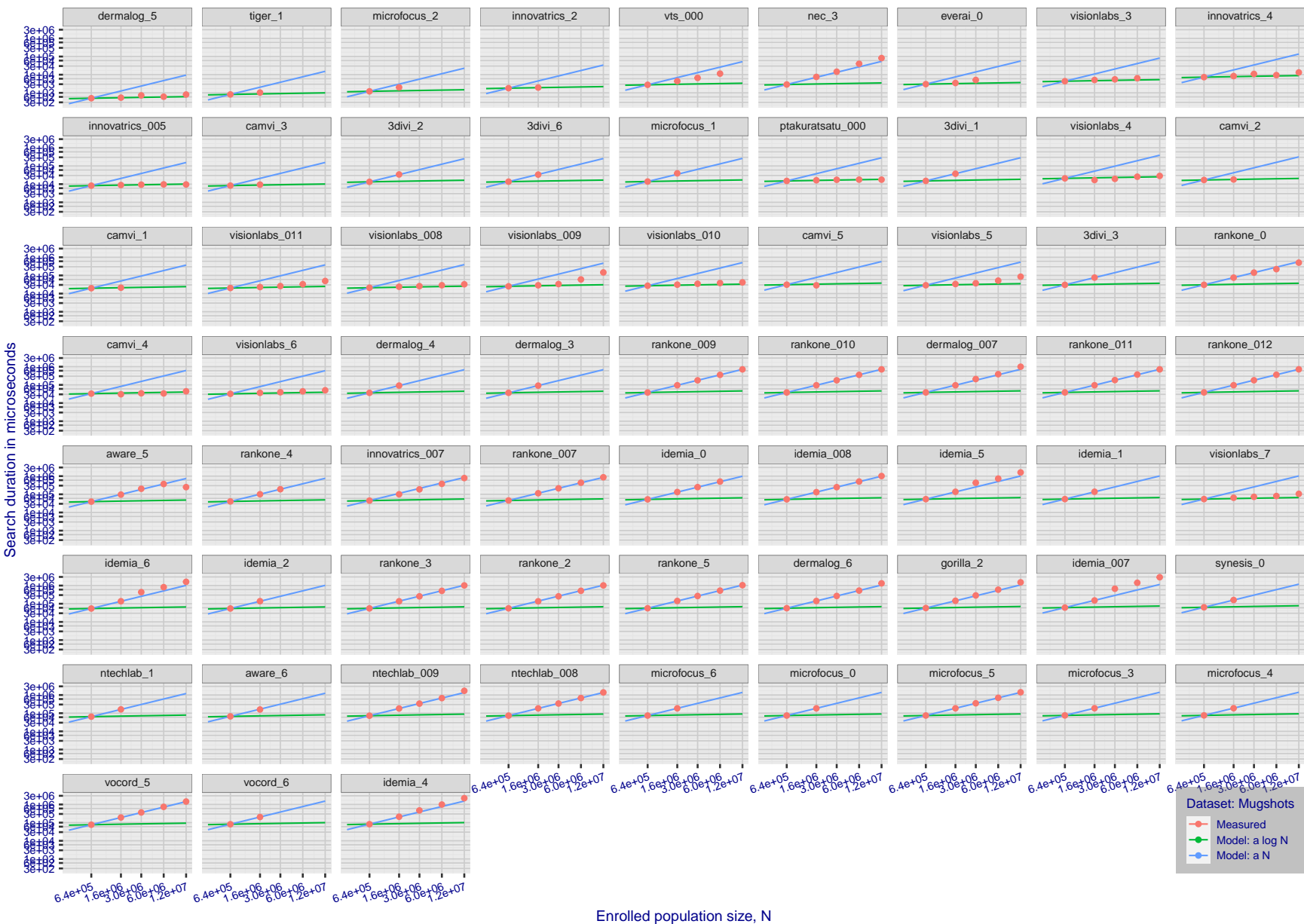
2022/02/23
14:06:29FNIR(N, R, T) = False neg. identification rate
FPFR(N, T) = False pos. identification rateN = Num. enrolled subjects
R = Num. candidates examined
T = ThresholdT = 0 → Investigation
T > 0 → Identification

Figure 131: [Mugshot Dataset] Search duration vs. enrolled population size. In red are the actual point durations measured on a single c. 2016 core. The blue shows linear growth from $N = 640\,000$. The green line shows logarithmic growth from that point to $N = 1\,600\,000$. Note the sublinear growth from algorithms from Camvi, Dermalog, EverAI, Innovatrics, and Visionlabs. The tiger_1 algorithm is also sublinear, but inaccurate and inoperable at $N \geq 3000000$. This capability sometimes comes at the additional expense of converting a linear gallery data structure into whatever fast-search data structure is used. Note that search times are sometimes dominated by the template generation times shown in Table 22.

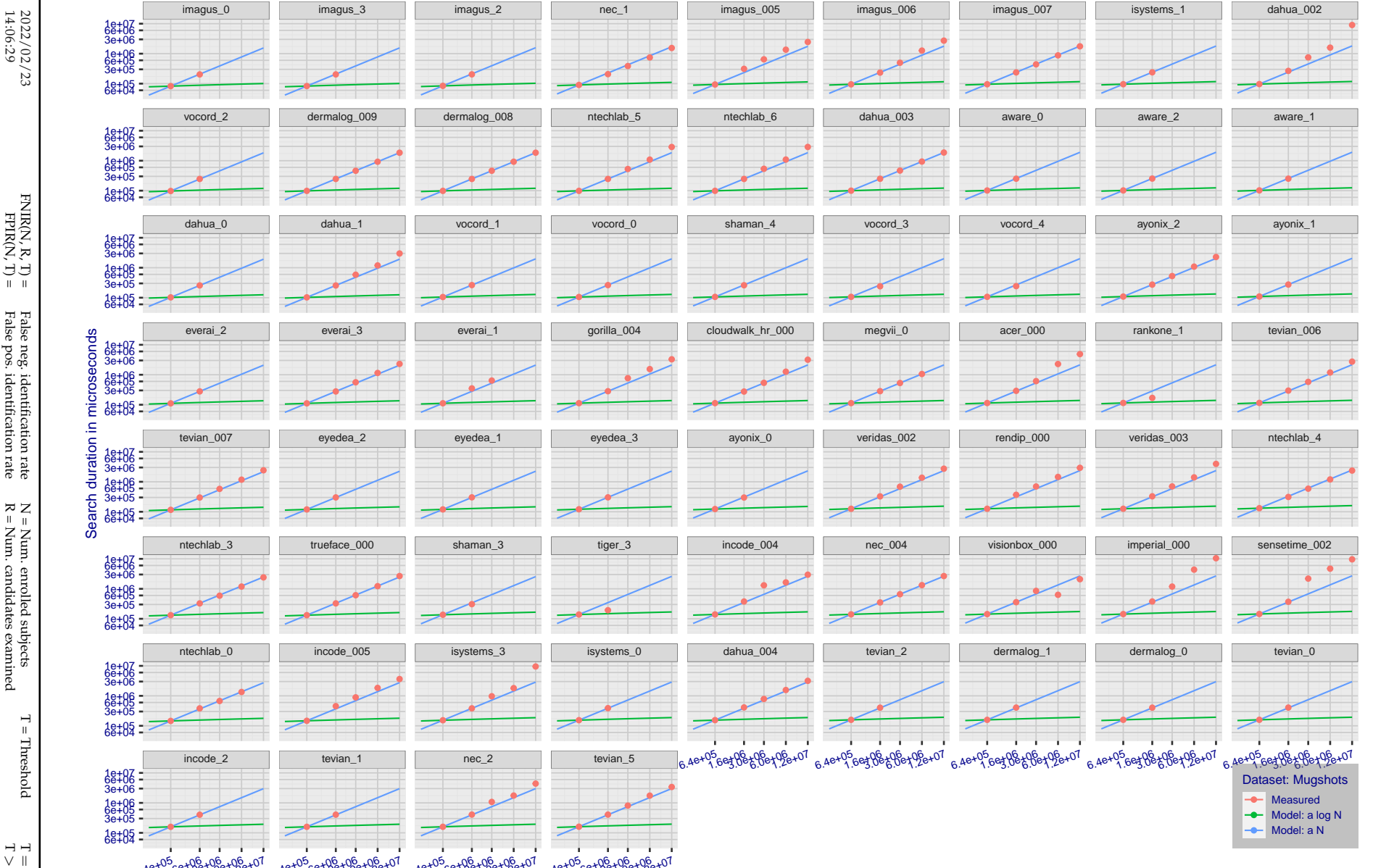


Figure 132: [Mugshot Dataset] Search duration vs. enrolled population size. In red are the actual point durations measured on a single c. 2016 core. The blue shows linear growth from $N = 640\,000$. The green line shows logarithmic growth from that point to $N = 1\,600\,000$. Note the sublinear growth from algorithms from Camvi, Dermalog, EverAI, Innovatrics, and Visionlabs. The tiger_1 algorithm is also sublinear, but inaccurate and inoperable at $N \geq 3000000$. This capability sometimes comes at the additional expense of converting a linear gallery data structure into whatever fast-search data structure is used. Note that search times are sometimes dominated by the template generation times shown in Table 22.

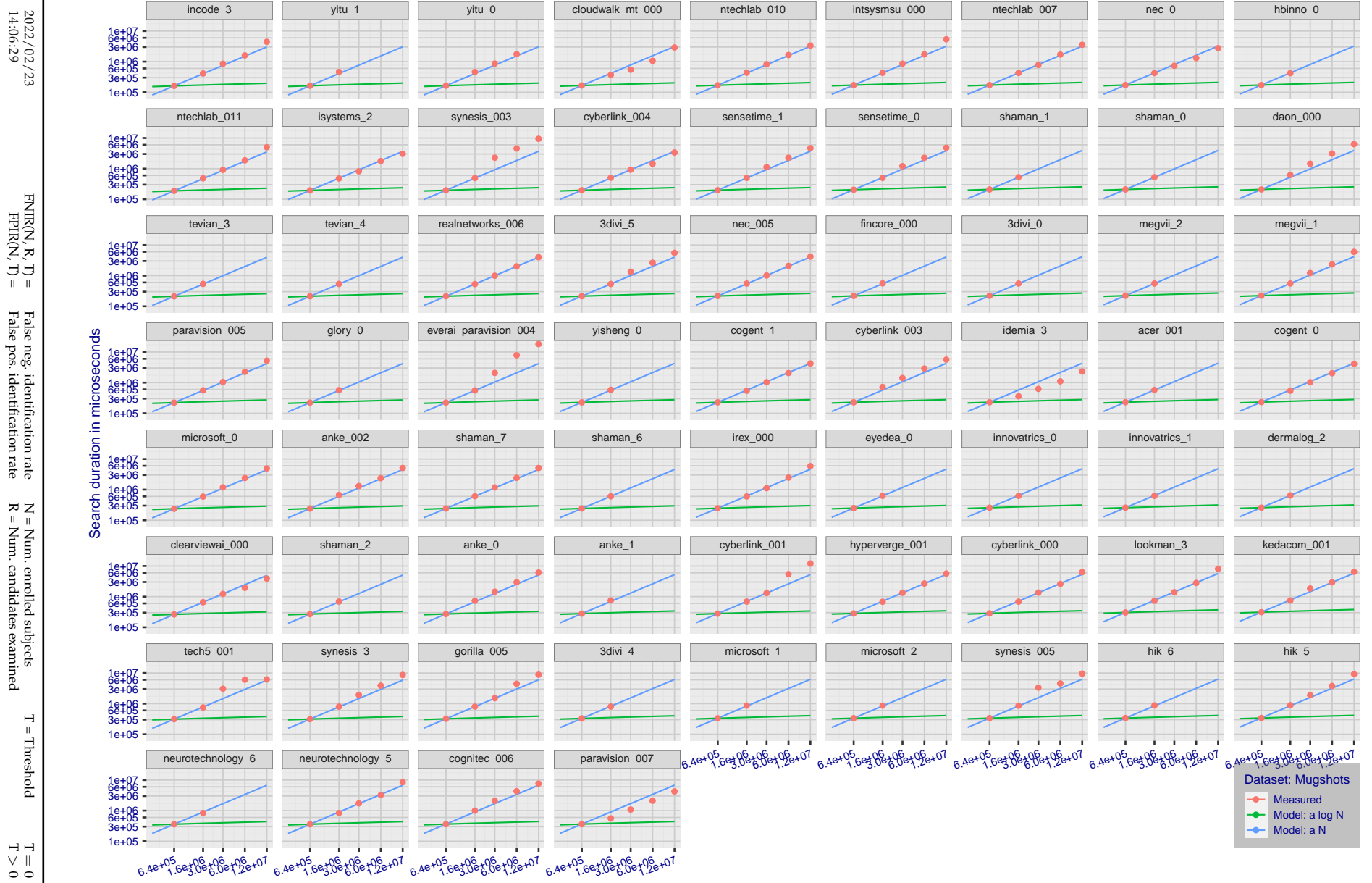


Figure 133: [Mugshot Dataset] Search duration vs. enrolled population size. In red are the actual point durations measured on a single c. 2016 core. The blue shows linear growth from $N = 640\,000$. The green line shows logarithmic growth from that point to $N = 1\,600\,000$. Note the sublinear growth from algorithms from Camvi, Dermalog, EverAI, Innovatrics, and Visionlabs. The tiger_1 algorithm is also sublinear, but inaccurate and inoperable at $N \geq 3000000$. This capability sometimes comes at the additional expense of converting a linear gallery data structure into whatever fast-search data structure is used. Note that search times are sometimes dominated by the template generation times shown in Table 22.

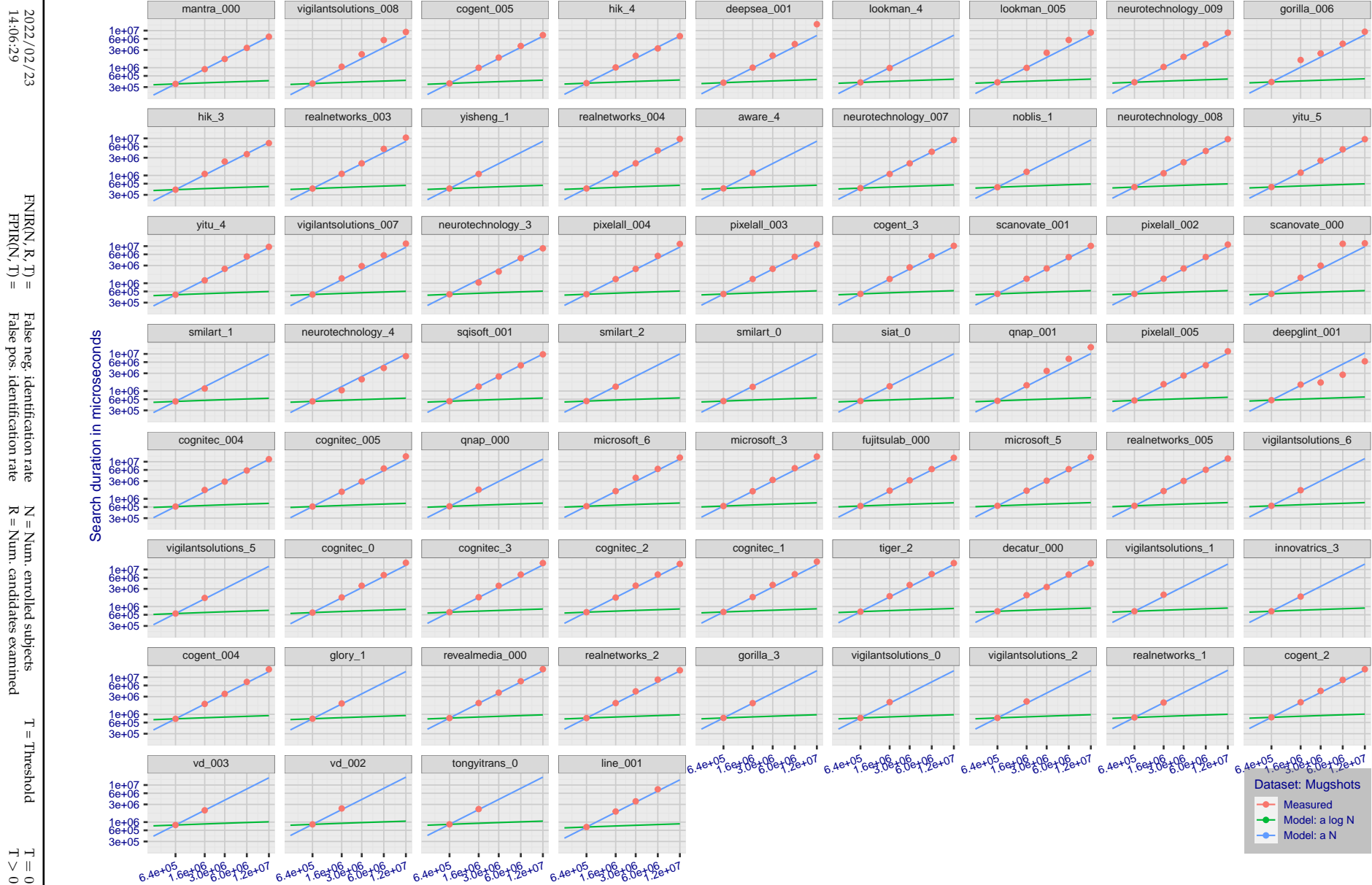


Figure 134: [Mugshot Dataset] Search duration vs. enrolled population size. In red are the actual point durations measured on a single c. 2016 core. The blue shows linear growth from $N = 640\,000$. The green line shows logarithmic growth from that point to $N = 1\,600\,000$. Note the sublinear growth from algorithms from Camvi, Dermalog, EverAI, Innovatrics, and Visionlabs. The tiger_1 algorithm is also sublinear, but inaccurate and inoperable at $N \geq 3000000$. This capability sometimes comes at the additional expense of converting a linear gallery data structure into whatever fast-search data structure is used. Note that search times are sometimes dominated by the template generation times shown in Table 22.

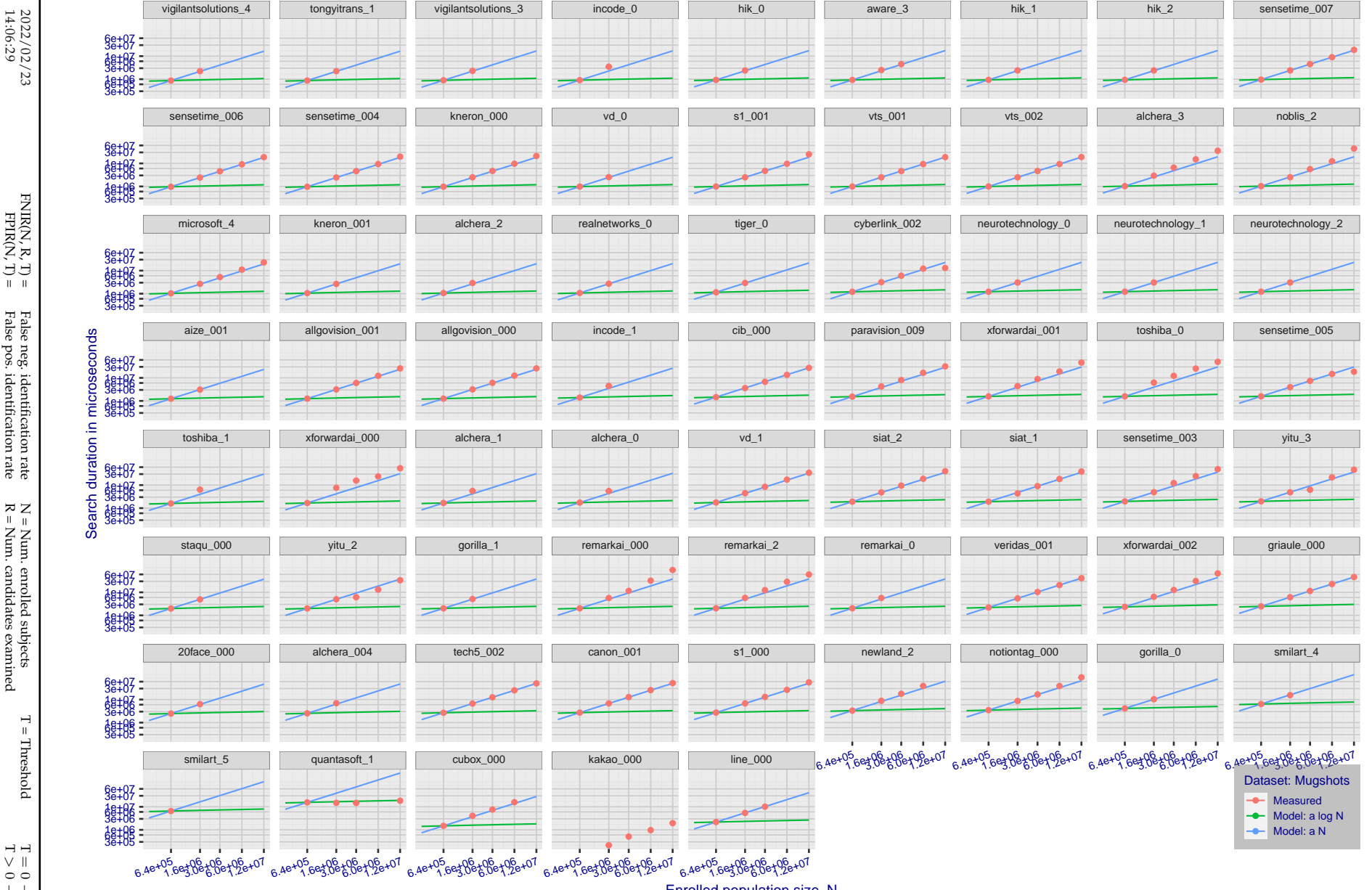


Figure 135: [Mugshot Dataset] Search duration vs. enrolled population size. In red are the actual point durations measured on a single c. 2016 core. The blue shows linear growth from $N = 640\,000$. The green line shows logarithmic growth from that point to $N = 1\,600\,000$. Note the sublinear growth from algorithms from Camvi, Dermalog, EverAI, Innovatrics, and Visionlabs. The tiger_1 algorithm is also sublinear, but inaccurate and inoperable at $N \geq 3000000$. This capability sometimes comes at the additional expense of converting a linear gallery data structure into whatever fast-search data structure is used. Note that search times are sometimes dominated by the template generation times shown in Table 22.

2022/02/23

FNIR(N, R, T) = False neg. identification rate

FPFR(N, T) = False pos. identification rate

N = Num. enrolled subjects

T = Threshold

T = 0 → Investigation

T > 0 → Identification

Appendix G Gallery Insertion Timing

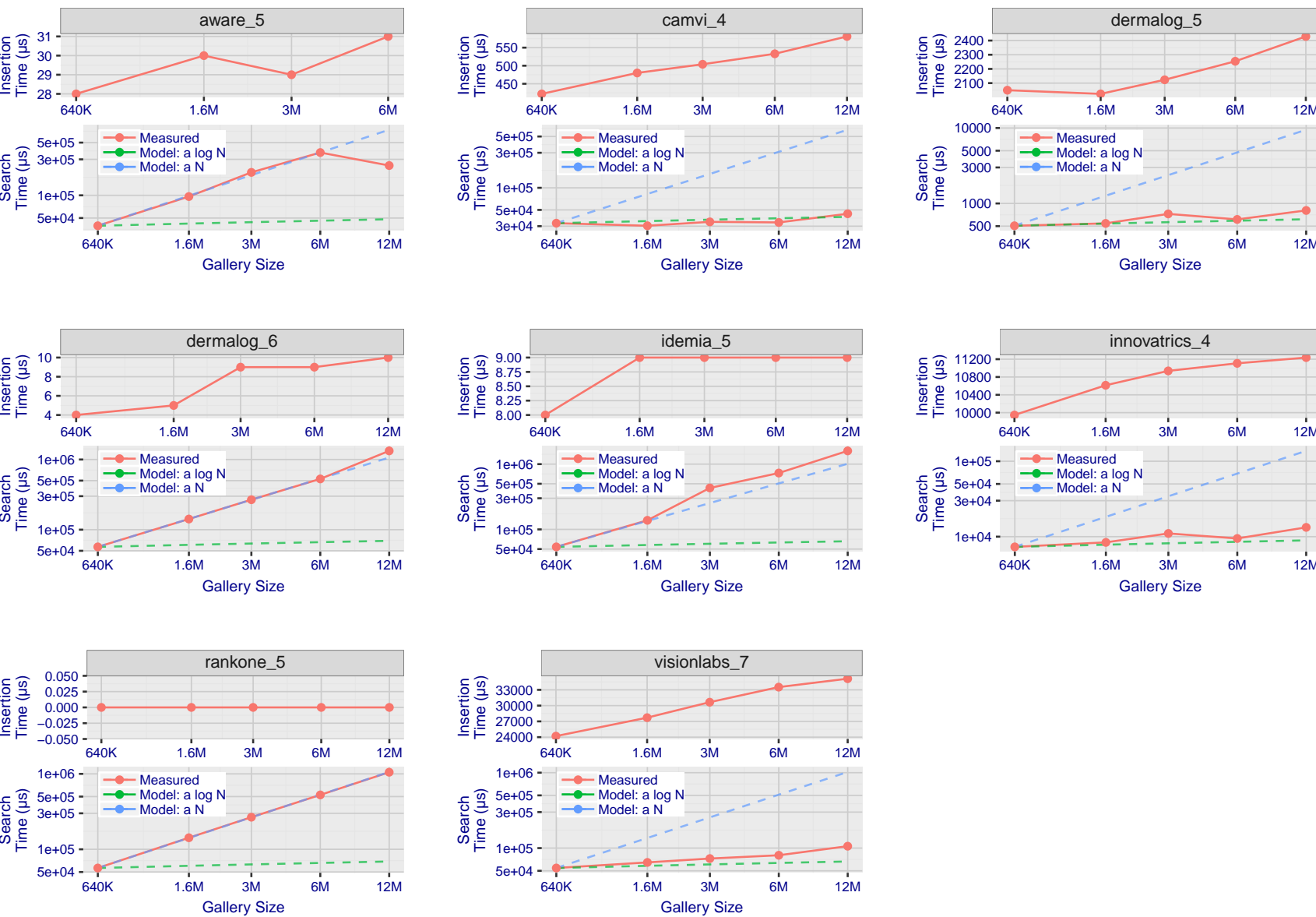
2022/02/23
14:06:29FNIR(N, R, T) = False neg. identification rate
FPIR(N, T) = False pos. identification rate
R = Num. candidates examinedN = Num. enrolled subjects
T = ThresholdT = 0 → Investigation
T > 0 → Identification

Figure 136: [Mugshot Dataset] Gallery insertion duration vs. enrolled population size. This chart plots the time it takes to insert a single template into a finalized gallery, illustrated over increasing gallery sizes. For reference, search times on finalized galleries of corresponding sizes are plotted right underneath. Gallery insertion time plots were generated on algorithms that 1) successfully implemented gallery insertion with no errors and 2) that were run on galleries with N up to 12 000 000. Generally, only the more accurate algorithms were run on galleries with N up to 12 000 000.

2022/02/23
14:06:29FNIR(N, R, T) = False neg. identification rate
FPFR(N, T) = False pos. identification rateN = Num. enrolled subjects
R = Num. candidates examinedT = Threshold
T = 0 → Investigation

T > 0 → Identification

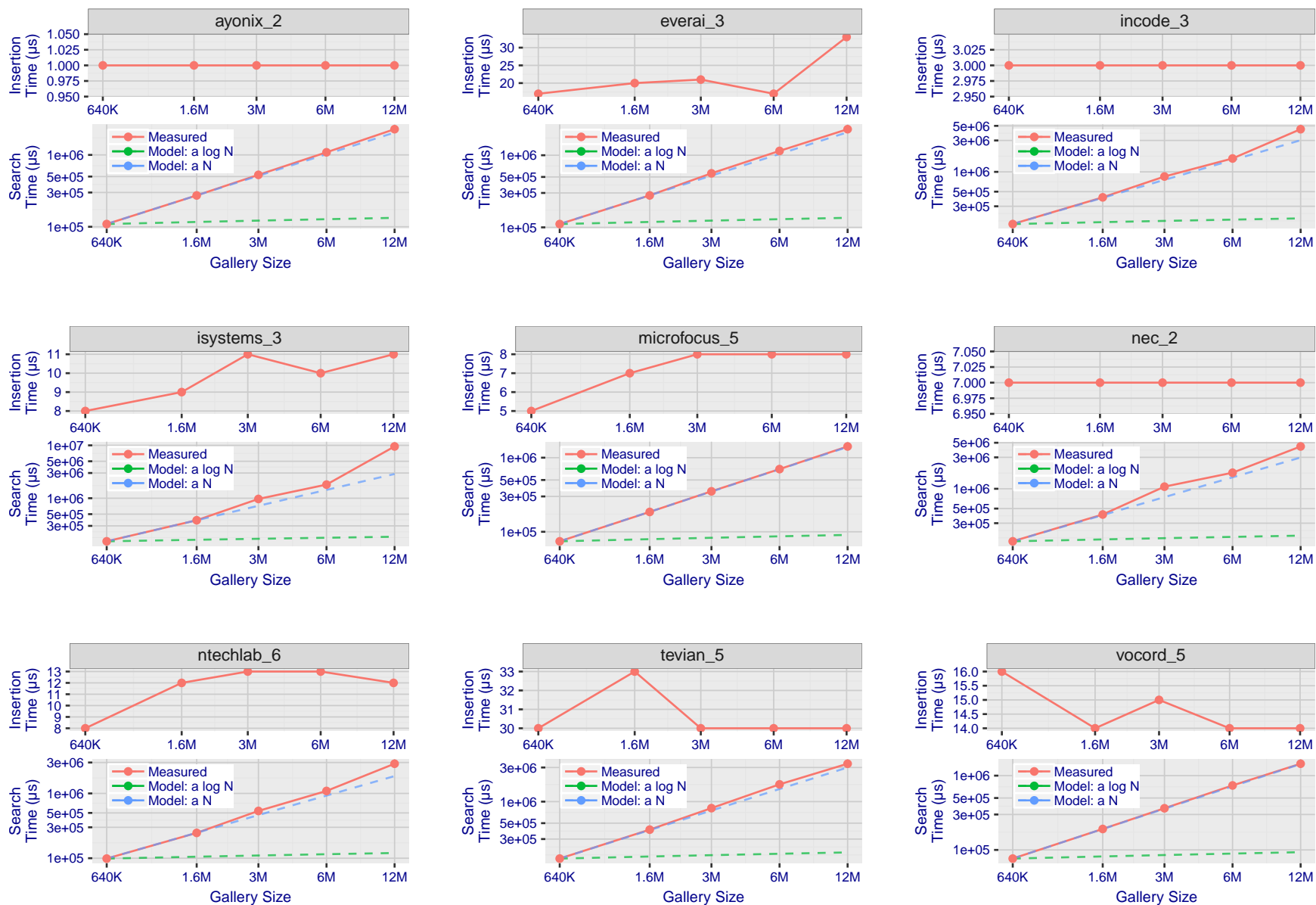


Figure 137: **[Mugshot Dataset] Gallery insertion duration vs. enrolled population size.** This chart plots the time it takes to insert a single template into a finalized gallery, illustrated over increasing gallery sizes. For reference, search times on finalized galleries of corresponding sizes are plotted right underneath. Gallery insertion time plots were generated on algorithms that 1) successfully implemented gallery insertion with no errors and 2) that were run on galleries with N up to 12 000 000. Generally, only the more accurate algorithms were run on galleries with N up to 12 000 000.

2022/02/23
14:06:29FNIR(N, R, T) = False neg. identification rate
FPTR(N, T) = False pos. identification rateN = Num. enrolled subjects
R = Num. candidates examinedT = Threshold
T = 0 → Investigation

T > 0 → Identification

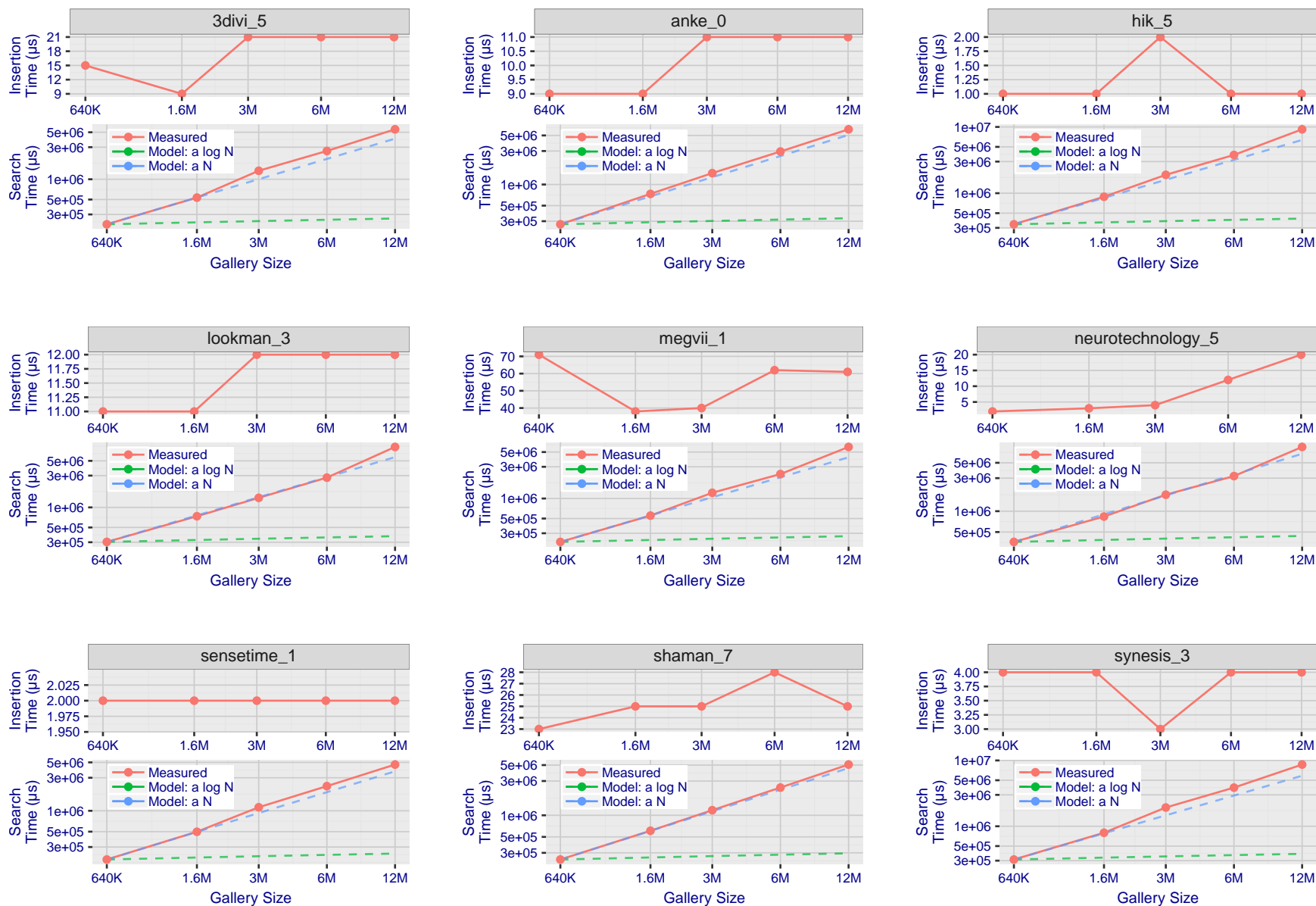


Figure 138: [Mugshot Dataset] Gallery insertion duration vs. enrolled population size. This chart plots the time it takes to insert a single template into a finalized gallery, illustrated over increasing gallery sizes. For reference, search times on finalized galleries of corresponding sizes are plotted right underneath. Gallery insertion time plots were generated on algorithms that 1) successfully implemented gallery insertion with no errors and 2) that were run on galleries with N up to 12 000 000. Generally, only the more accurate algorithms were run on galleries with N up to 12 000 000.

2022/02/23
14:06:29FNIR(N, R, T) = False neg. identification rate
FPTR(N, T) = False pos. identification rateN = Num. enrolled subjects
R = Num. candidates examinedT = Threshold
T = 0 → Investigation

T > 0 → Identification

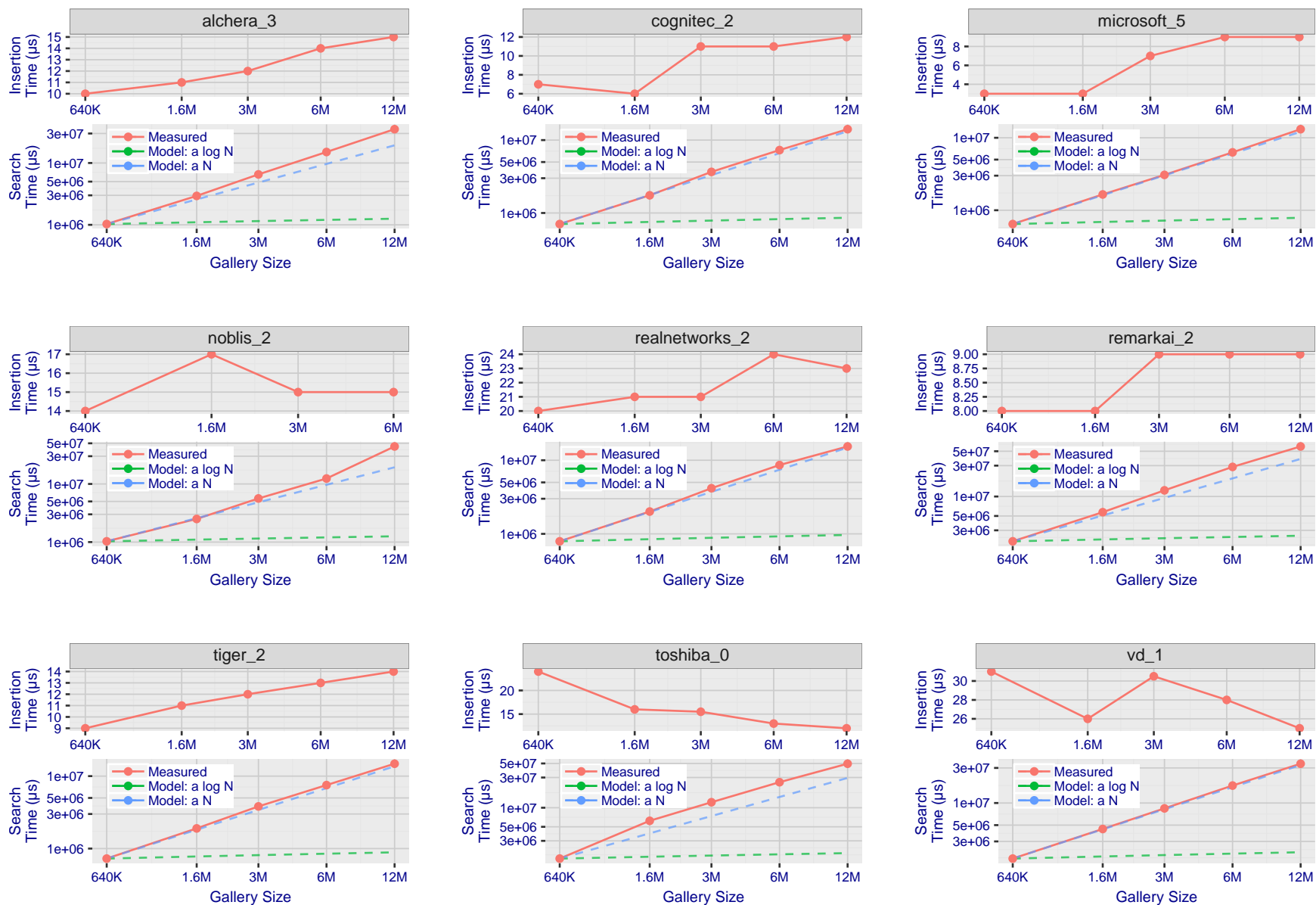


Figure 139: [Mugshot Dataset] Gallery insertion duration vs. enrolled population size. This chart plots the time it takes to insert a single template into a finalized gallery, illustrated over increasing gallery sizes. For reference, search times on finalized galleries of corresponding sizes are plotted right underneath. Gallery insertion time plots were generated on algorithms that 1) successfully implemented gallery insertion with no errors and 2) that were run on galleries with N up to 12 000 000. Generally, only the more accurate algorithms were run on galleries with N up to 12 000 000.

References

- [1] Artem Babenko and Victor Lempitsky. Efficient indexing of billion-scale datasets of deep descriptors. In *The IEEE Conference on Computer Vision and Pattern Recognition (CVPR)*, June 2016.
- [2] L. Best-Rowden and A. K. Jain. Longitudinal study of automatic face recognition. *IEEE Transactions on Pattern Analysis and Machine Intelligence*, 40(1):148–162, Jan 2018.
- [3] Blumstein, Cohen, Roth, and Visher, editors. *Random parameter stochastic models of criminal careers*. National Academy of Sciences Press, 1986.
- [4] Thomas P. Bonczar and Lauren E. Glaze. Probation and parole in the united statesm 2007, statistical tables. Technical report, Bureau of Justice Statistics, December 2008.
- [5] White D., Kemp R. I., Jenkins R., Matheson M, and Burton A. M. Passport officers' errors in face matching. *PLoS ONE*, 9(8), 2014. e103510. doi:10.1371/journal.pone.0103510.
- [6] P. Grother, G. W. Quinn, and P. J. Phillips. Evaluation of 2d still-image face recognition algorithms. NIST Interagency Report 7709, National Institute of Standards and Technology, 8 2010. <http://face.nist.gov/mbe> as MBE2010 FRVT2010.
- [7] P. J. Grother, R. J. Micheals, and P. J. Phillips. Performance metrics for the frvt 2002 evaluation. In *Proceedings of Audio and Video Based Person Authentication Conference (AVBPA)*, June 2003.
- [8] Patrick Grother and Mei Ngan. Interagency report 8009, performance of face identification algorithms. *Face Recognition Vendor Test (FRVT)*, May 2014.
- [9] Patrick Grother, George Quinn, and Mei Ngan. Face in video evaluation (five) face recognition of non-cooperative subjects. Interagency Report 8173, National Institute of Standards and Technology, March 2017. <https://doi.org/10.6028/NIST.IR.8173>.
- [10] Patrick Grother, George W. Quinn, and Mei Ngan. Face recognition vendor test - still face image and video concept, evaluation plan and api. Technical report, National Institute of Standards and Technology, 7 2013. http://biometrics.nist.gov/cs.links/face/frvt/frvt2012/NIST_FRVT2012.api_Aug15.pdf.
- [11] K. He, X. Zhang, S. Ren, and J. Sun. Deep residual learning for image recognition. In *2016 IEEE Conference on Computer Vision and Pattern Recognition (CVPR)*, pages 770–778, June 2016.
- [12] Gary B. Huang, Manu Ramesh, Tamara Berg, and Erik Learned-Miller. Labeled faces in the wild: A database for studying face recognition in unconstrained environments. Technical Report 07-49, University of Massachusetts, Amherst, October 2007.
- [13] Masato Ishii, Hitoshi Imaoka, and Atsushi Sato. Fast k-nearest neighbor search for face identification using bounds of residual score. In *2017 12th IEEE International Conference on Automatic Face & Gesture Recognition (FG 2017)*, pages 194–199, Los Alamitos, CA, USA, May 2017. IEEE Computer Society.
- [14] Jeff Johnson, Matthijs Douze, and Hervé Jégou. Billion-scale similarity search with gpus. *CoRR*, abs/1702.08734, 2017.

- [15] Ira Kemelmacher-Shlizerman, Steven M. Seitz, Daniel Miller, and Evan Brossard. The megaface benchmark: 1 million faces for recognition at scale. *CoRR*, abs/1512.00596, 2015.
- [16] Yury A. Malkov and D. A. Yashunin. Efficient and robust approximate nearest neighbor search using hierarchical navigable small world graphs. *CoRR*, abs/1603.09320, 2016.
- [17] Joyce A. Martin, Brady E. Hamilton, Michelle J.K. Osterman, Anne K. Driscoll, , and Patrick Drake. National vital statistics reports. Technical Report 8, Centers for Disease Control and Prevention, National Center for Health Statistics, National Vital Statistics System, Division of Vital Statistics, November 2018.
- [18] O. M. Parkhi, A. Vedaldi, and A. Zisserman. Deep face recognition. In *British Machine Vision Conference*, 2015.
- [19] P. Jonathon Phillips, Amy N. Yates, Ying Hu, Carina A. Hahn, Eilidh Noyes, Kelsey Jackson, Jacqueline G. Cava-zos, Géraldine Jeckeln, Rajeev Ranjan, Swami Sankaranarayanan, Jun-Cheng Chen, Carlos D. Castillo, Rama Chellappa, David White, and Alice J. O'Toole. Face recognition accuracy of forensic examiners, superrecognitioners, and face recognition algorithms. *Proceedings of the National Academy of Sciences*, 115(24):6171–6176, 2018.
- [20] Florian Schroff, Dmitry Kalenichenko, and James Philbin. Facenet: A unified embedding for face recognition and clustering. *CoRR*, abs/1503.03832, 2015.
- [21] Jeroen Smits and Christiaan Monden. Twinning across the developing world. *PLOS ONE*, 6(9):1–5, 09 2011.
- [22] Yaniv Taigman, Ming Yang, Marc'Aurelio Ranzato, and Lior Wolf. Deepface: Closing the gap to human-level performance in face verification. In *Proceedings of the 2014 IEEE Conference on Computer Vision and Pattern Recognition, CVPR '14*, pages 1701–1708, Washington, DC, USA, 2014. IEEE Computer Society.
- [23] A. Towler, R. I. Kemp, and D White. *Unfamiliar face matching systems in applied settings*. Nova Science, 2017.
- [24] Working Group 3. Ed. M. Werner. *ISO/IEC 19794-5 Information Technology - Biometric Data Interchange Formats - Part 5: Face image data*. JTC1 :: SC37, 2 edition, 2011. <http://webstore.ansi.org>.
- [25] David White, James D. Dunn, Alexandra C. Schmid, and Richard I. Kemp. Error rates in users of automatic face recognition software. *PLoS ONE*, 10:1–14, October 2015.
- [26] Bradford Wing and R. Michael McCabe. Special publication 500-271: American national standard for information systems data format for the interchange of fingerprint, facial, and other biometric information part 1. Technical report, NIST, September 2015. ANSI/NIST ITL 1-2015.
- [27] Andreas Wolf. Portrait quality - (reference facial images for mrtd). Technical report, ICAO, April 2018.
- [28] D. Yadav, N. Kohli, P. Pandey, R. Singh, M. Vatsa, and A. Noore. Effect of illicit drug abuse on face recognition. In *2016 IEEE Winter Conference on Applications of Computer Vision (WACV)*, pages 1–7, Los Alamitos, CA, USA, mar 2016. IEEE Computer Society.